

OVERVIEW OF MINERAL MATTER IN U.S. COALS

R. D. Harvey and R. R. Ruch

Illinois State Geological Survey
Champaign, IL 61820

INTRODUCTION

Minerals in coal have been a subject of much interest during the past 20 years. Early studies approached the subject somewhat indirectly by means of chemical analysis of high temperature ash and back calculation to obtain estimates of the mineral matter (1). Others supplemented chemical studies by hand picking the coarser minerals or making density separations for chemical tests and optical microscopic study (2,3). With the advent of radio frequency ashing at low temperature (<150°C) it became possible to directly investigate all the mineral constituents (4). This led to progress in quantitative analyses of the mineral composition by x-ray diffraction methods (5-8). This paper summarizes some geological aspects related to minerals, their classification and occurrences in coal, and presents a compilation of available data on the mineralogical composition in coals from some of the major coal basins in the United States.

CLASSIFICATION OF MINERAL MATTER IN COAL

Coal is a sedimentary rock composed of three categories of substances: organic carbonaceous matter, termed macerals, inorganic (mainly crystalline) minerals, and fluids. The latter occur in pores within and between the other two solid constituents. The fluids in coal prior to mining are mainly moisture and methane. Applied to coal, the term mineral matter is an inclusive term that refers to the mineralogical phases as well as to all other inorganic elements in the coal; that is, the elements that are bonded in various ways to the organic (C,H,O,N,S) components. The term mineral refers only to the discrete mineral phases.

Because coal is a type of sedimentary rock, 100 or so different minerals can occur in coals; however, only about 15 are abundant enough to have high importance. These are listed in table 1 along with the stoichiometric chemical formula of each. It must be noted that minor impurities commonly substitute for the major cations as well as some anions which account for a considerable fraction of the minor and trace elements reported in coals (9-10).

Minerals in coal occur as discrete grains or flakes in one of five physical modes: (1) disseminated, as tiny inclusions within macerals; 2) layers or partings (also lenses) wherein fine-grained minerals predominate; 3) nodules, including lenticular or spherical concretions; 4) fissures (cleat and fracture fillings and also small void fillings); 5) rock fragments, megascopic masses of rock replacements of coal as a result of faulting, slumping, or related structures.

The minerals listed in table 1 are classified by their physical modes of occurrences. Description of mineral impurities in coal deposits, based on this classification is useful in a number of ways. Thick layers and abundant nodules or rock fragments hamper mining operations, but are easily removed by standard coal preparation (cleaning) facilities. On the other hand, disseminated minerals and the thinner (microscopic) layers are not much removed by existing preparation facilities. The latter two modes are dominated by mixtures of illite, quartz, and pyrite (table 1).

Useful also is a genetic classification of minerals in coal, wherein they are classified according to Mackowsky (11) as detrital, syngenetic, or epigenetic (table 1). Detrital minerals are those that were deposited in a coal forming peat swamp from slowly moving water or wind currents. Flakes of illite clay and microscopic grains of quartz, feldspars, zircon, apatite, rutile and perhaps others were deposited as discrete grains which became interbedded with peat and ultimately with the resultant coal. Most wind deposited minerals are recognized as such by the presence of certain high temperature phases. These are therefore, dust particles derived from distant volcanoes. Layered deposits of these dusts are termed tonsteins.

Syngenetic minerals are those that formed within the peat during the early stages of its coalification - before the peat was deeply buried by other sediments, probably by not more than about 50 feet. Under these conditions disseminated pyrite is thought to have formed in sulfate bearing peat by bacterial reduction of the sulfur. Much of this type of pyrite has a spherical form and is described as framboidal pyrite. Nodules of peat mineralized with various carbonates and nodules comprised of microcrystalline quartz and/or hematite formed early in the development of coal. Ultra-small crystallites of some minerals disseminated within macerals may also be syngenetic in origin, notably micrometer sized crystals of kaolinite and possibly illite observed by Strehlow, et al. (12) and by Wert and Hsieh (13). These crystallites, as well as some of the tiny disseminated grains of quartz are thought by some to have crystallized from inorganic matter inherited from the original plant material (2,3,14).

Epigenetic minerals are mainly those found in fissures and void fillings. Much of the calcite in coals as well as part of the pyrite and kaolinite in coals are recognized as epigenetic. This class of minerals formed long after the peat was consolidated and coalified enough to allow joints to develop where in these minerals precipitated. For most coals, this precipitation probably occurred during the late lignite or early subbituminous stages of coalification.

DISTRIBUTION OF MINERALS IN COALS

Typically, different layers of a seam vary considerably in their mineral matter as well as specific mineral components (fig. 1). The thin layer labeled BB is a carbonaceous shale and it contains the highest amount of mineral matter, which is mainly comprised of clay (illite, kaolinite, and smectite minerals) and quartz. At one site in the mine studied this layer was enriched in pyrite (see lower part of the figure). The pyrite distribution at the four sites is fairly consistent in the upper layers at each site, but this epigenetic type of mineral is enriched in the lowest layer at three of the four sites (fig. 1). At this mine, and elsewhere, the conditions under which peat accumulated are thought to have been fairly consistent over regional geographical areas, much as they are today in existing peat swamps. Therefore, comparisons of mineral matter between coals are usually made by comparing analyses of channel samples that represent all layers in the seam (10).

ANALYTICAL TECHNIQUES

There are numerous instrumental techniques that can be applied to the characterization of mineral matter in coal. Probably the most widely used technique is x-ray diffraction analysis because of its availability and extensive development by mineralogists (5,6,7). Infrared spectroscopy has been successfully applied toward the analyses of common minerals found in coal (15). Differential Thermal Analysis (DTA) under nitrogen atmosphere can be used for the identification of certain minerals (16) by monitoring decomposition temperatures. Scanning electron microscopy with an energy dispersive x-ray analysis accessory unit has been used to identify various minerals as hosts for specific elements in coal (17,18). The

ion microprobe has also been applied to the study of minerals in coal (19). Mössbauer Spectroscopy has recently become very important in the study of iron sulfide minerals in coal (20). Preconcentrating the mineral matter in coal by radio frequency low-temperature ashing has been well established and is extensively practiced (4,9,14,22). It effectively removes the carbonaceous matter while causing only minor changes in the remaining minerals. The advantages are higher sensitivity for most instrumental techniques used.

Extensive elemental analyses has primarily been carried out on coal samples or ashes of coals for purposes of distribution studies and has been reviewed (21). Chemical analyses of separated coal minerals are also available confirming element-mineral associations derived from float-sink studies (14,22).

MINERAL COMPOSITION IN SOME SAMPLES FROM VARIOUS COAL BASINS

Results of mineralogical analyses of low temperature ashes by x-ray diffraction were compiled from the files of the Illinois State Geological Survey (table 2). Samples representative of the two most mined coals in the Illinois Basin provide a good statistical bases for evaluating this basin; however, this is not the case for results listed for other basins. To date, there is insufficient mineralogical data on these coal basins to draw many conclusions. Nonetheless, these data were generated in one laboratory, using the same procedures, and they provide a basis for some preliminary comparisons. The results show the following increasing compositional trends of the mean values, expressed by the state abbreviations given in table 1.

Mineral matter: AZ<TN<MT,ND,WY = So.WV<No.WV<IL<AL<IA

Pyrite (FeS_2): AZ = MT,ND,WY = So.WV<TN<AL = IL<No.WV<IA

The samples from the Black Mesa Basin in Arizona indicate the seams mined there are lowest in mineral matter and pyrite contents; those in Iowa appear to be the highest in both of these constituents. However, the range of mineral contents is generally high and dictates that the quality of each deposit be considered on its own quality parameters for possible feed stock to coal processing plants.

REFERENCES

1. S. W. Parr, University of Illinois Engineering Experiment Station Bull. 180, 1928, 62 pp.
2. C. G. Ball, Illinois State Geological Survey Report Invest. 33, 1935, 106 pp.
3. G. C. Sprunk and H. J. O'Donnell, U.S. Bureau of Mines Technical Paper 648, 1942, 67 pp.
4. H. J. Gluskoter, Fuel, 44, 285-291 (1965).
5. C. Prasada Rao and H. J. Gluskoter, Illinois State Geological Survey Circular 476, 1973, 56 pp.
6. J. J. Renton, U.S. Dept. Energy, Morgantown Energy Research Center MERC/CR-77/10, 1977, 20 p.
7. S. J. Russell and S. M. Rimmer, "Analysis of Mineral Matter in Coal, Coal Gasification Ash, and Coal Liquefaction Residues by Scanning Electron Microscopy and X-ray Diffraction," in Analytical Methods for Coal and Coal Products, C. Kan Jr., ed., Academic Press, NY, 1979, pp. 133-162.

8. A. S. Pavlovic, J. M. Cook, and J. J. Renton, Proc. International Conference on Coal Science, Düsseldorf 7-9.9, 1981, pp. 828-834.
9. J. V. O'Gorman and P. L. Walker, Jr., Fuel, 50, 1971, 135-151.
10. H. J. Gluskoter, R. R. Ruch, W. G. Miller, R. A. Cahill, G. B. Dreher, and J. K. Kuhn, Illinois State Geological Survey, Circular 477, 1977, 154 pp.
11. M.-Th. Mackowsky, in E. Stach, et al. "Coal Petrology," 3rd revised ed., Gebruder Borntraeger, Berlin, 1982, pp. 153-171.
12. R. A. Strehlow, L. A. Harris, and C. S. Yust, Fuel, 57, 1979, 185-186.
13. C. A. Wert and K. C. Hzieh, Proc. International Conference on Coal Science, Düsseldorf 7-9.9, 1981, p. 780-785.
14. C. B. Cecil, R. W. Stanton, and F. T. Dulong, U.S. Geological Survey Open-File Report 81-953-A, 1981, 92 pp.
15. P. A. Estep, J. J. Kovach, and Clarence Karr, Jr. Anal. Chem., 40 (2) 358-363 (1968).
16. James V. O'Gorman and P. L. Walker, Fuel 52, 71-79 (1973).
17. R. R. Ruch, H. J. Gluskoter, and N. F. Shimp, Illinois State Geological Survey Environ. Geology Note No. 72, 1974.
18. H. J. Gluskoter and P. C. Lindahl, Science, 181 264-166 (1973).
19. P. H. Ribbe, Abstr. Geol. Soc. Am. Abstracts with Programs, 7 (7) 1244 (1975).
20. Gerald V. Smith, Juei-Ho Lin, Mykola Saporoschenko, and Richard Shiley, Fuel 57 (1), 41-45 (1978).
21. Harold J. Gluskoter, Neil F. Shimp, and Rodney R. Ruch, "Coal Analyses, Trace Elements, and Mineral Matter," in Chemistry of Coal Utilization, Second Supplementary Volume, Martin A. Elliott, ed., John Wiley and Sons, 1981, pp. 369-424.
22. R. D. Harvey, R. A. Cahill, C.-L. Chou, and J. D. Steele, US EPA Grant R 806654, Final Report, 1983, 162 pp.

Table 1. Minerals frequently occurring in coals, their stoichiometric compositions, their modes of occurrences, and relative abundance (11).

Mineral	Composition	Chief occurrences		Abundance in min. matter
		Physical*	Genetic**	
Clay minerals				
illite (sericite, K-mica)	$KAl_2(AlSi_3O_{10})(OH)_2$	D,L	d,s(?)	common
smectite (mixed layered)	$Al_2Si_4O_{10}(OH)_2 \cdot H_2O$ (with Na, Mg and Others)	D,L	d,s(?)	common
kaolinite group	$Al_4Si_4O_{10}(OH)_8$	L,F	e,d,s(?)	common
Sulfides				
pyrite	FeS_2 (isometric)	D,N,F	s,e	variable
marcasite	FeS_2 (orthorhombic)	D(?)	s(?)	rare
sphalerite	ZnS	F	e	rare
others: greigite, galena, chalcopyrite and pyrrhotite are reported as very rare				
Carbonates				
calcite	$CaCO_3$	N,F	e,s	variable
dolomite, incl. ankerite (Fe)	$Ca(Mg,Fe)(CO_3)_2$	N	s,e	variable
siderite	$FeCO_3$	N	s,e	variable
Oxides				
hematite	Fe_2O_3	N	s	rare
quartz	SiO_2	D,L,N	d	common
others: magnetite and rutile are reported as very rare				
Others				
limonite-goethite	$FeOOH$	N	e	rare
apatite, incl.	$Ca_5(PO_4)_3(F,Cl,OH)$	D	d,s(?)	rare
sulfates, mainly gypsum, barite, and several iron-rich ones				
feldspars	$K(Na)AlSi_3O_8$	D,L	d	rare
zircon	$ZrSiO_4$	D,L	d	rare
others: many others reported as very rare (11)				

* D = disseminated; L = layers (partings); N = nodules; F = fissures (cleat).
Each mineral listed may often occur in rock fragments within coal beds.

** d = detrital; e = epigenetic, second state of coalification (mainly along joints (cleat) in coal beds); s = syngenetic, first stage of coalification (disseminated, intimately intergrown with macerals). The first listed occurrence is the more common one in U.S. coals; others are reported in some coal fields.

Table 2. Mineral composition of channel samples in various US coals*

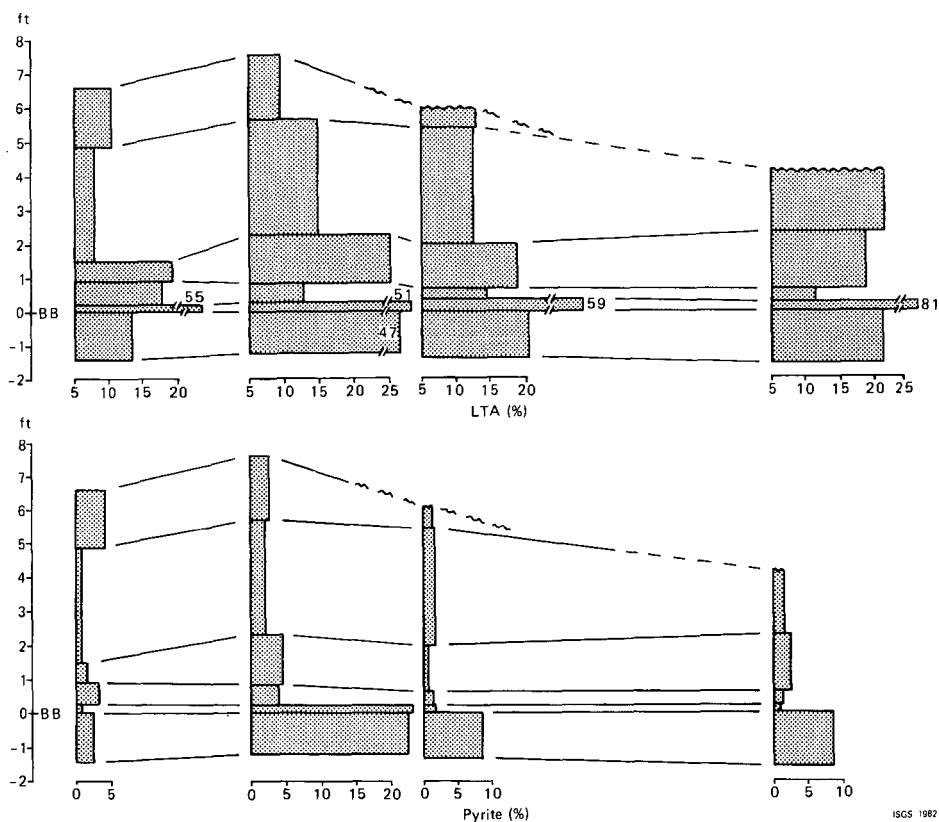
Minerals	Great Plains Basins MT, ND, WY		Western Interior Basin IA		Illinois Basin IL, IN, W-KY		Central Appalachian Basin			
	%	(range)	%	(range)	%	(range)	Southern WV		Northern WV+PA	
No. Samples	23		3		107		3		6	
LTA**	13	(7-27)	28	(23-34)	16	(9-28)	13	(13-14)	14	(10-15)
Pyrite	<1	(0-2)	8	(7-9)	2	(<1-12)	<1	(<1-1)	4	(2-5)
Quartz	2	(<1-6)	4	(1-7)	2	(<1-5)	1	(<1-3)	2	(1-2)
Calcite	<1	(0-3)	4	(1-7)	1	(<1-5)	<1	(0-<1)	1	(<1-3)
Clays†	11	(4-25)	13	(9-16)	9	(3-19)	11	(10-12)	8	(6-9)
Others (traces)	sulfates &/or nitrates feldspar aragonite chlorite		none det.		sulfates marcasite sphalerite feldspar hematite		siderite ankerite		siderite feldspar	

Southern Appalachian Basin						
No. Samples	Black Mesa Basin AZ		TN			
	%	(range)				
LTA	9	(5-12)	18	(13-28)	12	(10-16)
Pyrite	<1	(<1)	2	(0-6)	1	(<1-1)
Quartz	2	(2-3)	2	(<1-4)	1	(<1-2)
Calcite	<1	(0-1)	<1	(0-1)	none det.	
Clay†	6	(2-9)	18	(12-21)	11	(9-14)
Others (traces)	none det.		siderite apatite sericite		none det.	

* Mean weight percent and range on a whole coal basis.

** Total mineral matter by low temperature ashing methods.

† By difference.



ISGS 1982

Figure 1. Vertical variation of mineral matter within a seam at four sites in a large mine: the total mineral matter content is shown in the upper diagram and the pyrite (FeS₂) fraction below. Geological analysis of the layers indicated that the upper most layer at three sites was not present at the fourth, shown on the right.

Influence of Environments of Deposition on the Inorganic Composition of Coals

S. M. Rimmer¹ and A. Davis²

¹Department of Geology, University of Kentucky, Lexington, KY 40506

²Department of Geosciences, The Pennsylvania State University, University Park, PA 16802

Introduction

The mineral composition of coal is the result of physical, chemical and biological processes acting on the system from the time of peat accumulation, through burial and subsequent increase in rank, to the present. With respect to origin, inorganic constituents may be classified as: inherent (being derived from inorganic components within the peat-forming plants) or adventitious (being derived from outside the peat swamp and forming either during or after peat accumulation); and detrital (those transported into the peat swamp) or authigenic (those formed within the environment). Mackowsky (1) further differentiates between syngenetic minerals, formed during the accumulation of peat, and epigenetic minerals, which formed later.

In recent years considerable controversy has surrounded the origin of minerals in coal: the question is whether most of these materials are derived from inorganic substances originally contained within peat-forming plants (inherent), or from sources outside the peat swamp (detrital).

Studies of modern peat-forming environments have emphasized the importance of detrital influx (2,3), syngenetic formation of pyrite (4) and biogenic silica (2,5), and in-situ mixing with underlying sediments (2,6) to account for mineral constituents in coal. Within the peat environment certain unstable detrital clays may undergo alteration or dissolution (3,7); other clays, such as kaolinite, may form authigenically; and biogenic silica dissolves, possibly contributing to later authigenic mineralization (3,5). In coals, authigenic kaolinite formation along cleats is common (8,9). Clays may also form by alteration of volcanically-derived material (10). Opposing the concept of a major detrital input, Cecil and his co-workers (11,12) consider the major source of ash components to be the inorganic fraction of peat-forming plants, and total mineral content to be a function of the degree of peat degradation.

While this controversy still lingers, it appears that several origins are possible for minerals in peat and coal, including detrital influx, biogenic input, and precipitation either during or after peat accumulation, including some contribution from inorganic substances derived from plants. Various studies have attempted to relate inorganic composition to conditions existing at the time of peat accumulation. Pyrite has frequently been associated with marine and brackish peats (4,13), and the pyrite content of coal has been related to roof lithology (14,15). Clay assemblages of coals and underclays also have been related to depositional environment (9,16).

The purpose of this paper is to describe variability in the inorganic content of a single coal and attempt to explain the distribution of minerals in a framework of depositional environments. In western Pennsylvania, the Lower Kittanning seam provides an opportunity to study coal that was influenced by freshwater, brackish and marine conditions, as indicated by a previous study of the overlying shale (17). Several geologic controls are thought to have influenced deposition during this time: differential subsidence resulted in a thickening of sediments (and coal) towards the center of the basin; a basement high to the north of the field area may have supplied clastic material, adding

to a predominantly eastern sediment source; and active folds and variations in paleotopography may have also influenced sedimentation patterns (18).

Sampling and Methods

Forty-three channel samples of the Pennsylvanian-aged Lower Kittanning coal (Kittanning Formation, Allegheny Group) were collected in western Pennsylvania. Samples are representative of all three suggested depositional environments (Figure 1) and also of the increase in rank from high volatile bituminous in the west to low volatile bituminous in the southeast. Analyses included major and minor elements, total sulfur and sulfur forms, and low-temperature ashing. LTA's were obtained according to standard procedures (19). X-ray diffraction analysis of LTA's provided qualitative, quantitative (for quartz and pyrite), and semi-quantitative (for clays in the $< 2 \mu\text{m}$ fraction) data using procedures modified from Russell and Rimmer (20). Kaolinite was quantified using infra-red spectroscopy. Mineral composition was also calculated by normative techniques modified from Pollack (21) and Given *et al.*, (22).

Results and Discussion

The major mineral components of this coal include quartz, pyrite (and marcasite), and clays (predominantly kaolinite and illite/mica, with lesser amounts of expandable clays). Total mineral content (percent LTA) varies considerably across the basin, with very high ash contents occurring in the center of the basin and along sections of the Allegheny Front. To further understand these variations, individual mineral distributions were examined.

Pyrite distribution shows a definite basinal trend, with high pyrite contents occurring across the center of the basin (Figure 2). Whereas much of this area underlies marine and brackish roof rocks, the relationship is not perfect. Highest pyrite content appears to be most closely related to the eastern brackish zone. Factors influencing the distribution of sulfur in peat and coals include availability of iron and sulfate, and pH. Sulfate is thought to be introduced by marine and brackish waters (4). Recent work on pyrite distribution in the Florida Everglades (23) indicates highest pyrite content is associated with brackish environments rather than marine, and this has been related to the availability of iron. In freshwater, iron is transported in organic colloids which flocculate quickly upon entering brackish water, resulting in a higher availability of iron in brackish environments (24). pH is also a factor, as much of the pyrite appears to form as a by-product of sulfate-reducing bacteria (4). Compared to the more acidic freshwater environments, higher levels of microbial activity would occur in the neutral to basic pH conditions existing in marine or brackish waters. Pyrite content is therefore highest in areas that were influenced at least by brackish conditions.

The central part of the basin was experiencing more rapid subsidence than the margins, thus any marine influence would be greater in this area. Apparent discrepancies in the relationship between pyrite content and roof lithology may be explained on the basis of iron availability. (Data to be discussed later suggest a detrital influence towards the eastern margin of the basin, providing clay-rich sediments which may have contributed to the supply of iron). Other workers have also commented on this lack of correlation and suggest epigenetic pyrite formation along cleats and joints may be responsible (25). A third alternative is that the zone of maximum brackish and marine influence shifted during the history of the peat swamp.

Quartz content is highest in the north-central part of the basin, with isolated quartz-rich pods along the Allegheny Front. The origin of quartz in coal has been debated at length. Detrital quartz has been distinguished by many

authors (1,3) while other workers (11,12) believe much of this quartz is derived from silica originally contained within the plants. Petrographic observations of quartz in this coal revealed an association with attrital bands, suggesting a detrital origin. The distribution may be related to the basement high that existed to the north during this time (18). Transportation within the swamp of quartz-rich sediments derived from this high was possibly restricted by the baffling effect of vegetation, a phenomenon noted in modern swamps (2). In addition, lesser amounts of quartz may have been carried in from the east. Sediment derived from this latter source appears to have been predominantly clay. Comparable quartz distributions were noted in the underclay (26), thus the influence of in-situ mixing also exists.

Kaolinite is the major clay constituent of the coal and occurs in highest concentrations along the basin margins, with illite increasing towards the central part of the basin. Once again a similar distribution was noted in the underclays (26). Differential flocculation within the basin, together with chemical regrading of clays, could be used to explain this distribution. Holbrook (26) argues against this mechanism for the underclays on the basis of flocculation studies in modern environments, and suggests differential leaching related to variations in paleotopography may have been important. Another control could be the effect of peat chemistry on the clay assemblage. Kaolinite appears to be highest in freshwater environments where, under lower pH conditions, it would be the most stable clay mineral. Thus, in these areas not only could kaolinite be detrital, but also the product of clay alteration and authigenesis. The presence of high-temperature polytypes suggest a detrital origin for illite/mica in the Lower Kittanning coal and underclay, as discussed by Davis et al. (3) and Holbrook (26). Detrital illite/mica would be better preserved in more basinward areas.

One additional control on the clay mineral assemblage could be rank. With the increase in rank exhibited by this coal, certain diagenetic changes might be expected. No consistent trends in mineralogy were observed, however a general lack of smectite and highly-expandable clays (which can be seen in lower rank coals) was noted. This could be related to rank, or be a function of provenance.

Summary

The distribution of minerals within the Lower Kittanning coal can be related to depositional environments. Total mineral content varies considerably across the basin, and variations can be explained by examining the distributions of individual minerals.

Pyrite content is controlled by availability of sulfate and iron, and pH. Highest concentrations are seen towards the center of the basin where subsidence was more rapid and marine and brackish influences (affecting sulfate availability and pH) were felt during and after peat accumulation. Iron availability may have been associated with the transport of organic colloids or clay into the basin.

Quartz appears to be limited to the northern part of the field area and isolated areas along the Allegheny Front. It is suggested that quartz-rich sediments were derived from a positive area to the north. Much of the sediment brought in from the east appears to have been clay-rich.

The chemistry of the peat may have had a strong influence on clay mineral assemblage. Kaolinite may have been both detrital and authigenic, whereas illite/mica appears to be detrital. Rank has had little effect on the overall clay assemblage.

References

- (1) Mackowsky, M-Th. (1968). In "Coal and Coal-Bearing Strata" (D. Murchison and T.S. Westoll, eds.), pp. 325-345, American Elsevier, New York.
- (2) Otte, L.J. (1984). Geol. Soc. Am., Abstr. Programs 16, 3, 185.
- (3) Davis, A., Russell, S.J., Rimmer, S.M., and Yeakel, J.D. (1984) Int. J. Coal Geol., 3, 293-314.
- (4) Casagrande, D.J., Siefert, K., Berschinski, C., and Sutton, N. (1977) Geochim. Cosmochim. Acta, 41, 161-167.
- (5) Andrejko, M.J., Raymond, R. Jr., and Cohen, A.D. (1983). In "Mineral Matter in Peat: Its Occurrence, Form, and Distribution" (R. Raymond, Jr., and M.J. Andrejko, eds.), pp. 25-37, Proc. Workshop, Los Alamos Natl. Lab., Los Alamos, New Mexico.
- (6) Andrejko, M.J., Cohen, A.D., and Raymond, R. Jr. (1983). In "Mineral Matter in Peat: Its Occurrence, Form, and Distribution" (R. Raymond, Jr., and M.J. Andrejko, eds.), pp. 3-24, Proc. Workshop, Los Alamos Natl. Lab., Los Alamos, New Mexico.
- (7) Staub, J.R., and Cohen, A. (1978). J. Sed. Pet., 48, 203-210.
- (8) Ball, C.G. (1934). Econ. Geol., 29, 757-776.
- (9) Gluskoter, H.G. (1967). J. Sed. Pet., 37, 205-214.
- (10) Bohor, B.F., Pollastro, R.M., and Phillips, R.E. (1978) 27th. Ann. Clay Min. Conf., Prog. and Abstr., 47.
- (11) Renton, J.J., and Cecil, C.B. (1980). In "Carboniferous Coal Short Course and Guidebook, Vol. 3" (A.C. Donaldson, M.K. Presley, and J.J. Renton, eds.), AAPG Seminar, pp. 103-128, Morgantown, W.Va.
- (12) Renton, J.J., Cecil, C.B., Stanton, R., and Dulong, F. (1980). In "Carboniferous Coal Short Course and Guidebook, Vol. 3" (A.C. Donaldson, M.K. Presley, and J.J. Renton, eds.), AAPG Seminar, pp. 57-101, Morgantown, W.Va.
- (13) Spackman, W., Cohen, A.D., Given, P.H., and Casagrande, D.J. (1976) A Field Guide to Aid in the Comparative Study of the Okefenokee Swamp and the Everglades-Mangrove Swamp-Marsh Complex of Southern Florida: The Pennsylvania State University Coal Research Section Short Course, University Park, PA.
- (14) Williams, E.G., and Keith, M.C. (1963). Econ. Geol., 58, 720-729.
- (15) Kravits, C.M., and Crelling, J.C. (1981). Int. J. Coal Geol., 1, 195-212.
- (16) Parham, W.E. (1966). Proc. Int. Clay Conf., 1, 135-145, Jerusalem, Israel.
- (17) Williams, E.G. (1960). J. Paleontol., 34, 908-922.
- (18) Williams, E.G. and Bragonier, W.A. (1974). Geol. Soc. Am. Spec. Paper 148, 135-152.
- (19) Gluskoter, H.G. (1965) Fuel, 44, 285-291.
- (20) Russell, S.J., and Rimmer, S.M. (1979). In "Analytical Methods for Coal and Coal Products, Vol. III" (C. Karr, Jr., ed.), pp. 133-162, Academic Press, New York.
- (21) Pollack, S. (1979). Fuel, 58, 76-78.
- (22) Given, P.H., Weldon, D., and Suhr, N. (1980). Investigation of the Distribution of Minerals in Coal by Normative Analysis: Tech. Rept. 2, Pennsylvania State University to U.S. Dept. Energy, Rept. No. FE-2494-TR-2.
- (23) Cohen, A.D., Spackman, W., and Dolson, P. (1983). In "Mineral Matter in Peat: Its Occurrence, Form and Distribution" (R. Raymond, Jr., and M.J. Andrejko, eds.), pp. 87-112, Proc. Workshop, Los Alamos Natl. Labs., Los Alamos, New Mexico.
- (24) Sholkovitz, E.R., Boyle, E.A., and Price, N.B. (1978). Earth and Planet. Sci. Newsletter, 40, 130-136.
- (25) Davies, T.D., and Raymond, R. Jr. (1983). In "Mineral Matter in Peat: Its Occurrence, Form and Distribution" (R. Raymond, Jr., and M.J. Andrejko, eds.), pp. 123-139, Proc. Workshop, Los Alamos Natl. Labs., Los Alamos, New Mexico.
- (26) Holbrook, P.W. (1973) Geologic and Mineralogic Factors Controlling the Properties and Occurrences of Ladle Brick Clays: Unpubl. PhD. Thesis, The Pennsylvania State University, University Park, PA.

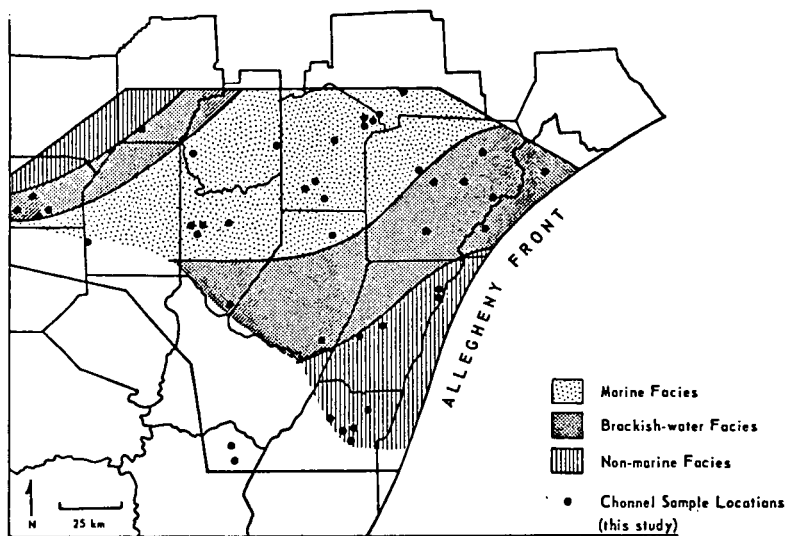


FIGURE 1. DISTRIBUTION OF SAMPLES IN WESTERN PENNSYLVANIA IN RELATION TO SUGGESTED ENVIRONMENTS OF DEPOSITION FOR THE OVERLYING SHALE

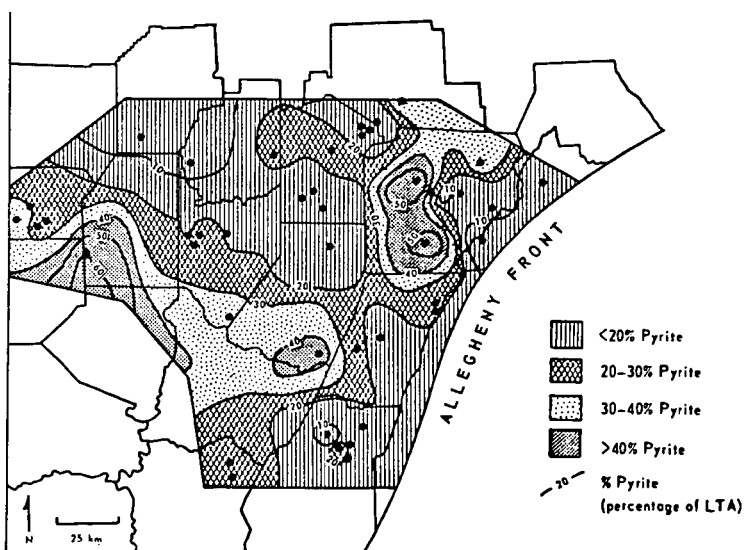


FIGURE 2. LATERAL VARIABILITY IN PYRITE CONTENT (LTA BASIS), AS DETERMINED BY X-RAY DIFFRACTION ANALYSIS

The Origin of Quartz In Coal

Leslie F. Ruppert, C. Blaine Cecil, and Ronald W. Stanton
U.S. Geological Survey, National Center, MS 956, Reston, Va. 22092

Introduction

Mineral matter in coal can originate as (1) inorganic elements from plants that were incorporated during peat formation, (2) wind- or water-borne detritus that settled in the peat-forming environment, and (3) epigenetic minerals that formed during or after burial of the peat (Stach and others, 1982). The latter two processes generally are considered to be the principal contributors to the amount and variety of minerals in coal of commercial quality. Certain physical properties, such as the shape of quartz grains, have led some workers to postulate that quartz in coal is primarily of detrital origin (Finkelman, 1981a, 1982b; Davis and others, 1981); however, evidence for such a hypothesis may be highly subjective and inconclusive. In contrast, Cecil and others (1982) suggested that mineral matter in the Upper Freeport coal bed is dominantly authigenic, on the basis of statistical relationships among major-, minor-, and trace-element, maceral, and mineral data. Mineral matter in coal, exclusive of pyrite and calcite, was probably derived from plants that contributed to peat formation (Stevenson, 1913; Cecil and others, 1982).

Cathodoluminescence (CL) petrography was used in the present investigation to obtain quantitative data on the amounts of authigenic and detrital quartz in the Upper Freeport coal bed. CL is the emission of visible light during electron bombardment. It is used widely as a tool in sandstone petrology to distinguish between detrital and authigenic quartz grains. CL in quartz results from molecular or other lattice imperfections; molecular imperfections which include the addition of "activator" ions (Al^{+3} or Ti^{+3} that substitute for Si^{+4}), and other lattice imperfections are related to temperature (Zinkernagel, 1978). Zinkernagel observed three distinct types of luminescence in quartz grains that included (1) "violet" luminescing quartz (spectral peaks at 450 and 610-630 nm), (2) "brown" or orange luminescing quartz (spectral peaks at 610-630 nm), and (3) non-luminescing quartz. He examined quartz from 46 localities and ranging in age from Precambrian to Tertiary, and in all cases the CL color was dependent on the temperature of crystallization. "Violet" or blue luminescing quartz was characteristic of fast-cooled volcanic, plutonic, and high-grade metamorphic rocks that were formed at temperatures greater than 573°C. "Brown" or orange luminescing quartz was characteristic of high-grade slow-cooled metamorphic rocks formed at temperatures ranging from 573°C to 300°C. Quartz that was formed at temperatures below 300°C and that was not heat tempered did not luminesce in the visible range. The origin of quartz can be inferred from CL data because detrital quartz, which has a high-temperature origin (>300°C), luminesces in the visible range whereas authigenic quartz, formed at low temperatures (<300°C) does not luminesce.

Methodology

Both a scanning electron microscope (SEM) and an electron microprobe (EMP) were used in this study to analyze the CL properties of quartz grains in samples of the Upper Freeport coal bed because quartz grains in coal are small (silt sized) and below the resolution capabilities of a standard luminescope. Quartz grains were identified by the detection of silicon alone with energy dispersive X-ray units attached to both the SEM and the EMP.

The SEM was used to observe and photograph the quartz grains. The EMP which was equipped with both a photomultiplier tube (spectral response 185-930 nm) and a monochromator, was used to measure wave length and intensity of CL. The EMP, instrument conditions were calibrated using a reference sample of the upper part of the Raleigh Sandstone Member of the New River Formation (Pennsylvanian age), which contained both orange and blue luminescent detrital quartz grains and non-luminescent authigenic overgrowths of low-temperature origin (fig. 1).

Quartz grains from the Upper Freeport coal bed were analyzed in (1) ash samples that were prepared by low-temperature plasma ashing (LTA) of facies channel samples, (2) pulverized coal samples of size-gravity separates, and (3) oriented blocks of mineral-rich bands, vitrain, fusain, clay-rich parting material, and roof-shale that were each cut from a coal core. All samples were mounted in epoxy and polished prior to analysis.

Results

All the Upper Freeport coal bed samples examined contained both luminescent and non-luminescent quartz grains (table 1, fig. 2). More than 200 grains were visually examined, and 76 measured spectra were obtained.

In the LTA samples, 95 percent of the quartz particles examined were non-luminescent and 5 percent were luminescent. Most grains luminesced in the orange range.

Twenty-nine measured spectra of quartz grains were obtained from the lightest (1.275 float) and the heaviest (1.800 sink) size-gravity separates. Only nine grains were analyzed in the lightest gravity separates because of the paucity of mineral matter. All nine grains were non-luminescent and were associated with vitrain. In the heaviest gravity separates, 60 percent of the quartz was non-luminescent; this quartz is petrographically associated with both vitrain, mineral-rich bands, and shale partings. The remaining 40 percent of the quartz grains in the heavy gravity separates were luminescent and are associated with mineral-rich bands and shale parting material.

Data from CL analyses of the blocks of coal from the core revealed that luminescing quartz was relatively rare and is associated only with mineral-rich bands. Of the 29 quartz grains analyzed, only 17 percent luminesced. The non-luminescent grains are petrographically associated with both vitrain and mineral-rich bands.

Roof-shale samples from the core were also examined. Ninety-three percent of the quartz analyzed was luminescent and only 7 percent was non-luminescent. The quartz grains analyzed were similar in size to the quartz grains in coal.

Conclusions

Seventy-six percent of the quartz grains examined in the Upper Freeport coal samples are non-luminescent; therefore the quartz is interpreted to be dominantly authigenic. The authigenic quartz is petrographically associated with both vitrain and mineral-rich bands. The remaining 23 percent of the quartz analyzed luminesced in the visible range and is therefore interpreted to be detrital in origin. Detrital quartz was petrographically associated with mineral-rich bands and clay-parting material.

In contrast, quartz grains in the samples of shale directly overlying the Upper Freeport coal bed are interpreted to be predominantly detrital in origin. The quartz grains are in the same size range as quartz grains in the coal samples.

Data from CL petrography support the interpretation of Cecil and others (1982) that quartz in Upper Freeport coal bed is primarily authigenic and derived from plant ash. Although it is impossible to ascertain the ash content of Pennsylvanian plants that grew in the Upper Freeport paleo-peat forming environment, it seems reasonable that the plants did contain silica, as do most modern plants. Biogenic silica can be preserved as phytoliths (Smithson, 1956; Baker, 1960; and Jones, 1964; Andrejko and others, 1983) and quartz grains in coal are similar in size to plant phytoliths (Wilding and Drees, 1974).

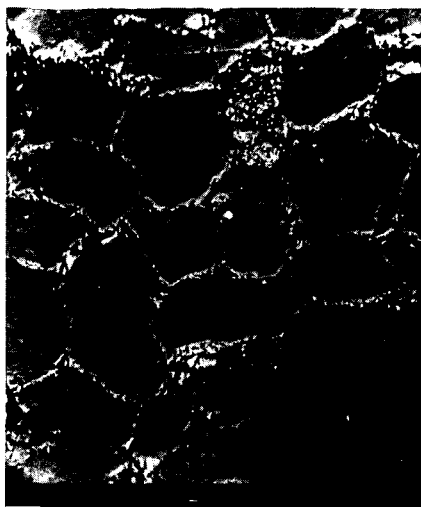
Most quartz grains in the commercial-quality Upper Freeport coal bed samples are authigenic in origin, but this interpretation does not rule out a detrital source for areas of the bed containing higher amounts of ash (approximately 20 percent) or for other high ash bituminous coal beds. The percentage of detrital quartz would be expected to increase approaching stream channels and the margins of the paleoswamp environment, but vegetal matter is probably the dominant source for quartz in interior portions of the paleoswamp.

Table 1. CATHODOLUMINESCENT AND PETROGRAPHIC CHARACTERISTICS OF QUARTZ GRAINS IN COAL AND SHALE

[Determined by using an electron microprobe (EMP). TNA, Total number of grains analyzed; Nonlum, nonluminescent grains; Lum, Luminescent grains; *, data was not obtained because coal was crushed; N/A, not applicable.]

	LOW-TEMPERATURE ASH		SIZE-GRAVITY SEPARATES			
	(Facies channel samples)		Float 1.275 (TNA = 9)		Sink 1.800 (TNA = 20)	
	Nonlum	Lum	Nonlum	Lum	Nonlum	Lum
Number of grains	39	2	9	0	12	8
Grain size range (in μm)	*	*	6-22	N/A	5-14	9-32
Mean grain size (in μm)	*	*	9.9	N/A	8.4	18.9
Percent of total	95	5	100	N/A	60	40
Association	*	*	Vitrain	N/A	Vitrain Mineral-rich band Shale parting	Mineral-rich band Shale parting

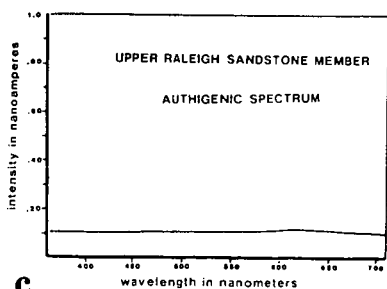
	COAL BLOCKS (TNA = 9)		ROOF-SHALE (TNA = 15) BLOCKS	
	Nonlum	Lum	Nonlum	Lum
Number of grains	24	5	1	14
Grain size range (in μm)	8-20	7-22	N/A	6-32
Mean grain size (in μm)	12	14.8	7	13.5
Percent of total	83	17	7	93
Association	Vitrain	Mineral-rich	Shale	Shale



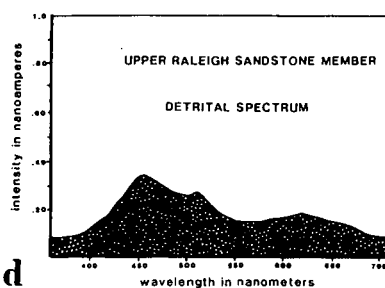
a



b



c



d

Figure 1 - Reference sample for EMP. (a) SEM backscatter electron photomicrograph, (b) CL SEM photomicrograph. Note luminescing detrital quartz grains, (c) EMP CL spectrum of non-luminescing authigenic overgrowth, (d) EMP CL spectrum of blue luminescing detrital quartz grain.

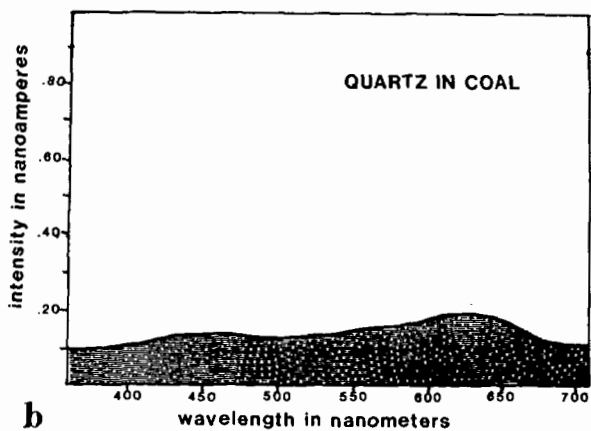
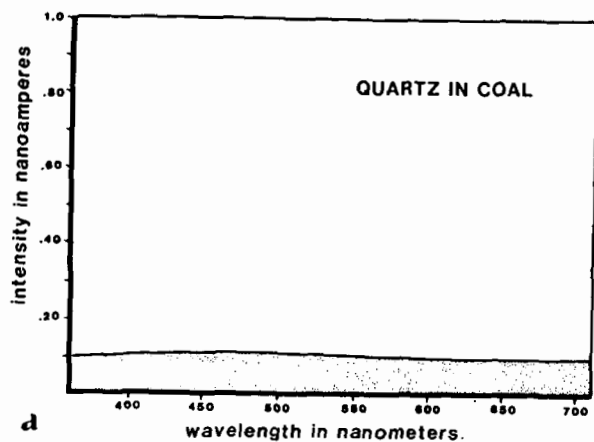


Figure 2 - EMP CL spectra of quartz in the Upper Freeport coal bed. (A) Non-luminescing authigenic spectrum, (B) Luminescing detrital spectrum.

References

- Andrejko, M.J., Raymond, R., and Cohen, A.D., 1983, Biogenic silica in peats: Possible Sources for Chertification in Lignite: in Raymond, R., and Andrejko, M.J., eds., *Mineral Matter in Peat: Its Occurrence, Form, and Distribution*: Los Alamos National Lab., Los Alamos, N.Mex., 1983.
- Baker, G., 1960, Opal phytoliths in some Victorian soils and "red rain" residues: *Australian Journal of Botany*, v. 7, p. 64-87.
- Cecil, C.B., Stanton, R.W., Dulong, F.T., and Renton, J.J., 1982, Geologic factors that control mineral matter in coal; in Filby, R.H., Carpenter, B.S., and Ragina, R.C., eds., *Atomic and Nuclear Methods in Fossil Research*: Plenum Press, New York, p. 323-325.
- Davis, A., Rimmer, S.M., Russell, S.J., and Yeakel, J.D., 1981, Some observations on the origin of common minerals in coals and their relationship to the organic petrology [abs]: *Geological Society of America, Abstracts with Programs*, v. 13, no. 7, p. 436.
- Finkelman, R., 1981a, The origin, occurrence, and distribution of the inorganic constituents in low-ranked coals, in *Proceedings of the Basic Coal Science Workshop*, Houston, Texas, Dec. 8-9, 1981, p. 69-90.
- 1981b, Recognition of authigenic and detrital minerals in coal [abs]; *Geological Society of America, Abstracts with Programs*, v. 13, no. 7, p. 451.
- Jones, R.L., 1964, Note on the occurrence of opal phytoliths in some Cenozoic sedimentary rocks; *Journal of Paleontology*, v. 38, p. 773-775.
- Smithson, F., 1956, Silica particles in some British soils: *Journal of Soil Science*, v. 7, no. 1, p. 122-129.
- Stach, E., Mackowsky, M-Th., Teichmuller, M., Taylor, G.H., Chandra, D., and Teichmuller, R., 1982, *Stach's textbook of coal petrology*: Gebruder Borntraeger, Berlin, p. 156.
- Stevenson, J.J., 1913, Formation of coal beds: *Proceedings of the American Philosophical Society*, v. 52, p. 100-108.
- Wilding, L.P., and Drees, L.F., 1974, Contributions of forest opal and associated crystalline phases of fine silt and clay fractions of soils; *Clay Mineralogy*, v. 22, p. 295-306.
- Zinkernagel, U., 1978, Cathodoluminescence of quartz and its application to sandstone petrology: *Contributions to Sedimentology*, no. 8, 69 p.

SEMI QUANTITATIVE DETERMINATION OF COAL MINERALS BY X-RAY DIFFRACTOMETRY

John J. Renton

Department of Geology
West Virginia University
Morgantown, West Virginia 26506

INTRODUCTION

The purpose of this paper is to present and support the argument that abundance estimates of the minerals in coal based upon x-ray diffraction data can only be considered semi-quantitative with expected errors of determination of 10 percent or more of the reported values. The compositional and physical characteristics of the low temperature ash components of coal relative to the preparation and mounting of ash for XRD analysis must also be considered.

MINERALS IN COAL

The minerals commonly found in coal are listed in Table 1. In the average coal, clay minerals may constitute up to 60 weight percent of the mineral matter (1,2). Quartz is usually the second most abundant mineral, with up to 20 weight percent being common. The carbonate minerals (calcite, siderite and to a lesser extent, dolomite and ankerite) and the iron disulphide minerals (pyrite and marcasite) make up, on the average, about 10 weight percent each group. Sulphate minerals of calcium and iron and the feldspar minerals are commonly present but rarely in concentrations of more than a few weight percent. Except for unusual cases such as the sulphide rich coals of the northern Illinois Basin, the occurrence of the other minerals in concentrations exceeding a few percent is rare. It must, however, be kept in mind that the mineralogy of the inorganic portion of coal shows systematic variation both geographically and locally reflecting the geochemistry of the original peat forming environment (3). As a result, "average" values of concentration may have little practical meaning.

Most coals considered for conversion processes such as liquifaction, and thereby those of prime interest to chemists, are generally high in ash (>10 weight percent) and sulfur (>1 weight percent). In such coals, illite would invariably be the dominant clay material, constituting, in some coals, up to half or more of the mineral content. Most of the sulfur contained in these coals will be in the form of pyrite although marcasite may be locally dominant (4).

QUANTIFICATION BY X-RAY DIFFRACTION

The most commonly employed quantitative XRD procedure used to evaluate the concentration of mineral components in a multicomponent mixture of minerals compares the Bragg intensity data of unknowns to those generated from a suite of known standard samples. Mineral specimens are acquired to represent each of the minerals expected in the unknowns. The specimens are ground to a uniformly small size (less than 44 microns) and mixed together in concentrations which represent the range of concentrations expected for each mineral. An internal standard such as calcium fluoride, aluminum oxide or powdered aluminum is usually added in order to monitor and correct for variations in sample absorption and instrumental variables. Working curves are then prepared by plotting the ratio of intensity (preferably integrated intensity) of the Bragg reflection chosen to quantify the mineral to that chosen for the standard versus the weight percent of the mineral in the standard samples.

This procedure will provide analyses of high precision provided certain basic assumptions are met: (1) the high composition and crystallinity (degree of ordering) of the individual minerals in the unknowns are both reasonably constant from sample to sample and (2) the composition and crystallinity of the standard minerals chosen for the preparation of the standard samples reasonably duplicate the composition and crystallinity of the respective minerals in the unknowns. The purpose of the following discussion is to demonstrate that, in the case of coal minerals, neither of the above assumptions is valid and as a result, any such quantitative procedure will reflect the inherent degree of departure from these basic assumptions and will therefore be semi-quantitative. Other procedures using data normalized to the total integrated intensity and quantification procedures utilizing weighting factors based upon standard chemical formulae for the minerals can be used but with no improvement in quantitative errors (5,6).

Illite and pyrite were specifically cited in the above discussion to make a point relative to the precision and accuracy with which coal minerals can be quantified by XRD. First, illite is NOT a mineral. Illite is "...a general term for the clay mineral constituents of argillaceous sediments belonging to the mica group (7). To a clay mineralogist, the term illite is synonymous with variability in both composition and crystallinity (8). The situation is even further complicated by the fact that much of the material in coal referred to as "illite" is actually an illite dominated mixed layered clay wherein the illite lattices are randomly interstratified with 14A clay lattices; usually chlorite. This mixing of clay mineral lattices further adds to the inherent variability in both composition and crystallinity of the illite material. The constitution of "illite" can therefore be expected to vary significantly from sample to sample. It should be quite apparent from the above discussion that no "standard" illite exists that could be used to represent illite in standard samples.

The iron disulphides may represent 10 weight percent or more of high ash-sulphur coal ashes. Usually, pyrite is the major disulphide. Pyrite occurs in coal in a number of morphological forms and sizes (9). Not only does the pyrite in coal vary in morphology and size but also in stoichiometry and crystallinity. Studies have been conducted in the author's laboratory on cut and polished surfaces of coal blocks wherein the blocks have been exposed to the atmosphere and the pyrites observed over a period of time. Some pyrite grains, the

ehedral forms, remain bright and show little tendency to react. The massive forms of pyrite, on the other hand, show a wide variation in apparent reactivity with crystals of iron sulfates being observed to form on some pyrite surfaces within a matter of hours and in some cases, within minutes.

Another study involved in quantification of pyrite in different coal lithotypes. Coals are described megascopically based upon the degree of bright and dull banding. Zones are delineated within the coal and designated as a "lithotype" based on the relative percentage of bright and dull bands within the zone (10). Dominantly bright bands are called "VITRAIN", dull bands, DURAIN and those intermediate between the two; "CLARAIN". Although the designation as to lithotype is solely made depending upon megascopic description, the lithotypes differ in basic organic composition as illustrated by the data for the Waynesburg Coal shown in Table 2.

TABLE 2. COMPOSITION OF LITHOTYPES OF THE WAYNESBURG COAL

LITHOTYPE	%VITRINITE	%EXINITE	%INERTINITE	%MINERAL MATTER
Vitrain	93.1	1.8	2.4	2.7
Clarain	84.2	4.4	5.6	5.8
Durain	43.4	17.8	24.9	13.9

The low temperature ash of each lithotype was then submitted to XRD analysis. The integrated intensities of each of the selected analytical Bragg reflections selected for the individual minerals were summed for all minerals present in each sample to give a "total integrated intensity". This value was then divided into the integrated intensity of the pyrite analytical Bragg reflection to give the "percent of total integrated intensity". The data are summarized in Figure 1. It is apparent that there is a systematic relationship between the composition/crystallinity of the pyrite and the basic organic makeup of the coal. Most important is the observation that equal concentrations of pyrite give different intensity responses. Volume for volume, the pyrite contained within the bright coal (Vitrain) showing significantly higher Bragg intensities than the pyrite contained in the duller coals.

To compound the problem, marcasite for reasons unknown to the author, does not show the intensity response, volume for volume as pyrite. It has been the author's experience that the marcasite coals that have been shown by optical examination to be insignificant concentration show almost no indication of being present on a diffractogram generated from the low temperature ash.

It must be apparent from the above discussion that the great number of variables other than concentration affect the intensities of mineral pattern as observed on a diffractogram. Inasmuch as they cannot be monitored and compensated for mathematically, these variations must be reflected in the error of determination. This would be true regardless of the quantification procedure employed. The conclusion, therefore, is that the inherent variability in composition and/or crystallinity that exists within the major mineral components of the low temperature ashes of coal will be reflected in the statistical error of determination and that error will be of sufficient magnitude to preclude the use of the term "quantitative" to describe the procedure. Therefore, any procedure using x-ray diffraction to determine the minerals in coal must be considered semi-quantitative at best.

SAMPLE PREPARATION & MOUNTING

Any procedure for the preparation and mounting of coal low temperature ashes for XRD analysis MUST take two properties of the material into account: (1) minerals exist which react with water to produce acidic solutions (the iron disulphides) which in turn dissolve acid soluble components such as calcite and (2) the clay minerals by virtue of exceptionally well developed (001) cleavage surfaces have a dominant platey crystal form. The significance of the first attribute is that the ashes cannot be placed in water thereby precluding certain sample preparation techniques such as dispersion in water followed by vacuum mounting on filters or ceramic blocks. The second characteristic, possession of a platey crystal form, precludes the attainment of the theoretically required randomly oriented sample. Those who work with the clay minerals, realizing a random sample cannot be prepared and that the clay particles will deposit in preferred orientation, purposely prepare and mount the samples such that the preferred orientation of the individual platelets is maximized and thereby minimize any variations in diffraction intensity due to variations in particle alignment within the sample. The orientation of the clay platelets parallel to the sample surface positions the "C" crystallographic axis perpendicular to the sample surface. Because the diagnostic interplanar spacing for the clay minerals is along the "C" crystallographic direction, such an orientation is ideal for clay mineral identification. The simplest method to mount a low temperature ash for XRD analysis is to press the ash onto the surface of a pellet prepared from the coal from which the ash was derived.

FUTURE PROSPECTS

A few years ago, and ad hoc group of workers interested in coal minerals, The Mineral Matter in Coal Group, prepared and distributed a round-robin low temperature ash to ten laboratories. Each laboratory was to prepare, mount and quantify the mineral components in the ash by their respective XRD techniques. The data were then compared. Even though a wide variety of techniques was used for each phase of the analysis, with the exception of the clay mineral estimates made by one laboratory (significantly lower than the others) and the pyrite estimate made by another (too high), the data compared reasonably well. The averages of all the submitted estimates are summarized in Table 3.

TABLE 3. RESULTS OF ROUND ROBIN L.T.A. ANALYSIS

MINERAL	AVE. CONC. WT%	S.DEV.	C.V.
Illite+Mix L	30	7.07	0.24
Kaolinite	18	4.85	0.27
Quartz	21	6.31	0.30
Calcite	10	3.59	0.36
Pyrite	18	4.93	0.27

Another objective of the exercise was to discuss the results and procedures used and come to some agreement on a "standard" procedure for sample preparation, mounting and quantification that would be acceptable to all the workers. The agreement that was reached was that no agreement would be forthcoming on any of the phases of the analysis. With no one procedure demonstrably better than the other, each laboratory was expected to maintain their own procedure. As long as a procedure is scientifically and analytically sound and reflects a thorough understanding of the characteristics of minerals contained in coal and the requirements and limitations of x-ray diffraction, one procedure will probably be as good as another but none will be better than semi-quantitative. With all its shortcomings, x-ray diffraction is still the best and most practical method for the estimation of the abundance of the individual minerals in coal.

REFERENCES CITED

1. Renton, J. J., 1982, in Coal Structure, R. Meyers ed., Academic Press, p. 283-326.
2. Renton, J. J., 1978, Energy Sources, Vol. 43, No. 2, p. 91-112.
3. Renton, J. J., C. B. Cecil, 1979, in "Carboniferous Coal Guidebook", A. C. Donaldson, M. W. Presley and J. J. Renton, eds., West Virginia Geological and Economic Survey, Morgantown, W. Va., p. 103-128.
4. King, H. M., 1978, Masters Thesis, Dept. of Geology, W. Virginia.
5. Renton, J. J., 1977, U. S. Dept. of Energy, MERC/CR-77/10, 20pp.
6. Renton, J. J., 1979, U. S. Dept. of Energy, METC/CR-79/5, 22pp.
7. Grim, R. E., et al, 1937, Amer. Min., Vol. 22, pp. 813-829.
8. Brown, G., 1961, Mineralogical Soc. of London, Clay Mineral Group, London, 544pp.
9. Grady, W. C., 1977, AIME Transactions, Vol. 262, p. 268-274.
10. Stopes, M. C., 1919, Proc. Roy Soc. B., 90, 470-487, London.

TABLE 1
COMMON COAL MINERALS

Major	Silicates	Clay Minerals	<div> <div>Kaolinite</div> <div>Illite</div> <div>Mixed Layer</div> <div>Chlorite</div> <div>Quartz</div> </div> <div> $\text{Al}_2\text{Si}_2\text{O}_5(\text{OH})_4$ ^a ^b $(\text{Mg}\text{fFeAl})_6(\text{SiAl})_4\text{O}_{10}(\text{OH})_8$ SiO_2 </div>
Minor		Carbonates	<div> <div>Calcite</div> <div>Dolomite</div> <div>Ankerite</div> <div>Siderite</div> </div> <div> CaCO_3 $(\text{Ca},\text{Mg})(\text{CO}_3)_2$ $\text{Ca}(\text{Fe},\text{Mg})\text{CO}_3$ FeCO_3 </div>
		Disulfides	<div> <div>Pyrite</div> <div>Marcasite</div> </div> <div> FeS_2 (cubic) FeS_2 (orthorhombic) </div>
		Sulfates	<div> <div>Coquimbite</div> <div>Szmolnokite</div> <div>Gypsum</div> <div>Bassanite</div> <div>Anhydrite</div> <div>Jarosite</div> </div> <div> $\text{Fe}_2(\text{SO}_4)_3 \cdot 9\text{H}_2\text{O}$ $\text{FeSO}_4 \cdot \text{H}_2\text{O}$ $\text{CaSO}_4 \cdot 2\text{H}_2\text{O}$ $\text{CaSO}_4 \cdot \frac{1}{2}\text{H}_2\text{O}$ CaSO_4 $\text{KFe}_3(\text{SO}_4)_2(\text{OH})_6$ </div>
		Feldspars	<div> <div>Plagioclase</div> <div>Orthoclase</div> </div> <div> $(\text{NaCa})\text{Al}(\text{AlSi})\text{Si}_2\text{O}_8$ KAlSi_3O_8 </div>

^aIllite has a composition similar to muscovite-
 $\text{KAl}_2(\text{Si}_3\text{Al})\text{O}_{10}(\text{OH})_2$, except for less K⁺ and more SiO₂ and H₂O

^bMixed layered clays are usually randomly interstratified
 mixtures of illitic lattices with montmorillonitic and/or
 chloritic lattices.

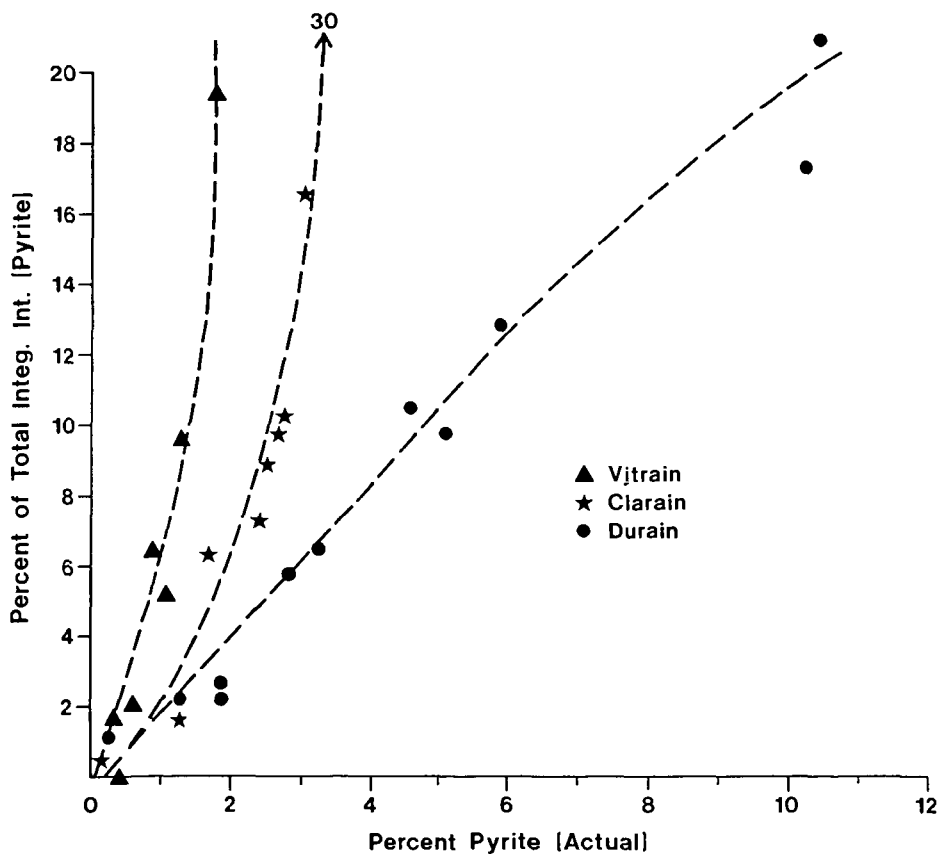


Figure 1. Relationship between actual pyrite composition and relative percent total integrated intensity of pyrite in low temperature ashes of Waynesburg coal lithotypes.

FACTORS INFLUENCING TRACE ELEMENT VARIATIONS IN U.S. COALS

Peter C. Lindahl

Analytical Chemistry Laboratory
Chemical Technology Division
Argonne National Laboratory
9700 South Cass Avenue
Argonne, IL 60439

Robert B. Finkelman

Reservoir and Facies Division
Exxon Production Research Company
P.O. Box 2189
Houston, TX 77001

INTRODUCTION

Although trace element data exist for thousands of coal samples, more will be required to better elucidate trace element trends within coal basins and to help decipher the geological and geochemical controls on trace element distribution and mode of occurrence. However, increased numbers of analyses will not necessarily provide all the answers. We run the risk of ending up information rich but knowledge poor.

The purpose of this paper is to give our analysis of coal trace element data in the literature. Several valuable compilations of trace element data exist for U.S. coal (1-4). We have borrowed freely from these compilations to illustrate their value in elucidating just one aspect of coal geochemistry: the factors influencing trace element variations.

Trace elements are generally defined as those elements with concentrations below 0.1 wt. % (1000 ppm). Despite concentrations in the parts-per-million range, certain trace elements can have a significant impact on coal utilization. For example, the chalcophile elements As, Cd, Hg, Pb, and Se, which are released during coal combustion or leached from coal waste products, can present significant environmental hazards; halogens such as Cl and F can cause severe boiler corrosion, and volatilized Ni or V can cause corrosion and pitting of metal surfaces. Moreover, although not strictly a trace element, sodium, even in small concentrations, can contribute to boiler fouling or to agglomeration of fluidized-bed reactors. On the positive side, some trace elements (e.g., Ge, Zn, U, Au) may eventually prove to be economic by-products, and others may be useful in helping to understand depositional environments (e.g., B) and to correlate coal seams (5,6).

In early studies of trace elements in coal (7-11), coal ash was analyzed using emission spectroscopy. Recent studies (3,4,12,13) have employed quantitative multi-element instrumental methods. Because a particular analytical technique is better suited for certain elements than for others, a combination of methods is usually necessary to determine all elements of interest. Methods for determining trace elements in coal must be accurate and precise. In addition, if possible, they should determine a large number of elements of interest simultaneously, require relatively little sample preparation, be capable of automation, produce an output compatible with computerized data processing, and be rapid.

Trace element concentrations in coal show variations from a microscopic to a worldwide scale. From a resource evaluation perspective, the most significant variations occur within and between coal basins. The rest of the paper will discuss factors that cause these variations.

DISCUSSION

Ash Related Variations

The amount of ash in a coal is a major factor influencing trace element content. In general, trace element concentrations increase as ash content increases. This relationship reflects the fact that most inorganic elements in coal are associated with minerals (5). Figures 1 and 2 illustrate this relationship for K in eastern Kentucky coals and for Ti in coals from the Uinta Region.

The above relationship also holds when comparing trace element concentrations among coal basins. Table I compares trace element data for coals from the Black Mesa Field, the Powder River Region, and the San Juan Region. As shown in Table I, the concentrations of the following elements increase as the ash contents of the coals increase: Si, Al, Na, K, Cu, Th, V, Li, Pb, and Se. The reason for the variation of these elements with ash content is that most are, or were, associated with the silicate (detrital) minerals brought into the depositional basins during the formation of the coals. Chemical alteration of minerals within the coal basin can remobilize some elements, which then precipitate as authigenic nonsilicate minerals, e.g., Cu and Pb, as sulfides or selenides (14). The good correlation between element concentration and ash content indicates that most elements have remained within the coal basin despite remobilization (15).

Table I. Concentrations of Selected Elements in Coal Samples from Black Mesa, Powder River, and San Juan Regions¹

	<u>Black Mesa</u>	<u>Powder River</u>	<u>San Juan</u>
Ash, %	8.0	9.9	21.1
Si, %	1.1	1.5	5.4
Al, %	0.69	0.78	2.7
Ca, %	0.78	1.1	0.67
Mg, %	0.1	0.2	0.1
Na, %	0.09	0.1	0.2
K, %	0.04	0.05	0.16
Fe, %	0.31	0.54	0.54
Ti, %	0.05	0.04	0.11
Cu, ppm	5.5	11.2	13.3
Th, ppm	2.2	4.3	5.9
Zn, ppm	5.6	20	15.1
Cr, ppm	3	7	5
Ni, ppm	2	5	3
V, ppm	7	15	20
Mn, ppm	9.7	51	29
Li, ppm	3.9	5.9	19.7
Pb, ppm	2.7	5.6	13.1
Se, ppm	1.6	1.7	2
Ba, ppm	300	300	300
Sr, ppm	150	200	100
Nb, ppm	1.5	1.5	3
Zr, ppm	15	15	50

¹Data from Reference 4; results are calculated on a moisture-free coal basis (mf coal).

Elements not increasing in concentration with ash content are generally those with (a) organic affinities (Ca, Mg, Sr, Ba); (b) sulfide affinities (Fe, Zn); (c) carbonate affinities (Ca, Mn, Mg); or (d) sulfate affinities (Ba, Sr, Ca). Sulfides, carbonates, and sulfates are generally epigenetic phases. Presence of these phases affects element concentration more than ash content. The concentrations of Zr and Nb would be expected to increase with ash content. The reason that this

behavior is not apparent in Table I may be the poor resolution of the technique (semiquantitative spectrographic analysis) used to obtain the data.

Rank-Related Variations

Several elements exhibit a distinct variation in concentration with coal rank. Table II illustrates the general decrease in concentration of alkaline-earth elements (Mg, Ca, Sr, Ba), Na, and B with increasing coal rank. It is generally accepted that these elements are associated with organic functional groups (e.g., carboxylic acids) in low-rank coals. With increasing coal rank, these groups are destroyed, thus displacing organically associated inorganic trace elements.

Table II. Rank-Related Variations¹

	<u>Anthracite</u>	<u>Bituminous</u>	<u>Subbituminous</u>	<u>Lignite</u>
Ca, %	0.07	0.33	0.78	1.2
Mg, %	0.06	0.08	0.18	0.31
Na, %	0.05	0.04	0.10	0.21
B, ppm	10	50	70	100
Ba, ppm	100	100	300	300
Sr, ppm	100	100	100	300

¹Data from Reference 1; mf coal.

Organic association has been proposed for other trace elements, such as Be, Sb, Ge, U, and some halogens (3,16). Finkelman (15) suggests that organic association of these elements is significant mainly for low-rank, low-ash coals.

Concentrations of organically bound elements in coal can decrease with increasing amount of detritus (Figure 3). Also, note that the concentrations of boron decrease with increasing ash contents (Table I).

Variations Due to Geochemical Factors

Geochemical factors, such as Eh and pH during and subsequent to coal formation, can have dramatic effects on trace element contents. The effect of these geochemical factors can be seen in Table III, in which selected data for Appalachian and Interior Province coals are compared. Coals from both areas are similar in rank and ash content, but the Interior Province coals have significantly higher contents of all six trace elements. The higher content of Ca is perhaps due to carbonate mineralization (high pH), whereas that of Fe, Cd, Pb, and Zn is attributable to sulfide mineralization (low Eh). The higher content of B is perhaps attributable to greater marine influence (high salinity).

Table III. Concentrations of Selected Elements in Coal Samples from Appalachian and Interior Coal Basins

	<u>Appalachian</u> ¹	<u>Interior</u> ²
Ash, %	13.3	15.7
Ca, %	0.12	1.2
Fe, %	1.9	3.3
Cd, ppm	0.7	7.1
Pb, ppm	15.3	55
Zn, ppm	20	373
B, ppm	30	100

¹Data from Reference 2; mf coal.

²Data from Reference 4; mf coal.

The occurrence of cleat-filling sphalerite and galena in the Interior Province coals is a classic example of how epigenetic mineralization can affect trace element content (17). Dramatic intra- and interseam variations are common. Cobb (18) reports that zinc content from benches of the Herrin (No. 6) coal varied from 20 to 14,900 ppm.

Variations Due to Geologic Factors

Ash chemistry is another important factor affecting trace element variations. Its influence is, however, generally more subtle than the other factors. In Table IV the trace element contents are compared for Appalachian Province coals and Wasatch Plateau coals. Both are bituminous coals with similar ash contents and rank. However, with a few exceptions, the trace element contents of the Wasatch coals are lower than those of Appalachian coals. The lower content of chalcophile elements in Wasatch coals may be due to a lower pyrite content. The lower concentration of lithophile elements (e.g., Li, Zr, Nb, Th, Sc, Y) but higher Si content may reflect a higher quartz content in the detrital component of Wasatch coals; this, in turn, may be a reflection of differences in the mineralogy of the source rocks.

Table IV. Concentrations of Selected Elements in Coal Samples from Appalachian Province and Wasatch Coal Field

	<u>Appalachian¹</u>	<u>Wasatch²</u>
Ash, %	13.3	11.3
Ca, %	0.2	0.41
Fe, %	1.9	0.26
Cd, ppm	0.7	0.06
Li, ppm	27.6	16
Pb, ppm	15.3	5.8
U, ppm	1.4	1.2
Zn, ppm	20	11
B, ppm	30	100
Nb, ppm	5	0.3
Ni, ppm	15	5
Zr, ppm	50	30
As, ppm	27	0.8
Cu, ppm	24	9.3
F, ppm	80	67
Th, ppm	4.9	1.8
Ba, ppm	100	70
Co, ppm	7	1.5
Cr, ppm	20	10
Mo, ppm	3	0.7
Sc, ppm	5	3
V, ppm	20	15
Y, ppm	10	7

¹Data from Reference 6; mf coal.

²Data from Reference 19; mf coal.

Other Factors Affecting Trace Element Content

Other factors that could modify the ash chemistry or the availability of trace elements include the salinity of waters in contact with the coal or peat, the type of chemical weathering process (arid vs. humid), and hydrologic conditions (Br and Cl may be especially sensitive to this factor). In general, these factors are still poorly understood.

CONCLUDING COMMENTS

In this paper, we made several broad generalizations regarding factors that influence trace element variations. We urge that in interpretative work these generalizations be applied carefully.

A critical evaluation of existing trace element data would probably result in identification of anomalous values and elimination of suspect data. Several questions might be answered by such an evaluation; for example, do the two K values in the high-ash region of Figure 1 deviate significantly from the trend of the other data because of analytical errors or recording errors? Are they legitimate geochemical anomalies? We encourage analytical chemists and geologists to interact closely because this is one of the best ways to improve the quality of analytical methodology and data, and geological interpretation.

The nature of trace element variations, for whatever cause, highlights the need to more judiciously select representative samples for reliable quantitative analyses.

Statistical techniques, such as principal component analysis, should help in resolving the influence of the factors affecting trace element variations in coal.

It is hoped that this paper will encourage more detailed study of factors influencing trace element variations in coals.

ACKNOWLEDGMENT

Portions of this work were performed under the auspices of the U.S. Department of Energy.

REFERENCES

1. Swanson, V. E., Medlin, J. H., Hatch, J. R., Coleman, S. L., Wood, G. H., Jr., Woodruff, S. D., Hildebrand, R. T. Geol. Surv. Open-File Rep. (U.S.) 1976, No. 76-468.
2. Zubovic, P., Oman, C., Coleman, S. L., Bragg, L., Kerr, P. T., Kozey, K. M., Simon, F. O., Rowe, J. J., Medlin, J. H., Walker, F. E. Geol. Surv. Open-File Rep. (U.S.) 1979, No. 79-665.
3. Gluskoter, H. J., Ruch, R. R., Miller, W. G., Cahill, R. A., Dreher, G. B., Kuhn, J. K. Circ.-Ill. State Geol. Surv. 1977, No. 499.
4. Hatch, J. R., Swanson, V. E. Resour. Serv. (Colo. Geol. Surv.) 1977, 1 (Geol. Rocky Mt. Coal-Symp., 1976), 143-164.
5. Finkelman, R. B. Ph.D. Dissertation, University of Maryland, College Park, MD, 1980.
6. Swaine, D. J. In "The Significance of Trace Elements in Solving Petrogenetic Problems and Controversies," Theophrastus Publications S.A.; Athens, Greece, 1983; p. 521-532.
7. Abernethy, R. F., Peterson, M. J., Gibson, F. H. Bur. Mines Rept. Inv. (U.S.) 1969, No. 7281.
8. Zubovic, P., Stadnichenko, T., Sheffey, N. B. Geol. Surv. Bull. (U.S.) 1961, No. 1117-A.
9. Zubovic, P., Stadnichenko, T., Sheffey, N. B. Geol. Surv. Bull. (U.S.) 1964, No. 1117-B.
10. Zubovic, P., Stadnichenko, T., Sheffey, N. B. Geol. Surv. Bull. (U.S.) 1966, No. 1117-C.
11. Zubovic, P., Sheffey, N. B., Stadnichenko, T. Geol. Surv. Bull. (U.S.) 1967, No. 1117-D.
12. Swanson, V. E., Huffman, J. C. Geol. Surv. Circ. (U.S.) 1976, No. 735.
13. Ruch, R. R., Gluskoter, H. J., Shimp, N. F. Environ. Geol. Notes (Ill. State Geol. Surv.) 1974, No. 72.
14. Cecil, C. B., Stanton, R. W., Allhouse, S. C., Finkelman, R. B. "Abstracts of Papers," Chemical Congress - 177th National Meeting of the American Chemical Society and 39th National Meeting of the Chemical Society of Japan, Honolulu, HI, April 1979; American Chemical Society: Washington, DC, 1979; FUEL 48.
15. Finkelman, R. B. "Proceedings," Basic Coal Science Workshop, Houston, TX, Dec. 1981; Energy Resources Co., Inc.: Cambridge, MA, 1982; 69-90.
16. Miller, R. N., Given, P. H. State College, PA, 1978, DOE Report FE-2494-TR-1.
17. Hatch, J. R., Gluskoter, H. J., Lindahl, P. C. Econ. Geol. 1976, 71, 613-624.
18. Cobb, J. C., Masters, J. M., Treworgy, C. G., Helfinstine, R. J. Ill. Mineral Note 1979, No. 71.
19. Hatch, J. R., Affolter, Davis, F. D. Spec. Stud.-Utah Geol. Miner. Surv. 1979, No. 49, 69-102.

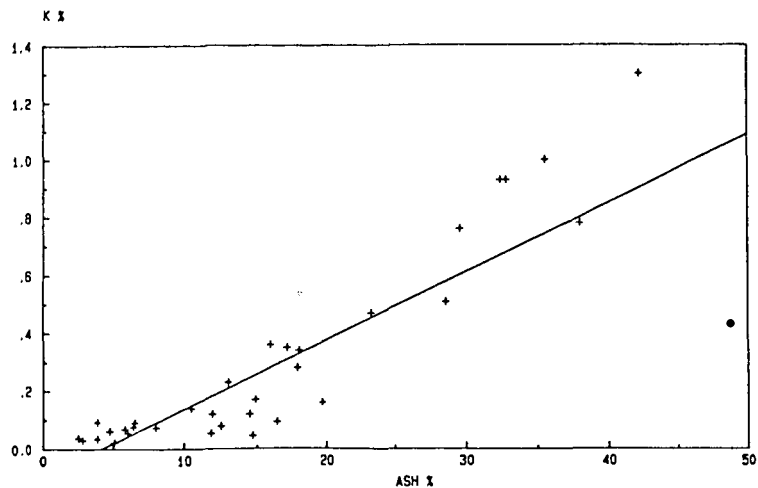


Figure 1. Relationship between K concentration in the coal and ash content for 34 coals from eastern Kentucky. $R = 0.86$. Data from Reference 1.

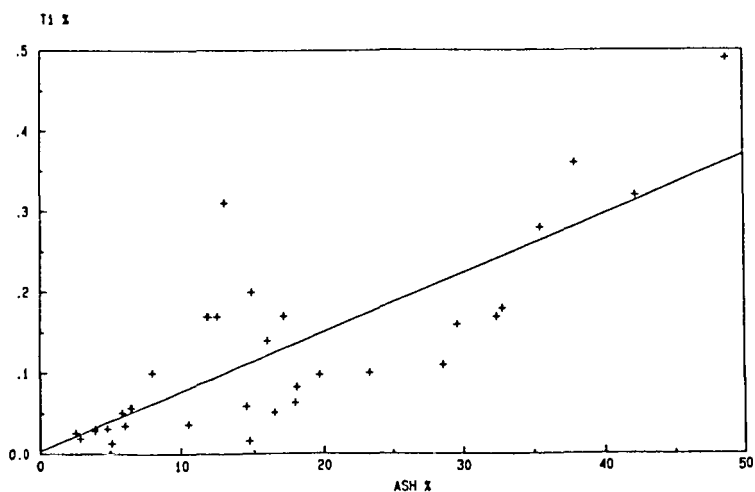


Figure 2. Relationship between Ti concentration in the coal and ash content for 26 coals from the Uinta Region. $R = 0.86$. Data from Reference 1.

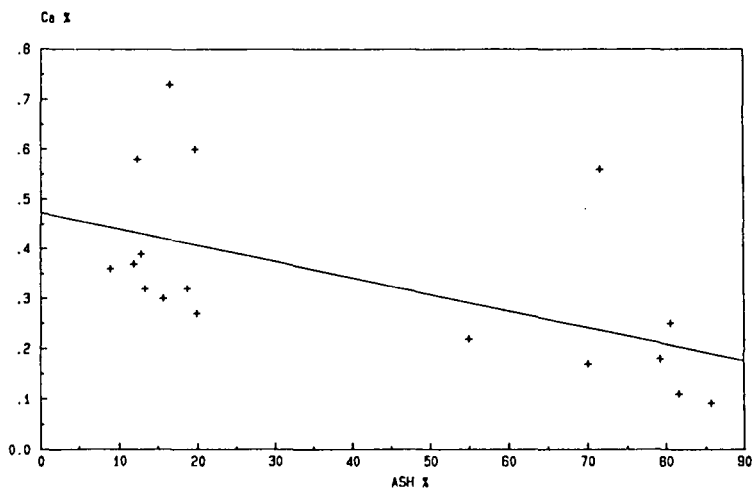


Figure 3. Relationship between Ca concentration in the coal and ash content for 17 coals and shales from the Emery Coal Field. $R = -0.57$. Data from Reference 18.

ELEMENTAL DISTRIBUTION AND ASSOCIATION WITH INORGANIC AND ORGANIC COMPONENTS IN TWO NORTH DAKOTA LIGNITES

S.A. Benson, S.K. Falcone, and F.R. Karner

University of North Dakota
Energy Research Center
Box 8213, University Station
Grand Forks, North Dakota 58202

Introduction

The associations of major, minor, and trace elements in lignite-bearing strata of the Fort Union Region present a challenge in understanding their geochemical relationships and history. In an earlier work (1), the spatial patterns of elemental distribution within a lignite-bearing sequence were examined and were related to factors of accumulation of vast amounts of plant materials and to the depositional and post-depositional influx of inorganic matter. Lignite-bearing sediments, including the lignite, lignite overburden, and underclay, were sampled from two beds, the Kinneman Creek and the Beulah-Zap, which are part of the Sentinel Butte Formation of North Dakota. These samples were examined to determine the spatial patterns of elemental distribution within the lignite seam, modes of elemental occurrence, and organic/inorganic affinities of the inorganic constituents.

The inorganic constituents within lignites from the Fort Union Region have been classified as being very heterogeneous (2), which leads some investigators to believe that the study of geochemical relationships is futile. The modes of occurrences of the elements are generally similar from one mine to another within the Fort Union Region lignites (3). The inorganic matter in the lignites is distributed as adsorbed ions on the organic acid groups, coordinated species, detrital minerals, and authigenic minerals. The distribution of elements is determined by natural processes, and, therefore, is expected to be systematic even though complex.

The methods to qualitatively identify the interrelationships of major, minor, and trace elements include examining the spatial patterns of distribution of elements within a stratigraphic sequence (1), consideration of results of chemical fractionation procedures (4), and evaluation of organic/inorganic affinities (5,6). The spatial pattern of elemental distribution was correlated with the chemical fractionation behavior, organic/inorganic affinities, and ionic potentials of elements to infer the association or combination of associations an element may have within these coals.

Methods and Procedures

The samples were collected from freshly exposed faces within open pit mines. The lignite, lignite overburden, and underclay were collected from two pits at the Beulah Mine where lignite is mined from the Beulah-Zap seam. Samples were also collected from the Kinneman Creek seam in the Center mine. The sample collection procedures have been summarized by Karner (7) and Benson (8). Bulk channel samples were also collected and homogenized to provide large quantities for additional experiments.

The lignite samples collected at various intervals within the stratigraphic sequence were subjected to the following analyses: proximate, ultimate, heating value, ash analysis, and trace element analysis by neutron activation analysis (NAA) (9) and x-ray fluorescence (10). Minerals in the coal and the associated sediments were determined by x-ray diffraction and by scanning electron microscopy and electron microprobe analysis. A split from the bulk sample was examined by chemical

fractionation to selectively extract inorganic constituents based on how they are bound in the coal. Briefly, the chemical fractionation procedure involves extracting the coal with 1M ammonium acetate to remove soluble and ion-exchangeable inorganic components. The coal is subsequently extracted with 1M hydrochloric acid to remove elements present as carbonates, oxides, or coordinated species. The extracts and residues from the chemical fractionation procedure are analyzed by a combination of NAA, XRF, inductively coupled argon plasma (ICAP), and atomic absorption spectroscopy (AA).

Results and Discussion

The major, minor, and trace element determinations along with locations within the seams and lithology of the stratigraphic sequence are summarized in Tables I and II for the Beulah coals. The data from Center Mine stratigraphic sequence was summarized in a previous report by Karner and others (1).

In previous work (1), the spatial distribution of elemental constituents has been described as fitting into several patterns: 1) concentration at one or both margins, 2) even distribution, and 3) regular patterns. The various ways inorganic constituents accumulated in the lignite during and after deposition affect where certain elements will concentrate within the seam. The detrital constituents carried in by wind and water will most likely be enriched near the margins of the coal seam. Included in this group of inorganic constituents are clay minerals, quartz, and volcanic ash. Solutions containing ions flowing through the lignite can exchange with the coal matrix and precipitate as stable authigenic phases. Inorganic constituents are also present in the original plant material that was deposited. Even patterns of elemental distribution are characteristic of organically bound elements. Irregular distribution patterns are characteristic of concentrated occurrences of authigenic minerals.

Table I includes data from two seams within the south Beulah mine. Table II summarizes the data from a high-sodium pit (Orange Pit) of the Beulah mine. The Center mine data used in this work was reported by Karner and others (1).

In this study, the spatial patterns of enrichment and depletion of major, minor, and trace elements have been expanded to include four categories: 1) even distribution, 2) enrichment at margins (top, bottom, or both), 3) enrichment at the center of the seam, and 4) irregular. The patterns of enrichment and depletion are listed in Table III for Beulah and Center mine lignite seams.

The bulk coals were subjected to chemical fractionation analysis (3) which can be used to categorize how a particular element is associated in the coal. The elemental associations within the coal were divided into three categories: 1) ion-exchangeable, 2) acid-soluble, and 3) residual. The elements are associated in the coal in one or more of the groups described above. The categories for the elements are listed in Table III.

The organic and inorganic affinities of elemental constituents have been determined by a number of investigators (5,6). The relationship between the concentration of an element in moisture-free coal and the ash content can be used as a guide to the affinity of that element for, or incorporation in, the mineral matter or the carbonaceous material. If the concentration of an element increases with increasing ash content that element may be characterized as being associated with the inorganic species that form ash, or in other words may be said to have an inorganic affinity. If the concentration shows no correlation with ash content, that element may be said to have an organic affinity. Linear least squares correlation coefficients were calculated for the concentrations of the elements versus the ash content. For example, organic and inorganic affinities for elements from the Center mine indicate the following affinities. Seven elements - Na, Ca, Mn, Br, Sr, Y, and Ba - had correlation coefficients below 0.200 and thus show organic affinity in this suite of samples. An additional seven elements - Mg, K, Cu, As, Rb, Ce, and Eu - had correlation coefficients ranging from 0.201 to 0.600

and may be associated with both the carbonaceous and mineral portions of the coal. The remaining 24 elements show inorganic affinity.

The ionic potentials of all the elements, Z/r , where Z is the ionic charge and r is the ionic radius, are summarized in Table III. The ionic potentials of elements have a large effect on the association of the element in mineral-forming processes (13). Elements having low ionic potential ($Z/r < 3$), such as sodium, magnesium, and calcium, associate as hydrated cations. Insoluble hydrolysates have ionic potential of $3 < Z/r < 12$, which include, for example, the elements aluminum, silica, and titanium.

The elements displaying an even distribution within the coal seams have the following characteristics: 1) ion-exchangeable, 2) organic affinity or both organic and inorganic, and 3) ionic potential less than 3. The elements that are included in this group are Na, Mg, Ca, Mn, Sr, and Ba. Slight variations in distribution patterns and chemical fractionation behavior may be indicated; these generalizations were made on the basis of average trends. The elements showing enrichment of the margins in the lignite seams display the following characteristics: 1) chemical fractionation suggests association with the acid soluble and residue portions or, in some cases, distribution in all three groups, 2) inorganic affinity, and 3) ionic potential $3 < Z/r < 12$. The elements that have these characteristics include Al, Si, Cl, K, Sc, Ti, V, Cr, Co, Br, Zr, Ra, Cs, La, Ce, Sm, Eu, Yb, Th, and U. These elements are primarily associated with detrital constituents. The elements that have a random or irregular distribution within the coal seams, for the most part, have the following characteristics: 1) chemical fractionation behavior which suggests that the elements are insoluble and remain in the residue, 2) inorganic affinity, and 3) formation by authigenic mineralization. The elements included in this group are Fe, Ni, Zn, As, Se, Cd, and Sb. The irregular distribution of these elements is the result of syngenetic and epigenetic mineralization in the formation of sulfides. All of these elements have chalcophilic characteristics.

The possible associations of the elements included in this study are given in Table IV which summarizes distribution patterns, chemical fractionation behavior, organic and inorganic affinities, and ionic potential.

Acknowledgment

The authors would like to thank Robin G. Roaldson for his assistance in sample preparation and data handling.

Literature Cited

1. Karner, F.R.; Benson, S.A.; Schobert, H.H.; and Roaldson, R.G. ACS Div. Fuel Chem. Preprints, 28 (4), 123-137 (1983).
2. Sondreal, E.A.; Kube, W.R.; and Elder, J.L. BuMines R.I. 7158, 94 pp. (1968).
3. Hurley, J.P.; and Benson, S.A. ACS Div. Fuel Chem. Preprints, to be presented at the Philadelphia ACS Meeting, August 1984.
4. Benson, S.A.; and Holm, P.L. ACS Div. of Fuel Chem. Preprints, 28 (2), 234 (1983).
5. Gluskoter, H.J.; Ruch, R.R.; Miller, W.G.; Cahill, R.A.; Dreker, G.B.; and Kuhn, J.K. Trace Elements in Coal: Occurrence and Distribution, Illinois State Geological Survey Circular 499, p. 109 (1977).
6. Nicholls, G.D. The Geochemistry of Coal-Bearing Strata in Murchison, D., and T.S. Westoll, editors. Coal and Coal-Bearing Strata: American Edition, New York, American Elsevier, p. 269-307 (1968).
7. Karner, F.R.; White, S.F.; Brekke, D.W.; and Schobert, H.H. Geologic Sampling of Lignite Mines in Mercer and Oliver Counties, North Dakota. DOE/FC/FE-1, 1983 (in preparation).
8. Benson, S.A.; Kleesattel, D.; and Schobert, H.H. ACS Div. of Fuel Chemistry Preprints, 29 (1), pp. 108-113, 1984.

9. Weaver, J.N. in Analytical Methods for Coal and Coal Products, Vol. 1, p. 377-401, Karr, C., Jr. (Ed.), Academic Press, Inc., New York (1978).
10. Benson, S.A. Proceedings, North Dakota Academy of Science, 34 (10), 1980.
11. Mason, B. Principles of Geochemistry. John Wiley and Sons Inc., New York, 2nd Ed., 1964, pp. 155-157.
12. Kleesattel, D.R. "Distribution, Abundance, and Maceral Content of the Lithotypes of the Beulah-Zap Bed of North Dakota." For Presentation at the Rocky Mountain Coal Symposium. Bismarck, North Dakota, October 2-4, 1984.

Table I. Elemental Analysis of a Stratigraphic Sequence Containing Two Lignite Seams at the Beulah Mine, North Dakota,
part per million unless otherwise indicated, dry coal basis

ID	Lithology	Height, m ^a	Ash, % ^f	Na	Mg	Al	Si**	P**	S**	Cl	K	Ca	Sc	Ti
3-1-A	Underclay	-0.3	--	1964	10364	84699	321178	436	2803	750	10062	3398	11.7	3574
3-2-A	Lignite	0.0	17.0	7767	722	8394	19572	679	17182	100	530	6888	11.9	829
3-3-A	Lignite	0.1	8.47	14348	678	1935	5068	332	10142	8	500	6101	2.1	207
3-4-A	Lignite	0.5	7.30	3479	642	2584	3139	286	8302	100	500	7249	4.9	100
3-5-A	Lignite	0.9	22.20	753	1598	27082	34145	387	13513	100	1908	2191	10.6	438
3-6-A	Clay	1.0	--	1821	13741	113270	298737	0	8009	750	13269	3720	15.0	4211
3-7-A	Clay	1.6	--	2159	12454	111945	307620	0	3204	750	13585	2559	16.1	4560
2-1-A	Lignite	1.7	10.80	3991	671	9428	10956	282	8823	16	500	7062	10.8	125
2-2-A	Lignite	2.1	7.20	7497	707	5192	3971	471	7698	100	500	5281	0.9	119
2-3-A	Lignite	2.6	7.60	9482	717	4542	5045	364	8522	100	713	6206	0.8	140
2-5-A	Lignite	2.9	7.10	6598	731	3431	3086	0	8046	100	500	6031	1.7	226
2-6-A	Lignite	3.3	7.40	6988	571	3886	4981	355	9720	100	500	3973	0.5	59
2-7-A	Lignite	3.4	5.60	6692	564	2664	11048	122	3453	24	500	4615	0.3	100
2-8-A	Lignite	3.6	15.28	6583	3386	7312	10072	800	20071	100	500	8261	0.8	502
2-10-A	Lignite	4.2	6.40	5907	472	4308	5475	223	6561	100	500	12635	2.4	77
2-11-A	Lignite	4.8	12.0	5631	1242	7557	12398	366	10476	100	500	8927	6.1	121
2-13-A	Top of Lignite	5.1	9.10	5561	914	5937	5360	436	10823	100	500	6423	11.5	196
2-14-A	Clay	5.2	--	3518	16012	118373	290790	436	4405	750	16692	4520	15.5	3647
2-15-A	Clay	6.3	--	4385	14031	88995	293127	0	1201	750	15654	4983	13.9	3630
2-16-A	Silt	7.3	--	3440	14605	88403	288453	0	2803	750	9177	2880	12.0	3082
2-17-A	Chert	7.5	--	464	3800	13052	56100	0	9211	1250	1000	1709	12.1	1000
2-18-A	Sandstone	7.8	--	4084	9826	49621	250117	0	2803	750	7608	27085	8.3	2426
2-19-A	Clay	8.9	--	1771	14771	81163	287518	436	4405	750	4162	6110	14.5	4017

Table I. Elemental Analysis of a Stratigraphic Sequence Containing Two Lignite Seams at the Beulah Mine, North Dakota,
part per million unless otherwise indicated, dry coal basis (Continued)

ID	Lithology	V	Cr	Mn	Fe	Co	Ni	Cu	Zn	As	Se	Br	Ru	Cd	Sb
3-1-A	Underclay	99	66	177	24853	5.9	>25	150	66	2.51	0.20	1.10	86.00	2.50	0.65
3-2-A	Lignite	66	37	44	15358	5.5	>20	58	19	21.8	1.42	1.70	12.00	1.00	4.61
3-3-A	Lignite	4	5	42	6580	4.0	9	10	25	22.5	0.69	4.98	5.00	1.00	0.05
3-4-A	Lignite	6	6.5	40	2561	1.7	>25	11	25	2.17	0.55	1.69	5.00	1.00	0.04
3-5-A	Lignite	148	39	57	26129	13.0	90	25	9	374	4.28	3.28	16.00	1.00	5.74
3-6-A	Clay	205	91	96	15258	18.0	95	150	30	24.1	0.20	0.77	108.00	1.00	1.78
3-7-A	Clay	181	94	98	11929	2.7	>25	150	94	6.66	4.12	0.76	126.00	2.50	1.35
2-1-A	Lignite	25	16	36	3100	1.9	>25	52	33	11.5	0.43	1.73	3.26	1.20	1.33
2-2-A	Lignite	3	2.8	41	1502	1.2	>25	25	8	3.55	0.10	1.18	5.00	1.00	0.12
2-3-A	Lignite	2	2.9	46	1467	1.1	>25	25	25	5.18	0.52	1.25	5.00	1.00	1.28
2-5-A	Lignite	5	3.1	46	1489	0.7	>25	48	0	2.22	1.00	1.29	5.00	1.00	0.04
2-6-A	Lignite	3	2.5	31	6193	1.0	>25	25	25	31.5	0.39	0.45	1.42	0.65	0.01
2-7-A	Lignite	1	1.3	36	1035	1.1	>25	25	25	0.66	0.32	0.53	5.00	1.00	0.03
2-8-A	Lignite	1	4.4	58	2928	0.6	>25	25	25	4.37	0.59	0.46	5.00	1.00	0.21
2-10-A	Lignite	6	8.6	27	8711	5.2	>25	25	20	21.2	1.27	0.55	5.18	1.00	0.34
2-11-A	Lignite	5	6.5	79	2821	1.5	7	25	19	3.45	0.56	1.24	5.00	1.00	0.29
2-13-A	Top of Lignite	34	9.3	70	2405	3.0	10	10	25	7.03	0.20	1.16	5.00	1.00	0.60
2-14-A	Clay	177	81	212	22282	17.0	121	150	30	14.8	0.20	0.50	115.00	2.50	1.52
2-15-A	Clay	144	64	735	27448	12.0	15	150	30	2.63	0.20	0.50	90.00	2.50	1.04
2-16-A	Silt	136	56	1000	28123	11.0	>20	150	30	2.75	0.20	0.89	77.80	2.50	0.63
2-17-A	Chert	73	18.9	8046	273475	2.7	>25	300	200	0.50	0.20	0.89	10.00	2.50	0.49
2-18-A	Sandstone	73	55	611	15853	8.6	>20	150	52	6.09	0.54	0.25	50.64	2.50	0.19
2-19-A	Clay	134	68	738	35592	12.0	>20	150	30	2.48	3.22	1.12	87.00	2.50	0.73

Table 1. Elemental Analysis of a Stratigraphic Sequence Containing Two Lignite Seams at the Beulah Mine, North Dakota, part per million unless otherwise indicated, dry coal basis (Continued)

ID	Lithology	Cs	Ba	La	Ce	Sm	Eu	Yb	U
3-1-A	Underclay	4.96	786	32.18	48.66	2.51	1.36	1.59	1.91
3-2-A	Lignite	5.50	746	8.07	19.81	1.31	0.71	2.22	2.09
3-3-A	Lignite	0.02	756	1.29	8.46	1.42	0.36	1.37	0.50
3-4-A	Lignite	0.05	1114	2.95	9.21	1.04	0.46	1.62	0.23
3-5-A	Lignite	4.56	683	45.36	71.90	8.29	1.95	1.38	3.32
3-6-A	Clay	8.10	676	45.36	41.00	2.45	1.13	1.20	3.32
3-7-A	Clay	10.00	644	36.00	45.32	2.58	0.98	1.60	2.34
2-1-A	Lignite	1.49	1005	2.49	8.32	1.05	0.49	1.41	1.86
2-2-A	Lignite	0.05	988	9.75	14.35	0.52	0.21	0.40	0.41
2-3-A	Lignite	0.05	1158	3.75	6.98	0.35	0.12	0.38	0.36
2-5-A	Lignite	0.05	1284	11.36	16.00	0.43	0.11	0.41	0.56
2-6-A	Lignite	0.16	844	0.84	1.00	0.17	0.07	0.11	0.23
2-7-A	Lignite	0.12	1041	0.58	1.66	0.17	0.06	0.07	0.10
2-8-A	Lignite	0.05	21	2.07	4.08	0.42	0.26	0.63	0.50
2-10-A	Lignite	1.15	3045	7.47	39.27	0.63	0.55	0.42	0.24
2-11-A	Lignite	0.34	1749	4.06	9.69	0.81	0.37	1.11	0.90
2-13-A	Top of Lignite	0.02	226	3.52	6.77	0.82	0.43	1.39	2.08
2-14-A	Clay	8.50	811	36.20	52.50	2.73	1.11	1.72	2.88
2-15-A	Clay	5.31	813	35.00	45.61	3.28	1.30	1.83	1.82
2-16-A	Silt	4.35	613	28.00	39.00	2.54	1.06	1.17	2.30
2-17-A	Chert	0.40	274	11.60	10.00	1.27	0.40	1.09	0.20
2-18-A	Sandstone	3.00	725	26.70	37.00	2.65	1.18	1.26	1.54
2-19-A	Clay	5.28	851	25.60	46.70	2.63	1.43	1.81	1.75

*Height from base of first seam.

**Determined by x-ray fluorescence.

†Ash on a moisture-free basis

Table II. Elemental Analysis of a Stratigraphic Sequence Containing One Lignite Seam from the Orange Pit of the Beulah Mine,
North Dakota, ppm (dry basis)

ID	Lithology	Height, m*	Ash, %	Na	Mg	Al	Si**	S**	Cl	K	Ca	Sc	Ti	V
B-1	Lignite	-0.5	7.1	7041	1041	2824	10800	65890	44.3	500	7317	2.16	132	3.02
B-2	Lignite	0.00	6.8	5178	1004	3107	12950	46240	43.9	500	9072	0.64	132	2.84
B-3	Lignite	0.50	6.7	5833	1150	3472	7940	50030	52.8	500	8891	0.57	138	2.73
B-4	Lignite	1.00	6.8	6018	1043	2675	16760	51530	41.8	500	7803	0.57	144	2.22
B-5	Lignite	1.50	13.0	5826	3526	6710	12580	65160	132.7	500	8016	0.38	326	5.84
B-6	Lignite	2.00	6.9	5313	1238	2793	39940	59750	49.2	500	7828	0.36	150	2.20
B-7	Lignite	2.50	8.5	6169	1292	4348	93000	64240	63.2	500	11998	0.43	162	2.50
B-8	Lignite	3.00	15.7	6278	1449	5869	44510	64070	70.9	500	10872	0.48	167	2.12
B-9	Lignite	3.50	10.4	5096	1483	7929	104700	56470	54.1	500	11876	1.05	226	4.85
BR-1	Overburden	3.60	--	2246	15718	9198	275900	3130	750	9724	7094	15	2390	136.00
BR-3	Overburden	4.14	--	2773	13226	89901	259700	1100	750	14994	6673	18	4256	165.00
BR-5	Overburden	4.80	--	3098	15480	97158	281400	497	100	8653	7342	16	3880	158.00
BR-6	Overburden	5.10	--	2619	15475	84833	288900	1480	100	10800	6197	5.1	3674	134.00
BR-9	Overburden	6.10	--	2389	16774	88663	294000	1350	750	14971	9553	15.8	4557	142.00
BR-11	Overburden	6.70	--	2082	9982	51610	187700	3220	750	14971	9465	18.7	2760	119.00
BR-13	Overburden	7.30	--	2842	12634	66743	277400	12710	750	6441	12042	8.97	3796	80.1
BR-13A	Overburden	7.35	--	3028	14339	78427	284900	840	150	8994	123401	12.9	4131	117.0
BR-18	Overburden	8.90	--	3028	12471	75153	286200	1070	750	8994	13916	14.0	4360	117.0
BR-19	Overburden	9.20	--	2863	12793	78030	290700	<100	750	10006	14862	14.0	3451	117.0

Table 11. Elemental Analysis of a Stratigraphic Sequence Containing One Lignite Seam from the Orange Pit of the Beulah Mine,
North Dakota, ppm (dry basis) (Continued)

ID	Lithology	Cr	Mn	Fe	Co	Ni	Cu**	Zn	As	Se	Br	Sr**	Y**	Zr**
B-1	Lignite	2.24	22	5147	1.68	5.75	53	12.62	10.67	0.05	1.62	360	6	8
B-2	Lignite	1.62	28	3261	0.75	10.23	33	5.48	3.90	0.40	1.40	445	6	11
B-3	Lignite	1.41	29	3462	0.70	10.71	53	6.08	3.52	0.39	1.49	480	4	13
B-4	Lignite	1.37	28	3289	0.39	13.17	58	4.78	3.34	0.50	1.04	410	2	9
B-5	Lignite	2.08	136	2202	0.37	5.00	23	25.00	27.18	0.91	0.84	320	2	<5
B-6	Lignite	1.89	37	3308	0.80	15.34	64	25.00	5.24	0.54	0.99	360	2	8
B-7	Lignite	2.30	33	1706	0.59	11.36	59	3.46	3.55	0.49	0.55	520	2	15
B-8	Lignite	2.60	48	30530	0.69	15.66	30	25.00	39.17	0.79	0.81	330	2	10
B-9	Lignite	3.51	47	2897	0.70	9.36	62	8.57	7.85	0.36	0.92	520	6	17
BR-1	Overburden	86.2	611	36878	14.02	28.88	86	30.00	12.66	1.56	0.92	262	26	112
BR-3	Overburden	93.2	2092	50756	13.57	72.84	73	30.00	2.50	0.57	1.05	223	28	94
BR-5	Overburden	92.4	467	30865	10.97	22.93	87	30.00	5.25	1.40	0.27	239	26	109
BR-6	Overburden	32.4	979	14308	3.99	95.69	81	25.00	6.23	0.42	0.55	234	31	126
BR-9	Overburden	88.0	885	39106	13.78	63.45	84	30.00	3.52	1.25	0.92	230	25	108
BR-11	Overburden	72.3	3542	147377	11.26	39.66	46	30.00	2.50	0.20	1.07	104	18	66
BR-13	Overburden	63.0	308	36902	10.14	50.09	64	30.00	27.16	1.01	1.41	255	22	169
BR-13A	Overburden	78.7	424	26437	9.95	20.00	71	30.00	5.01	0.84	1.46	274	28	165
BR-18	Overburden	90.8	670	31472	11.33	45.09	80	30.00	5.01	0.53	1.46	285	25	131
BR-19	Overburden	90.8	435	28566	11.44	36.64	73	30.00	3.34	1.08	1.08	265	27	164

Table II. Elemental Analysis of a Stratigraphic Sequence Containing One Lignite Seam from the Orange Pit of the Beulah Mine,
North Dakota, ppm (dry basis) (Continued)

10	Lithology	Ru	Ag	Cd	Sb	Cs	Ba	La	Ce	Sm	Eu	Yb	Th	U
B-1	Lignite	2.00	0.15	5.00	0.01	0.01	714	7.84	8.30	0.53	0.11	0.36	0.57	0.40
B-2	Lignite	1.37	0.53	5.00	0.04	0.04	917	3.30	5.61	0.49	0.09	0.28	0.75	0.24
B-3	Lignite	2.00	0.48	5.00	0.10	0.03	943	3.62	6.39	0.43	0.06	0.24	0.81	0.23
B-4	Lignite	2.00	0.79	0.34	0.10	0.03	844	3.24	4.92	0.24	0.05	0.09	0.83	0.75
B-5	Lignite	2.00	0.05	1.10	0.07	0.01	930	12.78	13.14	0.34	0.03	0.01	0.78	0.40
B-6	Lignite	2.00	0.53	0.19	0.01	0.03	704	0.98	2.42	0.26	0.01	0.06	0.49	0.31
B-7	Lignite	2.00	0.75	5.00	0.06	0.03	1138	1.52	3.18	0.31	0.05	0.09	1.01	0.56
B-8	Lignite	2.00	0.37	1.87	0.04	0.05	1242	2.20	9.98	0.28	0.07	0.08	1.12	1.26
B-9	Lignite	2.00	0.15	5.00	0.22	0.08	720	2.38	4.97	0.55	0.12	0.38	1.75	0.99
BR-1	Overburden	114.48	0.08	2.50	0.44	6.57	1075	12.19	63.46	1.17	1.30	1.07	10.37	1.51
BR-3	Overburden	131.48	0.08	2.50	0.50	7.56	732	14.58	67.26	1.23	1.29	1.77	10.14	1.03
BR-5	Overburden	164.19	0.08	2.50	0.49	7.53	685	13.82	61.24	1.25	1.12	1.33	9.50	0.80
BR-6	Overburden	35.87	0.49	5.00	0.51	0.79	285	12.70	18.50	1.26	0.31	0.73	3.26	0.76
BR-9	Overburden	127.44	0.08	2.50	0.38	6.38	567	12.31	61.70	1.12	1.33	1.59	9.39	1.09
BR-11	Overburden	77.75	0.00	2.50	0.69	4.50	401	16.88	82.93	1.59	1.37	1.46	7.02	2.99
BR-13	Overburden	72.16	0.08	2.50	0.40	3.39	444	12.36	69.63	1.15	1.26	1.15	7.84	1.12
BR-13A	Overburden	108.76	20.08	2.50	0.38	4.53	619	14.57	63.00	1.28	1.35	1.50	9.35	0.80
BR-18	Overburden	101.83	0.08	2.50	0.38	5.10	567	14.00	63.00	1.35	1.43	1.52	9.45	1.27
BR-19	Overburden	94.82	0.08	2.50	0.30	4.69	511	13.55	64.46	1.22	1.46	1.71	10.18	1.13

*Height from base of first seam.

**Determined by x-ray fluorescence.

† Ash on a moisture-free basis

Table III. Qualitative Geochemical Relationships Between Geochemical Properties and Elemental Distribution Within Seams

Distribution Within Lignite Seams at the Beulah Mine						Distribution Within Lignite Seam at the Center Mine			
	Beulah		Chemical Fractionation Behavior	Affinity	Center	Chemical Fractionation Behavior*		Affinity	Ionic Potential Z/r
	Beulah Orange Pit	Upper Seam				Center			
Na	E	E	CE	IE	Organic	E	IE	Organic	1.0
Mg	E	E	IE	IE	NC	E	IE>>AS	NC	3.0
Al	T-MA	MA	B-MA	AS, RS	Inorganic	MA	AS, RS	Inorganic	5.9
Si	T-MA	IR	E	RS	Inorganic	MA	RS	Inorganic	9.5
P	ND	IR	B-MA	ND	Inorganic	IR	ND	Inorganic	14.3
S	IR	IR	MA	RS, IE	Organic	MA	RS, IE	Organic	17.1
Cl	E	E	E	ND	NC	B-MA	ND	Inorganic	
K	E	E	E	RS, AS	Inorganic	B-MA	IE, AS, RS	Inorganic	0.13
Ca	E	CE	E	IE, AS	NC	E	IE, AS	NC	2.0
Sc	MA	MA	MA	RS, AS	NC	MA	AS, RS	Inorganic	3.7
Ti	T-MA	IR	B-MA	RS	Inorganic	B-MA	RS	Inorganic	5.9
V	E	MA	B-MA	AS	NC	B-MA	AS, RS	Inorganic	4.0
Cr	MA	MA	B-MA	RS	Inorganic	B-MA	RS	Inorganic	4.8
Mn	E	T-MA	T-MA	AS, IE	NC	E	AS, IE	NC	2.5/6.7
Fe	IR	IR	B-MA	RS, AS	Inorganic	MA	AS	Inorganic	2.7/4.7
Co	B-MA	ND	ND	AS, RS	Inorganic	MA	AS, RS	Inorganic	2.8
Ni	IR	E	MA	RS	Inorganic	MA	RS	Inorganic	3.0
Cu	IR	E	B-MA	ND	Inorganic	B-MA	RS	Inorganic	1.0/2.8
Zn	IR	ND	ND	RS	Inorganic	MA	ND	Inorganic	.88/2.7
Ge	ND	ND	ND	ND	ND	B-MA	ND	ND	2.7/7.5
As	IR	IR	IR	RS	Inorganic	MA	RS	NC	10.8
Se	CE	IR	B-MA	RS	Inorganic	B-MA	RS, IE	Inorganic	14.3
Br	B-MA	MA	CE	ND	NC	ND	ND	Organic	
Rb	ND	ND	ND	ND	ND	IR	RS, AS	ND	0.68
Sr	E	ND	ND	IE	Organic	E	IE	Organic	1.8
Y	MA	ND	ND	ND	ND	IR	ND	ND	3.4
Zr	T-MA	ND	ND	RS	ND	MA	ND	Inorganic	5.1
Ru	E	E	B-MA	ND	Inorganic	B-MA	ND	Inorganic	6.0
Ag	IR	ND	ND	ND	ND	MA	ND	Inorganic	2.2
Cd	ND	E	E	RS	NC	IR	ND	Inorganic	.87/2.1
Sb	IR	B-MA	B-MA	RS	Inorganic	B-MA	AS, RS	Inorganic	4.0
Cs	T-MA	B-MA	B-MA	RS	Inorganic	B-MA	RS	Inorganic	0.6
Ba	E	T-MA	T-MA	IE, AS	NC	MA	IE, AS	NC	1.5
La	B-MA	IR	MA	AS, RS	Inorganic	B-MA	AS, RS	Inorganic	2.6
Ce	B-MA	IR	B-MA	AS, RS	Inorganic	MA	AS, RS	NC	2.9
Sm	MA	MA	E	AS, RS	Inorganic	MA	AS	Inorganic	3.1
Eu	MA	MA	MA	AS, RS	Inorganic	MA	AS	NC	3.2
Yb	MA	MA	MA	AS, RS	NC	MA		Inorganic	
Th	T-MA	MA	B-MA	RS	Inorganic	MA	RS	Inorganic	3.9
U	T-MA	MA	B-MA	AS, RS	Inorganic	MA	AS, RS	Inorganic	4.2

Patterns of Distribution

E - Even Distribution
 MA - Enrichment at both margin
 T-MA - Enrichment at top margin
 B-MA - Enrichment at bottom margin
 CE - Enrichment at the center of the seam
 IR - Irregular

*Chemical Fractionation Behavior

IE - Ion-exchangeable
 AS - Acid soluble
 RS - Remains in the residue
 NC - No Correlation
 ND - Not Determined

Table IV. Association of Elements in North Dakota Lignites

Element	Possible Association
Na	- Organically bound
Mg	- Organically bound, carbonates
Al	- Clay minerals, possibly hydroxide or coordinated
Si	- Clay minerals, quartz
P	- Organically bound, phosphates*, associated with rare earth elements
S	- Sulfides, sulfates, organically bound
Cl	- Inorganic association
K	- Associated with illite and other k-bearing minerals, organically bound
Ca	- Organically bound, carbonates
Sc	- Inorganic association, clay minerals
Ti	- Rutile, associated with quartz
V	- Possibly has both an organic and inorganic association
Cr	- Totally an inorganic association
Mn	- Organically bound, carbonate minerals
Fe	- Oxides, hydroxides, sulfides
Co	- Inorganic association, possibly sulfides
Ni	- Inorganic association, possibly sulfides
Zn	- Inorganic association, possible sulfides
As	- Inorganic association, possible sulfides
Se	- Inorganic association, possibly sulfides
Br	- May have an organic association
Rb	- Organically bound
Sr	- Organically bound
Y	- Inorganic association, possibly carbonates
Zr	- Zircon
Ru	- Inorganic
Ag	- Inorganic, possibly sulfides
Cd	- Inorganic, possibly sulfides
Ba	- Organic, sulfates
La	- Detrital inorganic, phosphates*
Ce	- Detrital inorganic, phosphates*
Sm	- Detrital inorganic
Eu	- Detrital inorganic
Yb	- Detrital inorganic
Th	- Detrital inorganic
U	- Detrital inorganic

*Monazite has been found in Beulah lignite samples (12).

VOLCANIC ASH LAYERS IN COAL: ORIGIN, DISTRIBUTION, COMPOSITION AND SIGNIFICANCE

Don Triplehorn and Bruce Bohor

Geology/Geophysics Program, University of Alaska, Fairbanks, Alaska
99701, and U.S. Geological Survey, Federal Center, Denver, Colorado
80225

INTRODUCTION

The main purpose of this paper is to call attention to volcanic eruptions as a source of mineral matter in coal. Volcanic material is apt to have mineral and chemical compositions as well as patterns of distribution different from the more usual types of mineral matter in coal. Recognition of volcanic material requires some understanding of the process of origin, an awareness of the considerable variety of materials involved, and an appreciation of the tendency of volcanic materials to undergo substantial alteration so that their genesis is obscured.

Some comments on terminology are necessary. "Volcanic ash partings" here refers to sedimentary units bounded by organic-rich material (coal, lignite, or organic shale) and which were deposited as air-fall volcanic ash with essentially no subsequent transport or mixing with terrigenous detrital silicates (clay, mud and sand). No specific grain size or composition is implied. The term "tephra" is now commonly used for modern, unaltered, uncompacted material, while the term "tuff" is used for the compacted (rock) equivalent.

A volcanic origin is obvious where there is glass, volcanic phenocrysts, characteristic mineralogy, or absence of terrigenous detritus and lack of sedimentary structures formed by moving water. With increasing age, however, there is progressive alteration and loss of recognizable volcanic features; the product is generally some kind of clay unit. As a general term they might be called altered tuffs. In marine shales they are known as bentonites; these are usually montmorillonitic (smectitic), light-colored, and sticky when wet. In coals, particularly Carboniferous coals, they are usually kaolinitic, light-colored and firm. We prefer the general term "altered volcanic ash" because there is considerable range in physical appearance, original and secondary mineralogy, as well as in the type of enclosing sediment.

ORIGIN

Volcanic ash partings in coals should not be surprising. The recent eruption of Mt. St. Helens spread volcanic ash across several western states and traces of the dust traveled around the world. Consider, however, where a recognizable layer of this ash is likely to be preserved. On land, almost all of it will be eroded by wind and water, mixed with terrigenous sand and clay, and ultimately dispersed into lakes or the ocean. An important exception is to be found in marshes or swamps, the general setting in which plant material accumulates to eventually become coal. Once deposited in a coal swamp, an ash fall has a good chance of

remaining undisturbed because the shallow water, low stream gradients, lack of relief, and sediment baffling effects of vegetation minimize processes that could cause reworking. Portions of such swamps may be so distant from major streams that they receive little or no mud from over-bank floods. Thus it is likely that some ash falls would be buried in organic debris (coal) and remain free of non-volcanic material from fluvial sources.

It follows then that there is a genetic relationship between volcanic ash partings and the coals that contain them: environments of coal deposition provide one of the best places for preservation of air-fall volcanic materials.

Not all kinds of volcanic ash have the same chance of such preservation, however. Many volcanoes, such as those in Hawaii, are characterized by relatively quiet eruptions of mostly fluid lava. Though spectacular on a human scale, these involve only minor injection of fine-grained material into the upper atmosphere where it can be carried long distances by prevailing winds. Only volcanoes characterized by particularly violent eruptive styles are likely to be important in producing the thin, widespread units of ash most commonly preserved in the geologic record. The explosiveness of eruptions is related to several factors, including gas content and geometry of the vent. Of most importance here, however, is silica content: silica increases the viscosity of magma and the tendency toward explosive eruptions rather than quiet flows. Thus volcanic ash partings in coals are primarily the product of such silica-rich eruptions; this has important consequences in terms of the composition of the ash, as will be discussed later.

FIELD APPEARANCE OF VOLCANIC ASH PARTINGS IN COALS

Most volcanic ash partings are thin, ranging from 1 mm to a few cm. A few, however, attain thicknesses of more than 1 m. Some are uniform in thickness and have either sharp or gradational boundaries with the enclosing coal. Many, however, pinch and swell rapidly and may consist of a series of lenses rather than continuous beds, a feature they share with Carboniferous tonsteins (Williamson, 1970). Light shades of gray, brown, or yellow are most common, reflecting a lower organic content than the adjacent coal. Black and dark brown partings also occur, and sometimes these become obvious only after weathering; the oxidation of organic matter then results in a light-colored surface layer of siliceous material. Figure 1 shows the most common field appearance; in this case for a Cretaceous example from southern Alaska.

To a large extent the grain size and degree of induration of these partings depends upon the amount of post-depositional alteration; this in turn is largely a function of age and depth of burial. For example, lignites almost 4-5 m.y. old in southern Alaska contain partings that are loose and sandy; in fact they are clearly recognizable volcanic ash consisting mostly of glass shards. In contrast, 300 m.y. old partings in Kentucky bituminous coal are hard and very fine grained. The latter probably was similar to the Alaskan example at first, but has completely altered to a compact variety of kaolin known as flint clay.

COMPOSITION

Composition of the partings is a function of both the original materials and conditions, and the kind and extent of post-depositional modification. Therefore it is necessary to consider the primary composition (original) separately from the secondary composition (altered).

Primary Composition

The solid products of explosive volcanism include individual glass fragments, individual crystals (phenocrysts), and aggregates of these known as rock fragments. Glass is perhaps the most common component but there is a great variety among modern volcanics. A given volcano may eject different material over its eruptive lifespan. Even a single eruption, lasting perhaps only a few days, may involve changes in ash composition.

Volcanic ashes are characterized by a limited suite of mineral components. By far the most abundant are quartz, sanidine and plagioclase feldspars, certain pyroxenes and amphiboles, magnetite, apatite, biotite, and zircon. The presence of these minerals and the absence of others constitute evidence of a volcanic origin. Certain crystal forms, such as the beta form of quartz and hexagonal prisms of biotite, are particularly useful indicators of origin. Similarly, the presence of sanidine, the high-temperature form of potassium feldspar, suggests a volcanic origin. On the other hand, the presence of non-volcanic minerals such as muscovite and garnet indicates a non-volcanic origin or at least some admixture of non-volcanic (probably fluvial) material.

The specific minerals present reflect the original compositions of the magma. As noted earlier, explosive behavior, the kind most likely to produce ash partings in coals, is characteristic of silica-rich magmas. Thus the minerals cited above, and those to be expected in volcanic ash partings, are those associated with silica-rich magmas. The glass phase will, of course, also reflect this silica-rich tendency.

Original grain size of an ash parting reflects the texture of the material produced by a given volcano plus the progressive loss of coarser and denser components as an ash cloud moves downwind. In other words, texture is in part a function of distance from the source volcano. By far the most common ash partings in coal are thin, uniform and widespread. These probably were derived from distant volcanoes and consisted originally of silt- and clay-sized particles carried by high-altitude winds. Conversely, where ash partings are coarse-grained, thick, and abundant, the volcanic source is assumed to have been relatively close.

Secondary Composition

The primary composition discussed above is important here in that it determines in part the final products of alteration. It should be noted, however, that the factors controlling the degree and direction of alteration have not been thoroughly studied. In our opinion, chemical alteration in the environment of deposition and the length of time involved are probably more important than original composition in determining the final product.

The main secondary products are clay minerals, either smectite or kaolinite. These clay minerals are derived mainly and most readily from glass, but feldspars, amphiboles, pyroxenes, and biotite also alter in part to clay minerals. The alteration to kaolinite involves essentially complete removal of soluble components such as Na, Ca, Mg, K and Fe as well as considerable silica. Pure kaolinite consists of equal parts of silica and alumina and virtually nothing else--this is thus the product of very intensive leaching. Smectite on the other hand requires some Mg and more silica; it is thus the product of less intensive leaching than that which produces kaolinite.

It is uncertain whether the path of alteration can lead directly to kaolinite or must pass through a smectite intermediate stage. Certainly the thickness of the original ash can play a role: thin partings may be altered completely to kaolinite while adjacent thicker partings contain substantial smectite (Triplehorn and Bohor, 1981; Reinink-Smith, 1982). Given more time and further leaching, these smectitic partings presumably would eventually be altered to kaolinite. On the other hand, individual minerals such as feldspars and biotite can be observed altering directly to kaolinite without any smectite involvement.

A variety of other secondary minerals may occur in altered volcanic ash partings. Some of these may be related to modification of the primary constituents but others are more likely introduced by ground water taking advantage of the higher permeabilities of volcanic ash layers relative to the adjacent organic material (now coal). Carbonate minerals in quantities too large to have been derived entirely from the primary volcanic material are not uncommon. Siderite is most abundant although dolomite sometimes is present. Such cementation may obscure the volcanic origin of the original layer because well cemented partings are similar in appearance to the purely sedimentary carbonate layers that are very commonly associated with coals.

Recently occurrences of unusual aluminum phosphate minerals have been found with ash partings in coals (Triplehorn and Bohor, 1983). Since that report we have found a number of occurrences in Alaska and one in the Appalachian area. These minerals were grouped by Palache et al. (1951) as the plumbogummite series, with the general formula $X Al_2(PO_4)_2(OH)_2 \cdot H_2O$. End members of interest here include qoyazite (where $X = Sr$), gorcsekite (Ba), crandallite (Ca), and florencite (Ce, U, and other rare earths). Some layers in Alaska are sufficiently radioactive to give a distinct reading on hand-held radiation detectors in the field.

DISTRIBUTION

Because many geologists are not aware that volcanic ash partings occur in coals it is difficult to interpret the absence of published reports regarding their occurrences. The abundance of such partings is probably much greater than presently recognized. The following generalities regarding their distribution are mainly limited to North America and are based primarily on our own observations, discussions with others, and interpretation of published reports. Specific references to recognized volcanic ash partings in coals are relatively few and restricted mostly to the past few years.

In simple terms ash partings are relatively abundant in Cretaceous and Tertiary coals of the West and rare in Carboniferous coals of the East. We are less certain of the Gulf Coast Tertiary lignites but they appear to have at least a moderate abundance of such partings. To a degree this apparent distribution is related to the fact that the volcanic origin of the younger ash beds is more apparent, while older partings commonly appear as kaolinitic clay beds with little evidence of their volcanic heritage (see Bohor and Triplehorn, 1981). Even so, there is no question that the absolute frequency is higher in the West.

Locally the abundance can be highly variable. Where many coals are present ash partings may be distributed sparsely but uniformly or concentrated in just a few coals. Figure 2 shows an example in Southwestern Washington, in this case including both kaolinitic and smectitic partings (Reinink-Smith, 1982). In the West, where most of our work has been, volcanic ash partings are known from numerous coals in Utah, New Mexico, Colorado, Wyoming, Montana and Washington (Bohor, et al. 1978; Triplehorn and Bohor, 1981). Again, the frequency is highly variable. Individual coals in Montana and Colorado contain up to twenty or more ash partings, while the unusually thick coals of the Powder River Basin contain almost none. In Alaska, volcanic ash partings are present in all of the Cretaceous and Tertiary coals we have examined, but appear to be particularly abundant in the Cook Inlet area.

In the Appalachian coal basin and the Eastern Interior Basin, where we have had less experience, ash partings appear to be rare (Bohor and Triplehorn, 1982). The lack of ash partings in Carboniferous coals of eastern North America contrasts with their abundance in European coals of the same age. These have been studied for over a century although their volcanic origin was not generally accepted until the last few decades. Bouroz, et al. (1983) provides a good recent summary of some of this work in English.

SIGNIFICANCE

The geologic importance of volcanic ash partings in coals has been summarized previously by Triplehorn (1976). Of greatest importance is their use in correlation, the process of determining the time relationships among rocks exposed at different localities. The simplest use is as marker beds, where individual ash falls can be recognized and distinguished from others on the basis of some textural or compositional aspect. Beds containing the same ash layer (whether in coal or any other rock type) are the same age, although the absolute age (in years) is not indicated. Happily, the absolute age can sometimes be determined by radiometric age dating of certain minerals in the ashes. Potassium-argon dating is used for such minerals as feldspar and hornblende, while fission-track dating may be used for zircon and apatite.

It may be of interest here to note that Williamson (1970) mentioned the high radioactivity of certain ash partings (he called them tonsteins) that made them useful in bore-hole studies because they appeared as sharp maxima on gamma-ray logs of coal beds. Such maxima are conspicuous because coals are generally known for their absence of radioactivity.

He ascribed the high radioactivity of these partings to an unusual abundance of zircons. We have no specific knowledge of these occurrences, but suggest that the high radioactivity might instead be related to uranium-bearing phosphate minerals.

Thus far geologists have paid little attention to the significance of ash partings as indicators of processes and conditions in the coal-forming environment. For example, thin widespread partings without penetrating plant material suggest that these originated as ashes that fell into shallow standing water. Thick ashes should have affected the kind and amount of vegetation, and indirectly the nature of the coal immediately overlying thick ash beds. As yet there is little data in these aspects because geologists have not recognized the potential value of such studies.

For those interested in mineral matter in coal an awareness that some partings may be of volcanic origin may be useful in explaining the distribution of some of these layers and the occurrences of some unusual components, such as strontium, phosphate, or uranium. Volcanic ash partings are likely to be more widespread and uniform in texture, composition and thickness than the more common partings of fluvial origin. They are also more likely to show marked differences from layer to layer, and more likely to contain exotic mineral or chemical components.

REFERENCES

- Bohor, B.F., R.M. Pollastro, and R.E. Phillips, 1978, Mineralogical evidence for the volcanic origin of kaolinite partings (tonstein) in Upper Cretaceous and Tertiary coals of the Rocky Mountain region (abstr.): The Clay Mineral Soc., 15th Ann. Mtng., 27th Ann. Clay Minerals Conf. Bloomington, Indiana, Program and Abstracts, p. 47.
- Bohor, B.F., and D.M. Triplehorn, 1982, Volcanic origin of the Flint Clay parting in the Hazard #4 (Fire Clay) coal bed of eastern Kentucky, field trip guidebook, Geological Society of America Ann. Mtng., Oct., 1981, issued by Kentucky Geological Survey, 1982, p. 49-53.
- Bouroz, A., D.A. Spears, and F. Arbey, 1983, Review of the formation and evolution of petrographic markers in coal basins: Societe Geologique du Nord, Memoires Tome XVI, 115 pp.
- * Triplehorn, D.M., 1976, Volcanic ash partings in coals: characteristics and stratigraphic significance, The Neogene Society, Spring, 1976, Pacific Section, Society of Economic Paleontologists and Mineralogists, p. 9-12.
- Triplehorn, D.M. and B.F. Bohor, 1981, Altered volcanic ash partings in the C-coal, Ferron Sandstone member of the Mancos Shale, Emery County, Utah, U.S. Geol. Surv. Open-File Report 81-775, 49 pp.
- Triplehorn, D.M., and B.F. Bohor, 1983, Goyazite in kaolinitic altered tuff beds of Cretaceous age near Denver, Colorado: Clays and Clay Minerals, 31/4, p. 299-304.
- Triplehorn, D.M., D.L. Turner, and C.W. Naeser, 1977, K-Ar and fission-track dating of ash partings in Tertiary coals from the Kenai Peninsula, Alaska: a radiometric age for the Homerian-Clamgulchian stage boundary: Geological Society of Am. Bull, 88, pp. 1156-1160.
- Turner, D.L., D.M. Triplehorn, C.W. Naeser, and V.A. Wolfe, 1980, Radiometric dating of ash partings in Alaskan coal beds and upper Tertiary paleobotanical stages: Geology, 8, p. 92-96.
- Williamson, I.A., 1970, Tonsteins--their nature, origin, and uses: The Mining Magazine, 112, p. 119-125, 200-209.
- * Reinick-Smith, L., 1982, The Mineralogy, Geochemistry and Origin of Bentonite Partings in the Eocene Skookumchuck Formation, Centralia Mine, S. W. Washington. Unpublished M. S. Thesis, W. Washington Univ., 1/9 pp.

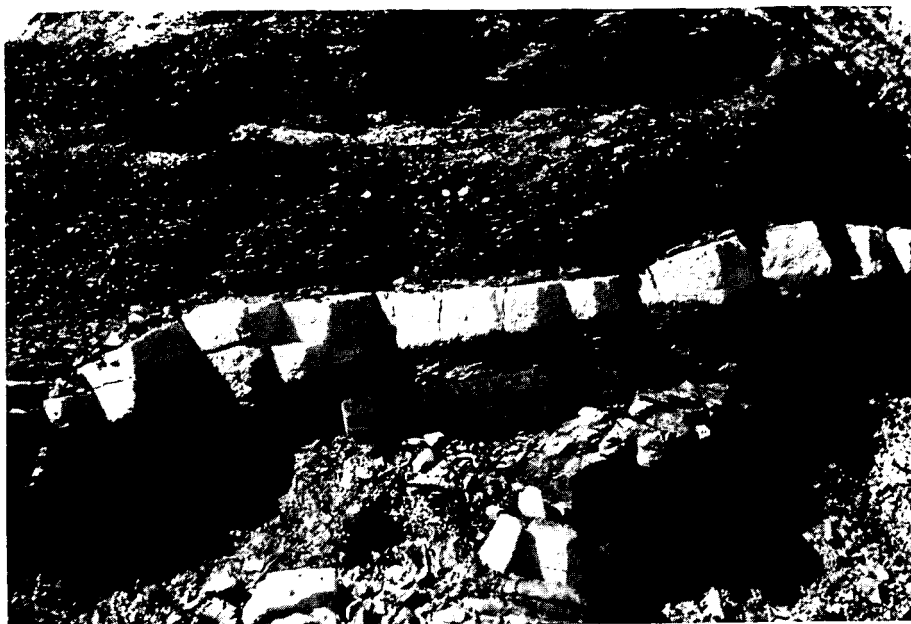


Figure 1. Light weathering kaolinite volcanic ash in coal, southern Alaska.



Figure 2. Multiple smectitic and kaolinitic ash partings in the Big Seam, southeastern Washington.

REACTIONS AND TRANSFORMATIONS OF COAL MINERAL MATTER AT ELEVATED TEMPERATURES

G. P. Huffman and F. E. Huggins

U. S. Steel Corporation Technical Center
Monroeville, PA

Introduction

Coal contains a variety of inorganic constituents that exhibit deleterious behavior in most processes that attempt to convert the energy in coal to a useful form. As coal is heated, the inorganic phases undergo transformations and reactions that yield a complex mixture of solid, molten, and volatile species. These species give rise to slagging and fouling deposits, corrosion, pollution, and other problems. Although such problems are usually associated with the combustion of coal to produce electrical power, they are also common in coal gasification and liquefaction, cokemaking, and iron production.

The current paper will briefly review research on this topic.

Nature of the Inorganic Constituents of Coal

It is common practice to make a distinction between the inorganic constituents of so-called "Eastern" and "Western" coals. By definition, Western coals are those for which the $\text{CaO}+\text{MgO}$ content exceeds the Fe_2O_3 content of the ash, while the reverse is true for Eastern coals. The inorganic constituents in Eastern coals, which are principally bituminous in rank, are predominantly in the form of discrete mineral particles. Clay minerals (kaolinite, illite) are usually dominant, followed by quartz and pyrite. The range and typical values of the mineral distribution and ash chemistry of Eastern coals are shown in Table I. These data were determined from computer-controlled scanning electron microscopy (CCSEM), Mössbauer spectroscopy, and other measurements on over a hundred coals.

Western coals are usually lignites or subbituminous coals. The range and typical values of the inorganic phase distribution and ash chemistry of approximately 20 Western coals examined in this laboratory are shown in Table II. In a recent paper, we discussed the differences between the inorganic constituents of low-rank coals and those of bituminous coals. These differences occur in the calcium-, iron-, and alkali-containing phases. In bituminous coals, the calcium content is typically low (CaO < 5% of ash) and all calcium is contained in the mineral, calcite. The calcium content of lignites is high (CaO ~10 to 30% of ash) and the calcium is molecularly dispersed throughout the coal macerals as salts of carboxylic acids. The latter point has been directly confirmed by EXAFS (extended X-ray absorption fine structure) spectroscopy. Similar differences occur for the alkali elements. Minerals such as illite, which accounts for most of the potassium in bituminous coal, are usually low in lignite and subbituminous coal (see Tables I and II). In lignites, sodium and potassium are believed to occur as salts of humic or carboxylic acids. Montmorillonite and halite (NaCl) are the dominant Na-containing minerals, and they occur in both bituminous and lower rank coal. The iron-bearing minerals in unoxidized bituminous coals include pyrite, ferrous-bearing clays (illite, chlorite), and carbonates (siderite, ankerite). In lignites, only pyrite and its weathering products (iron sulfates and oxyhydroxides) are normally observed.

The diversity of transformations and reactions that such complex assemblages of inorganic matter can undergo when coal is combusted or otherwise converted to a more useful form of energy is too complex to be discussed in any detail in a short article. Our intention, therefore, is simply to outline some of the major phenomena and to provide the reader with useful references. Most of the article will deal with reactions and transformations related to coal combustion, with a short section devoted to other conversion processes.

Slagging Behavior; Ash Melting

During pulverized-coal combustion, atmospheric conditions within the coal flame are considered to be reducing in the sense that the stable ionic form of iron is ferrous. After ash particles have left the flame region, they encounter a more oxidizing environment, yielding deposits and fly ash in which the iron may be predominantly ferric or a mixture of ferrous and ferric, dependent on the air-to-fuel ratio. Consequently, it is important to understand the high temperature reactions of ash constituents in both types of environment. This point is recognized in the ASTM ash-fusion test⁵⁾ which specifies measurement of the fusion temperatures of ash cones in both a reducing (60% CO, 40% CO₂) and an oxidizing (air) atmosphere. Numerous empirical formulae have been developed to predict ash-fusion temperatures (AFTs) and the viscosities of molten coal-ash slags at higher temperatures from ash composition. Detailed discussions of these formulae and their physical basis have been given by Winegartner and his associates,^{1,6,7)} by Watt and Fereday,^{8,9)} and in a recent review article by Reid.¹⁰⁾ The dominant parameter in these relationships is usually the base-to-acid ratio, where "base" and "acid" are simply the sums of the weight percentages of the basic and acidic oxides:

$$\text{Base} = \text{Fe}_2\text{O}_3 + \text{CaO} + \text{K}_2\text{O} + \text{Na}_2\text{O} + \text{MgO} \quad (1)$$

$$\text{Acid} = \text{SiO}_2 + \text{Al}_2\text{O}_3 + \text{TiO}_2 \quad (2)$$

Recently, we examined the behavior of ash fusion temperatures in the context of ternary phase diagrams.¹¹⁾ Significant similarities were observed between the dependence of AFTs on chemical composition and the liquidus curves in appropriate regions of the FeO-SiO₂-Al₂O₃, CaO-SiO₂-Al₂O₃, and K₂O-SiO₂-Al₂O₃ phase diagrams. The development of the Base-SiO₂-Al₂O₃ phase diagrams for the prediction of ash behavior appears to be a fruitful area for future research. An example of such a phase diagram is shown in Figure 1 where ash-softening temperatures (ST, reducing) are plotted in what is effectively the "mullite" region of a Base-SiO₂-Al₂O₃ phase diagram. The curves of equal ST exhibit great similarity to the liquidus curves in true ternary diagrams.

The arrow in Figure 1 illustrates the use of the phase diagram to predict STs. In this instance, a bituminous coal with a low ST was blended with two other coals to yield a product with a much higher ST. The blend was chosen with the aim of moving the composition of ash in a direction approximately normal to the equal ST curves. The predicted and observed STs of the original coal and the blend are shown in the inset of Figure 1. The predicted values are probably not as accurate as could be obtained with existing empirical formulae,⁶⁾ but they are nevertheless quite reasonable.

Ternary and more complex phase diagrams can also contribute to interpretation of the reactions that lead to ash melting. In a reducing environment

(60%CO-40%CO₂), the important reactions for Eastern coals occur primarily within the FeO-SiO₂-Al₂O₃ phase diagram.^{13,14} Using a variety of techniques [Mossbauer spectroscopy, computer-controlled scanning electron microscopy (CCSEM), X-ray diffraction (XRD)] to investigate quenched ash samples heat treated under conditions similar to the ASTM ash-fusion test, it was established that most Eastern coal ashes exhibit behavior similar to that shown in the schematic diagram of Figure 2. Here, phases that are molten at elevated temperatures appear as glass phases in the quenched specimens. The potassium-containing clay mineral, illite, appears to be the first phase converted to a partially molten form; presumably this is because of the numerous low-temperature eutectic points in the K₂O-SiO₂-Al₂O₃ phase diagram. At approximately 900°C, wustite, derived from pyrite and other iron-rich minerals, begins to react with quartz and aluminosilicates derived from clay minerals to produce a mixture of wustite, fayalite (Fe₂SiO₄), and ferrous-containing melt phase. At somewhat higher temperatures (~1050°C), fayalite has been largely incorporated into the melt phase, and ferrous iron may react with aluminosilicates to form hercynite (FeAl₂O₄). This reaction retards melting somewhat and its importance is related to the Al₂O₃ content of the ash. Essentially all of the iron is contained in the melt phase for samples quenched from above 1200°C, as shown in Figure 3. Above 1200°C, reducing, most Eastern ashes (%Base <30%) are a mixture of molten aluminosilicates, mullite, quartz, and minor constituents such as iron sulfide, which is also molten, but is immiscible with the viscous silicate melt.

Similar, but less extensive experiments¹³ have also been performed on ash samples quenched from high temperatures in air. Below approximately 1200°C, essentially all of the glass observed in the samples is derived from the potassium-bearing clay mineral illite. Melting accelerates above approximately 1300°C and approaches completion for most Eastern ashes at temperatures of the order of 1500°C. In an oxidizing environment, calcium appears to be a more effective flux than ferric iron.

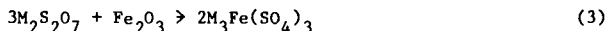
In both reducing and oxidizing atmospheres, significant partial melting of ash occurs at temperatures well below the initial deformation temperature (IDT). It is not uncommon to observe up to 50 percent of the ash in the form of glass at quenching temperatures as low as 200 to 400°C below the IDT. Such partial melting is important in deposit formation. Not surprisingly, the amount of glass observed at a given temperature in an oxidizing atmosphere is significantly less than that in a reducing atmosphere.^{13,14}

Fouling; Volatile Species

Fouling generally refers to the formation of deposits on convective heat-transfer surfaces at relatively low temperatures (600 to 1000°C). Excellent discussions of this problem have recently been given by Wibberly and Wall¹⁵ and in the general review article by Reid.¹⁶ Alkali elements (Na, K) are the principal culprits in the formation of such deposits. Within the flame, these elements become volatilized. The ease of volatilization is related to the form in which the alkalis are present in the coal. Organically bound alkalies would be expected to be easily volatilized at typical flame temperatures (1400-1500°C), as would NaCl, the most common form of sodium in bituminous coal. Potassium contained in illite would not be expected to volatilize as readily; illite should rapidly convert to a molten slag at these temperatures. For this reason, the water-soluble alkali content of coal is considered to be a more reliable indicator of fouling than the total alkali content, at least for Eastern coals. Wibberly and Wall list Na, NaOH, and NaCl as likely gaseous species, dependent on chlorine content of

the coal, flame temperature, and oxygen potential. Nonchloride species are probably rapidly converted to oxides (Na_2O , K_2O) on leaving the flame front. The volatile alkalis may condense on the surfaces of fly-ash particles carried by the flue gas or on cooler boiler surfaces. Wibberly and Wall¹⁵⁾ performed drop-tube experiments in which silica particles were exposed to synthetic combustion gases containing sodium at temperatures of 1200 to 1600°C. Sodium silicate layers ranging in thickness from 0.03 to 0.3 μm were observed on the particle surfaces, and sintered deposits formed rapidly on stainless steel probes inserted into the lower part of the furnace. Such alkali-silicate layers are molten at the temperatures of interest. The thickness of the sodium silicate layers was decreased by a factor of three when the sodium was introduced in the form of NaCl , rather than in chlorine-free forms.

An excellent review of the role of alkali sulfates is given by Reid.¹⁰⁾ Below 1100°C, alkali oxides and chlorides react rapidly with SO_2 and O_2 or SO_3 to form condensed sulfates on fly-ash particles and metal surfaces. Because of their low melting points, alkali sulfates are very corrosive, and form strongly bonded deposits. The melting points of the most easily formed sulfates, Na_2SO_4 and K_2SO_4 , are 882°C and 1075°C, respectively, and the minimum melting point of Na_2SO_4 - K_2SO_4 mixtures is 833°C. K_2SO_4 - CaSO_4 and Na_2SO_4 - CaSO_4 are also commonly observed mixtures, which exhibit melting points in the range from 870 to 970°C. If the SO_3 content of the atmosphere is sufficiently high, the pyrosulfates, $\text{K}_2\text{S}_2\text{O}_7$ and $\text{Na}_2\text{S}_2\text{O}_7$, may be formed from K_2SO_4 and Na_2SO_4 . These phases melt at very low temperatures: 400°C for $\text{Na}_2\text{S}_2\text{O}_7$ and 300°C for $\text{K}_2\text{S}_2\text{O}_7$. Crossley¹⁶⁾ has suggested that rapid metal wastage is caused by the reaction of the pyrosulfates with Fe_2O_3 to form low-melting point (<600°C) alkali-iron trisulfates:



where $\text{M} = \text{Na}$ or K . This point of view is supported by the work of Coats et al.¹⁷⁾ which established that liquid melts containing up to 90 percent pyrosulfate can be formed from Na_2SO_4 - K_2SO_4 mixtures in SO_3 pressures of 100 to 300 ppm at temperatures down to 335°C. Such SO_3 levels¹⁶⁾ can be readily reached via catalytic oxidation of SO_2 in the presence of Fe_2O_3 .

CCSEM analyses of fouling deposits from a boiler furnace in which a North Dakota lignite had been fired are given in Table III. Although the deposits consisted principally of calcium-enriched aluminosilicates, they also contained small but significant amounts of alkali sulfates, intermixed with calcium sulfate. Recently, we conducted potassium K-edge X-ray absorption spectroscopy (XAS) measurements on one of these samples at the Stanford Synchrotron Radiation Laboratory. The X-ray absorption near-edge structure, or XANES, shown in Figure 4, is nearly identical to that of a $\text{K}_2\text{S}_2\text{O}_7$ standard sample. It appears that XAS will be a very useful method of investigating the structure of individual elements in complex deposits.

Reactions and Transformations of Interest for Other Coal Conversion Processes

In this section, examples of the high-temperature behavior of inorganic phases in other conversion processes will be given.

Liquefaction - Montano et al.¹⁸⁾ have investigated the transformation of pyrite to pyrrhotite in coal liquefaction environments. They conducted in situ Mossbauer

spectroscopy measurements on coals maintained at 1.24 MPa nitrogen pressure and observed changes in the isomer shift at approximately 300°C that signalled the beginning of the transformation of pyrite to pyrrhotite. The transformation accelerated between 300 and 400°C, and from 20 to 80 percent of the pyrite in four different coals was transformed after one hour at 440°C. From close examination of both the in situ spectra and the spectra of cooled residues, they concluded that the pyrrhotite underwent covalent bonding to the coal molecules, causing a catalytic effect on coal liquefaction.

Carbonization - When coal is heated to temperatures ~900 to 1200°C in the absence of air, most of the volatile matter is driven off, leaving a char, or, in the case of metallurgical bituminous coal, a coke. The atmosphere in a coke oven consists principally of hydrogen and methane. Consequently, pyrite is reduced to a mixture of iron sulfide (troilite and pyrrhotite) and iron metal.¹⁹ The amount of iron metal formed depends on both the temperature and the composition of the coke-oven gas. The reduction of iron sulfide to iron metal is desirable since blast furnace operation is more efficient with low sulfur coke. Calcite reacts with the liberated sulfur to form calcium sulfate, thus retaining sulfur in the coke. In Figure 5, the calcium XANES spectrum of a coke produced from a Pittsburgh seam coal in which all calcium was initially present as calcite is shown. The spectrum establishes that approximately 70 percent of the calcite was converted to calcium sulfate during coking.

Gasification

Iron exhibits a great diversity of reactions at elevated temperatures when the reaction environment encompasses both reducing and oxidizing conditions at different stages of the process. For example, it is not unusual to observe five or six different iron-bearing compounds in three different oxidation states in char and ash samples obtained from coal-gasification systems. In Figure 6, the Mossbauer spectrum of a char residue from a bench-scale gasification system at the Institute of Gas Technology is shown. The input atmosphere to the gasifier was approximately 5.2% O₂, 21.2% H₂O, and the remainder N₂, and the average temperature was 1800°F. As indicated in Figure 6, six iron-bearing phases exhibiting three different oxidation states are observed: iron metal, iron sulfide (principally FeS), fayalite (Fe₂SiO₄), magnetite (Fe₃O₄), hematite (Fe₂O₃), glass, wustite, and possibly other minor phases.²⁰ A more detailed discussion of this work has been given by Mason et al.

Conclusions

Even from this brief overview, it is clear that much remains to be done in the area of understanding mineral-matter behavior in coal combustion and other conversion technologies and even more in combating the sticky problems arising from this component in coal. In particular, we feel there is a great need for much more detailed investigations of full-scale technological processes, especially now that a number of relatively new and sophisticated techniques are available that can be used to characterize mineral-matter related phenomena in ways that were not possible a few years ago. Such techniques include Mossbauer and EXAFS spectroscopies, which we have highlighted in this article, that have the ability to focus on specific critical elements (Fe, K, S, etc.), and reveal very detailed information about the behavior of that element. However, the observed phenomena in full-scale processes will also need to be interpreted in terms of both kinetic¹¹ (e.g., drop-tube experiments¹³) and thermodynamic (e.g., phase diagram analysis¹¹) approaches, as

well as to take into account the form of the mineral matter and its distribution in the original coal. These areas, we feel, should be important areas for research on mineral-matter related problems in the immediate future.

Acknowledgements

We are grateful to Ken Ho of the Babcock and Wilcox Company and Dave Mason of the Institute of Gas Technology for providing several of the samples discussed in this paper. We would also like to acknowledge the Stanford Synchrotron Radiation Laboratory for providing beam-time for the XAS experiments and our collaborators in those experiments, F. W. Lytle and R. B. Greegor of The Boeing Company.

References

1. Coal Fouling and Slagging Parameters, E. C. Winegartner, Ed., ASME Special Publication, 1974.
2. G. P. Huffman and F. E. Huggins, "Analysis of the Inorganic Constituents in Low-Rank Coals," to be published in Chemistry of Low-Rank Coal, H. H. Schobert, Ed., ACS Advances in Chemistry Series.
3. F. E. Huggins, G. P. Huffman, F. W. Lytle, and R. B. Greegor, Proceedings of the International Conference on Coal Science, International Energy Agency, NY, 1983, 679-682.
4. G. P. Huffman and F. E. Huggins, Fuel, 1978, 57, 592-604.
5. 1976 Annual Book of ASTM Standards, Pt. 26, American Society for Testing and Materials, Philadelphia, PA, 263-268.
6. E. C. Winegartner and B. T. Rhodes, Trans. ASME, J. Eng. for Power, (Series A) 1975, 97, 395-406.
7. E. C. Winegartner and A. A. Ubbens, Trans. AIME 1976, 260, 67-70.
8. J. D. Watt and F. Fereday, J. Inst. Fuel 1969, 42, 99-103.
9. J. D. Watt, J. Inst. Fuel 1969, 42, 131-134.
10. W. T. Reid, "Coal Ash--Its Effect on Combustion Systems," Chap. 21, 1389-1446 in Chemistry of Coal Utilization, M. A. Elliott, Ed., J. Wiley, NY, 1981.
11. F. E. Huggins, D. A. Kosmack, and G. P. Huffman, Fuel 1981, 60, 577-584.
12. E. M. Levin, H. F. McMurdie, and H. P. Hall, Phase Diagrams for Ceramists, Amer. Ceramic Soc., Inc., Columbus, Ohio, 1964.
13. G. P. Huffman, F. E. Huggins, and G. R. Dunmyre, Fuel 1981, 60, 585-597.
14. G. P. Huffman and F. E. Huggins, Fouling and Slagging Resulting from Impurities in Combustion Gases, R. W. Bryers, Ed., pp. 259-280, Engineering Foundation, New York, NY, 1983.

15. L. J. Wibberly and T. F. Wall, Fouling and Slagging Resulting from Impurities in Combustion Gases, R. W. Bryers, Ed., pp. 493-513, Engineering Foundation, New York, NY, 1983.
16. H. E. Crossley, J. Inst. of Fuel 1967, 40, 342-347.
17. A. W. Coats, D. J. A. Dear, and D. Penfold, J. Inst. of Fuel 1968, 41, 129-132.
18. A. S. Bommannavar and P. A. Montano, Fuel, 1982, 61 523-528.
19. G. P. Huffman and F. E. Huggins, Chapter 12, 265-301 in Mossbauer Spectroscopy and Its Chemical Applications, J. G. Stevens and G. K. Shenoy, Eds., ACS Adv. in Chem. Series 194, 1981.
20. Coal Gasification Research Studies, Proj. 61063, Quart. Report for Aug. 1983 through Nov. 1983, DOE/MC/19301-5.

Table 1
Inorganic Constituents of Eastern Coals

Mineral Distribution			Typical Ash Chemistry	
Mineral	Range	Typical	Species	Weight %
Quartz	5-44	18	SiO ₂	54
Kaolinite	9-60	32	Al ₂ O ₃	29
Illite	2-29	14	Fe ₂ O ₃	8
Chlorite	0-15	2	CaO	2
Mixed Silicates	5-31	17	MgO	1
Pyrite	1-27	8	K ₂ O	2
Calcite	0-14	3	Na ₂ O	1
Siderite/Ankerite	0-11	2	TiO ₂	1
Other Minerals	0-12	4	P ₂ O ₅	0.2
			SO ₃	2

Table II
Inorganic Constituents of Western Coals

Mineral Distribution			Typical Ash Chemistry	
Mineral	Range	Typical	Species	Weight %
Quartz	7-22	15	SiO ₂	30
Kaolinite	13-45	30	Al ₂ O ₃	15
Illite	0-12	2	Fe ₂ O ₃	10
Mixed Silicates	0-22	8	CaO	20
Pyrite	1-26	7	MgO	8
Fe Sulfates	0-5	1	K ₂ O	0.7
Fe-rich*	0-14	2	NaO	0.6
Ca-rich**	7-49	25	TiO ₂	0.7
Other minerals***	1-10	7	P ₂ O ₅	0.4
			SO ₃	15

*Principally iron oxyhydroxide.

**Principally calcium bonded to carboxyl groups in the macerals.

***Barite, apatite, montmorillonite, and others.

Table III

CCSEM Analyses of Fouling Deposits

<u>CCSEM Category</u>	<u>Sec. Superheater, 990-1050°C</u>	<u>Preheater 750°C</u>
Ca-rich aluminosilicate*	55	63
Ca- and Fe-rich aluminosilicate**	7	6
Alkali sulfate***	2	2
Calcium sulfate + alkali sulfate	4	6
SiO ₂	3	2
Ca-rich	10	6
Hematite	2	1
Ca-Fe ferrite	2	1
Ca-Mg sulfate	3	2
Al-Si rich	5	2
Unidentified, mixed phases	7	5

*Approximate average composition (mole %) determined from CCSEM energy dispersive X-ray fluorescence spectra was 37% Ca, 8% Mg, 4% Fe, 41% Si, 10% Al.

**Average composition - 31% Ca, 7% Mg, 21% Fe, 32% Si, 9% Al.

***Average composition - Na₃₃Ca₁₆K₃S₄₈.

U. S. STEEL CORPORATION, TECHNICAL CENTER, MONROEVILLE, PA

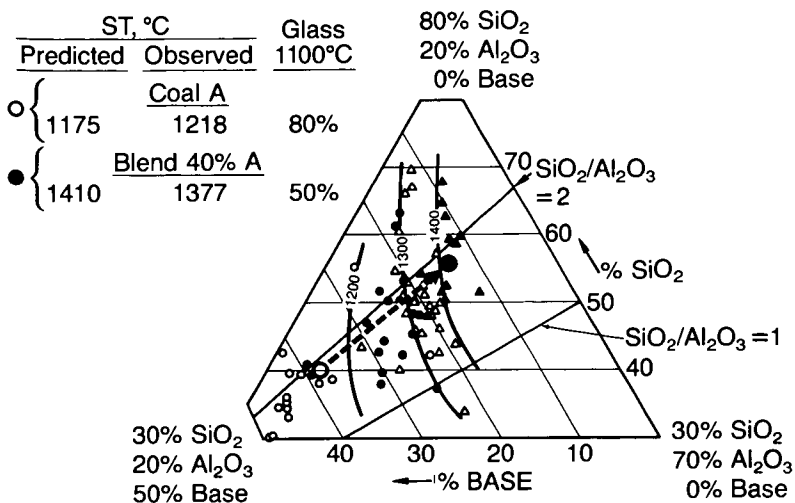


Figure 1 Pseudoternary phase diagram (Base - Al_2O_3 - SiO_2) showing spherul temperature (ST) contours. See text for discussion of points connected by arrow.

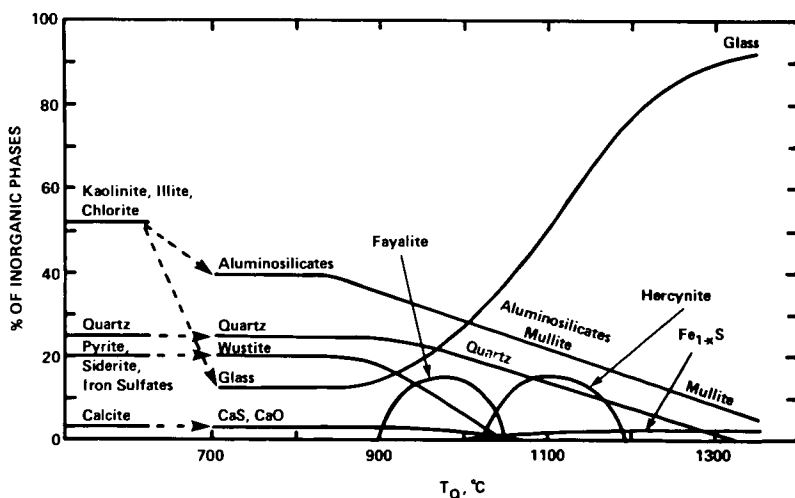


Figure 2 Schematic diagram illustrating high-temperature reactions for minerals in an Eastern-type coal under reducing conditions.

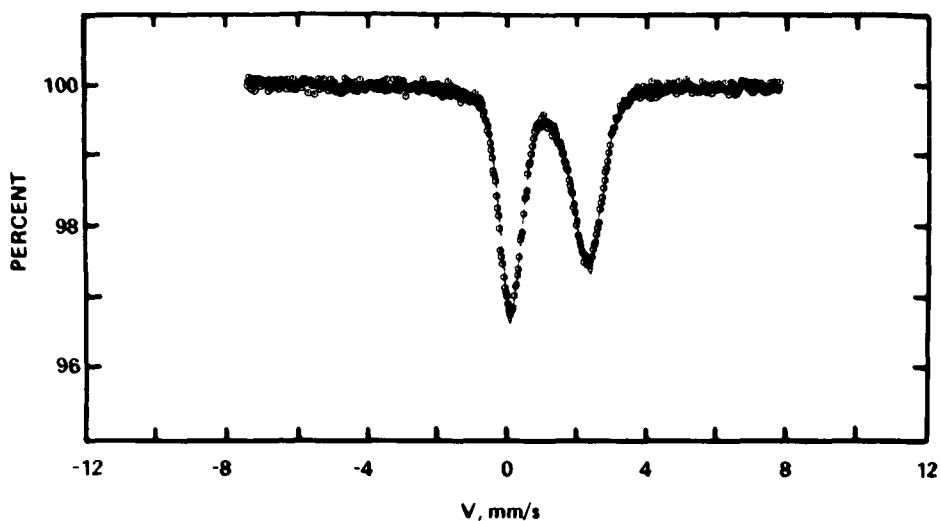


Figure 3 Mössbauer spectrum of Somerset C ash quenched from 1260°C under reducing conditions. Absorption derives entirely from Fe^{2+} in glass.

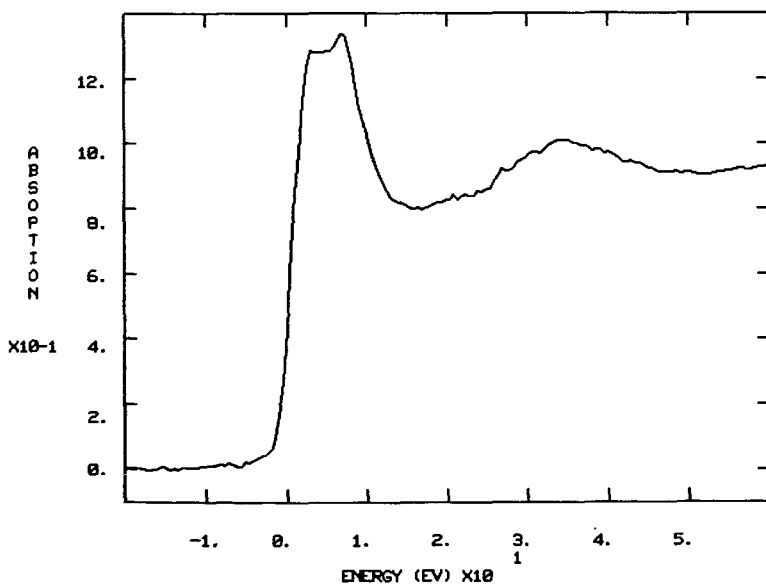


Figure 4 XANES for potassium (K edge) in the fouling deposit resulting from lignite combustion.

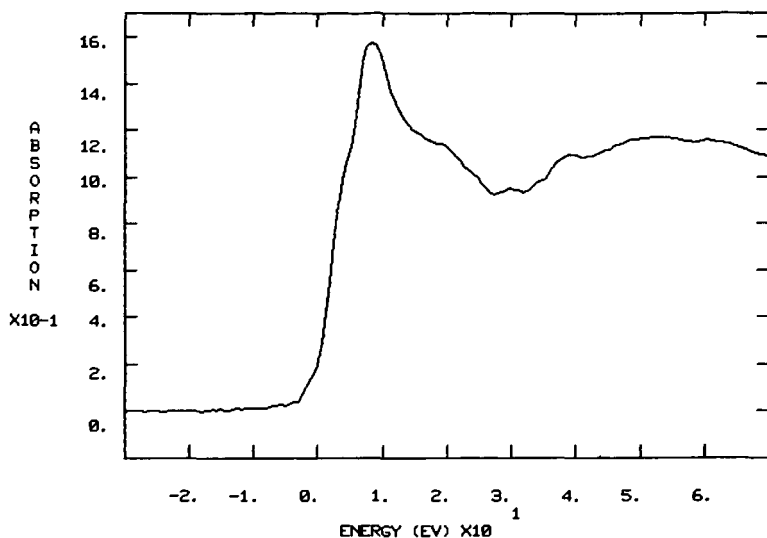


Figure 5 XANES for calcium (K edge) in coke made from high-sulfur coal from Pittsburgh seam.

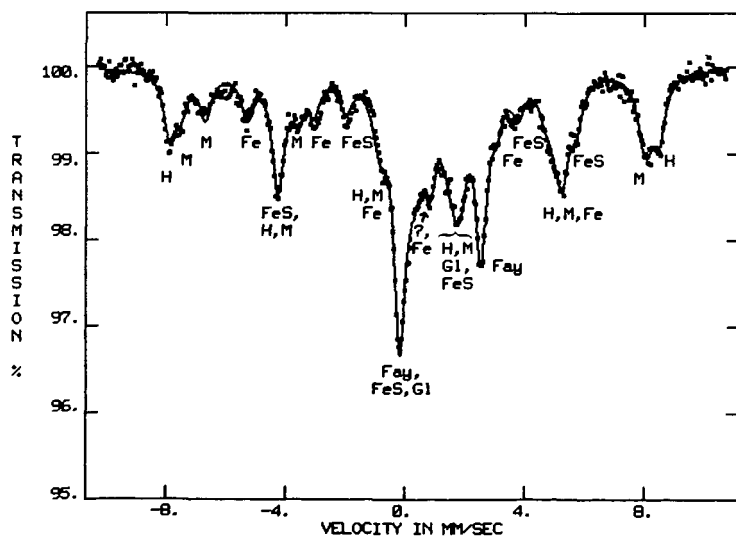


Figure 6 ⁵⁷Fe Mössbauer spectra of gasification char residue showing peaks from hematite (H), magnetite (M), iron metal (Fe), iron sulfides (FeS), fayalite (Fay), glass ± wustite (Gl), and an unknown phase (?).

Microstructural Changes in Coal During Low-temperature Ashing*

R. W. Carling, R. M. Allen

Sandia National Laboratories
Livermore, CA 94550

and

J. B. VanderSande

Massachusetts Institute of Technology
Cambridge, MA 02139

Introduction

In the present work, the microstructural changes occurring in two U. S. coals during low temperature ashing (LTA) have been examined using a scanning transmission electron microscope (STEM) and automated image analysis in an electron microprobe. The latter, a computer based technique, can be used to provide a quantitative analysis, by species, of the mineral particles $>0.2 \mu\text{m}$ in diameter in petrographic samples of powdered coal. A full description of the operation of automated image analysis routines for coal science application may be found elsewhere(1-5). The STEM, by comparison, with its high spatial resolution for imaging and compositional analysis, can be used to examine ultra-fine mineral particles (diameters $<0.2 \mu\text{m}$) in coal(6-9), and also to directly determine the principal inorganic elements chemically bound in the organic coal matrix(9). These two techniques therefore can be used together in a complementary manner to provide a detailed characterization of the mineral matter in coal samples(9). For the present task, their ability to work directly on either raw coal or ash samples was also a great advantage.

In support of the electron optical analysis of LTA transformations, complex thermochemical calculations have also been made. These calculations serve two purposes. The first is to provide a more fundamental thermodynamic understanding of mineral matter behavior under LTA conditions. Secondly, the calculations assist the electron microscopist in identifying species by predicting the possible products of observed reactants. This serves as guide when it becomes necessary to distinguish various species by electron diffraction, rather than energy-dispersive X-ray spectrometry (as when dealing with the many oxides, sulfides, and sulfates of iron). The limitation on this computational technique is that chemical equilibrium is assumed but may not be reached over the duration of a typical LTA experiment.

*This work supported by U.S. Department of Energy, DOE, under contract DE-AC04-76DP00789.

Experimental

The coals used in the present experiments were PSOC 98, a high-volatile-C bituminous coal from Wyoming (Bed #80 seam), and PSOC 279, a high-volatile-B bituminous coal from Indiana (Indiana #3 seam) obtained from the Penn State Coal Bank. The low temperature asher used in the present work was an LTA-504 from LFE Corporation. During ashing, small specimens were removed from a sample of each coal after 1, 3, 6, 12, 24, 48, and 72 hours of ashing. These partially-ashed samples were used for subsequent STEM analyses.

Thermochemical Modeling

The complex equilibrium code used in this work was an extension of the code originally developed by Erickson(10-12) and later modified by Bessman(13). The code, SOLGASMIX-PV, has been interfaced with a data base that is a compilation of thermodynamic data from JANAF(14) and the U.S. Geological Survey(15).

The elements included in the equilibrium calculations were: H, C, O, Mg, Al, Si, S, Ca, and Fe. The numbers of moles of each element (based on the analyses of each coal) were entered as oxides. An excess of oxygen was included to simulate the oxygen-rich environment of the LTA. The equilibrium temperature was set at 150°C with a pressure of one atmosphere. The list of species investigated for equilibrium stability is too long to present here, but included all of the combinations of the above elements given in the JANAF data base as well as many carbonates, sulfates, alumino-silicates, and sodium-aluminum silicates tabulated by the U.S. Geological Survey.

Results

PSOC 98

Low temperature ashing produced radical structural changes in PSOC 98 which resulted in individual ash particles having a gauzy appearance in the STEM. Stereomicroscopic examination revealed that the "gauze" was a fine three-dimensional network with denser particles suspended within the ash matrix. STEM microanalysis showed these dense particles to be the same sort of mineral inclusions observed in the raw coal. Electron diffraction patterns taken of the ash showed crisp rings characteristic of crystalline material. Analysis of the ash matrix in the STEM revealed Ca and S, as in the raw coal matrix. With this additional compositional information, the diffraction patterns were indexed and the presence of the mineral bassanite, $\text{CaSO}_4 \cdot 1/2\text{H}_2\text{O}$, was established. The grain size of the bassanite networks forming the matrices of the ash particles was on the order of 30 nm, as determined from standard dark field images formed from portions of the bassanite ring pattern.

Subsequent X-ray diffraction analysis of the material ashed for 72 hours showed bassanite to be one of the three principal minerals found after LTA (together with quartz and kaolinite).

PSOC 279

The raw particles of PSOC 279 were similar in appearance to those of PSOC 98. The most commonly observed type of ash particle, however, consisted of an agglomeration of mineral particles, principally quartz, clays, and pyrite. These were the predominant mineral species found in the raw coal by the electron microprobe analysis. These were also the three major species found by X-ray diffraction in the material ashed for 72 hours.

"Gauzy" ash particles, very similar in appearance to those in the PSOC 98 ash, were less common than the agglomerate type but were also found in the STEM samples. The characteristic inorganic signature of the organic matrix of raw PSOC 279 particles was a combination of an Al and a Si signal. Again, the same combination was carried over into the matrices of the gauzy type or ash for this coal.

STEM examination of the low temperature ash of PSOC 279 showed that much of the pyrite in the starting coal survived the full 72 hours of ashing. This was confirmed by the X-ray diffraction analysis of the ash, as mentioned earlier. STEM analysis was also done on particles of small (<80 nm diameter) crystals. These particles were Fe and S rich, but with much lower S:Fe ratios than pyrite. A significant portion of these particles had a cubic morphology. No minerals of this type were observed during STEM examination of the raw Indiana coal.

Modeling Results

Figure 1 illustrates the stable condensed phases predicted by the equilibrium calculations for low temperature ashing conditions. The results shown are for PSOC 98 but apply as well for PSOC 279 except for the relative amounts of each specie.

Discussion

Bassanite formation is commonly observed during low temperature ashing, particularly for western coals. It is believed to form by three means: dehydration of gypsum ($\text{CaSO}_4 \cdot 2\text{H}_2\text{O}$) found in the raw coal (16,17), reaction of organic S and the mineral calcite (CaCO_3) (18), and direct reaction of organic Ca and S (19,20). These reactions have proven to be hard to distinguish, because of the difficulty of analyzing the starting mineral content of raw coal samples by conventional techniques, and the inability of these same techniques to find and examine partially-ashed

particles to observe the reaction in progress. The use of the electron-optical analysis techniques described in this paper, however, overcame both of these problems, as will now be described.

The STEM results for PSOC 98 indicate that the organic matrix of the raw coal contained Ca and S in a non-crystalline form. This is consistent with the Penn State sulfur-forms analysis which indicates that most of the S in the coal is in an organic form. It also explains the relatively small percentages of Ca-bearing minerals found by the electron microprobe, since other information indicates that PSOC 98 contains a relatively large amount of calcium.

Apparently, the organic matrix of the coal itself was the origin of the Ca and S needed for bassanite formation. The fact that calcium sulphate would form under these conditions was confirmed by the results of the thermochemical calculations (see Fig. 1) which indicated that sufficient sulfur was present in the coal to react with the calcium and prevent the formation of other species, such as calcium carbonate (calcite).

The details of this LTA reaction process were brought to light by the STEM examination of the partially-ashed samples. In general, these samples were simply made up of mixtures of raw coal and fully-ashed particles in varying proportions, based on the amount of ashing time they had seen. However, it was still possible to find individual particles which themselves were only partially ashed.

In such a particle it appears that the fine bassanite network forms continuously as the organic material is burned away and the Ca and S are freed from the matrix. Mineral inclusions originally present in the raw coal particle often remain entrapped within this network as it forms. The bassanite network created thus determines the structure of the low temperature ash of PSOC 98.

It is interesting to speculate on the possible origin of the "gauze" developed by this reaction. It is well known that for coals from the western U.S., organic Ca is readily ion-exchangeable(21). This indicates that the Ca has ready access to the pore structure of the coal. If, during LTA, the Ca in the raw coal reacts in place with the organic S and the oxygen plasma, it could be that the bassanite gauze produced has a network structure related to the pore structure of the raw coal. The 30 nm size of the bassanite crystallites is also comparable to the diameters of a significant portion of the pores likely to be found in coal(22). It may therefore be possible to obtain heretofore unobtainable topographical information of the pore structure of pulverized coal particles by careful LTA experiments. This information would be of great use for modeling the combustion of such particles in commercial boilers. Further work is under way to investigate this possibility.

Although most of the ash produced from PSOC 279 consisted of particles

which appeared to be agglomerates of the mineral inclusions found in the raw coal, some "gauzy" particles were also generated during ashing. In analogy to the results from PSOC 98 just described, this suggests that the gauze was produced from inorganic elements chemically bound in the organic matrix of the starting coal. Unlike the Wyoming coal, however, the coal from Indiana had a matrix that contained primarily Al and Si. This combination of elements has been found by STEM analysis in the matrix of another midwestern coal as well(9). The STEM analysis of the gauzy ash particles for PSOC 279 also showed principally Al and Si. It appears that for this coal, the Al and Si from the organic matrix could react during ashing to produce new crystalline mineral matter. This transformation during LTA has not been previously reported.

The thermochemical modeling of the system indicated that Al and Si should preferentially react together with the oxygen of the LTA plasma to form one or more alumino-silicate compounds, as opposed to the separate formation of alumina and silica. This could not be directly confirmed by electron diffraction in the STEM, for several reasons. First, the mineral inclusion content of the gauzy particles was much higher for this coal than for PSOC 98. In addition, the microprobe results show that nearly 30 percent of these inclusions were alumino-silicates of various types. Selected area diffraction patterns of portions of gauzy particles therefore tended to be quite complex, and not readily amenable to interpretation. An attempt was made to use microdiffraction on the small regions of the network matrix which appeared to be relatively inclusion-free. However, the material was quickly destroyed by the high beam currents involved. The most that can be said from the present work is that STEM microanalysis supports the prediction of the thermochemical model by confirming the combined presence of Al and Si in the matrix of the gauzy ash particles from PSOC 279.

The thermochemical modeling also predicts another LTA transformation for PSOC 279. The modeling results indicate that pyrite is not a stable phase under the low temperature ashing conditions, and is expected to transform to an $\text{Fe}_2(\text{SO}_4)_3$ -type compound. Sulfur is expected to leave the system as SO_3 vapor.

A variety of LTA transformations involving Fe- and S-bearing compounds have been reported previously. Pyrite has been reported as either remaining unchanged(16,25), reacting to form coquimbite and other Fe^{3+} sulfates(17,24,25), or oxidizing to hematite(19). It is generally accepted that rozenite and other Fe^{2+} sulfates oxidize to Fe^{3+} sulfates during LTA(17,23-25). Indeed, in the most recent of these papers it was shown by Mossbauer spectroscopy that, for the LTA conditions used, all of the Fe^{3+} sulfate produced during LTA originated from the Fe^{2+} sulfate in the starting coal, while the pyrite remained unaffected(23).

The STEM results of the present work indicate that a significant amount of pyrite did appear to react during LTA. The pyrite that survived the LTA retains its dense appearance under STEM examination, along with its cubic morphology and high sulfur to iron ratio. By comparison, the

decomposition product has a highly porous structure, a much lower S:Fe ratio, and, in many (but not all) instances, has apparently lost its overall cubic shape. It was difficult to obtain electron diffraction patterns from these latter particles because of their unstable nature under the electron beam. In the few instances where a diffraction pattern was successfully recorded, the best fit for indexing the pattern appeared to be the Fe³⁺ sulfates, coquimbite and para-butlerite. The large proportion of these low S:Fe ratio particles (relative to surviving pyrite particles) observed in the ashed PSOC 279 rules out the possibility of their formation being completely the result of the oxidation of the starting iron sulfates in this coal. Only a very small fraction of the starting mineral matter in the coal was present in the form of Fe²⁺ sulfate.

For the LTA conditions used in the present work, pyrite in the starting coal did partially decompose. This appeared to occur on a particle-by-particle basis; no intermediate reaction products were observed. The rather sporadic nature of the decomposition of pyrite during LTA has been shown previously in tests where pyrites from different sources were subjected to LTA(19). The reason for this behavior is still not known.

One additional prediction of the thermochemical modeling requires comment. SiO₂ is not thermodynamically stable under LTA conditions, but instead should be reacting with other compounds to form aluminosilicates. However, silica particles were still easily identifiable as a species surviving LTA. There are at least two possible explanations for this. The first is that silica was generally found in relatively large particles, and so was not able to mix intimately with other compounds. Secondly, the kinetics of many reactions may be too slow for them to take place in the time frame of a LTA experiment. As was pointed out earlier, the thermodynamic models assume that equilibrium is reached.

References

1. Walker, P. L., Jr., Spackman, W., Given, P. H., White, E. W., Davis, A., and Jenkins, R. G., "Characterization of Mineral Matter in Coals and Coal Liquefaction Residues", 1st Annual Report to EPRI, Project RP-366-1 (Palo Alto, CA, 1975).
2. Walker, P. L., Jr., Spackman, W., Given, P. H., White, E. W., Davis, A., and Jenkins, R. G., "Characterization of Mineral Matter in Coals and Coal Liquefaction Residues", EPRI AF-417, Project RP-366-1 (Palo Alto, CA, 1977).
3. Lee, R. J., Huggins, F. E., and Huffman, G. P., in Scanning Electron Microscopy/1978/1 (Ed. O. Johari), Scanning Electron Microscopy, Inc. (AMF O'Hare, IL, 1978) p. 561.

4. Huggins, F. E., Kosmack, D. A., Huffman, G. P., and Lee, R. J., in Scanning Electron Microscopy/1980/1 (Ed. O. Johari), Scanning Electron Microscopy, Inc. (AMF O'Hare, IL, 1980) P. 531.
5. Huggins, F. E., Huffman, G. P., and Lee, R. J., in Coal and Coal Products: Analytical Characterization Techniques (Ed. E. L. Fuller, Jr.), ACS Symposium Series, No. 205, ACS (New York, 1977) p. 239.
6. Harris, L. A., Braski, D. N., and Yust, C. S., in Microstructural Science, Vol. 5 (Ed. J. D. Braun, H. W. Arrowsmith, and J. L. McCall), Elsevier North-Holland, Inc. (New York, 1977) p. 351.
7. Hsieh, K. C. and Wert, C. A., Mat. Sci. Eng., 50, 117 (1981).
8. Heinemann, H. in Proceedings of the International Conference on Coal Science, Dusseldorf, 7-9 Sept. 1981, Verlag Gluckauf (Essen, 1981) p. 567.
9. Allen, R. M. and VanderSande, J. B., Fuel, 63, 24 (1984).
10. Erickson, G., Acta Chem. Scand., 25, 2651 (1971).
11. Erickson, G. and Rosen, E., Chemica Scripta, 4, 193 (1973).
12. Erickson, G., Chemica Scripta, 8, 100 (1975).
13. Bessman, T. M., "SOLGASMIX-PV, a Computer Program to Calculate Equilibrium Relationships in Complex Chemical Systems", ORNL/TM-5775, Oak Ridge National Laboratory (1977).
14. JANAF Thermochemical Tables, 2nd edition, Ed. D. R. Stull and H. Prophet, U. S. Dept. of Commerce, National Bureau of Standards Publication NSRDS-NBS 37 (1971).
15. Robie, R. A., Hemingway, B. S., Schafer, C. M., and Haas, J. L., Jr., "Heat Capacity Equations for Minerals at High Temperatures", U.S. Geological Survey Rep. 78-934, U.S. Dept. of the Interior (1978).
16. Gluskoter, H., Fuel, 44, 285 (1965).
17. Mitchell, R. S. and Gluskoter, H. J., Fuel, 55, 90 (1976).
18. Painter, P. C., Coleman, M. M., Jenkins, R. G., Whang, P. W., and Walker, P. L., Jr., Fuel, 57, 337 (1978).
19. Miller, R. N., Yarzab, R. F., and Given, P. H., Fuel, 58, 4 (1979).
20. Morgan, M. E., Jenkins, R. G., and Walker, P. R., Jr., Fuel, 60, 189 (1981).
21. Durie, R. A., Fuel, 40, 407 (1961).

22. Gan, H., Nandi, S. P., and Walker, P. L., Jr., Fuel, 51, 272 (1972).
23. Guilianelli, J. L. and Williamson, D. L., Fuel, 61, 1267 (1982).
24. Montano, P. A., Fuel, 56, 397 (1977).
25. Huggins, F. E. and Huffman, G. P., in Analytical Methods for Coal and Coal Products, Vol. III, (Ed. C. Karr, Jr.), Academic Press (New York, 1979) p. 371.

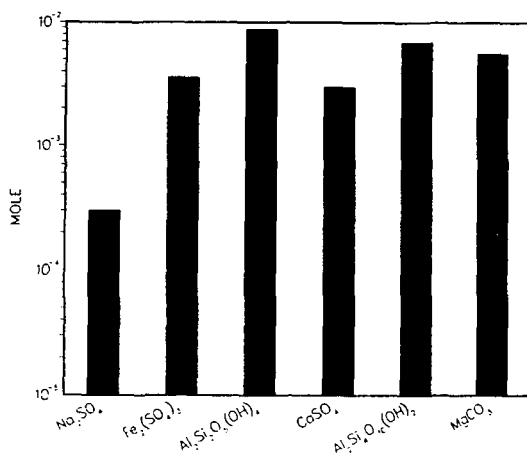


Figure 1 - Thermodynamically stable condensed phase species as predicted by the equilibrium thermochemical modeling. The plot shows the number of moles of each stable species that would be produced after equilibrium was reached under LTA conditions. The starting material was 100 g of PSOC 98.

MINERAL TRANSFORMATIONS DURING ASHING AND SLAGGING OF SELECTED LOW-RANK COALS

S.K. Falcone, H.H. Schobert, D.K. Rindt, and S. Braun

University of North Dakota Energy Research Center
Box 8213, University Station
Grand Forks, North Dakota 58202

Introduction

Inorganic species are incorporated in low-rank coals in many ways: as ion-exchangeable cations, as coordination complexes, and as a diverse array of discrete minerals. In some cases an element will be present in more than one form; potassium, for example, occurs both as an exchangeable cation and in association with clay minerals. The variation in association of inorganics among the multiple modes of occurrence results in a very complex series of reactions and mineral transformations when low-rank coals are ashed or slagged. The behavior or the inorganic components can be at least as important to effective operation as the behavior of the carbonaceous portion in low-rank coal utilization processes. The determination of the extent of the changes in bulk composition and in mineral phases during controlled laboratory ashing is very important in developing an understanding of ash or slag behavior during coal processing and how such changes are related to process conditions.

In the past, mineralogical determinations using ash formed at the standard temperature of 750°C identified minerals which were not originally present in the raw coal but which were artifacts of the ashing procedure. This was due to the alteration of minerals by oxidation, dehydration and other processes at high temperatures. Recent studies by Miller et al (1), Frazer and Belcher (2), and O'Gorman and Walker (3) have concentrated on relating raw coal mineralogy to ash mineralogy generated at low temperatures. Low-temperature ashing (LTA) theoretically would enable one to obtain the true mineralogical composition of a coal since little mineral alteration occurs up to 125°C. Mitchell and Gluskoter (4) expanded this concept to study low to high temperature mineral transformations in ash of subbituminous and bituminous coals. With few exceptions the application of LTA in ash mineralogy studies has been primarily associated with subbituminous and bituminous coals (5). In fact, Miller et al (1) and Frazer and Belcher (2) state that LTA may be unsuitable for obtaining the original mineralogy in lignites without appropriate pretreatment. This is due to the high organic oxygen content with associated inorganic exchangeable cations characteristic of lignites. The presence of organically-bonded inorganics drastically increases the ashing time thereby increasing the chances of mineral alteration by oxidation. In addition, the release of organically-bound cations and organic sulfur in contact with mineral matter can alter the original coal mineralogy with an extended period of low-temperature ashing.

The purpose of this study is to identify mineral transformations in low to high temperature ashes (125°, 750°, and 1000°C) and slags (1300°C) characteristic of lignites. The processes responsible for certain mineral transformation are also examined.

Twelve low-rank coals were selected from the northern Great Plains and Gulf Coast. Nine North Dakota lignites, two Gulf Coast (Texas and Alabama) lignites, and one subbituminous coal from Montana were studied (Table I).

Experimental

The mineral matter composition of each coal sample was determined directly by X-ray diffraction (XRD) of low temperature ash (LTA). A LFE Model 504 four-chamber oxygen

Table I. Location and Inorganic Analyses (XRF) of Coals Studied. All Coals are Lignites Except for Absaloka Subbituminous

Coal Name	Locality	Major and Minor Elements (Percent)									
		Si	Al	Fe	Mg*	Ca	Na*	S	K	Ti	Ba*
+ Absaloka	Big Horn Co., Montana	< 3.5	1.61	2.58	0.08	0.37	0.33	3.92	0.12	0.06	0.03
Beulah Low Sodium	Mercer Co., North Dakota	0.90	0.54	1.02	1.18	1.57	0.14	2.01	0.09	0.05	0.02
Beulah High Sodium	Mercer Co., North Dakota	0.35	0.29	0.52	0.67	1.81	0.46	0.75	ND	0.06	0.04
Center	Oliver Co., North Dakota	0.66	0.44	0.89	0.94	1.70	0.40	0.65	0.08	0.32	0.04
Choctaw	Choctaw, Alabama	1.06	0.49	1.87	0.56	0.84	0.09	2.50	0.10	0.04	ND
Falkirk	McLean Co., North Dakota	0.86	0.50	0.48	0.91	2.60	0.01	0.55	0.15	0.04	0.02
Gascoyne Blue	Bowman Co., North Dakota	1.09	0.73	0.25	0.38	2.28	0.27	0.93	0.14	0.05	0.13
Gascoyne Red	Bowman Co., North Dakota	2.86	0.87	0.39	0.59	1.74	0.13	1.12	0.13	0.12	0.06
Indian Head	Mercer Co., North Dakota	0.71	0.49	0.68	0.97	1.56	0.62	0.44	0.12	0.04	0.05
Pike	Pike County, Alabama	1.11	0.66	0.36	0.11	1.77	NA	2.28	0.10	0.65	NA
San Miguel	Atascosa Co., Texas	3.58	1.06	0.47	ND	1.20	0.60	1.88	0.35	0.08	NA
Velva	McHenry Co., North Dakota	0.56	0.33	0.26	0.11	0.98	0.09	NA	0.05	0.02	0.03

*Concentrations measured by neutron activation analyses (NAA).

+Absaloka coal analysis completely by NAA.

NA (Not Available) ND (Not Detected)

plasma low temperature asher was used. The ashing procedures used were modified after Miller and Givens' (6) technique for low temperature ashing of subbituminous and bituminous coals. One set of samples was ion-exchanged in 1N ammonium acetate at 70°C for 24 hours and freeze-dried prior to low temperature ashing. This procedure was repeated three times to ensure removal of ion-exchangeable cations. Another, but untreated, sample set was also ashed. Preliminary comparison of sample sets showed the exchanged samples to have reduced ashing time and identical mineralogy except for the presence of bassanite in non-exchanged samples. This difference will be discussed later.

Modifications in operating procedures are as follows: an RF Power of approximately 150W and an oxygen flow of 100cc/min at 2 psi were maintained along with a chamber pressure of 1mm Hg. Samples were stirred once every 2 hours during the first eight hours and every eight hours during the remaining ashing time.

Samples were also ashed at 750°C in accordance with ASTM procedure D3174-73 and will be referred to as ASTM samples (7). Samples were then ashed at 1000°C following the same procedure for 750°C coal ashing and will be referred to as HTA (high temperature ash) samples. Finally raw coal samples were heated to 1300°C forming slag. All slag samples were air quenched.

Mineralogical composition of ash samples was analyzed by XRD. X-ray fluorescence (XRF) analysis was also used for bulk ash analysis. Raw coal analysis was performed by XRF and neutron activation (NAA). XRF elemental analyses of raw coal samples are listed in Table I.

Results and Discussion

Mineralogical phases formed at different temperatures for each coal sample are summarized in Table II. The major mineral phases detected by XRD in LTA samples are quartz, pyrite, bassanite, kaolinite and plagioclase. The processes responsible for mineral transformations include oxidation, vaporization, sulfur fixation, dehydration, solid-state interactions, and recrystallization. The temperatures at which specific transformations occur are based on previous experimental work by Mitchell and Gluskoter (4) and published chemical data in the Handbook of Chemistry and Physics (8). In addition to mineral-mineral interactions it is believed that reactions between minerals and exchangeable cations occur (9).

Pyrite (FeS_2) is present in all LTA samples. While Miller et al (1) stated that pyrite may be oxidized with increased low temperature ashing time in lignites no evidence of oxidized forms of iron was seen by XRD. This may be attributed to the pretreatment of samples with ammonium acetate, thereby reducing ashing times as much as 50%. In ASTM samples pyrite is oxidized to hematite (Fe_2O_3) and magnetite (Fe_3O_4). According to Miller and Gluskoter (4), pyrite oxidizes at 500°C. With the oxidation of pyrite to iron oxide rather than iron sulfate, pyritic sulfur is released. The formation of sodium and calcium sulfates, detected in ASTM ash, may be associated with the release of pyritic sulfur. The source of such sulfates may be the interaction of pyritic sulfur released during pyrite oxidation with carbonates as well as with organically-bound calcium and sodium.

Bassanite ($\text{CaSO}_4 \cdot 0.5\text{H}_2\text{O}$) is present in some of the sample LTAs. Bassanite most likely forms from the dehydration of gypsum ($\text{CaSO}_4 \cdot 2\text{H}_2\text{O}$) at 65°C. Gypsum was detected by scanning electron microscopy (SEM) in raw coal samples. Another source of calcium or sodium sulfate may be the fixation of organic sulfur by organically-bound calcium or sodium cations (9, 10). In this case, bassanite is simply an artifact of the low temperature ashing procedure. This phenomenon is typical of coals having abundant alkali cations associated with carboxyl groups. Continued increases in ashing temperature results in complete dehydration of bassanite to anhydrite (CaSO_4) at 400°C. Anhydrite is a major mineral phase in ASTM and HTA samples and is present in most slags.

Kaolinite ($\text{Al}_2\text{Si}_2\text{O}_5(\text{OH})_4$) is present in only LTA samples. Kaolinite dehydration occurs approximately from 400° to 525°C (4). With removal of water by dehydration, the kaolinite structure collapses, retaining some degree of order forming

Table II. Mineralogical Composition of Ash and Slag Samples Determined by XRD*

Sample	LTA (~125°C)	ASTM (750°C)	HTA (1000°C)	Slag(1300°C)
Absaloka	Quartz Pyrite Kaolinite Plagioclase Bassanite	Quartz Anhydrite Hematite	Anhydrite Magnetite Hematite Quartz Melilite Plagioclase Nepheline	Plagioclase Hematite Magnetite Quartz
Beulah-Low Sodium	Quartz Pyrite Kaolinite Bassanite	Quartz Hematite Magnetite Anhydrite	Anhydrite Pyroxene Magnetite Hauyne Hematite Quartz	Anhydrite Pyroxene Magnetite
Beulah-High Sodium	Quartz Bassanite Kaolinite Pyrite	Anhydrite Hematite Magnetite Quartz Melilite Hauyne	Anhydrite Melilite Magnetite Hematite Hauyne Quartz Corundum	Melilite Hauyne Nepheline Magnetite Quartz Corundum
Center	Quartz Bassanite Pyrite Kaolinite	Anhydrite Hematite Quartz	Anhydrite Hauyne Pyroxene Melilite Hematite Quartz	
Choctaw	Quartz Pyrite Kaolinite Bassanite Plagioclase	Anhydrite Quartz Hematite Magnetite Plagioclase Pyroxene	Anhydrite Hematite Quartz Magnetite Plagioclase	
Falkirk	Quartz Kaolinite Pyrite	Anhydrite Quartz Hematite Magnetite Melilite (trace)	Anhydrite Quartz Melilite Hematite Magnetite Hauyne	Melilite (Akermanite) Anhydrite Pyroxene Hematite
Gascoyne Blue- High Sodium	Quartz Kaolinite Pyrite Calcite Sodium Sulfate (trace)	Anhydrite Quartz Hematite Magnetite Nosean Melilite	Anhydrite Melilite Hauyne Quartz	Anhydrite Pyroxene Spinel Melilite Magnetite

Table II. Mineralogical Composition of Ash and Slag Samples Determined by XRD*--
Continued

Sample	LTA (~125°C)	ASTM (750°C)	HTA (1000°C)	Slag(1300°C)
Gascoyne Red- Low Sodium	Quartz Kaolinite Pyrite	Quartz Anhydrite Hematite Magnetite	Quartz Anhydrite Pyroxene Hematite Hauyne	(Amorphous)
Indian Head- High Sodium	Quartz Pyrite Kaolinite Bassanite	Anhydrite Quartz Hematite Nosean Melilite Hauyne Sodium Sulfate (?)	Melilite Hematite Anhydrite Hauyne Magnetite Pyroxene	
Pike	Quartz Pyrite Kaolinite	Anhydrite Quartz Pyrite	Anhydrite Hematite Melilite Anorthite Quartz	
San Miguel	Zeolite (Heulandite) Quartz Kaolinite Pyrite Bassanite Plagioclase	Zeolite Anhydrite Hematite Quartz Plagioclase (Anorthite) Melilite	Plagioclase (Anorthite) Hematite Quartz Magnetite Anhydrite	(Amorphous)

*Minerals listed in decreasing order of peak intensities and occurrence.

metakaolin. No metakaolin was detected by XRD in ASTM samples perhaps due to its poorly defined crystalline structure. However, it is believed that the basic kaolinite components are present in an amorphous form in ASTM ash. With increasing temperature the collapsed kaolinite structure forms corundum ($\gamma\text{-Al}_2\text{O}_3$). While mullite ($3\text{Al}_2\text{O}_3 \cdot 2\text{SiO}_2$) and cristobalite (SiO_2) have been reported to form from well-ordered kaolinites in bituminous coals at 1000°C (4) neither were observed in HTA samples. According to Grim (11), the absence of mullite suggests that the original kaolinitic structure was poorly defined. It has also been suggested by Grim (11) that the presence of impurities in the form of alkali ions, such as in lignites, retards the development of mullites and cristobalite. The mechanism for this is not fully understood.

The collapsed kaolinitic structure acts as a source or framework for several different aluminosilicate complexes formed in HTA and slag samples. Common minerals found are as follows: anorthite ($\text{CaAl}_2\text{Si}_2\text{O}_8$), pyroxenes ($(\text{Ca},\text{Na})(\text{Mg},\text{Fe},\text{Al})(\text{Si},\text{Al})_2\text{O}_6$), melilites ($(\text{Na},\text{Ca})_2(\text{Mg},\text{Fe},\text{Al})(\text{Si},\text{Al})_2\text{O}_7$), hauyne ($(\text{Na},\text{Ca})_{4-8}(\text{AlSiO}_4)(\text{SO}_4)_{1-2}$), nosean ($\text{Na}_8\text{Al}_6\text{Si}_6\text{O}_{24}\text{SO}_4$) and nepheline ($(\text{Na},\text{K})\text{AlSiO}_4$). At 1000°C aluminosilicates minerals form from solid-state reactions of kaolinitic material with cations derived from carbonates, oxides, or sulfates. Interstitial substitution of alkali cations occurs within the dehydrated kaolinite structure with increasing temperature due to thermal expansion. In some coals, particularly those high in sodium, these aluminosilicates are also seen in ASTM samples.

At 1300°C inorganics are in a liquid phase. Upon quenching some sample slags remain amorphous due to rapid cooling thereby inhibiting nucleation of elements preventing the formation of crystalline structures. Other samples recrystallized upon cooling forming previously existing and new aluminosilicate structures. Differences between sample slagging behavior can be traced to silica content of the raw coal. Samples high in silica, such as Gascoyne Red and San Miguel coals, formed amorphous slags upon cooling. Samples having relatively low silica contents such as Absaloka, Beulah High and Low Sodium, Falkirk and Gascoyne Blue coals, formed crystalline slags when cooled. Anhydrite and magnetite are still present at 1300°C .

Minor amounts of calcite (CaCO_3) were detected in raw coal samples by SEM. XRD failed to detect calcite in LTA samples possibly due to extraction by ammonium acetate or because the amounts of calcite were below detection limits ($\sim 5\%$). For the most part, calcium is supplied to the system by gypsum and organically-bound calcium. As previously discussed, calcium whether in the form of bassanite, calcite, or cations in LTA samples forms anhydrite in ASTM samples. In HTA samples calcium reacts primarily with dehydrated kaolinite forming aluminosilicates discussed under kaolinite reactions.

Quartz (SiO_2) is stable throughout the ash samples at varying temperatures up to 1000°C . In slag analysis, quartz is not always present in crystalline form but forms an amorphous substance along with other compounds.

With increasing temperature quartz peak intensities in HTA samples decrease or disappear while various aluminosilicate peaks increase in intensity and number. According to Rindt et al (12) localized reducing areas are present within coal particles during combustion. In these areas, reactions between volatilized sodium and quartz occur forming sodium silicates (13). The sodium is fixed and not readily released on further heating.

Figure 1 displays a typical X-ray diffractogram sequence from LTA sample through slagging of the Beulah High Sodium lignite. Predominant peaks are identified according to the mineral phases present. Mineral transformations at higher temperatures are characterized by the presence of numerous aluminosilicate solid-solution series. Often several members of a particular solid-solution series have almost identical diffractogram patterns making identification by XRD difficult. When comparing several of these diffractograms there is little difference between LTA samples while ASTM, HTA, and slag samples are quite different. When comparing mineralogical differences to raw coal elemental compositions of various coals samples containing higher amounts of sodium tend to form aluminosilicates at lower temperatures (750°C) than samples high in calcium. High sodium coals such as Beulah

High Sodium and Gascoyne Blue develop complex silicates in ASTM samples and are known to be high fouling coals. Typical of such aluminosilicates in ASTM, HTA and slag samples are melilites, hauyne, nepheline, nosean and pyroxenes. Commonly these are minerals found in combustion fouling deposits of most lignites.

Concluding Remarks

The results of this study reflect the preliminary stage of investigation into the mineral phase transformations seen in low-rank coals. The original mineralogies of coals sampled do not vary a great deal. Quartz, kaolinite, pyrite, and bassanite are found in abundance in each LTA sample. Greater differences between samples are apparent at higher temperatures where complex aluminosilicates predominate. Perhaps this is a reflection of differences not so much in original mineral matter but in the total inorganic composition of the coal, specifically the presence of exchangeable alkali cations. The interactions of such organically-bound cations with crystalline inorganic phases in lignites account for differences in ashing and slagging behavior between coal samples (9).

The processes responsible for most reactions identified are oxidation, dehydration, sulfur fixation, solid-state interactions, vaporization, and recrystallization. Isolating specific reactions occurring in a multi-component system is difficult at best. Understanding the thermodynamics of mineral transformations is a necessity and will be pursued in future study. In addition, future studies isolating mineral pairs to observe phase transformations at various temperatures will support or refute results presented here.

Literature Cited

1. Miller, R.N.; Yarab, R.F.; and Given, Peter. Fuel 1979, 58, 4.
2. Frazer, F.W.; and Belcher, C.B. Fuel 1973, 52, 41.
3. O'Gorman, J.V.; and Walker, P.L. Fuel 1973, 52, 71.
4. Mitchell, R.S.; and Gluskoter, H.J. Fuel 1976, 55, 90.
5. Gluskoter, J.J. Fuel 1965, 44, 285.
6. Miller, R.N.; and Given, Peter. 'A Geochemical Study of the Inorganic Constituents in Some Low-Rank Coals' Technical Report, Pennsylvania State University to the U.S. Department of Energy, Rep. FE-2494-TR-1, 1978.
7. Annual Book of American Society of Testing Materials Standards 1979, Part 26: Gaseous Fuels; Coal and Coke; Atmospheric Analysis.
8. Handbook of Chemistry and Physics 54th edition, Chemical Rubber Company, 1973.
9. Morgan, M.E.; Jenkins, R.G.; and Walker, P.L. Jr. Fuel 1981, 60, 189.
10. Painter, P.C.; Coleman, M.M.; Jenkins, R.G.; and Walker, P.L. Jr. Fuel 1978, 57, 125.
11. Grim, R.E. Clay Mineralogy, McGraw-Hill, New York, 1968, Chapter 9.
12. Rindt, D.K.; Selle, S.J.; and Beckering, W. 1979 American Society of Mechanical Engineers, Corrosion and Deposits Division, Reprint 79-WA/CS-5.
13. Boow, J. Fuel 1972, 51, 170.

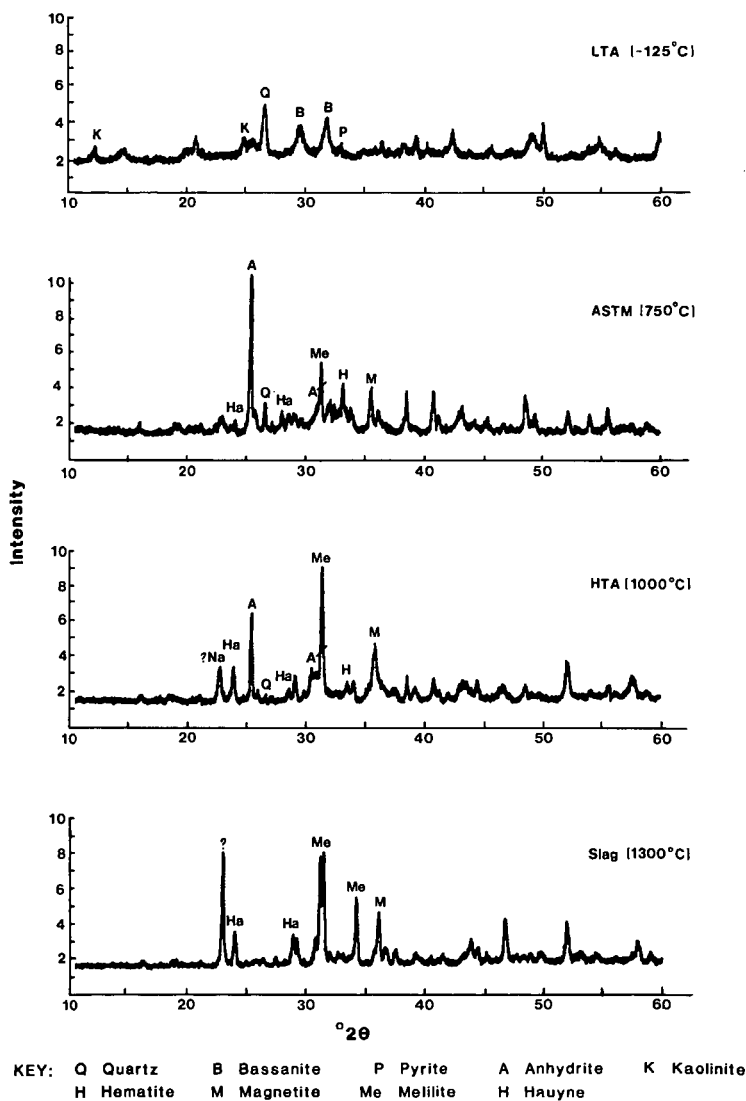


Figure 1. X-ray diffractograms of LTA, ASTM, HTA, and slag samples of Beulah high sodium coal.

HIGH TEMPERATURE INTERACTIONS AMONG MINERALS OCCURRING IN COAL

BY
DONALD L. BIGGS AND CURTIS G. LINDSAY

AMES LABORATORY*, IOWA STATE MINING AND MINERAL
RESOURCES RESEARCH INSTITUTE, AND
THE DEPARTMENT OF EARTH SCIENCES,
IOWA STATE UNIVERSITY
AMES, IOWA 50011

INTRODUCTION

Mineral impurities in coal are known to be primary contributors to the slagging and fouling of utility boilers, fly ash and bottom ash production as well as atmospheric pollution. They also produce undesirable effects in some parts of hydrogenation processes such as liquifaction and gasification (1,2,3). Despite a long history of investigation prompted by these observations, many questions remain unanswered.

Simple empirical relationships between fusion temperature of the furnace deposits and the mineralogy of coals have been proposed (4,5,6). More recently attempts have concentrated on a physico-chemical view of the problem comparing ash fusion temperatures with phase relations in three-component chemical systems (7,8). This method of attack has yielded some significant results, but at least some researchers (8) have questioned the assumption that these processes occur under conditions of equilibrium.

The aim of the research described here is to observe interactions between minerals known to occur in coals in the most direct fashion possible and in the simplest conditions consistent with causing the reactions to occur. It is considered that observation of simple mixtures of minerals observed to enter into reaction may make possible a better accounting of the processes by which slag and fouling deposits form in furnaces.

EXPERIMENTAL METHODS

ISOLATION AND IDENTIFICATION OF COAL MINERALS. Two coal samples collected from different coal basins in the United States (see Table I), were subjected to low-temperature ashing as described by Gluskoter (9). This process avoids destruction of the minerals while oxidizing the organic portion of the coal. This ashing procedure occurs at a much lower temperature than that of the American Society for Testing and Materials (ASTM) method it is given the name of "low-temperature ash" and generally abbreviated, LTA. In formation of a mineral concentrate by low-temperature ashing (LTA) a few changes are anticipated; some clays are reversibly dehydrated, hydrated sulfates are reduced to the hemihydrate form, for instance gypsum is converted to bassanite. Because these changes are known in advance, due allowance can be made for them.

*Operated for the U. S. Dept. of Energy by Iowa State Univ. under contract No. W-7405 Eng-82.

TABLE I

Coal Samples, Localities of Origin, and Analyses
(all samples run-of-mine)

Seam: Illinois #6

Locality: St. Clair County, Illinois

Analysis:

	9 mesh x 0 Raw	9 x 32 mesh Float	9 x 32 mesh Sink
Moisture (%):	5.31	5.44	2.55
Ash, ASTM (%):	32.86	7.10	68.05
Pyritic Sulfur (%):	2.46	0.76	5.08
Total Sulfur (%):	4.57	4.57	5.94
Heating Value (BTU/lb.):	9,039	13,248	3,574

Seam: Upper Freeport

Locality: Grant County, West Virginia

Analysis:

	9 mesh x 0 Raw	9 x 32 mesh Float	9 x 32 mesh Sink
Moisture (%):	0.30	0.68	0.93
Ash, ASTM (%):	35.90	7.26	72.10
Pyritic Sulfur (%):	1.58	0.27	2.62
Total Sulfur (%):	2.18	1.06	3.00
Heating Value (BTU/lb.):	9,695	13,365	3,086

Mineral constituents of the LTA concentrates were identified by x-ray diffraction techniques. Illite, kaolinite, quartz and pyrite are ubiquitous in the mineral suites; calcite occurs in most concentrates. Many other minerals have been identified in coals, but were not observed in these specimens.

HEATING-STAGE MICROSCOPIC OBSERVATIONS. Following the characterization of the mineral suites by x-ray diffraction techniques, each LTA concentrate was heated in a heating stage mounted on a microscope fitted for observation in vertically incident light. Concentrates examined in this way and the product phases are found in Table II.

TABLE II

LTA Samples and Heating Products

<u>LTA Sample</u>	<u>T_{max} (°C)</u>	<u>Phases Identified</u>
Upper Freeport raw	560	quartz, illite, pyrrhotite
	1410	quartz, mullite ^a
Upper Freeport 1.40 float	1031	quartz ^b
	1250	quartz ^b
Upper Freeport 1.40 sink	635	quartz, illite, pyrrhotite
	1150	quartz, pyrrhotite, illite ^c
Illinois #6 raw	880 ^d	quartz, illite, pyrr- hotite, oldhamite(?)
Illinois #6 1.40 float	625	quartz, illite, pyrr- hotite, troilite (?)
	1370	quartz, pyrrhotite
Illinois #6 1.40 sink	920	quartz, illite, pyrr- hotite, oldhamite
	1334	quartz, pyrrhotite, oldhamite

NOTES:

^aXRD peaks occurred at the correct diffraction angles for mulite, but were too weak to permit accurate intensity comparisons.

^bThe overall pattern was similar to the one for the illite-kaolinite pair heated to 1410°C, except that stronger peaks for quartz were found in the LTA XRD pattern.

^cPeaks were detected at some of the diffraction angles for illite, but the intensities were not comparable with standard patterns; it is possible that these were relict peaks of illite as it began to alter.

^dAnother sample of Illinois #6 raw LTA was heated to 1421°C; it formed a hard, dark-coloured glass at about 1400°C, and this material could not be removed from the heating-stage crucible.

The heating stage is limited to inert atmosphere or vacuum operation. Therefore, reactions sensitive to atmospheric conditions, such as partial pressure of oxygen cannot be studied. Furthermore, the extremely small particle size of the sample resulted in inability to observe changes occurring below the mount surface, and to resolve the specific minerals entering into a reaction at any point in the run.

These difficulties were met by obtaining samples of the minerals identified in the LTA concentrate before heating, grinding them to approximately the same size consist as the concentrate, and mounting them in separate domains in the heating stage crucible. The geometry of these mounts is shown in Fig. 1.

EXPERIMENTS WITH KNOWN MINERALS

EXPERIMENTS WITH INDIVIDUAL MINERALS. Single mineral mounts in the heating-stage crucible yielded the expected products, that is, pyrite yielded pyrrhotite and troilite, calcite gave lime and carbon dioxide, and clays reacted under high temperature conditions to yield a silicate glass.

EXPERIMENTS WITH PAIRS AND TRIPLETS OF KNOWN MINERALS. In these experiments, known minerals were ground and placed in the heating-stage crucible in separate domains as pairs or triplets of minerals. The pairs and triplets were heated and the behavior at their boundaries observed. Table III lists the minerals used in pair mounts and the reaction products obtained by heating.

TABLE III

Mineral Pairs and Heating Products

Mineral Pair	t_{\max} ($^{\circ}\text{C}$)	Products Identified ^a
calcite-illite	1310	lime (CaO)
calcite-kaolinite	1322	lime (CaO)
calcite-montmorillonite	1285	(indeterminate) ^b
calcite-pyrite	1253	lime, pyrrhotite (Fe_{1-x}S), oldhamite (CaS)
calcite-quartz	1467	quartz (SiO_2), lime (CaO)
illite-kaolinite	1410	mullite ($\text{Al}_6\text{Si}_2\text{O}_{13}$)
illite-montmorillonite	662	(indeterminate) ^b
illite-montmorillonite	1212	(indeterminate) ^b
illite-pyrite	1519	pyrrhotite, troilite (FeS)
illite-quartz	1450	quartz
kaolinite-montmorillonite	1403	mullite (poorly-crystalline) ^c
kaolinite-pyrite	1445	mullite
kaolinite-quartz	1220	quartz
montmorillonite-pyrite	1053	(indeterminate)
montmorillonite-quartz	1492	quartz
pyrite-quartz	1571	quartz

Notes:

^a Only those products are listed which could be positively identified by XRD; no attempt is made here to deduce the composition of amorphous products.

^b XRD patterns for these heating products did not match any standard pattern closely; attempts to match with computer routines produced results of low reliability.

^c "Poorly crystalline" means that diffraction maxima were found corresponding to the indicated phase, but peaks were not sharp and did not have the correct relative intensities in all cases.

Because the most reactive phases found in the experiments with pairs of minerals were clays, calcite, and pyrite, these were prepared in triplet mounts. In trials using either montmorillonite or illite with calcite and pyrite, a liquid formed at the mutual boundary of the latter pair at 600 - 650°C. Pyrite and calcite had, of course, previously reacted and this liquid therefore occurred between the product phases pyrrhotite and lime. Subsequent x-ray analysis showed the presence of pyrrhotite, lime, and oldhamite. In both instances, the temperature of this reaction was lower than that obtained in the pair mount of calcite and pyrite, 1140°C. When kaolinite was in the mount with calcite and pyrite, the same reaction occurred at 750 - 760°C. Though the fluxing action of the clays is not presently understood, the differences in reaction temperature with and without clay is considered significant.

The most obvious reaction of the clays themselves during these experiments was a darkening beginning with pyrite decomposition. This was more marked in the case of illite and montmorillonite. It is considered that in all cases, the clay mineral present formed a silicate glass, much like those found in furnace slags, but having, perhaps, less oxygen.

SUPPORTING EXPERIMENTS. To examine the effect of oxidizing and reducing atmosphere on these materials, graphite crucibles 10mm in diameter and 5mm deep were packed in the same manner described above and heated in a furnace fitted to permit introduction of controlled gases during heating. After heating, the samples were examined by scanning electron microscopy and energy dispersive x-ray spectroscopy (SEM/EDS). Samples treated in this way are listed in Table IV.

TABLE IV
Subjects of Supporting Experiments

<u>Assemblage</u>	<u>Atmosphere</u>	<u>T (°C)</u>	<u>Duration (min)</u>
calcite-kaolinite	inert	1400	60
calcite-quartz	inert	1400	60
pyrite-quartz	oxidizing	1200	30
pyrite-quartz	reducing	1200	30
pyrite-calcite	reducing	1200	30
pyrite-kaolinite	oxidizing	1200	30
pyrite-kaolinite	reducing	1200	30
pyrite-montmorillonite	inert	800	15
pyrite-montmorillonite	reducing	800	15
py.-calc.-kao.	reducing	1200	30
py.-calc.-mont.	inert	800	15
py.-calc.-mont.	reducing	800	15

NOTE:

The indicated temperature was the steady-state temperature for the trial. The indicated duration was the period of time for which that steady-state temperature was maintained.

In all these cases where pyrite was used with a clay, iron was found to have migrated from the region that was originally iron sulfide into the clay. Elemental mapping showed the presence of iron to have completely pervaded the region formerly occupied by clay. In the calcite-pyrite pair mount, the iron was lost. EDS mapping showed the presence of abundant calcium and sulfur, but iron was present in small amount. In all mounts containing calcite and pyrite, the calcium and sulfur peaks were present in the region originally occupied by calcite, and sometimes found in the region that had been pyrite-filled.

SUMMARY AND CONCLUSIONS

It is apparent that the phenomena described here are not complete processes terminating in equilibrium assemblages. The times of reaction are too short for many of the products of silicates such as clays and quartz to come to thermodynamic equilibrium at the new temperature. That this is indeed the case in operation of power-plant boilers is obvious from the consideration of the amount of glass found in furnace slags and fly-ash.

Illite and montmorillonite are similar in structure and differ slightly from kaolinite in this regard. The first two are composed of two silicon-oxygen layers per octahedral layer containing iron, magnesium and aluminum and in kaolinite the ratio of tetrahedral and octahedral layers is 1. In these crystals, thermal modification is easier because the bonds formed between the Al, Fe, and Mg atoms and oxygen are weaker than the Si-O bonds. Clays, therefore are expected to be more reactive than the silica crystals. There is evidence that some glass is formed in the clay mineral domains during thermal treatment and that iron diffuses into the mass. Further inquiries are in progress to answer these questions.

Calcite appears largely inert until temperatures approaching 600°C in the presence of some of the clay minerals and inert until about 900°C in their absence. The cause of this fluxing is not well understood at this time, but investigations are planned to elucidate this behavior. At whatever temperature, the reaction observed is for the calcite to decompose to lime (CaO) and carbon dioxide. The extent to which carbon dioxide fluxes further reaction is not known, but must be considered as an important step in complete explanation.

Like calcite, pyrite is quite reactive and its thermal behavior is influenced by the presence of clay minerals. The initial reaction temperature of pyrite alone or in the presence of calcite alone is to produce pyrrhotite, (Fe_{1-x}S) and at the highest temperature, troilite (FeS). The loss of sulfur is obvious and continues over an appreciable temperature range. T

The most important reaction products are those of the iron enrichment of the clay minerals, probably a precursor of the iron oxide and glass mixtures commonly observed in slags and fly-ashes, and the formation of the sulfide of calcium, oldhamite. That oldhamite is observed in all experiments where calcite and pyrite interact, and that anhydrite is observed only where they have reacted in the presence of an oxygen-rich atmosphere supports the conclusion that oldhamite, formed in the reducing part of a flame, is a necessary precursor to the formation of the sulfate, anhydrite.

Acknowledgements

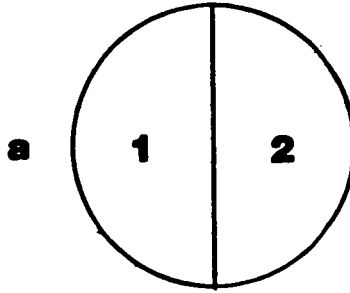
This material is based, in part, on work supported by the U.S. Bureau of Mines, Department of the Interior, under Grant No. G1106002. Any opinions, findings, and conclusions or recommendations expressed in this publication are those of the authors and do not necessarily reflect the views of the U.S. Bureau of Mines, Department of the Interior.

Work on other parts of this publication was performed in Ames Laboratory and was supported by the Assistant Secretary of Fossil Energy, Division of Coal Utilization through the Pittsburgh Energy Technology Center, Coal Preparation Branch.

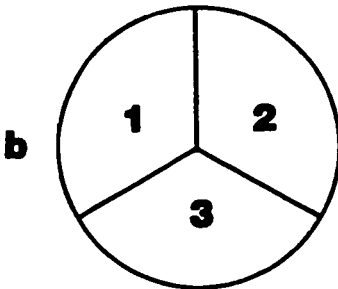
REFERENCES

- (1) Mukkherjee, D.K., and Chowdhury, B. : Fuel, 55, pp.4-8 (1976).
- (2) Wakely, L.D., Davis, A., Jenkins, R.G., Mitchell, G.D., and Walker, P.L.Jr. : Fuel, 58, pp.379-385 (1979).
- (3) Gray, D. : Fuel, 57, pp.213-216 (1978).
- (4) Moody, A.H., and Langhan, D.D. : Combustion, 6, pp.13-20 (1935)
- (5) Gauger, A.W. : Procedures of the American Society of Testing Materials 37, Part I, pp.376-401 (1937).
- (6) Palmenburg, O.W. : Industrial and Engineering Chemistry, 31, pp. 1058-1059. (1939).
- (7) Electric Power Research Institute (EPRI) Report CS-1418, Research Project 736; prepared by Battelle, Columbus Laboratories (1980).
- (8) Huggins, F.E., Kosmack, D.A., and Huffman, G.P. : Fuel, 60, pp. 577-584 (1981).
- (9) Gluskoter, H.J. : Fuel, 44, pp. 285-291 (1965)

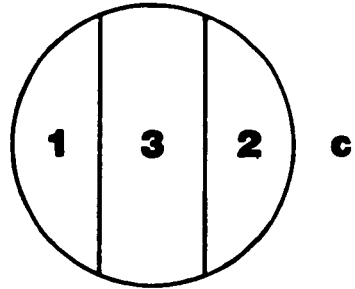
Pair Mounts



Triplet Mounts



Triple-Junction
Mount



Parallel-Boundary
Mount

Figure 1. Geometric arrangements of mineral pairs and triplets used in heating-stage microscopic experiments and in supporting experiments. Approximate diameters of actual mounts: for heating-stage experiments--5 mm; for supporting experiments--11 mm. In all triplet mounts, mineral "3" was a clay mineral.

FLAME VITRIFICATION AND SINTERING CHARACTERISTICS OF SILICATE ASH

ERICH RAASK

Technical Planning and Research Division of Central Electricity Generating Board,
Kelvin Avenue, Leatherhead, Surrey, UK

The silicate species constitute the bulk of the mineral matter in most coals, and the formation of boiler deposits depends largely on the physical and pyrochemical changes of the ash residue constituents. In this work the mode of occurrence of coal silicate minerals, and the flame induced vitrification and sodium initiated sintering mechanisms have been studied. The pulverized coal flame temperature is sufficiently high to vitrify the quartz particles. On cooling some devitrification occurs and the rate of sintering depends largely on the ratio of glassy phase to crystalline species in the ash. The flame volatile sodium captured by the vitrified silicate particles can initiate the coalescence of deposited ash by viscous flow and the rate of sintering is markedly increased by the alkali-metal dissolved in the glassy phase.

The flame imprinted characteristics of pulverized coal ash relevant to boiler slagging, corrosion and erosion have been discussed previously (1,2). The silicate minerals constitute between 60 and 90 per cent of ash in most coals and boiler deposits are largely made up from the silicious impurity constituents. This work sets out first to examine the mode of occurrence of the silicate mineral species in coal followed by a characterization assessment of the flame vitrified and sodium enriched silicate ash particles. The ash sintering studies are limited to investigations of the role of sodium in initiating and sustaining the bond forming reactions leading to the formation of boiler deposits.

SILICA (QUARTZ) AND SILICATE MINERAL SPECIES IN COAL

The quartz and aluminosilicate species found in most coals constitute the bulk of combustion ash residue. The aluminosilicates include muscovite and illite which contain potassium, and kaolinite species (3,4,5,6). The silica (SiO_2) and alumina (Al_2O_3) as determined by chemical analysis are present in aluminosilicates on an average weight ratio of 1.5 to 1 as reported by Dixon et al. (6). The excess of silica represents the amount of quartz in coal mineral matter:

$$(\text{SiO}_2)_q = (\text{SiO}_2)_t - 1.5(\text{Al}_2\text{O}_3) \quad 1)$$

Where $(\text{SiO}_2)_q$, $(\text{SiO}_2)_t$ and (Al_2O_3) denote respectively the quartz, total silica and alumina contents of ash.

An approximate amount of potassium aluminosilicates in coal mineral matter can be obtained from the potassium oxide (K_2O) content of ash. The amount of non-silicate potassium species is small in most coals and the silicate minerals contain on average 11 per cent K_2O by weight (6). Thus the potassium aluminosilicate content of coal mineral matter ($K_{\text{AL-SIL}}$) by weight per cent is:

$$K_{\text{AL-SIL}} = \frac{K_2\text{O}}{0.11} = 9.1 K_2\text{O} \quad 2)$$

where $K_2\text{O}$ denotes the potassium oxide content of ash.

The total amount of silicate minerals equals approximately the sum of SiO_2 , Al_2O_3 and K_2O in ash, and an estimate of kaolinite species is thus given by:

$$\text{Kaolinite} = (\text{SiO}_2 + \text{Al}_2\text{O}_3 + \text{K}_2\text{O}) - (\text{Quartz} + \text{Potassium Silicates})$$

3)

Table 1 gives the SiO_2 , Al_2O_3 and K_2O contents of some US and British bituminous coal ashes (4,7) which were used to calculate the approximate amounts of quartz, potassium aluminosilicate and kaolinite species in the mineral matter.

Table 1: Silicate Species in Mineral Matter of British and
US Bituminous Coals

Type of Coal		Ash Constituents, Weight Per Cent of Ash			Mineral Species, Weight Per Cent of the the Total		
		SiO_2	Al_2O_3	K_2O	Quartz	Pot. Alum. Silicates	Kaolinite
Low Silica	British	31.1	18.1	1.2	3.9	10.9	26.2
	US	29.2	14.2	1.5	7.9	13.6	23.6
Medium Silica	British	46.5	22.8	2.8	12.3	25.5	34.3
	US	46.6	27.8	1.1	4.9	10.0	60.6
High Silica	British	55.5	30.0	2.7	10.5	24.5	53.2
	US	56.5	32.2	2.6	8.0	23.6	59.7

Table 1 shows that the kaolinite species constitutes up to 60 per cent of the coal mineral matter. The amount of potassium aluminosilicates, chiefly muscovite and illite is between 10 and 25 per cent, and the quartz content is usually below 12 per cent. The aluminosilicate minerals contain frequently iron, calcium, magnesium and sodium as part replacement for potassium and partly incorporated in the kaolinite structure. Also, the silicate minerals occur as hydrated species with the inherent water content of between 2 to 5 per cent, thus the silicious mineral contents are likely to be about 5 per cent higher than those given in Table 1.

The silica and alumina contents of the first two samples are exceptionally low for bituminous coal ashes. The usual concentration range of silica is 35 to 55 per cent and that of alumina is 20 to 30 per cent thus the aluminosilicate species together with quartz constitute between 60 to 90 per cent of the bituminous coal mineral matter.

The silicate species occur in coal chiefly as separate strata and large particle inclusions, and this mode of occurrence is termed the "adventitious" mineral matter. Fig. 1a shows a typical sample of the adventitious silicate mineral particles, density separated from pulverized coal. The density separation technique does not remove the small silicate particles, chiefly aluminosilicate species dispersed in the coal substance (Fig. 1b). The average ash content of bituminous coals utilized in electricity generating power stations is usually between 12 and 20 per cent (4,8) and about one quarter, 3 to 5 per cent fraction is present as the inherent ash.

The mineral elements can be held in the coal substance as organo-metal salts, and also as a result of molecular adsorption and co-valent bonding. The mineral species dissolved in coal pore water, chiefly chlorides can also be considered as a part of the inherent mineral matter. The lignites and sub-bituminous coals can have a high fraction of the mineral elements, chiefly sodium, calcium and also aluminium and iron chemically combined in the fuel substance (9,10). The chemical reactivity and porosity of the fuel matrix decreases with the increase of coal age from lignite to bituminous rank. The loss of carboxyl, hydroxyl and quinone bonding sites in the fuel matrix results in a low "chemical" mineral matter content of bituminous coals.

CHLORIDE IN COAL PORE AND SEAM WATER

Chloride minerals are rarely found in coal in the form of solid species because of high solubility of sodium, calcium and trace metal chlorides in coal strata waters. The "inherent" water content of coal is related to its porosity and thus the moisture content of lignite deposits can exceed 40 per cent decreasing to below 5 per cent in fully matured bituminous coals (11). Chlorides, chiefly associated with sodium and calcium constitute the bulk of water-soluble matter in British bituminous coals (12) and Skipsay (13) has found that the distribution of chlorine coals was closely related to the salinity of mine waters. Hypersaline brines with concentrations of dissolved solids up to 200 kg m⁻³ occur in several of the British coalfields.

The mode of formation of hypersaline brines has been discussed by Dunham (14) concluding that the connate waters were of marine origin formed by the osmotic filtration through clay and shale deposits. The salinity of the brine ground waters increases with depth and when they are in contact with fuel bearing strata, correspondingly more chloride is taken up by the fuel. However, according to Skipsey (13) the high rank bituminous coals because of their low porosity are unable to take up large amounts of the chloride and associated cations, and the chlorine content rarely exceeds 0.2 per cent. The chlorine content of low rank bituminous coals can reach one per cent and correspondingly the sodium fraction associated with chlorine will amount up to 0.4 per cent of coal. That is, the ash from a high chlorine coal can contain up to 3 per cent of flame volatile sodium. The chlorine content of lignites and sub-bituminous coals is usually low, below 0.1 per cent, and sodium is held chiefly in the fuel substance in the form of organo-metal components (9,10).

All coals contain some sodium combined in the aluminosilicate species which will remain largely involatile in the flame. The ratio of the silicate sodium to non-silicate sodium varies over a wide range. The alkali-metal is present chiefly in the silicates in low chlorine bituminous coals, but in the high chlorine bituminous coals and in many lignites and sub-bituminous coals it is present mainly in a flame volatile form.

FLAME VITRIFICATION OF SILICA MINERALS

A characteristic feature of flame heated ash is that the particles are spherical in shape as shown in Fig. 2. The transformation of the angular silicate mineral particles in pulverized coal to spherical particle ash is a result of the surface tension force acting on the vitrified species. The stress (f) on a non-spherical surface section of the particle is:

$$f = 2\gamma/\rho \quad (4)$$

where γ is the surface tension of glassy silicate and ρ is the radius of curvature. It is evident from equation (4) that the stress is inversely proportional to the radius of curvature and thus the small sharp-edged particles are first to take a spherical form.

Frenkel (15) has shown that time (t) required to transform an angular particle to sphere is given to first approximation by:

$$r = r_0 e^{-t/z} \quad 5)$$

where

$$z = 4\pi\eta r_0/\gamma \quad 6)$$

and r is the distance of a point on the original surface from the center of a sphere of equivalent volume having radius r_0 , η is the viscosity and γ is the surface tension.

Equation 5 can be used to calculate the approximate time required for a particle to assume a spherical shape when the surface tension, viscosity, size and initial shape of particle are known. Alternatively, an estimate of the viscosity for the change to take place, can be made when the residence time of particles at a given temperature is known. Table 1 gives the calculated values of viscosity when the time for the change is one second. It was assumed that the thickness of moving surface layer was about ten per cent of the radius, and the surface tension of fused ash was taken to be 0.32 N m^{-1} as measured previously (16).

Table 2: Calculated Viscosities for Spheridization of Different Size

Silicate Particles					
Particle Radius, μm	0.01	0.1	1	10	100
Viscosity, N s m^{-2}	2.5×10^7	2.5×10^6	2.5×10^5	2.5×10^4	2.3×10^3

Table 2 shows that the small irregularly shaped particles transform to spheres in a coal flame when the viscosity of the material is several orders higher than that required for bulk flow under gravity, which is about 25 N s m^{-2} . A laboratory technique was used to determine the minimum temperature at which coal mineral species are transformed to spherical shapes (17). Particles of 10 to $200 \mu\text{m}$ in diameter were introduced into a gas stream and then passed through a vertical furnace. The temperature of the furnace was varied from 1175 to 2025 K and was measured by a radiation pyrometer and by thermocouples placed in the furnace. The residence time of particles in the furnace was between 0.2 and 0.5 sec. depending on the particle size.

Fig. 3a shows a surface-fused silicate particle heated to a temperature some 25 K lower than that required for its spheridization. Fig. 3b shows a spheridized particle heated in the laboratory furnace. Fig. 4 shows the temperature range at which the shape change of different coal mineral particles occurred. The chlorite mineral contain some quartz and the two species spheridized at markedly different temperatures as shown by curves D_1 and D_2 .

The temperature of mineral particles in the pulverized coal flame exceeds 1800 K (Fig. 5), and it is therefore to be expected that all particles with the exception of large size quartz will vitrify and change to spherical shapes. Fig. 6a shows a surface-fused but non-spherical quartz particle found in a sample of fly ash captured in the electrical precipitator. Occasionally ellipsoidal particles of aluminosilicates (Fig. 6b) can be found in the ash indicating that the high temperature residence time was slightly too short for complete spheridization. However, the majority of the ash particles appear to be spherical as shown in Fig. 2.

The spherical silicate ash particles, when viewed at close-up range appear to host a large number of sub-micron particles at the surface (Fig. 6c). The microvoids could be silicate crystalloids precipitated from the vitrified phase or sulphate fume particles formed from the non-silicate coal minerals (18). The latter are soluble in a dilute acid (HCl) solution and Fig. 6d shows the acid etched particles. Clearly, most of the microvoid particles were dissolved and the leach solution contained sodium and potassium sulphates.

Another diagnostic test for silicate ash is to treat the particles with hydrofluoric (HF) acid solution (18,19,20). The acid will dissolve the glassy phase revealing skeletons of crystalline species which may be in the form of mullite needles (Fig. 6e) or quartz crystalloids (Fig. 6f). The ratio of the glassy phase to crystalline species varies from particle to particle depending on the original composition of the silicate minerals, the capture of volatile sodium and the rate of cooling of the flue gas borne ash.

The flame imprinted characteristics of silicate mineral species from the point of view of subsequent sintering are summarized in Table 3.

Table 3: Flame Vitrification and Recrystallization of Silicates

Constituent Species	Particle Vitrification		Recrystallization Tendency	Glass Content
	Temperature Range, K	Extent		
Quartz	1700 to 1900	Medium	Low	Medium
Kaolinite	1600 to 1700	High	High	Medium
Potassium Alumino-silicates	1400 to 1600	High	Low	High

The relative amount of coal mineral quartz surviving in the pulverized fuel flame depends on the particle size and temperature. In the intense combustion of cyclone fired boilers the flame temperature exceeds 2000 K and the quartz particles of all sizes will vitrify. Some quartz particles in the crystalline form will survive the flame treatment in pulverized coal fired boilers and the ash may contain 25 per cent of the original coal quartz in the crystalline form (21).

The kaolinite mineral species in coal contain some sodium, calcium and iron in the crystalline structure (6) and the presence of fluxing metals enhances vitrification of the flame heated particles. The high temperature crystalline form of kaolinite species is mullite and the characteristic needle shapes of mullite (Fig. 6e) are frequently found in large, above 5 μ m diameter particles. The mullite needle crystals in ash are always embedded in a glassy phase of the large particles and it appears that the small, below 5 μ m diameter particles of the flame heated kaolinite species are not extensively recrystallized on cooling. The crystalline species of illite and muscovite are not found in the flame heated ash and thus it is likely that the potassium alumino-silicates remain on cooling largely in the form of glassy particles.

The inherent silicate ash (Fig. 1b) will coalesce on combustion first to a sintered matrix inside the burning coal particle and also to small slag globules at the surface of coke residue. Fig. 7a shows the slag globules on a coke particle separated from pulverized coal ash and Fig. 7b shows a lace skeleton of sintered ash in another coke particle revealed after combustion at 900 K.

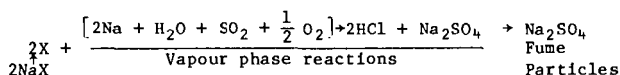
During combustion of the mineral rich coal particles in the pulverized fuel flame ash envelopes may be created which can take the form of cenospheres as shown in Fig. 7c and d. The gas bubble evolution leading to cenosphere formation has been discussed previously (16,22) and the fly ash usually contains between 0.1 and 2 per cent by weight of the lightweight ash. The mineral rich coal particles may leave the combustion ash residue also in the form of plerosphere (spheres-inside-sphere) as shown in Fig. 7e.

The above examples show that the inherent silica ash particles undergo extensive coalescence by sintering and slagging during combustion of the host coal particles. However, the adventitious ash retain the particle identity in the flame and the processes of sintering and slagging take place after deposition on boiler tubes.

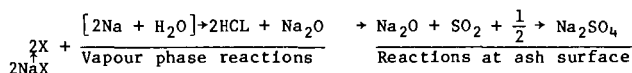
TRANSFER OF FLAME VOLATILE SODIUM TO SILICATES.

The coal sodium originally present as chloride or organo-metal compounds is rapidly volatilized in the pulverized coal flame (23). Subsequently the volatile species are partly dissolved in the surface layer of flame heated silicate particles and partly sulphated in the flue gas (8). The formation of sodium sulphate can proceed via two routes:

Route 1 - In the Flue Gas



Route 2 - At the Surface of Ash Particles



Route 1 for genesis of sodium sulphate fume can be described as the non-captive formation and route 2 as the captive formation.

Some potassium sulphate can also be formed via the two routes. Potassium is present in coal chiefly in the form of potassium aluminosilicates (Table 1) and a large part of the alkali-metal will remain involatile in the flame heated silicate particles. Some 5 to 20 per cent of the potassium is released for sulphation (24) which takes place partly at the surface of the parent particles (25) and partly via the volatilization routes as described above. However, sodium sulphate content of fly ash and chimney content of fly ash and chimney solids is always higher than that of potassium sulphate.

The distribution of the flame volatile sodium between the ash silicate and sulphate phases is markedly influenced by the temperature and residence time of the ash particles in the flame. The high temperature of large boiler flame reduces the viscosity of vitrified silicate particles and as a result a large fraction of the volatile sodium is dissolved in the silicate phase. On average 60 per cent of the sodium is dissolved in the silicate ash particles (6) the remainder being present as sulphate fume particles in the flue gas (20).

THE MECHANISM AND MEASUREMENTS OF SODIUM ENHANCED SINTERING

The formation of sintered ash deposits on boiler tubes requires first a close, molecular distance contact between the particles followed by a growth of particle-to-particle bridges chiefly by viscous flow. Sodium sulphate phase together with some potassium sulphate may play a significant role in the initial stage of sintering by bringing the silicate particles together as a result of surface tension. Sodium sulphate melts at 1157 K but mixed alkali-metal sulphates can form a molten phase at lower temperatures (26).

Once the close contact between the silicate particles has been established a viscous flow of the particle surface layer can commence and the sinter bonds are established according to Equation 7 as discussed by Frenkel (15):

$$\frac{x^2}{r^2} = \frac{3\gamma t}{2\eta r} \quad 7)$$

where x is the radius of neck growth between the spherical particles of radius r , γ is the surface tension, η is the viscosity of fused ash, and t is the time. The $(x/r)^2$ ratio can be taken as a criterion of the degree of sintering, i.e. the strength of boiler deposit (s) developed in time t , that is:

$$s = k \left(\frac{x}{r}\right)^2 \quad 8)$$

and the rate of deposit strength development is:

$$\frac{ds}{dt} = \frac{3k\gamma}{2\eta r} \quad 9)$$

where k is a constant.

Equation 9 shows that the rate of ash sintering, i.e. the development of cohesive strength of a deposit matrix is proportional to the surface tension and inversely proportional to the viscosity. The surface tension and particle size are not markedly changed by dissolution of sodium, iron or calcium oxides in the glassy phase of silicate ash. However, the viscosity is markedly changed by the oxides. In particular, an enrichment of sodium in the surface layer of the silicate ash particles can lead to a high rate of sintering.

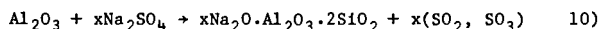
Some of the flame volatile sodium is dissolved in the vitrified silicate ash particles before deposition and an additional amount of sodium is transferred from the sulphate to silicate phases during sintering. The reaction between sodium sulphate and silicates at ash sintering temperatures has been monitored by thermo-gravimetric measurements. Some of the results are given in Table 4.

Table 4: Weight Loss of Sulphates and Sulphate/Silicate Mixtures

Sample	Na_2SO_4	$\frac{\text{Na}_2\text{SO}_4}{\text{Kaolin}}$	$\frac{\text{Na}_2\text{SO}_4}{\text{Ash}}$	CaSO_4	$\frac{\text{CaSO}_4}{\text{Kaolin}}$	$\frac{\text{CaSO}_4}{\text{Ash}}$
Loss Initiation Temperature, K	1425	1085	1175	>1525	1275	1275

Anhydrous sulphate samples and the sulphate/silicate mixtures (50 per cent by weight sulphate) were heated in air at the rate of 6 K per minute.

The results in Table 4 show that the reaction between sodium sulphate and kaolin commenced at 1085 K with the release of SO_2 and SO_3



A typical bituminous coal ash required a higher temperature of 1175 K for the sulphate decomposition reaction.

The transfer of sodium from the sulphate of silicate phase will reduce the viscosity of the glassy material resulting in an enhanced rate of sintering. At higher temperatures, above 1275 K, calcium sulphate starts to dissociate in the presence of kaolin and thus calcium oxide will be available for the sintering reactions. The specific roles of coal calcium and also the iron mineral species in ash sintering and slag formation have been discussed previously (2).

The sintering rates of bituminous, sub-bituminous and lignite coal ashes of different sodium contents can be determined by the electrical conductance measurements. In this method the conductance across an ash compact is measured and it is an indication of the degree of sintering (27). The sodium ions in the low viscosity glass and molten sulphate are the conductive species and the conductance continuity is provided by the sinter bridges between the particles.

Fig. 8 (curve B) shows that sub-bituminous coal ash of high (6.3 per cent) sodium oxide content commenced sintering at 1100 K as determined by the conductance measurements. The results (27) suggest that the amount of sodium in some ashes are sufficiently high both to initiate and sustain a rapid rate of sintering below 1200 K. In contrast, with low sodium coals the rate of ash sintering and the formation of boiler deposits are related to the calcium and iron contents of coal mineral matter. Several empirical formulae have been proposed for predicting the deposit forming propensity of the lignitic and bituminous coal type ashes based on the sodium content (28). These formulae indicate that a rapid build-up of boiler deposit is to be expected when sodium (Na_2O) content of bituminous coal exceeds 2.5 per cent, and that of lignite and sub-bituminous coal ashes is above 4 per cent.

The lignite type ashes have comparatively low fouling propensity when the sodium content is below 4 per cent because of the limited amount of clay minerals available for sintering reaction. That is, in some lignite and sub-bituminous coals there is an excess of sodium and calcium available for the high temperature reactions, and the rate of deposit formation depends on the silicate content of ash (2,9,30). The bituminous coal type ash has an excess of silicates, i.e. the ash is pyrochemically acidic and the rate of sintering depends on the availability of sodium, calcium and iron species in the flame heated deposit material.

The formation of sintered ash deposits is governed chiefly by viscous flow, and the rate of sintering (S_r) can be expressed in terms of the ratio of glassy material to crystalline species of silicate ash ($R_{g/c}$) and the viscosity of the glassy phase (η):

$$S_r = \kappa_1 (R_{g/c}) \frac{1}{\eta} \quad (11)$$

where κ is a constant. The characteristics of flame heated silicate particles, (Fig. 4 and Table 3 in Sect. 4) suggest that the vitrified potassium aluminosilicate particles and the below 5 μm diameter kaolinite particles are first to sinter after deposits. The particles will have a high glass content and the small size enhances sintering as evident from equation (10). It is therefore to be expected that the presence of floor material (6) should enhance sintering and

large particle quartz particles would retard the deposit formation. This applies in the absence of large concentrations of the flame volatile sodium, and non-silicate calcium and iron compounds. The flux material oxides will both increase the ash glass content and reduce the viscosity for sintering, Equation 11, and the composition of original silicate species is less important.

CONCLUSIONS

Silicate Minerals in Coal

The silicate minerals, kaolinite and potassium aluminosilicate species together with quartz constitute the bulk of mineral matter in most coals. The approximate amounts of different silicate species of the bituminous coal mineral matter can be estimated from ash analysis.

Flame Volatile and Silicate Sodium in Coal

Sodium is rapidly volatilized in the flame when it occurs in a non-silicate compound form, chiefly associated with chlorine in bituminous coals and combined with organic compounds in the lignite and sub-bituminous fuels. The fraction of sodium combined with coal silicates remains largely involatile in the pulverized fuel flame.

Flame Vitrification and Spheridization of Silicate Particles

The aluminosilicate particles vitrify and take a spherical shape in the flame and are partially recrystallized on cooling. Micro-needles of mullite up to 10 μm long and crystalloids of quartz are the principal devitrification products enveloped in a glassy material matrix. Large quartz particles originally present in coal are only surface vitrified and do not spheridize in the flame. The coalescence by sintering and fusion of the small aluminosilicate particles dispersed in the fuel substance occurs when the host coal particles burn in the flame. The products are sintered ash skeletons, cenospheres and plerospheres up to 250 μm in diameter.

Sodium Transfer to Silicate and Sulphate Phases

The flame volatile sodium is partly dissolved in the surface layer of vitrified silicate ash particles and partly sulphated. The sulphate particles, 0.1 to 2 μm in diameter can form on the surface of ash particles or in the flue gas via vapour phase reactions followed by sublimation on cooling. Some potassium sulphate is also formed from a fraction of the alkali-metal released on vitrification of potassium aluminosilicates in the flame.

Initial Stage in Ash Sintering

The sulphate phase can initiate ash sintering by bringing the silicate particles to close contact as a result of the surface tension force. Subsequent sintering proceeds by viscous flow and the rate of sinter bond growth is proportional to the surface tension of silicate glassy phase and inversely proportional to the particle size and the viscosity. The latter changes exponentially with temperature and thus the viscosity of silicate ash particles governs the rate of sintering at different temperatures.

Decomposition of Sulphate on Silicate Ash Sintering

Sodium sulphates in the initial material deposited on boiler tubes will be decomposed by the pyrochemically acidic silicates in ash when the deposit temperature exceeds 1085 K. The transfer of sodium from the sulphate to silicate

phase reduces the viscosity of the glassy material of silicate ash thus increasing the rate of sintering.

Sintering of High Sodium Coal Ashes

Some lignite and sub-bituminous coal ash contain sufficiently high quantities of the flame volatile sodium to initiate and subsequently to sustain a high rate of ash sintering leading to a rapid build-up of boiler deposit. With most bituminous coal ashes the volatile sodium plays a role in initiating sintering but the subsequent deposit and slag formation depends largely on the presence of calcium and iron flux oxides. In general terms, the rate of ash sintering is governed by the ratio of glassy material to crystalline species and the viscosity of the glassy phase.

ACKNOWLEDGEMENT

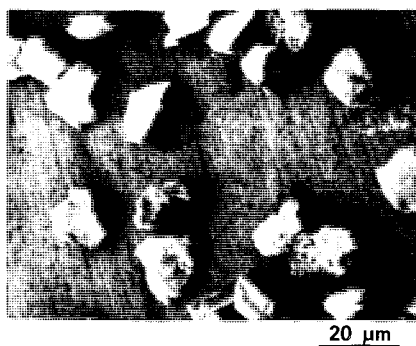
The work was carried out at the Central Electricity Research Laboratories and the paper is published by permission of the Central Electricity Generating Board.

LITERATURE CITED

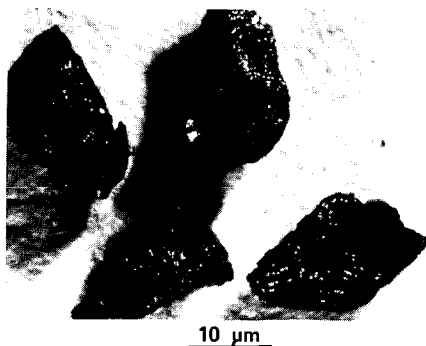
1. Raask, E., "Flame Imprinted Characteristics of Ash Relevant to Boiler Slagging, Corrosion and Erosion", Jour. Eng. Power (1982), 104, 858.
2. Raask E., "Mineral Impurities in Coal Combustion - The Behaviour, Problems and Remedial Measures", Hemisphere Publishing Corp., New York (1984).
3. Gumz, W., Kirsch, H. and MacKowsky, M-T., "Slagging Studies: Investigations of Minerals in Fuel and Their Role in Boiler Operation", Springer-Verlag, Berlin (1958).
4. O'Gorman, J.V. and Walker, P.L. "Mineral Matter and Trace Elements in US Coals", Dept. Interior Office of Coal Res. and Dev. Report No. 61, Washington, USA (1972).
5. Rao, C.P. and Gluskoter, J.H., "Occurrence and Distribution of Minerals in Illinois Coals", III. State Geol. Survey, Circular No. 476, Urbana, USA (1973).
6. Dixon, K., Skipsey, E. and Watts, J.T., "The Distribution and Composition of Inorganic Matter in British Coals: Part 2 - Alumino-Silicate Minerals in the Coal Seams of the East Midlands Coalfields", Jour Inst. Fuel (1970), 43, 124.
7. BCURA, "The Chemical Composition and the Viscometric Properties of the Slags Formed from Ashes of British Coals", British Coal Utilization Research Association, Leatherhead, UK (1963).
8. Raask, E., "Sulphate Capture in Ash and Boiler Deposits in Relation to SO₂ Emission", Prog. Energy Combust. Sci., (1982), 8, 261.
9. Sondreal, E.A., Kube, W.R. and Elder, J.L., "Analysis of the Northern Great Province Lignites and Their Ash: A Study of Variability", US Bureau of Mines, Report No. 7158, Washington, USA (1968).
10. Kiss, L.T., "The Mode of Occurrence and Distribution of Inorganic Elements in Australian Brown Coal", Coal Science Conference, E7 p. 774, Dusseldorf, W. Germany (1981).

11. Francis, W., "Coal, its Formation and Deposition", Arnold, London (1961).
12. Daybell, G.N., "The Relationship between Sodium and Chlorine in Some British Coals", Jour. Inst. Fuel (1967), 40, 3.
13. Skipsey, E., "Relationship between Chlorine in coal and the Salinity of Strata Waters", Fuel (1975) 54, 121.
14. Dunham, K.C., "Mineralization by Deep Formation Waters: A Review", Trans. Inst. Min. Metal, (1970), 79, B127.
15. Frenkel, J.S., "Viscous flow at Crystalline Bodies under the Action of Surface Tension", Jour. Phys. (Moscow) (1945), 9, 385.
16. Raask, E., Slag-Coal Interface Phenomena, ASME Jour Eng. Power (1966), Jan. p. 40.
17. Raask, E., "Fusion of Silicate Particles in Coal Flames", Fuel (1969), 48, 366.
18. Raask, E. and Goetz, L., "Characterization of Captured Ash, Chimney Stack Solids and Trace Elements", Jour. Inst. Energy, (1981), 54, 163.
19. Raask, E. and Bhaskar, M.C., "Pozzolan Activity of Pulverized Fuel Ash", Concrete Res., (1975), 5, 363.
20. Raask, E., "Surface Properties of Pulverized Coal Ash and Chimney Solids", (1981), 1, 233.
21. Raask, E., "Quartz, Sulphates and Trace Elements in PF Ash", Jour. Inst. Energy, (1980), 53, 70.
22. Raask, E., "Cenospheres in Pulverized Fuel Ash", Jour. Inst. Fuel (1968), 43, 339.
23. Halstead, W.D. and Raask, E., "The Behaviour of Sulphur and Chlorine Compounds in Pulverized Coal Fired Boilers", Jour. Inst. Fuel (1969), 42, 344.
24. Raask, E., "The Behaviour of Potassium Silicates in Pulverized Coal Firing", VGB Mitteilungen (Essen Germany) (1968) 48, 348.
25. Stinespring, C.D. and Stewart, G.W., "Surface Enrichment of Alumino-Silicate Minerals and Coal Combustion Ash Particles", Atm. Envir. (1981), 15, 307.
26. Adams, A.M. and Raask, E., "Complete Sulphates in Coal Fired Boiler Plant", Conf. Mechanism of Corrosion by Fuel Impurities, p. 196, Marchwood U.K., Butterworths Publ., London (1963).
27. Raask, E., "Sintering Characteristics of Coal Ashes by Simultaneous Dilatometry and Electrical Conductance Measurements", Jour. Therm. Anal. (1979), 16, 91.
28. Winegartner, E.C., "Coal Fouling and Slagging Parameters", ASME Research Committee Publication on Corrosion and Deposits from Combustion Gases, New York (1974).

29. Tufte, P.H., Gronhovd, G.H., Sondreal, E.H. and Selle, S.J., "Ash Fouling Potentials of Western Sub-Bituminous Coal as Determined in a Pilot Plant Test Furnace", Am. Power Conf., Chicago, USA (1976).
30. Sondreal, E.A., Gronhovd, G.H., Tufte, P.H. and Beckering, W., "Ash Fouling Studies of Low Rank Western US Coals", Conf. Ash Deposition and Corrosion due to Impurities in Combustion Gases, p. 85, Edited by R.W. Bryers, Hemisphere Publishing Corp. Washington (1978).



(a) ADVENTITIOUS



(b) INHERENT-WHITE PARTICLES

FIG. 1 MINERAL MATTER IN COAL

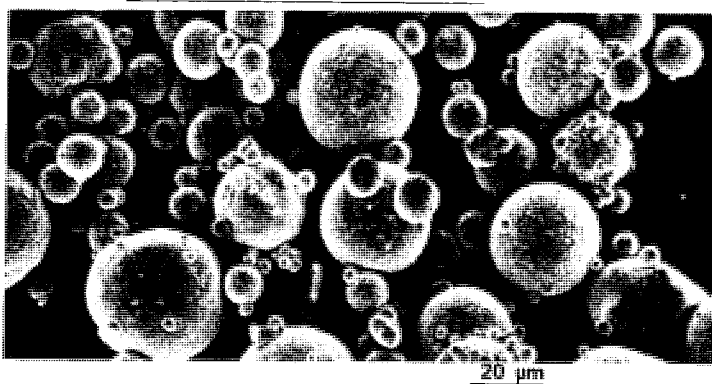
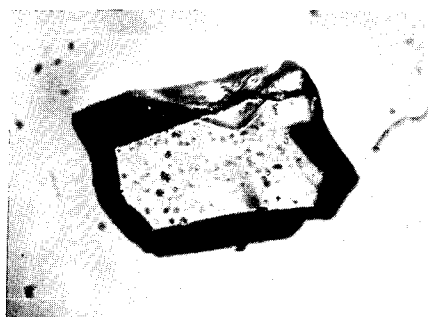
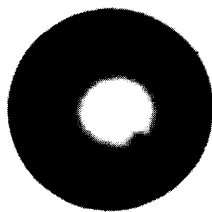


FIG. 2 PULVERIZED COAL ASH



(a)



(b)

FIG. 3 SURFACE FUSED (a) AND SPHERIDIZED (b) SILICATE PARTICLES

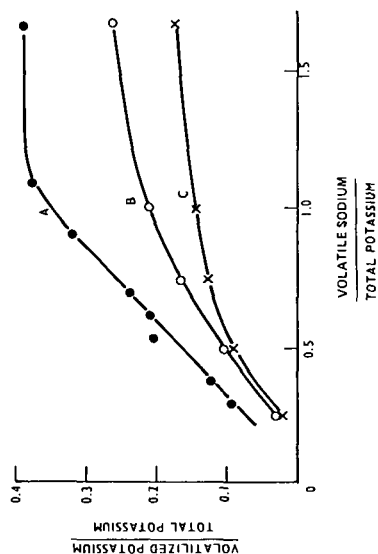


FIG. 4 THE EFFECT OF SODIUM CHLORIDE ON RELEASE
POTASSIUM FROM SILICATES

A - COAL SILICATES
B - MUSCOVITE
C - ORTHOCLASE

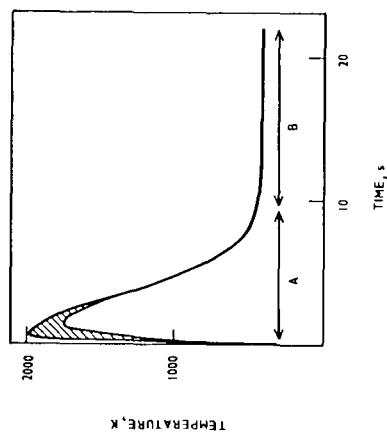


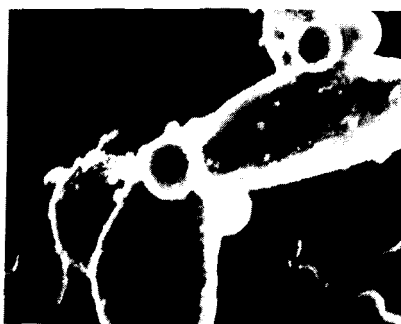
FIG. 5 TEMPERATURE/TIME PLOT FOR ASH PARTICLES IN A 500 MW
PULVERIZED COAL FIRED BOILER - 0.1 μ m (TOP CURVE) TO
100 μ m (LOWER CURVE) SIZES

SECTION A COMBUSTION AND HEAT EXCHANGE CHAMBERS
SECTION B ELECTRICAL PRECIPITATORS AND CHIMNEY



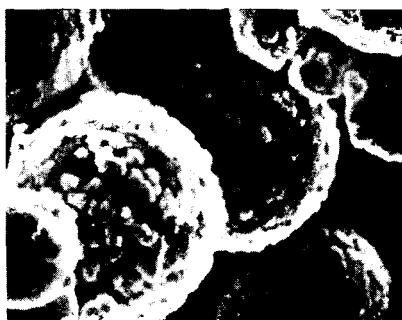
5 μ m

(a) UNFUSED QUARTZ PARTICLE



25 μ m

(b) ELONGATED SILICATE PARTICLES



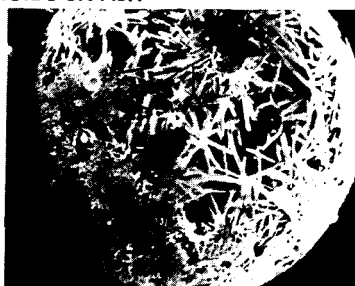
1.5 μ m

(c) MICROIDS ON ASH



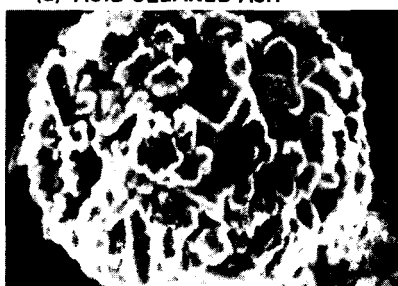
1.5 μ m

(d) ACID CLEANED ASH



10 μ m

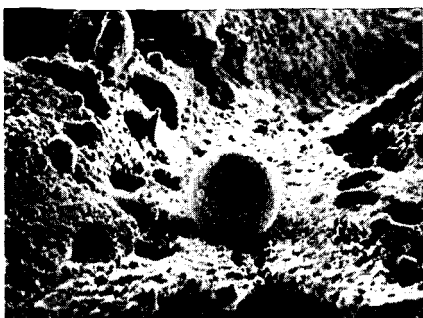
(e) MULLITE NEEDLES IN ASH



2 μ m

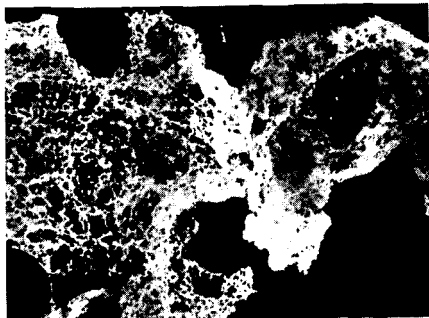
(f) QUARTZ CRYSTALLOIDS

FIG. 6 DIAGNOSTIC FEATURES OF FLAME HEATED ASH



10 μ m

(a) ASH PARTICLES ON COKE



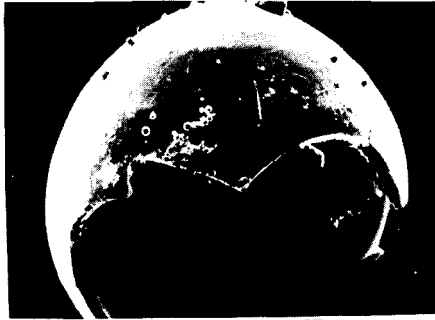
20 μ m

(b) ASH SKELETON IN COKE



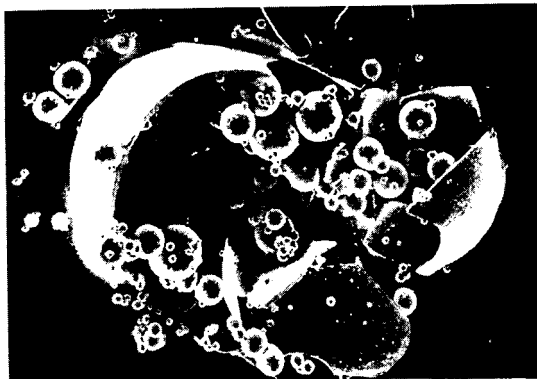
25 μ m

(c) CENOSPHERES



25 μ m

(d) FRACTURED CENOSPHERE



(e) PLEROSPHERE

25 μ m

FIG. 7 COALESCENCE PRODUCTS OF INHERENT ASH IN FLAME

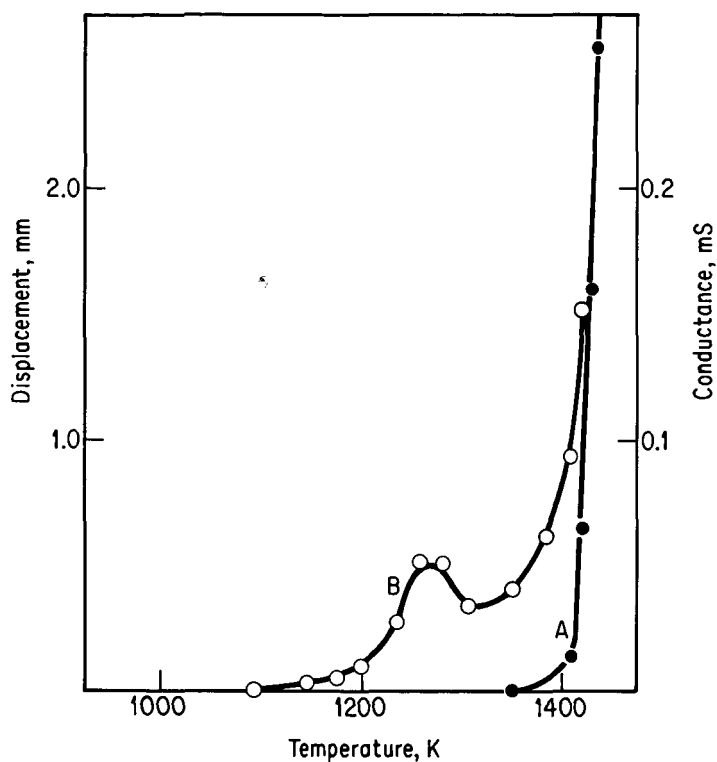


FIG.8 SIMULTANEOUS SHRINKAGE AND CONDUCTANCE MEASUREMENTS
LEIGH CREEK (AUSTRALIA) COAL ASH

A - SHRINKAGE
B - CONDUCTANCE

VISCOSITY OF SYNTHETIC COAL ASH SLAGS

Karl S. Vorres and Sherman Greenberg†

Chemistry Division, Building 211
†Materials Science and Technology Division, Building 212
Argonne National Laboratory
9700 South Cass Avenue
Argonne, Illinois 60439

INTRODUCTION

Coal used for energy conversion contains a considerable amount of mineral matter. During the conversion process the mineral matter is heated, and in the higher temperature reactors is converted to a molten material which flows from the reactor at a rate dependent on the viscosity of the slag. In studies of coal slags obtained from electric utility boilers (1,2,3) this behavior has been studied and correlations have been determined between the viscosity of the slag and the chemical composition. These studies have been carried out in a range of gaseous environments typical of the combustion furnace with a range of oxygen concentrations from almost zero to 15%.

The purposes of this study included a determination of the viscosity behavior of synthetic slags over a range of compositions and temperatures characteristic of slagging gasifier operation. The compositions were chosen to be broadly representative of a range of coals from both the eastern and western U.S. The temperatures were chosen to be in the range of satisfactory gasifier operation, and within the limits of the experimental equipment. The gaseous environments were selected to have the low oxygen partial pressure (about 10^{-8} to 10^{-9} atm) typical of the slagging gasifier.

The viscosity data were to be used as input for an associated refractory/slag corrosion program. Accordingly, the data obtained for the first few slags were compared with correlations developed by Watt and Fereday (1,2) based on chemical composition and by Hoy, Roberts and Williams (3), using a modified version of the silica ratio. In order to simplify the systems for study, the synthetic slags were limited to the five components: SiO_2 , Al_2O_3 , FeO , CaO and MgO . Since they contained no Na_2O or K_2O , the slag compositions were outside the range of the earlier correlations. If this difference was neglected, then the composition of all but four of the synthetic slags used in this program fell outside the range of the compositions for which the correlations were developed (10% Al_2O_3 or 0% MgO or low silica ratio or high $\text{SiO}_2/\text{Al}_2\text{O}_3$ ratio) and the correlations did not, in general, represent the data obtained for the synthetic slags.

EXPERIMENTAL

Slag: The viscosities of 21 synthetic slags, covering the range of compositions expected in slags derived from American coals were determined in this

study. The synthetic slags were prepared from reagent grade chemicals. The synthetic slags were mixed with water and pressed into pellets using a pressure of 15000 psig. The pellets had a slightly smaller diameter than that of the containment crucible. The composition of the slags is given in Table 1.

Viscometer: The apparatus and technique have been described in detail (4). Essentially a Brookfield Rheolog(TM) was used to replace the sample head in the rotating cylinder slag corrosion apparatus used in slag/refractory corrosion studies at ANL (5). Appropriate seals and ceramic structural components permit maintenance of the desired low oxygen activity within the measuring chamber. The viscosity measuring "bob" was a cylinder 12.7 mm diameter and 11.1 mm high. For measurement at lower oxygen partial pressures the "bob" and connecting shaft were fabricated of molybdenum; in an air environment the molybdenum was replaced by platinum. The slag was contained in Al2O3 crucibles. The "bob" and measuring system were calibrated at room temperature using a series of NBS oils ranging from 10 to 600 poise.

Procedure: Viscosity measurements were usually made in a decreasing temperature mode at 50 C. intervals after the slag sample had been slowly heated to the desired temperature, typically about 1400-1550 C. The slag was kept at each temperature long enough to demonstrate constant viscosity (about 30-60 minutes). In one case, slag 12, measurements were also made in an increasing temperature mode to determine if there were hysteresis effects. None were observed in this slag and other work confirmed this (4). Measurements made in other laboratories with other slags have shown hysteresis (6). The desired oxygen partial pressure was maintained by flowing H₂-CO₂-N₂ (or A) mixtures of the required composition through the interior of the measuring chamber throughout the experiment. The variation of oxygen partial pressure with gas composition and temperature was calculated using a NASA-developed code (4).

RESULTS AND DISCUSSION

The data obtained were plotted as viscosity versus temperature for the different materials and displayed the expected exponential increase in viscosity as the temperature decreased. In most of the runs a characteristic sudden increase in viscosity was noted, as in some related studies (1,3). Some typical results are shown and compared with the Watt-Fereday and modified silica ratio projections, assuming a liquid phase, in Figures 1 and 2, (slags 1 & 12).

To understand the Newtonian characteristics of the slags, plots of logarithm of viscosity versus temperature were made. These indicated straight lines or two line segments. For runs with a sudden increase in viscosity at lower temperatures, two segments were observed. Shear rates were not varied and the various types of non-Newtonian behavior were not explored. The observed straight lines are consistent with Newtonian behavior.

Arrhenius plots were then made. These plots typically involve the logarithm of a rate constant and the reciprocal of the absolute temperature. Viscosity is not a rate parameter, but is defined as the shear stress divided by the shear rate. The reciprocal of the viscosity is the shear rate per unit shear stress and was used in the plots. A typical example is shown in Figure 3. Slag 1 shows a typical high temperature low activation energy regime with a transition to a high activation energy, low temperature regime. This behavior was noted in most of the

runs. The other behavior was, as in the case of slag 12, a single straight line covering the range of the data. The slopes and activation energies for runs without the transition tended to be intermediate in the range of the values for runs with the transition.

In order to compare the viscosity behavior of the different compositions for the higher temperature regime and the slags with no transitions, separate plots superimposing the sample series with a constant weight % SiO₂ were made and are shown in Figures 4,5 and 6. Note the vertical change in scale in Figure 6. The solid portion of the lines represents the actual range of data. The dashed part of the lines was added to facilitate visual comparison. Examination of the plots shows two general tendencies. The reciprocal viscosities or fluidities tend to increase for series with lesser amounts of SiO₂ in them. Although the envelopes of data are broad, this observation can be made. Additionally, for a given series with a fixed weight % SiO₂, the fluidities are greater for the lower amounts of Al₂O₃.

A similar study of the lower temperature regime will be made later.

Activation energies and the temperature range of data are given in Table 2. Initial statistical analyses have not shown a strong correlation of activation energies with any of the slag constituents.

A wide range of activation energies with very high values was obtained for the lower temperature regime. The transition from the higher to the lower temperature regime generally occurred in the 1300-1400 C range. In order to interpret the data the ternary equilibrium phase diagrams for the systems SiO₂-Al₂O₃-MO were examined where MO is either CaO, FeO, or MgO. The mole fractions of each of the constituents were calculated as also shown in Table 2, and the ternary diagram corresponding to the major base in the group CaO, FeO or MgO was selected. Usually a ternary eutectic was found in the temperature region which would be expected for a system most closely corresponding to the sample composition. This eutectic temperature was close to the observed transition temperatures in the viscosity data. Many of the highest temperatures used were significantly below those associated with the appearance of a solid phase from the melt. This solid phase could have been present through the entire series of measurements on the slag.

CONCLUSIONS

A series of 21 synthetic coal ash slags were studied. It was observed that: (1) Plots of the logarithm of viscosity versus temperature showed one or two straight line segments, indicating Newtonian behavior in the temperature range studied. (2) Plots of the logarithm of the reciprocal of viscosity versus reciprocal of absolute temperature also showed one or two straight line segments, indicating one or two mechanisms were operative over the temperature range. (3) For three series, varying in SiO₂ content, those with the greatest SiO₂ content had the highest viscosities. (4) Within a series of given SiO₂ content, those members with the highest Al₂O₃ content had the highest viscosity. (5) For slags exhibiting a transition in behavior, the transition temperature could usually be associated with a ternary eutectic temperature in the phase equilibrium diagram for the most closely related ternary system. (6) Many of the slags probably had a

solid phase precipitating from the liquid phase during the cooling period before the transition temperature.

ACKNOWLEDGMENTS

The authors gratefully acknowledge the support of the U. S. Department of Energy. KSV acknowledges support from the Chemical Sciences Division of the Office of Basic Energy Sciences, while SG acknowledges support from the Surface Gasification Materials Program.

REFERENCES

1. J. D. Watt and F. Fereday, "The Flow Properties of the Slags Formed from the Ashes of British Coals. Part 1. Viscosity of Homogeneous Liquid Slags in Relation to Slag Composition", J. Inst. Fuel 42, 101 (1969).
2. J. D. Watt, "The Flow Properties of Slags Formed from the Ashes of British Coals. Part 2. The Crystallizing Behavior of the Slags", J. Inst. Fuel 42, 131 (1969).
3. H. R. Hoy, A. G. Roberts, and D. M. Williams, "Behavior of Mineral Matter in Slagging Gasification Processes", IGE Journal 5, 444 (1965).
4. J. Chen, S. Greenberg, and R. Poeppel, "The Viscosity of Coal Slags as a Function of Composition, Temperature and Oxygen Partial Pressure", ANL/FE-83-30 (in press).
5. S. Greenberg, R. Poeppel et al, "The Corrosion of Ceramic Refractories in Synthetic Coal Slags Using the Rotating Cylinder Technique: An Interim Report", ANL/FE-83-31 (in press).
6. R. C. Streeter, E. K. Diehl and H. H. Schobert, "Measurement and Prediction of Low-Rank Coal Viscosity", Preprints Am. Chem. Soc. Div. Fuel Chem. 28(4) 174 (1983).

TABLE 1 SLAG COMPOSITIONS

COMPOSITION	NO.						
	1	2	3	4	5	6	7
SiO ₂	50	50	50	50	50	50	50
CaO	5	5	5	5	5	5	5
Al ₂ O ₃	10	10	20	20	20	30	30
FeO	15	25	25	15	5	15	5
MgO	20	10	0	10	20	0	10

	8	9	10	11	12	13	14
SiO ₂	40	40	40	40	40	40	40
CaO	15	15	15	15	15	15	15
Al ₂ O ₃	10	10	20	20	20	30	30
FeO	15	25	25	15	5	15	5
MgO	20	10	0	10	20	0	10

	15	16	17	18	19	20	21
SiO ₂	30	30	30	30	30	30	30
CaO	25	25	25	25	25	25	25
Al ₂ O ₃	10	10	20	20	20	30	30
FeO	15	25	25	15	5	15	5
MgO	20	10	0	10	20	0	10

Table 2. Activation Energies, Range of Temperatures and Mole Fractions

Slag #	Ea	Temperature	Mole Fractions				
		Range	SiO ₂	Al ₂ O ₃	CaO	FeO	MgO
1	43.9	1440-1332	.483	.057	.052	.121	.288
2	44.2	1460-1314	.515	.061	.055	.215	.154
3	42.0	1456-1350	.568	.134	.061	.237	.000
4	40.1	1513-1337	.529	.125	.057	.133	.158
5	60.2	1462-1312	.495	.117	.053	.041	.295
6	366	1550-1500	.584	.209	.063	.147	.000
7	65.2	1515-1415	.543	.192	.058	.045	.162
8	77.6	1353-1192	.384	.056	.154	.120	.286
9	13.1	1455-1297	.409	.060	.164	.214	.152
10	55.5	1454-1335	.451	.133	.181	.235	.000
11	37.6	1439-1310	.420	.124	.169	.132	.156
12	103	1436-1262	.393	.116	.158	.041	.293
13	36.9	1535-1447	.464	.205	.186	.145	.000
14	50.8	1484-1401	.431	.190	.173	.045	.161
15	104	1434-1339	.286	.056	.255	.119	.284
16	77.6	1390-1265	.272	.060	.272	.212	.151
17	29.5	1451-1299	.335	.132	.299	.234	.000
18	106	1448-1377	.313	.123	.279	.131	.155
19	20.0	1459-1352	.293	.115	.261	.041	.291
20	55.1	1402-1294	.345	.203	.308	.144	.000
21	116	1532-1415	.321	.189	.286	.045	.159

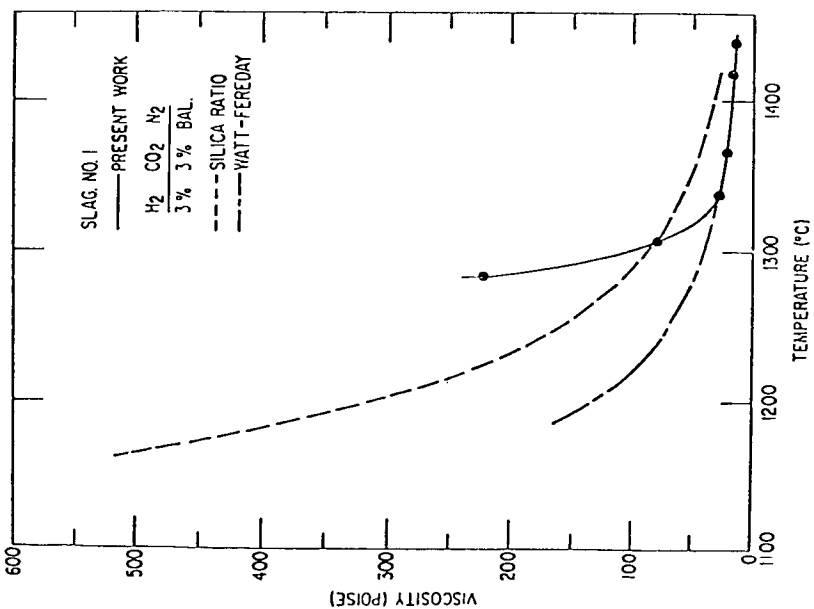


Figure 1. Viscosity of Slag 1

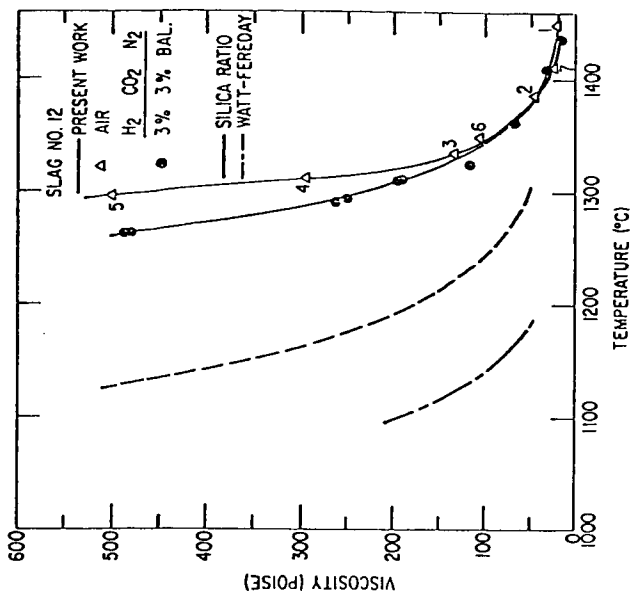


Figure 2. Viscosity of Slag 12

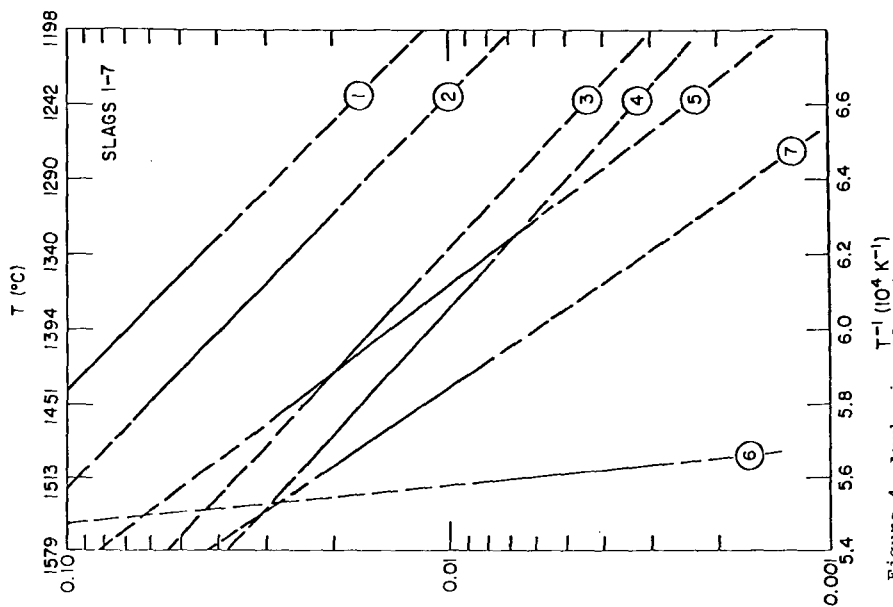


Figure 4. Arrhenius Plot for Slags 1-7

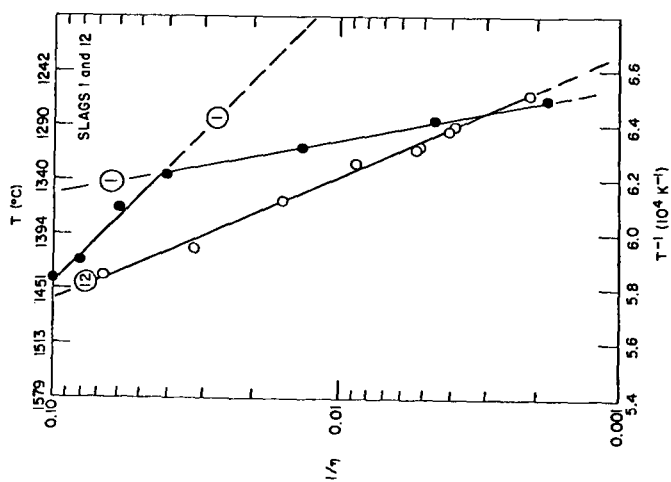
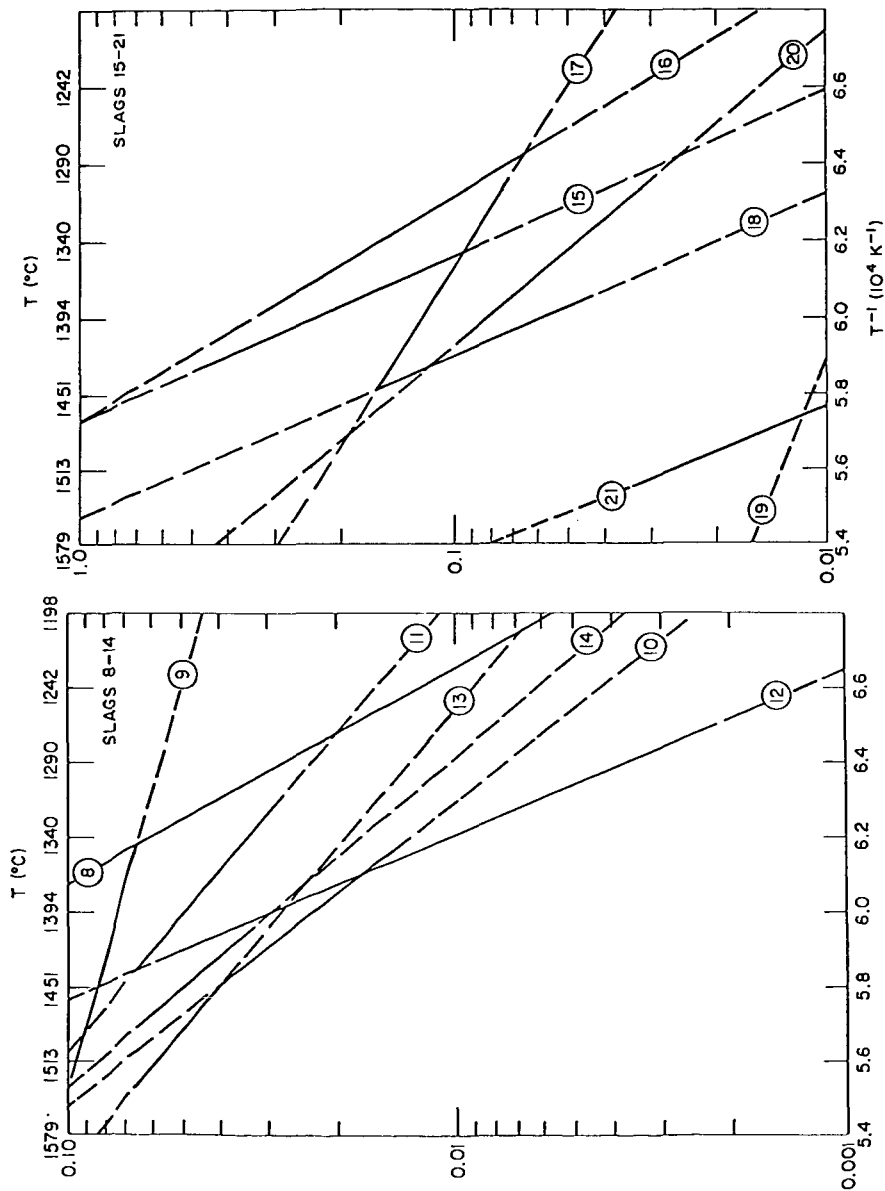


Figure 3. Typical Arrhenius Plots



Arrhenius Plots of Logarithm of Reciprocal Viscosity and Reciprocal Absolute Temperatures for Slags 8-14 and 15-21

SULFUR SOLUBILITY IN SLAGS FOR CYCLONE COAL COMBUSTORS

by

David H. DeYoung

Smelting Process Development Division
Alcoa Laboratories
New Kensington, PA 15068

I. INTRODUCTION

This study was conducted to select potential slag compositions for use in a slagging, staged, cyclone coal combustor, and to obtain the necessary data to evaluate the desulfurizing ability of the combustor. The first stage of such a combustor would be operated quite reducing to facilitate sulfur removal by a slag formed from the coal ash and inorganic additives (e.g., lime). A tangential motion imparted to the gas would throw ash, coal, and additives to the combustor wall where they would combine to form a molten slag. This slag, containing some dissolved sulfur, would continually drain out of a taphole at the exit end of the horizontally-placed cylindrical combustor. Advantages of this type of combustor are removal of some sulfur, low particulate emissions, and low NO_x emissions.

This paper will be divided into three parts. First, the selection of slag compositions will be outlined. Second, sulfide capacity measurements of these slags will be discussed. Third, the desulfurizing potential of a slagging, cyclone combustor will be evaluated using these measurements.

II. SLAG COMPOSITION SELECTION

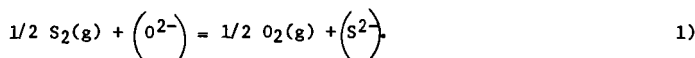
The strategy was first to select possible additives, then locate phase diagrams for systems of major ash components plus additives, and finally, select low-melting eutectic compositions as candidate slags. Additives were chosen for their known ability to form low-melting silicates (e.g., the alkalis) or for their known ability for desulfurization (e.g., the alkaline earth elements). An eastern coal was used for tests of a pilot combustor. Its ash composition, used to calculate additive compositions, is given in Table I. Major components, SiO_2 , Al_2O_3 , and Fe_2O_3 , account for approximately 80% of the ash.

Ternary phase diagrams for the SiO_2 - Al_2O_3 -additive and SiO_2 - FeO -additive systems were investigated for possible slag compositions. Unless otherwise noted, all phase diagrams were taken from Levin, et al (1-3) or Roth, et al (4). The selected compositions which were tested are given in Table II, as are estimated liquidus temperatures. Obviously, the liquidus temperature of the slag consisting of coal ash and the additive will be different from those given by the phase diagrams because of the minor components of the ash. However, the phase diagrams provide reasonable initial selections. Additive compositions and quantities are given in Table III.

III. SULFIDE CAPACITY MEASUREMENTS

Sulfide capacities of the selected slag compositions were measured to rate the slags and to provide data for evaluation of the operation of a combustor with these slags.

Chemistry of Sulfur in Slags: There has been considerable research on the chemistry of sulfur in slags reported in the literature. Most was aimed toward understanding and improving the desulfurization of iron and steel. These studies (5-7) have shown that at high oxygen potentials sulfur dissolves in slags as a sulfate, and at low oxygen potentials, the condition relevant to the two-stage combustor, sulfur dissolves as a sulfide. This can be represented by the reaction,



A quantity called the sulfide capacity (6) can be defined as:

$$C_S \equiv (\text{wt } \% S) \left(\frac{P_{O_2}}{P_{S_2}} \right)^{1/2} \quad 2)$$

where wt % S refers to sulfur dissolved in the slag, and P_{O_2} and P_{S_2} are the partial pressures of oxygen and sulfur in the atmosphere with which the slag is equilibrated. The sulfide capacity for many slags has been found (5,6) to be independent of sulfur and oxygen potentials for wide ranges, and therefore is a useful quantity for rating slags. One exception relevant to this study is that, for slags containing FeO, C_S is expected to change with oxygen potential as the ratio of ferrous to ferric ions in the slag changes.

A review of the literature (5-22) showed that virtually all work on sulfur in slags was on systems relevant to the desulfurization of iron and steel and at temperatures ranging from 1400-1600°C. No data were found for low-melting slags (liquidus temperatures, approximately 1000-1100°C), and particularly for the iron-alkali-aluminosilicates from which many of the proposed compositions are composed. Therefore, experimental measurements were necessary to obtain the data needed for selection of slags.

Experimental Method: An equilibration technique was chosen to measure the sulfide capacities of the candidate slags. Slag samples were equilibrated with a CO-CO₂-SO₂ gas mixture having fixed oxygen and sulfur potentials, quenched to room temperature, and analyzed for sulfur. Sulfide capacities were then calculated from the sulfur concentrations using Equation 2. This technique was chosen because it is a direct method, and because the oxygen and sulfur potentials could be accurately controlled, and, if necessary, these could be set to match the activities for oxygen and sulfur which were anticipated in the actual coal combustor. The apparatus used for sulfide capacity measurements is shown schematically in Figure 1.

Slags were prepared by mixing preweighed amounts of additives and coal ash. The coal ash was obtained from Bituminous Coal Research, Inc. It was prepared by ashing Loveridge Seam, West Virginia coal in air at 750°C, followed by a reduction in a 60%CO-40%CO₂ gas at 1000°C, then cooled under nitrogen.

The gas compositions for each experiment were chosen to obtain as low an oxygen potential as possible, without reducing FeO to Fe metal. They were also chosen to obtain as low a sulfur potential as possible to match anticipated conditions in the actual combustor, yet large enough so that they could be prepared by mixing gases. The equilibration time for slag samples was determined by periodic analyses of the gas exiting the reactor. Quenched slag samples were analyzed for sulfur using a Leco titrator, and were analyzed for Si, Al, Fe, Na, K, Ca, Mg, Ti, and P by atomic absorption.

Results: Table IV gives the results for all sulfide capacity measurements. Figures 2 and 3 show ternary phase diagrams for selected systems on which the results are shown. Compositions shown were obtained by taking the three major components from the slag analyses and normalizing to 100%. The sulfide capacities are shown as a function of basicity in Figure 4, which summarizes all results of this study. Molar basicities (Σ mole fraction bases/ Σ mole fraction acids) were calculated from the slag analyses.

It was found that after equilibration with the sulfurizing gas, certain slags in the $\text{FeO-Al}_2\text{O}_3\text{-SiO}_2$ system consisted of two immiscible liquids at 1100°C. One phase was a glass. The other phase had a metallic appearance and will be referred to as the "matte phase". The sulfide capacities for these slags should be considered as "apparent" because the sulfide capacity is defined for a single liquid phase. The matte phase in all of these double-phased slags contained 27-31% S, while the glass phase contained from 0.2 to 13% S. X-ray diffraction analyses showed the glass phase to be amorphous and the matte phase to contain FeS and FeS_2 .

Discussion: Slag compositions 2-A-1, 2-A-7, 2-B-2, 2-C-1, 2-D-2, and 2-E-1 were closest to the coal ash composition given in Table I, containing 25-38% additive. As seen from Table IV, $\log C_S$ ranged from approximately -3.8 to -5.5 at 1100°C. Using the basicity of the ash calculated from Table I and the data shown in Figure 4, the sulfide capacity for pure ash is estimated to be approximately $\log C_S = -5.2$. This is quite low as compared to results obtained for slags containing significant quantities of additives. As will be demonstrated later in the report, sulfur captured by coal ash slag with this sulfide capacity would be insignificant even at very favorable conditions - very low oxygen potential and low temperature.

There is a general correlation between sulfide capacity and basicity for a given system, as shown in Figure 4. There is a sharp drop in sulfide capacity between basicities of 1.0 to 0.5, which corresponds to the metasilicate to disilicate compositions in a binary silicate. For a given basicity, systems 2-A (FeO) and 2-C (FeO , CaO) have significantly higher sulfide capacities than systems 2-D (Na_2O) and 2-E (CaO), so that for a given basicity, FeO is superior to CaO and Na_2O as an additive. This is not what would be expected considering the standard free energies of formation of the sulfides and oxides of Fe, Ca, and Na.

Considering standard free energies for the formation of metal sulfides from metal oxides, FeO and CaO should be approximately equivalent desulfurizers and Na_2O should be superior. However, slags are far from ideal solutions because of the strong interactions among species -- particularly with SiO_2 . This is why experimental measurements of sulfide capacities were needed. Free energy of mixing data (24) for Na_2O , CaO , and FeO binary silicates show that the chemical interaction with silica decreases in the order Na_2O , CaO , FeO , and for a given basicity, the activity of the basic oxide in the silicates increase in the order Na_2O , CaO , and FeO . On this basis, FeO should be a better desulfurizer than CaO or Na_2O . This is consistent with the present results. Not surprisingly, the metal oxide-silica interaction is a major factor in the desulfurization ability of the slag.

Several modifications of slags based on the $\text{FeO-Al}_2\text{O}_3\text{-SiO}_2$ system were tested to determine if a less expensive additive could be substituted for some of the iron or if additives could be used to reduce liquidus temperatures. Figure 4 shows that replacing a portion of the iron oxide in slags of the $\text{FeO-Al}_2\text{O}_3\text{-SiO}_2$ system with CaO (5 wt %) or MgO (12 wt %) had no effect on the sulfide capacities. Results for composition 2-C-1 also support this conclusion, because for this composition approximately 14% of the FeO of an equivalent composition in the $\text{FeO-Al}_2\text{O}_3\text{-SiO}_2$ system was replaced by CaO , with only a slight decrease in sulfide capacity. Replacement of portions of the SiO_2 in $\text{FeO-Al}_2\text{O}_3\text{-SiO}_2$ slags by B_2O_3 or P_2O_5 has no effect on sulfide capacities; therefore, these additives are potentially useful for reducing slag liquidus temperatures.

Figure 5 compares some results of this study to those found in the literature for similar slags at higher temperatures. These literature data were adjusted to a basicity of 1.65 using data given in Figure 4. The data from this study are quite consistent with the literature data. The linearity of the sulfide capacity with inverse temperature is consistent with the theoretical relationship,

$$\frac{d \ln C_S}{d (1/T)} = -\Delta H^\circ/R + H_{FeO}^M/R - H_{FeS}^M/R \quad (3)$$

where ΔH° is the standard enthalpy change for the reaction,



and H_{FeO}^M and H_{FeS}^M

are the partial molar enthalpies of mixing of FeO and FeS in the slag. This relationship can be derived from Equation 2, the equilibrium constant for Equation 4 and the Gibbs-Helmholtz equation.

Most of the slags tested were found to have been partially or completely melted at 1100°C. However, at 1000°C, all slags from the FeO-Al₂O₃-SiO₂ system were not molten. It is thought that for these compositions the entire additive reacted with sulfur species in the atmosphere while none reacted with the SiO₂ or with other components in the ash. Hence, sulfide capacities measured from this experiment are not true sulfide capacities of the slags. Another point which supports this is that the "measured" sulfide capacities at 1000°C are greater than those at 1100°C, while Figure 5 shows the opposite trend for results for molten slags. Also, other literature data show that sulfide capacities generally increase with temperature.

This points out an inherent disadvantage in using a coal ash slag for desulfurization. When silica reacts with the desulfurizing agent, e.g., lime, the effectiveness of the desulfurizing compound is greatly reduced. Hence, it is desirable to design a desulfurizing combustor in which the ash does not react with the desulfurizing material.

IV. EVALUATION OF A PILOT COMBUSTOR

Calculations: The measured sulfide capacities were used to estimate sulfur emissions from a staged, slagging, cyclone combustor operating close to equilibrium. To calculate sulfur emissions, an equation for gas-slag chemical equilibrium for sulfur (Equation 2) and a mass balance for sulfur are solved simultaneously. First, the equilibrium gas compositions were calculated for the combustion of coal with air for a range of sulfur concentrations in the coal. This was done using Alcoa's Chemical Equilibrium Computer Program (23). Next, the concentrations of sulfur in the slags for equilibrium with the combustion gases were calculated. Finally, the quantity of additives needed to obtain these compositions were calculated from sulfur mass balances.

Results: Figure 6 shows an example of the results for these calculations, for combustion with 55% of stoichiometric air (stage 1) at 1100°C. A reasonable goal for the sulfur capture, considering projections of future EPA regulations, is 70%. The slag mass can vary between 85 and 350 g/kg coal (the upper limit was

established from a heat balance for Alcoa's pilot combustor), so the necessary $\log C_S$ for a 70% sulfur removal is between -2.75 and -3.3. A sulfide capacity of $\log C_S = -3.3$ at 1100°C was obtained for certain slags based on the FeO-Al₂O₃-SiO₂ system, e.g., compositions 2-A-3 or 2-A-10.

As the combustion stoichiometry is decreased, the curves in Figures 6 are rotated counterclockwise about the origin, i.e., the sulfur removal is increased. An increase in temperature will have the opposite effect. The curves are rotated clockwise about the origin. However, for a particular slag composition the sulfide capacity increases with temperature, as shown in Figure 5. The net result of the two opposing effects (using the temperature behavior shown in Figure 5) is that the sulfur removal decreases with increasing temperature. In the range of coal-sulfur contents investigated, 2-6%, the fraction of sulfur removed by slag does not change with sulfur content in the coal. The total sulfur emitted increases with increasing sulfur concentration in the coal, but the sulfur removal by the slag also increases.

A final point to note regarding sulfur removal is that as the concentration of hydrogen in the combustion gases is decreased, the sulfur removal by the slag will increase. This is due to the high stability of the hydrogen-sulfur species, such as H₂S(g), as compared to the carbon-sulfur species, such as COS. Thus, drying and charring of coal would significantly increase the theoretical removal of sulfur by the slag.

These calculations assume gas-slag equilibrium with respect to sulfur. This is probably only approached at the gas-slag surface near the exit of the first stage. At the entrance end of the combustor, the conditions would probably be more oxidizing than conditions calculated from the overall combustion stoichiometry, ϕ , and thus sulfur solubility in the slag would be less than that calculated. At some depth below the slag surface near this entrance end of the first stage, the conditions would be more reducing than those calculated from the overall combustion stoichiometry. This would result in increased sulfur solubility. The actual combustion process and sulfur removal processes are quite complex, and the extent of sulfur removal will depend on the combustion kinetics. For example, consider two extreme situations. In one, where most coal is combusted after it hits the slagged wall, sulfur removal should be relatively good. In the other extreme, where all the coal is combusted before it reaches the slagged wall, sulfur removal would be relatively poor because it would be dependent on mass transport through the gas phase, and the gas has a relatively short residence time.

In summary, the kinetics of the combustion process is important with regard to sulfur removal. The kinetics must be considered either by modelling or experimentation before a final judgment on desulfurization in a slagging, cyclone combustor can be made. The results of this study show that it is theoretically possible.

V. CONCLUSIONS

Sulfide capacity measurements of relatively low melting (approximately 1100°C in most cases) slags based on the FeO-Al₂O₃-SiO₂, FeO-Na₂O-SiO₂, FeO-CaO-SiO₂, Na₂O-Al₂O₃-SiO₂, and CaO-Al₂O₃-SiO₂ systems but composed of coal ash + additives, have shown that the FeO-Al₂O₃-SiO₂-based slags had the highest sulfide capacities. For a given basicity, the sulfide capacities could be ranked in the following order: FeO-Al₂O₃-SiO₂ > FeO-CaO-SiO₂ > FeO-Na₂O-SiO₂ > CaO-Al₂O₃-SiO₂ > Na₂O-Al₂O₃-SiO₂. The chemical interaction of the basic oxides with silica appears to be a dominant factor controlling the sulfide capacity. There was good correlation between sulfide capacity and slag basicity, and sulfide capacities increased with temperature.

Calculations of the equilibrium sulfur removal for a commercial combustor using the measured sulfide capacities, showed that it was theoretically possible to remove 70% or more of the sulfur in coal. The sulfur removal increases with decreasing temperature, decreasing combustion stoichiometry in the first stage of the burner, increasing slag flow, and decreasing content of hydrogen in the fuel. This work showed that a slagging, cyclone combustor can remove sulfur into the slag, but kinetic modelling and/or experimentation is needed to prove whether or not the concept will work.

VI. ACKNOWLEDGEMENT

This work was sponsored by the U.S. Department of Energy under Contract No. DE-AC07-78CS40037, "Pulverized Coal Firing of Aluminum Melting Furnaces."

VII. REFERENCES

1. E. M. Levin, C. R. Robbins, and H. F. McMurdie: Phase Diagrams for Ceramists, American Ceramic Society, Columbus, OH (1964).
2. E. M. Levin, C. R. Robbins, and H. F. McMurdie: Phase Diagrams for Ceramists, 1969 Supplement, American Ceramic Society, Columbus, OH (1969).
3. E. M. Levin and H. F. McMurdie: Phase Diagram for Ceramists, 1975 Supplement, American Ceramic Society, Columbus, OH (1975).
4. R. S. Roth, T. Negas, and L. P. Cook: Phase Diagrams for Ceramists, Volume IV, American Ceramic Society, Columbus, OH (1981).
5. G. R. St. Pierre and J. Chipman: Trans. AIME, v. 206, pp. 1474-1483 (1956).
6. C.J.B. Fincham and F. D. Richardson: Proc. R. Soc. Series A223, 40 (1954) and J. Iron Steel Inst. 178, 4 (1954).
7. F. D. Richardson: Physical Chemistry of Melts in Metallurgy, v. 2, pp. 291-304, Academic Press, London (1974).
8. P. T. Carter and T. G. McFarlane: J. Iron Steel Inst., 185, 54 (1957).
9. K. P. Abraham, M. W. Davies, and F. D. Richardson: J. Iron Steel Inst., v. 196, pp. 309-312 (1960).
10. K. P. Abraham and F. D. Richardson: J. Iron Steel Inst., v. 196, pp. 313-317 (1960).
11. E. W. Dewing and F. D. Richardson: J. Iron Steel Inst., v. 194, pp. 446-450 (1960).
12. R. A. Sharma and F. D. Richardson: J. Iron Steel Inst., v. 198, pp. 386-390 (1961).
13. R. A. Sharma and F. D. Richardson: J. Iron Steel Inst., v. 200, pp. 373-379 (1962).
14. G.J.W. Kor and F. D. Richardson: J. Iron Steel Inst. v. 206, pp. 700-704 (1968).
15. G.J.W. Kor and F. D. Richardson: Trans. AIME, v. 245, pp. 319-327 (1969).
16. R. J. Hawkins, S. G. Meherali, and M. W. Davis: J. Iron Steel Inst., v. 209, pp. 646-657 (1971).
17. A. Bronson and G. R. St. Pierre, Met. Trans. B, v. 10B, pp. 375-380 (1979).
18. A. Bronson and G. R. St. Pierre: Met. Trans. B, v. 12B, pp. 729-731 (1981).
19. H. B. Bell: Can. Met. Quart., v. 20 (2), pp. 169-179 (1981).
20. J. D. Shim and S. Ban-ya: Tetsu-to-Hagane, v. 68, pp. 251-60 (1982).
21. S. D. Brown, R. J. Roxburgh, I. Ghita, and H. B. Bell: Ironmaking and Steelmaking, v. 9, pp. 163-67 (1982).
22. I. Ghita and H. B. Bell: Ironmaking and Steelmaking, v. 9, pp. 239-43 (1982).
23. W. E. Wahnstedler: "Chemical Equilibrium Package Users Manual," Alcoa Laboratories Report No. 7-78-25.
24. D. R. Gaskell: Metallurgical Treatises, J. K. Tien and J. F. Elliott, ed., p. 60, TMS-AIME, Warrendale, PA (1981).

TABLE I. ASH FROM LOVERIDGE SEAM (WEST VIRGINIA) COAL

Component	Wt Pct.	Ash Analysis
		Normalized (excluding sulfur and taking iron as FeO)
Al ₂ O ₃	18.4	24.1
SiO ₂	44.5	47.8
Fe ₂ O ₃	15.9	17.4 (FeO)
CaO	4.56	4.9
MgO	1.08	1.2
Na ₂ O	1.10	1.5
K ₂ O	1.11	1.3
TiO ₂	1.20	1.1
SO ₃	9.02	--
P ₂ O ₅	0.33	0.5

TABLE II. NORMALIZED COMPOSITIONS OF CANDIDATE SLAGS -
MAJOR COMPONENTS ONLY

Slag No.	Composition, Wt. Pct.					Liquidus Temperature (°C) (Major Components Only)
	SiO ₂	Al ₂ O ₃	FeO	Na ₂ O	CaO	
2-A-1	46.0	19.9	34.1			1205
2-A-2	40.0	12.0	48.0			1083
2-A-3	18.1	5.9	76.0			1148
2-A-7	43.3	19.8	36.9			1220
2-A-8	35.3	14.1	50.6			1200
2-A-9	27.0	8.3	64.4			1150
2-A-10	23.6	5.9	70.4			1155
2-B-1	39.3		48.0	12.7		1000
2-B-2	56.4		21.8	21.8		?
2-B-3	33.2		26.2	40.6		1050
DSE-1	42.5		28.9	28.6		900
DSE-2	37.0		26.0	37.0		
2-C-1	37.7		46.4		15.7	1093
2-D-1	43.8	18.2		37.9		915
2-D-2	62.7	23.2		14.0		1063
2-D-3	61.6	12.2		26.2		732
2-E-1	42.1	20.1			37.8	1265
2-I-1	55.3	21.5	10.0	13.1		990

TABLE III. ADDITIVE COMPOSITIONS FOR CANDIDATE SLAGS

Slag No.	Additive Mass g/g Ash	Additive Composition, Wt. Pct.				
		SiO ₂	Al ₂ O ₃	Fe ₂ O ₃	Na ₂ CO ₃	CaO
2-A-1	0.34	22.9		77.1		
2-A-2	1.20	27.0		73.0		
2-A-3	3.52	7.4		92.6		
2-A-4	3.74	7.0		87.2		5.8 % CaF ₂
2-A-5	3.52	1.6		92.6		5.8 % B ₂ O ₃
2-A-6	3.52	1.6		92.6		5.8 % P ₂ O ₅
2-A-7	0.36	13.9		86.1		
2-A-8	0.89	13.9		86.1		
2-A-9	2.19	13.9		86.1		
2-A-10	3.47	13.9		86.1		
2-A-10b	4.07	11.8		73.5		14.7 % MgO
2-A-11	3.49	7.5		86.7		3.4 % CaF ₂
2-A-12	4.99	13.9		86.1		
2-B-1	0.69			65.7	34.2	
2-B-2	0.30			3.9	96.1	
2-B-3	1.20			18.9	81.1	
DSE-1	0.69			24.2	75.8	
DSE-2	0.97			18.5	81.5	
2-C-1	0.61			75.5		24.5
2-D-1	0.93	10.9			89.1	
2-D-2	0.40	43.8			56.2	
2-D-3	1.60	46.3			53.7	
2-E-1	0.43	6.3				93.7
2-I-1	0.99	49.1	13.5		37.4	

TABLE IV. SULFIDE CAPACITY MEASUREMENTS

Exp't. No.	T (°C)	Run Time (h)	Slag Composition	Wt % S	Log C _S	Comments
2*	1100	24	DSE-1	4.22	-4.31	
			"	5.34	-4.21	
			2-B-1	6.05	-4.16	
			2-B-2	0.26	-5.52	
			2-D-1	0.96	-4.96	
			2-D-2	0.87	-5.00	Did not melt
4**	1100	115	2-D-3	0.69	-5.10	
			DSE-1	4.31	-4.06	
			2-A-1	4.80	-4.01	
			2-A-2			Sample crept out
			2-A-3	22.5	-3.34	2 phases
			2-A-4	23.5	-3.32	2 phases
5**	1100	144.6	2-C-1	7.91	-3.79	
			2-A-5	20.2	-3.38	2 phases
			2-A-6	13.4	-3.56	2 phases
			2-A-7	5.06	-3.99	
			2-A-8	9.81	-3.70	
			2-A-9	16.6	-3.47	2 phases
			2-A-10	19.1	-3.41	2 phases
			2-A-11			Sample crept out
			2-B-3	2.65	-4.27	
7***	1000	168.75	2-A-3	25.4		Did not melt
			2-A-4	25.1		" " "
			2-A-5	25.5		" " "
			2-A-6	24.1		" " "
			2-A-10	23.6		" " "
			2-A-11	24.2		" " "
			2-A-12	25.8		" " "
			2-A-3a	26.3		" " "
			2-I-1	0.44	-5.04	
11****	1300	70.0	2-A-3	2.67	-2.86	
			2-A-10	1.97	-3.00	
			2-A-10b	3.10	-2.80	

* Gas Composition - 70%CO-29.5% CO₂-0.5%SO₂

$$X_{O_2} = 7.2 \times 10^{-14}, X_{S_2} = 5.4 \times 10^{-4}$$

** Gas Composition - 70.2%CO-29.6%CO₂-0.25%SO₂

$$X_{O_2} = 6.8 \times 10^{-14}, X_{S_2} = 1.6 \times 10^{-4}$$

*** Gas Composition - 74.5%CO-25.3%CO₂-0.18%SO₂

$$X_{O_2} = 6.8 \times 10^{-14}, X_{S_2} = 1.6 \times 10^{-4}$$

**** Gas Composition - 66.3%CO-33.6%CO₂-0.14%SO₂

$$X_{O_2} = 4.9 \times 10^{-11}, X_{S_2} = 1.9 \times 10^{-4}$$

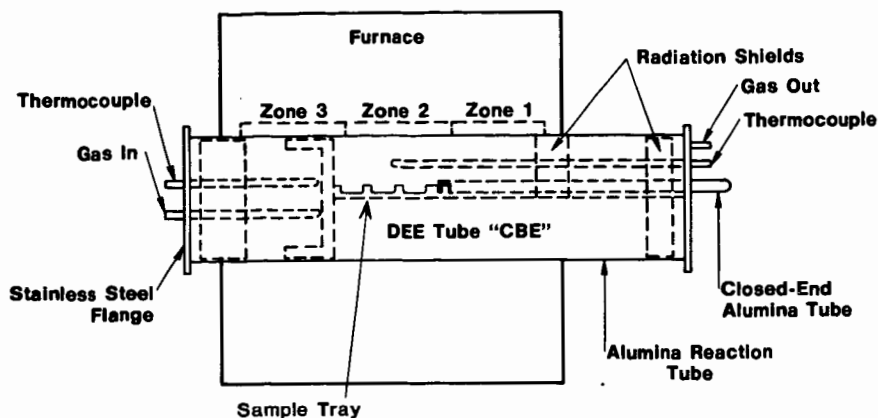


FIGURE 1. REACTOR USED FOR SULFIDE CAPACITY MEASUREMENTS.

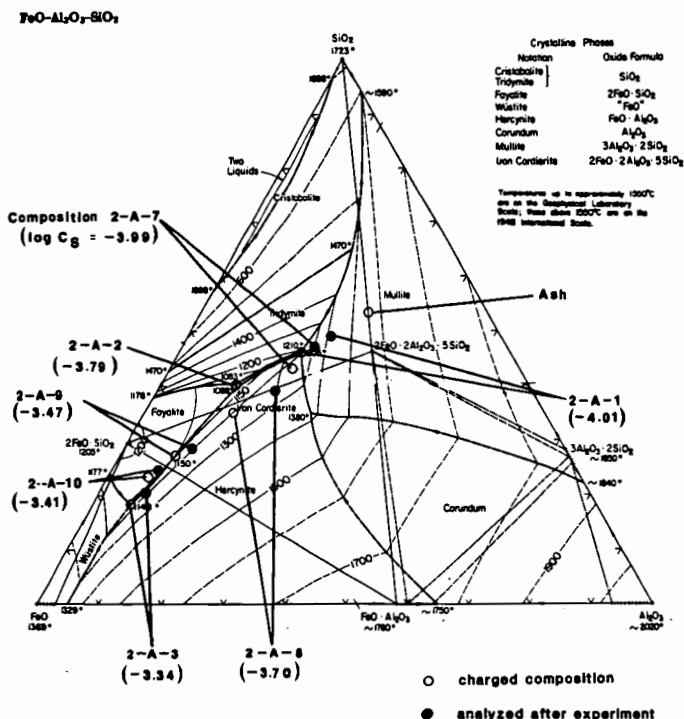


FIGURE 2. THE $\text{FeO}-\text{Al}_2\text{O}_3-\text{SiO}_2$ SYSTEM (2-A) WITH MEASURED SULFIDE CAPACITIES INDICATED. PHASE DIAGRAMS TAKEN FROM REFERENCE (1). OXIDE PHASES IN EQUILIBRIUM WITH METALLIC IRON.

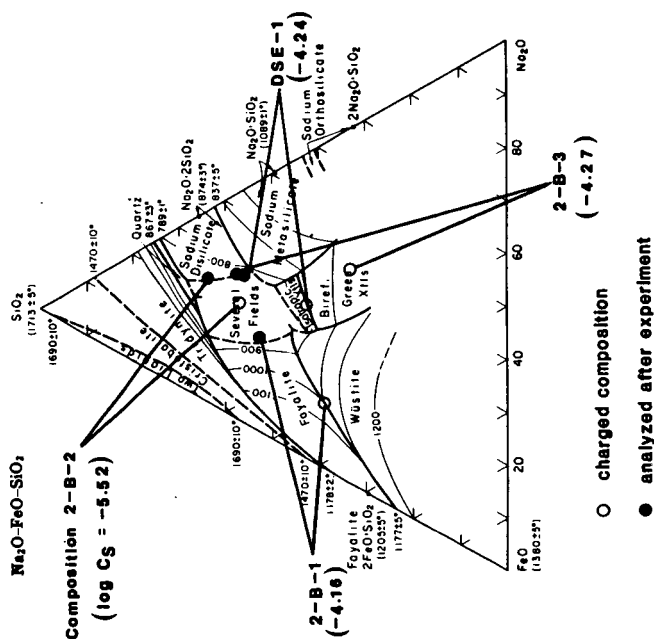


FIGURE 3. THE $\text{FeO-Na}_2\text{O-SiO}_2$ SYSTEM (2-B) WITH MEASURED SULFIDE CAPACITIES INDICATED. PHASE DIAGRAM TAKEN FROM REFERENCE (2). OXIDE PHASES IN EQUILIBRIUM WITH METALLIC IRON.

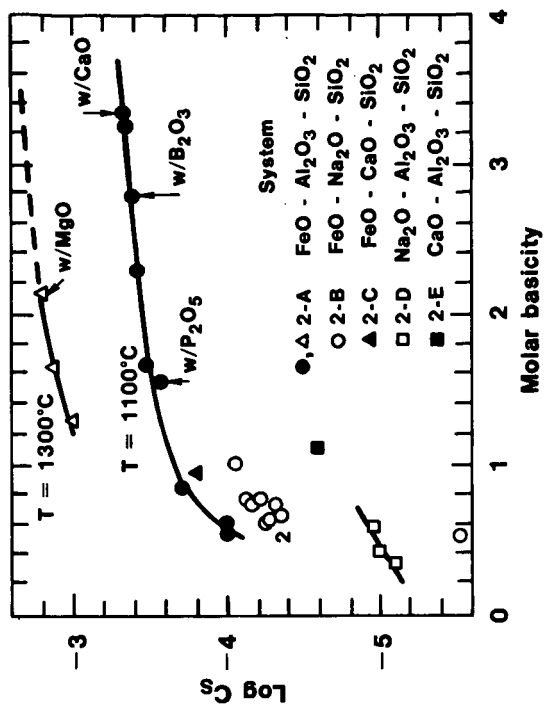


FIGURE 4. MEASURED SULFIDE CAPACITIES OF CANDIDATE SLAGS. BASICITY CALCULATED FROM CHEMICAL ANALYSES. POINTS DENOTED BY w/P₂O₅ AND w/B₂O₃ REPRESENT SLAGS IN WHICH 5% SiO₂ WAS REPLACED BY 5% OF THESE OXIDES. POINT DENOTED BY w/CaO IS FOR SLAG TO WHICH 5% CaF₂ WAS ADDED, BUT ALL FLUORINE WAS LOST DURING EXPERIMENT. POINT DENOTED BY w/MgO FOR SLAG TO WHICH 12% MgO WAS ADDED.

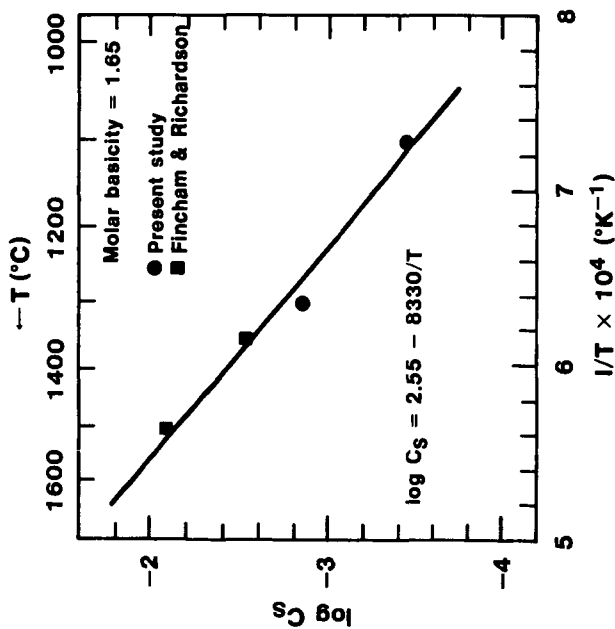


FIGURE 5. COMPARISON OF RESULTS FROM THIS STUDY TO THOSE OF FINCHAM AND RICHARDSON (6) FOR AN IRON SILICATE WITH MOLAR BASICITY OF 1.65. DATA FROM FINCHAM AND RICHARDSON WERE FOR PURE IRON SILICATES WHILE THESE FROM THE PRESENT STUDY CONTAINED SOME COAL ASH. DATA FROM FINCHAM AND RICHARDSON WERE CORRECTED FOR BASICITY USING DATA FROM THE PRESENT STUDY.

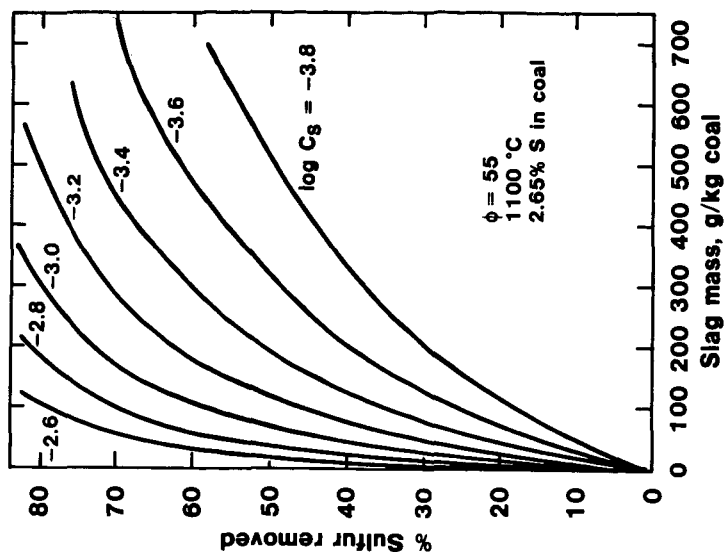


FIGURE 6. EQUILIBRIUM SULFUR REMOVAL BY SLAG FOR A COMBUSTOR OPERATING WITH LOVERIDGE SEAM (WEST VIRGINIA) COAL.

The Thermodynamic Properties of Molten Slags

Milton Blander* and Arthur D. Pelton†

INTRODUCTION

Silica based slag systems are highly ordered liquids which have been a difficult class of materials on which to perform thermodynamic analyses.¹⁻⁵ To our knowledge, no satisfactory, self-consistent prior method of analysis has been developed for systems as ordered and complex as silicates which incorporates all known data in a meaningful way. In this paper, we discuss the results of a method of analysis which permits one to simultaneously analyze a large amount of different types of data on binary systems. The calculations lead to a small set of parameters which permit one to calculate the thermodynamic properties of slag solutions as a function of temperature and composition. The thermodynamic self-consistency and the form of the equations used provide some confidence in the use of the results for interpolations and extrapolations outside the range of data. In addition, for systems in which silica is the only acid constituent, we propose a theoretically justified combining rule to calculate the properties of ternary systems based solely on data for the three subsidiary binaries. The results are in good agreement with available data.

The ionic nature of molten silicates suggests that many of the theories and correlations developed for molten salts⁶ can be applied to the development of correlations between the relative magnitudes of the deviations from ideal solution behavior in terms of ionic radii, charges, polarizabilities, dispersion interactions and ligand field effects.

CALCULATIONAL METHOD⁷

The molar free energy of mixing, ΔG_m of a silicate is represented by the expression

$$\Delta G_m = \sum_i RTX_i \ln X_i + \sum_i RTX_i \ln \gamma_i = \Delta G_m^{ideal} + \Delta G^E \quad (1)$$

where X_i is the mole fraction of component i , γ_i , the activity coefficient, represents deviations from ideal solution behavior of component i , ΔG_m^{ideal} is the molar free energy of mixing of a hypothetical ideal solution and ΔG^E is the molar excess free energy of mixing which represents the deviations from ideality of the molar free energy of solution. The conventional representation of $\ln \gamma_i$ and ΔG^E is a power series in mole fractions. The complexity of ordered solutions would require a very long power series in order to obtain a reasonable representation of their properties. This arises from the tendency of such solutions to have a "V" shaped dependence of the enthalpy of mixing and an "m" shaped dependence of the entropy of mixing on concentration.¹ The fitting of data using a long polynomial will generally be poor and ambiguous in such systems. In order to obtain reasonable fits, one must use equations which inherently have the concentration and temperature dependence of ordered solutions built in.

We have deduced a set of equations with such properties based on empirical modifications of the quasi-chemical theory. An energy parameter in the theory, W , is represented by a power series

*Argonne National Laboratory, Argonne, IL 60439

†Ecole Polytechnique, Université de Montréal, Montréal, Québec, Canada, H3C3A7

$$W = \sum_{j=0} C_j y^j \quad (2)$$

where y is an equivalent fraction of one of the components (silica is always chosen if present). For binary systems, the parameters C_j are deduced from a complex optimization procedure which performs a global and simultaneous analysis of all thermodynamic data on a system. This includes liquidus phase diagrams, activity data, data on miscibility gaps, enthalpies of fusion, free energies of formation of compounds, etc. The small set of resultant parameters (seven at most including temperature coefficients of some) are then used to recalculate the input data to double check the accuracy of the curve fitting procedure and the efficacy of the use of the equations for representing the data. The results were generally very good.

For multicomponent systems, we developed an asymmetric combining rule such that *e.g.* for a system 1-2-3 where 1 is silica, W_{12} and W_{13} which represent energies related to interactions of silica with the other two components, are a function only of y_1 , and W_{23} is related to the ratio $y_3/(y_2 + y_3)$. A partial theoretical justification for such a method can be based on theories for ternary systems.⁸

RESULTS OF THERMODYNAMIC ANALYSES

We have performed analyses of ten of the fifteen binary systems and six of the twenty ternary systems containing the components MgO, FeO, CaO, Na₂O, Al₂O₃, and SiO₂.^{7,9}

Table I
Systems Which Have Been Analyzed

<u>Binary Systems</u>		<u>Ternary Systems</u>
CaO-SiO ₂	CaO-AlO _{1.5}	CaO-AlO _{1.5} -SiO ₂
FeO-SiO ₂	NaO _{0.5} -AlO _{1.5}	NaO _{0.5} -CaO-SiO ₂
MgO-SiO ₂	MgO-FeO	NaO _{0.5} -AlO _{1.5} -SiO ₂
NaO _{0.5} -SiO ₂	MgO-CaO	CaO-FeO-SiO ₂
AlO _{0.5} -SiO ₂	CaO-FeO	CaO-MgO-SiO ₂
		MgO-FeO-SiO ₂

We illustrate our calculations for one ternary system below. The analysis of the three binary subsystems and the ternary system CaO-FeO-SiO₂ was performed using as input the liquidus phase diagram,¹⁰ activities of CaO,¹¹ and SiO₂,¹² the free energies of formation of CaSiO₃ and Ca₂SiO₄,¹³ and the miscibility gap¹⁴ in the CaO-SiO₂ system, measured activities of FeO in the CaO-FeO system,¹⁵ and the activities of FeO,^{16,17,18} the phase diagram¹⁹ and the free energy of formation of Fe₂SiO₄²³ in the FeO-SiO₂ system. To illustrate some of the results, we exhibit (1) the calculated phase diagram of the FeO-SiO₂ system in Fig. 1 along with measured values of the invariant points and (2) a comparison of activities of "FeO" measured in the iron saturated molten FeO-SiO₂ system with calculated values in Fig. 2.

Using our "asymmetric" combining rules, the data for the binary systems were combined and led to the results for ternary systems given in Fig. 3; this figure illustrates the correspondence between calculated and measured values²⁰ of the activities of FeO in the CaO-FeO-SiO₂ system. The differences are well within the uncertainties in the measurements. We find that this method essentially permits us to make predictions in ternary systems based solely on data for the three

subsidiary binary systems for cases in which silica is the only acid component. When alumina and silica are both present, a more complex representation is necessary.

The good correspondence of calculations with the complex concentration dependence of activities in the CaO-FeO-SiO₂ system illustrates the fact that our equations properly take into account the kinds of ternary interaction terms known to exist in such systems.^{8,21} This feature lends confidence in the use of our equations for predictions in multicomponent systems (containing only silica as an acid component) based solely upon the subsidiary binaries. If, as it appears, this is generally true, our method provides an important predictive capability.

CORRELATIONS OF PROPERTIES

Theories and concepts which have been developed for molten salt solutions can be used to correlate the thermodynamic properties of silicates.⁶ Coulomb interactions lead to a dependence of thermodynamic functions on the inverse of the cation-anion interatomic distance. Thus, by analogy with molten salts, one would expect a linear dependence of the magnitudes of free energies of mixing on this parameter which is in a direction such that negative deviations from ideality increase in the order Li⁺, Na⁺, K⁺, Rb⁺, Cs⁺, and Mg⁺⁺, Ca⁺⁺, Sr⁺⁺, and Ba⁺⁺. In addition, monovalent alkali oxides should exhibit more negative deviations from ideality than divalent alkaline earth oxides. The polarizability of oxide anions leads to an additional contribution with a similar dependence on cations. The magnitude of cation-cation dispersion interactions are related to the polarizabilities, ionization potentials and interaction distances. Thus, the dissolution of oxides of cations with large dispersion interactions leads to a loss of this negative energy and hence to a positive contribution to deviations from ideality. In addition ligand field effects for divalent transition metals tend to contribute to negative deviations from ideal solution behavior in molten salts with monovalent cations. The effective charge of Si is greater than two and one would thus expect a positive contribution to deviations from ideal solution behavior from this source. The effect for Mn²⁺ which has a half filled shell for example, should be much less positive than for Fe²⁺.

The data for testing these influences on solution behavior are too sparse to reach quantitative conclusions. However, the general trends are in the right direction. Measured deviations from ideality of silicates with divalent oxides become more negative (or less positive) in the order Fe²⁺, Mn²⁺, Pb²⁺, Mg²⁺, Ca²⁺.^{1,7,9,22} In this view, ligand field effects lead to Fe²⁺ preceding Mn²⁺ and Mn²⁺ preceding even Mg²⁺ which has a smaller radius; dispersion interactions lead to Pb²⁺ preceding even Mg²⁺ even though its radius is larger than Ca²⁺ and Sr²⁺; finally, coulomb and polarization interactions lead to Mg²⁺ preceding Ca²⁺. With careful measurements of a larger number of binary silicate systems, it should be possible to develop useful correlations and a means of making reasonable predictions of the magnitudes of thermodynamic properties of silicates.

CONCLUSIONS

There are several significant conclusions which can be reached.

1. We have performed analyses of thermodynamic data on binary silicate systems which lead to a unique and accurate mathematical representation of their known properties.
2. Our use of equations which have the properties of ordered liquids built in appears to have the innate capability for representing a mass of different types of data on binary systems measured in various ranges of temperature and composition. This result lends confidence in the use of our analyses for interpolations and extrapolations outside the range of measurements.

3. We can theoretically justify an "asymmetric" combining rule which, for cases in which silica is the only acid component, leads to *a priori* predictions for ternary systems based on data for the three subsidiary binaries. It appears likely that such predictions would be valid for multicomponent systems.
4. A preliminary examination of thermodynamic data on silicates indicates that correlations developed for molten salts may be useful in understanding and ultimately in predicting magnitudes of the thermodynamic solution properties of silicates.

FIGURE CAPTIONS

1. Calculated phase diagram of the FeO-SiO₂ system. Numbers in parentheses are measured values from Muan and Osborne¹⁰ and Robie, et al.¹³
2. Activities of "FeO" measured in iron saturated molten FeO-SiO₂ at 1325°C (Δ)¹⁷, 1785°C (O)¹⁶, 1880°C (\diamond)¹⁶, and 1960°C (\square)¹⁶. The two solid lines represent calculated points at 1325°C and 1880°C. The filled circles along one solid line represent individual calculated points and the three filled circles labeled 1960, 1880, and 1785 represent calculated points at three temperatures and fixed composition which illustrate the calculated temperature dependence.
3. Activities of FeO in iron saturated CaO-FeO-SiO₂ at 1550°C. Dashed lines are from Timucin and Morris²⁰ and the solid lines represent our calculations.

REFERENCES

1. P. L. Lin and A. D. Pelton, *Metall. Trans.* **10B**, 667-676 (R1979).
2. C. R. Masson, I. B. Smith, and S. G. Whiteway, *Can. J. Chem.* **48**, 1456-1464 (1977); *Proc. 11th International Congress on Glass*, J. Gotz, Ed., Vol. 1, pp. 3-41, Prague (1977).
3. D. R. Gaskell, *Metall. Trans.* **8B**, 131-145 (1977).
4. C. J. B. Fincham and F. D. Richardson, *Proc. Roy. Soc.* **223**, 40 (1954).
5. G. W. Toop and C. S. Samis, *Trans. TMS-AIME* **224**, 878-887 (1962).
6. M. Blander, "Thermodynamic Properties of Molten Salt Solutions," *Molten Salt Chemistry*, M. Blander, Ed., Interscience, N.Y., pp. 127-237 (1964).
7. M. Blander and A. D. Pelton, Computer Assisted Analyses of the Thermodynamic Properties of Slags in Coal Combustion Systems, ANL/FE-83-19, Argonne National Laboratory, Argonne, IL (1983) Available from NTIS, U.S. Dept. of Commerce, Washington, D.C.
8. M.-L. Saboungi and M. Blander, *J. Chem. Phys.*, **63**, 212-220 (1975); *J. Amer. Ceram. Soc.* **58**, 1-7 (1975).
9. A. D. Pelton and M. Blander, in preparation.
10. A. Muan and E. F. Osborne, Phase Equilibria Among Oxides in Steelmaking, Addison-Wesley Publishing Co., Reading, Mass. (1965).
11. R. A. Sharma and F. D. Richardson, *J. Iron Steel Inst.* **200**, 373 (1962); **198**, 308 (1961).
12. R. H. Rein and J. Chipman, *Trans. AIME* **233**, 415-425 (1965).
13. R. A. Robie, B. S. Hemingway, and J. R. Fisher, Thermodynamic Properties of Minerals and Related Substances at 298.15 K and 1 Bar Pressure and at Higher Temperatures, Geologic Survey Bulletin 1452, U.S. Govt. Printing Office, Washington, D.C. (1978).
14. Ya. I. Ol'shanskii, *Dokl. Akad. Nauk. SSR* **76**, 94 (1951); J. D. Tewhey and P. C. Hess, *Phys. Chem. Glasses*, **20**, 41-53 (1979).
15. J. F. Elliott, *Trans. AIME*, **203**, 485 (1955).
16. P. A. Distin, S. G. Whiteway, and C. R. Masson, *Can. Met. Quart.*, **10**, 73(1971).
17. R. Schuhmann and P. Ensio, *J. Metals*, **3**, 401 (1951).
18. C. Bodsworth, *J. Iron and Steel Inst., London*, **193**, 13 (1959).
19. E. M. Levin, C. R. Robbins, and H. F. McMurdie, Phase Diagrams for Ceramists, Am. Ceram. Soc., Columbus, Ohio (1964); Supplement, (1969); E. M. Levin and H. F. McMurdie, Supplement (1975).
20. M. Timucin and A. E. Morris, *Met. Trans.*, **1**, 19 (1970).
21. M. Blander, "Some Fundamental Concepts in the Chemistry of Molten Salts" in Molten Salts, G. Mamantov, ed., Marcel Dekker, New York (1969).
22. H. Gaye and P. Riboud, Données Experimentales sur les Activités des Constituants de Laitiers, IRSID PCM-RE 337, St. Germain-en-Laye, France (1976).

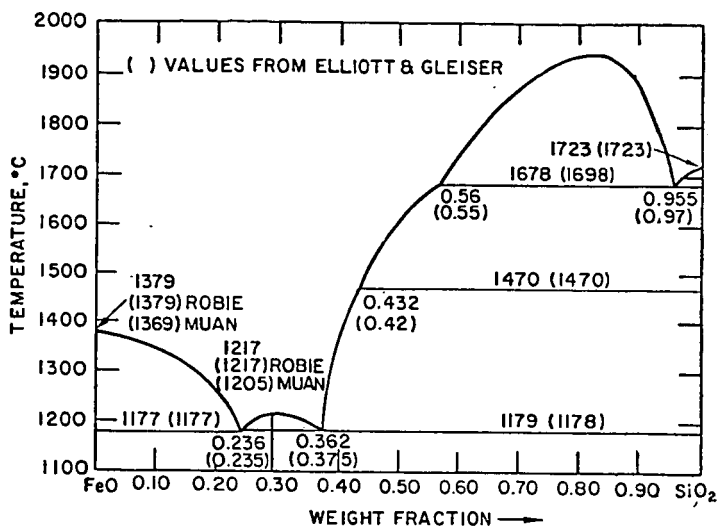


Fig. 1

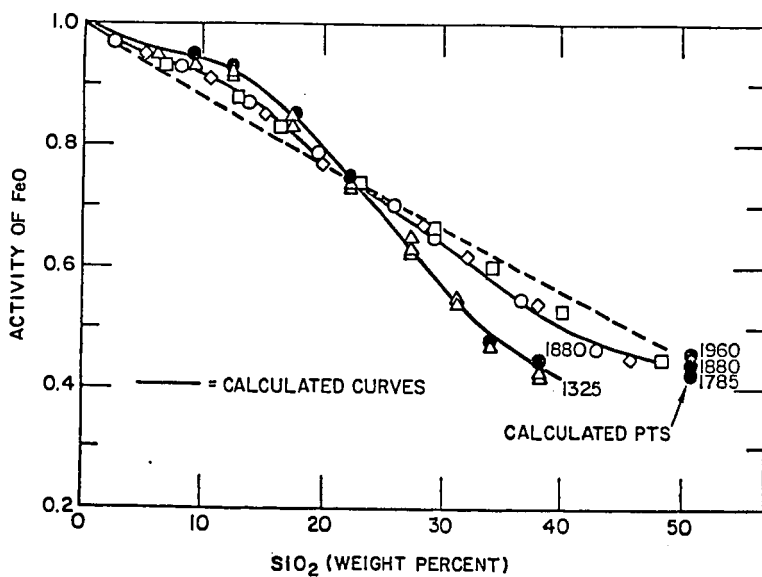


Fig. 2

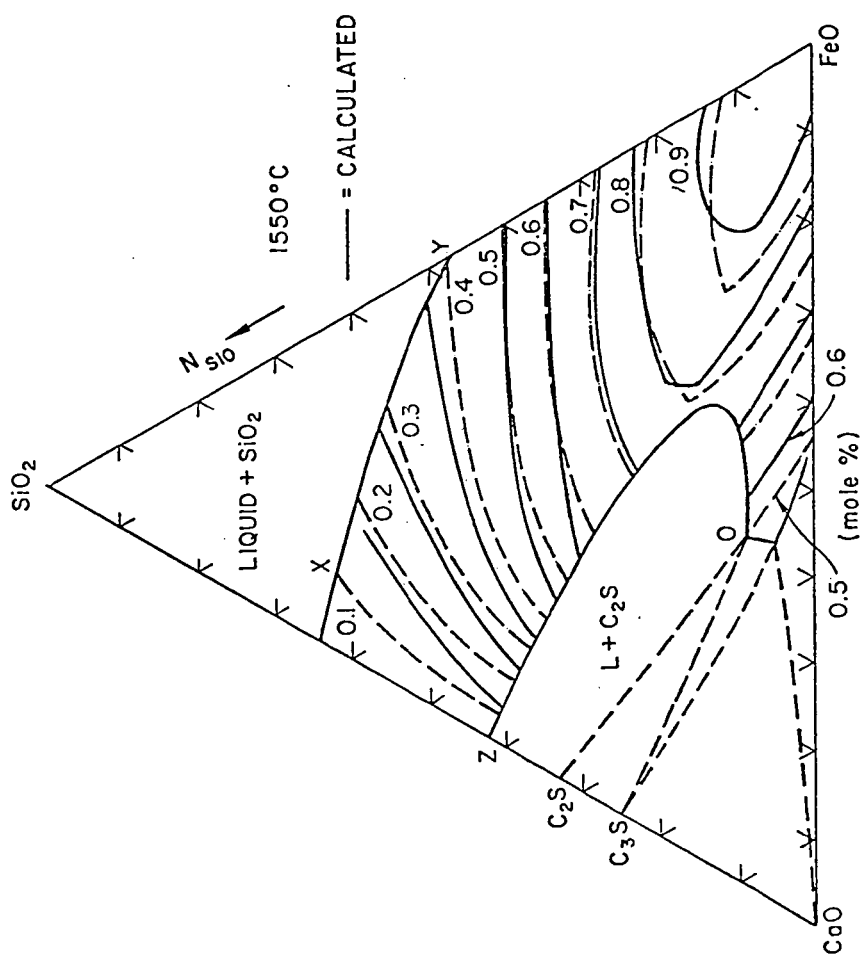


Fig. 3

ESTIMATION OF PHYSICO-CHEMICAL PROPERTIES OF COAL SLAGS AND ASHES

K C MILLS

National Physical Laboratory, Teddington, Middx, TW11 0LW, UK.

1. INTRODUCTION.

Slags formed during the gasification of coal usually contain SiO_2 , Al_2O_3 , iron oxides, CaO , Na_2O and K_2O with minor amounts of various other oxides. A knowledge of the physico-chemical properties of these slags can improve the control of the process eg. the amount of flux required to bring the slag viscosity to a level suitable for tapping can be calculated from viscosity-composition relations. Physical property data for the coal slags can also improve process design by the development of reliable mathematical models of the process eg. thermal properties of the slags are needed for heat balance calculations. There is an appreciable variation in the compositions of slags formed from various coals and even from different batches of the same stock on occasions and these compositional variations can give rise to considerable differences in the physical properties. As the chemical analysis is frequently available on a routine basis it would be particularly desirable to have reliable models for the prediction of physico-chemical properties from their chemical composition. Furthermore such models would have the further advantage that they would eliminate the need for arduous interpolations on pseudo-ternary plots for slags which are really multicomponent and interactive systems.

The properties of slags are dependent not only upon chemical composition, but upon other factors also. The most pronounced deviations from additivity rules based on composition arise in the estimation of those properties which involve ionic transport such as electrical conductivity. However surface tension values estimated from additivity rules are frequently in error as bulk thermodynamic properties do not apply at surfaces. Furthermore, virtually all the physical properties of slags are, to some extent, dependent upon the structure of the slag (viz. the length of silicate chains, degree of crystallinity etc.) thus estimation procedures have to accommodate these structural factors, where possible.

There is only a limited amount of physical property data available for coal slags and consequently it has been necessary to examine a much broader range of silicates including magmatic liquids and those slags encountered in steelmaking, glassmaking and non-ferrous processes. Thus the models cited here should have a much wider range of application than coal gasification.

A critical evaluation of the extant physical property data has shown that virtually every physical property is markedly dependent upon the distribution of iron in the slag between FeO , Fe_2O_3 and free iron. Frequently these distributions are not reported and they can not be easily predicted as they are very dependent upon (i) the partial pressure of oxygen, p_{O_2} (ii) temperature, T and (iii) the nature of the other oxides present, eg CaO , Na_2O and K_2O . Increase the amount of Fe_2O_3 and SiO_2 increases the amount of FeO present. Even when the iron distributions are cited they are vulnerable to error owing to difficulties in chemical analysis and the possibility of some redistribution of the $\text{Fe}^{2+}/\text{Fe}^{3+}$ ratios during the quench. Nevertheless it is strongly recommended that all future physical property determinations on coal slags should be accompanied by chemical analysis for $\text{Fe}(\text{free})$, FeO and Fe_2O_3 on the quenched specimen as the surface tension, absorption coefficient, melting range etc. fluctuate dramatically with the iron distribution.

2. MODELS FOR ESTIMATING PHYSICO-CHEMICAL PROPERTIES.

2.1 Melting Range

Empirical rules have been formulated⁽⁴⁻⁶⁾ for the estimation of melting range on the basis of the basicity of the slag or ash. However the various constants used in the calculations are applicable to very narrow compositional ranges and thus a large number of constants are required to represent the slags formed from different coals.

A more universal approach has been adopted recently by Gaye^(7,8) who expressed, the dependency of liquidus temperature, T_{liq} , upon chemical composition as polynomial for each of the phases (or compounds^{11g}) formed by the slag. The maximum calculated value of T_{liq} value for the various phases is the T_{liq} value. Good agreement was obtained between the calculated and experimental values for T_{liq} for the $SiO_2 + Al_2O_3 + MgO + FeO$ and the $SiO_2 + Al_2O_3 + MgO + CaO$ systems. However development of this model to cover the multicomponent coal slags could prove difficult.

A second model due to Gaye⁽⁹⁾ would appear to offer more promise; it is based on the Kapoor-Frohberg model for the estimation of activities and assumes that both acidic and basic oxides are made up of symmetrical cells and that these interact to form assymetrical cells. The activities of the various oxides calculated for quaternary slags with this model are in excellent agreement with those determined experimentally. Values of T_{liq} for a given composition can be derived by determining the temperature at which the solid phase formed has an activity of one. The model has been developed for systems based on seven components, SiO_2 , Al_2O_3 , CaO , MgO , FeO , Fe_2O_3 and MnO . The model will have to be enlarged to include Na_2O etc. before it can be used for the reliable estimation of T_{liq} of coal slags² but it would seem to have considerable promise and has the decided advantage that it also produces activity data for the various component oxides.

2.2 Viscosity (η)

Several models have been reported for the estimation of viscosities (η) of silicate melts to cover the compositional ranges of glasses^(10,11) steelmaking slags⁽¹²⁻¹⁴⁾, magmas⁽¹⁵⁻¹⁸⁾ and coal slags and ashes⁽¹⁹⁻²⁴⁾. The temperature (T) dependence of the viscosity is expressed in the form of the Arrhenius relationship (equation 1)) or the Frenkel relationship (equation 2) which is sometimes known as the Weymann equation) where A and B are constants, E is the activation energy and R is the Gas Constant.

$$\eta = A \exp. (E/RT) \quad 1)$$

$$\eta = AT \exp.(E/RT) \quad 2)$$

Estimated viscosities have been calculated using these various models and the closest agreement with experimental values was obtained with the models due to Riboud et al⁽¹³⁾ and Urbain et al^(17,18). These estimation procedures use the Frenkel relationship and thus their superiority may be largely due to the use of equation 2). The model due to Schobert which involves petrographic classification of the coal slag has not been checked and this procedure may provide reliable estimates of viscosity for coal slags but could not be applied to slags covering a wide range of composition. Thus effort in the present study was focussed predominantly on the Riboud and Urbain models.

Model due to Riboud et al⁽¹³⁾

The slag constituents are classified in five different categories in this model. The mole fractions (x) for those categories being given by

$$(i) \quad x("SiO_2") = x(SiO_2) + x(PO_2) + x(TiO_2) + x(ZrO_2)$$

$$(ii) \quad x("CaO") = x(CaO) + x(MgO) + x(FeO) + x(FeO_{1.5})$$

$$(iii) \quad x(Al_2O_3)$$

$$(iv) \quad x(CaF_2) \text{ and}$$

$$(v) \quad x("Na_2O") = x(Na_2O) + x(K_2O).$$

The parameters A and B of equation 2) are calculated from the mole fraction of the five categories by using equations 3) and 4).

$$A = \exp(-19.81 + 1.73x("CaO") + 5.82x(CaF_2) + 7.02x(Na_2O) - 33.76x(Al_2O_3)) \quad 3)$$

$$B = +31140 - 23896x("CaO") - 46356x(CaF_2) - 39159x("Na_2O") + 68833x(Al_2O_3) \quad 4)$$

Subsequently, from the values of A and B it is possible to calculate the viscosity for the temperatures in question by use of equation 2).

Model due to Urbain et al⁽¹⁸⁾

In this model the parameters A and B are calculated by dividing the slag constituents into three categories (i) "glass formers", $x_G = x(SiO_2) + x(P_2O_5)$ (ii) "modifiers", $x_M = (CaO) + x(MgO) + x(Na_2O) + x(K_2O) + 3x(CaF_2) + x(FeO) + x(MnO) + 2x(TiO_2) + 2x(ZrO_2)$ (iii) "amphoterics", $x_A = x(Al_2O_3) + x(Fe_2O_3) + x(B_2O_3)$.

However we consider that Fe_2O_3 behaves more like a modifier than an amphoteric and in our revised programme $1.5 x(FeO_{1.5})$ has been added to x_M and $x(Fe_2O_3)$ deducted from x_A . "Normalized" values x_G^* and x_M^* and x_A^* are obtained by dividing the mole fractions, x_G , x_M and x_A by the term $(1 + 2x(CaF_2) + 0.5 x(FeO_{1.5}) + x(TiO_2) + x(ZrO_2))$. Urbain proposed that the parameter B was influenced both by the ratio, $\theta = [x_M^*/(x_M^* + x_A^*)]$ and by x_G^* . The parameter B can be expressed in the form of equation (5) where B_1 , B_2 and B_3 can be obtained by equation (6).

$$B = B_0 + B_1 x_G^* + B_2 (x_G^*)^2 + B_3 (x_G^*)^3 \quad 5)$$

$$B_i = a_i + b_i \theta + c_i \theta^2 \quad 6)$$

B_0 , B_1 , B_2 and B_3 can be calculated from the equations listed in Table 1 and these parameters are then introduced into equation 5) to calculate B. The parameter A can be calculated from B by equation 7) and the viscosity of the slag (in PaS) can then be determined using equation 8).

$$- \ln A = 0.2693 B + 11.6725 \quad 7)$$

$$\eta = 0.1 [AT \exp(10^3 B/T)] \quad 8)$$

TABLE 1

B_0	$= 13.8 + 39.9355 \theta - 44.049 \theta^2$
B_1	$= 30.481 - 117.1505 \theta + 129.9978 \theta^2$
B_2	$= -40.9429 + 234.0486 \theta - 300.04 \theta^2$
B_3	$= 60.7619 - 153.9276 \theta + 211.1616 \theta^2$

Modifications to the Urbain model

Urbain⁽¹⁸⁾ has recently modified the model to calculate separate B values for different individual modifiers, CaO, MgO and MnO. The global B value for a slag containing all three oxides can be derived using equation 9)

$$B(\text{global}) = \frac{x(\text{CaO})B(\text{CaO}) + x(\text{MgO})B(\text{MgO}) + x(\text{MnO})B(\text{MnO})}{x(\text{CaO}) + x(\text{MgO}) + x(\text{MnO})} \quad 9)$$

Assessment of the viscosity models

These two models have been used to calculate the viscosities of slags with widely-varying compositions and it has been found that both give values which agree well with experiment.

The model of Urbain gives a slightly better fit than the Riboud model. The discrepancies between the experimental values and the predicted values are of the order of $\pm 30\%$ which are of similar magnitude to the experimental uncertainties for viscosity measurements.

2.3 Density (ρ)

Recently Keene⁽²⁵⁾ has reported that the density at 1673K of molten slags can be obtained within $\pm 5\%$ using the equation 10)

$$\rho / \text{gcm}^{-3} = 2.46 + 8.018 (\% \text{FeO} + \% \text{Fe}_2\text{O}_3 + \% \text{MnO} + \% \text{NiO}) \quad 10)$$

An additive method for the estimation of densities (ρ) in slags has been widely used for some time^(26,27). In this method, the molar volume, V , can be obtained from equations 11) and 12) below, where M , x and \bar{V} are the molecular weight, mole fraction and the partial molar volume, respectively, and 1, 2 and 3 denote the various oxide constituents of the slag.

$$V = M_1x_1 + M_2x_2 + M_3x_3 \quad 11)$$

$$V = x_1\bar{V}_1 + x_2\bar{V}_2 + x_3\bar{V}_3 \quad 12)$$

The partial molar volume is usually assumed to be equal to the molar volume of the pure component (V^0). Bottinga and Weill⁽²⁸⁾ produced a series of values of \bar{V} for various oxides assuming a constant value for $\bar{V}(\text{SiO}_2)$ and it was claimed that good estimations of the density could be obtained for compositions containing between 40 and 80% SiO_2 . Two more recent studies^(29,30) also concluded that $\bar{V}(\text{SiO}_2)$ was independent of composition and have revised the \bar{V} values for the various oxides. However it has been pointed out^(31,32) that the density of the slag is also related to its structure. Silicate slags contain a mixture of chains, rings and basic silicate units, which are dependent upon the silica concentration and upon the nature of the cations present. Thus the densities of silicate slags estimated using a constant value for $\bar{V}(\text{SiO}_2)$ will be subject to error as the arrangement of these silicate chains varies with silica concentration.

Furthermore Grau and Masson⁽³¹⁾ pointed out that for the series $M_2\text{O}$, $M_2\text{SiO}_2$ the partial molar volume of SiO_2 is not constant. They calculated a $\Delta\bar{V}$ term for the differences between any two members of the series and in this way calculated values were derived for the systems $\text{FeO} + \text{SiO}_2$, $\text{PbO} + \text{SiO}_2$, $\text{FeO} + \text{MnO} + \text{SiO}_2$ and $\text{FeO} + \text{CaO} + \text{SiO}_2$ for compositions in the range $x_{\text{SiO}_2} = 0.5$ to 1.0. However this method is not suitable for calculating densities of multicomponent systems.

Very recently, Bottinga et al⁽³³⁾ have presented a model in which the partial molar volumes of alumina-silicate liquids were considered to be composition-dependent.

New model for calculating the densities of slags

Slags containing SiO_2 , Al_2O_3 and P_2O_5 consist of chains, rings and complexes which are dependent upon the amount and nature of the cations present. Thus it is necessary to make the partial molar volumes dependent upon composition for oxides of this type. If in a binary system, equation 12) were applicable and if $\bar{V}_1 = \bar{V}_1^0$ ie. \bar{V} is independent of composition, then the curve of V as a function of composition will be that shown by the solid line in Figure 1a and the two $x_1\bar{V}_1$ contributions by the dotted lines. If we now consider a binary silicate system the molar volume (V) would have the form shown as a solid line in Figure 1b. It is reasonable to assume that $\bar{V}(\text{M.O})$ is independent of composition and would have the form of $x_1\bar{V}_1$ in Figure 1b. The parameter $x_2\bar{V}_2$ can be derived for SiO_2 by use of equation 13) below.

$$x_2\bar{V}_2 = V - x_1\bar{V}_1 \quad 13)$$

Thus $x_2\bar{V}_2$ will have the form of the curve shown in Figure 1b.

It is possible to derive $x\bar{V}$ for SiO_2 in ternary and quaternary slags by using equation 14). Values for $x\bar{V}$ (SiO_2) have been derived using experimental density data for the systems, $\text{FeO} + \text{SiO}_2$, $\text{CaO} + \text{SiO}_2$, $\text{MnO} + \text{SiO}_2$, $\text{Na}_2\text{O} + \text{SiO}_2$, $\text{K}_2\text{O} + \text{SiO}_2$ and $\text{CaO} + \text{FeO} + \text{SiO}_2$ and are plotted against $x(\text{SiO}_2)$ in Figure 2. It can be seen from this figure that there is excellent agreement between the $x\bar{V}(\text{SiO}_2)$ calculated from different sources, with the exception of that for the $\text{MnO} + \text{SiO}_2$ system; however the reliability of the experimental data for this system, have been questioned previously. From this curve for $x\bar{V}(\text{SiO}_2)$ we can derive the relationship, $V(\text{SiO}_2) = 19.55 + 7.966.x(\text{SiO}_2)$. The recommended values for \bar{V} for the various oxides at 1500°C are given in Table 2.

$$x\bar{V}(\text{SiO}_2) = V - x_1\bar{V}_1 - x_2\bar{V}_2 - x_3\bar{V}_3 \quad 14)$$

Values for $x\bar{V}$ (Al_2O_3) were determined in a similar manner by using experimental density data for the systems, $\text{CaO} + \text{Al}_2\text{O}_3$, $\text{CaF}_2 + \text{Al}_2\text{O}_3$, $\text{CaF}_2 + \text{Al}_2\text{O}_3$, $\text{SiO}_2 + \text{Al}_2\text{O}_3$, $\text{MgO} + \text{CaO} + \text{Al}_2\text{O}_3$ and $\text{MnO} + \text{SiO}_2 + \text{Al}_2\text{O}_3$. The $x\bar{V}$ (Al_2O_3) results are plotted in Figure 3 and the relationship $x\bar{V}(\text{Al}_2\text{O}_3) = 28.31 + 32 x(\text{Al}_2\text{O}_3) - 31.45 x^2(\text{Al}_2\text{O}_3)$ was derived from this curve.

There are few experimental data for the density of phosphate slags, $x\bar{V}(\text{P}_2\text{O}_5)$ values were derived from data for the systems $\text{CaO} - \text{FeO} - \text{P}_2\text{O}_5$ and $\text{Na}_2\text{O} - \text{P}_2\text{O}_5$. A constant value of $\bar{V} = 65.7 \text{ cm}^3 \text{ mol}^{-1}$ was obtained from the selected linear relationship.

TABLE 2

Recommended values for the partial molar volumes, \bar{V} ,
of various slag constituents at 1500°C

SiO_2	$19.55 + 7.966 x(\text{SiO}_2)$	FeO	15.8	K_2O	51.8
Al_2O_3	$28.31 + 32 x(\text{Al}_2\text{O}_3) - 31.45 x^2(\text{Al}_2\text{O}_3)$	Fe_2O_3	38.4	CaF_2	31.3
CaO	20.7	MnO	15.6	P_2O_5	65.7
MgO	16.1	Na_2O	33	TiO_2	24

$$\text{Units of } \bar{V} = \text{cm}^3 \text{ mol}^{-1} = 10^{-6} \text{ m}^3 \text{ mol}^{-1}$$

In order to provide a temperature coefficient, the temperature dependencies of

the molar volumes (dV/dT) of many slag systems were examined and a mean value of $0.01\% K^{-1}$ was adopted.

Assessment of density models.

An analysis of the uncertainties associated with the estimated of densities with this model has not been completed yet. However on the basis of those values obtained so far the standard deviation of the factor $[(\text{est} - \text{expt})/\text{expt}]$ is between 1 and 2% and less than that recorded vary the method due to Bottinga et al⁽³³⁾. The experimental uncertainties associated with density measurements for slags are i.e. $\pm 2\%$.

2.4 Surface tension (γ)

Methods for estimating the surface tension of slags based on the addition of the partial molar contributions (γ_i) of the individual constituents have been reported by Appen⁽³⁴⁾ by Boni and Derge⁽³⁵⁾ and by Popel⁽³⁶⁾. All these methods make use of equation 13a where 1,2,3 etc denote the various slag constituents.

$$\gamma = x_1 \bar{\gamma}_1 + x_2 \bar{\gamma}_2 + x_3 \bar{\gamma}_3 + \dots \quad 13a)$$

Values of $\bar{\gamma}_i$ are often taken to be the surface tension of the pure components, γ_i^0 , and have also been obtained by reiterative procedures. Figure 4a shows a typical plot of γ as a function of x for a binary slag and the individual $x_i \bar{\gamma}_i$ contributions have been included. These methods work well for certain slag mixtures but break down when surface-active constituents, such as P_2O_5 , are present. Surface active components migrate preferentially to the surface and cause a sharp decrease in the surface tension and only very small concentrations are required to cause an appreciable decrease in γ if the constituent is concentrated in the surface layer. Thus some unreported or undetected impurity could have a marked effect on the surface tension of the slag and consequently produce an apparent error in the value estimated by the model. In this aspect surface tension differs from all the other physical properties which are essentially bulk properties.

Model for calculating the surface tension of slags

Figure 4a shows the surface tension of two slag constituents which are not surface active. For a binary mixture with one surface active component the surface tension-composition relationship will have the form of that shown in Figure 4b where 2 denotes the surface-active constituent. If we assume that $x_1 \bar{\gamma}_1$ for component 1 is unaffected then the term $\bar{\gamma}_2 x_2$, the partial molar contribution of the surface active material, can be calculated by equation 14a below. The term $(x_2 \bar{\gamma}_2)$ can similarly be calculated for ternary and quaternary systems providing there is only one surface active component. The compositional dependence of the $(x_2 \bar{\gamma}_2)$ term is shown in

$$x_2 \bar{\gamma}_2 = \gamma - x_1 \bar{\gamma}_1 \quad 14a)$$

Figure 4b and it should be noted that as $x_2 \rightarrow 1$ then $x_2 \bar{\gamma}_2 \rightarrow \gamma^0$. Values of $(x \bar{\gamma})$ for various surface active materials derived from experimental surface tension data are shown in Figures 5a. It is possible to deal with the compositional dependence of these $(x \bar{\gamma})$ values by considering two curves viz. one operating up to the point N and the other representing values of x where $x > N$. The partial surface tension for non-surface active constituents is shown in Table 3 and the equations for calculating $\bar{\gamma}$ for surface active components and values of N are given in Table 4. There is a considerable discrepancy in the $x_2 \bar{\gamma}_2 - (x_2)$ relationships for B_2O_3 obtained from experimental data on two different systems,

consequently a mean value has been adopted until further data become available.

TABLE 3
Partial molar surface tension, $\bar{\gamma}$, at 1500 °C
for different slag constituents

Oxide %/mNm ⁻¹	SiO ₂ 260 ²	CaO 625	Al ₂ O ₃ 655 ²	MgO 635	FeO 645	MnO 645	TiO ₂ 360 ²
------------------------------	--------------------------------------	------------	--	------------	------------	------------	--------------------------------------

TABLE 4
Values of $x_1 \bar{\gamma}_1$ at 500 °C for surface-active constituents

Slag Constituent	$x_1 \bar{\gamma}_1$ for $x < N$	N	$x_1 \bar{\gamma}_1$ for $x > N$
Fe ₂ O ₃	-3.7 - 2972 x + 14312 x ²	0.125	-216.2 + 516.2 x
Na ₂ O ³	0.8 - 1388 x - 6723 x ²	0.115	-115.9 + 412.9 x
K ₂ O	0.8 - 1388 x - 6723 x ²	0.115	-94.5 + 254.5 x
P ₂ O ₅	-5.2 - 3454 x + 22178 x ²	0.12	-142.5 + 167.5 x
B ₂ O ₃	-5.2 - 3454 x + 22178 x ²	0.10	-155.3 + 265.3 x
Cr ₂ O ₃	- 1248 x + 8735 x ²	0.05	-84.2 + 884.2 x
CaF ₂ ³	-2 - 934 x + 4769 x ²	0.13	-92.5 + 382.5 x
S	-0.8 - 3540 x + 55220 x ²	0.04	-70.8 + 420.8 x

The reported values of $(d\bar{\gamma}/dT)$ for various slag systems were examined and a mean value of -0.15 mN m⁻¹ K⁻¹ was applied as a temperature coefficient.

Assessment of the model

The standard deviation of the factor $[(\bar{\gamma}_{est} - \bar{\gamma}_{expt})/\bar{\gamma}_{expt}]$ was ca. $\pm 10\%$. Undoubtedly much of the uncertainty arises from experimental errors, where the effect of unreported surface active impurities and the nature of the gaseous atmosphere could have a marked effect on the value of surface tension.

Another major source of error is the amount of Fe₂O₃ present in the slag, this investigation has shown clearly that Fe₂O₃ is very surface active. Few investigators cite the (Fe³⁺/Fe²⁺) ratio which in turn is dependent upon, (i) p_{O₂}, (ii) T and (iii) the nature and amount of other oxides present and furthermore the ratio, when quoted, is vulnerable to error. Thus the problem arises if a decrease in $\bar{\gamma}$ is recorded when Na₂O is added to the slag, is this decrease due to a increase in Fe₂O₃ content or due to the surface activity? In this investigation attempts were made to compensate $\bar{\gamma}$ for an increase in Fe₂O₃ content but the effects of basic oxides on the Fe distribution are not well documented and some error may ensue.

A major unresolved problem concerns the situation where the slag contains more than one surface active component. It is possible that there is some competition for sites on the surface and hence the decrease in $\bar{\gamma}$ would not be as sharp as that calculated from the summation of $(x_A \bar{\gamma}_A + x_B \bar{\gamma}_B)$ where A and B denote surface active constituents. In this case the model may overestimate the decrease in $\bar{\gamma}$. There are no extant data to confirm this possibility, we have, however, considered (Na₂O + K₂O) as one contribution in the model.

2.5 Thermal Properties

The computation of the thermal losses in the converter by conductive and radiative processes requires knowledge of the following thermal properties, heat capacity, enthalpy, thermal conductivity, absorption coefficient and emissivity.

2.5.1 Heat capacity C_p and enthalpy ($H_T - H_{298}$) of slags

When a silicate liquid is cooled the structure of the solid formed is dependent upon the cooling rate and the thermal history of the sample. Consider a liquid at a temperature corresponding to the point C in Figure 6, a rapid quench will produce a glass and the enthalpy evolved will follow the path CLGA. By contrast, a very slow cooling rate will result in the formation of a crystalline slag, the enthalpy evolution following the path CL DB. It will be noted from Figure 6 that $(H_T - H_{298})_{\text{cryst}} = (H_T - H_{298})_{\text{glass}} + \Delta H_{\text{vit}}$, where ΔH_{vit} is enthalpy of the endothermic transformation of (crystal \rightarrow glass). The C_p values for the various phases can be summarized as:

$$C_p(\text{crystal}) = C_p(\text{glass}) < C_p(\text{supercooled liquid}) = C_p(\text{liquid})$$

It can be seen from Figure 6 that at the glass temperature (T_{gl}) there is a sudden increase in C_p (ΔC_p^{gl}) as the glass transforms into a supercooled liquid. Drop calorimetry studies on the glass phase at temperatures between T_{gl} and T_{liq} will produce progressively more crystallization as T_{liq} is approached and consequently the $(H_T - H_{298}) - T$ relationship will be similar to that depicted by the dots in Figure 6 and not the path, AGLC; the magnitude of the apparent enthalpy of fusion (ΔH_{fus}) will be dependent upon the fraction of the sample crystallized during annealing at temperatures between T_{gl} and T_{liq} . The C_p values for the liquid and supercooled liquids have been reported to be constant and independent of temperature⁽³⁷⁾. It follows from the triangle GEL in Figure 6 that $\Delta C_p^{\text{gl}}(T_{\text{liq}} - T_{\text{gl}}) = \Delta H_{\text{fus}}$. Thus it is possible to estimate the enthalpy of a slag with a glassy structure from estimates of $C_p(\text{glass})$, $C_p(\text{liq})$ and T_{gl} . However the estimation of T_{gl} is difficult as it can vary between 700 and 1700 K and the various estimation rules suggested are known to be prone to appreciable errors⁽³⁸⁾. Inspection of literature data^(38,39) indicates that the glass transformation occurs when C_p attains a value of ca. $1.1 \text{ J K}^{-1} \text{ g}^{-1}$; this rule has been used in the development of the following model for the estimation of $(H_T - H_{298})$ and C_p of slags with a glassy structure.

The C_p for glass, liquid and supercooled liquid phases can be estimated from the slag composition using partial molar heat capacities (\bar{C}_p) as shown in equation 15).

$$C_p = x_1 \bar{C}_{p_1} + x_2 \bar{C}_{p_2} + x_3 \bar{C}_{p_3} + x_4 \bar{C}_{p_4} \dots \quad (15)$$

For most materials the temperature dependence of C_p is usually expressed the form given by equation 16) where a , b and c are constants

$$C_p = a + bT - c T^{-2} \quad (16)$$

The enthalpy at T relative to 298 K (25 °C) is obtained from equation 17) for the glass phase

$$(H_T - H_{298}) = \int_{298}^T C_p = a(T-298) + \frac{b}{2}(T^2-298^2) + \frac{c}{T} - \frac{c}{298} \quad (17)$$

Values of a , b and c for the various slag components are given in Table 5 and it should be noted that the P_2O_5 and S in the slag were calculated as CaP_2O_6 and CaSO_4 , respectively. The amount of CaO used in the calculation of $x(\bar{C}_{p_2})$ (CaO) should be adjusted by the relationship $x(\text{CaO}) = x(\text{CaO}, \text{total}) - x(\text{P}_2\text{O}_5)^{\text{P}} - x(\text{S})$ to account for the CaO in CaP_2O_6 and CaSO_4 . The model also takes into account the presence of free iron in the slag.

TABLE 5

Slag Component	M	$\bar{C}_p(\text{glass})/\text{cal K}^{-1}\text{mol}^{-1} = a + bT - c/T^2$			$\bar{C}_p(\text{liq})$ $\text{cal K}^{-1}\text{mol}^{-1}$
		a	$b \cdot 10^3$	$c \cdot 10^5$	
SiO ₂	60.09	13.38	3.68	3.45	20.79
CaO ²	56.08	11.67	1.08	1.56	19.3
Al ₂ O ₃	101.96	27.49	2.82	8.4	35
MgO ³	40.31	10.18	1.78	1.48	21.6
K ₂ O	94.2	15.7	5.4	0	17.7
Na ₂ O	61.98	15.7	5.4	0	22
TiO ₂	79.9	17.97	0.28	4.35	26.7
MnO ²	70.94	11.11	1.94	0.88	19.1
FeO	71.85	11.66	2.0	0.67	18.3
Fe ₂ O ₃	159.7	23.49	18.6	3.55	45.7
Fe ² ₃	55.85	3.04	7.58	-0.6	10.5
P ₂ O ₅	141.91	43.63	11.1	10.86	58
CaF ² ₂	78.08	14.3	7.28	-0.47	23
SO ₃ ²	80.06	16.78	23.6	0	42

1 cal = 4.184 J; T in K

The values of \bar{C}_p for the liquid and supercooled liquid given in Table 5 are those reported by Carmichael et al.⁽⁴⁰⁾ except \bar{C}_p values for Al₂O₃ and Fe₂O₃, where other values have been preferred.

Thus $(H_T - H_{298})$ values for a liquid slag at temperature T can be estimated by determining T_{gl} (ie temperature at which $C_p = 1.1 \text{ J K}^{-1} \text{ g}^{-1}$) and calculating $(H_T - H_{298})_{gl}$ from equation (17) and $(H_T - H_T)_{gl}$ from $C_p(\text{liq}) \cdot (T - T_{gl})$.

Values of $C_p(\text{glass})$ obtained with this model lie within 2% of the experimental values and the $C_p(\text{liq})$ values also appear to agree with experimental data; values of ΔC_p^{gl} at T_{gl} calculated using the model lie within the range of experimental values^(38,39) of 0.15 to 0.30 $\text{J K}^{-1} \text{ g}^{-1}$. One major uncertainty would appear to lie in the calculation of T_{gl} , however it can be shown that an error in T_{gl} of 100 K would only produce an error of ca. 1% in the value of $(H_{1900} - H_{298})$ for the slag. The most serious source of error would thus appear to arise through crystallization of the sample during quenching, as few data are available for ΔH_{vit} , the magnitude of errors arising from this source have not been evaluated.

2.5.2 Heat transfer in slags

Heat is transferred through slags by a variety of mechanisms which include convection, radiation and various thermal conduction processes, viz. thermal ("phonon") conductivity, (k), electronic conductivity (k_e) and radiation conductivity (k_R). Methods for estimating the various physical properties involved in these processes are considered below.

2.5.3 Thermal conductivity (k)

Heat is transferred by phonons which are quanta of energy associated with each mode of vibration in the sample. Scattering of the phonons causes a decrease in the thermal conductivity and thus the conductivity is sensitive to the structure of the slag and consequently those factors affecting structure such as the basicity. Despite this structure dependence, estimation rules based on the additivity principle (equation 18)) have been proposed^(41,42). Other models have been developed which relate k to the volume concentration of the oxides in the

glass⁽⁴³⁾ and a third approach⁽⁴⁴⁾ relates the thermal resistance ($1/k$) to $x_i m_i$ where m_i is the effectiveness of modifier of component i in scattering phonons.

$$k = (\%i)k_i + (\%j)k_j + \dots \quad (18)$$

However in coal slags there is frequently an appreciable degree of crystallization and the thermal conductivity value varies with the thermal history of the sample⁽⁴⁵⁾, and consequently rules developed for glasses may not apply well for coal slags. Recent work carried out on a large number of silicate slags⁽⁴⁶⁾ indicated that the thermal diffusivity, a , ($a=k/C \cdot \rho$) of various slags was independent of both composition and temperature in the range (500-1300 K) with $a(\text{glass}) = 4.5(\pm 0.5) \times 10^{-7} \text{ m}^2 \text{ s}^{-1}$; $a(\text{cryst}) = 6 \times 10^{-7} \text{ m}^2 \text{ s}^{-1}$ and $a(\text{liq}) \approx a(\text{glass})$. These data are consistent with values reported for coal slags⁽⁴⁵⁾ and steelmaking slags⁽⁴⁷⁾. However, the values reported by Nauman et al⁽⁴⁸⁾ indicate that at high FeO contents ($> 20\%$) both k and a increase with increasing FeO content ($k = 0.8 + 1.7 \times 10^{-2} (\% \text{ FeO}) \text{ Wm}^{-1} \text{ K}^{-1}$).

2.5.4 Absorption coefficient (α)

Radiation conductivity (k_R) can be the predominant mode of heat transfer through semi-transport media like glasses and the magnitude of k_R is determined largely by the optical properties such as the absorption coefficient (α) and the refractive index (n). The value of k_R increases as the slag thickness (d) is increased until a critical point is attained, above this point k_R remains constant and independent of thickness. Above this critical point the slag is said to be "optically thick, this condition applies when $\alpha d > 3.5$ and values of k_R can be calculated using equation 19), where σ is the Stefan-Boltzmann constant.

$$k_R = \frac{16 n^2 T^3 \sigma}{3 \alpha} \quad (19)$$

No formulae exist for the calculation of k_R for optically thin conditions. The absorption coefficient (α) is markedly dependent upon the amounts of Fe^{2+} and Mn^{2+} present in the slag⁽⁴⁹⁾; levels for $\text{FeO} < 5\%$ the following relationship can be applied, $\alpha (\text{cm}^{-1}) = 11(\% \text{ FeO})$. Temperature appears to have little effect on the absorption coefficient of glasses but the absorption coefficients of magmas have been reported to increase with increasing temperature^(50,51). Crystallization of the slag will result in a large increase in the absorption (or extinction) coefficient which could reduce k_R to virtually zero.

The importance of radiation conduction in heat transfer through coal slags can readily be demonstrated, for a slag with an appreciable FeO content (7%) Fine et al⁽⁴⁷⁾ recorded $\alpha = 50 \text{ cm}^{-1}$ at 298 K using this value and equation 19), a value of $k_R = 0.9 \text{ Wm}^{-1} \text{ K}^{-1}$ can be calculated for 1873 K. As $k = 1.5 \text{ Wm}^{-1} \text{ K}^{-1}$ it can be seen that about 40% of the heat is transferred by radiation conduction.

2.5.5 Emissivity (ϵ)

The emissivity (ϵ) of a semi-transparent medium, is a bulk property of ϵ (metal) which is solely dependent upon the surface. In the basis of the spectral and total normal emissivity data reported for coal and metallurgical slags the value $\epsilon = 0.8 \pm 0.1$ can be adopted for coal slags in the range (1100 - 1900 K).

CONCLUSIONS

- 1) Estimation procedures based on the chemical composition of the slag have now been developed for the prediction of viscosity, surface tension, density and heat capacity.
- 2) The accuracy of these estimation routines for some physical properties (eg viscosity, surface tension) can be improved when more reliable experimental data become available.
- 3) The distribution of iron in the slag between free Fe, FeO and Fe_2O_3 has a pronounced effect of virtually all the physical properties and it is recommended that experimental data for the properties of the slag should always be accompanied by values for the distribution of iron.
- 4) The development of models for the prediction of some physical properties (thermal conductivities, absorption coefficient) is restricted by the limited amount of experimental data available.

REFERENCES

- 1) DARKEN, L.S. and GURRY, R.W. J. Am. Chem. Soc. 1946, 68, 798.
- 2) LARSON, H. and CHIPMAN, J. J. Metals, 1953, Sept., 1089.
- 3) BANYA, S. and SHIM, J.D. Canad. Metall. Q., 1982, 21, 319.
- 4) SONDREAL, E.A. and ELLMAN, R.C. Fusibility of ash from lignite and its correlation with ash composition. US Energy Res. and Develop. Admin. GFERC/RI-75-1, Pittsburgh, 1975.
- 5) WINEGARTNER, E.C. and RHODES, B.T. J. Eng. Power, 1975, 97, 395.
- 6) BRYERS, R.W. and TAYLOR, T.E. J. Eng. Power, 1976, 98, 528.
- 7) STEILER, J.M. Commission of the European Communities Research Contract, 7210 CA/3/3/03. Thermodynamic data for steelmaking. 1981, Eur N7820, BP 1003, Luxembourg 1982.
- 8) GAYE, H. Ironmaking and Steelmaking, 1984, in press.
- 9) GAYE, H. Paper presented at Metallurgical Conference, Centenary of Teaching of Metallurgy, held at Strathclyde University, 25/26 June 1984.
- 10) OCHOTIN, M.W. Steklo Keram., 1954, 11, 7.
- 11) LYON, K.C. J. Res. Natl. Bur. Stand., 1974, 78, 497.
- 12) MCCAULEY, W.D. and APELIAN, D. Canad. Metall. Quart., 1981 20, 247.
- 13) RIBOUD, P.V., ROUX, Y, LUCAS, L.D. and GAYE, H. Fachber. Huttenpraxis Metallveiterverarb., 1981, 19, 859.
- 14) MAIRY, B. Private communication, Centre Recherches Metallurgique, Liege, Belgium.
- 15) BOTTINGA, Y. and WEILL, D.F. Am. J. Sci., 1972, 272,
- 16) SHAW, H. Am. J. Sci., 1972, 272, 870.

- 17) URBAIN, G., CAMBIER, F., DELETTET, M. and ANSEAU, M.R. Trans. J. Brit. Ceram. Soc., 1981, 80, 139.
- 18) URBAIN, G. Private communication, CNRS, Laboratoire de Ultra-Refractaires, Odeillo, France. Jan. 1983.
- 19) WATT, J.D. and FEREDAY, D. J. Instr. Fuel, 1969, 338, 99.
- 20) BOKAMP, . Inst. of Gas Technol. Preparation of a coal conversion systems Technical Data Book. Energy Res. and Dev. Admin. Report FE-1730-21 (1976).
- 21) CAPPS, W. and KAUFFMAN, D. Natl. Bur. Stand. Quart. Prog. Rept. to Office of Coal Res., Dept. Interior, 30/9/74.
- 22) SCHOBERT, H.H. Div. Fuel Chem. Prep., 1977, 22, 143.
- 23) SCHOBERT, H.H. and WITTHOEFFT, C. Fuel Proc. Technol., 1981, 5, 157.
- 24) HENSLEE, S.P. and KELSEY, P.V. Jr. US Dept. of Energy Report, EGG-FM-6049, Sept. 1982.
- 25) KEENE, B.J. National Physical Laboratory Report, DMA(D)75, Feb. 1984.
- 26) MOREY, G.H. Properties of Glasses. Reinhold, New York, 1954, 217.
- 27) HUGGINS, M.L.; SUN, K.H. J. Am. Ceram. Soc. 1948, 26, 4.
- 28) BOTTINGA, H. and WEILL, D.E. Am. J. Sci., 1972, 272 438.
- 29) NELSON, S.A. and CARMICHAEL, I.S.E. Contrib. Mineral Petrol, 1979, 71, 117.
- 30) MO, Y., CARMICHAEL, I.S.E., RIVERS, M. and STEBBINS, J. Mineralog. Mag., 1982, 45, 237.
- 31) GRAU, A.E. and MASSON, C.R. Canad. Metall. Quart., 1976, 15, 367.
- 32) LEE, Y.E., GASKELL, D.R. Metall. Trans., 1974, 5, 853.
- 33) BOTTINGA, Y., WEILL, D.E. and RICHET, P. Geochim Cosmochim. Acta, 1982, 46, 909.
- 34) APPEN, A.A., SHISHKOV, K.A. and KAYALOVA, S.S. Zhur. Fiz. Khim, 1952, 26, 1131.
- 35) BONI, R.E. and DERGE, G. J. Metals, 1956, 8, 53.
- 36) POPEL, S.E. Metallurgy of slags and their use in building. 1962, 67.
- 37) RICHET, P. and BOTTINGA, Y. Geochim. Cosmochim Acta, 1984, 44, 1533.
- 38) BACON, C.R. Am. J. Sci., 1977, 277, 109.
- 39) MOYNIHAN, C.T., EASTEAL, A.J., TRAN, D.C., WILDER, J.A. and DONOVAN, E.P. J. Am. Ceram. Soc., 1976, 59, 137.
- 40) CARMICHAEL, I.S.E., NICHOLLS, J., SPERA, F.J., WOOD, B.J. and NELSON, S.A. Phil. Trans. Roy. Soc. (London), 1977, A286, 373.
- 41) MOREY, G.W. Properties of Glass. Reinhold, New York, 1954, 217.

- 42) ABAKOVA, I.G. and SERGEEV, O.A. Thermophysical properties of glasses. Proc. of Metrological Inst. of USSR, No.129 (189), Moscow-Leningrad, 1971, 13.
- 43) MISNAR, A. Thermal conductivity of solid, gases and composite materials. Leningrad, 1968.
- 44) VAVILOU, Y.V., KOMAROV, V.E. and TABUNOVA, W.A. Phys. Chem. Glasses, 1982, 8, 472.
- 45) GIBBY, R.L. and BATES, J.L. 10th Thermal Conductivity Conf. held Newton, Mass. Sept. 1970, IV-7,8.
- 46) TAYLOR, R. and MILLS, K.C. Unpublished work, 1984.
- 47) FINE, H.A., ENGH, T. and ELLIOTT, J.F. Metall. Trans. B. 1976, 7B, 277.
- 48) NAUMAN, J., FOO, G. and ELLIOTT, J.F. Extractive Metallurgy of Copper. Chapter 12, 237.
- 49) STEELE, F.N. and DOUGLAS, R.W. Phys. Chem. Glasses, 1965, 6, 246.
- 50) FUKAO, Y., MITZUTANI, H. and UYEDA, S. Phys. Earth Planet Interiors, 1968, 1, 57.
- 51) ARONSON, J.R., BELLOTI, L.H., ECKROAD, S.W., EMSLIE, A.G., MCCONNELL, R.K. and THUNA, P.C., von. J. Geophys. Res., 1970, 75, 3443.

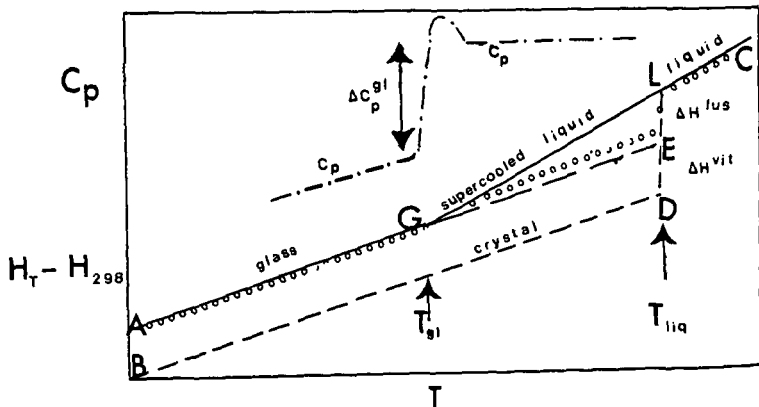
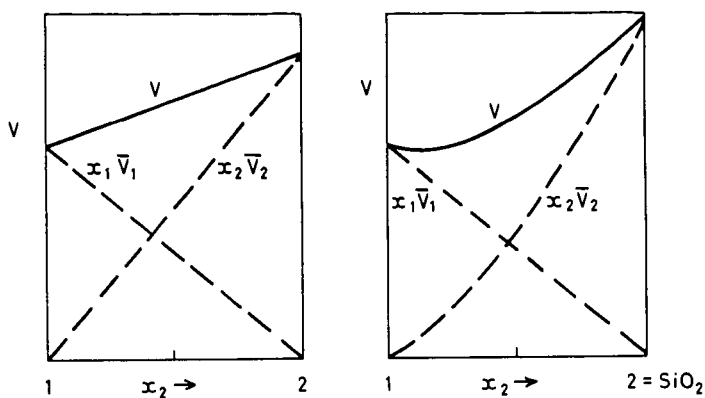


Figure 6 C_p and $(H_T - H_{298})$ for glassy and crystalline phases of a slag; O, indicates typical drop calorimetry results.



Figures 1a The molar volume of binary slag system as a function of composition and 1b. showing the individual $x_1 \bar{V}_1$ contributions.

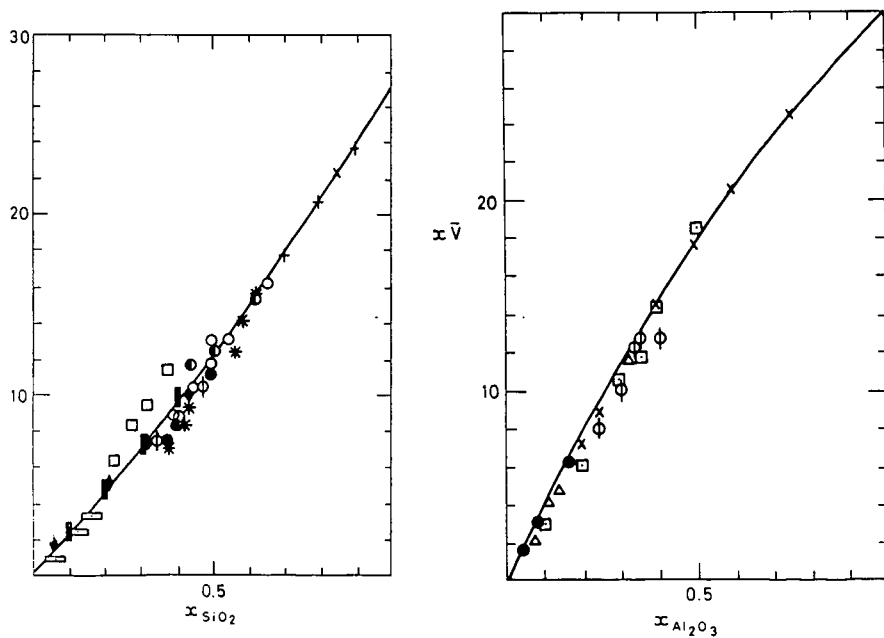


Figure 2. $x \bar{V}(\text{SiO}_2)$ as a function of $x(\text{SiO}_2)$

Figure 3. $x \bar{V}(\text{Al}_2\text{O}_3)$ as a function of $x(\text{Al}_2\text{O}_3)$

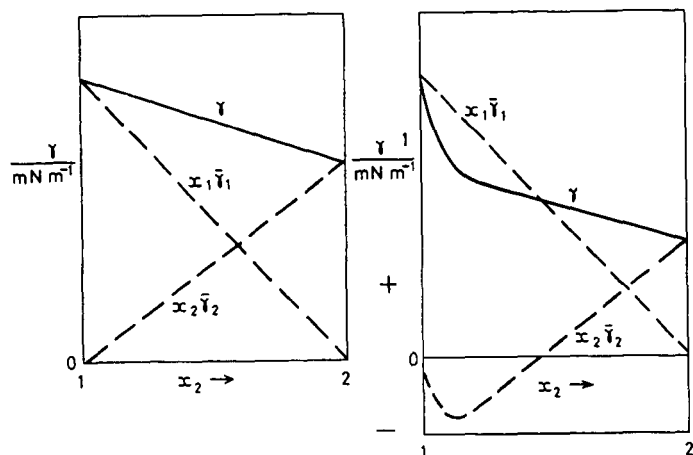


Figure 4a. The compositional dependence of γ , $x_1\bar{V}_1$ and $x_2\bar{V}_2$ for a binary slag system with non-surface active constituents

Figure 4b. with one surface active constituent (2).

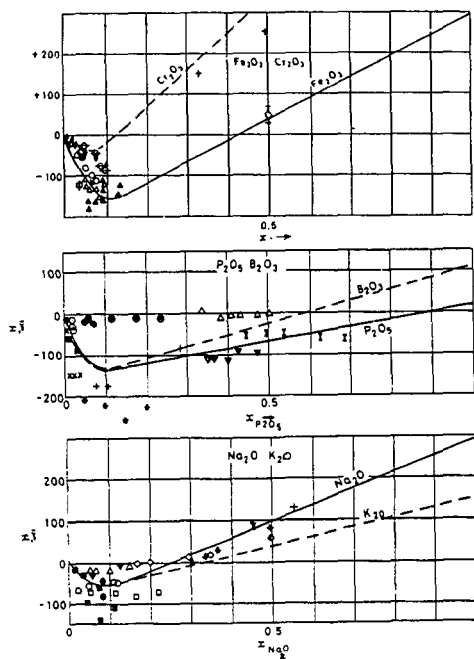


Figure 5 The compositional dependence of $x_1\bar{V}_1$ for various surface-active constituents.

Viscosity of Fluxes for the Continuous Casting of Steel

W. L. McCauley and D. Apelian

Materials Engineering, Drexel University, Philadelphia, PA, 19104

Mold fluxes are routinely used in both continuous casting and bottom pouring of steel. These fluxes are generally calcium-silicate based compositions with alkali oxides $[(Li, Na, K)_2O]$ and fluorides $[CaF_2, NaF]$ added as fluidizers. The compositions are sometimes based on the blast furnace slag $[Al_2O_3-SiO_2]$ system, but the fly ash $[CaO-SiO_2]$ system is more common.

A variety of properties of the flux must be controlled, including fusion characteristics (fusion temperature range and sintering characteristics, flow properties of the powder, viscosity of the molten flux, and non-metallic absorption ability. The viscosity influences the consumption rate of flux, heat transfer in the mold, and non-metallic dissolution rate, and has been the subject of a great deal of published and unpublished work over the last ten years. The purpose of this paper is to discuss the expression of viscosity as a function of composition and temperature in separate relations.

In a previously published work (1), fluxes based on the $CaO-SiO_2$ system were examined to determine the effects of basicity ratio and alkali oxide and fluoride additions on the viscosity of oxide melts in the mold flux composition range. Those results showed that for that range of compositions, the viscosity at a given temperature could be expressed as a function of the silica content squared. In this work, an expression for viscosity as a function of temperature is derived from the Claussius-Clapeyron equation.

Previous Work - Viscosity vs. Composition

The viscosity of twenty controlled composition fluxes was measured as a function of temperature. The compositions, given in Table 1, were selected to fit a second order statistical design in the variables V-ratio, $\%Na_2O$ and $\%CaF_2$. The V-ratio $[wt\%CaO/wt\%SiO_2]$ was varied from 0.6 to 1.3, Na_2O from 4 to 19wt%, and CaF_2 from 2 to 12wt%. Al_2O_3 was kept constant at 10wt%. The viscosity was measured using a rotating type viscometer with a molybdenum spindle in an argon atmosphere. Details of the experimental technique were reported earlier (1).

A summary of the experimental results is given in Table 2. Viscosity decreased with increasing V-ratio, CaF_2 content and Na_2O content as shown in Figures 1, 2 and 3, respectively. A plot of viscosity vs. silica content, Figure 4, shows that silica has a predominating effect on viscosity. A simple quadratic relation of viscosity with wt% silica or mole fraction of silicon cations produced a better fit of the data than a model containing the design variables. The best fit of data was obtained with a quadratic relation of the ratio of network forming cations $[Si, Al \text{ and } Zr]$ to total anion concentration $[O \text{ and } F]$. Specifically,

$$\eta_{1500^\circ C} = 6.338 - 43.44K + 75.03K^2$$

where

$$K = \frac{X_{Si} + X_{Al} + X_{Zr}}{X_O + X_F}$$

The log of viscosity versus reciprocal absolute temperature showed a distinct non-linearity as evidenced by the typical results shown in Figure 5. This is not a complete surprise, but a simple Arrhenius type equation is not adequate to describe the viscosity/temperature relationship.

Viscosity vs. Temperature

Viscosity can be considered as a measure of the ease of movement of molecules in a liquid undergoing shear. Several factors may influence this ease of movement including molecule size and intermolecular attraction, but a major factor is the amount of space available between the molecules, hence, the variety of models incorporating a free volume term.

The Claussius-Clapeyron equation relates pressure with temperature, enthalpy, and volume, and has been used to develop semi-theoretical expressions of vapor pressure (2). Many properties, including viscosity, can be related to an energy barrier, free volume and temperature. The attempt here is to express viscosity in the form of the Claussius-Clapeyron equation.

The Claussius-Clapeyron equation can be written

$$\frac{dP}{dT} = \frac{H}{T \Delta V} = \frac{\Delta H}{T(V - V_0)} \quad 1)$$

where P, T, and ΔH have their usual meaning. For this discussion, ΔV is a measure of free volume or the difference between the volume at temperature and the volume at some standard state, e.g., at absolute zero.

Equation 1 can be rewritten as

$$\frac{d(\ln P)}{d(1/T)} = - \frac{\Delta H}{R \Delta z} \quad 2)$$

where $\Delta z = PV/RT - PV_0/RT$

Expanding ΔH to the Taylor series form and integrating with respect to $1/T$ yields

$$\ln P = \frac{1}{R} \left(a - \frac{\Delta H_0}{T} + b \ln T + dT + \frac{e}{2} T^2 + \dots \right) \quad 3)$$

If the higher order terms are ignored, the expression reduces to

$$\ln P = A - \frac{B}{T} + C \ln T \quad 4)$$

Such a derivation was originally developed and used by Kirchoff [1858] and Rankine [1849] (2) to express the temperature dependence of vapor pressure. It was also successfully used by Brostow (3) to express the temperature dependence of the isothermal compressibility of a wide variety of organic liquids, some metallic liquids and water. By a similar analogy, we have used it to express the viscosity of liquid mold fluxes.

Regression Analysis

The flux viscosity data was fitted to the Kirchoff-Rankine equation as,

$$\eta = \exp(C_1 + \frac{C_2}{T} + C_3 \ln T) \quad 5)$$

and to the Andrade-Arrhenius equation

$$\eta = A \exp(E/RT) \quad 6)$$

using the Marquardt method of non-linear least squares regression in the Statistical Analysis Systems [SAS] program package (4). The results of the regression are given in Table 3. The standard deviation and an average difference between calculated and measured values are given in Table 4.

In some cases, viz., Fluxes 5, 6 and 13 in Table 3, the signs of the coefficients are reversed, and a concave downward curve is generated. This is most likely caused by the regression being trapped at a local minimum in the data and assuming convergence at that point. It is required for these cases that the size of the regression step should be increased to avoid the local minima, which SAS does not allow. Also, there may not be enough data points to expand the regression step as is probably true for Fluxes 6 and 13.

For the majority of fluxes evaluated, the standard deviation, s , and the average percent variation, $\Delta\bar{\eta}$, is lower for the Kirchoff-Rankine fitted equation vs. the Andrade-Arrhenius model, indicating a better fit of the experimental data. The average percent variation between calculated and experimental values is lower for the Kirchoff-Rankine equation, and the difference is most pronounced for those fluxes where the non-linearity of the experimental $\ln \eta$ vs. $1/T$ data is greatest.

Discussion

When the non-linearity of the log viscosity vs. reciprocal temperature data was first observed, tests were made to insure that the curvature was real and not an artifact of the experimental apparatus. Hysteresis curves and constant temperature for extended time tests showed that the non-linearity was not caused by volatilization of alkali or fluoride constituents or from thermal deviations in the furnace setup. The observed curvature of the data was not an artifact and represented the true physical behavior of the materials. The application of the Kirchoff-Rankine equation produced a more accurate description of the temperature dependence of viscosity.

Additional work on liquid metals, simple chloride salts and some small molecule organic liquids (5) indicates that the advantage of the Kirchoff-Rankine equation over the Andrade-Arrhenius equation improves as the size of the melt species increases. The improvement in the description of viscosity vs. temperature for metals and simple salts [e.g., NaCl and BiCl₃] is not great, but for materials with larger melt species, there is a distinct improvement.

References

- (1) W. L. McCauley and D. Apelian, *Canadian Metallurgical Quarterly*, 20(2) 1984, pp. 247-262.
- (2) G. W. Thomson, *Chemical Review*, 38, February 1946.
- (3) W. Brostow and P. Maynadier, *High Temperature Science*, 11 1979, pp. 7-21.

- (4) SAS User's Guide, SAS Institute, Inc., Cary, North Carolina, 1979.
- (5) W. L. McCauley and D. Apelian, "Temperature Dependence of the Viscosity of Liquids," to be presented at the International Symposium on Slags and Fluxes, TMS-AIME Fall Meeting, Lake Tahoe, NV, November 1984; to be published.

Table 1. Experimental Fluxes - Frit Composition, wt%

Flux	SiO ₂	Al ₂ O ₃	CaO	Na ₂ O	CaF ₂	MgO	ZrO ₂	Total	V-ratio
1	34.8	10.2	32.7	10.7	7.6	0.9	0.6	97.5	0.94
2	34.4	9.8	32.1	10.9	8.4	0.7	0.6	96.9	0.93
3	34.5	10.0	32.7	11.0	7.6	0.7	0.7	97.2	0.95
4	34.6	10.1	32.5	10.8	7.8	0.6	0.6	97.0	0.94
5	34.6	10.3	32.3	10.9	8.0	0.7	0.5	97.3	0.93
6	34.7	10.1	33.0	10.8	7.2	0.6	0.6	97.0	0.95
7	26.7	9.8	31.8	14.4	11.7	0.6	1.9	96.9	1.19
8	30.7	8.9	32.6	12.9	2.3	0.7	8.8	96.9	1.06
9	31.2	10.4	40.3	5.7	7.6	0.8	0.7	96.7	1.29
10	35.2	10.3	40.8	5.7	3.3	0.9	0.8	97.0	1.16
11	33.5	10.4	24.9	15.1	11.5	0.5	0.4	96.3	0.77
12	38.8	10.4	26.2	15.1	3.5	0.7	0.9	95.6	0.67
13	41.9	10.6	29.5	6.8	7.8	0.7	0.9	98.2	0.77
14	48.0	10.6	28.6	6.5	3.3	0.8	1.4	99.2	0.60
15	46.8	10.4	22.2	10.7	5.5	0.6	2.7	98.9	0.47
16	30.6	10.0	36.2	10.3	7.0	1.0	2.1	97.2	1.18
17	30.0	10.2	27.8	18.6	8.2	0.8	1.6	97.2	0.93
18	39.6	10.4	35.7	4.0	4.7	1.0	1.3	96.7	0.90
19	32.4	10.4	30.4	10.8	11.7	0.7	1.1	97.5	0.94
20	39.1	10.4	32.6	11.3	1.7	0.9	1.2	97.2	0.83

Table 2. Summary of Flux Viscosities

Flux	Viscosity at 1300°C, Ns m ⁻²	Viscosity at 1400°C, Ns m ⁻²	Viscosity at 1500°C, Ns m ⁻²
1	0.395	0.230	0.135
2	0.310	0.175	0.112
3	0.340	0.205	0.128
4	0.485	0.235	0.125
5	0.290	0.190	0.088
6	0.510	0.230	0.122
7	0.110	0.065	0.035
8	NA*	NA*	NA*
9	0.280	0.160	0.080
10	6.00	0.360	0.180
11	0.270	0.150	0.114
12	0.930	0.460	0.270
13	1.15	0.530	0.280
14	2.80	1.30	0.710
15	2.40	1.30	0.725
16	7.00	0.170	0.090
17	0.160	0.115	0.059
18	1.40	0.670	0.380
19	0.250	0.130	0.094
20	1.40	0.720	0.410

*Not available

Table 3. Regression Analysis Results

Flux	Andrade-Arrhenius Equation				Kirchoff-Rankine Equation					
	A	E	s [†]	$\overline{\Delta\%}^{++}$	C ₁	C ₂	C ₃	s	$\overline{\Delta\%}$	n ⁺⁺⁺
1	8.831E-6	33783	7.03E-3	2.40	-184.35	51341	20.502	6.36E-3	1.94	12
2	2.704E-6	36304	1.99E-2	7.98	-282.59	68183	32.337	1.27E-2	3.47	6
3	2.332E-6	30095	8.92E-3	2.08	-184.30	47516	20.792	5.68E-3	1.42	6
4	8.016E-7	41748	1.82E-2	2.73	-278.11	71633	31.502	1.67E-2	3.20	6
5	2.528E-5	29493	2.15E-2	4.14	132.94	-10764	-17.290	2.10E-2	3.91	14
6	8.079E-7	41814	2.33E-2	5.41	123.80	-5309	-16.447	2.29E-2	5.68	7
7	1.963E-7	41439	1.31E-2	7.01	-1511.91	297516	179.394	5.72E-3	3.91	5
9	1.496E-5	30736	1.22E-2	3.15	-1626.10	321853	192.942	1.11E-2	3.62	6
10	7.5E-3	36000*	-	-	-8603.16	1735752	1019.0	2.83E-2	3.97	18
11	7.820E-6	32510	1.43E-2	3.15	-276.14	63473	31.935	5.81E-3	1.52	7
12	4.828E-7	45110	6.00E-2	2.95	-239.51	62253	27.155	3.35E-2	1.10	12
13	2.661E-6	40700	5.19E-2	4.69	169.80	-13879	-21.843	5.00E-2	3.89	8
14	5.488E-8	48579	2.26E-1	13.00	-987.72	212141	116.012	9.85E-2	5.30	11
15	5.761E-6	40568	1.32E-1	5.57	-233.90	60668	26.660	6.26E-2	3.07	10
16	2.0E-2	30000*	-	-	-42701.6	8456727	5071.8	8.69E-2	15.8	17
17	5.469E-6	32981	8.65E-3	5.05	-483.18	105664	56.221	1.60E-3	0.84	5
18	4.126E-6	39880	2.66E-2	3.01	-200.79	56382	22.457	1.66E-2	1.84	6
19	7.393E-6	32313	1.48E-2	7.39	-377.12	85334	43.656	8.69E-3	4.89	7
20	1.493E-7	50240	1.62E-1	16.46	-517.30	116706	60.246	5.32E-2	4.46	8

$$+ \quad s = \sqrt{c(n_{\text{exp}} - n_{\text{calc}})/(n-1)}$$

* estimated

$$++ \quad \overline{\Delta\%} = \frac{1}{n} \left(\frac{n_{\text{exp}} - n_{\text{calc}}}{n_{\text{exp}}} \right) \times 100$$

+++ n = number of observations

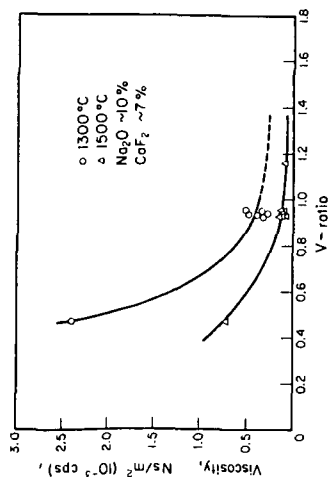


Figure 1. Viscosity vs. V-ratio

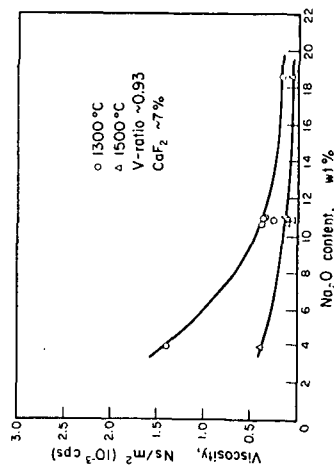


Figure 2. Viscosity vs. Na₂O Content

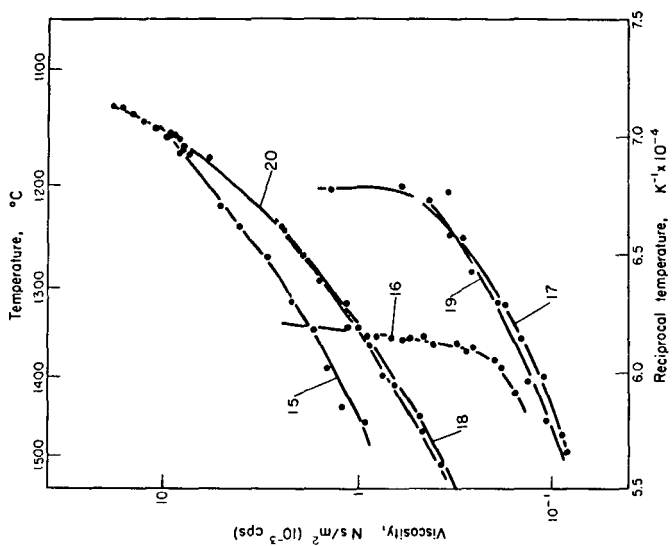


Figure 5. Typical viscosity results vs. reciprocal temperature

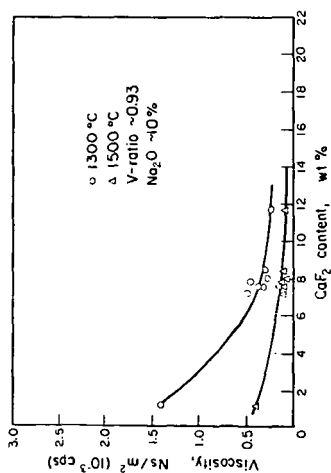


Figure 3. Viscosity vs. CaF_2 Content

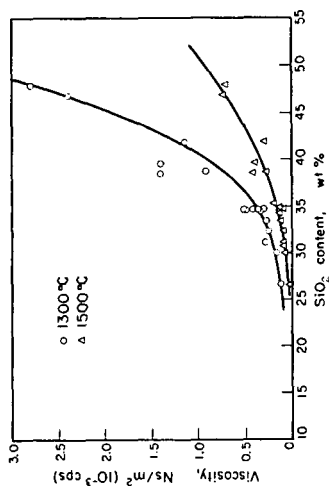


Figure 4. Viscosity vs. SiO_2 Content

RHEOLOGICAL PROPERTIES OF MOLTEN KILAUEA IKI BASALT CONTAINING SUSPENDED CRYSTALS

H. C. Weed, F. J. Ryerson, and A. J. Piwinski

University of California, Lawrence Livermore National Laboratory
Livermore, CA 94550

INTRODUCTION

In order to understand the flow behavior of molten silicates containing suspended crystals, we need to know the rheological behavior of the system as a function of volume fraction of the suspended crystalline phases at appropriate temperatures, oxygen fugacities and bulk compositions. This approach can be applied to magma transport during volcanic eruptions, large scale convective and mixing processes in magmatic systems, and fouling of internal boiler surfaces by coal ash slags in plants burning pulverized coal.

EXPERIMENTAL METHODS

We are currently determining the dynamic viscosity and crystallization sequence for a basalt from Kilauea Iki, Hawaii at 100 kPa total pressure. The oxygen fugacity is controlled by mixing CO and CO₂. The mixing proportions are chosen to yield oxygen fugacities corresponding to the high temperature extrapolation of quartz-fayalite-magnetite buffer (i.e. QFM, see Huebner (1)). Viscosities are being measured in an iron-saturated, Pt-30% Rh, rotating-cup viscometer of the Couette type from 1250° to 1150°C. The temperature interval for the crystallization sequence ranges from 1270° to 1130°C; the oxygen fugacity is maintained by flowing CO/CO₂ mixtures and is monitored by a ZrO₂ sensor cell. Low temperature limits on the investigated crystallization sequence are dictated by the sluggish kinetics encountered in this system.

RESULTS

The major element bulk composition of the starting material used in our experiments is given in Table 1:

TABLE 1. Analyses of Starting Material

Oxide	Kilauea Iki	Shaw et. al. ⁽²⁾
SiO ₂	46.29	50.14
Al ₂ O ₃	10.44	13.37
MgO	17.90	8.20
FeO*	11.34	10.13
Fe ₂ O ₃	-	1.21
CaO	8.49	10.80
Na ₂ O	1.84	2.32
P ₂ O ₅	0.22	0.27
K ₂ O	0.40	0.53
TiO ₂	1.89	2.63
MnO	0.19	0.17
TOTAL	99.90	99.77

*All iron as FeO

The crystallization experiments were carried out employing a specimen of Kilauea Iki whole rock powder. The experimental results obtained at the QFM buffer are listed in Table 2. Olivine and chrome spinel are the only crystalline phases which occur between 1240° and 1179°C; clinopyroxene and plagioclase feldspar crystallize at approximately 1170°C.

Approximately 30 weight per cent crystallization occurs between 1250° and 1180°C. The liquid line of descent is characterized by a slight SiO₂, Al₂O₃ and alkali enrichment and an FeO and MgO depletion.

The volume percentage of melt as a function of temperature is shown in Figure 1. The break in slope at approximately 1170°C, corresponds to the appearance of clinopyroxene and plagioclase feldspar (see Table 2).

TABLE 2. Results of Selected Kilauea Iki Liquidus Experiments

Exp't No.	Time (Hrs)	Temp (°C)	Experiment Products	Vol % Melt ^a	Wt % Melt ^b
14	93.0	1240	olivine, chrome spinel, glass	71.8	78.1
9	189.5	1230	olivine, chrome spinel, glass	80.2 ^c	76.1
8	24.0	1219	olivine, chrome spinel, glass	77.3	74.8
10	290.0	1209	olivine, chrome spinel, glass	76.2	74.2
12	289.0	1189	olivine, chrome spinel, glass	63.8	72.5
13	364.0	1179	olivine, chrome spinel, glass	71.8	71.5
16	380.0	1170	olivine, chrome spinel, clino-pyroxene, plagioclase, glass	69.6	68.5
19	400.0	1160	olivine, chrome spinel, clino-pyroxene, plagioclase, glass	54.7	53.5
20	400.0	1149	olivine, chrome spinel, clino-pyroxene, plagioclase, glass	40.7	49.8

a) Volume percent of melt was determined by a 1000 point mode on metallograph.

b) Weight percent of melt was determined by constrained least squares analysis of phase compositions.

c) Volume percent glass was determined by 850 point mode on metallograph.

This volume percentage of melt, V_m , is given by Equations 1 and 2:

$$V_m (Ol+Chsp) = 0.157 T(^{\circ}C) - 114.0, \text{ where } T(^{\circ}C) \geq 1170, \quad 1)$$

$$V_m (Ol+Chsp+Cpx+Plag) = 1.36 T(^{\circ}C) - 1522.7, \text{ where } T(^{\circ}C) \leq 1170. \quad 2)$$

Extrapolation of Equation 1 to $V_m = 100$ corresponds to $T = 1360^{\circ}C$ for the liquidus.

Extrapolation of Equation 2 to $V_m = 0$ yields $T = 1119^{\circ}C$ for the disappearance of liquid, the solidus temperature.

The measured apparent viscosities of the Kilauea Iki molten basalt between 1250° and 1150°C varied from 30 to 2000 Pa.s. Sigmoidal torque versus rotation speed curves were obtained at all investigated temperatures. The curves are linear at low rotation speeds, less than 0.4 revolutions/second, with a positive slope. This corresponds to Newtonian behavior. However, at higher rotation speeds, the curves are concave toward the rotation speed axis, indicating pseudoplastic behavior. This pseudoplastic behavior becomes more

pronounced at low temperature as the volume per cent of suspended crystals increases. We have analyzed the results in terms of an extended the power law indicated by Equation 3:

$$\log \tau_{yx} = A_1 + A_2 \left(\log \left(\frac{du}{dx} \right) \right) + A_3 \left(\log \left(\frac{du}{dx} \right) \right)^2 \quad (3)$$

where τ_{yx} is the stress, and $\left(\frac{du}{dx} \right)$ the strain rate. The apparent viscosity, μ , is given by Equation 4:

$$\mu = \tau_{yx} / \left(\frac{du}{dx} \right) \quad (4)$$

Figure 2 is a plot of Equation 3 portraying experimental results obtained at the 1236°C isotherm. Figure 3 is a log-log plot of apparent viscosity as a function of shear rate at the same temperature. The apparent viscosity decreases with increasing shear rate, which is common for pseudoplastic liquids. The log of the viscosity at unit shear rate, $\log \mu_0$, is calculated from Equation 3 as $\log \mu_0 = A_1$.

$\log \mu_0$ is plotted as a function of reciprocal temperature in an Arrhenius diagram given in Figure 4. The log viscosity curves illustrated there show a sharp break in slope with decreasing temperature. Data above and below this break have been fitted by limiting straight lines from which apparent activation energies can be calculated. The apparent activation energy in the temperature interval 1250° - 1170°C is 65 + 30 kcal mol⁻¹. For temperatures below 1170°C where appreciable crystallization occurs (see Table 2 and Figure 1) and the system exhibits strongly pseudoplastic behavior, the apparent activation energy is 341 + 42 kcal mol⁻¹. Also shown in Figure 4 are the results of Shaw (3) obtained on a Hawaiian basalt similar to our Kilauea Iki specimen (see Table 1). The general trend of the two sets of data is similar, but the break in the slope of Shaw's data occurs at a lower temperature than it does in ours, presumably because of the change from Newtonian to pseudoplastic behavior in his system. In both studies, the break in the slope of the viscosity curves occurs at 20 to 30 volume percent of suspended crystals. The non-Newtonian behavior of these molten silicate suspensions appears to arise from the increasing volume of suspended crystals in the melt. This suggests that in modeling fluid flow in silicate liquids, power law behavior should be considered when the suspended crystal volume exceeds 20 percent.

REFERENCES

- (1) Huebner, J. S. (1971) in Research Techniques for High Pressure and High Temperature, Ulmer, E. C. ed., Springer-Verlag (1971), p. 146.
- (2) Shaw, H. R., Wright, T., Peck, D. L. and Okamura, R. (1968) Amer. Jour. Sci., Vol. 266, p. 225-264.
- (3) Shaw, H. R. (1969) Jour. Petrology, Vol. 10, p. 510-535.

This work was performed under the auspices of the U. S. Department of Energy by the Lawrence Livermore National Laboratory, under Contract No. W-7405-ENG-48.

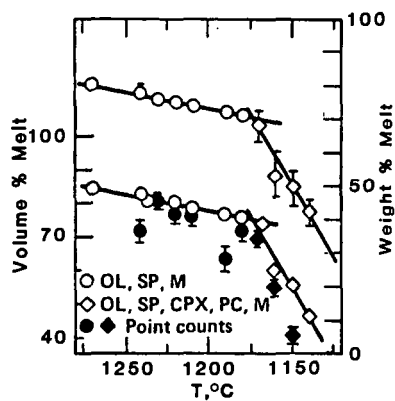


Fig. 1. Volume percent and weight percent melt as a function of temperature for Kilauea Iki basalt. The upper curve gives weight percent melt, indicated by the right ordinate. Open symbols on the lower curve give volume percent melt remaining (left ordinate), calculated from weight percent data and densities of phases. Solid symbols are from modal analyses.

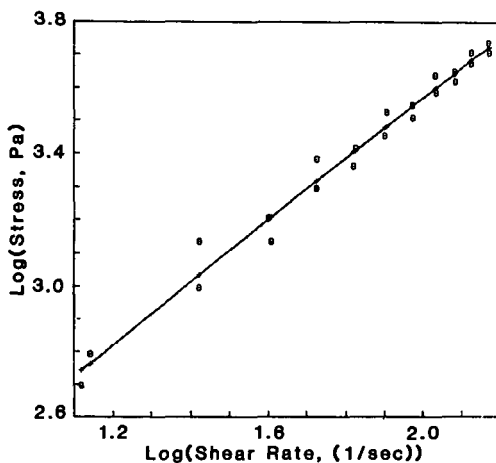


Fig. 2. Log (Stress) as a function of log (Shear Rate) for Kilauea Iki basalt melt at 1236°C.

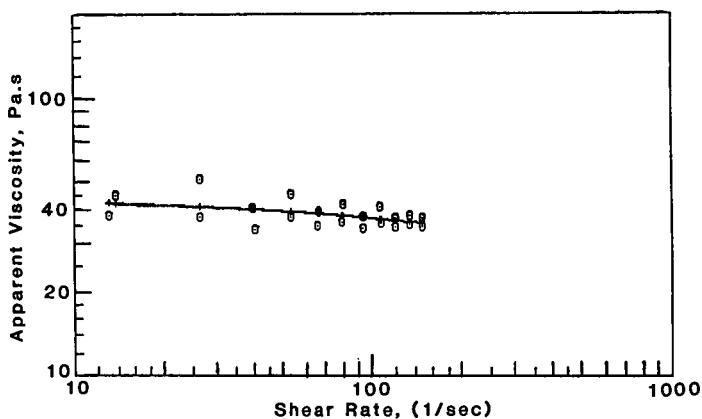


Fig. 3. Apparent viscosity of Kilauea Iki basalt melt as a function of shear rate at 1236°C.

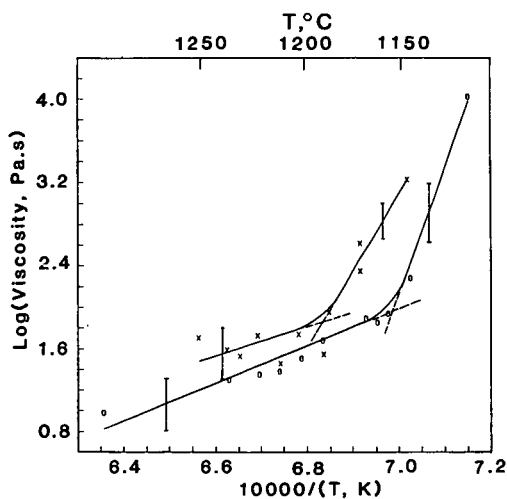


Fig. 4. Log (Apparent Viscosity) as a function of a reciprocal temperature. Present study, X; Shaw (1969), O.

CRYSTALLISATION OF COAL ASH MELTS

David P. Kalmanovitch and J. Williamson⁺

Energy Research Laboratories, CANMET, 555 Booth St., Ottawa, K1A 0G1, Canada

⁺Department of Metallurgy and Materials Science, Imperial College of Science and Technology, Prince Consort Rd., South Kensington, London, SW7, England.

The formation of ash deposits within p.f. coal-fired boilers may cause severe reduction in heat transfer and thermal efficiency. These deposits vary in nature from friable, slightly sintered fouling to dense, semi-vitreous slags. Utility boiler designers and operators use a variety of methods (9) to ascertain various design criteria or the likelihood of the ash to form deposits (its slagging or fouling propensity). The major technique used is the standard ash fusion test (2) in which a cone or pyramid of coal ash is heated at a given rate, both in air and a mildly reducing atmosphere, while the temperatures at which various degrees of deformation occur are recorded. This method is known to give inaccurate indications of slagging propensity due mainly to the subjective nature of the test and the fact that the technique does not duplicate the thermal history experienced by coal matter in a p.f. boiler.

Various laboratory studies, (5,6) have shown that significant fusion of coal mineral matter, the precursor to ash, occurs within a very short time-frame at temperatures analogous to those in the combustion zone of a boiler (about 1550-1650°C). This is confirmed by microscopical studies of p.f. fly ash. Despite total flight times of about 2s (6) and a temperature gradient ranging from 1650°C to about 300°C the characteristic nature of fly ash, that of hollow cenospheres is due to the presence of significant liquid phase at some stage of the particles' histories. This is further confirmed by mineralogical studies of the particles which sometimes reveals the presence of a refractory phase which had crystallised from a liquid and was not the product of thermal decomposition of an individual coal mineral (4,6). Raask has shown that the growth of deposits is by initial adhesion of fly ash particles to the surface of deposits already present. This adhesion is due to the liquid phase present and the rate of assimilation of the captured particle will be by sintering by viscous flow. From the theory of sintering (6) the rate of increase in strength (s) i.e. growth, of the deposit is given by:

$$\frac{ds}{dt} = \frac{3\gamma k}{2\eta r}$$

Where γ is the surface tension coefficient of the viscous phase, k a constant, r the initial radius of the particles and η the viscosity of the liquid. It can be seen that the nature of a deposit can be described by the degree of sintering which has taken place. For a given coal ash the parameters r and γ are effectively constant with respect to the variability of the viscosity. Therefore the factors which affect the rheological behaviour will determine to a great extent the rate of growth by viscous flow. For homogeneous melts the determining factors are temperature and chemical composition. Lauf has observed that the amount of fly ash particles collected at the outlet of various boilers was inversely proportional to the calculated viscosity (taking account of the different ash contents between the parent coals). (4) The viscosity was calculated by two methods based on the chemical composition; those of Watt and Fereday and Reid. (7,8) The observations confirm the viscosity relation above, albeit qualitatively and the assumption of complete melting of the coal mineral matter. A factor which has not received attention in the literature is the crystallisation of ash particles and/or the deposits already present. With devitrification of a phase from homogeneous melt the composition of the liquid phase will change depending on the precipitating phase and the degree of crystallisation. This in turn will directly affect the viscosity and hence the rate of growth of the deposits.

subjected to a series of crystallisation treatments within the reducing atmosphere. The quenched samples were analysed for phases present by X-ray diffraction and for the ratio of ferrous to ferric iron by a wet chemical technique.

The major observation of the crystallisation study of the ash melts was that the phase or phases which were precipitated contained only the predominant components, the minor components remaining in the liquid phase. Another observation was the reluctance of the melt to crystallise to the expected number of phases; only anorthite ($\text{CaO} \cdot \text{Al}_2\text{O}_3 \cdot 2\text{SiO}_2$) was determined to crystallise for the two western type ashes and mullite ($3\text{Al}_2\text{O}_3 \cdot 2\text{SiO}_2$) as the primary phase with a secondary phase of iron spinel; a member of the solid solution series magnetite ($\text{FeO} \cdot \text{Fe}_2\text{O}_3$) - hercynite ($\text{FeO} \cdot \text{Al}_2\text{O}_3$), only for the eastern type ash.

The crystallisation of the ternary compositions is discussed with respect to that predicted for each from the phase diagram for the system. The normalized ternary compositions of the two western type ashes were plotted on the phase diagram and the observed crystallisation compared with that predicted from the diagram and the behaviour of the model compositions. The system was found not to be able to correctly predict the primary crystalline phase for one of the two ashes but could account for the crystallisation of anorthite only for the other ash.

As quaternary systems are quite complex both the representation and crystallisation of compositions are discussed in the presentation. Planes of constant MgO content was used as the method of representation of the $\text{CaO-MgO-Al}_2\text{O}_3\text{-SiO}_2$, with planes at 5, 10 and 15 wt% prepared from literature sources and results of this study (3). The observed crystallisation of the glasses studied is discussed in terms of the equilibrium system, a striking observation being the apparent low solubility of magnesia in the compositions studied; a magnesia bearing phase precipitating for nearly all the glasses as primary or secondary phase. The corresponding normalised composition of the western type ashes were plotted on the 5% plane and the observed behaviour compared with the predicted crystallisation behaviour. As with the ternary system the four-component system only correctly predicted the primary crystalline phase for one of the ashes. Also the system would predict that a secondary phase containing magnesia would be expected to crystallise; behaviour which was not observed.

The true representation of the system $\text{CaO-Al}_2\text{O}_3\text{-SiO}_2\text{-iron oxide}$ is as a quinary system which is too complex for normal analysis. The results of the ferrous to ferric ratio of the quenched samples showed significant amount of ferric iron present. Fortunately analysis of the crystalline phases shows that predominantly the ferrous iron is taken up by the iron bearing phase (there was some evidence of solid solution of ferric iron in the iron spinel phase) and therefore the system could be approximated by the quaternary system $\text{CaO-FeO-Al}_2\text{O}_3\text{-SiO}_2$. Planes of constant FeO content (5-30 wt% at 5% increments) have been prepared from literature sources and the results of the crystallisation studies of the glasses are discussed in terms of the system. Unlike the quaternary system above the iron oxide remains in solution compared with magnesia. This would be predicted from the planes of the system and was observed in the crystallisation studies; no primary phase containing iron oxide was determined even for the glasses containing 20 wt% equivalent FeO. The corresponding normalised composition of the three ashes (iron oxide expressed as equivalent FeO) was plotted on the relevant plane of the system and the observed behaviour compared with that predicted from the phase diagram and the behaviour of the model compositions. The system correctly predicted the primary crystalline phase for all the ashes and could account for the crystallisation of anorthite only for the two western type ashes. While initially the system could not predict the crystallisation of iron spinel as the secondary phase for the eastern type ash analysis of the

Thus it will be of great value to be able to predict to some extent the crystallisation behaviour of coal ash melts. For simplicity it is initially necessary to consider that the crystallisation will be from a homogeneous melt. The data obtained can be extended to the phenomena of boiler deposits by using an accurate model of viscosity of ash melts based on chemical composition. The main aim of the study presented here was to obtain relevant crystallisation data of coal ashes and to model the behaviour so as to be able to predict the devitrification of a given ash. Coal ash is usually described as a mixture of up to 11 oxide components and though various investigators (1) have attempted to simplify the system by using certain equivalences the authors have chosen to use the major three or four components to model the observed behaviour.

For eastern type coal ashes the major components are silica, alumina, iron oxide and lime, whereas for western type ashes the major components are silica, alumina, lime and iron oxide or magnesia. In both cases these may comprise 90 wt% or more of the total composition of the ash. Sanyal and Williamson have shown that the initial crystallisation of two western type ashes of low iron oxide content (5% or less) could be described by the normalised composition on the ternary equilibrium diagram of the system $\text{CaO-Al}_2\text{O}_3\text{-SiO}_2$. The study presented here has extended the investigation to the devitrification of eastern type ash as well as two western type ashes and the crystallisation of model compositions corresponding to the normalised compositions of coal ashes. The systems studied were; $\text{CaO-Al}_2\text{O}_3\text{-SiO}_2$, $\text{CaO-MgO-Al}_2\text{O}_3\text{-SiO}_2$ and $\text{CaO-Al}_2\text{O}_3\text{-SiO}_2\text{-iron oxide}$, to ascertain which system or systems govern the behaviour most adequately.

The crystallisation of three coal ashes (two western and one eastern type) was determined under laboratory conditions by fusing a sample in an electric muffle furnace to achieve complete melting of the coal minerals. Devitrification was induced by reducing the temperature to a given level and leaving the sample for a given time. The sample was then quenched, effectively freezing the phases present at the elevated temperatures. The sample was analysed by petrographic microscopy and X-ray diffraction. The treatment was repeated over a range of temperatures and times for each sample.

For the study of the crystallisation of the model compositions five ternary CaO , Al_2O_3 and SiO_2 compositions were chosen which were expected to exhibit different behaviour (from the corresponding phase diagram) while being in the compositional region relevant to coal ashes. Homogenous glasses were produced by fusing the correct mixture of the oxide components. The crystallisation of the glasses was determined in an analogous manner to that used for the ash melts. The same five compositions were used as the basis for the study of the crystallisation of the system $\text{CaO-MgO-Al}_2\text{O}_3\text{-SiO}_2$. Two series of compositions were prepared based on the ternary compositions with 5 and 10 wt% MgO respectively. Glasses were produced and the liquidus and crystallisation behaviour determined by a quenching technique.

As iron oxide exists in two oxidation states (ferrous and ferric) in p.f. ash deposits it was necessary to study the crystallisation of glasses in the system $\text{CaO-Al}_2\text{O}_3\text{-SiO}_2\text{-iron oxide}$ in a controlled atmosphere; the same as that used in the reducing part of the standard ash fusion test i.e. $\text{CO}_2\text{:H}_2$ mixture 1:1 v/v. The range of iron oxide content in coal ashes is wider than that of magnesia and hence glasses were prepared with up to 20 wt% equivalent FeO . Two series of glasses were produced based on the five ternary compositions with 5 and 10 wt% equivalent FeO with another two series of glasses based on three of the five composition with 15 and 20 wt% equivalent FeO . The glasses were ground to a fine powder and each was

results of the model compositions indicated that ferric iron present in the liquid phase reduced the solubility of iron oxide which could account for the behaviour.

CONCLUSIONS

Therefore the system $\text{CaO-FeO-Al}_2\text{O}_3\text{-SiO}_2$, governs the initial crystallisation of the ash melts studied. The major aim of this study was to be able to predict the crystallisation of ash melts and relate the behaviour to boiler deposit growth. The phases present in six boiler deposits are compared with that predicted from the corresponding normalised composition in the presentation and shows that for all six (three western and three eastern type) the quaternary system predicts the primary phase. Furthermore the change in composition of the liquid phase for two of the ashes (one slagging the other non-slagging) for a range of degrees of crystallisation shows a great difference in terms of the relative concentration of the components which govern viscosity. While the liquid phase for the non-slagging ash became enriched predominantly in silica (the major viscosity-increasing component) the slagging ash became enriched in viscosity reducing components. This relates directly to the model of deposit growth discussed above and is a confirmation of the model.

The results of the study presented indicate the use of phase equilibria data to be phenomena of p.f. boiler deposits and the possible extension to the prediction of boiler fouling and slagging.

REFERENCES:

1. Barrett, E. P., "The fusion, flow and clinkering of coal ash. A survey of the chemical background." Chemistry of Coal Utilization, Ed. E. Lowry, Vol. 1, 1945, Ch. 15, pp 496-576.
2. British Standard 1016, Pt. 15, 1970. "Methods for the analysis of coal and coke, Fusibility of coal ash and coke ash", pp 14.
3. Kalmanovitch, D. P., "Reactions in coal ash melts", PhD Thesis, Univ. London 1983.
4. Lauf, R. J., "cenospheres in fly ash and conditions favouring their formation". Fuel, 60, 1981, p. 1177-79.
5. Padia, A. S., "The behaviour of ash in pulverised coal under simulated combustion conditions". D.Sc. Thesis, M.I.T., 1976.
6. Raask, E., "Flame imprinted characteristics of ash relevant to boiler slagging, corrosion, and erosion". J. Eng. Power, 104, 1982, p. 858-66.
7. Reid, W. T., method given in "Influence of coal mineral matter on slagging of utility boilers". E.P.R.I. report 736, 1981, p. D-1-4.
8. Watt, J. D. & Fereday, F., "The flow properties of slags formed from the ashes of British coals. Pt. I. Viscosity of homogeneous slags in relation to slag composition". J. Inst. Fuel, 42, 1969, p. 99-103.
9. Winegartner, E. C. "Coal fouling and slagging parameters". A.S.M.E. Special Publication, 1974.

THERMAL CONDUCTIVITY AND HEAT TRANSFER IN COAL SLAGS

K C MILLS

National Physical Laboratory, Teddington, Middlesex, TW11 0LW, UK

1. INTRODUCTION

During the gasification of coal, both molten and solid slags are formed in the converter, and the heat transfer within the gasification chamber is governed to a large extent by the thermal properties of the slag phase. Thus in order to carry out either heat balance or modelling calculations it is necessary to have reliable data for the thermal properties of both solid and liquid coal slags. However, the thermal transfer mechanisms in high temperature processes involving slags are exceedingly complex since heat can be transported by convection, radiation and thermal conduction. The total thermal conductivity (k_{eff}) is, in turn, made up from contributions from (i) the thermal ("phonon") conductivity, k_c , (ii) radiation conductivity, k_R and (iii) electronic conductivity, k_{el} . Heat balance calculations must take account of all these thermal transport mechanisms; consequently it is necessary to study the effects of the various mechanisms for not only do they determine the heat transfer in the gasifier, but they can also critically affect the experimental values derived for the thermal conductivity of the slag. Hence the factors affecting the thermal conductivity of slags will be examined and their effect on the various methods available for the measurement of thermal conductivities will be assessed. Finally, experimental data for the thermal conductivity of slags, glasses and magmas will be evaluated to provide a reliable data base for the thermal conductivity of slags, and to determine the likely effects of variations in chemical composition upon values for coal slags.

2. THERMAL CONDUCTION MECHANISMS

2.1 Thermal "phonon" conductivity (k_c)

Heat is transferred through a medium by phonons, which are quanta of energy associated with each mode of vibration in the sample. This mode of conduction is thus referred to as thermal, phonon or lattice conduction. Scattering of the phonons causes a decrease in the thermal conductivity and hence the conductivity is sensitive to the structure of the sample. Scattering of the phonons can occur by collisions of the phonons with one another, or by impact with grain boundaries or crystal imperfections, such as pores. Thus a low-density, highly-porous material will have a low thermal conductivity. In glassy, non-crystalline materials it has been suggested (1) that thermal conductivity decreases as the disordering of the silicate network increases.

2.2 Radiation conductivity (k_R)

Measurements of the thermal conductivity of glasses were found to be dependent upon the thickness of the specimens used, and this is shown in Figure 1. This behaviour was ascribed to the contribution from radiation conductivity, k_R , which can occur in semi-transparent media like slags and glasses. Radiation conductivity occurs by a mechanism involving absorption and emittance of radiant energy by various sections through the medium. Consider a thin section in the slag, radiant energy absorbed by the section will cause it to increase in temperature and consequently radiant heat will be emitted to cooler sections. This process can occur right through the medium and it is obvious that the energy transferred in this way will increase with increasing number of sections (ie increasing thickness) until the point where k_R attains a constant value. At this point the slag is said to be "optically thick", and this is usually considered to occur when $\alpha d > 3.5$, where α and d are the absorption coefficient and thickness of the slag, respectively.

At high temperatures, radiation conductivity can be the predominant mode of conduction, eg in glassmaking more than 90% of the total conductivity occurs by radiation conduction. The radiation conductivity can be calculated for an optically-thick sample if steady-state conditions apply and if it is assumed that the absorption coefficient of the medium, α , is independent of wavelength, λ , ie grey-body conditions obtain. For these conditions k_R can be calculated by use of equation 1), where σ and n are the Stefan-Boltzmann constant and refractive index, respectively.

$$k_R = \frac{16\sigma n^2 T^3}{3\alpha} \quad 1)$$

Values of k_R cannot be calculated for optically-thin samples ($\alpha d < 3.5$) and for some measurement techniques involving non-steady state conditions. Thus it is obvious that reliable values of thermal conductivity can only be obtained when either k_R is negligible, or where it can be calculated reliably for optically-thick conditions.

Absorption coefficient (α)

The absorption coefficient is a very important parameter, as it determines (i) the magnitude of k_R (equation 1) and (ii) the thickness at which a slag becomes optically thick ($\alpha d > 3.5$). Hence increasing α has the effect of decreasing k_R and decreasing the depth at which a slag becomes optically thick. If a particular slag sample were optically thin, these two factors would operate in opposition to one another.

The absorption coefficient is markedly dependent upon the amounts of FeO and MnO present in the slag (2); although Fe_2O_3 absorbs infra-red radiation, its effect on α is much less pronounced than that of FeO. An empirical rule has been derived (2) for glasses containing less than 5% FeO, the absorption coefficient at room temperature is given by the relationship, $\alpha = 11. (\% \text{ FeO})$.

A basic assumption adopted in deriving equation 1) was that α was independent of wavelength; however, in practice the spectral absorption coefficient (α_λ) varies with the wavelength (λ) as shown in Figure 2 for a glass containing ca. 5% FeO (3). It can be seen from this figure that there is strong absorption by FeO at ca. $1 \mu m$ and by SiO_2 at ca. $4.4 \mu m$. At high temperatures this restricts absorption by the slag to a "window", in the wavelength range $1-4.4 \mu m$. However, even within this wavelength band there is some variation in α_λ and the average absorption coefficient, α_m , is determined by weighting of the α_λ values.

The average absorption coefficient, α_m , can be affected by temperature in two different ways. Firstly, the absorption spectrum, ie, (α_λ), can change markedly with temperature and consequently alter the value of α_m . Secondly, even if the absorption spectrum is unaffected by temperature, α_m would continue to be a function of temperature because the wavelength distribution used in deriving α_m is itself a function of temperature. This can be seen in Figure 3 where the fraction of total energy emitted in the "window" $1-4.4 \mu m$ constitutes 61.1%, 79.5% and 81.9% of the total energy emitted at 1073K, 1573K and 1773K, respectively. In a similar manner, the various α_λ values of the spectrum will have to be weighted differently in the calculation of α_m for the three temperatures in question.

It can be seen from Figure 2 that α_m increases with increasing temperature, and similar behaviour has been observed in rocks and minerals (4,5,6). By contrast, the absorption coefficients (α_m) of amber glass have been found to decrease with increasing temperature.

Extinction coefficient (E)

In solids, radiant energy can be scattered by grain boundaries, pores and cracks in the material. In these cases, it is necessary to use the extinction coefficient (E) which is given by the relationship $E = \alpha + s$, where s is the scattering coefficient.

2.3 Electronic conductivity (k_{el})

It has been reported that glasses which contain significant concentrations of Fe^{2+} ions behave in a similar manner to semi-conductors and hence thermal conduction via conduction electrons, holes, etc. could be significant, according to Fine et al.⁽⁷⁾. Little is known of this mechanism in relation to the heat transfer in slags and consequently the contribution of k_{el} to the measured thermal conductivities has been ignored in this review.

2.4 Total thermal conductivity (k_{eff})

In practice, the radiation and conduction contributions to the heat flux (Q) are interactive, and the interpretation of the combined conductive-radiative heat transfer is exceedingly complex. Various models have therefore been proposed to simplify the theory of the heat transfer process. One widely-used model is the diffusion approximation which assumes that the heat flux (Q) is given by equation 2), where k_{eff} is the effective thermal conductivity and is defined by equation 3) where x is the distance. Gardon (8) has pointed out that this model only applies strictly when (i) k_R is small and (ii) $\alpha d \gg 8$.

$$Q = -k_{eff} (dT/dx) \quad 2)$$

$$k_{eff} = k_c + k_R \quad 3)$$

3. EXPERIMENTAL METHODS FOR DETERMINING THERMAL CONDUCTIVITY

The experimental methods available for measuring thermal conductivities are summarised below; more detailed reviews of the experimental techniques are available elsewhere (3,9,10,11). The techniques can be divided into three classes: (i) steady-state methods, (ii) non-steady state methods, and (iii) indirect methods for the determination of k_R . The steady-state methods usually yield k_{eff} values and the non-steady state techniques usually produce thermal diffusivity (a_{eff}) values, which can be converted to thermal conductivity values by use of equation 4), where ρ and C_p are the density and heat capacity of the slag.

$$k = a \cdot C_p \cdot \rho \quad 4)$$

3.1 Steady-state methods

These methods all yield k_{eff} values provided that the specimen is optically thick.

In the linear heat-flow method two disc-shaped specimens are placed on either side of an electrically-heated plate and the temperature profiles across the samples are monitored by thermocouples sited on both faces of the specimens. The apparatus is well insulated to minimise heat losses. In some versions of this method, the total heat fluxes passing through the samples are determined by calorimeters in contact with the specimens. When high-temperature measurements are required, this technique is usually operated as a comparative method (12).

In the radial heat-flow method the specimen is in the shape of a hollow cylinder, which is sited in the annulus between two coaxial cylinders with the internal cylinder acting as a radial heat source (13). The temperature profile across the specimen is determined by thermocouples placed on the inside walls of the two cylinders. This method requires a large isothermal zone in the furnace, which is difficult to achieve at high temperatures. When this technique is used for measurements on liquids it is prone to errors from convective heat transfer.

3.2 Non-steady state methods

In the radial wave method the slag is placed in a cylindrical crucible sited in the isothermal zone of a furnace, and thermocouples are located on the walls and along the geometric axis of the crucible (the slag). The outside wall of the

of the crucible is then subjected to a sinusoidal variation of temperature and the variation in temperature of the central thermocouple is monitored. There is a phase shift between the input and output which is related to the thermal diffusivity of the slag. In the modification of this apparatus used by Elliott and co-workers^(7,14) the periodic variation in temperature is produced in a wire running along the central axis of the cylindrical crucible, and the phase shift is measured in the signal of the thermocouples sited on the walls of the crucible. The thermal diffusivity values obtained with this method may be vulnerable to errors arising from convective heat transfer.

In the modulated beam method the specimen is in the form of a disc, which is maintained at a constant temperature, whilst the front face of the disc is subjected to a laser beam which produces a periodic variation in temperature of constant frequency. The phase shift between this input and the signal from a temperature sensor in contact with the back face is determined. By carrying out measurements at two or more frequencies, Schatz and Simmons⁽⁶⁾ were able to derive values of both a_{eff} and the extinction coefficient. If this method were applied to measurements in liquids, it too would be prone to errors caused by convection.

The laser pulse method^(15,16) when applied to solids uses a disc-shaped slag specimen coated with metallic films on both planar surfaces. A laser pulse is directed on to the front face of the specimen and the temperature of the back face is monitored continuously. The maximum temperature rise of the back face (ΔT_{max}) usually occurs after ca. 10 seconds, and a_{eff} may be computed from the time taken ($t_{0.5}$) for the back face to attain a temperature rise of $(0.5 \Delta T_{max})$. The method has also been applied to measurements on liquid slags^(15,17) which were contained in Al_2O_3 or BN crucibles. The major advantage of this technique is that the short duration of the experiment minimises the errors due to convection. The major disadvantage is that the maximum specimen thickness is about 4 mm, and consequently optically-thick conditions only apply when the extinction coefficient is greater than 9 cm^{-1} . A second disadvantage is that the laser pulse method is a transient technique and k_R cannot be calculated by equation 1), which is applicable to steady-state conditions; at the present time no formulae exist for the calculation of k_R for this method. Thus this technique is most useful when applied to specimens which have (i) very small values of αd (ie $\alpha d \ll 3.5$) where $a_{eff} \approx a_c$, or (ii) large extinction coefficients where k_R is negligible and thus $a_{eff} = a_c$.

The line source method is also a transient technique and is the standard method for measuring the thermal conductivities of liquids at lower temperatures. In the high-temperature versions, this method consists of a fine Pt wire (ca. 0.1 mm dia) which is sited centrally in a crucible of molten slag. This wire acts as both heating element and temperature sensor. When an AC or DC current is applied to the wire, the temperature rise of the wire (ΔT) is monitored continuously during the heating period (ca. 1 second). A linear relationship exists between ΔT and $\ln(\text{time})$, the slope of which is proportional to $(1/k)$. This method has the advantage that convective heat transfer is eliminated (if convection does occur it results in a non-linear $\Delta T - \ln(\text{time})$ plot and can therefore be readily detected). Routines are available for calculating the value of k_R for optically-thick conditions⁽¹⁸⁾; however, de Castro et al.⁽¹⁹⁾ have recently proposed that k_R is negligible in the values of k_{eff} measured by this technique at ambient temperatures (ie $k_R \approx 0$, $k_{eff} = k_c$). There is evidence to support the view that $k_R \approx 0$, as measurements made with this technique at higher temperatures^(20,21,22) yield much lower values of k_{eff} for slags than those obtained by steady-state techniques. Furthermore, Powell and Mills⁽²³⁾ have pointed out that the thermal conductivity data for molten salts become more consistent if k_R is taken to be zero in the various line source determinations.

3.3 Indirect measurements of k_R

The absorption (or extinction) coefficient can be determined by measurement of the optical transmissivity (τ) of the slag as a function of wavelength; the absorption coefficient (α) is given by equation 5), where d is the thickness of the specimen.

Measurements at high temperatures are carried out by using

$$\alpha_{\lambda} = -\ln(\tau_{\lambda})/d \quad 5)$$

an assembly of mirrors to direct a beam of radiation of known frequency on to a disc-shaped specimen sited in a tube furnace. The transmitted beam is diverted into an infrared spectrophotometer where the transmissivity is determined. Blazek and Endrys⁽³⁾ have reported that k_R values for glasses calculated from absorption coefficient data are in good agreement with values of $(k_{eff} - k_c)$ determined experimentally.

3.4 Summary of experimental limitations

- (i) It is important to ensure that the thermal conductivity measurements on semi-transparent media should be carried out with optically-thick specimens, as k_R cannot be calculated for optically-thin conditions. It is recommended that absorption coefficient measurements should also be carried out to determine the slag thickness required to produce an optically-thick specimen.
- (ii) The non-transient techniques are prone to errors due to convective heat transfer.
- (iii) At the present time no reliable routines are available for calculating the k_R contribution to the overall thermal conductivity measured in transient techniques; there is some evidence to suggest that k_R is negligible in measurements obtained by the line source method.

4. REVIEW OF THE EXISTANT DATA FOR SLAGS

There is a paucity of data for coal slags; it is therefore necessary to study a much broader range of slags in order to determine the effects of compositional change on the thermal conductivity of the slag. One problem continually encountered is that the distribution of Fe in slags between (Fe^{3+}) , (Fe^{2+}) and free iron is not reported, and this can have a marked effect on the absorption coefficient and consequently k_R . Furthermore, the ratio of $((Fe^{2+})/(Fe^{3+}))$ is known to vary with (i) temperature, (ii) $p(O_2)$ and (iii) the composition of the slag, (Fe^{2+}) increasing with increasing SiO_2 and TiO_2 , and decreasing CaO and Na_2O .

4.1 $CaO + SiO_2 + FeO_x$

Fine et al⁽⁷⁾ determined the absorption spectra at room temperature of three slags containing 0, 7 and 14% FeO (Figure 4). The absorption coefficients of the slags containing 7 and 14% FeO will probably increase with increasing temperature as the (Fe^{2+}/Fe^{3+}) ratio increases with increasing temperature. An increase in α with increasing temperature can also be seen in Figure 2. Fine et al⁽⁷⁾ used the radial wave method to determine a_{eff} of solid and liquid slags containing 0 to 25% FeO; their results are summarised in equation 6), where B represents the basicity, ie (CaO/SiO_2) ratio and T is the temperature in $(^{\circ}C)$.

$$a_{eff} = 10^{-7} (1.5 - 0.5 B) + 1.8 \times 10^{-6} \frac{(T/1500)^3}{(\%FeO)^{0.8}} m^{-1} \quad 6)$$

This equation indicates that increasing the FeO content results in a reduction of a_{eff} ; this behaviour is due presumably to the increase in α and hence the consequent decrease in k_R with increasing FeO content. However, Nauman et al⁽²⁴⁾ using the same experimental technique as Fine et al⁽⁷⁾ obtained the $k_{eff} - (\%FeO)$ relationship shown in Figure 5 for molten slags with high FeO contents. The density of slags are known to increase with increasing (FeO_x, MnO) content, thus $k (= a.C_p.\rho)$ would be expected to increase as the level of FeO increases⁽²⁵⁾. However, calculations have shown that this increase in k would be ca. 30%, and this alone would not account for the increase in k shown in Figure 5. Thus it must be concluded that FeO additions do increase the thermal diffusivity of the

system. In these slags with high FeO content, the absorption coefficient must be very high and thus k_R must be negligible and $k_{eff} = k_C$.

4.2 CaO + Al₂O₃ + SiO₂

Measurements on solid slags have been reported by Kingery⁽¹²⁾ (comparative linear heat-flow method), Osinovskikh⁽²⁵⁾ and Susa *et al*⁽²¹⁾ (line source method), and for the liquid phase by Susa *et al*⁽²¹⁾ and Ogino *et al*⁽¹³⁾ (radial heat-flow); the results are summarised in Figure 6. The data recorded by Osinovskikh⁽²⁵⁾ appear to be too low, but there is some measure of agreement between the data obtained for the liquid near the liquidus temperature (T_{liq}). However, the reported, thermal conductivity values diverge as the temperature increases, and this is possibly due to the negligible contribution of k_R in the line source measurements⁽²⁰⁾ and the effects of k_R and convective heat transfer on the value due to Ogino⁽¹³⁾. The value due to Kingery⁽¹²⁾ for the compound 3Al₂O₃.SiO₂ is appreciably higher than that for the slags of the ternary system.

4.3 MgO + Al₂O₃ + SiO₂

Values for the various binary compounds occurring in this system have been reported by Rudkin⁽²⁶⁾ and by Kingery⁽¹²⁾ (comparative linear heat-flow method), and by Schatz and Simmons⁽⁶⁾ (modulated beam method) for temperatures up to 1300 °C; there is excellent agreement between the values due to the latter two groups of workers. Schatz and Simmons⁽⁶⁾ reported that extinction coefficient of 2MgO.SiO₂ increases from 5 cm⁻¹ at 270 °C to 25 cm⁻¹ at 1300 °C.

4.4 Na₂O + SiO₂

Susa *et al*⁽²¹⁾ (line source method) reported thermal conductivity data for solid and liquid slags for three compositions; the single value obtained by Ogino *et al*⁽¹³⁾ (radial heat-flow method) is in reasonable agreement with these data.

4.5 Glasses

Blazek and Endrys⁽³⁾ have reviewed the thermal conductivity data for glasses. The lattice thermal conductivity, k_C , for glasses is relatively unaffected by composition and was found to increase with temperature from 1Wm⁻¹K⁻¹ at 25 °C to 2.7 Wm⁻¹K⁻¹ at 1300 °C. However, the radiation conduction is frequently the dominant mode of heat conduction in glasses at high temperatures.

4.6 CaF₂-based slags

Extinction coefficients have been reported (1.3 cm⁻¹ for 1000-1300 °C) by Keene and Mills⁽²⁷⁾, and absorption coefficients (1.3 cm⁻¹) for the liquid state by Mitchell and Wadier⁽²²⁾.

The thermal conductivity values for polycrystalline (optically-thick) CaF₂ obtained by Kingery⁽¹²⁾ (comparative linear flow method) and by Taylor and Mills⁽¹⁶⁾ are in reasonable agreement (Figure 7). However, there is an appreciable discrepancy between the values of k obtained by the line source method⁽²⁰⁻²²⁾ and the single value due to Ogino *et al*⁽¹³⁾ (radial heat source method).

The reason for the discrepancy probably lies in the magnitude of the k_R values measured in the two experiments, as k_R is probably negligible for the line source technique, in contrast to the steady-state method where k_R would be appreciable despite the fact that the sample was probably optically thin ($\alpha d \approx 0.8$).

4.7 TiO₂-based slags

Values of thermal diffusivity, a_{eff} , of ca. 3×10^{-7} m²s⁻¹ have been reported by Raflovich and Denisova⁽²⁸⁾ for slags based on TiO₂ (>45%) and SiO₂ with small

amounts of Al_2O_3 and Fe_2O_3 . The data reported by Osinokikh *et al*⁽²⁵⁾ for slags with less than 15% TiO_2 are much lower, this is probably due to the high porosity of the sample used.

4.8 Continuous casting slags

These slags have the approximate composition ($\text{CaO} = \text{SiO}_2 = 35\%$; $\text{Al}_2\text{O}_3 \approx 7\%$; Na_2O (4-15%) and CaF_2 (5-8%). Olusanya⁽²⁹⁾ has reported that the absorption coefficients lie in the range (0.5 - 5 cm^{-1}) and thus k_R could be appreciable in these slags. Values for a_{eff} were obtained for ten glassy-slugs by Taylor and Mills⁽³⁰⁾ (laser pulse method) which lay between 4 and 5 $\times 10^{-7} \text{ m}^2\text{s}^{-1}$ (Figure 8); these slags were optically thin ($ud = 0.4$) and thus we might expect k_R to be small and $k_{\text{eff}} \approx k_C$. Some crystallisation of the samples occurred at temperatures above the glass temperature in these experiments, and this resulted in an initial decrease in a_{eff} , which was subsequently followed by an increase in the thermal diffusivity. Taylor and Mills reported that a_{eff} of a crystallised specimen had a value of 6 $\times 10^{-7} \text{ m}^2\text{s}^{-1}$, which is higher than that of the glassy specimens; the crystalline samples would have a higher extinction coefficient and thus k_R would be low and hence $a_{\text{eff}} = a_C$. Thermal conductivity values for the liquid phase have been obtained by Nagata *et al*⁽³¹⁾ and by Powell *et al*⁽³²⁾ (line source method), and by Taylor and Edwards⁽¹⁷⁾ (laser pulse method) and by Ohmiya *et al*⁽³³⁾ (interpretation of thermal flux data). As can be seen from Figure 8, the results from the line source technique are lower than the other data, and this probably reflects the fact that k_R is negligible in the line source experiments. The increase in k_{eff} observed by Taylor and Edwards⁽¹⁷⁾ above the solidus temperature is probably due to the decrease in α (and increase in k_R), as liquid is formed from crystallised slag.

4.9 Blast furnace slags

Values of k_{eff} have been reported by Ischenko⁽³⁴⁾ and by Vargaftik and Oleschuk⁽³⁵⁾ for temperatures in the range (200-1000 °C). The values cited are lower than those reported for other slags, which is presumably due to the high porosity of the samples used by these workers.

4.10 Rocks and Minerals

Absorption and extinction coefficients for several rocks and minerals^(4,5,6) were found to increase appreciably at high temperatures, eg α_M (peridot) increases from 0.5 cm^{-1} at 25 °C to 4.3 cm^{-1} at 1240°C. Values of k_{eff} (or a_{eff}) have been recorded by Kingery⁽¹²⁾, by Kawada⁽³⁶⁾ (comparative linear flow method), by Murase and McBirney⁽³⁷⁾ (radial heat flow), and Schatz and Simmons⁽⁶⁾ (modulated beam method). The results are given in Figure 9, and Schatz and Simmons⁽⁶⁾ reported that for forsterite and olivine at 1300 °C, approximately half of the measured k_{eff} value was due to the contribution of k_R . There is good agreement between the results reported by Kingery⁽¹²⁾ and by Schatz and Simmons⁽⁶⁾ for k_{eff} of forsterite. The values of k_{eff} reported by Murase and McBirney⁽³⁷⁾ are appreciably lower than those reported by other investigators, which may indicate systematic errors in the method, or may merely be due to the higher SiO_2 content of the samples studied by Murase and McBirney. The sharp increase in k recorded above 1100 °C for some samples probably indicates the onset of melting, which causes the extinction coefficient to decrease and hence k_R to increase appreciably. It is noticeable that Kawada⁽³⁶⁾ recorded no marked increase in k_{eff} for dunite (DU), which has an FeO content of 13% and where k_R would be negligible.

4.11 Coal slags

The experimental details of various investigations concerned with these slags are summarised in Table 1. The results are presented in Figure 10; only the upper and lower $a(T)$ curves reported by Gibby and Bates have been plotted.

The absorption coefficients of these slags are probably quite high, as they contain appreciable levels of FeO and free Fe. Thus the radiation contribution, k_R , will

be relatively small. There is good agreement between the results of the investigations when the appreciable differences in the composition of the slags is taken into account. Gibby and Bates⁽¹⁵⁾ reported that for solid slags the value of a_{eff} varied appreciably from run to run and appeared to be dependent upon the thermal history of the sample. This behaviour was attributed to the crystallinity of the sample and the fact that a_{eff} (crystalline) $>$ a (glass), which is in agreement with the observations on continuous-casting slags. Gibby and Bates⁽¹⁵⁾ also observed that K_2O additions resulted in a decrease in a_{eff} up to 900 °C, and that the a_{eff} -(T) relationship showed a sharp inflection around 950 °C, which was attributed to the crystallisation of the slags.

These workers also reported that a_{eff} appeared to decrease with increasing SiO_2 content or with the ratio $(SiO_2/(SiO_2 + Fe_2O_3 + MgO + CaO))$. This implies that k_c is probably dependent upon the structure of the silicate slag, and thus it should be possible to build up a reliable model for the estimation of k_c in due course. However, it is also possible that the decrease in a_{eff} with increasing SiO_2 content may simply reflect the lower fraction of crystalline phase present in the slag.

5. DISCUSSION

The thermal conductivity data for slags, magmas and glasses have been collated in Figure 11. It can be seen that k_{eff} values for solid coal slags are similar to those for slags from the systems $CaO + Al_2O_3 + SiO_2$ and $CaO + SiO_2 + FeO$ and for those used in continuous casting. Thus it would appear that the chemical composition of the slag has little effect on the values of k_{eff} ; however, certain oxides (eg SiO_2 , CaO) could exert some influence on the conductivity by altering the crystallinity of the slag. Furthermore, the radiation conduction will also be affected by the crystallinity of the sample as the extinction coefficient will be high for crystalline materials.

It is more difficult to evaluate the thermal conductivity of molten slags, although the data obtained for coal slags⁽¹⁵⁾ and for slags of the system $CaO + FeO + SiO_2$ ⁽⁷⁾⁽¹⁴⁾ indicate that k_{eff} for the liquid near the melting-point is similar to that for the solid phase. It is noticeable that the k_{eff} values obtained for liquid slags by the line source method are considerably lower than the values obtained with other techniques. It is possible that the line source method is prone to systematic errors when applied to molten slags, but a more likely explanation is that the k_R is negligible in these experiments. As coal slags contain relatively high levels of $(FeO + Fe_2O_3)$, it would be expected that the absorption coefficient of the slag would be high and that the k_R contribution would be small. However k_R increases dramatically with temperature and even a slag with a relatively high absorption coefficient of 100 cm⁻¹ would give rise to a contribution of k_R of 0.4 Wm⁻¹K⁻¹ at 1800 K.

However as the absorption coefficient is very dependent upon the (Fe^{2+}) concentration the value of k_R will be dependent upon the various factors affecting the (Fe^{2+}/Fe^{3+}) ratio in the slag viz, the ratio increases with (i) increasing temperature (ii) decreasing $p(O_2)$ (iii) increasing SiO_2 and TiO_2 contents and decreasing CaO , Na_2O and K_2O contents in the slag. This review has revealed the urgent need for absorption coefficient data for coal slags at high temperatures and for information relating the absorption coefficient to the FeO content of the slag.

The heat transfer process in the coal gasifier can also be affected by the layer of slag which lines the walls of the gasifier. Recently, Grieveson and Bagha⁽³⁸⁾ have developed a simple experiment for measuring the thermal flux (Q) in various slags used in the continuous casting of steel. A water-cooled, copper finger is lowered into a crucible containing molten iron covered with a layer of slag and a layer of solidified slag forms around the cold finger. The thermal flux is determined by measuring the

temperature rise of the cooling water flowing through the copper finger. It was found that the heat flux was related to (i) the thickness of the slag layer and (ii) the thermal resistance of the Cu/slag interface. The thickness of the slag layer is, in turn, dependent upon the viscosity of the slag and upon other factors determining the "melt back" of the slag layer. Grieveson and Bagha (38) observed that the thermal resistance of the Cu/slag interface appeared to be related to (i) the mineralogical constitution of the slag and (ii) the strength of the adhesion between the copper and the slag eg. Q (glass from CaO.SiO_2 field giving good Cu/slag adhesion) > Q (glass from $\text{CaO.Al}_2\text{O}_3.2\text{SiO}_2$ phase field with poor Cu/slag adhesion). Thus relatively simple experiments like these simulation tests can provide us with a valuable insight into the factors affecting heat transfer mechanisms occurring in industrial processes.

CONCLUSIONS

- (i) Experimental data for the thermal conductivities of slags must be carefully analysed to establish the boundary conditions of the experiment (eg. optical thickness of the specimen, magnitude of k_R etc.) This evaluation of the data allows one to determine the suitability of a specific thermal conductivity value for subsequent use in heat balance calculations for the gasifier.
- (ii) The thermal conductivities of coal slags are not very dependent upon the chemical composition of the slag.
- (iii) The thermal conductivity of a slag is dependent upon the degree of crystallization and consequently upon the thermal history of the specimen; the thermal conductivity of the crystalline phase is greater than that of the glassy phase.
- (iv) The radiation conduction, k_R , is principally determined by the magnitude of the absorption (or extinction) coefficient. As the absorption coefficient of the slag is largely dependent upon the (Fe^{2+}) concentration in the slag, it will also be dependent upon the factors affecting the $(\text{Fe}^{2+}/\text{Fe}^{3+})$ ratio viz. temperature, $p(\text{O}_2)$ and the SiO_2 , CaO and Na_2O contents of the slag.
- (v) Experimental data are required for the absorption coefficients of coal slags at high temperatures so that the relationship between α_m and the FeO content can be established.
- (vi) Heat transfer in the coal gasifier will be partially dependent upon the thermal resistance of the slag/wall interface and this, in turn, will be dependent upon the mineralogical constitution of the slag adjacent to the wall.

ACKNOWLEDGEMENTS

Valuable discussions with B J Keene, (National Physical Laboratory) Professor P Grieveson (Imperial College) and Dr R Taylor (UMIST) are gratefully acknowledged.

REFERENCES

- (1) AMMAR, M M., GHARIB, S, HALAWA, M M, E L BADRY, K, GHONEIM, N A and E L BATAL, H A. J. Non-Cryst. Solids 1982, 53, 165.
- (2) STEELE, F N and DOUGLAS, R W. Phys. Chem. Glasses 1965, 6, 246.
- (3) BLAZEK, A and ENDRYS, J. Review of thermal conductivity data in glass, Part II Thermal conductivity at high temperatures published Intl. Commission on Glass, 1983.

- (4) FUKAO, Y., MITZUTANI, H. and UYEDA, S. Phys. Earth Planet Interiors 1968, 1, 57.
- (5) ARONSON, J R, BELLOTI, L H., ECROAD, S W, EMSLIE, A G., MCCONNEL, R K and THUNA, P C von. J Geophys. Res. 1970, 75, 3443.
- (6) SCHATZ, J F and SIMMONS, G. J. Geophys. Res. 1972, 77, 6966.
- (7) FINE, H A; ENGH, T, and ELLIOTT, J H; Metall. Trans B, 1976, 7B, 277.
- (8) GARDON, R; paper presented at 2nd Intl. Thermal Conductivity Conference, Ottawa, 1962, 167.
- (9) GARDON, R Review of thermal conductivity data in glass, Part 1 Thermal conductivity at low and moderate temperatures published Intl. Commission on Glass, 1983.
- (10) TOULOUKIAN, Y S, POWELL, R W, H O, C Y and KLEMENS, P G. Thermophysical Properties of Matter, volumes 1 (1970) and volume 10 (1973) published by IFI/Plenum, New York
- (11) TYE, R P, Thermal conductivity, volumes 1 and 2, 1969, published by Academic Press, New York.
- (12) KINGERY, W D, FRANCL, J, COBLE, R L and VASILOS, T. J. Amer. Ceram. Soc., 1954, 37, 107.
- (13) OGINO, K, NISHIWAKI, A, YAMAMOTO, K and HAMA, S. Paper presented at Intl. Symp. Phys. Chem. Steelmaking, Toronto, 1982, III-33.
- (14) NAUMAN, J; FOO, G; and ELLIOTT, J F; Extractive Metallurgy of Copper, Chapter 12, 237.
- (15) GIBBY, R L and BATES, J L; 10th Thermal Conductivity Conference, held Newton, Mass., Sept. 1970, IV-7,8. see also BATES, J L, Final Report to National Science Foundation, Grant GI-44100 Properties of Molten coal slags relating to open cycle MHD, Dec. 1975.
- (16) TAYLOR, R and MILLS, K C; Arch. f. Eisenhuttenw., 1982, 53, 55.
- (17) TAYLOR, R and EDWARDS, R. cited by MILLS, K C and GRIEVESON, P, a paper presented at the Centenary Conference 1984, "Perspectives in Metallurgy" Sheffield University, July 1984.
- (18) SAITO, A; Bull. Jap. Soc. Mech. Engr., 1980, 23, 1459.
- (19) de CASTRO, C.A.N., L I, S.F.Y., MAITLAND, G.C. and WAKEHAM, W.A, in press Intl. J Thermophys. (1984)
- (20) MILLS, K C; POWELL, J S; BRYANT, J W and KEENE, B J, Canad. Metall. Q, 1981, 20, 93.
- (21) SUSAKI, M, NAGATA, K and GOTO, K S; Trans. Iron Steel Inst. Japan, 1982 22 B42.
- (22) MITCHELL, A and WADIER, J F; Canad. Metall. Q, 1981, 20, 373.
- (23) POWELL, J S, and MILLS, K C. Paper to be presented at the Ninth European Conference on Thermophysical Properties to be held in Manchester, Sept. 1984.

- (24) MILLS, K C. Paper entitled "Estimation of physico-chemical properties of coal slags and ashes" to be presented at this conference.
- (25) OSINOVSKIKH, L L, KOCHETOV, N N and BRATCHIKOV, S G; Trudy Urals N-I Chern. Met., 1968 (8), 71.
- (26) RUDKIN, R L; Report US AF., ASD-TDR-62-24 II.
- (27) KEENE, B J and MILLS, K C. Arch f Eisenhüttenw. 1981, 52, 311.
- (28) RAFALOVICH, I M and DENISOVA, I A; Fiz. Khim Rasplav. Schlakov, 1970, 181.
- (29) OLUSANYA, A, "The Fundamental Properties of Continuous Casting Fluxes" PhD Thesis, Imperial College, London, 1983.
- (30) TAYLOR, R, GRIEVESON, P, TAYLOR, R. Paper entitled "Thermal and Physico-chemical properties of continuous-casting slags" to be presented at Ninth European Conference on Thermophysical Properties to be held in Manchester, Sept. 1984.
- (31) NAGATA, K and GOTO, K S. private communication, Tokyo Inst. of Technology, 1984.
- (32) POWELL, J. S., MILLS, K C unpublished thermal conductivity data on casting powders, National Physical Laboratory, 1984.
- (33) OHMIYA, S; TACKE, K H and SCHWERTFEGGER, K; Ironmaking and Steelmaking, 1983, 10, 24.
- (34) VARGAFTIK, N B and OLESHCHUK, O N; Teploenergetika, 1955, 4, 13.
- (35) ISCHENKO, K D; Met. Kobosokhim, 1970, (21) 82.
- (36) KAWADA, K; Bull. Earthquake Res. Inst., 1966, 44, 1071.
- (37) MURASE, T, and McBIRNEY, A, R; Science, 1970, 170, 165.
- (38) GRIEVESON, P and BAGHA, S cited by MILLS, K C and GRIEVESON, P in a paper presented at the Centenary Conference 1984, "Perspectives in Metallurgy", Sheffield University, July 1984

Table 1

Reference	No	Slag composition					Sample	Method	Temperature Range °C
		%CaO + MgO	%SiO ₂	%FeO	%Fe ₂ O ₃	%Al ₂ O ₃			
Vargaftik (34)	A	12.8	35.9	29.0	5.3	14.3	Liquid, solidified slag; (10 mm) softening point ~ ca. 1000 °C	Radial heat flow method. Pt and stainless steel crucibles	25 - 1348
	B	3.8	53.5	14.1	6.0	22.7			25 - 1283
	C	2.2	50.8	21.0	-	13.0			25 - 1151
Gibby and Bates (15)			33-61	6-9	6-36	14-32	6 samples, liquid and solid	Laser pulse method	100 - 1600
Taylor (30)		27	34	6.5	4.5% free Fe	22 +% Na ₂ O	Glass, (1 mm)	Laser pulse method	200 - 950

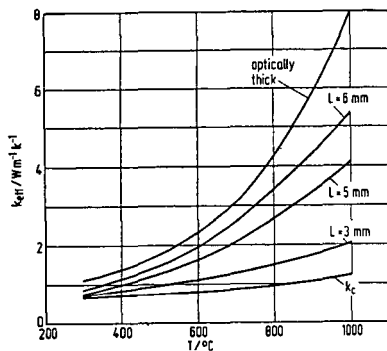


Figure 1. The dependence of k_{eff} upon the thickness of the sample.

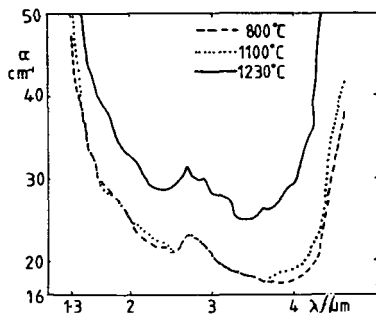


Figure 2. The wavelength of dependence of a glass containing 67 % SiO_2 , 16 % Na_2O + 9.% $(\text{FeO} + \text{Fe}_2\text{O}_3)$

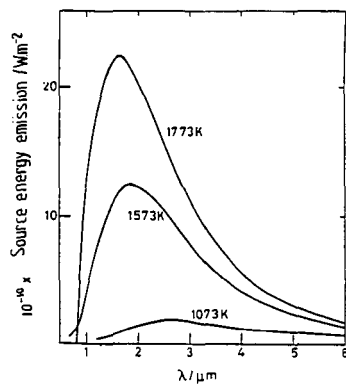


Figure 3. Wavelength distribution of the source energy emission for a black body.

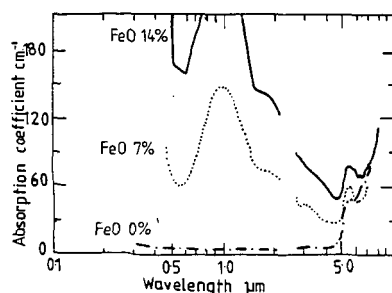


Figure 4. The absorption spectra at room temperature for slags containing FeO_x + CaO + SiO_2 .

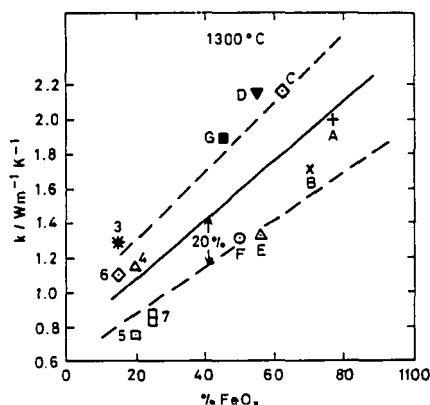


Figure 5. The thermal conductivity of slags of the system FeO_x + CaO + SiO_2 as a function of the FeO_x content. The letters and numerals refer to the specimen numbers (14).

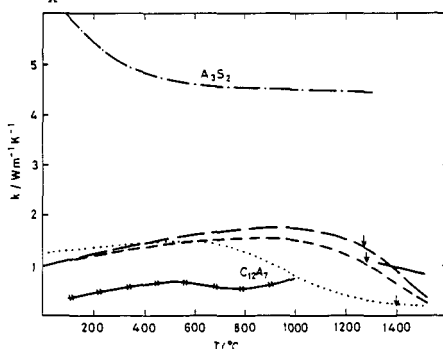


Figure 6. Thermal conductivities of slags from the system, CaO + Al_2O_3 + SiO_2 , —, Kingery for $3\text{Al}_2\text{O}_3 \cdot 2\text{SiO}_2$; —, Ogino et al; —, Susa et al, , 50% CaO + 50% Al_2O_3 ; —, —, —, 40% CaO + 40% SiO_2 + 20% Al_2O_3 ; —, —, 25% CaO + 60% SiO_2 + 15% Al_2O_3 ; —, —, Osinovskikh; —, —, T_{liq} .

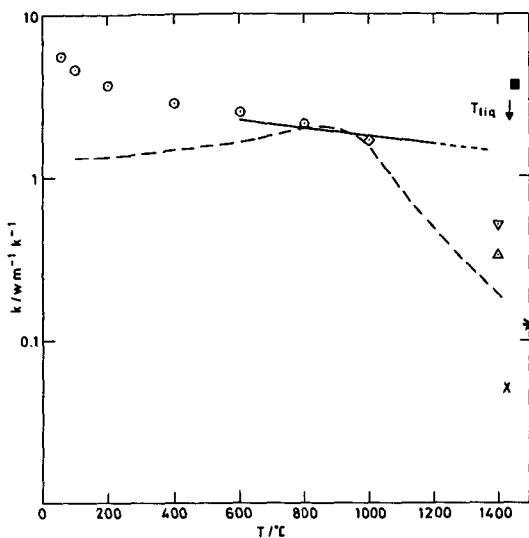


Figure 7. The thermal conductivity of CaF_2 and CaF_2 -based slags; CaF_2 ; *, Powell; \circ , Charvat; —, Taylor; x, Nagata; \blacksquare , Ogino; ∇ , Mitchell; CaF_2 -based slags, ---, Suga et al; Δ , Mitchell.

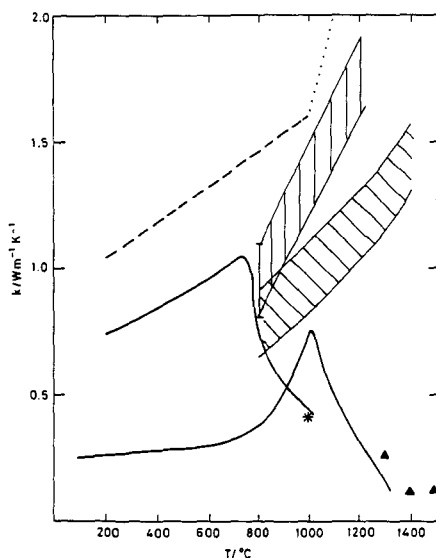


Figure 8. Thermal conductivity of continuous-casting slags; ---,, Taylor, and Taylor and Edwards; —, Nagata; |||| , Ohmiya; *, average k_c value, Ohmiya; \blacktriangle , Powell.

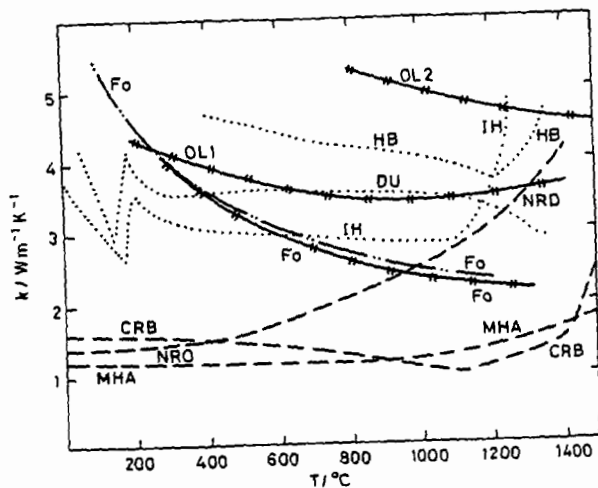


Figure 9. The thermal conductivity of rocks and minerals; — — —, Murase; — — —, Schatz; — — —, Kingery; ·····, Kawada; the letters refer to samples.

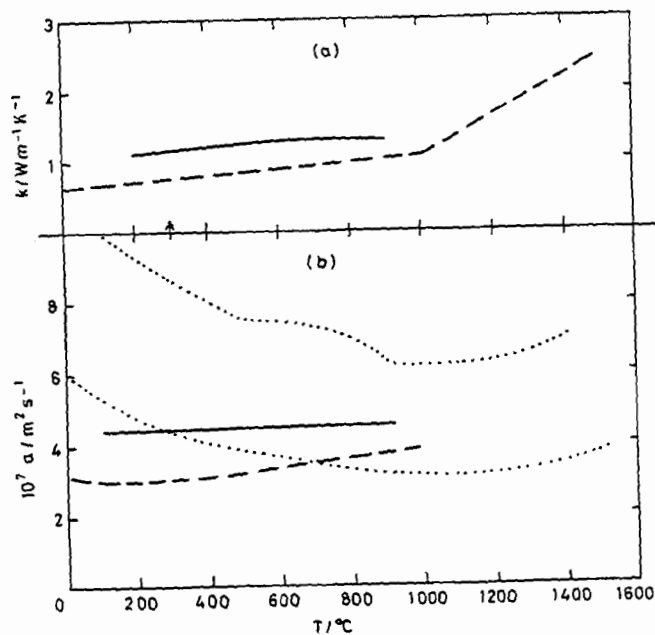


Figure 10. (a) Thermal conductivity (b) thermal diffusivity of coal slags; — — —, Taylor; — — —, Vargoftik; ·····, upper and lower limits of a values reported by Gibby and Bates.

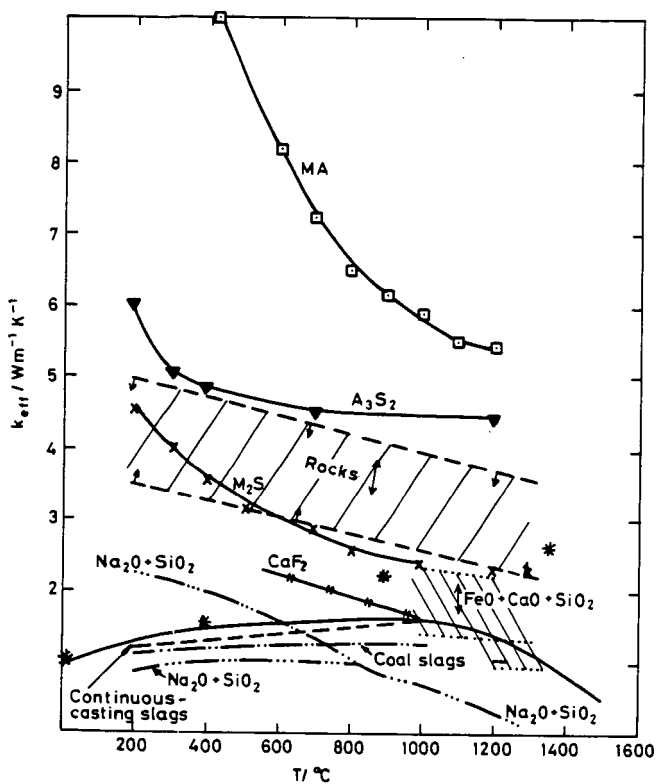


Figure 11. The thermal conductivity of various slag systems; —, $\text{MgO} \cdot \text{Al}_2\text{O}_3$; —, $3\text{Al}_2\text{O}_3 \cdot 2\text{SiO}_2$; —, $2\text{MgO} \cdot \text{SiO}_2$; —, upper and lower limits for data on rocks; —, CaF_2 ; —, data for the $\text{FeO}_x + \text{CaO} + \text{SiO}_2$ system; — ... —, $\text{Na}_2\text{O} + \text{SiO}_2$ system; —, $\text{CaO} + \text{SiO}_2 + \text{Al}_2\text{O}_3$ system; — — —, continuous casting powders; — — —, coal slags; *, k_c (glass).

SOLID-LIQUID-VAPOR INTERACTIONS IN ALKALI-RICH COAL SLAGS

L. P. Cook and J. W. Hastie

National Bureau of Standards, Washington, D.C. 20234

I. INTRODUCTION

Sodium and potassium are important constituents of the clay minerals found in most coals. As the coal is combusted these metals may be vaporized, transported and reabsorbed by slag in the cooler portions of the system, leading to the production of slags having concentrations of alkalis several times that of the primary mineral matter. Without doubt the most marked concentrations occur in slags from magnetohydrodynamic generators, where potassium is deliberately added to the combustion gases to enhance electrical conductivity of the plasma. Slags from MHD generators have K_2O concentrations approaching 20 wt%.

The corrosive effects of these high alkali slags on ceramic components of combustion systems are well known. Corrosion arises from the fact that such slags are good solvents for a wide range of materials. Furthermore, when many ceramics come into contact with high alkali slags, destructive reactions producing new solids may occur. For example, alumina, a widely used refractory, may react to produce $NaAlSiO_4$, $KAlSiO_4$ or beta alumina, depending upon the activities of silica and the alkalis. In most situations, reactions of this type would result in loss of structural integrity of the ceramic.

For these and related reasons, there is need for detailed knowledge of the physical chemistry of high alkali coal ash - derived slags. NBS has an ongoing theoretical and experimental program to systematically determine the nature of solid-liquid-vapor equilibria in high alkali coal slags. Given the wide variability of coal slag, this necessitates a close interaction between theory and experiment, if significant progress is to be made.

Experimentally, three principal methods are being utilized. Application of the high temperature quenching method, with examination of results by x-ray diffraction and electron microprobe methods, is facilitated by the fact that most silicate melts quench readily to glasses, preserving the textural and chemical relationships which prevailed under equilibrium at high temperatures. On the other hand, the relatively slow kinetics makes necessary great care in the determination of alkali vapor pressures by the Knudsen effusion/mass spectrometric method. Nonetheless the technique has been used successfully at NBS in determining vapor pressures by closely correlating effusion experiments with on-going quench experiments. Similarly, the application of the third principal experimental method, high temperature differential thermal-thermogravimetric analysis, requires a degree of caution.

There has long been interest in the development of models for the prediction of coal slag phase equilibria. While silicate phase diagrams of limited compositional range have been successfully modeled, a single model for accurate prediction of slag phase equilibria in general will require that considerably more progress be made not only in our understanding of the structural chemistry of slags but also in the availability of thermochemical data needed for such models. Progress to date is related to the realization that treatment of silicate liquids as polymerized melts may be necessary for very precise prediction of phase relationships. Also important is the discovery that alkali activities can be modeled over a wide range of compositions by treating slags as composed of mixtures of complex mineral melts such as $CaAl_2Si_2O_8$, $KAlSiO_4$, $NaAlSi_3O_8$, etc.

Thus coal slags, while not chemically ideal mixtures of the oxide components, appear to be much more ideal with respect to a choice of more complex components.

II. PHASE EQUILIBRIA IN COAL SLAGS

(A) Coal Slag As A 7-Component System

The variability of coal ash composition is directly related to variations in the proportions of mineral impurities such as SiO_2 , CaCO_3 , $\text{CaMg}(\text{CO}_3)_2$, $\text{CaSO}_4 \cdot 2\text{H}_2\text{O}$, Fe_2O_3 , FeS_2 , and the clay minerals which comprise a complex group of hydrated alkali aluminosilicates. Coal ashes may vary widely in their contents of iron, calcium and magnesium, but do not vary as greatly in the amount of silica and alumina they contain. In fact, of the 323 coal ash analyses reported in U.S. Bureau of Mines Bull. 567 (1), the great majority have a $\text{SiO}_2/(\text{SiO}_2 + \text{Al}_2\text{O}_3)$ mole ratio between .67 and .80, with a well defined maximum near .75 (2). The bulk chemistry of the ash is related to the conditions of formation of the coal. In general lignites and subbituminous coals of the western U.S.A. are high in calcium while bituminous coals of the eastern U.S.A. contain more iron. Table 1 gives typical analyses for ashes from these coals, and includes for comparison an analysis of coal slag from a magnetohydrodynamic generator. From this table, it can be seen that, in general, coal slag must be regarded as a seven component substance, if minor constituents such as TiO_2 and P_2O_5 are ignored and if sulfur is assumed to vaporize at high temperature.

Table 1. Typical Coal Ash Analyses (wt %).

	Montana Coal ⁽³⁾	Illinois Coal ⁽³⁾	MHD Slag ⁽⁴⁾
K_2O	0.4	1.4	20.2
Na_2O	0.4	1.6	0.5
CaO	11.9	8.2	3.9
MgO	3.9	0.8	1.1
Al_2O_3	21.4	16.2	12.4
Fe_2O_3	10.0	23.7	14.7
SiO_2	42.5	37.5	48.3
TiO_2	0.8	0.8	0.5
P_2O_5	0.3	0.1	-
SO_3	8.1	8.9	0.2

To account for the fact that Fe_2O_3 reduces partially to FeO with increasing temperature would require an added component. However this may be reduced again to seven if the oxygen partial pressure is included as an intensive variable along with temperature and composition. By doing this the need to specify both FeO and Fe_2O_3 in defining the bulk composition is eliminated; these are replaced by FeO_x , where x is determined by the oxygen partial pressure.

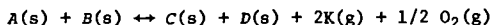
(B) Representation of Solid-Liquid-Vapor Equilibria

Ready visualization of a range of phenomena is one of the attributes making phase diagrams indispensable in understanding the chemistry of heterogeneous systems. However, although advanced multidimensional projective methods have been derived for the representation of n -component systems (5), these do not

in general lead to easily visualized diagrams. Thus for the seven component coal slag system, alternative methods must be used.

It is useful to subdivide the slag system into smaller systems. The system $\text{Al}_2\text{O}_3\text{-SiO}_2$ is perhaps the most fundamental system for all slags, and to this one may think of adding progressively combinations of the alkalis and CaO , MgO and FeO , until the desired degree of complexity is reached. Constituent systems making up the slag system are summarized in Table 2. Data are available for parts of many of these systems (6-10), but as the number of components increases, data become progressively fewer.

At NBS, experimental work is presently concentrating on the system $\text{K}_2\text{O-CaO-Al}_2\text{O}_3\text{-SiO}_2$. This along with $\text{K}_2\text{O-FeO-Al}_2\text{O}_3\text{-SiO}_2$ and $\text{K}_2\text{O-MgO-Al}_2\text{O}_3\text{-SiO}_2$, forms the basis for modeling potassium-rich slags. The approach has been to establish subsolidus equilibria (Figure 1) and then to combine these data with literature thermochemical data via solid state reactions of the type



At the temperature of minimum melting, such calculations provide direct links between the phase diagram and the measurements of potassium vapor pressure which are independent of any solution model (Figure 2). This approach aides greatly in the determination of an internally consistent set of thermochemical data.

As the systems investigated become more complex (more components), other techniques may be used to reduce the number of variables, so that results can be portrayed graphically. For example, in principle phase equilibria at 1 atm in the system $\text{K}_2\text{O-CaO-FeO-Al}_2\text{O}_3\text{-SiO}_2$ could be portrayed in three dimensions graphically as a tetrahedral diagram at constant $\mu_{\text{K}_2\text{O}}$ or $P_{\text{K}_2\text{O}}$, T and P_{O_2} .

Another way of reducing the dimensionality of the representational problem is to deal with saturation surfaces - this is actually a form of projection. For example by considering the equilibria in which Al_2O_3 participated as a phase, the need to use Al_2O_3 as a representational component would be eliminated.

(C) Role of Polymerization Theory

One of the major problems in prediction and calculation of phase equilibria is the formulation of accurate expressions for the free energy of mixing of silicate melts. Relatively few calorimetric measurements are available, and hence the importance of sound methods of estimation and prediction of mixing data to within the required degree of accuracy. Polymer theory, extended in the 1960's to include silicate melts by Masson (11) and others holds promise. It is perhaps the only general theory for silicate melts which deals quantitatively with the problem of melt structure. This has been used, with a surprising degree of success, to calculate phase equilibria in binary oxide systems (12,13). Preliminary calculations on multicomponent slags have shown that polymer theory, when treated in a quasicheical fashion, is highly flexible, and can accommodate seven component liquid immiscibility by making relatively few estimates and assumptions (Figure 3). However, attempts to fit liquidus surfaces in the system $\text{K}_2\text{O-CaO-Al}_2\text{O}_3\text{-SiO}_2$ have met with only partial success. Further applications and extensions of polymer theory in this quaternary system are hampered by a lack of experimental data, and an attempt is being made to rectify this situation.

Table 2. Breakdown of Lower Order Systems Comprising 7-Component Coal Slag System.

	(+CaO)	(+MgO)	(+FeO) _x	(+CaO +MgO)	(+CaO +FeO) _x	(+MgO +FeO) _x	(+CaO +MgO +FeO) _x
AL ₂ O ₃ -SiO ₂ BASE SYSTEM	CaO-Al ₂ O ₃ -SiO ₂	MgO-Al ₂ O ₃ -SiO ₂	FeO-Al ₂ O ₃ -SiO ₂	CaO-MgO-Al ₂ O ₃ -SiO ₂	CaO-FeO-Al ₂ O ₃ -SiO ₂	MgO-FeO-Al ₂ O ₃ -SiO ₂	CaO-MgO-FeO-Al ₂ O ₃ -SiO ₂
(+K ₂ O)	K ₂ O-CaO-Al ₂ O ₃ -SiO ₂	K ₂ O-MgO-Al ₂ O ₃ -SiO ₂	K ₂ O-FeO-Al ₂ O ₃ -SiO ₂	K ₂ O-CaO-MgO -Al ₂ O ₃ -SiO ₂	K ₂ O-CaO-FeO -Al ₂ O ₃ -SiO ₂	K ₂ O-MgO-FeO -Al ₂ O ₃ -SiO ₂	K ₂ O-CaO-MgO -FeO-Al ₂ O ₃ -SiO ₂
(+Na ₂ O)	Na ₂ O-CaO-Al ₂ O ₃ -SiO ₂	Na ₂ O-MgO-Al ₂ O ₃ -SiO ₂	Na ₂ O-FeO-Al ₂ O ₃ -SiO ₂	Na ₂ O-CaO-MgO -Al ₂ O ₃ -SiO ₂	Na ₂ O-CaO-FeO -Al ₂ O ₃ -SiO ₂	Na ₂ O-MgO-FeO -Al ₂ O ₃ -SiO ₂	Na ₂ O-CaO-MgO -FeO-Al ₂ O ₃ -SiO ₂
(+K ₂ O +Na ₂ O)	K ₂ O-Na ₂ O-CaO -Al ₂ O ₃ -SiO ₂	K ₂ O-Na ₂ O-MgO -Al ₂ O ₃ -SiO ₂	K ₂ O-Na ₂ O-FeO -Al ₂ O ₃ -SiO ₂	K ₂ O-Na ₂ O-CaO -MgO-Al ₂ O ₃ -SiO ₂	K ₂ O-Na ₂ O-CaO -FeO-Al ₂ O ₃ -SiO ₂	K ₂ O-Na ₂ O-MgO -FeO-Al ₂ O ₃ -SiO ₂	K ₂ O-Na ₂ O-CaO-MgO -FeO-Al ₂ O ₃ -SiO ₂
							COAL SLAG SYSTEM

III. SOLUTION MODEL FOR THE PREDICTION OF ALKALI VAPOR PRESSURES

(A) Basis of the Model

The model employed for prediction of vapor pressures in multicomponent coal slags has been outlined in (14). Briefly, large negative deviations from ideal thermodynamic activity behavior are attributed to the formation of complex liquids and solids (actual components) such as K_2SiO_3 , $KAlSiO_4$, etc. The free energies of formation (ΔG_f) are either known or can be estimated for these liquids and solids. By minimizing the total system free energy, one can calculate the equilibrium composition with respect to these components. Thus, for instance the mole fraction of K_2O present ($X^*_{[K_2O]}$) in equilibrium with K_2SiO_3 , and other complex liquids (and solids) containing K_2O , is known. As has been shown previously for the ternary systems, the component activities can, to a good approximation, be equated to these mole fraction quantities (15). From this assumption it also follows that potassium partial pressures can be obtained from the relationship

$$P_K = \left\{ 2 \cdot X^*_{[K_2O]} \right\}^{0.4}_p,$$

where K is the stoichiometric dissociation constant for pure K_2O (liquid or solid) to K and O_2 . In the following discussion the model is tested by comparing predicted P_K data determined in this manner with experimental values. Thermodynamic activities and phase compositions were also calculated using this model. The experimental K -pressure data were obtained by Knudsen effusion mass spectrometry as discussed in detail elsewhere (16).

(B) Method of Calculation

The SOLGASMIX computer program (17) used for calculation of the equilibrium composition and hence activities utilizes a data base of the type given in (14). The coefficients to the ΔG_f equation were obtained by fitting ΔG_f vs T data available in JANAF (18), Robie et al (19), Barin and Knacke (20), Rein and Chipman (21) and Kelley (22). In some cases no literature data were available and we estimated functions in the manner described earlier (16). Many of the compounds used in the calculation are mineral phases such as mullite ($Al_6Si_2O_{13}$), kaliophilite ($KAlSiO_4$), leucite ($KAlSi_2O_6$), feldspar ($KAlSi_3O_8$), and gehlenite ($Ca_2Al_2SiO_7$).

(C) Application to the K_2O - CaO - Al_2O_3 - SiO_2 System

Figure 4 shows results of calculations for potassium pressures made using the model. As can be seen these agree with experimental results within limits of experimental error over a wide range of temperature. The calculations also indicate temperatures of precipitation of various solids in the quaternary system. These predictions are being checked by experiment. Other potassium pressure calculations (not shown) show similarly good agreement with experiment in the system K_2O - CaO - Al_2O_3 - SiO_2 .

IV. SUMMARY

An integrated experimental/theoretical approach to the problem of non-condensed (solid-liquid-vapor) phase equilibria in multicomponent coal slags has been outlined, including methods for the presentation of results. This relies upon prediction as an important tool in planning experimental work. Theory in turn benefits from experimental feedback, resulting in a continual evolution of models. Hopefully this will lead to generalized solution models capable of predicting slag phase equilibria with a high degree of accuracy.

V. REFERENCES

1. Selvig, W. A. and Gibson, F. H.: 1956, Bureau of Mines Bull. 567.
2. Cook, L. P.: 1978, Proc. 17th Symposium on Engineering Aspects of Magnetohydrodynamics, Stanford Univ., Stanford, Calif., p. C.1.2-C.1.6.
3. Petrick, M. and Shumyatsky, B. Ya., editors: "Open-Cycle Magnetohydrodynamic Electrical Power Generation" (Argonne, Illinois: Argonne National Lab.), p. 420-421.
4. Long, W.: 1978, Pers. Commun., Univ. Tenn. Space Inst.
5. Palatink, L. S. and Landau, A. I.: 1964, "Phase Equilibria in Multicomponent Systems" (New York: Holt, Rinehart and Winston).
6. Levin, E. M., Robbins, C. R. and McMurdie, H. F.: 1964, "Phase Diagrams for Ceramists" (Columbus: The American Ceramic Society).
7. Levin, E. M., Robbins, C. R. and McMurdie, H. F.: 1969, "Phase Diagrams for Ceramists, 1969 Supplement" (Columbus: The American Ceramic Society).
8. Levin, E. M., Robbins, C. R. and McMurdie, H. F.: 1975, "Phase Diagrams for Ceramists, 1975 Supplement" (Columbus: The American Ceramic Society).
9. Roth, R. S., Negas, T. and Cook, L. P.: 1981, "Phase Diagrams for Ceramists, Volume IV" (Columbus: The American Ceramic Society).
10. Roth, R. S., Negas, T. and Cook, L. P.: 1983, "Phase Diagrams for Ceramists, Volume V" (Columbus: The American Ceramic Society).
11. Masson, C. K., Smith, I. B. and Whiteway, S. G.: 1970, Canad. J. Chem., 48 1456.
12. Fraser, D. G., editor: 1976, "Thermodynamics in Geology" (Oxford, England: NATO Adv. Study Inst.).
13. Lin, P. L. and Pelton, A. D.: 1979, Metall. Trans. 10B, 667.
14. Hastie, J. W., Bonnell, D. W. and Plante, E. R.: 1983, Proc. Annual Meeting of Electrochem. Society, San Francisco, Calif.
15. Hastie, J. W., Horton, W. S., Plante, E. R., and Bonnell, D. W.: Thermo-dynamic Models of Alkali Vapor Transport in Silicate Systems, IUPAC Conf., Chemistry of Materials at High Temperatures, Harwell, U.K., August 1981; High Temp. High Press, in press.
16. Hastie, J. W., Plante, E. R. and Bonnell, D. W.: 1982, Alkali Vapor Transport in Coal Conversion and Combustion Systems. ACS Symp. Series, 179, p. 543-600, Cole, J. L., and Stwalley, W. C., eds. Metal Bonding and Interactions in High Temperature Systems with Emphasis on Alkali Metals (see also NBSIR 81-2279).
17. Eriksson, G.: 1975, Chemica Scripta, 8, p. 100.
18. JANAF: 1971, Joint Army, Navy, Air Force Thermochemical Tables, 2nd Ed. NSRDS-NBS 37. See also later supplements for 1971-1981.
19. Robie, R. A., Hemingway, B. S., Fisher, J. R.: 1979, Thermodynamic Properties of Minerals and Related Substances at 298.15 K and 1 Bar (10^5 Pascals) Pressure and at Higher Temperatures, Geol. Survey Bull. 1452 (Washington, D.C.: U.S. Govt. Printing Office).
20. Barin, I. and Knacke, O.: 1973, "Thermochemical Properties of Inorganic Substances" (New York: Springer Verlag).
21. Rein, R. H. and Chipman, J.: 1965, Trans. Metall. Soc. AIME, 233, p. 415.
22. Kelley, K. K.: 1962, U.S. Bur. Mines Rep. Invest., No. 5901.
23. Cook, L. P.: 1980: Proc. Seventh International Conference on MHD Electrical Power Generation, MIT, Cambridge, Mass., p. 212-219.

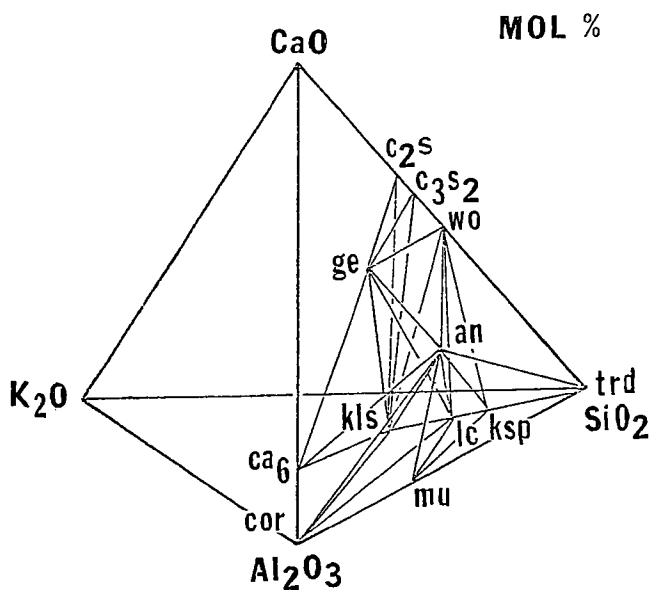


Figure 1. Experimentally determined subsolidus phase relations in the system K_2O - CaO - Al_2O_3 - SiO_2 .

$c_2s = Ca_2SiO_4$	$trd = SiO_2$
$c_3s_2 = Ca_3Si_2O_7$	$ksp = KAlSi_3O_8$
$wo = CaSiO_3$	$lc = KAlSi_2O_6$
$ge = Ca_2Al_2SiO_7$	$kl_s = KAlSiO_4$
$an = CaAl_2Si_2O_8$	$mu = 3Al_2O_3 \cdot 2SiO_2$
$ca_6 = CaAl_{12}O_{19}$	$cor = Al_2O_3$

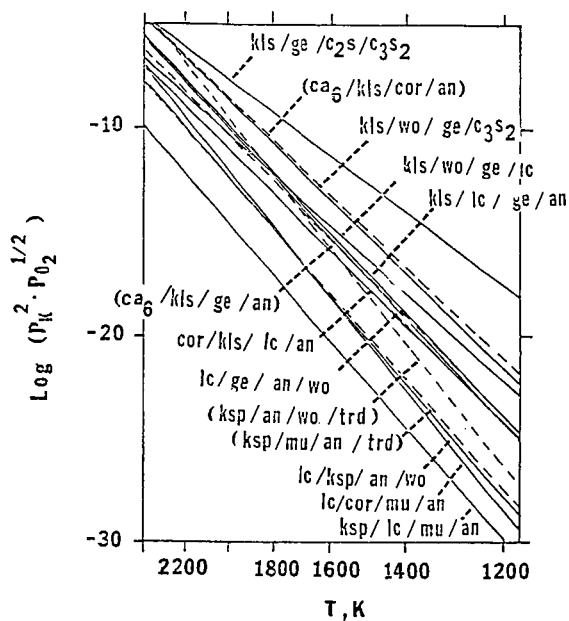


Figure 2. Calculated potassia pressures for solid assemblages in K_2O - CaO - Al_2O_3 - SiO_2 (see Figure 1). Thermochemical data used were from (19). Equilibria are metastable above the minimum melting temperatures.

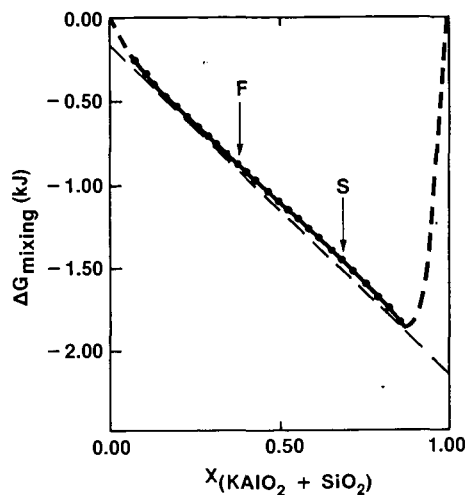


Figure 3. Calculated free energy of mixing along a compositional vector in the system $K_2O-CaO-MgO-FeO-Al_2O_3-SiO_2$ passing through experimentally determined compositions of immiscible melts (F and S). Calculations were made using the quasi-chemical melt polymerization theory (23). The compositions of predicted and observed immiscible melts can be made to agree reasonably well by adjustments in polymerization equilibrium constants and in the ratio $Fe^{+3}/(Fe^{+3} + Fe^{+2})$.

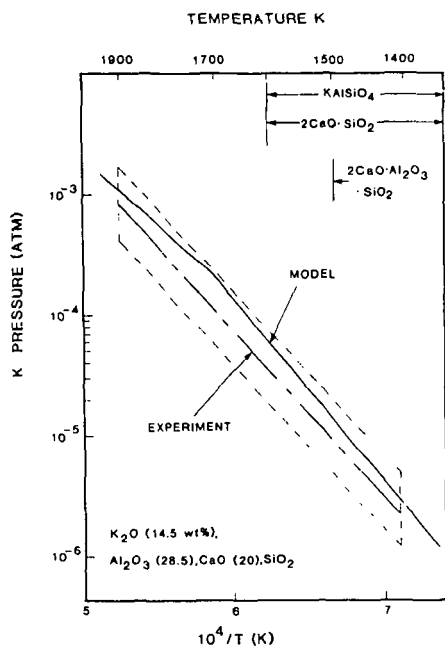


Figure 4. Comparison of ideal mixing of complex components solution model (solid curve) and experimental (broken curve) K-pressure data as a function of reciprocal temperature, for a composition in the K_2O - CaO - Al_2O_3 - SiO_2 system. Compounds listed are solid precipitates formed over the temperature interval indicated.

OVERVIEW OF COAL ASH DEPOSITION IN BOILERS

R. W. Borio and A. A. Levasseur

COMBUSTION ENGINEERING, INC.
1000 Prospect Hill Road, Windsor, CT 06095

INTRODUCTION

The management of coal ash in utility boilers continues to be one of the most important fuel property considerations in the design and operation of commercial boilers. The behavior of mineral matter in coal can significantly influence furnace sizing, heat transfer surface placement, and convection pass tube spacing. Ironically, many of the more reactive, low rank U. S. coals must have larger furnaces than the less reactive higher rank coals. This is strictly a requirement based on the mineral matter behavior; Figure 1 illustrates this point. Given the same mineral matter behavior the more reactive, lower rank coals would require less residence time and therefore smaller furnace volumes than the less reactive, higher rank coals.

Although pulverized coal has been fired for more than 50 years and much is known about combustion behavior there are still a number of boilers experiencing operational problems from coal ash effects. Ash-related problems are one of the primary causes of unscheduled outages, unit derating and unavailability. Because of variability in a given coal seam and since many boiler operators may experience changes in their coal supply during the life of a boiler, operational problems caused by changes in coal ash properties can significantly affect boiler performance. Not only must the initial boiler design be correctly determined based on the specification coal but reliable judgements must be made regarding the suitability of other candidate coals and their effect on operation during the lifetime of the boiler.

The increased emphasis on coal usage in this country and, indeed, the significant effort underway to consider coal water mixtures as possible oil substitutes in oil-designed boilers underscores the need to improve the prediction of mineral matter behavior in a boiler environment.

Coal is a very heterogeneous, complex material which produces heterogeneous, complex products during combustion. Since, during pulverized coal combustion, coal particles of various organic and mineral matter compositions can behave in completely different manners, prediction based upon the overall or average composition may be misleading. Like many of the currently-used ASTM coal analyses, the method for determining ash fusibility temperatures was developed when stoker firing was a predominant coal firing technique; the methodologies and conditions employed during many of the ASTM tests reflect this. It is not surprising that the usefulness of some ASTM test results may be limited when used for a pulverized coal firing application. In recent years researchers have developed methodologies for characterizing coal ash behavior that better reflect the fundamental mechanisms controlling behavior and more closely simulate the conditions that exist in a pulverized coal fired boiler.

Clearly there is a need for improved mineral matter behavior predictive techniques. This paper will provide a statement of the ash deposition problem in pulverized coal fired boilers, it will present an assessment of the older, traditional methods for predicting mineral matter behavior and it will address some of the newer techniques that have been suggested as better ways of characterizing coal ash behavior. Additionally some areas of uncertainty will be identified as requiring the development of better predictive techniques.

STATEMENT OF THE PROBLEM

The presence of ash deposits and flyash can create the following problems in a boiler:

1. Reduced heat transfer
2. Impedance of gas flow
3. Physical damage to pressure parts
4. Corrosion of pressure parts
5. Erosion of pressure parts

These problems can result in reduced generating capacity, unscheduled outages, reduced availability, and costly modifications.

Ash which deposits on boiler walls in the radiant section of a furnace is generally referred to as slagging. Ash deposition on convection tube sections downstream of the furnace radiant zone is typically referred to as fouling. Ash slagging and fouling can result in problems listed in items 1 through 4; item 5, erosion, is the result of impingement of abrasive ash on pressure parts. Often coal ash deposit effects are inter-related. For example, slagging will restrict waterwall heat absorption changing the temperature distribution in the boiler which in turn influences the nature and quantity of ash deposition in downstream convective sections. Ash deposits accumulated on convection tubes can reduce the cross-sectional flow area increasing fan requirements and also creating higher local gas velocities which accelerates flyash erosion. In situ deposit reactions can produce liquid phase components which are instrumental in tube corrosion.

One of the most common manifestations of a deposition problem is reduced heat transfer in the radiant zone of a furnace. Decreased heat transfer due to a reduction in surface absorptivity is a result of the combination of radiative properties of the deposit (emissivity/absorptivity) and thermal resistance (conductivity) of a deposit. Thermal resistance (thermal conductivity and deposit overall thickness) is usually more significant because of its effect on absorbing surface temperature.

Previous work has indicated that the physical state of the deposit can have a significant effect on the radiative properties, specifically molten deposits show higher emissivities/absorptivities than sintered or powdery deposits (Ref. 1). Although thin, molten deposits are less troublesome from a heat transfer aspect than thick, sintered deposits, molten deposits are usually more difficult to remove and cause frozen deposits to collect in the lower reaches of the furnace; physical removal then becomes a problem for the wall blowers.

Impedance to gas flow is the result of heavy fouling on tubes in the convective section. Problems of this type are most likely to occur with coals having high sodium contents, usually found in low rank coal deposits in Western U.S. seams. Hard, bonded deposits can occur which are resistant to removal by the retract soot-blowers.

Physical damage to pressure parts can occur if large deposits have accumulated in the upper furnace and proceed to become dislodged or blown off and drop onto the slopes of the lower furnace. Such deposits are usually characterized by their relatively high bonding strengths and their heavily sintered structure.

Fireside corrosion can occur on both waterwall and superheater tube surfaces. Normal sulfates and pyrosulfates are frequently the cause of waterwall corrosion, although reducing conditions can also cause depletion of protective oxide coatings on tube surfaces. On higher temperature metal surfaces, (superheaters/reheaters) alkali-iron-trisulfates are often the cause of corrosion. Chlorine can also be a contributing factor toward superheater metal corrosion. While exact mechanisms can be argued there have been examples of both liquid phase and gas phase corrosion when chlorides have been present (Ref. 2).

Erosion of convective pass tubes, while not a function of deposits, is caused by the abrasive components in flyash. Flyash size and shape, ash particle composition and concentration, and local gas velocities play important roles concerning erosion phenomenon. Recent work has shown that quartz particles above a certain particle size are very influential in the erosion process and that furnace temperature history plays an important role in determining erosive characteristics of the particles (Ref. 3 & 4).

FUNDAMENTAL CONSIDERATIONS IN ASH DEPOSITION

The coal ash deposition process is extremely complex and involves numerous aspects of coal combustion and mineral transformation/reaction. The following all play a role in the formation of ash and the deposition process.

- Coal Organic Properties
- Coal Mineral Matter Properties
- Combustion Kinetics
- Mineral Transformation and Decomposition
- Fluid Dynamics
- Ash Transport Phenomena
- Vaporization and Condensation of Ash Species
- Deposit Chemistry - Specie Migration and Reaction
- Heat Transfer To and From the Deposit

Despite considerable research in these areas, there are many gaps in our fundamental understanding of the mechanisms responsible for mineral matter behavior. Although substantial knowledge exists concerning the deposition process, the complexity of the subject does not allow detailed discussion here. However, the importance of furnace operating conditions on the combined results of each of the above areas must be stressed. For a given coal composition, furnace temperatures and residence times generally dictate the physical and chemical transformations which occur. The ash formation process is primarily dependent on the time/temperature history of the coal particle. The resultant physical properties of a given ash particle generally determine whether it will adhere to heat transfer surfaces. Local stoichiometries can also influence the transformation process and thereby the physical characteristics of ash particles; iron-bearing particles are a prime example of this.

Aerodynamics can play a role in the ash deposition process in all furnaces regardless of the type of firing; recent interest in microfine grinding of coal is testimony to this fact. It has been postulated that smaller ash particles will follow gas streamlines and be less likely to strike heat transfer surfaces. This is a logical hypothesis for those ash particles that cause deposition due to an impact mechanism. In addition to particle size, particle density and shape also affect aerodynamic behavior. Molten, spherical particles will be less likely to follow gas streamlines than angular or irregular particles of the same mass due to the difference in drag forces.

Most coal ash will result in deposits of increasing severity with increasing gas temperature. This is not a linear relationship, as illustrated in Figure 2, but rather shows a progressively more severe ash deposit condition with increasing gas temperature (Ref. 5). Boilers are normally designed so that cleanable, sintered deposits will be formed. This is a reasonable compromise between a very large, economically uncompetitive boiler that may produce very dry, dusty deposits and a very small, highly loaded boiler that would produce molten, running ash deposits.

The key governing factor, then, is determining how small a furnace can be, for a given MW output, and still result in deposits that are cleanable with conventional sootblowing equipment.

Because of the complexity of the ash formation and ash deposition process, it seems logical to deal first with those key coal constituents most responsible for ash deposition. The iron and sodium contents of an ash have typically been considered key constituents. Techniques have been developed to determine how these key constituents are contained in the coal, i.e., the particular mineral forms that are present or the grain size of the constituent in question. Obviously the remainder of the mineral matter has an effect, but depending on the concentration and form in which iron and/or sodium constituents are present, the remaining mineral matter often has second order effects.

As previously discussed, ash formation and the resulting ash size distribution is extremely complex and is dependent on several factors including initial coal size, coal burning characteristics, mineral content, mineral grain size, volatile ash species, melting behavior of the mineral matter, and temperature history of the particle. Generally, coal containing lower melting mineral matter has a greater potential for ash agglomeration as the particle burns and yields fewer ash particles per coal particle which results in coarser ash particles than those of coal with higher melting ash. Obviously things like ash quantity, and mineral grain sizes could influence this hypothesis. The way a coal particle burns may also influence the number of ash particles generated, i.e., a shrinking sphere burning mode may produce a different result from a constant diameter, decreasing density mode of burning; swelling coals may behave differently than non-swelling coals.

In reflecting on the above discussion, it becomes apparent that one cannot completely divorce the predictive techniques employed, from the particular coal burning application. Pulverized coal firing will require a sensitivity to different conditions than stoker firing, or a slagging combustor. Failure to address the specific conditions inherent in each type of firing system will lead to lower resolution in one's predictive abilities than desired.

ASSESSMENT OF TRADITIONAL PREDICTIVE METHODS

ASTM measurements such as ash fusibility (D1857) have formed the basis for traditional ash behavior predictive techniques. These bench-scale tests provide relative information on a fuel; this is used in a comparative fashion with similar data on fuels of known behavior. Unfortunately, the commonly used tests do not always provide sufficient information to permit accurate comparison.

The fusibility temperature measurement technique attempts to recognize the fact that mineral matter is made up of a mixture of compounds each having their own melting point. As a cone of ash is heated some of the compounds melt before others and a mixture of melted and unmelted material results. The structural integrity or deformation of the traditional ash cone changes with increasing temperature as more

of the minerals melt. However, more recent results indicate that significant melting/sintering can occur before initial deformation is observed (Ref. 6). The fact that the time/temperature history of laboratory ash is quite different from conditions experienced in the boiler can result in difference in melting behavior. In addition, the ash used in this technique may not represent the composition of ash deposits that actually stick to the tube surfaces. Often there is a major discrepancy between the composition of as-fired ash and that which is found as deposits (See Table I). This is a major criticism of the ash fusibility temperatures. The discrepancies between fusibility temperature predictions and actual slagging performance is usually greater on ashes that may look reasonably good based on fusibility temperature results. One can usually assume, with reasonable confidence, that the melting temperature of the waterwall deposits will be no higher than ASTM fusibility temperatures; but deposit melting temperatures can be and are often lower than ASTM melting temperatures. This is because selective deposition of lower melting constituents can and does occur; hence there is an enrichment of lower melting material in the deposit.

Ash viscosity measurements suffer similar criticism to the fusibility measurements. These tests are conducted on laboratory ash and on a composite ash sample. Viscosity measurements are less subjective and more definitive than fluid temperature determination for the assessment of ash flow characteristics. However, these measurements reflect the properties of a totally dissolved solution of ash constituents and may not be representative of slag deposit properties in pulverized coal-fired boilers. During pulverized coal firing, a severe problem may already exist before slag deposits reach the fluid/running state. Generally, only a small quantity of liquid phase material exists in deposits and it is the particle-to-particle surface bonding which is most important.

Much use is made of the ash composition which is normally a compilation of the major elements in coal ash expressed as the oxide form. From this compilation of elements, expressed as oxides, judgements are often made based on the quantity of certain key constituents like iron and sodium. Base/acid ratios are computed and used as indicators of ash behavior; normally lower melting ashes fall in the 0.4 to 0.6 range. It has been shown that base/acid ratios generally correlate with ash softening temperatures, so although base/acid ratios have helped explain why ash softening temperatures varied, it has not improved predictive capabilities in the authors' opinion. Other ratios such as Fe/Ca and Si/Al have been used as indicators of ash deposit behavior. Ratios like these have helped to explain deposit characteristics, but their use as a prime predictive tool is questionable especially since these ratios do not take into account selective deposition nor do they consider the total quantities of the constituents present. An Fe/Ca ratio of 2 could result from 6/3 or 30/15; the latter numbers would generally indicate a far worse situation than the former, but ratios don't show this.

Many slagging and fouling indices are based upon certain ash constituent ratios and corrected using such factors as geographical area, sulfur content, sodium content, etc. One commonly used slagging index uses Base/Acid ratio and sulfur content. Factoring in sulfur content is likely to improve the sensitivity of this index to the influence of pyrite on slagging. (As previously discussed, iron-rich minerals often play an important role in slagging.) However, the use of such "correction" factors is often a crude substitute for more detailed knowledge of the fundamental fuel properties. Another example of this is the use of chlorine content in a coal as a fouling index. This can be true if the chlorine is present as NaCl thereby indicating the concentration of sodium which is in an active form and that will, in fact, cause the fouling. Chlorine present in other forms may or may not adversely affect fouling.

Sintering strength tests have been used as an indication of fouling potential. Assuming that correct ash compositions have been represented (which is less of a problem in the convection section than in the radiant section) worthwhile information may be obtained relative to a time/temperature vs. bonding strength relationship. In order for sintering tests to accurately predict actual behavior it is necessary that tests be conducted with ash produced under representative furnace conditions (time-temperature history). Fouling behavior is often greatly influenced by sodium reactions. Sodium which vaporizes in the furnace can condense in downstream convection sections thereby concentrating on flyash surfaces. Particle surface reactions are primarily responsible for convection deposit bonding.

In summary, traditional methods for prediction ash deposit characteristics are heavily based upon ash chemistry. These convectional analyses do not provide definitive information concerning the mineral forms present in the coals and the distribution of inorganic species within the coal matrix. Such information can be extremely important in extrapolating previous experience, since the nature in which the inorganic constituents are contained in the coal can be the determining factor in their behavior during the ash deposition process.

ASSESSMENT OF NEW PREDICTIVE TECHNIQUES

Generally speaking the newer bench scale predictive techniques are far more sensitive to the conditions that exist in commercial furnaces than the older predictive methods. Selective deposition, for example, has been recognized as a phenomenon which cannot be ignored. More attention is being paid to fundamentals of the ash formation and deposition processes. New tools, such as Scanning Electron Microscopy (SEM), are being considered as ways to improve predictive capabilities. Other, more specialized bench scale apparatuses are being developed to simulate important aspects of commercial conditions and provide quantitative information on parameters that influence bonding strength.

Recent work has shown that pulverized coal, if separated by gravity fractionation, can yield important information relative to slagging potential due to the iron content. (Ref. 6, 7). Results of this work have shown that the percentage of iron in the heavy fractions correlates very well to the slagging behavior in commercial boilers. (See Figure 3). This technique appears to identify the proportion of relatively pure pyrites particles that are generated in the pulverized coal feed and that are capable of melting at relatively low temperatures and that would account for enrichment of iron in lower furnace waterwall deposits.

A method for measuring active alkalis has been developed as a means for improved prediction of fouling potential (Ref. 8). Previous wisdom held that fouling potential was directly related to the total sodium content. Much of this early work was done on low rank coals in which case it was not uncommon for all of the alkalis to be present as an active sodium form (Ref. 9). However, there were many occasions where the fouling potential was not adequately predicted by the total sodium content. (Table II provides some examples of anomalous fouling behavior.) The mechanism postulated for sodium-related fouling was one of a vaporization/condensation mechanism. Simple forms of sodium compounds resulted in the vaporization of sodium in the radiant zone of the furnace where peak temperatures are generated. Subsequent condensation of the sodium on the relatively cool tube surfaces effected a process for deposition of sodium. Sodium is a known, effective fluxing agent that can create hard, bonded deposits. The referenced method relied on the use of weak acid to preferentially leach out sodium from simple compounds like NaCl and/or organically-bound alkali as would be present in many of the lower rank coals. This method gives results that correlate well with field performance on coals having significant sodium contents (See Table II).

The use of new analytical techniques promises to give results that allow mineral matter to be identified according to composition, mineral form, distribution within the coal matrix, and grain size.

Techniques such as computer-controlled scanning electron microscopy (CCSCM) transmission electron microscopy (STEM), X-ray diffraction can be used to characterize these properties on individual particle by particle basis. New spectroscopies such as extended X-ray absorption of fine structure spectroscopy (EXAFS), and electron energy loss spectroscopy (EELS) are capable of determining electronic bonding structure and local atomic environment for organically associated inorganics like calcium, sodium and sulfur. Other new techniques such as Fourier transform infrared spectroscopy (FTIR), electron microprobe, electron spectroscopy for chemical analysis (ESCA), etc. all provide methods of improving present capabilities. By development and application of these techniques a much better fundamental assessment of coal mineral matter behavior is possible. The authors believe these results, coupled with those of other existing methods, can make a significant improvement to predictive capabilities.

AREAS OF UNCERTAINTY

Prediction of ash deposit characteristics based solely on bench-scale fuel properties always requires substantial judgement and allows only a certain level of confidence. As discussed, the ash deposition process is so complex that detailed modelling of commercial systems based on fundamental data is presently unrealistic. However, current techniques can provide relative data which in most cases is sufficient to make accurate assessment of slagging and fouling potentials relative to other fuels.

There remains many areas of uncertainty where experienced judgements must fill the gap between good laboratory results/predictions and boiler design decisions. One of these areas concerns the extent of deposit coverage in a boiler. Though the fuels researcher may adequately characterize a given coal ash in terms of its potential deposit effects, he is often at a loss to adequately describe the extent of coverage of deposits in the boiler. It is necessary to accurately describe furnace conditions in order to assess resulting deposits in particular boiler regions. Though some good work is underway in this area, the question of bonding strength and cleanability remains a problem as far as its prediction from bench scale tests. Though some good correlations have been developed between iron content of heavy gravity fractions and slagging, there does not exist a bench scale technique that can simulate what the ash deposit composition shall be when burned in a commercial boiler.

It is possible to increase the level of confidence for prediction of deposit effects by conducting pilot-scale combustion studies in test rigs which more closely simulate the conditions present in commercial boilers. Combustion testing allows evaluation of the ash formation and deposition process and permits detailed characterization of deposits generated. Results can allow determination of deposit characteristics as a function of fundamental boiler design parameters (such as gas temperature, velocity, etc.). Combustion test rigs also serve as valuable tools for assessment of fuels with very unusual properties and can significantly reduce uncertainties in extrapolation of their behavior from past experience.

Whenever test results are assessed and used to establish boiler design parameters, the representativeness of the test sample must be carefully considered. The degree of variability in the coal deposit and its impact on the day-to-day fuel properties

are very important factors which must be evaluated. Judgements are also required on long term coal supply properties.

In summary, it can be stated that the ash formation and deposition process is not fully understood. Traditional ASTM analyses do not always provide information that can be used to make predictive judgements at the confidence levels desired. Newer techniques have been developed and are being developed that are more sensitive to the conditions that exist in the boiler environment, and that recognize the heterogeneity of the inorganic constituents in the coal matrix. There appears to be a recognition that no one test can adequately describe coal ash behavior; a combination of tests, each designed to focus on a particular aspect of ash behavior seems to be a logical approach. Based on the results from many of these newer tests, on coals that are presently being burned in existing units, the authors feel certain that significant improvements have been made in predicting ash behavior. Finally the authors suggest that attention be given, by cognizant people, to the idea of standardizing some of the newer predictive techniques and incorporating them as supplements to existing ASTM tests.

REFERENCES

1. G. J. Goetz, N. Y. Nsakala, and R.W. Borio, "Development of Method for Determining Emissivities and Absorptivities of Coal Ash Deposits," paper presented at the 1978 Winter Annual ASME Meeting, Dec. 1978, TIS-5890.
2. R. W. Borio, et.al., "The Control of High Temperature Fireside Corrosion in Utility Coal-Fired Boilers," ORC R&D Report No. 41 (1969).
3. F. Raask, "Flame Imprinted Characteristics of Ash Relevant to Boiler Slagging Corrosion and Erosion," presented at the 1981 Joint Power Generation Conference, ASME Paper No. 81-JPGC-Fu-1.
4. W. P. Bauver, J. D. Bianca, J. D. Fishburn, and J. G. McGowan, "Characterization of Erosion of Heat Transfer Tubes in Coal-Fired Power Plants," paper to be presented at 1984 Joint Power Generation Conference, Toronto, Canada, September 1984.
5. R. W. Borio, G. J. Goetz, and A. A. Levasseur, "Slagging and Fouling Properties of Coal Ash Deposits as Determined in a Laboratory Test Facility," paper presented at the ASME Winter Annual Meeting, December 1977, Combustion Engineering publication TIS-5155.
6. J. P. Huffman and F.E. Higgins, "Investigations of Partial Ash Melting by Phase Analysis of Quenched Samples," presented at 1981 Engineering Foundation Conference-Fouling and Slagging Resulting From Impurities in Combustion Gases, July 1981, Henniker, NH.
7. R. W. Borio, R. R. Narciso, Jr., "The Use of Gravity Fractionation Techniques for Assessing Slagging and Fouling Potential of Coal Ash," paper presented at the ASME Winter Annual Meeting, December 10-15, 1978, San Francisco, CA; available as Combustion Engineering publications TIS-5823.
8. R. W. Bryers, "The Physical and Chemical Characteristics of Pyrites and Their Influence on Fireside Problems in Steam Generators," ASME Paper No. 75-WA/CD-2, 1976.

9. G. L. Hale, A. A. Levasseur, A. L. Tyler and R. P. Hensel, "The Alkali Metals in Coal: A Study of Their Nature and Their Impact on Ash Fouling," paper presented at Coal Technology '80, November 1980, TIS-6645.
10. G. H. Gronhovd, W. Beckering, and P. H. Tlufte, "Study of Factors Affecting Ash Deposition from Lignite and Other Coals," an ASME publication presented at the ASME Winter Annual Meeting, November 16-20, 1969, Los Angeles, CA.

FIGURE 1
EFFECT OF COAL PROPERTIES ON FURNACE SIZE

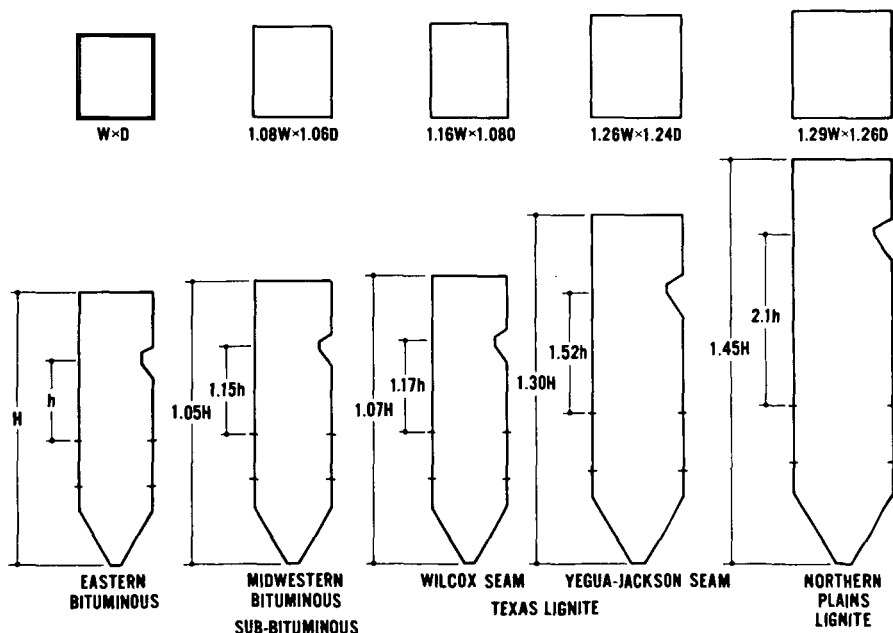


FIGURE 2

SUPERHEATER DEPOSIT BUILDUP vs FLUE GAS TEMPERATURE

DEPOSIT COLLECTED IN 8 HOUR PERIOD
 DEPOSIT WEIGHT NORMALIZED: (DEPOSIT WT. / (ASH INPUT
 * SURFACE AREA OF COLLECTION)

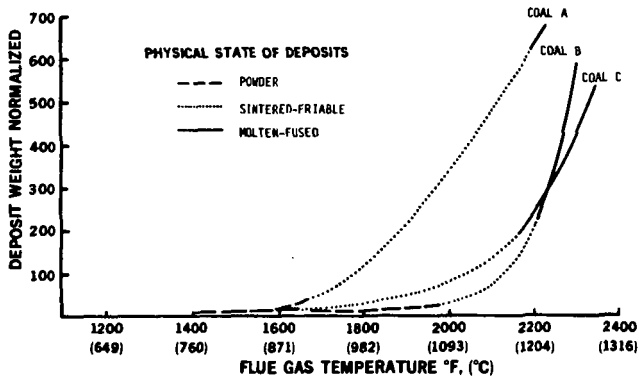


FIGURE 3

EFFECT OF SEGREGATED IRON ON COAL ASH SLAGGING
 SLAGGING POTENTIAL
 VERSUS
 PERCENT IRON IN 2.9 GRAVITY FRACTION

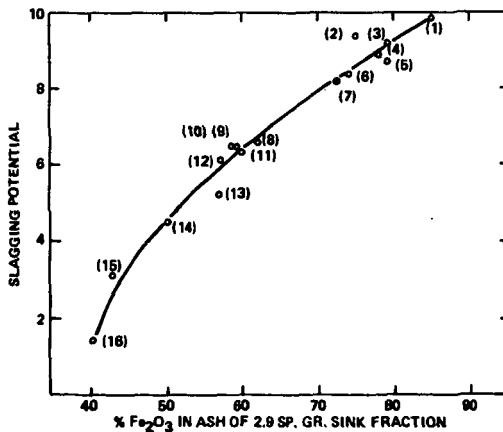


TABLE I
ENRICHMENT OF IRON IN BOILER WALL DEPOSITS
COMPARISON OF COMPOSITION OF ASH
DEPOSITS AND AS-FIRED COAL ASHES

UNIT SAMPLE	1		2		3	
	AS-FIRED COAL ASH	WATERWALL DEPOSIT	AS-FIRED COAL ASH	WATERWALL DEPOSIT	AS-FIRED COAL ASH	WATERWALL DEPOSIT
Ash Composition						
SiO ₂	47.0	33.3	50.2	55.1	49.7	41.8
Al ₂ O ₃	26.7	18.0	16.9	14.6	16.5	15.8
Fe ₂ O ₃	14.6	43.5	5.9	18.3	12.0	28.5
CaO	2.2	1.2	12.8	7.2	6.5	9.0
MgO	0.7	0.5	3.5	2.0	0.9	0.9
Na ₂ O	0.4	0.2	0.6	0.5	1.1	0.6
K ₂ O	2.3	1.6	0.8	0.6	1.5	0.9
TiO ₂	1.3	0.8	0.9	0.8	1.1	0.7
SO ₃	1.1	0.5	12.0	0.1	2.0	0.2

TABLE 2 ANALYTICAL DATA ON U.S. COALS

Rank Region	Lignite N. Dakota	Sub B Montana	Lignite Texas (Yegua)	Lignite Texas (Wilcox)	lvBb Utah	lvAb Penn	Lignite Texas (Wilcox)
(Dry Basis)							
Volatile	44.4	42.2	39.6	41.0	41.5	32.5	38.1
Fixed C	46.0	52.0	26.9	39.5	48.3	54.0	33.0
Ash	9.6	5.6	33.5	19.5	10.2	13.5	28.9
HHV (Btu/lb) (Dry Basis)	10640	12130	7750	9710	12870	13200	8420
Ash Fusibility							
I.D. (°F)	2130	1980	1940	2150	2190	2370	2210
S.T.	2180	2020	2200	2250	2270	2510	2300
H.T.	2190	2060	2430	2340	2390	2560	2420
F.T.	2200	2170	2610	2530	2620	2660	2620
Ash Composition							
SiO ₂ (%)	20.0	33.9	62.1	52.3	52.5	51.1	57.9
Al ₂ O ₃	9.1	11.4	15.1	17.4	18.9	30.7	21.8
Fe ₂ O ₃	10.3	10.8	3.5	5.3	1.1	10.0	3.9
CaO	22.4	21.0	6.2	9.4	13.2	1.6	7.1
MgO	6.4	2.7	0.7	3.2	1.3	0.9	2.1
Na ₂ O	5.0	5.8	3.6	0.9	3.8	0.4	0.9
K ₂ O	0.5	1.6	2.1	1.2	0.9	1.7	0.8
TiO	0.4	0.7	0.9	1.2	1.2	2.0	1.1
SO ₃	21.9	12.0	6.1	9.6	6.2	1.4	4.4
Total alkali, %, ash basis							
Na ₂ O	5.0	5.8	3.6	0.9	3.8	0.4	0.7
K ₂ O	0.5	1.6	1.9	1.2	0.9	1.7	0.8
Soluble Alkali, %, ash basis							
Na ₂ O	5.58	6.45	3.88	0.71	1.49	0.15	0.16
K ₂ O	—	—	0.44	0.04	0.08	—	0.05
Relative Soluble Alkali, %							
Na ₂ O	112%	111%	108%	79%	39%	38%	23%
K ₂ O	—	—	—	3%	9%	—	6%
Fouling Potential							
	Severe	High	High	Moderate	Moderate	Low	Low

DEPOSIT CONSTITUENT PHASE SEPARATION AND ADHESION

E. RAASK

Technology Planning and Research Division, Central Electricity Generating Board,
Kelvin Avenue, Leatherhead, Surrey, UK

The initial deposit material on coal fired boiler tubes consist largely of silicate, sulphate and iron oxide particles. The fused silicates and molten sulphates form immiscible phases at high temperatures first on the micro-scale in individual particles and subsequently as separate layers in the deposit. The adhesion of ash deposit constituents to boiler tubes starts with the small particle retention as a result of the van der Waals, electrostatic and liquid film surface tension forces. Subsequently a strong bond will develop between the oxidized metal surface and iron saturated layer of ash deposit.

The pulverized coal fired boilers at electricity utility power stations are designed for "dry" ash operation where the bulk of mineral matter residue is removed in the electrical precipitators in the form of particulate ash. However, it is inevitable that some deposits of sintered ash and semi-fused slag form on the heat exchange tubes and between 20 and 30 per cent of coal ash is discharged from the combustion chamber as clinker. The high temperature cyclone fired boilers are designed for "wet" ash operation and up to 80 per cent of coal ash is discharged from the furnace as molten slag.

The build-up of sintered ash and fused slag deposits depends chiefly on the rate of ash particle impaction and the adhesive characteristics of the collecting surface. The initial deposit on the heat exchange tubes in pulverized coal fired boilers consists of ash particles of diameter ranging from less than 0.1 μm to 100 μm . Subsequently the deposited ash may be re-entrained in the flue gas or it may form first a sintered matrix and later a fused slag deposit chiefly by viscous flow. For the deposit formation the ash particles must be first held at the collecting surface and subsequently the deposit matrix bonded to the boiler tubes by adhesive forces sufficiently strong to overcome the gravitational pull, boiler vibration and eventually the sootblower jet impaction. This work sets out to examine the adhesive characteristics of different constituents of the flame heated ash and the formation of sintered deposits and slag bonded to the heat exchange tubes.

INITIAL DEPOSIT CONSTITUENTS

The mineral matter in coal consists chiefly of silicate, sulphide, carbonate species, and chlorides and organo-metal compounds associated with the fuel substance (1,2). The silicate mineral particles vitrify partially or completely, in the pulverized coal flame (3), and thus the silicate ash fraction of the initial deposit consists of particles of variable amounts of a glassy phase and crystalline species (4).

The sulphide, carbonate, chloride and organo-metal species dissociate and oxidize in the flame. The oxides may remain as discrete particles, chiefly iron oxide (magnetite), can dissolve in the glassy phase of silicates, and a fraction of calcium and sodium oxides are sulphated (5). Thus the initial deposit material will contain some calcium, sodium and potassium sulphate. The latter originates from the release of potassium in the flame heated aluminosilicate particles (6).

The relative concentrations of flame heated ash constituents, namely silicates, iron oxide and sulphate can be estimated from the ash analysis. However, the composition of the initial deposit material can be markedly different as a result of selective deposition. In particular, the deposit material can be enriched in sulphate as shown in Fig. 1. The relative concentrations of different deposit constituents were obtained by analysing the material on a cooled metal tube probe inserted in boiler flue gas for short, 2 to 15 minute duration (7). The sulphate content of the flue gas borne ash and probe deposits in a cyclone fired boiler was higher than that in the pulverized coal fired boiler ash and deposits. This was because in cyclone boilers the bulk of silicate ash is discharged as molten slag but the residual ash is relatively rich in sulphate.

The rate of alkali-metal sulphate deposition will decrease when the temperature of collecting target surface exceeds 1075 K as shown in Fig. 2. The decrease in the deposition of alkali-metal sulphates is related to the concentration of the volatile alkali-metals in the flue gas and the saturation vapour pressure of sodium and potassium sulphates (8). The initial deposit on cooled surfaces contains a small amount of chloride as shown in Fig. 2.

In a reducing atmosphere the deposit material may contain iron sulphide (FeS) formed on dissociation of coal pyrite mineral. This is likely to occur on the combustion chamber wall tubes near the burners where the reaction time is short, below one second, for oxidation of FeS residue to the oxide. It has been suggested that calcium sulphide (CaS) may also be present in the ash material deposited from a reducing atmosphere gas stream as a result of sulphidation of calcium oxide (9).

THERMAL STABILITY OF SULPHATES AND IMMISCIBILITY WITH SILICATES

Bituminous coals usually leave a highly silicious ash on combustion. That is, fused aluminosilicates constitute an acidic media at high temperatures that is capable of absorbing large quantities of basic metals in the form of oxides, chiefly those of sodium, calcium and magnesium. At lower temperatures the corresponding sulphates are thermodynamically more stable in the presence of sulphur gases. The equilibrium distribution of alkaline oxides between molten sulphates and fused silicates at different temperatures can be calculated from the appropriate thermodynamic data. However, the residence time of the flame borne mineral species before deposition is short and the alkali-metal distribution does not reach the equilibrium state.

The fused silicate particles will absorb the flame volatilized sodium to the depth of about 0.05 μm (10), and the remainder is converted to sulphate partly in the flue gas and partly at the surface of ash particles. The distribution of sodium in the silicate and sulphate phases can be expressed in a form:

$$m_{\text{sul}} = m_o - kw^{2/3} \quad \dots 1)$$

$$\text{where } m_{\text{sil}} + m_{\text{sul}} = m_o \quad \dots 2)$$

m_{sil} , m_{sul} and m_o denote the amount of sodium in silicate and sulphate fractions, and the total sodium in ash respectively; k is a constant and w is the ash content of coal. When the sodium to ash ratio is below 1 to 100 the bulk of sodium is captured by the silicate particles and equation 2 reduces to:

$$m_{\text{sil}} \approx m_0$$

... 3)

and consequently the amount of sodium available for the formation of sulphate is small.

The molten sodium sulphate/sodium silicate system of composition $\text{Na}_2\text{SO}_4/\text{Na}_2\text{O}-\text{SiO}_2$ has one liquid phase at 1475 K, but as the proportion of silica increases, the melt separates into two layers (11,12). The change from the miscible to immiscible phase of the system has been explained by alterations in the silicate structure as the ratio of Na_2O to SiO_2 decreases. In more basic, less viscous melts, the silicate ions exist in the form of SiO_4^{4-} tetrahedrons which have the same mobility as sulphate ions, and thus homogeneity of the system is to be expected. As the silica content is increased the complexity of the silicate structure reaches a point where the silica anions become relatively immobile for a separation of sulphate from silica to take place.

The miscibility of the corresponding potassium sulphate-silicate system has been studied by the usual crucible method as well as by a technique of a hanging droplet (13). The droplets of potassium sulphate/silicate mixtures, 3 mm in diameter, were suspended from 0.5 mm platinum wire which had a semi-spherical head 1.5 mm in diameter. Separation of the silicate (internal) and sulphate phases in the droplets can be observed directly in the Leitz heating microscope which is used, in its conventional mode of operation, to assess the fusion characteristics of coal ashes (14). Fig. 3 shows the two phase separation of $2\text{K}_2\text{SO}_4-\text{K}_2\text{O}-2.1\text{SiO}_2$ system at 1575 K where the outside envelope is the transparent sulphate phase through which the platinum wire heats (top) and a globule of molten silicate (bottom) can be seen. As the temperature was increased to 1725 K the two phases became miscible because of the increased solubility of sulphate in the silicate melt at the higher temperature.

The $\text{K}_2\text{SO}_4-\text{K}_2\text{O}-\text{SiO}_2$ phase diagram is depicted in Fig. 4 which shows that the system is miscible at 1575 K when the molar ratio of K_2O to SiO_2 is above 0.5. As in the corresponding sodium sulphate/sodium silicate system, less basic melts separate into two immiscible liquids. This is the case with most coal ash slags where the molar ratio of basic oxides (sum of Na_2O , K_2O , CaO and MgO) to SiO_2 is well below 0.5. Exceptions to this are the sodium and calcium rich ashes of some lignite and non-bituminous coals, which can have sufficient amounts of alkalis to form a single phase melt of miscible sulphates and silicates at high temperatures.

ADHESION BY VAN DER WAALS AND ELECTROSTATIC FORCES

The ash particles deposited on boiler tubes are initially held in place by surface forces, i.e. van der Waals and electrostatic attraction forces. Van der Waals forces become important when molecules or solid surfaces are brought close together without a chemical interaction taking place. For a hemispherical particle of radius (r) held at a distance of nearest approach (h) from a plane, the resultant forces (F) is given by:

$$F = \frac{Ar}{6h^2} \quad \dots 4)$$

where A is the Hamaker constant (15).

Equation 4 applies over short distances, up to 150 Å (1.5×10^{-8} m) and for longer distances the "retarded" van der Waals forces decay rapidly (16). An equation based on the dielectric properties of solids for the retarded

van der Waals forces (F') between a sphere of radius (r) at the distance (h) from a flat surface is (17):

$$F' = \frac{2B\pi r}{3h^3} \quad \dots 5)$$

where B is the appropriate constant for the given material.

The changeover from the unretarded to retarded van der Waals forces occurs at a distance of about 150 \AA ($1.5 \times 10^{-8} \text{ m}$), and the corresponding value of the Hamaker constant (A) in equation 4 was found to be 10^{-19} N (Newton), and that of the Lifshitz constant (B) in equation 5 was $8.9 \times 10^{-29} \text{ N m}$ (16,18). These values have been used to compute the ratio of van der Waals forces to the gravitational force on small ash particles approaching a flat surface.

The gravitational force (F_g) on an ash particle of radius (r) and the density (D) is given by:

$$F_g = \frac{4\pi r^3 Dg}{3} \quad \dots 6)$$

where g is the gravity acceleration constant (9.81 m s^{-2}). Thus, the ratio (F_r) of the short distance van der Waals forces (F) to the gravitational force (F_g) on a particle is:

$$\frac{F}{F_g} = F_r = \frac{A}{8\pi Dgr^2 h^2} = \frac{1.62 \times 10^{-25}}{r^2 h^2} \quad \dots 7)$$

where the value of D for ash was taken to be 2500 kg m^{-3} and when $h < 1.5 \times 10^{-8} \text{ m}$. The corresponding ratio (F_r') of the retarded van der Waals forces (F') to the gravitational force is given by:

$$\frac{F'}{F_g} = F_r' = \frac{2B}{Dgr^2 h^3} = \frac{8.15 \times 10^{-34}}{r^2 h^3} \quad \dots 8)$$

where $h > 1.5 \times 10^{-8} \text{ m}$.

Fig. 5 shows a comparison of van der Waals and the gravitational forces on small ash particles as these approach a collecting surface. Plots A and B indicate that the sub-micron sized particles are readily held on a surface by van der Waals forces. The capture of small particles of ash on boiler tubes is further enhanced by surface irregularities of oxidized metal (19). Also, it has been suggested that an electrostatic attraction force enhance the transport and retention of sub-micron sized particles on steel probes inserted in the flue gas of coal fired boilers (7,20). A layer of electrically precipitated deposit of ash can have a cohesive strength between 5 and 40 times higher than that formed by sedimentation because particles in an electric field have permanent dipole characteristics which lead to these being orientated to form a cohesive layer of ash (21). It appears therefore that the combined effects of van der Waals and electrostatic forces of attraction, and surface irregularities are sufficient to hold the sub-micron diameter particles on the surface of boiler tubes for the subsequent liquid phase adhesion, and chemical and mechanical bond formation.

ADHESION BY SURFACE TENSION FORCE

The formation of strong adhesive bonds of enamel coatings and glass/metal seals on heating requires the presence of a liquid phase (22,23,24). The role of the liquid film is to provide the initial adhesion of solid particles as a result of surface tension. The work of adhesion (W_a) is given by:

$$W_a = \pi + \gamma (1 + \cos \theta) \quad \dots 9)$$

where γ is the surface tension of the liquid, and θ is the contact angle at the solid/liquid interface. With perfect wetting, i.e. when θ equals zero, W_a has the highest value:

$$W_a = \pi + 2\gamma \quad \dots 10)$$

The work of cohesion of a liquid (W_c) is given by:

$$W_c = 2\gamma \quad \dots 11)$$

With wetting liquids, therefore, W_a can be higher than W_c and failure will take place within the liquid layer, whereas with non-wetting liquids the rupture occurs at the solid/liquid interface.

Alkali-metal sulphates frequently constitute a liquid phase in ash deposits, and the molten sulphates readily wet and spread on the surface of boiler tubes. In a reducing atmosphere and when in contact with carbon, sulphates are reduced to sulphides which wet and spread on any surface. The coefficient of surface tension of sulphates is fairly high, 0.20 N m^{-1} for Na_2SO_4 and 0.14 N m^{-1} for K_2SO_4 near their respective melting point temperatures (25,26). Thus work of cohesion of molten sulphate layer in boiler deposit is between 0.3 and 0.4 N m^{-1} and the work of adhesion is higher because of a low contact angle at the sulphate/tube surface interface. It is therefore to be expected and it is observed in practice that when the deposit is removed, e.g. by sootblowing, there remains a film of sulphate adhering to boiler tubes. The surface tension of coal ash slag has been measured previously by the sessile drop method (27) and a typical value was 0.3 N m^{-1} . It is about twice that of sulphates and thus the work of adhesion (Equation 9) and the cohesive bond strength are corresponding higher at the slag/solid interface.

Only a small amount of liquid, about a hundred molecule thick layer, is sufficient for the adhesion contact of sub-micron diameter particles (28). In the case of a volatile liquid, the equilibrium thickness of the film, and thus the adhesion, varies with partial pressure of the vapour in the surrounding atmosphere. When evaporation from a liquid film occurs, as a result of increased temperature, the adhesion first rises to a maximum value due to the meniscus effect but it breaks down as the film thickness is reduced to molecular dimensions. However, before the break-down of the surface tension chemical and mechanical bonds may develop between the deposited ash and boiler tube surface.

MECHANICAL AND CHEMICAL BONDING

Ash deposits on boiler tubes can be keyed to the surface of metal oxide by mechanical and chemical bonds. Mechanical bonding is enhanced by extending surface at the interface as shown in Fig. 6a. Boiler tubes are not polished and thus have an extended surface that is further increased by oxidation and chemical reactions between the oxide layer and ash deposits. It is therefore evident that a comparatively rough surface of boiler tubes constitute an anchorage for keying ash deposits to the heat exchange elements.

Dietzel (29) and Staley (30) have proposed that the chemical reactions at a enamel/metal interface can be considered in terms of electrolytic cells set up between the metals of different electro-chemical potential. It has been suggested that cobalt or nickel precipitated in the enamel when in contact with steel surface, forms short-circuited local cells in which iron is the anode. The current flows from iron through the melt to cobalt and back to iron. The result is that iron goes into solution, the surface becomes roughened, and the enamel material anchors itself into the cavities as shown in Fig. 6b.

The galvanic reactions will take place at a much faster rate in the low viscosity phase of sulphates in boiler deposit than that in highly viscous silicate glass. However, rapid reactions at the tube surface/deposit interface may not be necessary or appropriate for development of a strong bond between the ash deposit and boiler tubes. In metal/glass seal and metal/enamel coating technology, the adhesive bonds formed on heating have to be completed in a few hours, whereas those in boiler deposits can form over a period of days or weeks. The adhesive bond between the metal surface and a silicate material can be high when there is a gradual rather than abrupt change in the glass phase composition near the interface (31).

When the ash deposit is brought in intimate contact with the surface of boiler tubes either by the action of surface tension or by the galvanic reactions, the controlling parameter in mechanical bonding is the strength of the glassy phase at the narrowest cross sectional area of contact cavities (Fig. 6b). The annealed glass may have a tensile strength of around 50 MN m^{-2} giving a maximum bond strength of 35 MN m^{-2} . However, the glass at the interface may be stronger or weaker depending on whether the conditions in the keying cavities increase or decrease local flaws and resultant stresses.

Chemical bonds, covalent or ionic as shown in Fig. 6c and d, at the metal oxide/deposit surface are potentially strong with theoretical values over 10^9 N m^{-2} . It is, however, impossible to estimate the number of sites and the size of contact areas at the interface where the chemical bonds may be effective. In any case, the cohesive strength of the deposit matrix is the limiting factor since it is lower than that of chemical bonds by several orders of magnitude. In practice, this means that when a strongly adhering deposit is subjected to a destructive force, e.g. sootblower jet, failure occurs within the deposit matrix and there remains a residual layer of ash material firmly bonded to the tube surface.

ADHESION OF ASH DEPOSITS ON FERRITIC AND AUSTENITIC STEELS

The adhesion bond strength of soda glass on a metal substrate has been determined by heating a glass disc sandwiched between two metal discs in a vertical furnace (32). The technique has been adopted for measuring the strength of the adhesive bond developed when a boiler deposit was sandwiched between two discs of ferritic or austenitic steels (33). The deposit material was taken immediately after boiler shut-down from the superheater tubes of a pulverized coal fired boiler fuelled with a mixture of East Midlands, UK coals. The flue gas temperature in the superheater prior to boiler shut-down was about 1300 K and the tube metal temperature was 850 K. The deposit material consisted of 30 per cent of alkali-metal sulphates in weight ratio of 2 to 1 of Na_2SO_4 to K_2SO_4 , the remainder being silicate ash. A layer of deposit, 3 mm thick, was sandwiched between two metal discs, 20 mm in diameter, made of boiler tube steels and then heated in a vertical furnace. After a time interval lasting from one to 25 days the bond was ruptured by applying a tensile force without prior cooling.

The results in Fig. 7 show that the strength of adhesive bond between the ferritic steel sample and boiler deposit increased exponentially with

temperature in the range of 775 to 900 K. Similar results were obtained by Moza et al. (34) who used a droplet technique to measure the adhesive bond of coal ash slag on a ferritic steel target in the temperature range of 700 to 950 K.

The results plotted in Fig. 8 shows that the strength of adhesive bond of ash deposit on both the ferritic and austenitic steels increased approximately linearly with time at 900 K. However, the bond strength of deposit on the austenitic steel (Type 18Cr13NiNb) was significantly lower than that between the deposit and 9Cr-ferritic steel. The latter resulted from the thermal and chemical compatibility of the steel oxide layer and deposit material (35). Table 1 shows approximate values of the coefficient of thermal expansion of the ferritic and austenitic steels, some oxides and silicate materials (36).

Table 1: Coefficient of Thermal Expansion of Boiler Tube Steels, Oxides and Silicates

Material	Thermal Expansion, $\frac{\Delta m}{m} K^{-1}$
<u>Steels</u>	
Mild Steel and Ferritic Steels	11 to 12 $\times 10^{-6}$
Austenitic Steels	16 to 18 $\times 10^{-6}$
<u>Oxides</u>	
Tube Metal Oxides (Fe_3O_4 , Cr_2O_3 , NiO)	8 to 10 $\times 10^{-6}$
<u>Deposit Constituents</u>	
Glassy Material	6 to 9 $\times 10^{-6}$
Quartz (Crystalline)	5 to 8 $\times 10^{-6}$
Silicates in Fired Brick	7 to 8 $\times 10^{-6}$

The data in Table 1 show that the coefficient of thermal expansion of mild steel and ferritic steels is not greatly different from that of their oxides and the ash deposit constituents. It is therefore evident that there is no gross incompatibility in the thermal expansion characteristics and strongly bonded ash deposits once formed on mild steel tubes are not easily dislodged on thermal cycling.

In contrast, the thermal expansion of austenitic steel is significantly higher than that of the oxides and deposit material. In the absence of boiler deposit, the oxide material in the form of thin layer is able to absorb thermal stresses and the adhesive layer remains intact on cooling. However, it appears that the oxide layer is unable to absorb thermal stresses in a similar manner when contaminated and constrained by bonded ash deposits. It is therefore a usual occurrence that ash deposits peel off the austenitic steel tubes on cooling whereas the deposit formed on ferritic steels under the same conditions remain firmly attached to the tubes.

King et al. (22) have suggested that in order to obtain good adherence of enamel coatings on metals, the enamel material at the interface must become saturated with the metal oxide, e.g. FeO of ferritic steels. Coal ash deposit on boiler tubes contains between 5 and 25 per cent iron oxide (Fig. 1) and thus the layer at the tube/deposit interface becomes saturated with FeO . The chromium and nickel contents of ash deposit are low and thus the same chemical compatibility stage is not reached at the austenitic steel/deposit interface.

The adhesive bond between boiler ash deposit and the surface of ferritic steels can attain exceptionally high strengths. This was found on examining the deposits formed on different steel specimens tested in an experimental superheater loop. Favourable conditions for the formation of firmly bonded deposits were as follows:

- (a) The iron oxide content of coal was above 20 per cent expressed as Fe_2O_3 giving an iron saturated layer of deposit on the tube specimens.
- (b) The ash collecting surface was a 5 per cent chromium ferritic steel which formed an oxide layer strongly adhering to metal for a firm anchorage of deposits.
- (c) The tube metal temperature was high, 950 K, which enhanced the formation of strong adhesive bond. The flue gas temperature at that position was approximately 1250 K.
- (d) The ferritic test piece in the experimental loop was sheltered from direct action of sootblower. Weak turbulence caused by the jet removed some of the unsintered silica ash leaving iron rich deposit firmly bonded to the tube. The iron rich deposit had grown in thickness to about 20 mm after nine months, and cohesive strength of the deposit material increased towards the surface of tube metal. The microscopic examination showed that there was no marked interface boundary between the ash deposit and metal oxide.

FORMATION OF LAYER STRUCTURE DEPOSITS AND SLAG MASSES

The coal ash deposits on boiler tubes have frequently a separate zone structure with a sulphate rich layer up to 2 mm thick under the matrix of sintered ash (35). The outer layer is porous and it constitutes a pathway for the enrichment of alkali-metals in the deposit layer next to tube surface. The diffusible species may be sulphate, chloride, oxide or hydroxide, but the thermodynamic data (8) and the results of deposition measurements in coal fired boilers (Fig. 3) suggest that sodium and potassium sulphates are the principal vapour species which diffuse through a porous matrix of silicate ash deposit.

The relative amounts of Na_2SO_4 and K_2SO_4 which diffuse through the sintered matrix of silicate ash depend on the temperature gradient across the deposit layer, vapour pressure of the species and thermodynamic stability of the sulphates in the presence of silicates. Potassium sulphate has a higher temperature stability limit when compared with that of sodium sulphate and as a result K_2SO_4 can be preferentially transported to the surface of cooled boiler tubes when there is a steep temperature gradient across the ash deposit. The K_2SO_4 rich phase, when molten, can cause severe corrosion of tube metal.

The corrosion product, a mixture of oxide, sulphide at the metal interface and sulphate outside, has a weak adhesive bond to the metal surface and cannot support large deposit masses. It is therefore unusual to find excessive amounts of sintered ash deposits and fused slag in the exact localities where severe high temperature corrosion occurs. Conversely, a strongly adhering matrix

of sintered ash deposit in the absence of sulphate, sulphide or chloride phases is not markedly corrosive.

The build-up of boiler tube deposits is a continuously changing process as depicted in Fig. 9. When the deposit material reaches a thickness of 2 to 3 mm (Fig. 9a) the separate sulphate and silicate phases occur (Fig. 9b). Subsequently, the sulphate layer disappears in the middle section (Fig. 9c) allowing a strong bond to be established between the sintered ash deposit and ferritic steel boiler tubes. This is the "classical" mode of formation of superheater tube deposit when the metal temperature is in the range of 750 to 900 K. Above 950 K the layer structured deposits are less likely to occur and a strong adhesive bond is rapidly formed between the silicate ash deposits and the high temperature tube surface.

A notable feature of slag formed in pulverized coal fired boiler is its variable gas hole porosity. Burning coal particles are encapsulated in the deposit layer and generate CO and CO₂ inside the silicate material (27) resulting in a highly porous slag. The density of slag will increase when the encapsulated coal particles are consumed and gas bubbles have escaped.

It has been observed that new boilers have an "immunity" period lasting weeks or months before severe slag build-up occurs. This is partly due to the fact that during the commissioning period the boiler rarely reaches full load output. However, it may also be partly due to a slow rate of formation of the interface layer on boiler tubes which is able to have a strong adhesive bond to rapidly forming ash slag and thus able to support large masses of deposit.

CONCLUSIONS

Initial Deposit

The initial deposit material on cooled tubes in coal fired boilers consists largely of flame vitrified silicate ash, iron oxide, and calcium and alkali-metal sulphates. Trace amounts of chloride will also deposit and under reducing conditions some iron and calcium sulphides can be present.

Phase Separation

Most coals leave an ash residue which is pyrochemically acidic, and the alkali-metals and calcium are distributed in the silicate and sulphate phases under oxidizing conditions. The fused silicates and molten sulphates are immiscible and separate into two phases. The phase separation enhances the adhesion of ash to boiler tubes and leads to the formation of layer structured deposits.

Initial Particle Adhesion

Initially the small particles of ash, below 1 μm in diameter are held at the surface of boiler tubes by the van der Waals and electrostatic attraction forces. Subsequently a film of molten sulphate may form at the tube surface/deposit interface and only a small amount of liquid, about one hundred molecules thick is sufficient for bonding.

Strong Adhesive Bond of Deposits on Ferritic Steels

Strong adhesive bonds can form between the oxidized surface of ferritic steels and iron rich ash because of the composition and thermal expansion compatibility of the metal oxide and silicate ash deposit. The adhesive bond strength increases exponentially with temperature of the target surface in the

range of 750 to 950 K. The bond strength can reach high values, that is, higher than the cohesive strength of sintered ash deposits at temperatures above 850 K.

Weak Adhesive Bond of Deposits on Austenitic Steels

The adhesive bond between the austenitic steel surface and ash deposit is relatively weak as a result of the composition and thermal incompatibility of the steel oxide and the silicate material. The temperature fluctuations on changeable boiler load conditions can cause sufficiently high thermal stresses for deposit to skid off the austenitic steel tubes.

Boiler Tube/Ash Deposit Interface

The boiler tube/ash deposit interface layer which can support large masses of slag formed in the combustion chamber takes several months to develop. Thus the full extent of boiler slagging may not become evident during the commissioning period of new boiler plant.

ACKNOWLEDGEMENT

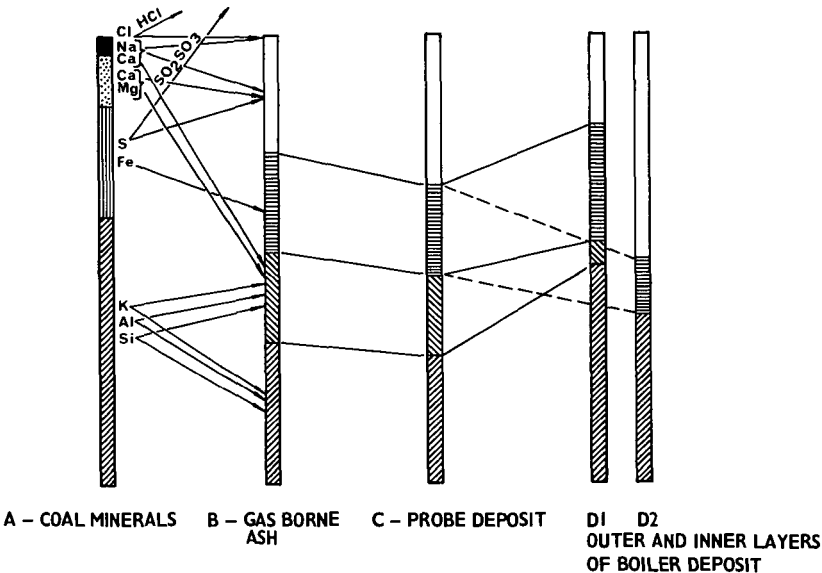
The work was carried out at the Central Electricity Research Laboratories and the paper is published by permission of the Central Electricity Generating Board.

LITERATURE CITED

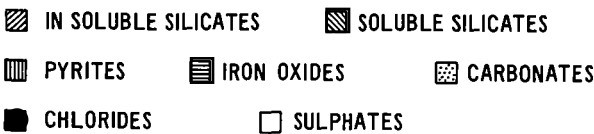
1. Lowry, H.H., Editor, "Chemistry of Coal Utilization", John Wiley and Sons, Inc., New York, (1963)
2. Francis, W., "Fuels and Fuel Technology", Vol. I, Pergamon Press, London, (1965)
3. Raask, E., "Fusion of Silicate Particles in Coal Flames", Fuel, (1969), 48, 366
4. Raask, E. and Goetz, L., "Characterization of Captured Ash, Chimney Stack Solids and Trace Elements", Jour. Inst. Energy, (1981), 54, 163
5. Raask, E., "Sulphate Capture in Ash and Boiler Deposits in Relation to SO₂ Emission", Proc. Ener. Comb. Sci., (1982), 8, 261
6. Raask, E., "The Behaviour of Potassium Silicates in Pulverized Coal Firing", VGB Mitteilungen, (1968), 18, 348
7. Raask, E., "Reactions of Coal Impurities during Combustion and Deposition of Ash Constituents on Cooled Surfaces", Conf., Mechanism of Corrosion by Fuel Impurities, p. 145, Marchwood, UK, Butterworth Publ., London, (1963)
9. Halstead, W.D. and Raask, E., "The Behaviour of Sulphur and Chlorine Compounds in Pulverized Coal Fired Boilers", Jour. Inst. Fuel, (1969), 43, 344
9. Hein, K., "Chemical and Mineralogical Aspects of Fouling of Heat Exchange Surfaces in Non-Bituminous Coal Fired Boilers", VGB Kraftwerkstechnik, (1979), 59, 576
10. Hosegood, E.A. and Raask, E., "Reactions and Properties of Alkalis and Ash in Pulverized Fuel Combustion", CERL Note No. RD/L/N 49/64, Leatherhead, UK, (1964)

11. Kordes, E., Zofelt, B. and Proger, H.J., "Reactions in the Melting of Glass with Na_2SO_4 : Immiscibility Gap in Liquid State between Na-Ca-Silicates and Na_2SO_4 ", *Zeitschr. Anorg. Allgem. Chem.*, (1951), 264, 255
12. Pearce, M.L. and Beisler, J.F., "Miscibility Gap in the System Sodium Oxide-Silica-Sodium Sulphate at 1473 K", *Jour. Am. Cer. Soc.*, (1965), 48, 40
13. Raask, E. and Jessop, R., "Miscibility Gap in the Potassium Sulphate-Potassium Silicate System at 1575 K", *Phys. and Chem. Glasses*, (1966), 7, 200
14. DIN, "Determination of Ash Fusion Behaviour", German Standard, DIN 51 730, (1976)
15. Casimir, H.B.G. and Polder, D., "The Influence of Retardation on the London-van der Waals Forces", *Phys. Rev.*, (1948), 73, 360
16. Tabor, D., "Surface Forces", *Chem. Ind.*, (1971), No. 35, p 969
17. Lifshitz, E.M., "The Theory of Molecular Attractive Forces Between Solids", *Soviet Physics, JETP*, (1956), 2, 73
18. Tabor, D. and Winterton, R.S.H., "Surface Forces: Direct Measurement of Normal and Retarded van der Waals Forces", *Nature*, (1968), 219, 1120
19. Pfefferkorn, G. and Vahl, J., "Investigation of Corrosion Layers on Steel Using Electron Microscopy and Electron Diffraction", *Conf., Mechanism of Corrosion by Fuel Impurities*, p. 366, Marchwood, UK, Butterworths Publ., London, (1963)
20. Steel, J.S. and Brandes, E.A., "Growth and Adhesion of Oxides in Furnace Deposits and Their Influence on Subsequent Deposition of Ash Particles as Combustion Products", *Conf., Mechanism of Corrosion by Fuel Impurities*, p 374, Marchwood, UK, Butterworths, London, (1963)
21. Penney, G.W. and Klinger, E.H., "Contact Potentials and the Adhesion of Dust", *Trans. A.I.E.E.*, (1962), 81, 200
22. King, B.W., Tripp, H.P. and Duckworth, W.H., "Nature of Adherence of Porcelain Enamels to Metals", *Jour. Am. Cer. Soc.*, (1959), 42, 504
23. Holland, L., "The Properties of Glass Surfaces", Chapman and Hall, London, (1964)
24. Klomp, J.T., "Interfacial Reactions Between Metals and Oxides During Sealing", *Am. Ceram. Soc. Bull.*, (1979), 10, 887
25. International Critical Tables, "Surface Tension of Molten Sulphates", 4, 443, McGraw-Hill Book Co., New York, (1928)
26. Bertozzi, G. and Soldani, G., "Surface Tension of Molten Salts, Alkali Sulphate and Chloride Binary Systems", *Jour. Phys. Chem.*, (1967), 71, 1536
27. Raask, E., "Slag/Coal Interface Phenomena", *Trans. ASME for Power*, Jan., (1966), p 40
28. Cross, N.L. and Picknett, R.G., "Particle Adhesion in the Presence of Liquid Film", *Conf. Mechanism of Corrosion by Fuel Impurities*, p 383, Marchwood, UK, Butterworths, Publ., London, (1963)

29. Dietzel, A., "Explanation of Adhering Problem in Sheet Iron Enamels", Emailwaren-Industrie, (1934), 11, 161
30. Staley, H.F., "Electrolytic Reactions in Vitreous Enamels and Their Reaction to Adherence of Enamels to Steel", Jour. Am. Ceram. Soc., (1934), 17, 163
31. Weyl, W.A., "Wetting of Solids as Influenced by Polarizability of Surface Ions", Structure and Properties of Solid Surfaces, p 147, Edited by R. Gomer and C.S. Smith, University of Chicago Press, USA, (1953)
32. Oel, H.J. and Gottschalk, A., "The Adhesion Temperature Between Glass and Metals", Glastechnische Berichte, (1966), 39, 319
33. Raask, E., "Boiler Fouling - The Mechanism of Slagging and Preventive Measures", VGB Kraftwerkstechnik, (1973), 53, 248
34. Moza, A.K., Shoji, K. and Austin, L.G., "The Sticking Temperature and Adhesion Force of Slag Droplets from Four Coals on Oxidized Mild Steel", Jour. Inst. Fuel, (1980), 53, 17
35. Raask, E., "Mineral Impurities in Coal Combustion", Hemisphere Publishing Corp., New York, (1984)
36. Hodgman, C.D., (Editor), "Handbook of Chemistry and Physics", The Chemical Rubber Publishing Co., Ohio, USA, (1962)



**FIG. 1 ASH COMPOSITION CHANGES ON ROUTE FROM MINERAL
MATTER TO BOILER TUBE DEPOSITS**



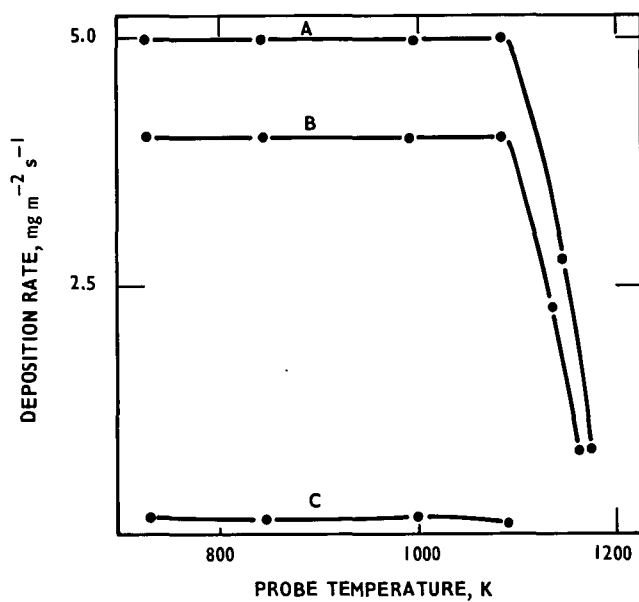


FIG. 2 DEPOSITION OF SULPHATE AND CHLORIDE IN
CYCLONE FIRED BOILER - 0.28 PER CENT
CHLORINE IN COAL

A - Na₂SO₄ B - K₂SO₄ C - NaCl

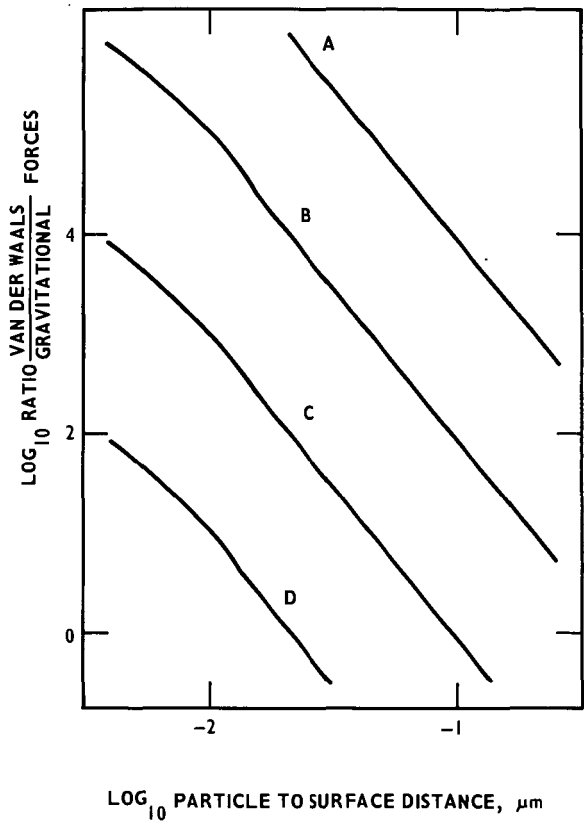
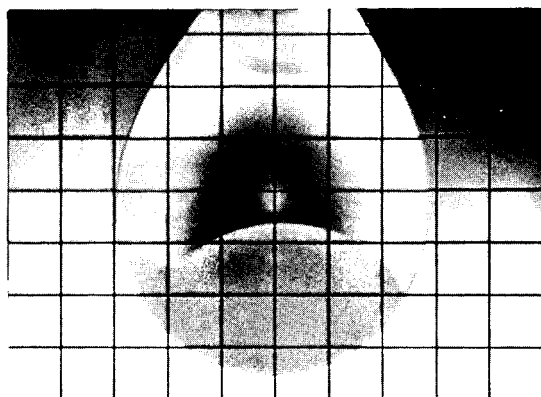


FIG. 5 COMPARISON OF VAN DER WAALS AND GRAVITATIONAL FORCES ON ASH PARTICLES NEAR COLLECTING SURFACES

PARTICLE DIAMETER, μm
A - 0.01; B - 0.1; C - 1.0; D - 10.0



TWO PHASES AT 1575K

FIG. 3 $2K_2SO_4 - K_2O - 2.1 SiO_2$ DROPLET IN HEATING MICROSCOPE (0.5 mm GRID)

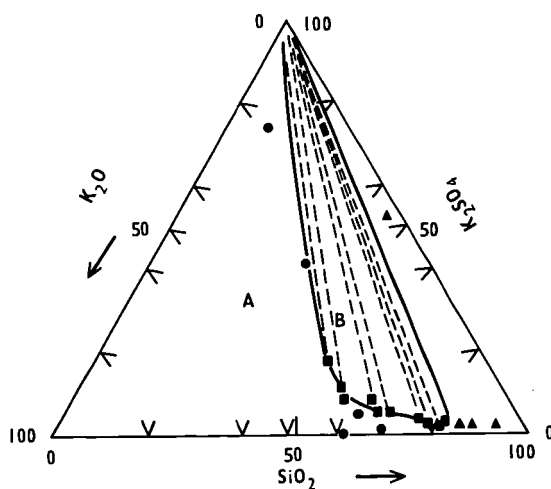


FIG. 4 MISCIBILITY GAP IN K_2SO_4 - K_2O - SiO_2 SYSTEM AT 1575 K
 A, SINGLE PHASE B, TWO PHASES C, LIQUID + SOLID SiO_2

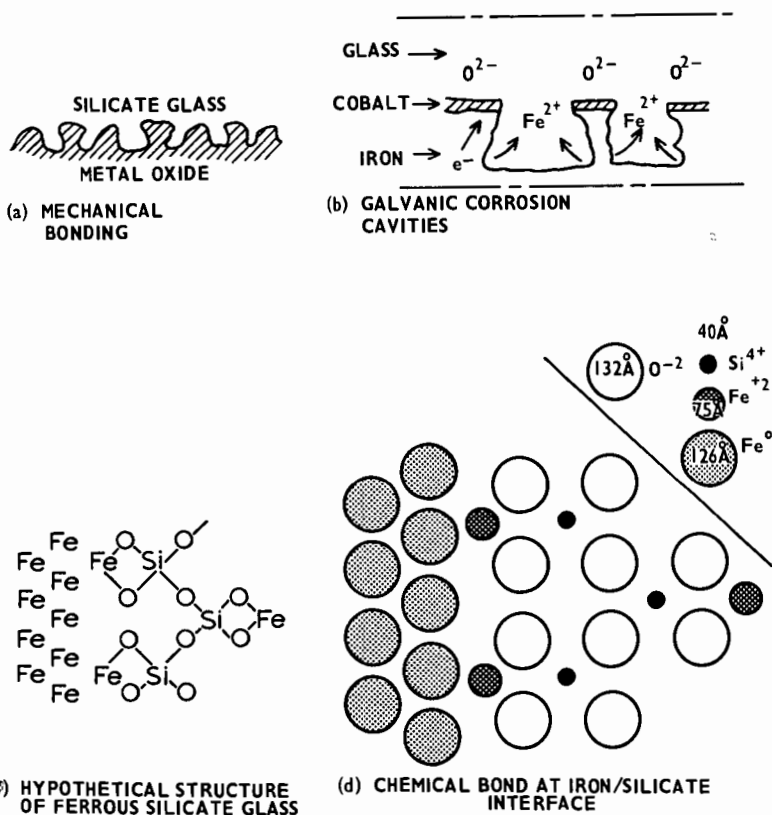


FIG. 6 SCHEMATIC REPRESENTATION OF MECHANICAL AND CHEMICAL BONDS AT
BOILER TUBE/ASH DEPOSIT INTERFACE

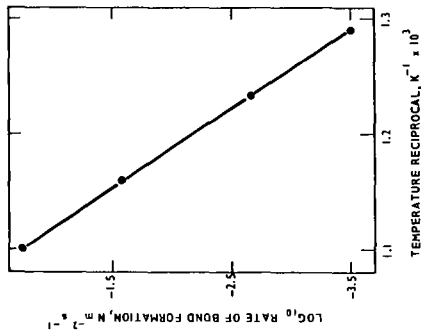


FIG. 7 THE EFFECT OF TEMPERATURE ON ASH DEPOSIT/FERRITIC STEEL BOND

BR/AWS(23.11.81)RL 4.3.3795

(R)

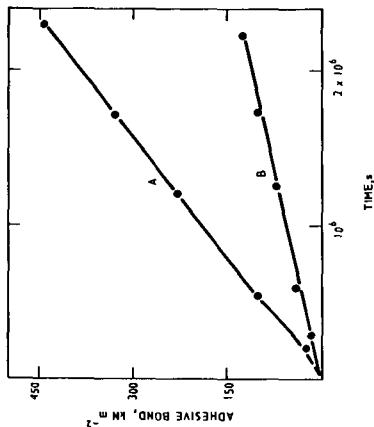


FIG. 8 BOND STRENGTH BETWEEN ASH DEPOSIT AND BOILER TUBE STEELS AT 900 K

A - FERRITIC STEEL B - AUSTENITIC STEELS

BR/AWS(23.11.81)RL 4.3.3794

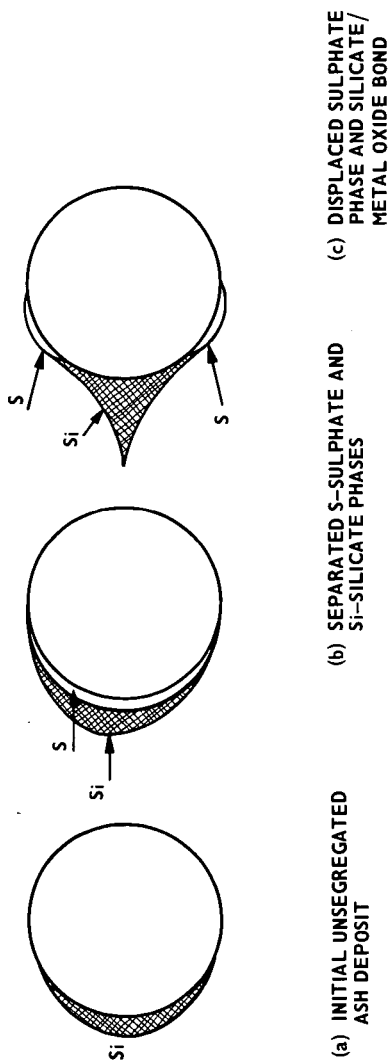


FIG. 9 SEQUENTIAL STAGES IN THE FORMATION OF LAYER-STRUCTURED AND FIRMLY
ADHERING SUPERHEATER DEPOSIT

USE OF GLASS FOR MODELING THE DEPOSITION OF
COAL ASH IN HOT CYCLONES

D. M. Mason and A. G. Rehmat

Institute of Gas Technology
IIT Center
3424 South State Street
Chicago, Illinois 60616

K. C. Tsao

University of Wisconsin — Milwaukee
P.O. Box 7841
Milwaukee, Wisconsin 53201

ABSTRACT

Tests have been conducted in a laboratory hot cyclone to obtain an estimate of the temperature below which spherical glass particles do not form a firmly attached deposit. A temperature of 800° to 850°C, corresponding to a viscosity between 6.3×10^5 and 2.9×10^6 poises, as calculated from the composition of the glass, was found. We take this viscosity to be approximately that of coal ash above which particles will not deposit in cyclones of fluidized-bed coal gasifiers.

INTRODUCTION

A cyclone operating at temperatures near those of the fluidized bed of the reactor has been used in the gasifier of the U-GAS® pilot plant to remove entrained char particles from the product gas and return them to the bed. Essentially pure coal ash has been found to deposit in this hot cyclone (1). The deposits have been analyzed chemically and examined by optical and scanning electron microscopy. Ferrous sulfide is responsible for deposition under adverse conditions, but deposition of iron-rich ferrous aluminosilicates is the more serious problem. In deposits from Western Kentucky coal, for example, the selective deposition of high-iron siliceous particles is indicated by an $\text{Fe}_2\text{O}_3/\text{Al}_2\text{O}_3$ ratio (calculated after excluding the iron contribution of iron sulfide) ranging from 2.2 to 4.6 in the ash of deposits, compared with a ratio of 1.2 in the ash of the coal. The effect of gas temperature (which equals particle temperature) and cyclone-wall temperature on the deposition of such particles was studied in a laboratory hot cyclone in the laboratories of the Mechanical Engineering Department of the University of Wisconsin at Milwaukee (1,2). The particles used in these tests were prepared from pilot plant deposits. The results indicated that the borderline temperature, below which the particles do not form a firm deposit, is about 900°C when gas and wall temperatures are equal.

We envision that the mechanism of deposition involves viscous or plastic flow following collision of particle and deposition surface to create a neck exerting enough surface tension to prevent rebound. We consider that the main cause of flow is impact. Flow driven by surface tension, as postulated by Raask (3) for deposition of coal ash on heat exchange surfaces of boilers, constitutes an additional mechanism leading to firm adhesion. Deposition at the inlet impingement area in the laboratory hot cyclone tests, massiveness of deposits at regions of high gas velocity and acceleration in or near the pilot plant cyclone, and virtual absence of deposits at low-gas-velocity regions of the gasification reactor all indicate that impact of deposition-prone particles plays an important role in the mechanism.

For both mechanisms, however, the effect of temperature on deposition can be attributed to change in viscosity, as surface tension does not vary much with temperature. Investigation of the effect of viscosity with ash particles is difficult, because little is known about the viscosities of iron aluminosilicates and ferrous sulfide at temperatures from 850° to 1050°C and, in any case, the ash particles vary in composition and presence of high melting phases. Therefore, we have chosen to use glass spheres as a homogeneous model material of known viscosity for the study of deposition. We report here a few results of a preliminary nature.

EXPERIMENTAL

The test apparatus consists of a natural gas burner to provide hot flue gas, a dust feeder, and a 9.68-cm ID cyclone (Figure 1). Calculations indicate that the residence time of particles in the hot flue gas is sufficient to heat the particles to the temperature of the flue gas at the cyclone entrance. The inlet section of the cyclone is jacketed to allow cooling of the wall; or alternatively, it can be heated to achieve substantially equal gas and wall temperatures. Temperature readings of the gas during a run are taken by a bare wire thermocouple projecting into the gas just upstream from the inlet section of the cyclone; it is calibrated before the run by an aspiration thermocouple in the inlet section. Temperature of the wall is measured by a thermocouple embedded in it at the spot where the entering gas impinges, where coherent deposits typically form (1,2). The surface of the inlet section is smoothed with No. 320-grit emery paper before each test.

The feed dust in these tests was supplied by the Cataphote Division of Ferro Corporation as Class IV-A uncoated Unispheres of soda-lime glass in a nominal 13-44 μm diameter. A Coulter counter size distribution analysis indicated that the size ranged only between 20 and 51 μm , with 14% greater than 40 μm and 3% smaller than 25 μm .

To determine the borderline of deposition we have made a total of nine runs with the glass spheres, of which seven were within about 50°C of a borderline region obtained by plotting wall temperature against gas temperature (Figure 2). The burner was operated to yield an oxidizing atmosphere at rates giving cyclone inlet velocities ranging from 30 to 50 f/s; these velocities are comparable to those of laboratory tests with particles of pilot plant deposits. Very light but firm deposits of the spheres were observed at the jet impingement area in three of these tests. The results indicate that the borderline for firm deposition with equal gas and wall temperatures is between 800° and 850°C. The slope of the borderline, which should depend mostly on the specific heat of the dust, is assumed to be parallel to the better-established borderline for the pilot plant deposits, which is also shown in Figure 2. In the future, we expect to make additional tests to establish the borderline more precisely and to determine the effect of variables such as velocity and size of particles.

We have chemically analyzed the glass spheres and from this estimated the viscosity at 800° and 850°C by means of the correlation equations of Lyon (4,5). The range of viscosity thus obtained over the above temperature range is 6.3×10^5 to 2.9×10^6 poises. This is near the geometric mean of the viscosities at the softening and working temperatures of glass (5).

DISCUSSION

According to Dietzel's correlation of the surface tension of glasses, glazes, and enamels with composition (6), the surface tension of the pilot plant deposits is up to about 25% higher than that of the glass used here. Neglecting this difference and the effect of particle shape, we may conclude that the effective viscosity of the pilot plant deposit for borderline deposition in the laboratory hot cyclone is in the range reported above for the glass spheres. In the pilot plant or in a commercial plant with much larger cyclones, considerable scale-up is required for application of our results, but we think it likely that they apply there also.

REFERENCES CITED

1. Mason, D. M.; Rehmat, A.; Tsao, K. C. "Chemistry of Ash Deposits in the U-GAS Process." In Fouling of Heat Exchange Surfaces, Bryers, R. W., Ed. Engineering Foundation: New York, 1983.
2. Tsao, K. C.; Tabrizi, H.; Rehmat, A.; Mason, D. M. "Coal-Ash Agglomeration in a High-Temperature Cyclone," Am. Soc. Mech. Eng. [Pap], ASME Annual Meeting, November 1982, ASME Preprint No. 82-WA/HT-29.
3. Raask, E. VGB Kraftwerkstechnik 1973, 53(4), 248.
4. Lyon, K. C. J. Res. Nat. Bur. Stand. Section A, 78A, 1974, 497.

5. Boyd, D. C.; Thompson, D. A. "Glass," in Encyclopedia of Chemical Technology, 11, 807-80. Wiley: New York, 1980.
6. Scholze, H. "Glas-Natur, Struktur and Eigenschaften," 213-21. Vieweg: Braunschweig, 1965.

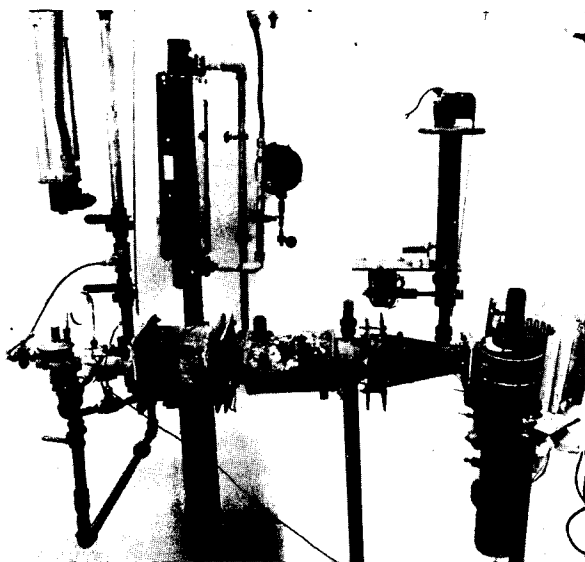


Figure 1. LABORATORY HOT CYCLONE APPARATUS

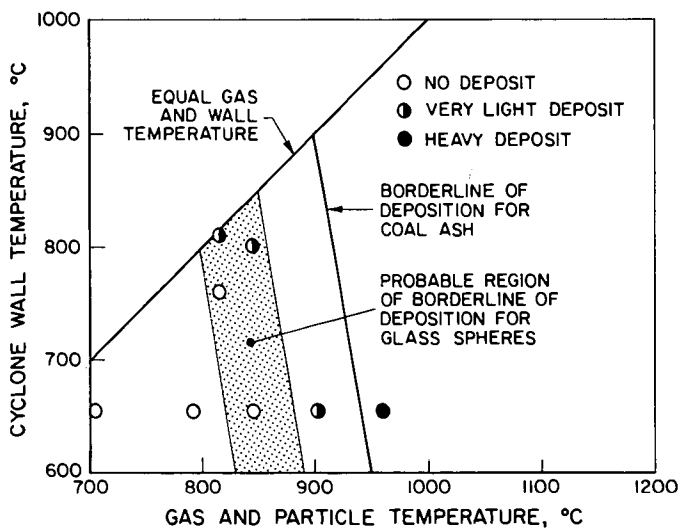


Figure 2. BORDERLINE OF DEPOSITION

A83111582

A STUDY OF SLAG DEPOSIT INITIATION IN A DROP-TUBE TYPE FURNACE

Murray F. Abbott* & Leonard G. Austin

Fuel Science Section and Department of Mineral Engineering
The Pennsylvania State University
University Park, PA 16802

ABSTRACT

A drop-tube furnace was designed and constructed for the purpose of simulating the time/temperature environment for p.c. combustion in a utility furnace. The ash produced was impacted on oxidized boiler steel coupons at gas and metal temperatures similar to upper furnace waterwall tubes. Both fly ash and deposits were similar to those of a pilot-scale (7-9 kg/hr) combustor. Iron-rich slag droplets produced from pyrite-rich p.c. particles bonded strongly with the oxidized steel surface. These particle types were found at the base of ash deposits after removal of sintered and loose ash for both eastern and western coals. Adhesion of iron-rich droplets was a function of both flame and metal surface temperatures. Also, volatile species, i.e., alkali and exchangeable cations influenced the "sticking" behavior of the iron-rich droplets. These trends are in qualitative agreement with previous sticking test results.

INTRODUCTION

All coals contain inorganic matter which is converted to ash when the coal is burned. The management of this ash constitutes one of the principal limiting design considerations for a p.c. steam generator. Operational problems occur if ash deposition and build-up on heat exchange surfaces becomes unmanageable. A single day's outage for an 800 MW unit for ash removal and repair can cost the utility as much as \$600,000 in lost electrical generation (1). Derating of the boiler system to manage ash deposition problems can cost millions of dollars annually. This investigation is part of an ongoing research program to gain a better fundamental understanding of the initiation of slag deposits on the upper walls of a boiler furnace enclosure. This paper reports on the development of a gas-fired vertical muffle tube (drop-tube) furnace as a new research tool.

A previous laboratory test, the sticking test (2-7) led to a number of conclusions concerning the mechanism and chemistry of molten slag drop adhesion to oxidized boiler steels. However, this test had several inherent disadvantages. It required the use of comparatively large molten ash drops (2 mm in diameter) and there was no proof that the conclusions applied equally well to the smaller size droplets (submicron to 250 μ m) produced in p.c.-fired furnaces. Also, the large drops formed from a coal ash contained all of the constituents of the ash (mean ash composition) which cannot accurately simulate the variety of mineral associations occurring on a particle-by-particle basis in a pulverized coal (8). Thus, the purpose of the drop-tube furnace was to produce coal fly ash particles under the same time/temperature environment experienced in full-scale boiler combustion followed by impaction on an oxidized boiler steel coupon simulating an upper furnace waterwall surface.

EXPERIMENTAL

Three Pennsylvania bituminous coals, designated Keystone, Montour and Tunnelton and a Decker, Montana subbituminous coal were studied in this investigation. All are current steam coals. Semi-quantitative mineralogical analysis of LTA and spectrochemical analysis of ASTM HTA are given in Table 1 for the three

*Current Address: Babcock & Wilcox R&D, 1562 Beeson Street, Alliance, OH 44601

Pennsylvania coals and raw (untreated) and acid washed Decker coal samples.

The drop-tube furnace system in which the test coals were burned is shown in Figure 1. It consisted of four major component parts: (i) a gas-fired hot zone, (ii) a fluid-bed feeding system, (iii) a preheat section and injector, and (iv) a water-cooled ash collector probe. The conditions inside the heated muffle tube simulated those of a utility furnace combustion zone: (i) maximum gas temperatures of 1500 to 1750°C, (ii) particle residence times between one and two seconds, and (iii) ash sampling temperatures ranging from 1000 to 1300°C. The fluid-bed feeder delivered between 0.2 and 0.3 grams of pulverized coal with slightly less than 1 liter of primary air per minute. In the preheat section the secondary air stream (roughly 2 liters/min) was heated to about 1000°C before a honeycomb flow straightener distributed it in streamlines across the muffle tube cross-section. The cold p.c./primary air mixture was carried by the injector to the hot combustion zone. A thin pencil-like p.c. stream was burned as it passed through the heated muffle tube. The fly ash produced was accelerated and impacted onto a water-cooled boiler steel coupon at surface temperatures of 300 to 450°C.

The ash deposits were characterized physically by observation under both a Zeiss optical and IDS-130 scanning electron microscope (SEM). Chemical characteristics were determined by energy dispersive x-ray fluorescence equipment associated with the SEM.

RESULTS AND DISCUSSION

Physical characteristics for all ash deposits were similar. Figure 2 shows a typical ash deposit structure on both a macro and microscale. The top photograph (A) shows an ash deposit collected from the raw Decker coal on a Croloy 1/2 steel coupon. The lower optical photomicrograph shows the strongly bonded material remaining on the surface after the comparatively loosely adhered ash had been brushed away. The opaque black droplets are rich in iron (85 to 100 wt. %) and the light colored transparent glassy spheres are predominantly aluminosilicates. The deposit build-up mechanism appeared to be similar for all coals. All originated with the relatively strong bonding of iron-rich slag drops to the oxidized steel surface. Aluminosilicates were only found in this layer for the raw Decker coal. In addition, there was always a layer of very fine particles (submicron) covering the entire coupon surface. It was not possible to brush or blow this layer from the surface. A region of loosely bonded ash particles often containing most all of the major constituents of the ash then built upon the more strongly adhered droplets. There was little if any interaction between the loose ash and adhesive particles. As the distance from the steel surface increased the ash particles began to sinter, eventually forming a fluid mass in some instances.

Preferential deposition of iron-rich species has been suggested by other investigators (9,10). It was also observed in a pilot-scale p.c. test combustor (11). The fine particle layer probably formed on the coupon surface due to convective diffusion to the relatively cold steel coupon (12). Presumably the scouring action of the ash laden gases in a utility furnace would prevent formation of the loose ash layer until the iron-rich layer is more extensively developed and interaction with successive layers can occur.

The iron-rich deposit base particles formed from the Keystone coal at flame temperatures of 1470 (A) and 1500°C (B) are shown in the SEM photomicrographs in Figure 3. The concentration of these particles increased with increasing flame temperature. Note that the particles flattened more on impact at the higher temperature, probably due to a decrease in particle viscosity. There appeared to be two different iron-rich particle types in each deposit: (i) a porous particle with a rougher surface texture, and (ii) a more glassy appearing particle with a very smooth surface texture. X-ray fluorescence spectrograms are also shown in Figure 3. The porous type particles were found to contain exclusively iron (see analysis of Point 1 in Figure 3B), whereas the more glassy particle types contained smaller amounts of silicon, aluminum and potassium (Point 2).

The two furnace operating parameters which most influenced ash deposition rates

were flame and coupon surface temperatures. Both of these trends are shown in Tables 2 and 3. Deposit build-up rates increased between two and six times with each increase in flame temperature and ten-fold for a 30 degree rise in coupon surface temperature. Removing exchangeable cations from the Decker coal caused a three-fold decrease in the ash deposition rate, see Table 4. The exchangeable cations appeared to play a significant role in both the initial iron-rich deposit and the sintering properties exhibited by the ash deposit. The sintered ash collected from the raw Decker coal was yellow-brown in color and comparatively difficult to break apart requiring a force of nearly 20 psi. The acid form sinter was coral colored and broke apart while removing the coupon from the collector probe.

CONCLUSIONS AND FUTURE WORK

The drop-tube furnace closely simulated the time/temperature history of a utility boiler furnace. One type of slag deposit initiating particle which strongly bonds to oxidized boiler steels is low melting iron-rich droplets produced from pyrite-rich p.c. particles. Flame and metal surface temperatures strongly influence ash deposit build-up rates. Sufficient evidence exists to suggest that alkalis and calcium enhance the "sticking" behavior of iron-rich and other fly ash droplets. This investigation revealed a qualitative relationship between results obtained from several different apparatus used to study slag initiation: (i) sticking apparatus, (ii) drop-tube furnace, and (iii) pilot-scale p.c. test combustor.

Future work in the drop-tube furnace will include: (i) developing a method for defining the relative adhesion properties of ash particle types, and (ii) more clearly defining the role of volatile species in deposit initiation and growth. This second goal can be accomplished by investigating controlled composition synthetic polymer/mineral combinations.

ACKNOWLEDGEMENTS

This study was funded by grants from the Department of Energy, Contract No. DE-FG22-80PC-30199 and Babcock and Wilcox.

REFERENCES

- 1) Williams, N., Sharbaugh, R., Van Tiggerler, D. and Kadlec, R., Electric Light and Power, 25 (1983).
- 2) Moza, A.K. and Austin L.G., Fuel, 60, 1057-64 (1981).
- 3) Abbott, M.F., Moza, A.K. and Austin, L.G., Fuel, 60, 1065-72 (1981).
- 4) Moza, A.K. and Austin, L.G., Fuel, 61, 161-5 (1982).
- 5) Abbott, M.F. and Austin, L.G., Fuel, 61, 765-70 (1982).
- 6) Abbott, M.F., Conn, R.E. and Austin, L.G., "Studies on slag deposit formation in pulverized coal combustors. 5. The effect of flame temperature, thermal cycling of the steel substrate, and time on the adhesion of slag drops to boiler steels", in preparation.
- 7) Abbott, M.F. and Austin, L.G., "Studies on slag deposit formation in pulverized coal combustors. 6. The sticking behavior of slag from three Pennsylvania steam coals", in preparation.
- 8) Moza, A.K., Austin, L.G. and Johnson, G.G., Jr., SEM/1979/1, p. 473, SEM Inc, AMF O'Hare, IL, 1979.
- 9) Borio, R.W. and Narcisco, R.R., Journal of Engineering for Power, 101, 500 (1979).
- 10) Bryers, R.W., Journal of Engineering for Power, 101, 517 (1979).
- 11) Austin, L.G., Abbott, M.F. and Kinneman, W.P., Jr., ASME 83-JPGC-Pwr-42.
- 12) Rosner, D.E., Chen, B.K., Fryburg, G.C. and Kohl, F.J., Combustion Science and Technology, 20, 87-106 (1979).

TABLE 1. MINERALOGICAL AND ELEMENTAL ASH COMPOSITION FOR TEST COALS

<u>Procedure/Coals</u>	<u>Montour</u>	<u>Keystone</u>	<u>Tunnelton</u>	<u>Raw Decker</u>	<u>Acid-Washed Decker</u>
Mineralogical (wt. % LTA)					
Quartz	25	25	22	20	30
Pyrite	15	10	15	5	10
Calcite	5	--	5	5	--
Gypsum	--	5	--	30	--
Kaolinite	17	30	18	11	16
Illite	30	20	30-40	--	--
Feldspar	--	--	5-10	--	--
LTA (wt. % as received coal)	18.0	21.6	22.9	6.3	3.3
HTA (wt. % as received coal)	15.8	18.0	20.1	4.0	2.2
Spectrochemical (wt. % HTA)					
SiO ₂	51.7	54.1	50.3	26.5	53.0
Al ₂ O ₃	25.6	25.9	26.8	15.5	28.5
TiO ₂	1.3	1.3	1.3	0.9	2.7
Fe ₂ O ₃	14.1	9.7	11.0	5.3	9.2
CaO	2.4	1.8	2.5	14.3	4.1
MgO	0.9	1.0	1.0	2.5	0.7
Na ₂ O	0.2	0.3	0.4	0.03	0.01
K ₂ O	2.4	2.9	2.9	5.0	0.4
SO ₃	1.5	1.1	2.3	0.97	0.6
P ₂ O ₅	0.4	0.4	0.4	21.6	--

TABLE 2. DEPOSIT BUILD-UP RATES FOR THE THREE PENNSYLVANIA STEAM COALS AT THREE FLAME TEMPERATURES

Coal	Flame Temperature °C	Deposit Mass mg	Relative Build-up Rates		Percent of Total Ash (Based on HTA)
			mg/min	mg/gr Coal	
Montour	1465	26.5	2.2	11.0	6.9
	1518	64.5	5.4	22.5	14.2
	1561	133.0	11.1	46.3	29.2
Keystone	1470	24.0	2.0	7.1	3.9
	1500	117.7	9.8	40.8	22.7
	1560	286.1	23.8	99.2	47.3
Tunnelton	1467	39.7	3.3	11.8	3.1
	1510	252.6	21.1	75.4	19.7
	1518	297.1	24.8	103.3	51.3

TABLE 3. DEPOSIT BUILD-UP RATES FOR THE KEYSTONE COAL AT A FLAME TEMPERATURE OF 1500°C AND TWO DIFFERENT COUPON SURFACE TEMPERATURES

Coupon Surface Temperature °C	Deposit Mass mg	Relative Build-up Rates		Percent of Total Ash (Based on HTA)
		mg/min	mg/gr Coal	
310-318	11.7	6.98	29.1	2.3
340-345	117.7	9.8	40.8	18.0

TABLE 4. DEPOSIT BUILD-UP RATES FOR RAW AND ACID WASHED DECKER COAL SAMPLES AT A FLAME TEMPERATURE OF 1500°C

Coal Sample	Deposit Mass mg	Relative Build-up Rates		Percent of Total Ash (Based on HTA)
		mg/min	mg/gr Coal	
Raw Decker	82	4.1	14.6	36.6
Acid Washed Decker	25	1.3	5.4	23.7

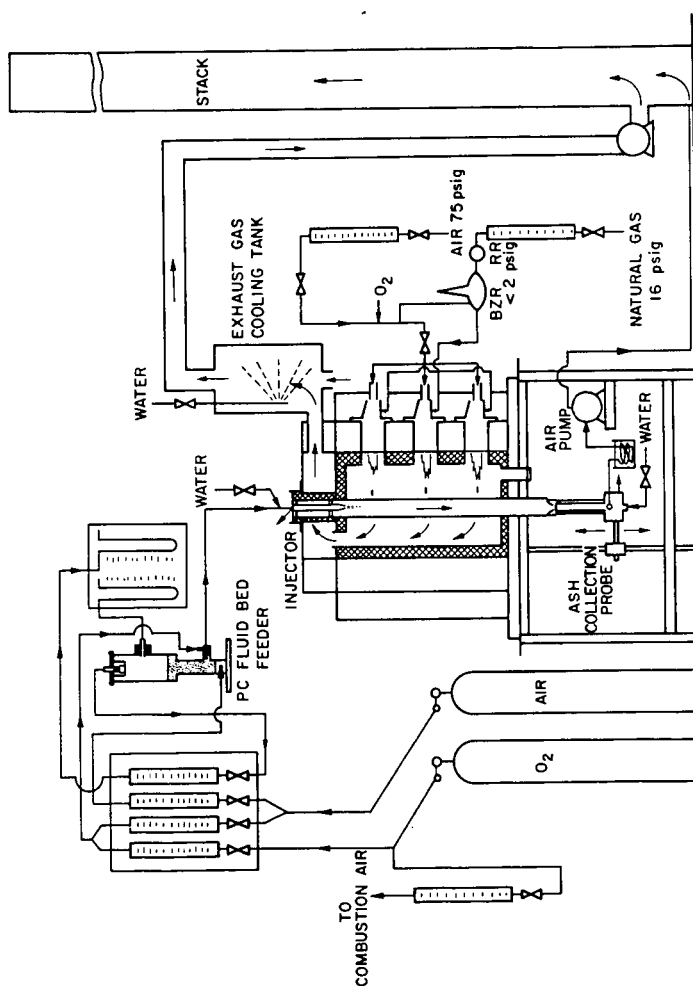


FIGURE 1 DROP-TUBE FURNACE SYSTEM

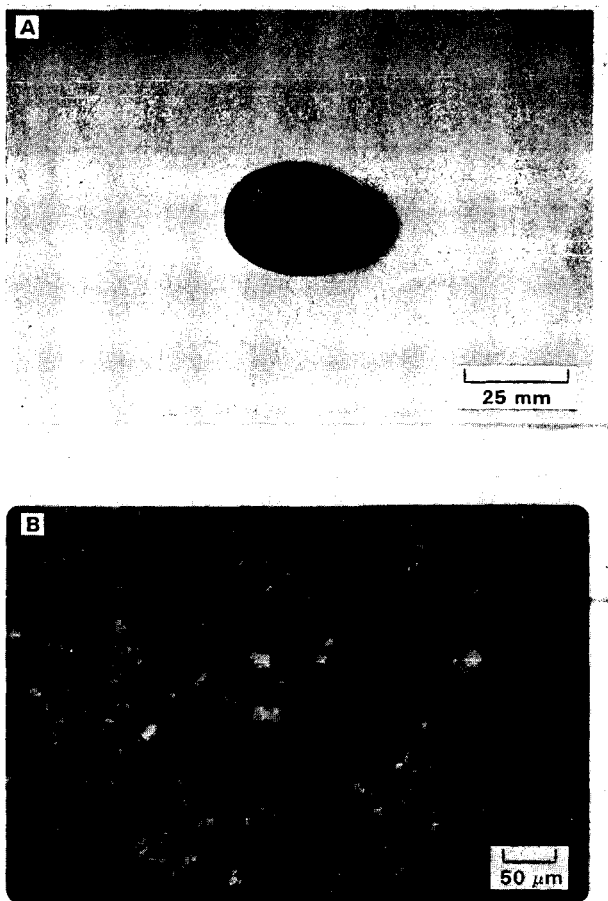


FIGURE 2 RAW DECKER COAL ASH DEPOSIT:
A) TOTAL DEPOSIT AFTER TWENTY MINUTES,
B) OPTICAL PHOTOMICROGRAPH OF BONDED
ASH PARTICLES

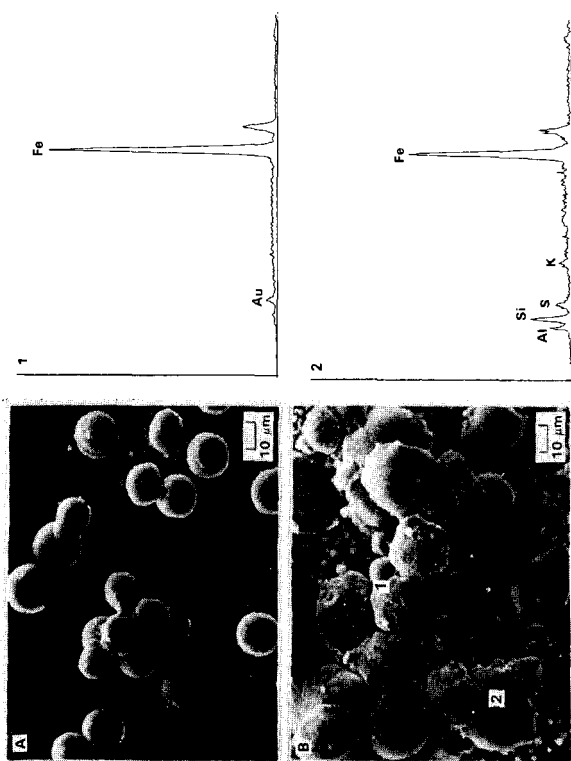


FIGURE 3 KEYSTONE COAL ASH DEPOSITS: A&B) SEM PHOTOMICROGRAPHS SHOWING IRON-RICH SLAG DROPLETS COLLECTED FROM FLAME TEMPERATURES OF 1470°C (A) AND 1550°C (B). X-RAY FLUORESCENCE SPECTROGRAMS CORRESPONDING TO POINTS 1 AND 2 IN PHOTO B.

INFLUENCE OF SEGREGATED MINERAL MATTER IN COAL ON SLAGGING

R. W. Bryers

Foster Wheeler Development Corporation
12 Peach Tree Hill Road
Livingston, New Jersey 07039

INTRODUCTION

The mineral content of any given rank of coal is a key factor in sizing and designing a steam generator or reactor. The mineral content becomes even more important as the premium solid fuels are consumed, leaving reserves with continual increasing mineral concentrations and lower quality ash. The problem of dealing with lower quality ash in coal is compounded by the increase in size of steam generators and refinements imposed by economic constraints. Empirical indices, based on coal ash chemistry and ASTM ash fusion temperatures or viscosity, are presently used to rank coals according to the fireside behavior of the mineral matter. Unfortunately, the indices are only marginally satisfactory, as they do not relate to operating or design parameters and frequently are based on a coal ash chemistry quite different from that deposited on the furnace wall. Frequently, different coals with identical ash chemistry produce decidedly different slagging conditions in steam generators of identical design operated in the same mode. Variations in composition of the slag, when compared with the coal ash, suggest specific minerals are being selectively deposited on furnace walls depending upon their specific gravity, size, composition, and physicochemical properties. It is quite apparent there is a need for a better understanding of the impact of mineral composition, its size, and its association with other minerals and carbonaceous matter on fireside deposits.

MINERAL MATTER IN COAL

Minerals occurring in coal may be classified into five main groups. These include shale, clay, sulfur, and carbonates. The fifth group includes accessory minerals such as quartz and minor constituents like the feldspars (1).

Shale, usually the result of the consolidation of mud, silt, and clay, consists of many minerals including illite and muscovite--these are forms of mica. Kaolinite is the most common clay material (1).

The sulfur minerals include pyrites with some marcasite. Marcasite has the same chemical composition as pyrites but a different mineralogical structure. Sulfur is also present as organic matter and occasionally as sulfate. The latter usually occurs in weathered coal such as in outcrops. The amount of sulfate sulfur in coal is generally less than 0.01 percent.

Generally, 60 percent of the sulfur in coal is pyritic, particularly when the sulfur concentration is low. At higher concentrations it may run as high as 70 to 90 percent. Pyrite occurs in coal in discrete particles in a wide variety of shapes and sizes. The principal forms are (1-6):

- Rounded masses called sulfur balls or nodules an inch or more in size.
- Lens-shaped masses which are thought to be flattened sulfur balls.
- Vertical, inclined veins or fissures filled with pyrite ranging in

thickness from thin flakes up to several inches thick.

- Small, discontinuous veinlets of pyrite, a number of which sometimes radiate from a common center.
- Small particles, <72 μ , or veinlets disseminated in the coal. Microscopic pyrite occurs in five basic morphology types: (a) framboids, (b) isolated euhedral crystals, (c) nonspherical aggregates of euhedral crystals, (d) irregular shapes, and (e) fractured fillings (7).

All coals contain some of the third and fifth forms of pyrite, and some coals contain all five of the principal forms (6,8,9).

The carbonates are mainly calcite, dolomite, or siderite. The occurrence of calcite is frequently bimodal. Some calcite occurs as inherent ash, while other calcite appears as thin layers in cleats and fissures. Iron can be present in small quantities as hematite, ankrite, and in some of the clay minerals such as illite. In addition to the more common minerals, silica is present sometimes as sand particles or quartz. The alkalis are sometimes found as chlorides or as sulfates but probably most often as feldspars, typically orthoclase and albite. In the case of lignites, unlike bituminous and subbituminous, sodium is not present as a mineral but is probably distributed throughout the lignite as the sodium salt of a hydroxyl group or a carboxylic acid group in humic acid. Calcium, like sodium, is bound organically to humic acid. Therefore, it too is uniformly distributed in the sample.

The term, "mineral matter," usually applies to all inorganic, noncarbonaceous material in the coal and includes those inorganic elements which may occur in organic combination. Physically, the inorganic matter can be divided into two groups--inherent mineral matter and extraneous mineral matter. Inherent mineral matter originates as part of the growing plant life from which coal was formed. Under the circumstances, it has a uniform distribution within the coal. Inherent mineral matter seldom exceeds 2 - 3 percent of the coal (10).

Extraneous mineral matter generally consists of large bits and pieces of inorganic material typical of the surrounding geology. In some cases the extraneous matter is so finely divided and uniformly dispersed within the coal it behaves as inherent mineral matter. Coal preparation can separate some of the extraneous ash from the coal substance, but it seldom removes any of the inherent mineral matter.

The physical differences between inherent and extraneous ash are important not only to those interested in cleaning coal but also to those concerned with the fire-side behavior of coal ash. Inherent material is so intimately mixed with coal that its thermal history is linked to the combustion of the coal particle in which it is contained. Therefore, it will most likely reach a temperature in excess of the gas in the immediate surroundings. The close proximity of each species with every other species permits chemical reaction and physical changes to occur so rapidly that the subsequent ash particles formed will behave as a single material whose composition is defined by the mixture of minerals contained within the coal particle. The atmosphere under which the individual transformations take place will, no doubt, approach a reducing environment. Figure 1 illustrates a model of the coal and mineral matter as fed to the combustor and the fate of the minerals after combustion (11).

Extraneous materials can behave as discrete mineral particles comprised of a single species or a multiplicity of species. As already indicated, a portion of this material may be so finely divided it can behave as inherent mineral matter.

During combustion the larger particles respond individually to the rising temperature of the environment. In the absence of carbon or other exothermic reactants, the particle should always be somewhat less than the local gas temperature. However, the particles may be subjected to either reducing or oxidizing conditions. As each particle rises in temperature, it loses water of hydration, evolves gas, becomes oxidized or reduced, and eventually sinters or melts, depending on its particular composition or temperature level.

It is evident, then, that there can be a great difference in the final state of each particle, depending upon its composition and whether it is inherent or extraneous ash. Figure 2 summarizes the phase transformations which pure mineral matter commonly found in coal undergoes during heating (12,13,14). Since this data was developed primarily by mineralogists performing differential thermal analysis under air at slow heating rates, it must be used only as a guideline for predicting the thermal behavior of minerals in coal. Thermal shocking these minerals in the presence of carbon and other mineral forms at very high temperatures, no doubt, will alter some of these transformations and may defer others until postcombustion deposition on heat transfer surfaces.

Clays and Shale

The melting temperatures of most pure minerals are in the vicinity of or greatly exceed the maximum flame temperature encountered during combustion. Therefore, the fused spheroidal fly ash, generated from the mineral matter in coal, primarily forms as the result of the fluxing action between pure minerals contained within each particle. Illite and biotite appear to be an exception. Both minerals contain small concentrations of iron and potassium and form a glassy phase at 950°C and 1100°C, respectively. Depending upon its fluidity, this glassy phase could be responsible for surface deformation at a relatively low temperature and provide the necessary sticking potential to prevent reentrainment upon contacting heat transfer surfaces. Low temperature ash of a gravity fraction containing illite was heated in a thermal analyzer under air to 600 and 1000°C, respectively, and compared to the low temperature ash of a gravity fraction void of illite. The scanning electron photomicrographs, appearing in Figure 3, indicate the minerals containing illite did, indeed, show signs of the formation of a melt.

Quartz

The inherent silica retained in the char as quartz or silica released from kaolinite and illite at low temperatures (i.e., 950°C) is partially reduced to silica monoxide. Unlike silica which boils at 2230°C, silica monoxide melts at 1420°C and boils at 2600°C (15). The vapor pressure of silicon is low--in the range of temperatures experienced during combustion. Honig reports values ranging from 0.01m Hg at 1157°C to 1m Hg pressure at 1852°C (15,16). The presence of other mineral matter and carbonaceous material appears to alter vapor pressure substantially. When a mixture of alumina silicate and graphite was heated, the volatilization of silicon monoxide began at about 1150°C and reached a maximum at 1400°C. Mackowsky reports that volatilization of silicon monoxide starts at about 1649°C in the presence of carbonates and clays and reaches a maximum at 1704°C (17). In the presence of pyrite or metallic iron, volatilization begins at about 1560°C and continues at a rapid rate as the temperature rises until practically all the silica in the mineral is volatilized. Sarofin has shown that about 1.5 to 2.0 percent of the ASTM ash in bituminous coals volatilize (18). Approximately 35 - 40 percent of the volatilized material was silica. The next largest component was iron. Extraneous quartz appears to be relatively innocuous unless contaminated by Fe_2O_3 , CaO , or K_2O .

Pyrites

The decomposition of pyrite has been examined by numerous investigators under oxidizing, neutral, and reducing environments. TGA, rather than DTA, has been used by most investigators. Acquisition of representative data is difficult, as the decomposition process is complex and sensitive to many variables including the chemical composition of pyrites, its grain size, its origin, the presence of adventitious impurities, the composition of the local environment, and diffusion rates through sulfated layers. Under oxidizing conditions it is believed that pyrites decompose directly to an iron oxide and SO_2 or SO_3 or iron sulfate and SO_2 , depending upon the final temperature level. Under reducing conditions pyrrhotite and either carbon or hydrogen sulfide form. Complete reduction results in elemental iron and carbon disulfide. There is also a possibility that pyrrhotite may form under oxidizing conditions as an intermediate step in the presence of sufficient adventitious carbon. Pure pyrites ignite at about 500°C in the thermal analyzer at $20^\circ\text{C}/\text{min}$ and burn out by 550°C in a single-step process, as shown in Figure 5. Pure pyrites do ignite as readily as bituminous coal; however, the burnout time is comparable. Although pyrrhotite ignites readily, it requires as much time as anthracite to complete combustion. Pyrites containing small quantities of adventitious carbon, as might be found in the -1.80 $+2.85$ gravity fraction, appear to form pyrrhotite, deferring burnout until 800°F . Within the combustor the problem is compounded by the fact that pyrite particles do not shrink during the combustion process as do coal particles, and hence, their burnout time is extended. The burnout time of particles in excess of 40μ appears to exceed the residence time available in most combustors.

TGA reveals decomposition rates but tells little about the physical state during the combustion process. Phase diagrams for the Fe-S-O and FeS-FeO system, representing transitory states at the particle surface, imply the formation of a temporary melt at low temperatures. SEM photomicrographs, appearing in Figure 5, of pure pyrites heated to 600°C , 800°C , and 1000°C under reducing conditions clearly reveal the formation of a melt at temperatures as low as 600°C . Large particles of partially-spent pyrites, which may be molten on contact with the heat transfer surface, complete the oxidation process in situ, forming a solid fused deposit with a very high melting temperature.

An examination of the thermal behavior of the mineral matter in coal indicates the mineral origin of the elements found in coal ash and their juxtaposition with regard to each other, as well as other mineral forms, and determines their physical fate during combustion. As indicated in Figure 1, the physical state (i.e., vapor or solid) and the size of solidified ash will determine the mode and rates of migration to the heat transfer surface. The physical state at the tube surface will depend upon the local surface temperature and the composition of the particulate depositing. In the case of pyrites residence time and environment conditions may also play a significant role.

CHARACTERIZATION OF MINERALS IN COAL

The fireside behavior of mineral matter in coal has been investigated by characterizing the mineral content of several bituminous coals, using size and gravity fractionation analysis of pulverized coal and then firing the coal in a vertically fired combustor. High sulfur coals containing pyrites of varying size and varying association with carbonaceous and other mineral forms were selected for examination. A comparison was also made with western subbituminous coals to assess the impact of potassium in the mineral illite on furnace slagging.

Each coal was analyzed for proximate, ultimate, ash chemistry, and ash fusion temperatures to permit evaluation using conventional data. The pulverized coal samples were then divided into four sizes representing equal weights (i.e., +105 μ , -105 μ +74 μ , -74 μ +44 μ , and -44 μ). Each size fraction was separated into four weight classes, thereby, partitioning the coal into groups dominated by coal, non-pyritic mineral matter, and pyrites. The partitioned coal was analyzed for ash chemistry, ash fusion temperature, combustion profile, and mineral content.

The analytical data is summarized in Figure 6. The enclosed data points represent the composite analysis. The open data points represent the fractionated species. Ash softening temperatures and percent basic constituents were selected as the variables to characterize the coal, as they appear most frequently in the indices used to express the slagging or fouling potential of the fuel. It is quite evident the combustor is exposed to ash with a wide range of chemical compositions and melting temperatures not adequately identified by a composite coal analysis. The data indicates slagging was most severe with coals having the highest melting temperature and demonstrating the greatest degree of separation of ash from coal and pyrites from other mineral matter. The two coals with the lowest composite ash softening, having the highest slagging index by conventional evaluation, caused the least slagging. Liberation of mineral matter from these two coals was also the lowest.

The data was replotted on fusibility diagrams, appearing in Figure 7, typifying the coal with the greatest partitioning of mineral matter and highest degree of slagging and the coal with the least liberation of mineral matter and degree of slagging. The fusibility diagram illustrates the size and weighted contribution of each ash specie. It also shows the degree of liberation of nonpyritic and pyritic mineral matter. By washing the worst coal at 1.80 sp. gr. and 14M x 0, thereby minimizing extraneous ash as well as total sulfur, the degree of slagging of the Upper Freeport coal was greatly reduced.

COMBUSTION TESTING

Deposits were removed from various locations in the combustor after firing each coal for \pm 14 - 16 hours. Samples were removed from slagging probes at 398 - 510°C, fouling probes at 510 - 537°C, and refractory surfaces at 537 - 1204°C and examined using the scanning electron microscope and energy dispersive x-ray. Fly ash samples were also examined for carbon loss, surface morphology, and chemical composition.

The deposits forming on the slagging probes were initiated by a thin layer of powdery fly ash, <8 μ in size, enriched with small quantities of potassium. Beads of slag formed on top of this thin layer when the surface temperature approached the initial deformation temperature of the deposit. Growth progressed with the formation of rivulets from which a continuous phase of molten slag formed. Deposits forming on the refractory surface represent an advanced stage of slag due to the higher surface temperatures which could only be achieved on the cooler probes after the initial dust layer formed. The composite ash chemistry and ash fusion temperatures of the slag resemble that of the heaviest gravity fraction (i.e., >1.80 sp. gr.) in most cases. Macrophotographs of the deposit formation on the furnace probes subjected to axial symmetric flow at low gas velocities (5 - 6 ft/s), illustrated in Figure 8, show that the initial layer of dust, upon which further slagging depends, formed only when firing coals whose ash contained more than 1 percent potassium. Continued deposit growth resulting in serious slagging is dependent upon the total pyrites liberated from the coal.

SEM microphotographs and EDAX scans of the cross section and outer surface of the slag deposit, illustrated in Figure 9, indicate the chemistry of the deposit is not uniform. The bulk of the fused material is rich in silica, low in iron, and virtually depleted of potassium. The outermost layers, no more than 2 to 3 μ thick, are very rich in iron and frequently also rich in calcium. On occasions, the outer surface is covered with small particulate several microns in diameter or undissolved cubic or octahedral crystals whose origin is pyrites. Similar formations have been observed in full-scale operation. The evidence indicates deposits form under axial symmetric flow conditions in the furnace by the fluxing action at the heat transfer surface of small particles, <8 μ in diameter, of decidedly different chemical composition and mineral source. Migration of the fly ash to the surface is by means of eddy diffusion, thermophoresis, or Brownian motion.

Sintered deposits form at the furnace exit at lower gas temperatures and in zones subject to rapid changes in direction. The deposit is composed of spheroidal particles <40 μ bound together by a molten substance. In those cases where substantial quantities of coarse pyrites are liberated from the pulverized coal, the spheroids are nearly pure Fe_2O_3 , as shown in Figure 10. The matrix contained silica, alumina, iron, and potassium and has an initial deformation temperature of 1000°C, as determined by differential thermal analysis. The heavier pure iron spheroids deposit as a result of inertial impact. The mineral source of the molten phase is most likely illite.

Deposits also form on the leading edge of the first row of tubes in the convection pass when firing coals which liberate pure, coarse pyrites. These tubes are subjected to high gas velocities and have moderate to high collection efficiencies for particles between 40 and 100 μ . The deposits are nearly pure Fe_2O_3 . They are hard and fused despite being at gas temperatures below their initial deformation temperature. No doubt, the final stages of decomposition of the pyrites takes place at the tube surface.

CONCLUSIONS

The formation of fireside deposits in furnaces depends on the composition, size, and association of mineral matter liberated from the coal. Selective deposition of specific mineral species depends on their size, thermal behavior, the local gas temperatures, and their mode of transport to the surface. Consequently, the composition of the sintered deposit or molten slag may vary with time at a given location and will most probably vary throughout the combustor, depending on local temperatures and fluidynamics. The composition of the slag may be substantially different from the composite coal ash, depending upon its heterogeneity. Illite is a likely candidate as the mineral most responsible for initiating deposits. The molten phases are frequently part of the FeO-SiO_2 or FeO-CaO-SiO_2 system and depend on the interaction of quartz, calcite, or pyrites at the heat transfer surface. Liberated pyrite crystals and small particles are primary candidates for slag formation subjected to parallel flow regimes at low velocities. Coarse pyrites can be selectively deposited and solely responsible for deposit formation on surfaces subjected to flue gas impingement at high velocities.

ACKNOWLEDGMENTS

Substantial portions of this study were sponsored by the U. S. Department of Energy, Pittsburgh Energy Technology Center, Contract DE-AC22-81PC40268, under the direction of Mr. J. Hickerson, Mr. H. Ritz, and Dr. R. Walker. I am grateful to Mr. O. R. Walchuk for supervising the combustion program; Mr. G. Lantos, who

directed laboratory analyses; Messrs. G. Stanko and I. Dojcsanszky for SEM and EDAX analyses; and Mrs. J. Betyeman for preparing the manuscript.

REFERENCES

1. R. W. Bryers, "The Physical and Chemical Characteristics of Pyrites and Their Influence on Fireside Problems in Steam Generators," Trans. of the ASME, Journal of Engineering for Power, October 1976.
2. F. E. Walker and E. F. Hartner, "Forms of Sulfur in U.S. Coals," IC830, Bu. Mines, U.S. Dept. of the Interior, 1966.
3. H. J. Gluskoter and J. A. Simon, "Sulfur in Illinois Coals," Circular 432, Illinois State Geological Survey, Urbana, Illinois, 1968.
4. P. Nicholls and W. A. Selvig, "Clinker Formation as Related to the Fusibility of Coal Ash," U.S. Bureau of Mines Bulletin 364, 1932.
5. J. F. Barkley, "The Sulfur Problem in Burning Coal," Technical Paper 436, Bu. of Mines, U.S. Dept. of the Interior, 1928.
6. "Sulfur Codes Pose Dilemma for Coal," Environmental Science and Technology, Vol. 11, No. 12, December 1970.
7. Hobart M. King and John J. Renton, "The Mode of Occurrence and Distribution of Sulfur in West Virginia Coals," Carboniferous Coal Guide Book, A. Donaldson, M. W. Presley, and J. J. Renton, Editors, West Virginia Geological and Economic Survey Bulletin B-37-1, 1929.
8. M. Deul, "Preliminary Observation of the Mode of Occurrence of Pyrite in Coal," Second Conference, Eastern American Anthraologist, University Park, Pennsylvania, May 26, 1958, p. 27.
9. Hobart M. King, "Sulfide Minerals in West Virginia Coals," Mountain State Geology, West Virginia Geological and Economic Survey, December 1980.
10. R. W. Bryers, "Influence of the Distribution of Mineral Matter in Coal on Fireside Ash Deposition," Trans. of the ASME, Journal of Engineering for Power, October 1979.
11. R. C. Flagan and A. F. Sarofim, "Transformation of Mineral Matter in Coal," Progress in Energy and Combustion, to be published.
12. H. R. Hoy, A. G. Roberts, and D. M. Wilkins, "Behavior of Mineral Matter in Slagging Gasification Processes," I.G.E. Journal, June 1965.
13. P. Jackson, "From Mineral Matter to Deposits in PF-Fired Boilers, Part I: The Behavior of Mineral Matter in the Flame," Pulverized Coal Firing - The Effects of Mineral Matter, T. Wall, ed., University of Newcastle, August 1979.
14. J. D. Watt, "The Physical and Chemical Behavior of the Mineral Matter in Coal Under the Conditions Met in Combustion Plants: A Literature Survey--Part I: The Occurrence, Origin, Identity, Distribution, and Estimation of the Mineral Species in British Coals," BCURA Industrial Laboratories, Leatherhead, Surrey, England, August 1979.

15. N. W. Nelson, et al., "A Review of Available Information on Corrosion and Deposits in Coal- and Oil-Fired Boilers and Gas Turbines," ASME, 1954.
16. R. E. Honig, "Sublimation Studies of Silicon in the Mass Spectrometer," Journal of Chemistry and Physics, Vol. 77, 1954, pp. 1610-1611.
17. M. Th. Mackowsky, "The Behavior of Coal Minerals at High-Combustion Temperatures with Consideration of Slow and Rapid Heating," Paper Given at The Annual Meeting of the Association of Large Boiler Owners, Nürnberg, Germany, July 1955.
18. R. J. Quann and A. F. Sarofim, "Vaporization of Refractory Oxides During Pulverized Coal Combustion," Nineteenth Symposium International on Combustion, The Combustion Institute, 1982.

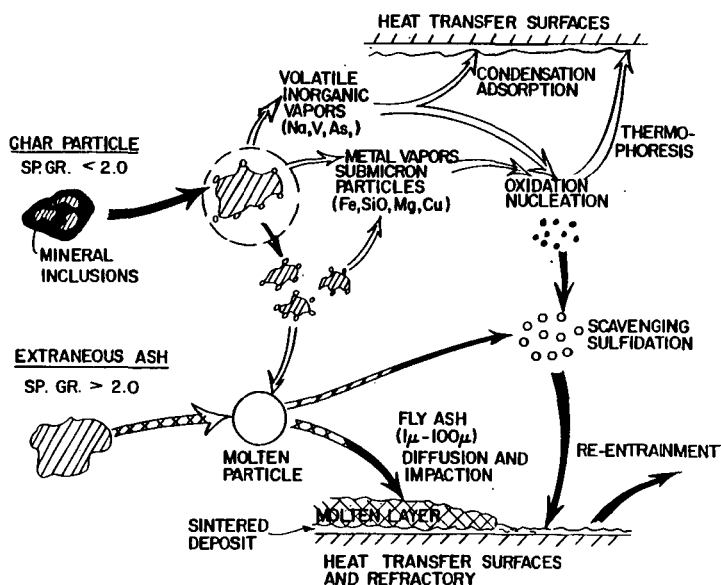


Figure 1 Fate of Mineral Matter in Coal During Combustion, as Proposed by Dr. Sarofim

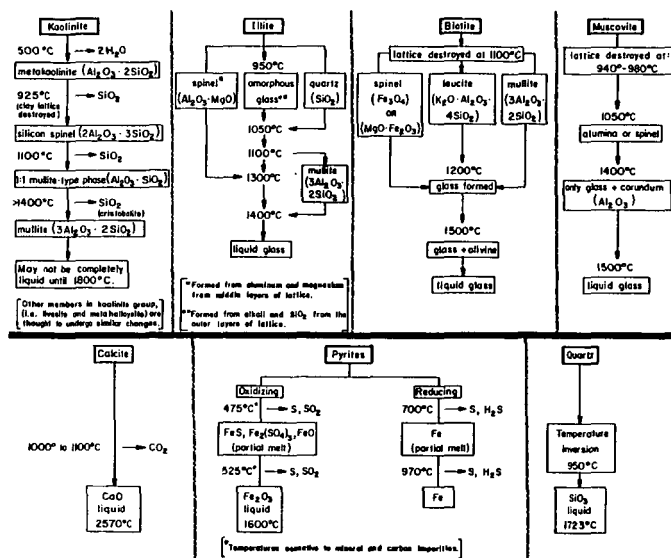


Figure 2 Phase Transformation of Some Mineral Matter Commonly Found in Coal

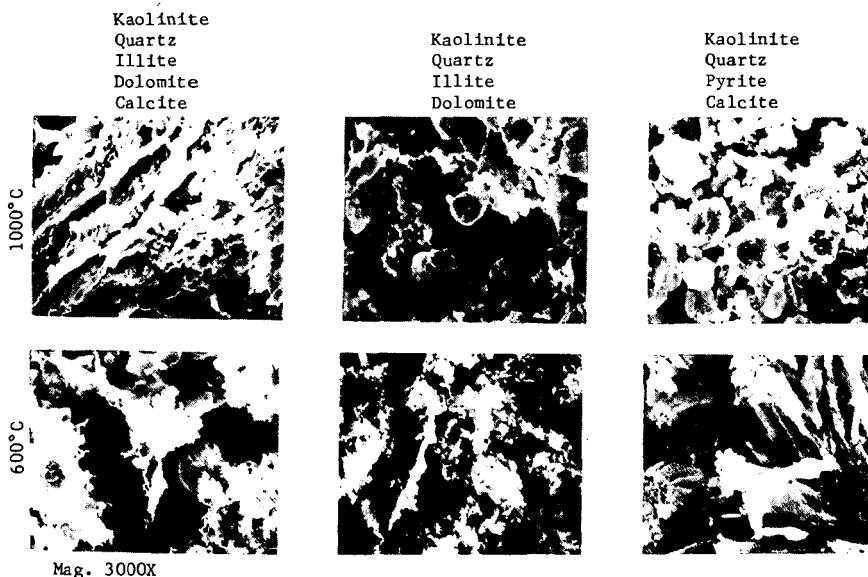


Figure 3 SEM Photomicrographs Showing the Impact of Illite on the Thermal Behavior of Low Temperature Ash

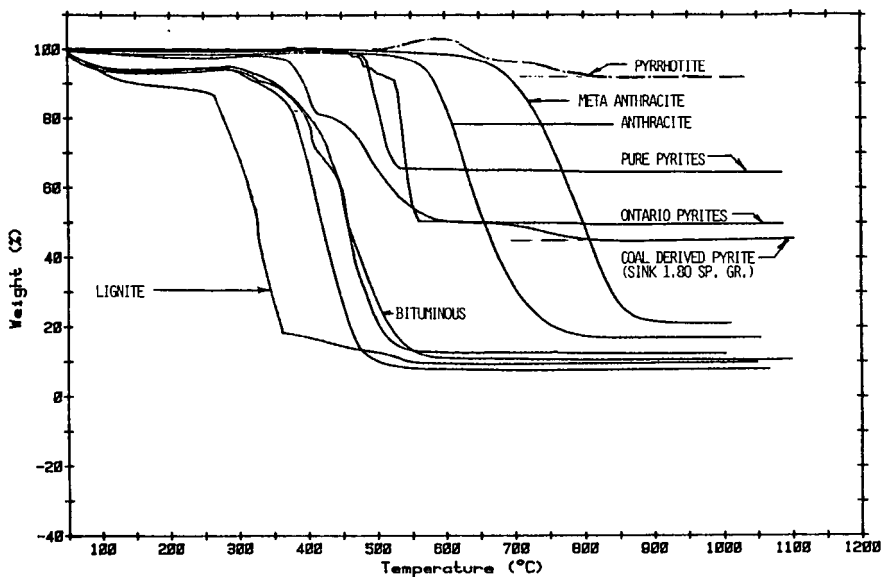


Figure 4 TGA Thermograms Comparing the Decomposition of Various Grades of Pyrites with Various Ranks of Coal

Mag. 3000X

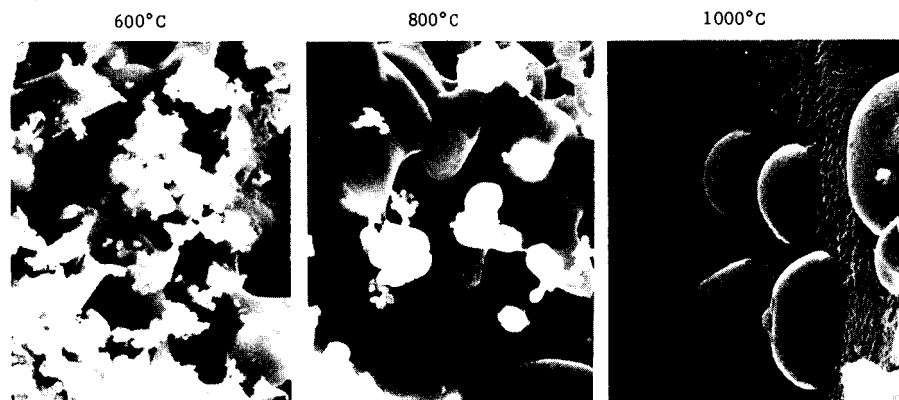


Figure 5 Pure Pyrites Heated Under Reducing Conditions to 600, 800, and 1000°C





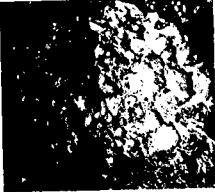
Ash Soften. (Red) and % Ash	% Liberated Fe_2O_3 in Coal			% Kin Ash	Ash Soften. Temp. (Red) and % Ash
2130°F 14.9	Kentucky No. 11 0.225			Western Fuel 1 0.2	2165°F 6.7
2080°F 9.4	Illinois No. 6 0.159			Western Fuel 2 1.0	2252°F 16.67
2443°F 16.4	Lower Freeport 1.56			Western Fuel 3 1.2	2232°F 25.73
2245°F 23.5	Upper Freeport 1.67			Lower Freeport 2.5	2443°F 16.4

Figure 8 Slagging on Furnace Probes after 14 - 16 Hours Operations

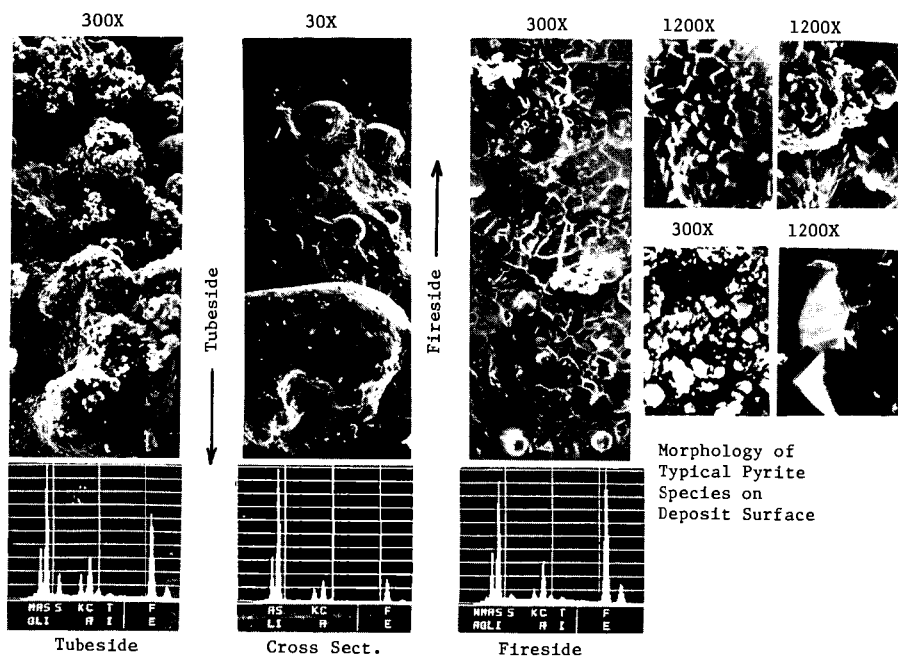


Figure 9 Slag Formation on Furnace Slag Probe

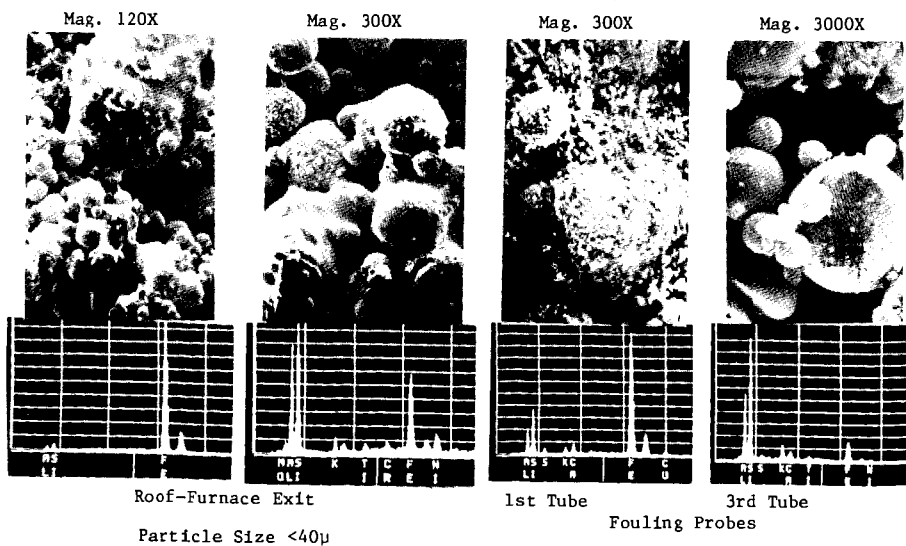


Figure 10 Iron-Rich Sintered Deposits Formed on Furnace Roof and 1st Tube of Convection Pass Probes by Coarse Pyrites

INFLUENCE OF THERMAL PROPERTIES OF WALL DEPOSITS ON PERFORMANCE OF P.F. FIRED BOILER COMBUSTION CHAMBERS

W. Richter, R. Payne, and M.P. Heap

Energy and Environmental Research Corporation
Irvine, CA 92714

1.0 INTRODUCTION

The build-up of ash deposit layers on tube walls and superheaters in dry bottom p.f. boiler combustion chambers not only deteriorates furnace and overall boiler efficiency; but increases the temperature level in furnace and convective passages and aggravates existing deposit problems. This can finally lead to expensive outages when deposit formation cannot be controlled by soot blowing alone. Since errors in furnace design with respect to slagging and fouling or wrong estimation of impact of fuel conversion on deposit formation are so costly in large boilers, there is considerable financial incentive to develop analytical methods in order to predict furnace performance for a wide range of coal types and operating conditions. It is clear that such methods must take quantitatively into account, among other things, the thermal properties of ash deposits.

The properties which determine heat transfer through a deposit layer of given thickness are thermal conductivity, emissivity, and absorptivity. The current paper presents results from various studies carried out by the authors at Energy and Environmental Research Corporation (EER) to show the sensitivity of overall furnace performance, local temperature and heat flux distributions on the properties of deposits in large p.f. fired furnaces.

2.0 PARAMETRIC STUDY OF OVERALL FURNACE PERFORMANCE

The most important parameters for overall furnace heat absorption are the adiabatic flame temperature, the firing density per heat sink area, the emissivity of the furnace volume, temperature and emissivity of the heat sinks and the flow and heat release patterns. Figure 1 shows how these quantities are related in a complex manner to each other, to fuel characteristics and to operating and boundary conditions of the furnace. Some of the relationships of Figure 1 were approximately quantified utilizing a simple well-stirred furnace model (1) which assumed transport of grey radiation. Two important results for furnace performance with respect to formation of deposits are shown in Figures 2 and 3, in which furnace efficiencies η_f ,

$$\eta_f \equiv 1 - \frac{\dot{M}_0 c_p \int_{T_0}^{T_{ex}} (T_{ex} - T_0)}{\dot{Q}_0} \quad (1)$$

are plotted over furnace height L with surface temperatures T_w of deposits and surface emissivities ϵ_w as parameters. The calculations were carried out for a rectangular furnace box of width $L/3$. Other input parameters are

listed in the Figures. The grey absorption coefficient K_a of 0.1 1/m used in the examples corresponds to an emissivity $\epsilon_f = 0.55$ for a furnace volume with a height of $L = 30\text{m}$. The effect of deposit surface temperature T_w on furnace efficiency η_f is considerable for values larger than 700 K (Fig. 2). For instance a furnace efficiency of 0.40 (corresponding to $T_{ex} = 1440\text{ K}$ according to Equation 1) was obtained for $T_w = 700\text{ K}$ (see Section 3 and 4). The L must be increased by 16.5m or 53% of the original height with clean walls to achieve the same furnace efficiency for a furnace with wall deposit of surface temperature 1300 K.* The impact of wall temperature on η_f will be even stronger for adiabatic flame temperatures less than 2200 K. Such adiabatic flame temperatures can occur when firing lignite or high-moisture coals. For furnaces operated with the same thermal input at low efficiencies, the presence of wall deposits requires only a moderate increase in size.

A reduction of surface emissivities from 1 (clean "sooty" walls) to 0.4 (which is the lowest range reported for ash deposits (see Section 3) also causes a drop of η_f (Fig. 2). However, the required increase in size to maintain η_f is smaller than for the change of deposit surface temperatures from 700 K to 1300 K mentioned above. The size changes non-linearly with changes of surface temperature but nearly linearly with ϵ_w between $\epsilon_w = 1$ and $\epsilon_w = 0.5$. Beyond $\epsilon_w = 0.2$, L must increase non-linearly to maintain furnace efficiency.

When a deposit layer is formed, surface temperature is increased and wall emissivity decreased. However, the superposition of these effects on η_f is less than a pure summation; since, by decreasing ϵ_w , the net heat flux to the layer is reduced, thus retarding the increase of surface temperature to a certain extent.

3.0 AVAILABLE DATA OF THERMAL PROPERTIES OF ASH DEPOSITS AND DATA ANALYSIS

Thermal Conductivity. A comprehensive review of literature data for thermal conductivity k of ash deposits was published by Wall et al. (2). The thermal conductance, k , of the ash material increases reversibly with temperature until sintering or fusion occurs. At this stage, a rapid and irreversible increase of k is observed. Typical values of k for non-sintered deposits from Australian coals in actual furnaces vary between $0.1 \cdot 10^{-3}\text{ KW/mK}$ at 500 K up to $0.4 \cdot 10^{-3}\text{ KW/mK}$ at 1300 K. The factors contributing to the thermal conductance in the powdered deposits are: Conductance in the solid particles; gas conduction in the voids and radiative transfer through the voids. Fetters et al. recently measured k for boiler deposits of an Indiana coal (3) and point out that the dominant mode of heat transfer through the deposit layer is by radiation at high temperature. The values of k measured for powdery deposits by Fetters et al. are about 2 times larger than those of

* 1m of furnace height corresponds to $\approx 500,000\$$.

Wall et al. (2) at the same temperature. This is contributed to the relative large particle sizes of the Indiana coal ash (75% in the 100 μ m range) compared to the Australian coal ash with mean weight particle diameters of 50 μ m and less.

Thermal conductivity of sintered and fused deposits found by the Australian researchers range from 0.5 10^{-3} KW/mK at 800 K to 1.2 10^{-3} KW/mK at 1500 K. This is consistent with the recent findings of Feters et al. (3) for crushed deposits from a boiler fired with Indiana coal and other literature values (4). The increase of thermal conductivity of sintered and fused deposits is due to a decrease of void space and increased transmissivity of the material. Assuming uniform mean conductivity, the thickness of a sintered deposit layer which maintains fusion at its surface can be estimated by

$$\Delta s_{fu} = \frac{k (T_{fu} - T_{t,a})}{\epsilon_w q_{in} - \epsilon_w \sigma T_{fu}^4} \quad 2)$$

where T_{fu} is the ash fusion temperature, $T_{t,a}$ the temperature of the outer surface of the tubes and q_{in} the incident heat flux density. With typical values $k = 0.8 \cdot 10^{-3}$ KW/mK, $T_{fu} = 1550$ K, $\epsilon_w = 0.7$, $T_{t,a} = 750$ K and $q_{in} = 400$ KW/m² the layer thickness with a wet surface would be about 8 mm. Wall et al. emphasize that values of k obtained from ground deposits in laboratory studies are questionable since bounding of the deposit occurs in situ which leads to an increase of k . This agrees with our results for a 700 MW_e boiler which yielded an overall value of $k = 3.2$ KW/m²K for deposits which could not be removed by soot blowing (see Section 4).

Emissivity and Absorptivity

Reviews of emissivity data of ash deposits were given by Wall et al. (2) and recently by Becker (5). The literature data has a considerable spread of emissivity, between values of $\epsilon_w = 0.9$ and $\epsilon_w = 0.3$ depending on temperatures, ash origin and probe preparation. However, general agreement exists that, for non-sintered material ϵ_w decreases reversibly with surface temperature. After sintering, the emissivity changes irreversibly to higher values (2). This agrees with measurements of furnace generated deposits of American coals carried out by Goetz et al. (6). These authors report values between 0.38 and 0.67 for powdery (initial) deposits, values between 0.76 and 0.93 for sintered deposits and values 0.65 and 0.85 for glassy and or molten deposits. The increase of emissivity with sintering and fusion is due to increased transmission of radiation into the surface of the deposit layer. In the range of surface temperatures of interest, namely between 800 K and 1400 K, measured total emissivities on probes of sintered real furnace deposits exhibit only slight variations with surface temperature (5), (6). However, measurements by Becker of spectral emissivities of deposits on laboratory prepared probes showed distinctive non-grey behavior. For typical flame temperatures of 1700 K and typical surface temperatures of 1100 K, up to 0.2 higher values were found for emissivities than for absorptivities. Non-greyness of emission and absorption is typical for glassy material and is due to the low spectral absorptivities at short wavelengths which becomes dominant for radiative transfer at more elevated flame

temperatures. The assumption of grey radiation of furnace deposits and consequent use of grey emissivity values for determination of absorption may lead to errors in heat transfer calculations for furnaces with moderate deposits since at lower surface temperatures absorption is several times larger than re-emission. By performing detailed one-dimensional spectral calculations, Becker showed that for a 10 m path length, typical of furnaces, and relatively cool walls errors up to +30% in predicted net heat flux densities would result from the assumption that the deposits were grey. However, these findings are based on spectral values found for laboratory prepared probes. Spectral measurements of real furnace deposits show reduced non-grey behavior (5), (6) and higher emissivities than the laboratory probes (6). Moreover, coloring agents such as unburnt carbon as well as the rough surface structure of real deposits and tube curvatures tend to make boiler surfaces more closely approximate grey behavior. Thus, the importance of non-grey deposits is uncertain in boiler chambers and, in any case, insufficient information is available to recommend replacing the assumption of grey radiation of deposits currently used in 3-D furnace models (see Section 4) by expensive more rigorous spectral models.

4.0 PREDICTIONS OF INFLUENCE OF WALL DEPOSITS ON HEAT TRANSFER IN EXISTING BOILERS

On the basis on the literature values of thermal properties discussed above a considerable number of performance predictions have been carried out for existing boiler combustion chambers in the past two years. Some results of those calculations with relevance to the impact of ash deposits on heat transfer follow. The tool used for the analysis is an extreme flexible 3-D Monte-Carlo type zone model (7), (8). In this model, the emissive power of each volume and surface zone is distributed into a discrete number of radiative beams. Taking multiple reflection at furnace walls into account, the beams are traced throughout the furnace volume until final absorption. Non-greyiness of the combustion products is modeled with a weighted grey gas approach. The radiating species considered are H_2O , CO_2 and particulates (soot, char and ash). Currently, char and ash particles are treated as grey radiators. The model of radiative exchange is directly coupled with a total heat balance of volume and surface (deposit) zones with unknown temperatures. The calculation of convective heat fluxes through the furnace is based on mass flow vectors at the boundary of each zone obtained from isothermal modeling. The heat release pattern is based on this flow field. The heat release due to volatile combustion is based on observed visible flame length and the heat release due to burnout of char particles is calculated from carbon and oxygen balances solved simultaneously with the heat balance.

Example 1: Tangentially Coal-Fired Boiler

This study was carried out to investigate the influence of ash deposits in a twin furnace of a boiler originally designed to fire No. 6 oil at a net thermal input of 1000 MW_t. However, the thermal input of the furnace was reduced to 590 MW_t to investigate the prospects of firing coal in this unit. The coal considered was a Utah coal with 8.8% ash content fired with 30% excess air. Figure 4 shows the zoning of the furnace and the assumed flow

patterns. The heat release due to combustion is indicated by the shaded area. The surface conditions were specified by the following input data:

- Case A Clean surfaces, emissivity of tubes $\epsilon_w = 0.9$
- Case B Powdery ash deposit, $\epsilon_w = 0.6$, $\Delta s = 0.5\text{mm}$, $k = 0.3 \cdot 10^{-3} \text{ KW/mK}$
- Case C Properties of ash deposit layer in upper part of the furnace (above heat-release zone) as specified for Case B; glassy ash deposit layer in lower part of the furnace with $\epsilon_t = 0.8$, $\Delta s = 7\text{mm}$, $K = 1 \cdot 10^{-3} \text{ KW/mK}$.

The properties for the powdery (primary) and for the glassy (molten) deposit layer of the Cases B and C correspond to average data from literature as cited above. The actual calculations were carried out with an effective emissivity of the tube walls taking the shadow effect of the gap between adjacent tubes into account.

Table 1 and Figures 5 through 7 show that the build-up of ash deposits seriously affects overall and local heat transfer. The difference ($\Delta\eta_f$) in computed furnace efficiencies for the extreme cases, A (clean walls) and C (highest thermal resistance), is 6.2 percentage points. The formation of a first initial deposit layer (Case B) has a stronger impact on heat transfer than subsequent increase of deposits in the lower furnace (Case C). The increase of the thickness of ash deposit opposite to the heat release zone displaces the peak heat fluxes up into the regions of the thinner deposits (Fig. 6). This is one reason why the build up of deposit layers, once started, spreads into adjacent wall zones. Once the deposit layers begin growing, surface temperatures can soon reach values in the range between softening (1400 K) and fusion temperature (1500 K) as indicated by shaded areas in Fig. 7. The furnace model is also able to predict, for a given coal ash fusion temperature approximately the development and extent of molten slag layers.

Another investigation showed for the same boiler fired with COM at a rate of 875 MW_t, showed that a decrease of surface emissivity from 0.9 (clean) to 0.6 (initial deposit) raised mean furnace exit temperature by 55 K.

Example 2 Opposed P.F. Fired Boiler

This study was carried out in order to verify the 3-D furnace heat transfer model with performance data available from a coal-fired, boiler combustion chamber of 1732 MW_t fuel heat input. The coal had a medium volatile content, an ash content of 6.6%, and was fired with 28% excess air. In this case, the flow pattern was based on detailed distribution of mass mean flow vectors measured in a physical isothermal model. However, turbulent components were superimposed on these vectors with the help of a simple model of turbulence. Fig. 8 shows a comparison of the profiles of gas temperatures measured and predicted for 100% Load in one half of the furnace outlet plane. The difference between predicted and measured values was less than 25 K. The good agreement is partially due to a reasonable assumption of the effective heat conduction coefficient $(k/\Delta s)_{\text{eff}}$ of the deposit layers. Fig. 9 shows how the predicted mean furnace exit temperature varied with $(k/\Delta$

s)eff and compares those predictions with two data points obtained from measured heat balances of the boiler immediately after soot blowing and 20 h after soot blowing. Since measurements and observations yielded approximately a 2mm deposit layer, which could not be removed by soot blowing an effective thermal conductivity of $3.2 \cdot 10^{-3}$ /mK can be deduced. An assumed value of $k = 0.8 \cdot 10^{-3}$ KW/mK for a dry partially sintered deposit would suggest the build-up of an additional layer of 1.5 mm, 20 h after soot blowing for a total layer of 3.5 mm thickness.

Fig. 9 also contains the relationship of $T_{ex} = f(k/\Delta s)$ for a similar boiler of 1250 MW_t heat input in which slagging and fouling problems are encountered. Further applications of the 3-D furnace model with respect to impact of wall deposits on heat transfer in CWM and COM fired furnaces may be found in (5), (10).

5.0 CONCLUSIONS

Thermal conductivity and emissivity of wall deposits have a considerable effect on heat transfer in large boilers. This results in temperature differences of furnace exit temperatures which influence furnace height, performance and costs. More exact values of deposit thermal properties, which vary over a wide range of temperatures and conditions, than currently available are needed for detailed prediction of the initial formation of deposit layers. However, gross characteristics of thermal properties can be assumed and are sufficient to estimate the performance of furnaces, since the model contains other major uncertainties such as, thickness and inhomogenous distribution of deposits at furnace walls and superheaters. This is especially true between soot blowing cycles. The 3-D heat-transfer model used in the present study has the potential to form the basis of a more comprehensive model of slagging and fouling because it can provide reliable predictions of flame and deposit temperatures. A model of ash transport is currently being coupled with the furnace heat transfer model which will account for time-temperature histories of ash and wall collisions.

6.0 LITERATURE

- (1) Richter, W.: Parametric Screening Studies for the Calculation of Heat Transfer in Combustion Chambers. Topical Report, prepared for Pittsburgh Energy Technology Center, Department of Energy, under Contract No. DE-AC22-80PC30297, January 1982.
- (2) Wall, T. F., A. Lowe, L. J. Wibberley, and McC. Stewart: Mineral Matter in Coal and the Thermal Performance of Large Boilers. Prog. Energy Combust., Science, Vol. 5, pp. 129, 1979.
- (3) Fethers, G. D., R. Viskanta, and F. P. Incropera: Experimental Study of Heat Transfer Through Coal Ash Deposits. 1982 ASME Winter Annual Meeting, Paper 82-WA/HT-30.
- (4) Singer, J. G., Editor: Combustion: Fossil Power Systems, 3rd Edition, Combustion Engineering Inc., Windsor, p. C-16, 1981.

- (5) Becker, H. B. : Spectral Band Emissivities of Ash Deposits and Radiative Heat Transfer in Pulverised-Coal-Fired Furnaces. Ph.D. Thesis, University of Newcastle, Australia, February 1982.
- (6) Goetz, G. J., N. Y. Nsakala, and R. W. Borio: Development of Method for Determining Emissivities and Absorptivities of Coal Ash Deposits. Journal of Engineering for Power, Vol. 101, pp. 607-619, 1979.
- (7) Richter, W., and M. P. Heap: A Semistochastic Method for the Prediction of Radiative Heat Transfer in Combustion Chambers. Western States Section, The Combustion Institute, 1981 Spring Meeting, Paper 81-17, 1981.
- (8) Richter, W., and M. P. Heap: The Impact of Heat Release Pattern and Fuel Properties on Heat Transfer in Boilers, 1981 ASME Winter Annual Meeting, Paper 81 WA/HT27, 1981.
- (9) England, G. C., Y. Kwan, W. Richter and K. Fujimura: Studies to Evaluate the Impact of Conversion from Fuel-Oil to Coal-Oil Mixtures on Thermal Performance and Pollutant Emissions. Pittsburgh Energy Technology Center, Proc. of the Fourth International Symposium on Coal Slurry Combustion, Vol. 3, 1982.
- (10) Payne, R., S. L. Chen and W. Richter: A Procedure for the Evaluation of the Combustion Performance of Coal-Water Slurries. Fifth International Symposium on Coal Slurry Combustion and Technology, Session VII, DOE, PETC, 1983.

Table 1. Thermal Performance of 590 MW_t Coal-Fired Combustion Chamber For Various Slagging And Fouling Conditions

No.	Case	Furnace Efficiency	Mean Furnace Exit Temperature	Mean Net Heat Flux Density	Max. Net Heat Flux Density	Vertical Position of Max. Net Heat Flux Density	Max. Flame Temp.	Max. Furnace Exit Temp.	Unburnt Cfix	Carbon Content of Fly Ash
		%	K	KW/m ²	KW/m ²	m	K	K	%	%
A	Clean Surfaces	40.3	1436	168	304	14.9	1661	1515	1.35	6.43
B	Powdery Ash Deposit	35.6	1519	148	235	16.7	1728	1582	0.89	4.33
C	Slagging Lower Half	34.1	1541	143	239	19.2	1776	1610	0.75	3.68

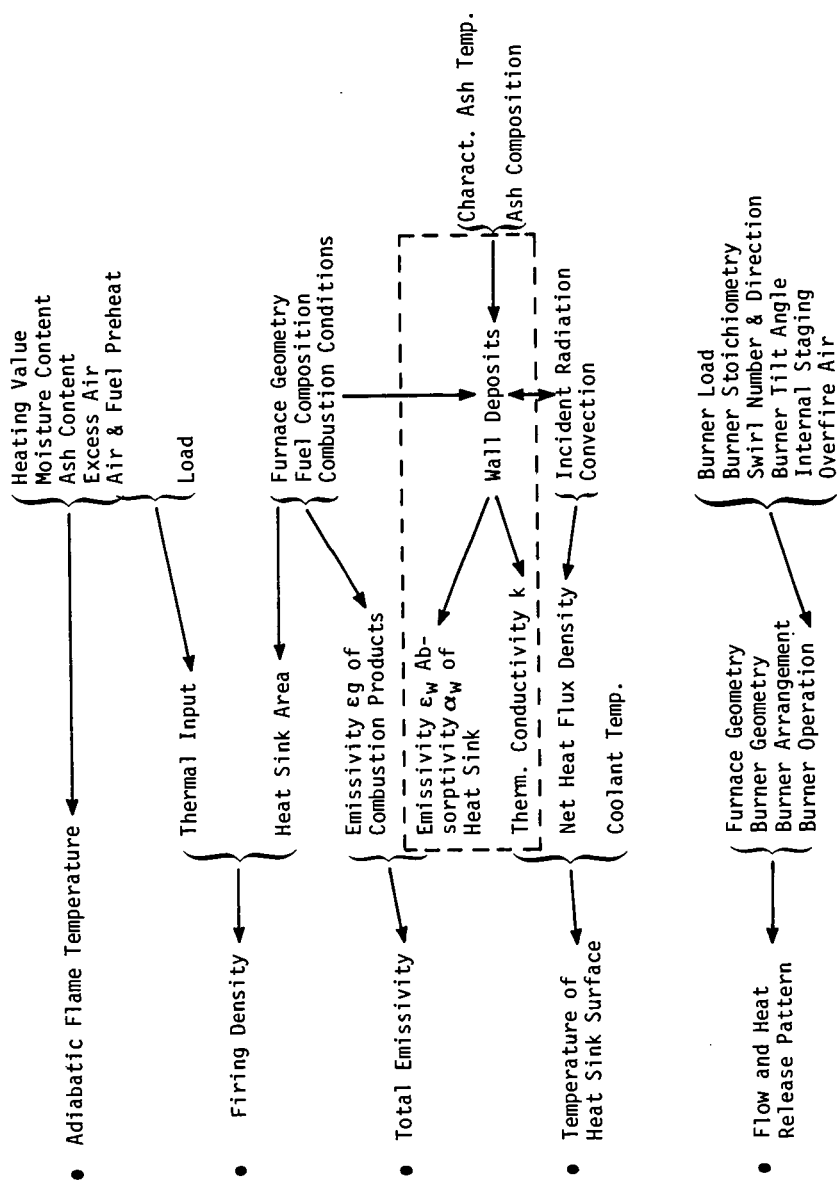


Figure 1. Major Factors Influencing Thermal Performance of Furnaces

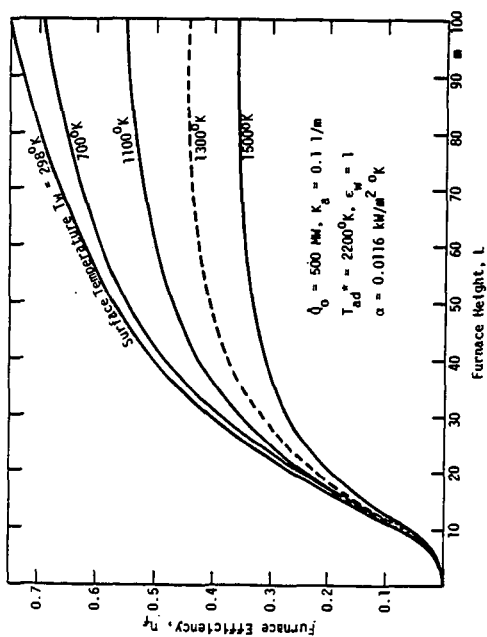


Figure 2. Dependency of Furnace Efficiency on Furnace Dimensions for Various Surface Temperatures.

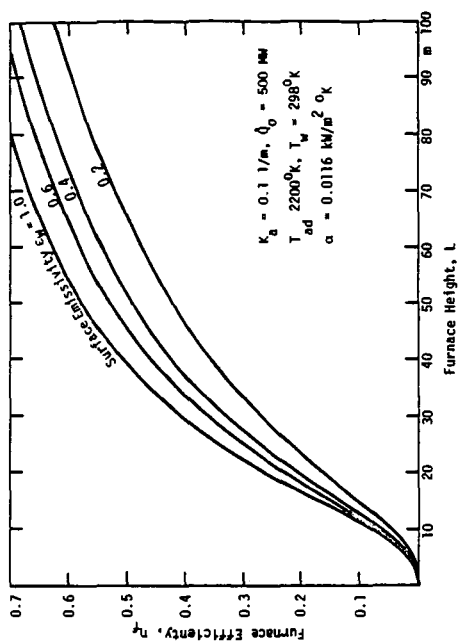


Figure 3. Dependency of Furnace Efficiency on Furnace Height With Surface Emissivity as Parameter.

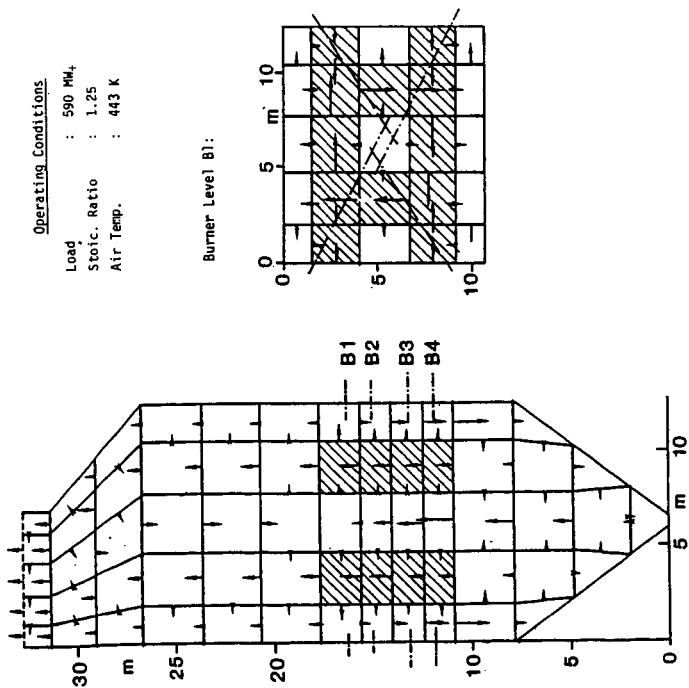


Figure 4. Geometry and Zoning of Tangentially Fired Boiler Originally Designed for Oil Firing with 1000 MW_t Thermal Input.

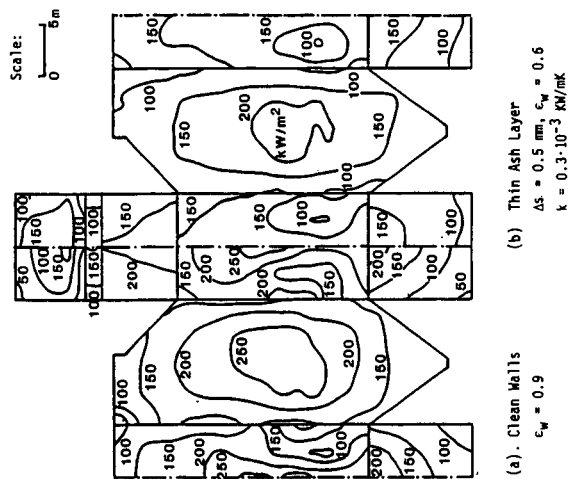


Figure 5. Influence of Wall Deposits on Predicted Net Heat Flux Distribution in Boiler Combustion Chamber Fired with Coal at a Rate of 590 MW_t.

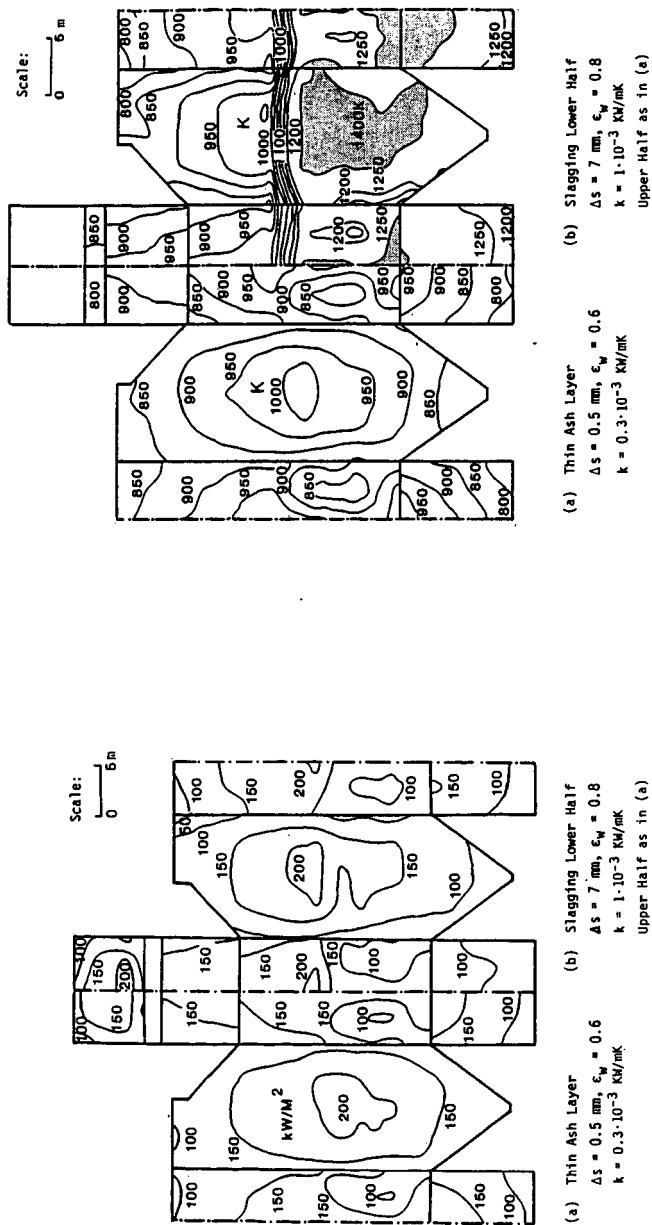


Figure 6. Influence of Slagging in Lower Furnace Half on Predicted Net Heat Flux Distribution in Boiler Combustion Chamber Fired with Coal at a Rate of 590 MW_t.

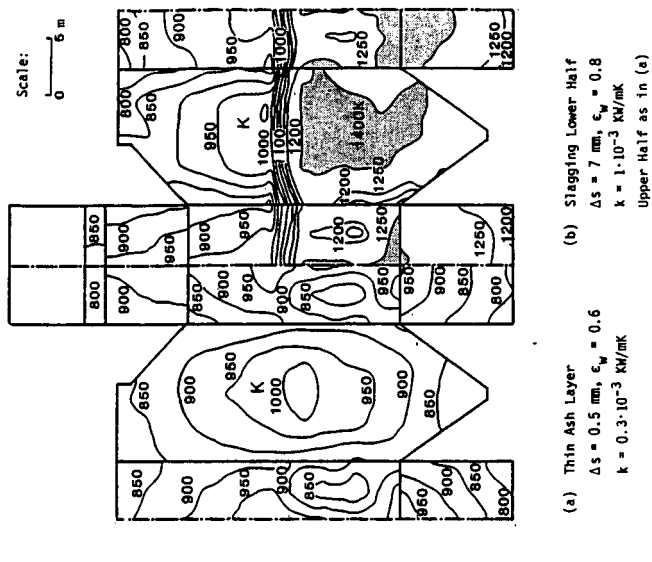


Figure 7. Influence of Slagging in Lower Furnace Half on Predicted Surface Temperatures of Deposits in Boiler Combustion Chamber Fired with Coal at a Rate of 590 MW_t.

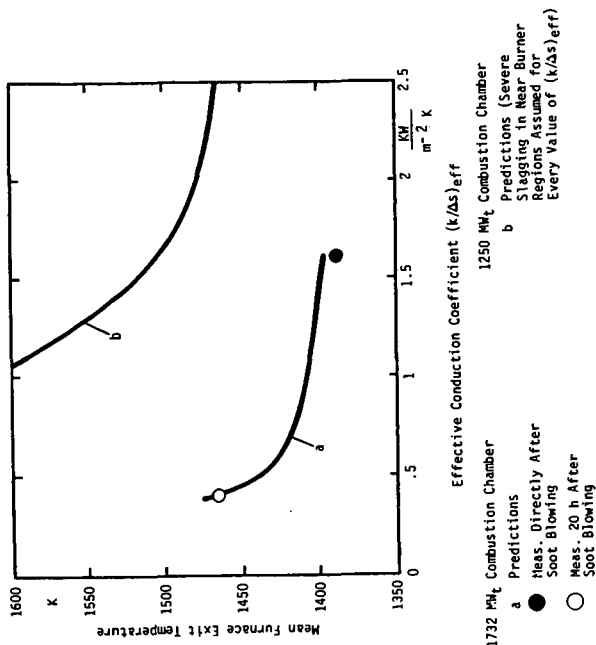


Figure 9. Dependence of Mean Furnace Exit Temperature on Effective Conduction Coefficient for Two Opposed Coal-Fired Boiler Combustion Chambers.

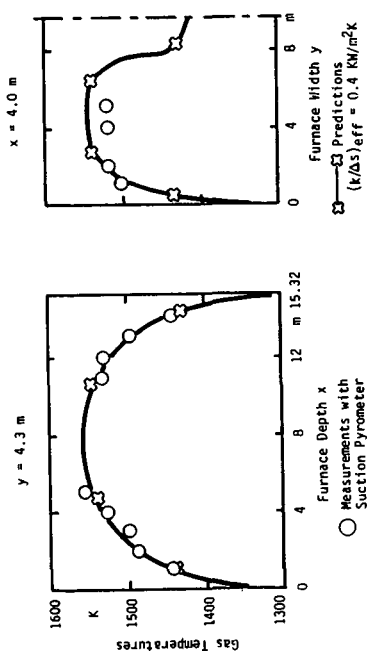


Figure 8. Comparison of Temperature Profiles Predicted and Measured Near Furnace Exit ($z = 68.6 \text{ m}$) of 1730 MW_t Opposed Coal-Fired Boiler Combustion Chamber.

The Prediction of the Tendency of Slagging and
Fouling of European Lignites by New Statistical
and Experimental Methods

W. Altmann
Technical University of Dresden
Mommenstrasse 13
8027 Dresden

German Democratic Republic

Communicated by:

John H. Pohl
Energy and Environmental Research Corporation
18 Mason
Irvine, California 92714

Introduction

Proper design and operation of coal-fired boilers requires prediction of the tendency of the fuels to foul and slag. A large number of correlations based on the oxides of an ash produced in the laboratory exist (1,2). The success of these correlations has been limited to the range of ash properties for which they were developed, and even then, these relationships may be unreliable. For instance, existing correlations can predict whether a fuel will create deposition problems in boilers rarely, occasionally, or frequently for approximately 50 percent of the fuels. An accuracy only slightly better than random guess (3).

Potential problems using available techniques have been discussed in the literature (2,3,4,5). The problems result from:

- Preparation and analysis of the ash (6)
- Ignoring the distribution and individual nature of mineral matter (4,6)
- Neglecting the influence of ash content (7)
- Ignoring the design of the boilers including heat release rate, heat fluxes and velocity profiles (3,8,9)

In addition the correlation should not be used for coals with properties outside the range for which the correlations were developed.

This paper describes the limited success of applying such techniques to predict performance, efforts to develop and verify new techniques to predict performance, and application of these techniques to predict the slagging and fouling behavior of European brown coals.

Prediction of Slagging Performance

Slagging performance of coals in boilers has been predicted by:

- temperature of critical viscosity,
- the base to acid ratio,
- and the base to acid ratio multiplied by the sulfur content of the coal.

Predictions of slagging and fouling using these relationships are compared to boiler performance for the six European brown coals listed in Table 1. The calculated indices and estimated and actual performance of the fuels are shown in Table 2.

The temperature of critical viscosity is the temperature at which the slag changes from plastic to Newtonian behavior. Plastic slags are difficult to remove by soot blowing. As a consequence, fuels with low temperatures of critical vis-

cosity are expected to form difficult to remove plastic and molten slags more readily than other fuels.

The temperature at critical viscosity can be measured in a viscometer, but the measurements are time consuming and expensive and the temperature at critical viscosity is usually estimated using empirical formulae. For instance, Watt and Fereday (10) developed

$$T_{cv} = \sqrt{\frac{107.7m}{2.398-c}} + 150 \text{ in } ^\circ\text{C} \quad 1).$$

$$\text{where } \text{SiO}_2 + \text{Al}_2\text{O}_3 + \text{Fe}_2\text{O}_3 + \text{CaO} + \text{MgO} = 1 \quad 2).$$

$$\text{and } m = 0.835 \text{SiO}_2 + 0.601 \text{Al}_2\text{O}_3 - 0.109 \quad 3).$$

$$c = 4.15 \text{SiO}_2 + 1.92 \text{Al}_2\text{O}_3 \quad 4).$$

The temperature at critical viscosity probably does not adequately predict slagging behavior of the six European brown coals of this study. The qualitative relationship between deposits formed in a boiler and the temperature of critical viscosity estimated by the technique of Watt and Fereday (10) is shown in Figure 1a. The data appear to correlate with observations, but predict improved performance at an intermediate temperature of critical viscosity. No reason is known for this and the correlation may be fortuitous.

The base to acid ratio is the reverse of the previous relationship and probably does not correlate the slagging data either. Figure 1b shows that the base to acid ratio appears to correlate the prediction of performance of brown coals in boilers. This relationship predicts optimum performance at a base to acid ratio of 0.3. This is quite possible with the formation of eutectics. However, comparison of Figure 1a and 1b shows the curves are reversed and the prediction of performance of all the fuels fall in the same relative position on both curves. This again leads to uncertainty as to the reasonableness and the reliability of the correlations in Figure 1.

The standard slagging factor, R_s , could not correlate the performance of all the fuels in the boilers. The slagging factor is defined as

$$R_s = B/A \cdot S \quad 5).$$

by Attig and Duzy (11). This equation is suggested for ashes which have $\text{Fe}_2\text{O}_3 > \text{CaO} + \text{MgO}$ but is applied to all ashes in this study. Only two of the ashes in this study have $\text{Fe}_2\text{O}_3 > \text{CaO} + \text{MgO}$. Leipzig has about equal amounts and Nordbohlen has greater Fe_2O_3 than $\text{CaO} + \text{MgO}$. The base to acid ratio (shown in Figure 2a) is recommended to correlate slagging behavior of ashes with $\text{CaO} + \text{MgO} > \text{Fe}_2\text{O}_3$ (11). Five of the fuels correlate reasonably with R_s but the slagging of Nordbohlen was greatly underestimated. However, this fuel was the only one with significantly greater Fe_2O_3 than $\text{CaO} + \text{MgO}$ and might not correlate with the other five fuels.

A good correlation of all six fuels was developed by modifying the slagging factor. The relationship is shown in Figure 2b where the slagging factor, f_s , is defined as:

$$f_s = 1.7 + 1.7 \text{SiO}_2^* + 0.8 \text{Al}_2\text{O}_3^* - 6.0 (\text{S})_{\text{Fe}}^{0.2} - 2.2 (\text{CaO}^* + \text{MgO}^*) - 1.9 \text{SiO}_3^* - 1.3 (\text{Alk})^* \quad 6).$$

where $f_s = 0$ is strong slagging

and $f_s = 1$ is no slagging

$$\text{and } [\]^* = \frac{[\]^*}{1 - \text{SiO}_2 + \text{SiO}_{2\text{corr}}} \quad (7).$$

$$\text{SiO}_{2\text{corr}} = 823 \Gamma_{\text{SO}_3}^{2.65} \cdot \exp(-9.45 \Gamma_{\text{SO}_3}) \text{Fe}_2\text{O}_3 \quad (8).$$

$$\Gamma_{\text{SO}_3} = \frac{\text{SO}_3}{1 - \text{SiO}_2} \quad (9).$$

where S is the weight percent sulfur in the coal as received and all other compositions are weight percent of the ash.

Predictions of Fouling Performance

The fouling performance of the six brown coals of this study could not be adequately predicted by existing or new techniques. The fouling performance of coals with $\text{CaO} + \text{MgO} > \text{Fe}_2\text{O}_3$ is usually predicted by the sodium content of the ash. Figure 3a shows the correlation of the qualitative observation of fouling in boilers with the alkali (Na_2O plus K_2O) content of the ash. All the coals except Ungarn correlate with the alkali content of the ash. However, no explanation is available for the fouling of the Ungarn which had 0.0 alkali content in the ash. A new fouling factor, f_F ,

$$f_F = \exp \left[\frac{-5 \cdot \text{Alk}^*}{\Gamma_S + 0.3} \right]$$

where Alk^* is defined by equation (7) was moderately successful, Figure 3b, in correlating the fouling performance of coals. However, considerable scatter still exists in the relationship.

Pilot Scale Prediction of Fouling and Slagging Performance

The limited success of predicting fouling and slagging performance based upon the analysis of the oxides of ashes produced in laboratory apparatus has prompted the Technical University of Dresden to develop pilot scale tests to predict slagging and fouling of ashes in boilers. Two tests are currently being evaluated which determine slagging and fouling characteristics of fuels not determined by current laboratory or other small scale tests. The first, determines the fouling and slagging of the fuel under different combustion conditions. In this test, the coal is burned in a small drop tube furnace. The level of oxygen and the thermal environment of combustion are changed. The particle temperatures are measured with thermographic techniques and the nature and deposition rate evaluated. Such a technique can simulate the limits of the time temperature concentration history in boilers and avoids production of an artificial mean ash. This technique does not account for ash trajectories in boilers.

The tendency of ash to follow streamlines or deposit on surfaces is determined in a second test. In this test, the coal is burned in a small cyclone combustion chamber. This chamber can also simulate the limits of time and temperature history of ashes in boilers. In addition, a cyclone chamber subjects the coal to centrifugal forces, which allows the ability of the fly ash particles to follow streamlines to be assessed.

The ability of these pilot scaled tests to predict the slagging and fouling performance of European brown coals is currently being evaluated. Preliminary results are promising.

TABLE I ASH COMPOSITION OF EUROPEAN BROWN COALS
WEIGHT PERCENT IN THE ASH

	UNGARN	LEIPZIG	NIEDERLAUSITZ	OBERLAUSITZ	NORDBOHMEN	SÜLZROHLE
SiO ₂	47.9	25.5	46.2	41.8	52.9	11.9
Al ₂ O ₃	26.1	3.5	6.8	30.0	25.3	6.9
Fe ₂ O ₃	8.6	24.0	13.4	8.3	12.6	3.0
CaO	8.0	19.5	11.4	9.5	3.4	15.2
MgO	1.7	3.5	7.6	4.0	1.5	2.2
SO ₃	4.8	22.5	12.9	3.6	2.5	31.5
Alkali	0.0	1.5	1.3	0.2	1.8	22.0
Not Determined	2.9	0.0	0.4	2.6	0.0	7.3

TABLE II COMPARISON OF ESTIMATED AND OBSERVED PERFORMANCE OF EUROPEAN BROWN COALS

Coal	Performance	slagging	fouling	Matt & Ferreday		Prediction		Slagging	f _s	Fouling	f _f	Fouling	% Alkali
				Critical	Viscosity	B/A	Slagging	R _s					
Ungarn	considerable	medium	medium	1395	0.247	low	high-severe	1.088	medium	0.384	medium	1.000	none
Leipzig	strong	strong	medium	904	1.621	high-severe	medium	4.539	very high	0.863	strong	0.863	low
Niederlausitz	medium	medium	low	1268	0.611	medium	medium	0.734	medium	0.456	medium	0.300	low
Oberlausitz	none	none	none	1312	0.304	low	low	0.061	little	0.963	none	0.988	none
Nordbohm	very strong	very strong	low	1440	0.224	low	low	0.246	little	0.086	very strong	0.627	medium
Salzkohle	strong	strong	very strong	963	1.085	high-severe	high-severe	3.038	very high	0.189	strong	0.091	very strong
													22.0

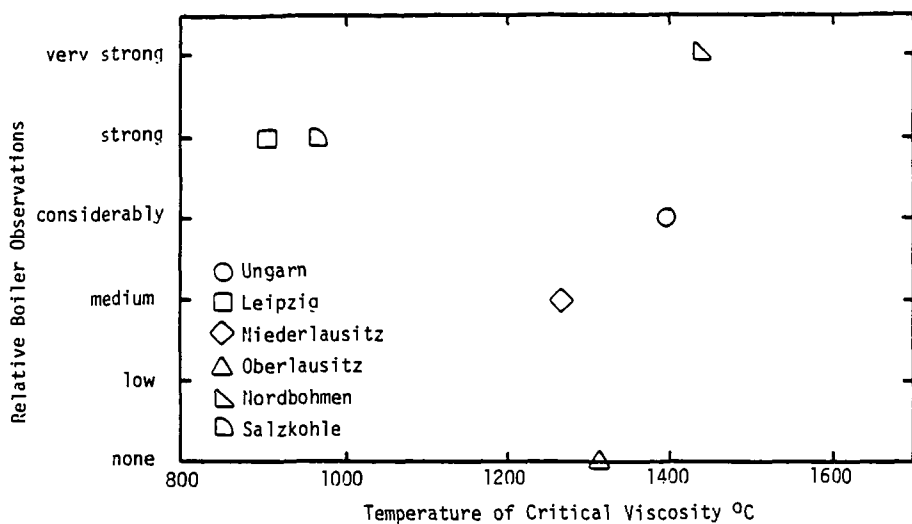


Figure 1a. Comparison of observed and predicted (T_{CV}) slagging performance of brown coal.

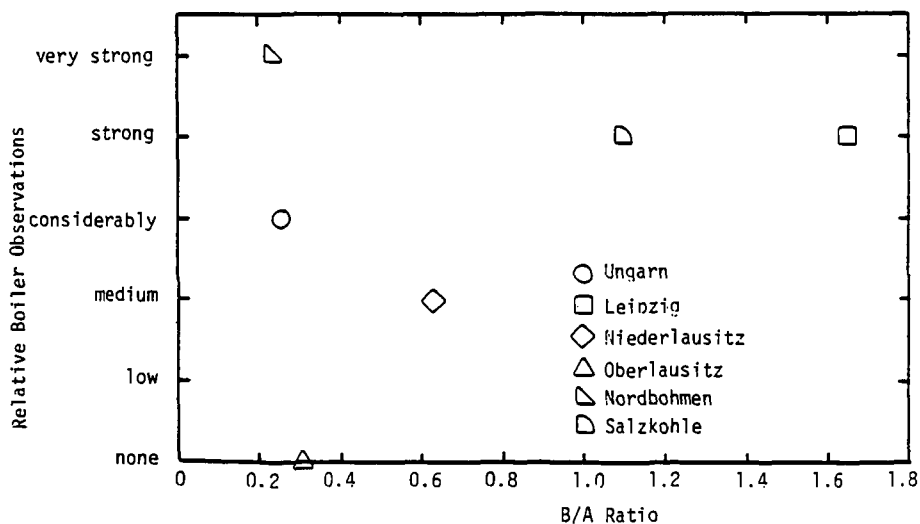


Figure 1b. Comparison of observed and predicted (B/A) slagging performance of brown coal.

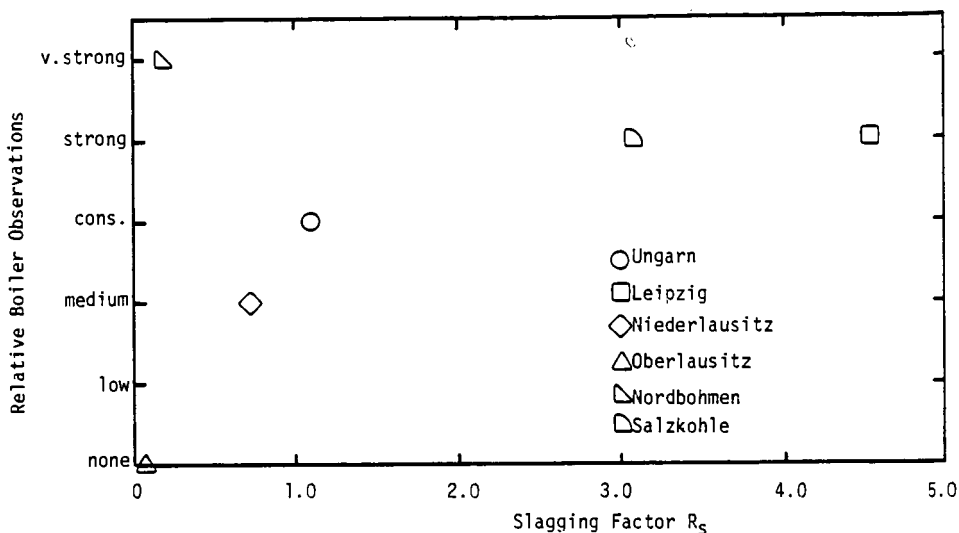


Figure 2a. Comparison of observed and predicted (R_s) slagging performance of brown coal.

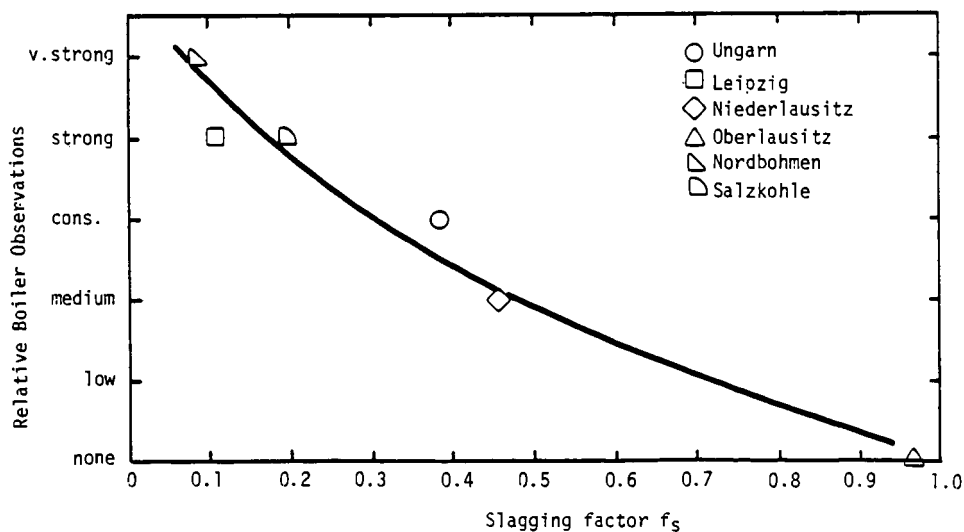


Figure 2b. Comparison of observed and predicted (f_s) slagging performance of brown coal.

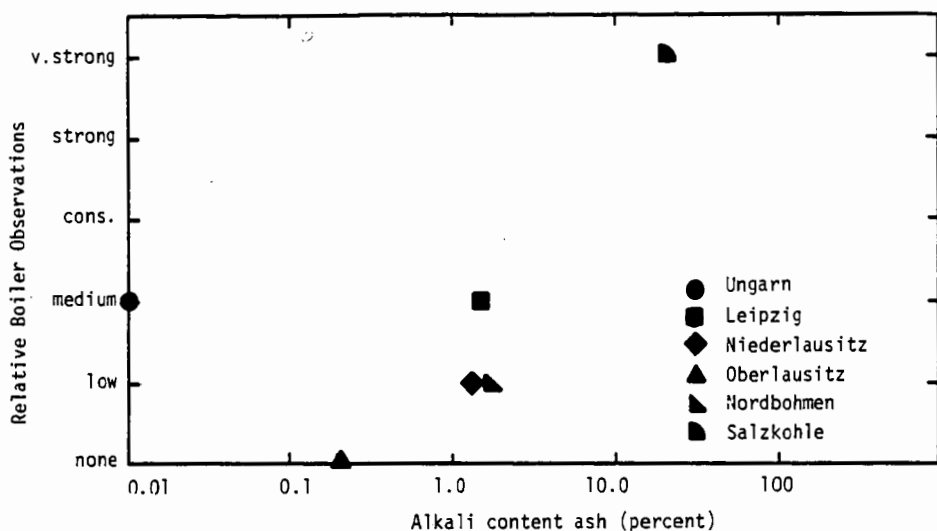


Figure 3a. Comparison of observed and predicted (Alkali content) fouling performance of brown coal.

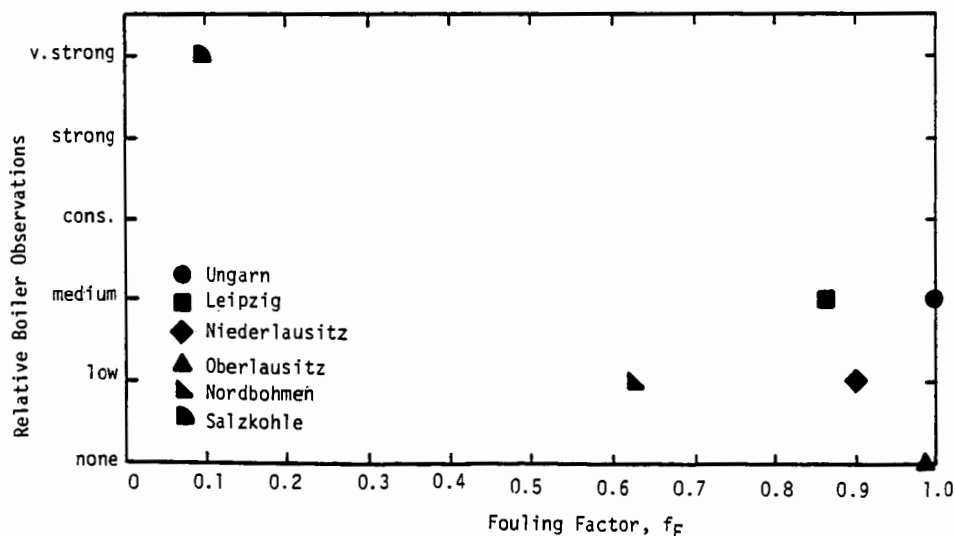


Figure 3b. Comparison of observed and predicted (f_F) fouling performance of brown coal.

References

- (1) Winegartheer, E. C., "Coal Fouling and Slagging Parameters," Book No. H-86 ASME, 1974.
- (2) Bryers, R. W., "On-Line Measurements of Fouling and Slagging (Full-Scale and Pilot Units) and Correlation with Predictive Indices in Conventionally Fired Steam Generators." Proceedings of the Low Rank Coal Technology Development Workshop, San Antonio, Texas, June, 1981.
- (3) Barrett, R. E., J. M. Murin, and G. A. Mack, and J. P. Dimmer, "Evaluating Slagging and Fouling Parameters," presented at the American Flame Research Committee Fall Meeting, Akron, Ohio, October, 1983.
- (4) Pollmann, S. and W. Albrecht, "Investigations of the Slagging Behavior of Bituminous Coals in Large Dry-Bottom Steam Generators," p. 85., in R. W. Bryers, "Fouling and Slagging Resulting from Impurities in Combustion Gases," Engineering Foundation, New York, 1983.
- (5) Altmann, W. "Beurteilung der Verschlackungs - und Verschmutzungsneigung fester Brennstoffe." XIV Kraftwerkstechnischen Kolloquium, Dresden, German Democratic Republic, October, 1982.
- (6) Pohl, J. H., "Errors in Predicting the Slagging and Fouling Behavior of Coals Based on Standard Techniques", XIV Kraftwerkstechnischen Kolloquium, Dresden, German Democratic Republic, October, 1982.
- (7) Blackmore, G., "Quality Coal for Electric Utility Use," Ninth Annual International Conference on Coal Gasification, Liquidification, and Conversion to Electricity," Pittsburgh, PA, August 1982.
- (8) Bryers, R. W., Private Communication, Foster Wheeler Development Corporation, 1984.
- (9) Richter, W., Private Communication, Energy and Environmental Research Corporation, 1984.
- (10) Watt, J. D. and F. Fereday, "The Flow Properties of Slags formed from the Ashes of British Coals: Part 1: Viscosity of Homogeneous Liquid Slags in Relation to Slag Composition." J. Inst. Fuel, v. 42, p.99, 1969.
- (11) Attig, R. C., and A. F. Duzy, "Coal Ash Deposition Studies and Applications to Boiler Design, Proceedings of the American Power Conference", v. 31, p. 299, 1969.

AN OVERVIEW OF MINERAL MATTER CATALYSIS OF COAL CONVERSION*

Thomas D. Padrick
Sandia National Laboratories, Albuquerque, NM 87185

INTRODUCTION

Since the 1920's, several studies have focused on the catalytic effects of inherent mineral matter on coal conversion.¹ In recent years, we have witnessed an increase in the level of coal research and the development of new coal utilization processes. In parallel with this activity, there have been reports on the effects of coal minerals on coal liquefaction, coal gasification, in-situ coal gasification, and other areas of coal utilization.²⁻⁵ This overview will deal primarily with recent results of mineral matter effects in coal liquefaction and coal gasification. The terms minerals, mineral matter, and ash will be used synonymously. An attempt will not be made to review the effects of all classes of minerals, but will only consider those minerals which have shown a large effect on coal conversion processes. A good review of the specific minerals present in a variety of coals can be found in the work of Gluskoter et al.⁶

COAL LIQUEFACTION

The Germans used coal liquefaction on a commercial scale from 1930 to the end of the second World War. They found that a catalyst could enhance liquid yields and help remove heteroatoms. The Bergius process used an iron oxide-aluminum catalyst at a 2-3% by coal weight concentration.

In recent years, it has been realized that mineral matter plays an important role in coal liquefaction,^{7,8,9} similar to the role of the added catalyst in the Bergius process. Several experimental techniques have been used to study the effects of minerals on coal liquefaction and to identify the specific catalytic phase.¹⁰ Most studies^{11,12} strongly imply that the iron sulfides are the most active species, and the other minerals appear to have little effect on enhancement of liquid yield or quality.

The specific role of pyrite (FeS_2) as a catalyst has been under investigation since pyrite was identified as the most active inherent mineral for coal liquefaction. Under liquefaction conditions, FeS_2 is transformed into a nonstoichiometric iron sulfide, Fe_{1-x}S ($0 \leq x \leq 0.125$). Thomas et al.¹³ studied the kinetics of this decomposition under coal liquefaction conditions, and concluded that the catalytic activity of FeS_2 is associated with radical initiation resulting from the pyrite-pyrrhotite transformation.

Several studies have investigated the possibility that defects in the pyrrhotite structure provide the sites for catalyst activity. A recent study¹⁴ found a linear correlation between the conversion to benzene or THF solubles and the atomic percent iron in

* This work supported by the U. S. Dept. of Energy at Sandia National Laboratories under contract no. DE-AC04-76DP00789.

the liquefaction residues. Montano *et al.*¹⁵ used *in situ* Mössbauer spectroscopy to study transformation of FeS_2 to Fe_{1-x}S . They observed a large pyrrhotite surface area at the reaction temperature (above 350°C).

Stohl and Granoff¹⁶ investigated the effects of pyrite particle sizes, pyrite defects and surface areas on coal liquefaction. They observed no effect due to surface area and concluded that the observed particle size effect was due to diffusional limitations in the transformation of pyrite to pyrrhotite.

While many studies indicate that pyrrhotites are probably involved in the liquefaction process, the exact mechanism by which pyrrhotite catalyzes the conversion of coal to oil is not clear. Based on the works of Thomas *et al.*¹³ and Derbyshire *et al.*,¹¹ one can suggest that a possible role of pyrrhotite is as a hydrogenation catalyst. However, more work is necessary on the surface properties of the pyrrhotites and the interaction with model compounds before a definite catalytic mechanism can be proposed.

COAL GASIFICATION

The gasification of coal involves two distinct stages: (1) devolatilization and (2) char gasification. Devolatilization occurs quite rapidly as the coal is heated above 400°C . During this period, the coal structure is altered, producing a less reactive solid (char), tars, condensable liquids and light gases. Nominally 40% of the coal is volatilized during this period. The less reactive char then gasifies at a much slower rate. We will discuss the effects of coal minerals on both devolatilization and char gasification.

A large volume of work has been reported on rapid devolatilization of coal (heating rates approximating process conditions).^{17,18} Recently, the effects of coal minerals on the rapid pyrolysis of a bituminous coal were reported by Franklin, *et al.*¹⁹ They found that only the calcium minerals affected the pyrolysis products. Addition of CaCO_3 reduced the tar, hydrocarbon gas and liquid yields by 20-30%. The calcium minerals also altered the oxygen release mechanism from the coal. Franklin, *et al.* attribute these effects to CaCO_3 reduction to CaO , which acts as a solid base catalyst for a keto-enol isomerization reaction that produces the observed CO and H_2O .

Walker and co-workers at the Pennsylvania State University have investigated the reactivity of a variety of coals during gasification in air, CO_2 , H_2 and steam.²⁰⁻²³ Hippo and Walker²¹ found a linear correlation between reactivity and CaO content in the ash. They also observed an increase in reactivity with MgO , up to about 1%. They found no correlation between reactivity and iron content or total K or Na content. In their studies on hydrogen and steam gasification, the Penn State group used coals demineralized by acid washing to study mineral matter effects. While changes were observed in these studies, it was difficult to attribute these changes to catalytic effects or physical effects.

Mahajan *et al.*²⁴ observed that the presence of pyrite in coal had a beneficial catalytic effect on hydrogenation at 570°C . They suggested that the catalytic activity was due to pyrrhotite formation. Hüttinger and Krauss²⁵ reached a similar conclusion concerning the catalytic activity of pyrite, and concluded that

above 850°C, iron enhanced the methane formation if the H₂ pressure was sufficiently high.

Padrick et al.²⁶ observed enhancement of the hydrogasification rate of a Pittsburgh Seam coal at 1000°C when various iron-containing minerals were mixed with the coal. They investigated the chemical effect of the minerals by measuring H₂/D₂ exchange rates, and also determined the physical effect of the mineral addition on the resultant surface areas and pore volumes of the chars. While the correlation of 1000°C hydrogasification rates with measured parameters was somewhat better including the chemical effects of the minerals, it was concluded that the gasification rates for the various sources of reduced iron were primarily due to the physical interaction of the minerals with the coal.

REFERENCES

1. Marson, C. B. and Cobb, J. W., Gas J. 171, 39 (1925).
2. Davidson, R. M., "Mineral Effects in Coal Conversion," Rept. No. ICTIS/TR22, IEA Coal Research, London, January 1983.
3. Otto, K., Bortosiewicz, L., and Shelef, M., Fuel 58, 85 (1979).
4. Fisher, J., Young, J. E., Johnson, J. E., and Jonke, A. A., Report ANL 77-7 (1977).
5. Plogman, H. and Kuhn, L., Proceedings of the International Conference on Coal Science, Düsseldorf, Germany, September 7-9 (1981).
6. Gluskoter, H. J., Shimp, N. F. and Ruch, R. R., in "Chemistry of Coal Utilization. 2nd Supplementary Volume," John Wiley and Sons, New York, NY, pp. 369-424 (1981).
7. Granoff, B. and Traeger, R. K., Coal Process. Technol. 15, (1979).
8. Mukherjee, D. K. and Chowdhury, P. A., Fuel 55, 4 (1976).
9. Gray, David, Fuel 57, 213 (1978).
10. Gray, J. and Shah, Y. T. in "Reaction Engineering in Direct Liquefaction," Adison Wesley Pub. Co., New York, NY (1981).
11. Derbyshire, F. J., Varghese, P. and Whitehurst, D. D., Preprints, Amer. Chem. Soc., Div. Fuel Chem. 26, No. 1, 84 (1981).
12. Whitehurst, D. D., Mitchell, F. U. and Farcasiu, M., in "Coal Liquefaction. The Chemistry and Technology of Thermal Processes," Academic Press, New York, NY, pp. 163-177 (1980).
13. Thomas, M. G., Padrick, T. D., Stohl, F. V. and Stephens, H. P., Fuel 61, 761 (1982).
14. Montano, P. A. and Granoff, B., Fuel 59, 214 (1980).

15. Montano, P. A., Bommanavar, A. S., and Shah, V., Fuel 60, 703 (1981).
16. Stohl, F. V. and Granoff, B., 90th Annual Meeting of the AIChE, Houston, TX (1981).
17. Anthony, D. B. and Howard, J. B., AIChE J. 22, 625 (1976).
18. Stangby, P. C. and Sears, P. L., Fuel 60, 131 (1980).
19. Franklin, H. D., Peters, W. A. and Howard, J. B., Preprints, Amer. Chem. Soc., Div. Fuel Chem. 26, No. 2, 121 (1981).
20. Jenkins, R. G., Nandi, S. P. and Walker, P. L. Jr., Fuel 52, 288 (1973).
21. Hippo, E. J. and Walker, P. L. Jr., Fuel 54, 245 (1975).
22. Tomita, A., Mahajan, O. P. and Walker, P. L. Jr., Fuel 56, 137 (1977).
23. Linares-Solano, A., Mahajan, O. P. and Walker, P. L. Jr., Fuel 58, 327 (1979).
24. Mahajan, O. P., Tomita, A., Nelson, J. R. and Walker, P. L. Jr., Fuel 56, 33 (1977).
25. Hüttinger, K. J. and Krauss, W., Fuel 60, 93 (1981).
26. Padrick, T. D., Rice, J. K. and Massis, T. M., Preprints, Amer. Chem. Soc., Div. Fuel Chem. 27, No. 3, 300 (1982).

EFFECTS OF EXCHANGEABLE CATIONS ON THE CONVERSION OF LOW RANK COALS TO GASES AND LIQUIDS

Robert G. Jenkins

Fuel Science Program
Department of Materials Science and Engineering
The Pennsylvania State University, University Park, PA 16802

INTRODUCTION

It has become evident that for low rank coals (generally of subbituminous C and lower) the inorganic constituents play major roles in their utilization. These coals are partly characterized by the presence of significant quantities of carboxyl and phenolic groups which are, to varying degrees, associated with alkali and alkaline-earth metal cations (1,2,3,4). As an example, in an earlier study (2) we reported that these exchangeable metal cations can account for approximately 3 wt% (dmmf) of a Montana Lignite. The dominant exchangeable metal cation in US low rank coals is calcium. However, appreciable concentrations of sodium and magnesium are found (2,3). Generally, approximately between 30 to 60% of the carboxyl groups are associated with metal cations (2,3).

It is important to differentiate between these exchangeable inorganic species and the mineralogical components when considering the behavior of low rank coals under processing conditions. The most significant differentiation is, of course, their dispersion throughout the coal matrix. In the case of the exchangeable cations, they are dispersed on an atomic basis; that is, each metal cation is associated with one or two carboxylic acid groups. There have been many electron microprobe studies (5), for example, which have shown that the inorganic elements under investigation are extremely uniformly distributed through a lignite. In essence, in that type of study, it is impossible to resolve precisely the distribution because the cations are of an atomic size, much lower than the resolution of the instrument. When considering the mineralogical species, it is well established that the great majority of the minerals exist in size ranges greater than 1 μm . Thus, they are several orders of magnitude greater in size than the cations. This size differentiation has, of course, ramifications on the chemical behavior of the species as well as physical considerations. It is extremely likely that the exchangeable metal cations are of much different chemical reactivity than a like atom in the lattice of some mineralogical species. Finally, it must be realized that on pyrolysis (which accompanies combustion, gasification and liquefaction processes) that the carboxylic acid salts will decompose to liberate a metal cation as some chemically reactive entity. Even after some degree of sintering, or agglomeration, the cation derived species will be finely dispersed, i.e., still much smaller than the vast majority of mineralogical particles.

It is the goal of this presentation to review several recent studies which have shown the importance of understanding the nature of the exchangeable cations in the utilization of low rank coals.

DIRECT LIQUEFACTION

It is well known that during direct liquefaction there is always some amount of material which appears as insoluble, residual solids (6,7). These solids are composed of a wide range of carbonaceous and inorganic materials. However, in this case we are only interested in those generated during the liquefaction of low rank coals. The most important feature of reactor deposits obtained from these coals is the formation of calcium carbonate as calcite and/or metastable vaterite (6,7,8,9). Detailed optical and SEM studies on these solids indicates that carbonate is precipitated and is not related to calcite grains which may occur in the feed low

rank coal (6,7). The source of the calcium is the exchangeable calcium present in these coals. A semi-quantitative relationship can be found between the amount of deposited solids and the ion-exchangeable calcium content of the feed coal (6). Liquefaction experiments made on an acid washed coal resulted in no production of calcium carbonate. A series of experiments were made on a Wyodak subbituminous coal which was first demineralized and then back exchanged with calcium acetate solution. The calcium loaded (5 wt%), dried coal was then reacted at 400°C in tetralin (N_2 , CO_2 and H_2S atmospheres) for periods varying from 10 to 60 min. The quantity of calcium carbonate was determined quantitatively by measuring the volume of CO_2 evolved on treating the reaction products with 1N HCl. The results of this series of experiments are shown in Figure 1. The data are expressed as a first-order plot in terms of the conversion of carboxylates to the theoretical amount of $CaCO_3$ that could be produced. It is obvious that these data fit the first order plot rather well. Under these conditions 50% of the exchangeable calcium is converted to carbonate after about 23 mins. The calculated rate constant is $5 \times 10^{-4} \text{ sec}^{-1}$. In all cases, the crystallographic form of calcium carbonate produced was found to be a mixture of calcite and vaterite. From the data plotted in Figure 1, it can be seen that the rate of conversion of calcium cations to carbonate, under these conditions, is not affected by the presence of the three gaseous atmospheres utilized (H_2O , N_2 and CO_2).

COAL PYROLYSIS

In any investigation dealing with the role of exchangeable metal cations in coal pyrolysis one has to be concerned with several gauges of pyrolysis behavior. As examples, it is important to gain understanding of the effects of the cations on total weight loss, tar evolution, product gas composition, decarboxylation and kinetics. Several investigations have been made into this general area. Tyler and Schafer (10), Franklin et al. (11), and Otake (12) studied the effects of exchangeable cations on total weight loss and tar yield over a wide range of reaction conditions. They found, in general, that replacement of the metal cations by protons leads to an increase in weight loss. Murray (14) and Schafer (15,16) studied the decarboxylation of low-rank coals in fixed-bed reactors at slow heating rates. They found that removing the metal cations does result in an increase in the amount of decarboxylation at any given temperature.

In recent studies in these laboratories (17,18,19), Morgan found profound effects of the metal cations on rapid pyrolysis of a Montana lignite in an entrained flow apparatus. Total weight loss, at 1173 K in N_2/He , was found to be a function of the presence of metal exchangeable cations for a residence time of about 250 ms (Table 1).

TABLE 1
EFFECT OF CATIONS ON MAXIMUM WEIGHT LOSS IN ENTRAINED
FLOW REACTOR, 1173 K, DICF* BASIS (17,18)

<u>Sample</u>	<u>mmoles cation/g DICF Coal</u>	<u>wt Loss</u>
Raw	0.94	31
Ca A	1.11	30
Ca B	0.84	29
Ca C	0.75	35
Ca D	0.49	39
Acid Washed	--	49

* DICF: Dry Inorganic Constituent Free

As can be seen from Table 1, as the loading of calcium increases there is a drop in the total yield. The most significant reductions takes place after the initial

loadings. After a certain level of calcium cations the effects become essentially constant. Morgan's studies also suggested that presence of exchangeable cations caused a reduction in the amount of tars evolved when compared to the acid-washed sample. FTIR spectra of the tars evolved in these cases indicated that tars from the raw coal contain three times the amount of aliphatic hydrogen as do the tars from the acid-washed sample. Finally, it was found that the presence of the metal cations retarded the decomposition of the carboxylic acid groups. In this study, the carboxylic acid concentrations were determined directly on the pyrolyzed lignite samples.

GASIFICATION REACTIVITY

It has been well recognized that the measured gasification reactivities of coal chars, prepared under similar conditions, are a function of the rank of the parent coal (20,21). The chars of highest reactivities are those derived from lignites. Correlation have been made between the reactivities and the amount of exchangeable calcium cations in the coals or calcium in the chars (20,21,22). However, it was not until the work of Radovic et al. (23,24,25,26,27) that it was shown, in the case of calcium loaded onto a North Dakota Lignite, the catalytic species was calcium oxide. In addition, it was established that the observation that reactivity was a function of the severity of pyrolysis conditions was due to catalyst crystallite growth (sintering). As pyrolysis severity increased then the measured reactivities were reduced. A correlation was drawn between the observed gasification reactivities and the dispersion (as measured by crystallite size) of the catalytically active calcium oxide. Thus, the gasification reactivity of lignite chars was shown to be dominated by the concentration of their inherent catalyst sites.

It is important to recognize that the aforementioned reactivity measurements have been made on chars and not the corresponding raw or pretreated lignites. It is becoming evident that the exchangeable cations can have significant effects on combustion and gasification of the coals themselves. Some data reported by Morgan and Jenkins (19) and Morgan and Scaroni (28) have indicated relationships between the presence/absence of exchangeable metal cation and the rates of gasification/combustion of lignites. It is apparent from their data that the effects of the cations on rapid pyrolysis rates can ultimately result in enhancements in oxidation reactivity.

SUMMARY

As research proceeds in the area of low rank coal utilization, it is becoming obvious that the inherent inorganic constituents of these coals have profound influences on their behavior. The reason for this influence is related to the fact that a significant proportion of the inorganic components are in the form of atomically dispersed exchangeable metal cations. It is evident that variations in the metal cation content can bring about significant differences in the performance and behavior of these coals. With that in mind, it may well be that we should be looking in more depth at the "beneficiation" of low rank coals by effecting alterations in the chemical distributions of the cations associated with their carboxylic acid functionalities.

ACKNOWLEDGEMENTS

The author would like to acknowledge all his colleagues with whom he has been associated. Financial support for the research studies were provided by the Gas Research Institute, Electric Power Research Institute, Department of Energy, and The Pennsylvania State University Cooperative Program in Coal Research.

REFERENCES

1. Schafer, H. N. S., Fuel 49, 197 (1970) and Fuel 49, 271 (1970).

2. Morgan, M. E., Jenkins, R. G., and Walker, P. L., Jr., Fuel 60, 189 (1980).
3. Bobman, M. H., Golden, T. C., and Jenkins, R. G., Solvent Extraction and Ion Exchange 1(4), 791 (1983).
4. Bobman, M. H., Golden, T. C., and Jenkins, R. G., Solvent Extraction and Ion Exchange 1(4), 813 (1983).
5. Fowkes, W. W., "Separation and Identification of Minerals from Lignites," Chapter 27, in Analytical Methods for Coal and Coal Products, Volume 2, Ed. C. Karr, Jr., Academic Press (1978).
6. Walker, P. L., Jr., Spackman, W., Given, P. H., Davis, A., Jenkins, R. G., and Painter, P. C., "Characterization of Mineral Matter in Coals and Coal Liquefaction Residues," Final Report to EPRI, AP-1634, November 1980.
7. Wakely, L. D., Davis, A., Jenkins, R. G., Mitchell, G. D., and Walker, P. L., Jr., Fuel 58, 379 (1979).
8. Brunson, R. J., Chabach, J. J., Chem. Geol. 25(4), 333 (1979).
9. Stone, J. B., Trachte, K. L., Poddar, S. K., Amer. Chem. Soc. (Fuel Chem. Div.) Preprints 24(2), 255 (1979).
10. Tyler, R. J. and Schafer, H. N. S., Fuel 59, 487 (1980).
11. Franklin, H. D., Cosway, R. G., Peters, W. A., and Howard, J. B., Ind. Eng. Chem. Process Des. Dev. 22, 39 (1983).
12. Otake, Y., M.S. Thesis, The Pennsylvania State University (1982).
13. Murray, J. B., Fuel 57, 605 (1978).
14. Schafer, H. N. S., Fuel 58, 667 (1979).
15. Schafer, H. N. S., Fuel 58, 673 (1979).
16. Morgan, M. E., Ph.D. Thesis, The Pennsylvania State University (1983).
17. Morgan, M. E., and Jenkins, R. G., Amer. Chem. Soc. (Fuel Chem. Div.) Preprints 28(4), 138 (1983).
18. Morgan, M. E., and Jenkins, R. G., Amer. Chem. Soc. (Fuel Chem. Div.) Preprints 29(2), 141 (1984).
19. Jenkins, R. G., Nandi, S. P., and Walker, P. L., Jr., Fuel 52, 288 (1973).
20. Hippo, E. J., and Walker, P. L., Jr., Fuel 54, 245 (1975).
21. Hippo, E. J., Jenkins, R. G., and Walker, P. L., Jr., Fuel 58, 338 (1979).
22. Radovic, L. R., Ph.D. Thesis, The Pennsylvania State University (1982).
23. Radovic, L. R., Walker, P. L., Jr., and Jenkins, R. G., Fuel 62, 209 (1983).
24. Radovic, L. R., Walker, P. L., Jr., and Jenkins, R. G., J. Catal. 82, 382 (1983).
25. Radovic, L. R., Walker, P. L., Jr., and Jenkins, R. G., Fuel 62, 849 (1983).

26. Radovic, L. R., Steczko, K., Walker, P. L., Jr., and Jenkins, R. G., submitted to Fuel.
27. Morgan, B. A., and Scaroni, A. W., Amer. Chem. Soc. (Fuel Chem. Div.) Preprints 28(4), 164 (1983).

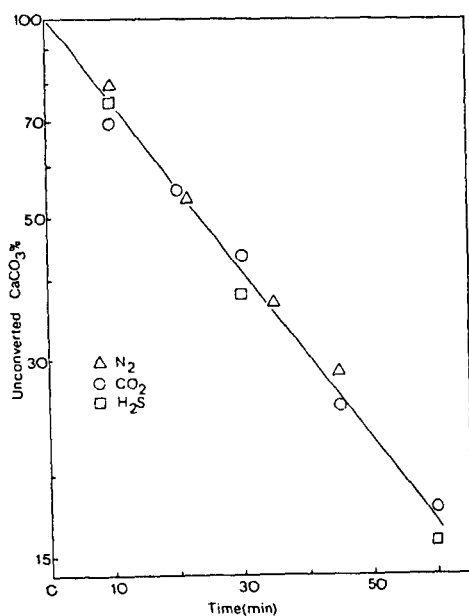


Figure 1. First Order Plot for Calcium Carbonate Formation at 400°C Under Pseudo-Liquefaction Conditions

Iron Sulfide Catalysis in Coal Liquefaction

P.A. Montano, Y.C. Lee, A. Yeye-Odu and C.H. Chien

Department of Physics, West Virginia University, P.O. Box 6023
Morgantown, WV 26506-6023

I. Introduction

The direct liquefaction of coal is a process that involves the interaction between coal, hydrogen, solvent, and catalysts. Mineral matter has been known to enhance the conversion of coal to liquid products.^(1,2,3) Addition of pyrite, pyrrhotite, and liquefaction residues to coal has been shown to affect the coal conversion yields and the viscosity of the products.⁽⁴⁾ Of all the minerals present in coal, pyrite (and marcasite) are the most important for coal utilization, especially in direct coal liquefaction.⁽⁵⁾ However, one has to remember that under coal liquefaction conditions pyrite rapidly transforms to a non stoichiometric iron sulfide Fe_{1-x}S ($0 < x < 0.125$). It is noted that the sulfur formed as a result of the decomposition of pyrite is able to extract hydrogen from poor donor solvents. The stoichiometry of the pyrrhotite formed from FeS_2 depends strongly on the partial pressure of H_2S .⁽⁶⁾

A correlation between the conversion of coal to benzene soluble, and the stoichiometry of the iron sulfides was observed by Montano and Granoff.⁽⁷⁾ Higher conversion is accomplished by a more iron-deficient pyrrhotite.⁽⁸⁾ Stephens et al studied the effect of additives to an IL#6 conversion to liquid products. Their work strongly suggests that Fe_{1-x}S and H_2S play a catalytic role in the conversion of coal to oils. These results, ^(9,10) in good agreement with the ones obtained from in situ Mössbauer measurements, where there was clear evidence of interaction between the iron sulfides and some coal components. Many questions remain unanswered concerning the catalytic roles of H_2S and Fe_{1-x}S . Lambert⁽¹¹⁾ suggested that the catalytic activity observed for pyrite is solely due to H_2S acting as a hydrogen-transfer catalyst. In a recent study by Anderson and Bockrath⁽¹²⁾ on direct coal liquefaction more conversion was obtained when the ratio of sulfur added to an iron solution (the catalyst) was equal to the one needed to obtain pyrrhotite (Fe_{1-x}S). A very recent work by Ogawa, Stenberg, and Montano⁽¹³⁾ reporting the hydrogenation of diphenylmethane in the presence of pyrrhotite clearly shows that maximum activity is obtained when the partial pressure of H_2S is enough to maintain an iron deficient surface. Too high a partial pressure of H_2S in the reactor moves the composition of the surface towards FeS_2 and the conversion of diphenylmethane is reduced. Too low a partial pressure of H_2S leads to the formation of troilite (FeS) and lower conversion. These results indicate that optimum conditions are obtained when the surface of the sulfide is rich in metal vacancies, where dissociation of H_2S can take place forming highly reactive species.⁽¹⁴⁾ It is obvious that the understanding of the catalytic role of the iron sulfides lies in the investigation of their surface properties. We report in the present paper such a study, where surface techniques were used to observe the reaction of gases found under liquefaction conditions with the sulfides surfaces. A special reactor was developed to study the surface composition of the iron sulfides after reaction with oxygen containing compounds using conversion electron Mössbauer spectroscopy (CEMS). Extended X-ray Absorption Fine Structure (EXAFS) and X-ray Absorption Near Edge Structure (XANES) were used for determining the environment of iron species in the residues obtained from the study of the interaction of iron sulfides ($\text{FeS}_2, \text{Fe}_7\text{S}_8$) with pyrene.

II. Experimental

Auger and electron energy loss spectroscopy measurements were performed using an UHV system with a base pressure of 10^{-10} torr. The system was attached to a reactor cell where the samples were exposed to high temperatures and gases. The reactions of FeS_2 , Fe_7S_8 , and FeS with CO , H_2 , O_2 , NH_3 , CH_4 , C_2H_4 , and higher hydrocarbons were studied between room temperature and 450°C . Figure 1 shows a schematic diagram of the system used in these measurements.

The CEMS measurements were carried out in a specially designed reactor to be described elsewhere. In this reactor the samples of ^{57}Fe foil were studied and treated with $\text{H}_2/\text{H}_2\text{S}$ to obtain the iron sulfides. The detector employed for the detection of the electrons was a $\text{He}/10\% \text{CH}_4$ flow counter connected in line with the reactor. The reaction of pure iron and iron sulfide with naphthoquinone were studied with this cell. The EXAFS and XANES measurements of the residues of the reactions of FeS_2 and Fe_7S_8 with model compounds were made at the Cornell High Energy Synchrotron Source.

Experimental Results

1. Auger and Electron Energy Loss Measurements on FeS_2 , Fe_7S_8 , FeS

Natural crystals of FeS_2 (pyrite) and Fe_7S_8 (monoclinic pyrrhotite) were used for the measurements. The (100) face of pyrite and the (0001) face of pyrrhotite were studied in the reactor, using a polycrystalline sample of FeS . All the samples show a characteristic $M_{2,3}$ VV Auger doublet with a separation of 5.0 eV (Figure 2). Two additional peaks (3 and 4 in Figure 2) are also observed for FeS . Peak 1 may correspond to transitions involving the s-3p ($2\sigma_v$) valence band while peak 2 may correspond to transitions involving the d-band. A typical set of Electron Loss spectra for FeS_2 is shown in Figure 3. Peak a is assigned to interband transitions from the $\text{Fe}-3d$ band to an empty state above the Fermi level. Peaks b and c may be assigned to transitions for one s-3p-like valence band (peak b to $1\pi_g \rightarrow 2\sigma_v$ and c to $2\sigma_g, 1\pi_u \rightarrow 1\sigma_u$ transitions.) Peaks d and e are attributed to collective oscillations of the conduction or valence electrons. Peaks f and g are assigned to surface and volume plasmons respectively. Peaks j and k are transitions involving the Fe-3p electrons ($M_{2,3}$ level). Peak l is due to transition from the M_1 level. The EEL spectra for the other sulfides are similar but the position and intensities of the peaks vary. In our measurements we observed EEL peaks with strong iron or sulfur character. Damaged iron sulfide surfaces show evidence of reconstruction through migration of sulfur after heating to 450°C . For undamaged sulfides, heating results in changes in the chemical composition of the surface; migration of sulfur also occurs. There is clear evidence of the presence of elemental sulfur on the pyrite and pyrrhotite surface but not on troilite (FeS). Since the maximum temperature attained was 450°C we do not expect that reduction of the FeS surface will take place. Essentially if the partial pressure of H_2S is low in the reactor the formation of FeS will occur by removal of sulfur from the Fe_{1-x}S surface. Once this state is reached no further loss of sulfur occurs and a fairly stable surface is obtained.

The interaction of the pyrrhotite with simple gases is more complex, damaged surfaces of FeS_2 and Fe_7S_8 react with CO at 450°C . We understand that as the result of the interaction of CO with Fe on the sulfide surface. This interaction is not detected with undamaged surfaces (pure single crystals) and with FeS . The formation of oxides on the surface is easily detected for FeS_2 and Fe_7S_8 after reaction with CO . It has been observed that CO undergoes a disproportionation reaction on Fe, $2\text{CO} \rightarrow \text{C} + \text{CO}_2$, with the formation of surface oxide due to the

dissociation of CO.⁽¹⁶⁾ The surface oxide is rapidly removed by H₂. The surfaces of the sulfides do not show any evidence in the Auger and EEL spectra of reactions with NH₃, CH₄, and C₂H₄. However, they interact strongly with molecular oxygen forming a surface oxide. Figure 4 shows the surface oxide formed on pyrite after interaction with oxygen, for comparison purposes the EEL spectrum for α -Fe₂O₃ is also shown. The present measurements indicate a high reactivity of the sulfide surfaces towards oxygen containing compound and very little towards light hydrocarbons and ammonia.

2. CEMS Measurements of the Surface Interaction of Naphthoquinone with Iron and Iron Sulfide Surfaces

A high purity ⁵⁷Fe foil was used for these measurements, such a foil was necessary in order to record rapidly a Mössbauer spectrum (less than one-half hour). The sample was placed in the holder inside of the reactor and H₂ was flown for 2 hours at 350 °C to reduce the surface and clean off any residual contamination. Figure 5a shows the Mössbauer spectrum at room temperature inside the reactor after cleaning. We studied the hydrogenation of naphthoquinone by introducing about 20 mg of the compound and flowing hydrogen at about 0.5 cc/sec. The temperature of the reaction was 305 °C and 405 °C and the time of reaction was one-half hour. After reaction the CEM spectrum was taken inside the reactor. No evidence of the formation of any known oxide was detected (Figure 5b). The same experiment was repeated using a sulfided sample (produced from the ⁵⁷Fe foil by flowing H₂/H₂S (10%) at 400 °C). The spectrum for such a sample is shown in Figure 6a before reaction. After reaction with naphthoquinone we see clear evidence of the formation of Fe₃O₄ on the surface (Figure 6b). Magnetite is formed at the expense of the iron sulfide. This observation is in very good agreement with our earlier *in situ* Mössbauer work,⁽¹⁷⁾ where a less surface sensitive technique was used for the measurements. We interpret these results as evidence of a greater reactivity of the iron sulfides surfaces towards oxygen containing organic molecules than the pure metal. It is noted that magnetite can be easily removed by further flow of H₂/H₂S. The magnetite layer is formed in the first few surface layers of the iron sulfide (see Figure 6).

3. EXAFS and XANES Measurements

Measurements were performed on the residues of the reaction of FeS₂ and Fe₇S₈ with pyrene. Pyrite and monoclinic pyrrhotite were used as chemical standards for the measurements. In Figure 7 the XANES spectra are shown for the residues of the reactions of pyrene with Fe₇S₈ and FeS₂. The reactions were performed⁽¹⁴⁾ at 440 °C in the presence of H₂. One notices that the near edge structure is different for both residues, we attributed the difference to the presence of FeS in the reaction residues of Fe₇S₈ and pyrene. A compound that is not present in the residues of the pyrite run. The total EXAFS spectrum were analyzed and the Fourier transform for the residues of the FeS₂ run is shown in Figure 8a. (The peak positions are not corrected for phase shifts.) For comparison purposes the Fourier transform for pure pyrite and monoclinic pyrrhotite are also shown. The first prominent peak in all the spectra is due to Fe-S distances (2.262 Å for pure FeS₂). The second peak in pyrite (Figure 8b) is due to the other iron neighbors. For Fe₇S₈ the spectrum is complicated since there are many iron distances present (Figure 8c). For the residues of the reaction of FeS₂ with pyrene practically no Fe-Fe can be identified. This means that the iron atoms and vacancies in the Fe_{1-x}S structure⁽¹⁴⁾ (atomic % iron is 47.8) are extremely disordered and randomly distributed and that the only well defined coordination of the iron ions are the sulfur atoms. This is a striking result since we should have expected as a result of the Mössbauer study⁽¹⁴⁾ a better defined pyrrhotite structure.

III. Conclusions

We have observed that the behavior of iron sulfide surfaces depends strongly on the stoichiometry. Iron deficient surfaces show a higher reactivity than the troilite surface. At high temperatures (450 °C) there is elemental sulfur present on the iron sulfide surfaces. The metal vacancies can serve as centers for the dissociation of H_2S thus facilitating the transfer of hydrogen to organic entities. The pyrrhotite surface shows a great reactivity towards oxygen containing compounds. The surface oxide formed on the pyrrhotite surface are easily reduced when H_2 and H_2S are present in the reactor. The interaction between the pyrrhotites surfaces and light hydrocarbons is minimal.

Acknowledgement: The authors wish to thank the U.S. DOE for their support.

REFERENCES

1. R.M. Davidson "Mineral Effects in Coal Conversion," Report No. ICTIS/TR22, IEA Coal Research London.
2. D.K. Mukherjee and P.B. Chowdbury FUEL 55, 4(1976).
3. W. Hodek, Chemical and Physical Valorization of Coal Meeting, Liege, EUR-5954-d/e/f/i, Luxembourg, 87, 1978.
4. B. Granoff, M.G. Thomas, P.M. Baca and G.T. Noles, Am. Chem. Soc. Div. FUEL Chem. Prepr. 23, 23(1978).
5. E. Illig, "Disposable Catalysts in Coal Liquefaction," DOE, Albuquerque, NM (1978).
6. P.A. Montano, A.S. Bommanavar and V. Shah, FUEL 60, 703(1981).
7. P.A. Montano and B. Granoff, FUEL, 59, 214(1980).
8. H.P. Stephens, F.V. Stohl and T.D. Padrick, Proc. Int. Conf. Coal Sci., Dusseldorf, Sept. 1981, Verlag Glück Auf Essen; pp368 (1981).
9. A.S. Bommanavar and P.A. Montano FUEL, 61, 1289(1982).
10. A.S. Bommanavar and P.A. Montano FUEL, 61, 523(1982).
11. J.M. Lambert, Jr., FUEL, 61, 777(1982).
12. R.R. Anderson and B.C. Bockrath, "Effect of Sulfur on Coal Liquefaction in the Presence of Dispersed Iron and Molybdenum Catalysts," PETC, Pittsburgh 1982.
13. T. Ogawa, V. I. Stenberg, and P.A. Montano, FUEL (in press).
14. P.A. Montano and A.S. Bommanavar, J. of Molecular Catalysis, 20, 393(1983).
15. Y.C. Lee and P.A. Montano, Surface Science 142, 27(1984).
16. K. Jagannathan, S. Srinivasan, M.S. Hedge and C.N.R. Rao Surface Sci. 99, 309(1980).

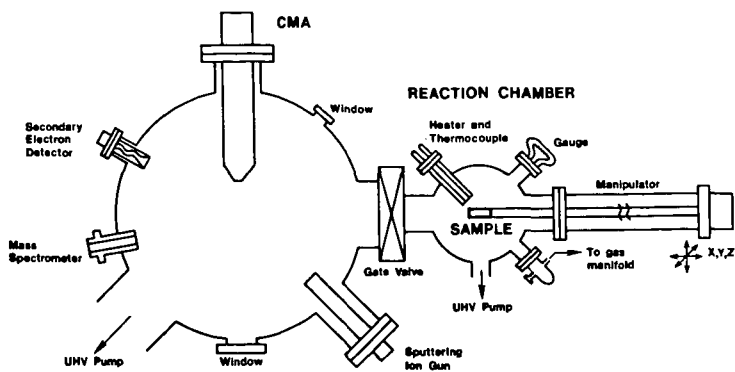


Figure 1. Schematic diagram of the UHV system used for the surface measurements

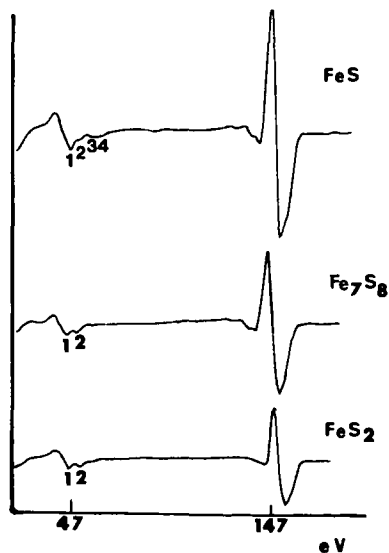


Figure 2. Low energy Auger spectra for the iron sulfides

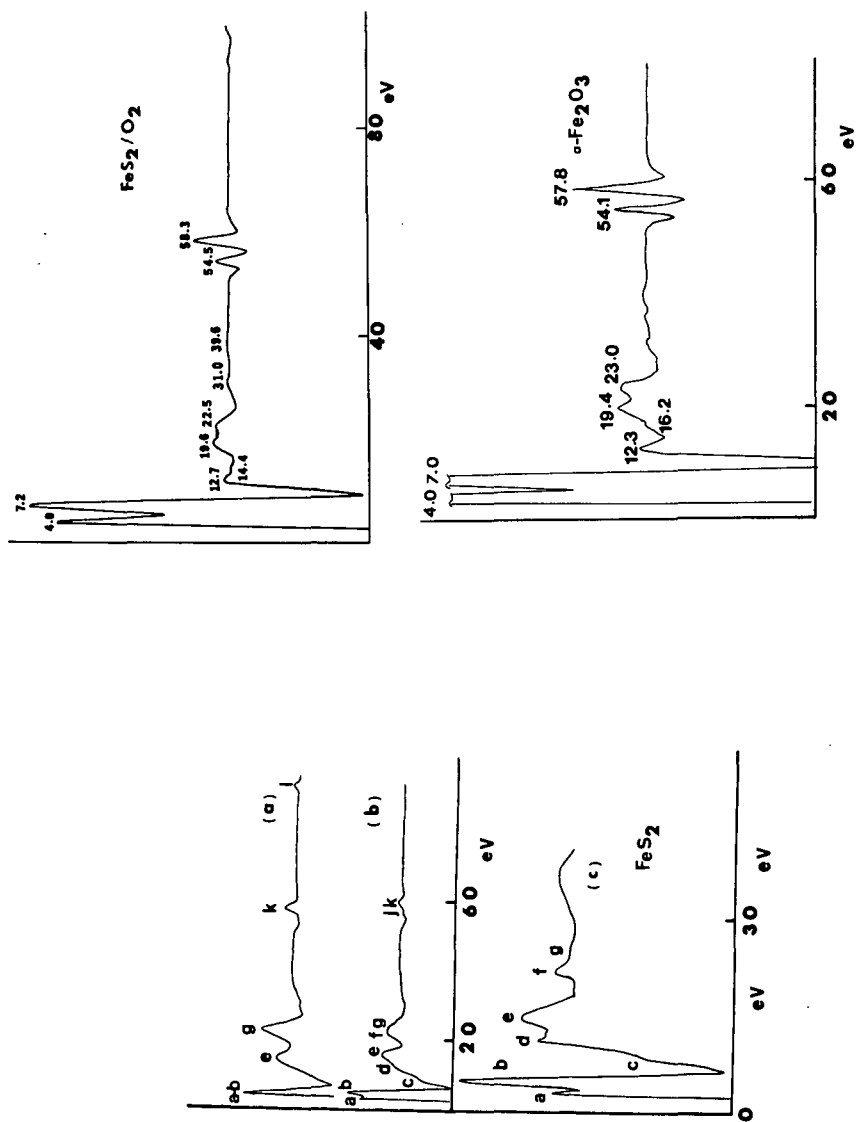


Figure 3. EEL spectra for FeS₂
a) E_p = 300 eV b) E_p = 150 eV c) E_p = 50 eV
Figure 4. EEL spectra of FeS₂ after reaction
with oxygen (a) and of α -Fe₂O₃ (b)

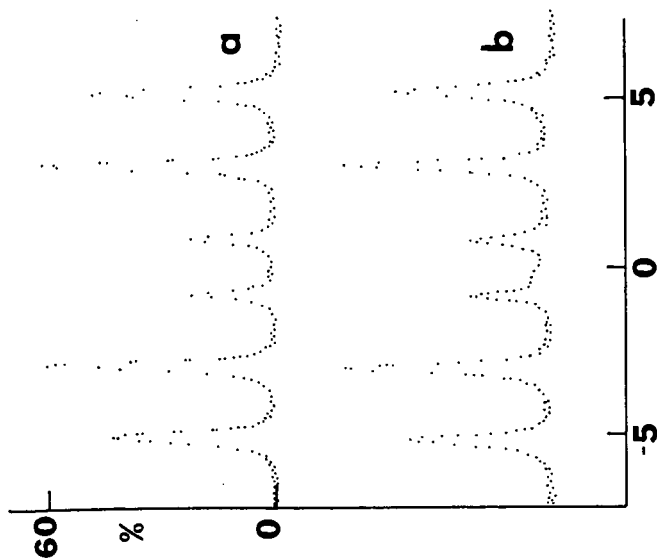


Figure 5. CEM spectra of ^{57}Fe foil (a) and after reaction with naphthoquinone (b). X-axis is in mm/sec.

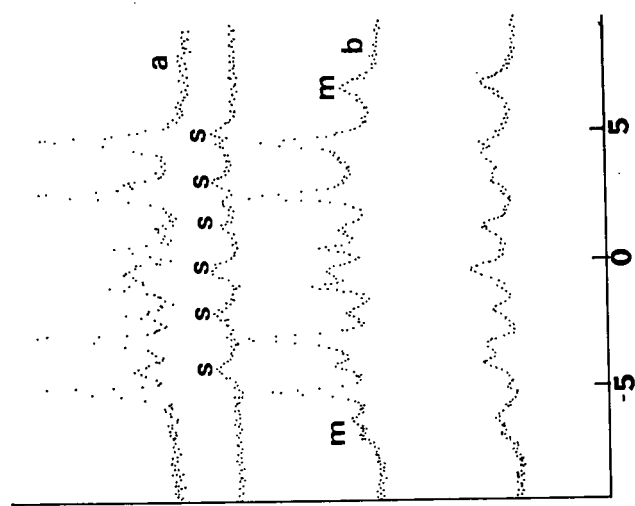
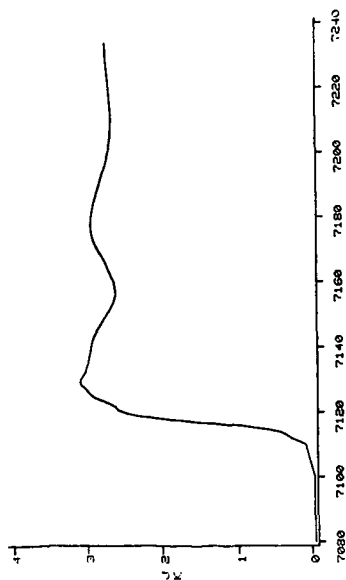


Figure 6. CEM spectra of a) sulfided ^{57}Fe foil, s: indicates the sulfide surface b) After reaction with naphthoquinone m: magnetic, bottom spectrum is the surface layers after reaction. X-axis is mm/sec.

FeS₂+H₂+PYRENE
AFTER BACKGROUND SUBTRACTION



Fe₇S₈+H₂+PYRENE
AFTER BACKGROUND SUBTRACTION

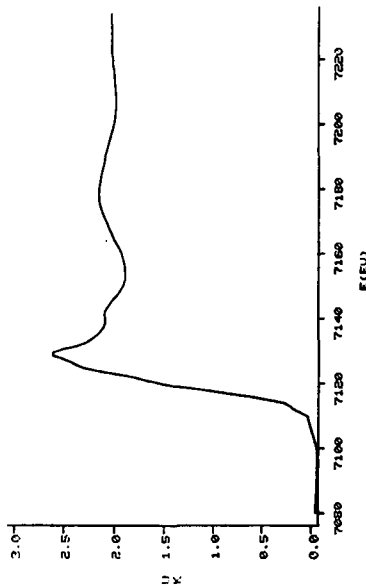


Figure 7. XANES spectra of the residues of the reactions of pyrene with a) FeS₂ and b) Fe₇S₈

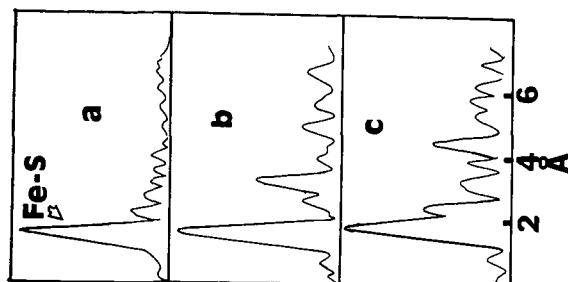


Figure 8. Fourier transforms of $\chi \cdot k$ (x EXAFS structure) for a) FeS₂ after reaction b) pure FeS₂ and c) Fe₇S₈ X-axis is in Å and without corrections for phase shifts.

NEW IRON OXIDE CATALYST REDUCTION ACTIVITIES WITH HYDROGEN SULFIDE AND HYDROGEN

H. Hattori, F.A. Jones, T. Ogawa, C.L. Knudson,
L.J. Radonovich and V.I. Stenberg

University of North Dakota Energy Research Center
and the Department of Chemistry
University of North Dakota, Grand Forks, ND 58202

INTRODUCTION

Various types of catalysts have been used for coal liquefaction. Among these catalysts, molybdenum and iron catalysts are most frequently used and they are usually combined with other metal oxides. Molybdenum catalysts, in the form of $\text{Co/Mo/Al}_2\text{O}_3$ wherein this notation represents some form of the metal oxides and the last species is the support, have been used in the H-Coal process. In others, iron catalysts have been used in the form of red mud which is mixed with elemental sulfur. The activity of iron catalysts has generally been regarded as low when compared with that of molybdenum catalysts. However, iron oxide catalysts became highly active for the conversion of coal-related model compounds when used in the presence of H_2S and H_2 . For coal liquefaction in the absence of a heterogeneous catalysts, the use of a mixture of H_2S and H_2 instead of H_2 resulted in an increase in conversion.¹ Because of the interaction of H_2S with Fe_2O_3 ² and the fact that iron is presently the lowest cost transition metal, iron was selected as the basis metal for a new set of heterogeneous catalysts specifically designed for coal liquefaction using the $\text{H}_2\text{S-H}_2$ reducing gas medium.

EXPERIMENTAL

A series of 26 iron oxide catalysts were designed and synthesized. The supported iron catalysts prepared are listed in Table 1. The selection of the supports were based on the following objectives.

1. To clarify the effect of SiO_2 surface area, SiO_2 supports for catalysts 1, 2, and 3 were prepared at different pH's from a Na-free SiO_2 source.
2. To examine the effect caused by use of a different starting material to prepare SiO_2 , catalysts 4, 5, and 6 were prepared from sodium metasilicate at different pH's and can be compared to catalysts 1-3.

3. To examine the effect of the precipitating reagent, catalysts 7 and 8 were prepared from $\text{Si}(\text{OC}_2\text{H}_5)_4$ with H_2SO_4 or NaOH , respectively. Catalysts 7 and 8 results are to be compared with those of catalysts 1 and 3.
4. To examine the effect of basic supports, metal oxides with basic properties were used for the supports of catalysts 9, 10, 11, 12, 13 and 14.
5. To examine the effect of the sulfate ion on the TiO_2 support, it was prepared in the presence of sulfate ions and the resulting catalyst 15 is to be compared with catalyst 14.
6. To examine the effect of additives to Fe/SiO_2 , small amounts of Mo, W, Co, and Ni oxides were added (catalysts 16, 17, 18, and 19) to the Fe_2O_3 on the surface of the catalyst.
7. To examine the effect of the sulfate and nitrate anions on the deposition of the iron layer, catalysts 20 and 21 were prepared.
8. To examine the effect of acidic sites on the Fe/SiO_2 catalyst, sodium- and potassium-poisoned catalysts were prepared (catalysts 22 and 23).
9. To examine the effects of the commercial TiO_2 and SiO_2 supports, catalysts 20 and 24 were prepared to be compared to catalysts 1 and 14, respectively.
10. To examine the effect of activated carbon which possesses an extremely high surface area as the Fe_2O_3 supports, catalyst 26 was prepared to be compared to catalyst 20 (SiO_2) and 24 (TiO_2).
11. To examine the effect of a simple admixture of Fe_2O_3 and SiO_2 , catalyst 28 was prepared to be compared with catalyst 20.
12. To enable comparison to a known commercial hydrogenation catalyst, $\text{Co/Mo/Al}_2\text{O}_3$ (catalyst 29) was included as a part of the series.

The catalysts were subjected to two reactions: hydrocracking of diphenylmethane to toluene and benzene, a model compound for the Ar-C bond cleavage of the coal structure, and hydrocracking of diphenyl ether to phenol and benzene, a model compound for the Ar-O bond cleavage of the coal structure. The reaction conditions for these reactions are summarized in Table 2.

RESULTS AND DISCUSSION

The design of the iron oxide catalysts was based on the following experimental findings.

1. For the hydrocracking of diphenylmethane, the effect of H_2S addition was augmented with iron oxide catalysts.³

2. The promotional effect of the H_2S addition on the catalytic activity varied with the preparative method for iron catalyst.³ Among Fe catalysts supported on SiO_2 , ZrO_2 , and TiO_2 , the Fe/SiO_2 showed the highest activity for the hydrocracking of diphenylmethane.
3. The Fe/TiO_2 catalyst was active not only for hydrocracking of diphenylmethane but also for hydrocracking of diphenyl ether.³

Besides these findings, it has been generally observed that the catalytic behavior of active components vary with the types of supports.

The time dependence of the diphenylmethane conversion is depicted in Figure 1. The value of 20 minutes reaction time was selected for the tubing bomb tests in order to differentiate catalyst effects.

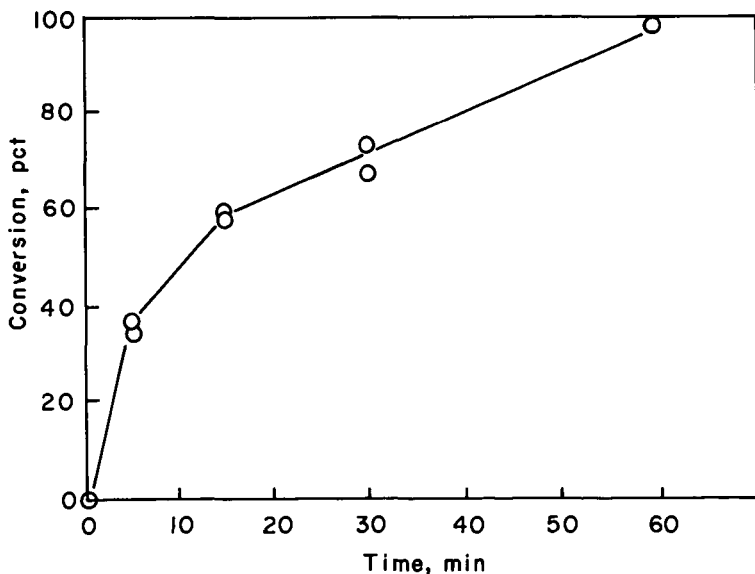


Fig. 1. Time dependence of conversion for hydrocracking of diphenylmethane. Catalyst, $\text{Fe}_2\text{O}_3/\text{SiO}_2$ (catalyst 20); catalyst/reactant, 50 mg/500 mg; reaction temperature, 425°C ; pressure at room temperature, H_2 700 psi, H_2S 100 psi; and reactor, 12-ml capacity.

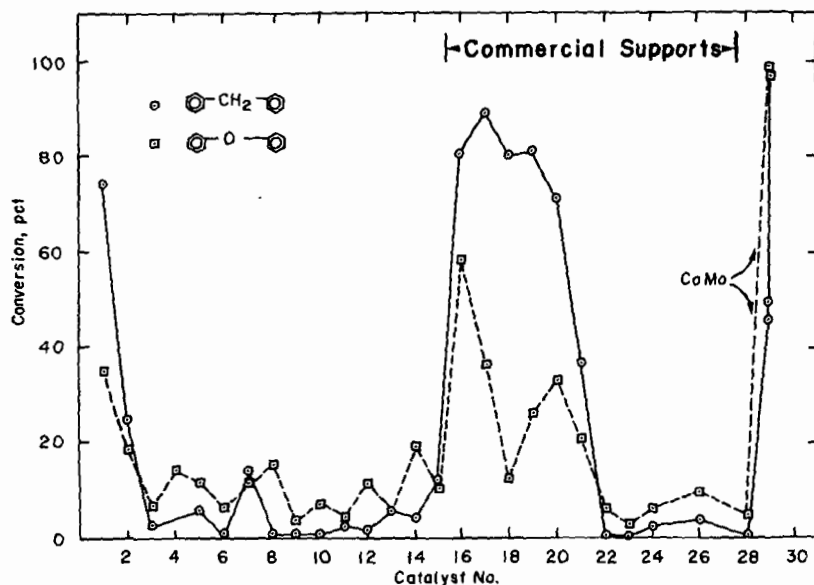


Fig. 2. Conversion of diphenylmethane (—) and diphenylether (---) with various catalysts.

The results of the catalytic reactions are given in Figure 2. For hydrocracking of diphenylmethane, the activities vary with different supports. This indicates that an interaction of Fe_2O_3 with the support occurred. The activity increased with an increase in surface area of support (catalysts 1, 2, and 3). Enhanced catalytic activity was observed by addition of Mo (no. 16), W (no. 17), Co (no. 18), and Ni (no. 19) oxides to the surface Fe_2O_3 as compared to Fe/SiO_2 (no. 20). The introduction of sodium or potassium to Fe/SiO_2 eliminated the catalytic activity (nos. 22 and 23 vs. no. 20). Similar phenomena were observed for catalysts 5, 6, and 8, which possibly contain sodium on the support. The sulfate ion had a negative influence on catalytic activity, cf. catalyst 5 with 2.

For the hydrocracking of diphenyl ether, the catalyst containing Mo and Fe (catalyst 16) was twice as active as the iron oxide catalyst. However, hydrogenated products such as methylcyclopentane and cyclohexane were produced in larger quantities with catalyst 16 than with 20. The Fe/SiO₂ catalyst activity increased with increased surface area of the support (catalysts 1-3), and was poisoned by sodium and potassium ions, cf. catalysts 22 and 23 with 20. The presence of the sulfate ion again retarded the Fe/SiO₂ activity, cf. nos. 15 to 14 and 20 to 21, as it did with diphenylmethane.

In general the catalysts required the presence of hydrogen sulfide⁴ and the commercially supplied sample of silica with its high surface area worked very well. The pH of the silica preparation method proved to be crucial to generating high surface area silica. The catalysts in which the iron oxides were deposited on silica exceeded or equaled the activity of a simple admixture of iron oxide and silica (catalyst 28). The iron oxide catalysts were the better than the commercial hydrogenation-hydrocracking catalyst Co/Mo/Al₂O₃ for the hydrocracking of diphenylmethane (e.g., catalyst 20 vs. 29) but the latter exhibited both hydrocracking and hydrogenation ability. However, the Co/Mo/Al₂O₃ was more active in the conversion of diphenyl ether.

ACKNOWLEDGEMENT

We are grateful for the financial support of the Department of Energy.

REFERENCES

1. (a) Sondreal, E.A.; Wilson, W.G., and Stenberg, V.I., Mechanisms Leading to Process Improvements in Lignite Liquefaction Using CO and H₂S, Fuel, 1982, 61, 926. (b) Baldwin, R.M. and Viciguerra, Fuel, 1982, 62, 498. (c) Abdel-Baset, M. and Ratcliffe, C.T., Preprints Amer. Chem. Soc. Div. Fuel Chem., 1979, 25, 1. (d) Satterfield, C.M. and Model, M., U.S. NTIS, P.B. Rept., 1975, 248101.
2. (a) Ogawa, T.; Stenberg, V.I., and Montano, P.A., Fuel, 1984, in press. (b) Stenberg, V.I.; Tanabe, K.; Ogawa, T.; Sweeny, P. and Hei, R., Iron-Based Catalysts, H₂S and Liquefaction, Preprints, Fuel Division, American Chemical Society, 1983, National Meeting of the American Chemical Society, Washington, D.C.
3. Stenberg, V.I.; Ogawa, T.; Willson, W.G. and Miller, D., Hydrocracking of Diphenylmethane, Fuel, 1982, 62, 1487.

4. (a) Stenberg, V.I.; Srinivas, V.R.; Sweeny, P.; Baltisberger, R.J. and Woolsey, N.F., Dealkylation of N,N-dimethylaniline with Sulphur and Hydrogen Sulphide, Fuel, 1983, 62, 913. (b) Baker, G.G.; Willson, W.G.; Farnum, B.W., and Stenberg, V.I., Homogeneous Catalysis of Lignite Liquefaction with Hydrogen Sulfide, 1983 Spring National AIChE Meeting, Utilizing Texas Lignite, Session 16D, Fuels and Petrochemicals Division, March 27-31, Houston, Texas.

Table 2. Reaction conditions

Reaction	Temperature (°C)	Ratio of reactant/catalyst by wt.	Pressure (psi cold charge)		Reaction time (1 min)
			H ₂ S	H ₂	
Hydrocracking of diphenylmethane	425	10/1	100	700	20
Hydrocracking of diphenyl ether	425	10/1	100	1400	60

Table 1. List of catalysts prepared

Catalyst			Source of Fe ₂ O ₃	Surface area (M ² /g)	Support	
No.	Composition (wt. ratio)	Starting Material			Precipitation Reagent	pH
1	Fe/SiO ₂ (1/9)	Fe(NO ₃) ₃	579	Si(OC ₂ H ₅) ₄	HNO ₃	1
2	Fe/SiO ₂ (1/9)	Fe(NO ₃) ₃	382	Si(OC ₂ H ₅) ₄	HNO ₃	5
3	Fe/SiO ₂ (1/9)	Fe(NO ₃) ₃	28	Si(OC ₂ H ₅) ₄	NH ₄ OH	11
4	Fe/SiO ₂ (1/9)	Fe(NO ₃) ₃	578	Na ₂ SiO ₃	H ₂ SO ₄	1
5	Fe/SiO ₂ (1/9)	Fe(NO ₃) ₃	349	Na ₂ SiO ₃	H ₂ SO ₄	5
6	Fe/SiO ₂ (1/9)	Fe(NO ₃) ₃	318	Na ₂ SiO ₃	H ₂ SO ₄	11
7	Fe/SiO ₂ (1/9)	Fe(NO ₃) ₃	568	Si(OC ₂ H ₅) ₄	H ₂ SO ₄	1
8	Fe/SiO ₂ (1/9)	Fe(NO ₃) ₃	39	Si(OC ₂ H ₅) ₄	NaOH	11
9	Fe/CaO (1/9)	Fe(NO ₃) ₃	1	Ca(OH) ₂	-(calined at 500°C)-	
10	Fe/La ₂ O ₃ (1/9)	Fe(NO ₃) ₃	11	La(NO ₃) ₃	NH ₄ OH	9
11	Fe/ZrO ₂ (1/9)	Fe(NO ₃) ₃	74	ZrOCl ₂	NH ₄ OH	9
12	Fe/ZnO (1/9)	Fe(NO ₃) ₃	5	Zn(NO ₃) ₂	NH ₄ OH	9
13	Fe/SnO ₂ (1/9)	Fe(NO ₃) ₃	28	SnCl ₂	NH ₄ OH	9
14	Fe/TiO ₂ (1/9)	Fe(NO ₃) ₃	41	TiCl ₄	NH ₄ OH	9
15	Fe/TiO ₂ (1/9)	Fe(NO ₃) ₃	56	TiCl ₄ + (NH ₄) ₂ SO ₄	NH ₄ OH	9

Table 1. (continued)

No.	Catalyst		Source of Fe_2O_3	Surface area (M^2/g)	Support		pH
	Composition (wt. ratio)				Starting Material	Precipitation Reagent	
16	Mo/Fe/SiO ₂ (1/9/90)		Fe(NO ₃) ₃ + (NH ₄) ₆ Mo ₇ O ₂₄	477			
17	W/Fe/SiO ₂ (1/9/90)		Fe(NO ₃) ₃ + (NH ₄) ₁₂ W ₁₂ O ₄₂	496	Commercial. Fisher Sci. Co. Catalog No. S-156. 14-20 mesh Lot No. 744571		
18	CoFe/SiO ₂ (1/9/90)		Fe(NO ₃) ₂ + Co(NO ₃) ₃	550			
19	Ni/Fe/SiO ₂ (1/9/90)		Fe(NO ₃) ₃ + Ni(NO ₃) ₂	502			
20	Fe/SiO ₂ (1/9)		Fe(NO ₃) ₃	521			
21	Fe/SiO ₂ (1/9)		Fe ₂ (SO ₄) ₃	344			
22	Na/Fe/SiO ₂ (2/10/90)		Fe(NO ₃) ₃	200			
23	K/Fe/SiO ₂ (2/10/90)		Fe(NO ₃) ₃	205			
24	Fe/TiO ₂ (1/9)		Fe(NO ₃) ₃	11	Commercial, MCB, TX068501, Anatase		
26	Fe/Activated C (1/9)		Fe(NO ₃) ₃	946	Commercial, Union Carbide, LCK, Columbia ^R		
28	Fe ₂ O ₃ + SiO ₂				Commercial JMC, Puratronic + Fisher SiO ₂		
29	Co/Mo/Al ₂ O ₃		(Co, 3%; Mo, 9%)		Harshaw Co-Mo-0401		

The Influence of Mineral Matter on
The Rate of Coal Char Combustion
John H. Pohl
Energy and Environmental Research Corporation
18 Mason
Irvine, California 92714

Introduction

The rate of coal combustion can, in some instances, influence the design of boilers. The intrinsic rate of char combustion is, however, poorly known. Figure 1 shows that estimated intrinsic rate of char combustion can vary by a factor of 10^4 (1). The largest uncertainties are (2):

Property	Factor of Uncertainty
Surface Area	100
Effectiveness Factor	50
Catalysis	100
Crystal Structure	30

Other uncertainties account for less than a factor of four in the estimated intrinsic rate of coal char combustion.

Changes in the apparent rate of char combustion by a factor of 10 can influence the predicted performance of boilers. An example of these changes for a 660 MWe boiler is shown in Table 1. These figures were calculated using a well tested model of boiler performance (3). Increasing the accepted apparent rate constant by a factor of 10 predicts slightly improved performance, but decreasing the accepted rate constant by a factor 10 predicts severely degraded and unacceptable boiler performance.

This paper assesses one of the major uncertainty in estimating intrinsic rate constants, the influence of catalysis of the combustion rate of coal char.

Mineral Matter

Mineral matter contained in the coal could influence the rate of char combustion by blocking part of the coal surface or by catalytically increasing the rate of combustion. Figure 2 shows that the measured rate of combustion of purified nonporous graphics is uncertain by less than a factor of 3. This is a small difference compared to the spread in the overall rate data and suggests that some of the scatter in the measured rates of coal combustion are caused by the mineral matter in the coal.

Blocking of the surface area of coal by ash is unlikely to significantly change the rate of char reaction. Calculations for a coal with 25 percent ash indicate that, except at high levels of burnout, much less than 1 percent of the surface area of char will be blocked with ash particles.

Experiments have shown that small amounts of certain metals can accelerate the rate of char combustion (4,5,6,7,8,9). A number of anions and cations have been shown to accelerate the combustion of carbons at concentrations of 10 to 1000 ppm. Table 2 shows the relative influence on the combustion rate of various salts added as solutions to purified graphite. Relatively small amounts of metals can accelerate the rate of combustion by many orders of magnitude. Metals which appear in coal in significant concentrations which will accelerate the combustion of coal are 1) sodium and 2) calcium. Sodium can be present in coal in concentrations of 100-6000 ppm and calcium at concentrations of 50-12,000 ppm. The in-

fluence of relatively minor levels of sodium on the combustion rate of graphite is shown in Figure 3. Addition of sodium to a concentration of 15 ppm accelerates the reaction by one to two orders of magnitude; higher levels of sodium accelerate the reaction at a lower rate. Calculations show that the sodium must be distributed on nearly the molecular level to be effective. In addition, the influence of catalysis will be less pronounced at the higher temperatures of combustion where noncatalytic combustion proceeds much faster. No data exists at these higher temperatures. The available data indicates that combustion of carbon is accelerated by up to two orders of magnitude by levels of sodium normally present in coals at temperatures only slightly lower than combustion temperatures.

Summary

Minerals present in coal can accelerate the rate of char combustion by as much as a factor of 100. Molecularly attached Sodium and Calcium Compounds are likely to increase the char combustion substantially at low temperatures. However, information is not available and work should be undertaken to assess the acceleration of char combustion by minerals at the temperatures of combustion.

References

- (1) Smith, I. W. "The Intrinsic Reactivity of Carbons to Oxygen." *Fuel*, Vol. 57, 1978, pp. 409-414.
- (2) Pohl, J. H., R. W. Richter, M. P. Heap and B. A. Folsom, "Influence of Coal Char Combustion Rate on Power Plant Performance," Special Report Prepared Under EPRI Contract EPRI RP 2256-1, 1983.
- (3) Pohl, J. H., W. Richter, R. Payne, K. Fujimura, T. C. Derbidge, "Coal Particle Size and the Performance of Coal-Water Slurries," Presented at ASME Winter Annual Meeting, New Orleans, Louisiana, December, 1984.
- (4) Smith, I. W. and R. J. Tyler, "Internal Burning of Pulverized Semi-Anthracite: The Relation Between Particle Structure and Reactivity." *Fuel*, Vol. 51, 1972, pp. 312-321.
- (5) Essenhigh, R. H. "Fundamentals of Coal Combustion." In M.A. Elliott, ed, Chemistry of Coal Utilization, Second Supplementary Volume. John Wiley & Sons, New York, 1981, pp. 1153-1312.
- (6) Patai, S., E. Hoffman, and L. Rajbenback. "The Oxidation of Carbon by Air I. Catalysis in the Oxidation of Carbon Black by Air." *J. Appl. Chem.*, Vol. 2, 1952, pp. 306-310.
- (7) Lang, F. M., P. Magnier, and S. May. "Etude de L'Oxydation des Carbones par et L'Anhydride Carbonique en Fonction de Leur Texture et d Leur Etat de Purete." 5th Proc. Conf. on Carbon, Vol. 1, 1961, pp. 171-191.
- (8) Heuchamps, C. and X. Duval. "Effet des Catalyseurs sur Les Caracteristiques Cinetiques de la Combustion du Graphite." *Carbon*, Vol. 4, 1966, pp. 243-253.
- (9) A Mariglio, H. and X. Duval. "Etude de la Combustion Catalytique du Graphite." *Carbon*, Vol. 4, 1966, pp. 323-332.

TABLE 1 INFLUENCE OF COMBUSTION RATE ON POWER PLANT PERFORMANCE
FOR A 660 MW_e COAL-FIRED BOILER

Kinetic Constant, g/cm ² s Atmosphere	Furnace Efficiencies (%)	Mean Furnace Exit Temp (°F)	Mean Heat Flux Btu/ft ² ·hr	Maximum Heat Flux Btu/ft ² ·hr	Position of Maximum Heat Flux (ft)	Maximum Flame Temp (°F)	Percent Unburned Fixed Carbon	Percent Combustibles In Ash (%)
40e ^{-21,450/RT} ^a	43.1	2190	39,000	61,500	116	2650	0.66	5.97
400e ^{-21,450/RT}	44.2	2160	40,300	62,800	102	2670	0.04	0.38
4e ^{-21,450/RT}	33.6	2200	26,000	64,700	224 ^b	2350	32.17	69.03

^aNormal Value

^bBoiler Exit Plane

TABLE 2 INFLUENCE OF METALS ON THE RATE OF
GRAPHITE COMBUSTION (9)

Metal	ppm	Relative Reactivity
Be	120	1
B	80	1
Al	70	3
Ca	120	4
Mg	120	6
Sr	120	8
Ni	150	32
Cd	120	90
Ba	120	100
Na	120	230
Au	120	240
V	120	340
Cu	120	500
Ag	120	1,340
Cs	120	64,000
Mn	80	86,000
Pb	130	470,000

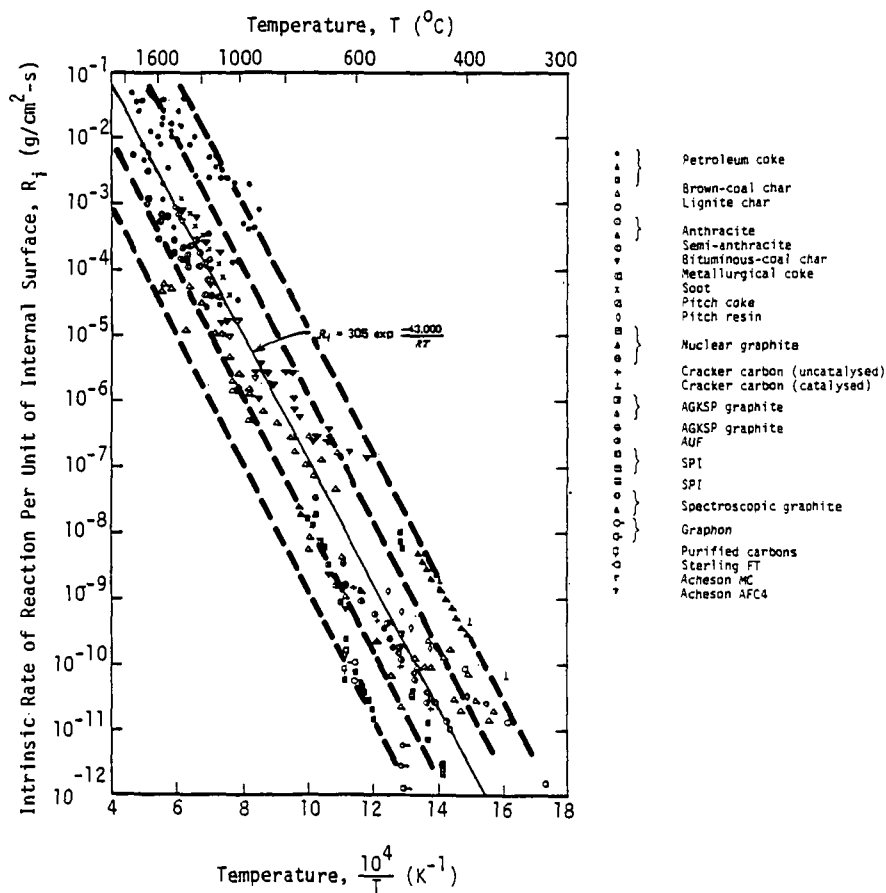


Figure 1. Intrinsic Rate of Reaction of Chars (1)

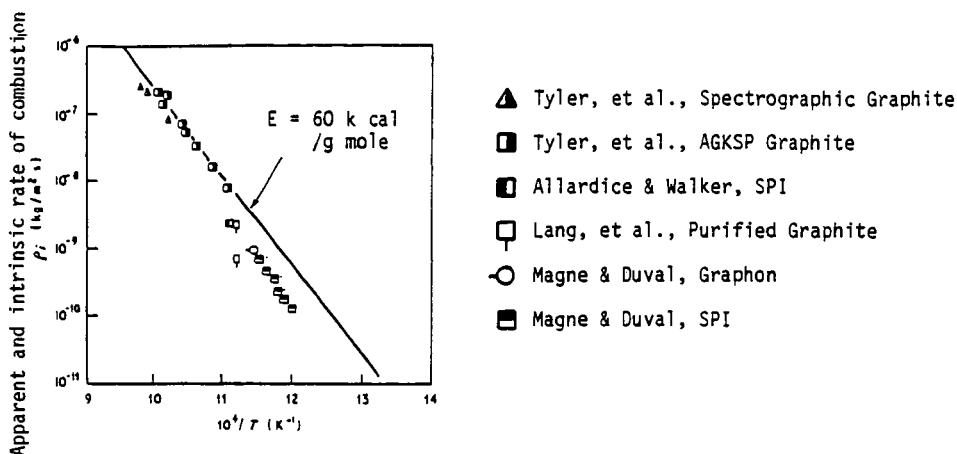


Figure 2. Combustion Rates of Highly Purified Graphite (4)

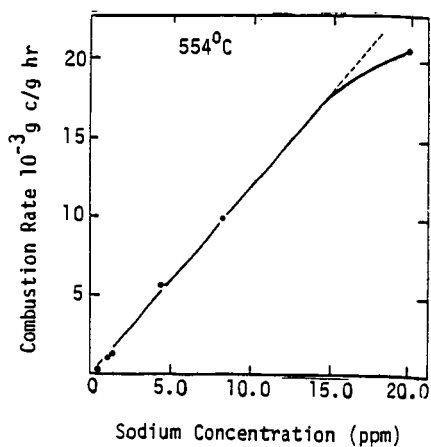


Figure 3: Catalysis of Graphite Combustion by Sodium (9)

BEHAVIOR OF MINERAL MATTER DURING COAL BENEFICIATION

Harold L. Lovell

The Pennsylvania State University
Department of Mineral Engineering
University Park, Pennsylvania 16802

Each coal beneficiation unit operation responds to the physical and chemical properties of its feed. The response is as a "collage" of the individual particles but specifically as the frequency distribution of the component particle properties. These particle responses are not totally independent with particle property-process parameter interactions, but are also significantly controlled by the overall distribution of particle properties. Diligence is appropriately applied to establish the "collage" distribution by certain particle properties of the plant feed. This distribution provides the design bases for each unit operation in the flow sheet - including its capacity, flow rate, and unit loading: thus ultimately defining the separational performance, efficiency, and unit costs. Each unit operation should be sized and operated such that its optimum performance is well within the sensitivity range of its feed property distribution. The concern that the feed distributions may, at times, exceed the sensitivity range for some unit operation within the system, is normally related to in situ coal variability, which can be extreme. The concern may extend to coal feeds from different seams and/or paleo-geological origin, mining system, or handling-storage system. Unfortunately, seldom are the concerns extensive and rarely are the feed characterizations detailed to each downstream operation.

The plant feed characterization usually is limited to particle size distribution and, if detailed, will include a particle gravity distribution for several size groupings greater than 28 or 16 mesh (washability). There is no generally accepted range for either the size or density groupings. The characterization of the individual particle fractions are usually limited to moisture, high temperature ash, and total sulfur content. In some unusual instances the low temperature ash and sulfide sulfur content may be determined. Pragmatism, procedures, and economics prevent the direct determination of minerals whose concentrations will be modified in the process. These levels are expressed in terms of ash content. If there is any characterization of the individual macerals or minerals, they are evaluated on the basis of the "total-composite" feed sample. Should flotation processes be anticipated, some "laboratory floatability" studies (1), may be carried out on some minus 16 or 28 mesh or other sized fraction. The origin of the particular fraction thus tested, seldom relates to that which will exist within the plant flow sheet. Feed hardness or friability tests (as Hardgrove Grindability Index, Drop-Shatter, etc.) may also be determined on the composite feed sample. If any comminution evaluations are made for the particular feed coal in the course of selecting a particular comminution device, they are usually made on a sample purported to be representative of the plant feed. Attempts to evaluate variations of particle strength or stability, maceral, mineral, or elemental composition, have been limited to research characterizations, as those reported by the author (2). We are almost totally devoid of pragmatic techniques to establish the particle sizes or volumes of individual components within a given individual coal particle (Richardson and Lovell (3)).

These observations can but lead to the conclusion that, in contrast, to typical unit operations in chemical engineering, the coal processing engineer assumes a feed to each unit operation within the plant system based upon the defined plant feed. Further, it is assumed that the collage of particles entering the plant as feed DOES NOT CHANGE in passing through the processing system and that the same number of particles 2 by 1-inch having densities between 1.40 and 1.45 gm/cc (or any other fraction) leaves the plant as enters! We know that this is not

correct even if we ignore the comminution operations within the plant designed to make such changes!

The composition of any individual coal beneficiation feed particle ranges from a nearly uniform metamorphized, phyto component through an almost infinite mixture series with macerals-minerals to an opposite end member as a nearly uniform mineral component. The behavior of a beneficiation feed during processing is determined by this almost limitless (and changing) distribution of individual particle compositions whose responses to process parameters are established by the particle properties as size, shape, density, hardness, porosity, and gas-liquid-solid interfaces. The particle responses establishes its direction and rate of movement toward one of the process product ports.

With coals as sedimentary rocks of paleophyto origin, their inorganic contents incorporate those components which were part of the original phyto system and associated substances, as well as those that have been introduced through all the subsequent geologic events. Accordingly, the mineral components found in coals reflect the nature of the originating plant systems, their environment, degree of water existing (whether of fresh or marine water character), oxidation-reduction conditions, temperatures, and pressures as well as those conditions to which the coal-forming strata have been subject during all the ensuing geologic epochs, including past and current circulating ground waters. Thus the observed complexity of the resulting physical characteristics is to be expected.

The minerals found in United States coals continue to be studied with the availability of improved instrumental procedures as X-ray diffraction, infrared absorption, and scanning electron microscopy beyond the traditional optical and chemical mineralogical techniques as applied to thin sections, polished pellets, and isolated particles. The minerals may be grouped into the silicates (kaolinite, illite, monmorillonite, and chlorite); the oxides (quartz, chalcedony, hematite); the sulfides (pyrite, marcasite, and sphalerite); the sulfates (jarosite, gypsum, barite, and numerous iron sulfate minerals); the carbonates (ankerite, calcite, dolomite, and siderite); and numerous accessory minerals as apatite, phosphorite, zircon, rutile, chlorides, nitrates, and trace minerals).

The greatest interest in mineral occurrences in coal particles for processing engineers relates to their potential liberation as an essential first step for their physical removal. Further the concern relates to the mineral behavior in each of the unit operations within the preparation plant and environmental implications within the preparation operations, for utilization of the clean coal product and the disposal of the refuse materials. The greatest attention has been given to the former interests, especially as applied to the liberation of pyrite in efforts to achieve the greatest possible sulfur reduction during processing.

Specific Responses of Coal Mineral Components During Processing

The "collage" of particles entering a coal processing plant are subject to a series of unit operations designed to achieve the desired level of quality improvement. The development of the initial set of particles is determined by the mining and preprocessing storage and handling systems. Undoubtedly these operations introduces stresses within the coal particles that lead to subsequent fracture failures. Any potential control of the nature of this particle set is usually extremely limited - being determined by production and economic factors. Situations which lead to oxidation, decrepitation, and absorption of excessive levels of moisture may be modified. The introduction of moisture prior to processing probably enhances clay swelling, tends to increase the amount of mineral fines (usually clays) into the plant stream, and may enhance localized heating, swelling, and oxidation. Initiation of dispersion of clays may begin here. Uncontrolled comminution during the handling and storage due to dropping from stackers, compaction by graders, etc. tend to create fines and probably selectively favors reduction of

the softer particles, especially certain clays. Other handling steps as particle movement through pumps, jigs, etc. tend to accent the production of fines. The oxidation of coal and temperature increases may favor the production of water soluble salts leading to acid plant waters and potential corrosion.

Primary crushing which usually involves breakers or single roll crushers may be preceded by a scalping operation to remove large particles of hard shales and sandstones. Such operations though not rejecting large amounts of refuse, do prevent wear, save energy, and prevent the introduction of additional refuse fines into the plant feed. The primary comminution devices usually are designed to control top size rather than achieve particle liberation, as such, they offer an opportunity to minimize fines production and show some selectivity toward the large, harder particles as shales and sandstones. Pre operational testing of comminution devices should consider the production of minimal amount of mineral fines. In coal processing systems where classifying rotating mills may be used, the selective build up of harder components within the mill can affect system performance.

In coarse coal sorting operations, as jigs and heavy media vessels, the softer minerals will tend to comminute due to attritional actions of particle movements and result in further dispersion into the plant circulating water system. In jigs, the production of mineral fines may be desirable to enhance hindered settling effects. In the Haldex heavy media system (4) and water only cyclones, the presence of mineral fines are essential to serve as an autogeneous heavy media system. Operational care must be taken to prevent the build up of unacceptable levels of fines leading to unacceptable fluid viscosity levels. Although quartz, clays, and other very fine mineral particles enhance these conditions, several type of clays, notably kaolinite and montmorillonite (especially sodium), are especially responsive. Suspended clay levels above five percent in such systems are most undesirable and may limit control of density in magnetite heavy media systems. The viscosity effect increases with decreasing particle size and with spherical shape which enhances settling rates. These concerns can also become critical in coal-water transport systems.

In fine coal sorting systems, heavy media cyclones, water only cyclones, tables and spirals the density and viscosity responses of suspensions are even more critical. In froth flotation the presence of clay fines is undesirable and usually require a desliming step ahead of flotation if their concentration becomes excessive.

It is in the water circuit that the build up of fines, especially clays must be controlled. The responses become evident in dewatering devices as centrifuges and filters. In the latter case, clays may enhance blinding resulting in unacceptable water contents of the filter cake, thin watery cakes, and unacceptable performance. Difficulties in the filtration of refuse fines has lead recently to the introduction of expensive processes as pressure and belt filters to meet environmental standards. In thickeners, excessive clay fines may reduce settling rates, minimize the formation of desirable underflow slurry densities, and lead to plant failure. It is in the dewatering stages and water circuit, as processes at the end of the flow sheet that these responses become acute. Although the use of one or more polymeric flocculants can usually control these situations, unexpected changes in plant feeds may require feed rate reductions or plant shut down.

Recent environmental regulations which essentially require closed water circuits make the problems of mineral fines buildup especially severe. Similar difficulties are associated with the disposal of refuse fines.

These examples describe some of the more prominent responses of mineral components in coal processing operations. Control of these problems can be achieved with better detection and analytical systems to identify the problems.

LITERATURE CITED

- 1a). Cavallaro, J. A. and A. W. Deurbrouck. Froth Flotation Washability Data of Various Appalachian Coals Using The Time Release Analysis Technique. Report of Investigations 6652. U. S. Bureau of Mines. 1965.
- 1b). Alderman, J. K. Evaluating Flotation Washability Data. Coal Mining and Processing. pp 70-73. 1981.
- 2). Lovell, Harold L. The Characteristics of American Coals. Final Report. U.S. Department of Energy. FE-2030-11. 1976.
- 3a). Richardson, D. and H. L. Lovell. Pyrite Liberation - Key to Sulfur Reduction During Beneficiation. Proceedings of Coal Conference and Expo V. Symposium on Coal Preparation and Utilization. October 1979.
- 3b). Richardson, D. L. A Study of the Occurrence of Pyrite in Coal and Its Relationship to Liberation in Coal Preparation and Mine Drainage Formation. M. S. Thesis in Mining Engineering. 1979. The Pennsylvania State University.
- 4). Anon. Investigation of the Haldex (Simdex) Process for Beneficiating Coal Refuse: Hungarian Practice - 1969. Special Report 80. The Coal Research Section. The Pennsylvania State University. University Park, Pennsylvania.

MINERALOGICAL CHARACTERISTICS OF COAL IN VARIOUS CLEANING CIRCUITS

Richard B. Muter and William F. Lawrence

Coal Research Bureau
College of Mineral and Energy Resources
West Virginia University, P. O. Box 6070
Morgantown, West Virginia 26506-6070

The optimum utilization of our national coal resources while still affording the protection of our environment can not be achieved without beneficiation. However, our most common ways of measuring the success or failure of beneficiation processes are not truly representative and may well be responsible for unnecessary economic and energy resource losses. This is the result of several factors, the most important of which are:

1. The analyses which we perform do not really measure the materials which are being beneficiated. Rather, they are indirect measurements.

One of the most common quality criteria is that of ash. However, we do not remove ash from coal during beneficiation processes; we really change distribution of the minerals or rock consist of the coal material, and thereby change the "ash" as measured. Also, we do not remove sulfur as such, we remove sulfur containing minerals such as pyrite, marcasite, etc.

2. Mineral properties, not elemental properties, are what effect combustion and beneficiation processes up until the time when the minerals are broken down; yet it is the elemental composition which we seem to be most concerned about.

Seemingly obvious, this point is often overlooked in all stages of beneficiation and utilization until major problems occur. Two coals may have the same SiO_2 content when analyzed, but the physical properties of quartz (sand) are quite different from those of clays (illite, kaolinite, etc.). Different minerals, even of similar compositions, require different cleaning processes and have different effects upon process equipment.

3. Common analytical methods, because they destroy the mineralogical structures, give the impression that coals are to a large extent homogeneous and consistent in mineral content. This impression is markedly false and often leads to major false assumptions.

The two most obvious, i.e. most studied, examples of this error are the forms of sulfur and the siliceous contents of coal. Conventional analyses will give the same silica content for a carbonaceous shale as for a calcareous one, but they will react quite differently during beneficiation and combustion. Total sulfur is the most common analysis for this element of environmental concern, but occasionally a "sulfur breakdown" analysis will be performed. Although knowing whether the sulfur is "pyritic", "organic" or "sulfate" is helpful; it is not enough. Knowing that the sulfur is predominately "pyritic" is insufficient, we must know other factors such as size, distribution within the coal matrix, and whether the particles are attached to the coal material as well as the degree of liberation. All these factors affect the beneficiation processes.

Physical beneficiation is generally considered to be a "mature" subject in that most changes which have occurred over the past few years have been in terms of equipment design or the order in which particular operations are performed. These

operations are generally based on physical characteristics such as specific gravity or hardness and brittleness difference between the minerals of interest and the coaly materials. However, these processes are still measured on element reduction bases rather than one of specific mineral concentration or reduction.

Froth flotation, considered a higher lever of sophistication in beneficiation, is also based on differences in mineralogical properties. Based upon particle surface characteristics it tends to be more chemical than physical in nature. Tendencies of particles to be hydrophilic or hydrophobic in nature are enhanced through the use of chemical additives and then a physical separation is made.

The next level of sophistication in coal beneficiation will most likely be that of chemical coal cleaning. It will also be the most costly level, especially when the large tonnage amounts involved in coal utilization are considered. In order to keep these costs to a minimum, while still attaining desired results, process operations will have to be carefully planned and closely monitored. Process designers will have to know exactly what minerals will be involved and in what amounts. Acquiring a better knowledge of what minerals occur in specific coals and how they are affected by less expensive physical beneficiation is an obvious first step.

As part of a much larger effort by the U. S. Department of Energy, the Coal Research Bureau of the College of Mineral and Energy Resources at West Virginia University has been characterizing the mineralogy and petrography of three major bituminous coals in an effort to determine whether the mineralogical associations can be closely followed through common physical beneficiation processes. A listing of the minerals commonly present in these coals is provided in Table 1. Also included are the chemical formulas with the elements of most interest to the beneficiation plant operator underlined. This listing is based upon bituminous coals as most sub-bituminous coals and lignites meet current emission specifications and are not cleaned to a large extent.

Mineralogical analyses were performed using a number of different techniques including x-ray powder diffraction analysis, infrared spectroscopy, normative calculations, and optical petrography. All met with limited success although each had limitations as to the number of minerals which could be identified or accurately quantified. X-ray powder diffraction proved to be the most versatile as to accuracy, ease of implementation and number of different minerals identified versus misidentifications. Mineralogical sink-float (washability) curves were prepared (Figure 1) and compared with actual equipment operations (Table 2). It can be seen, that their predicted value varied for specific minerals and specific processes. However, the indication is that further effort in this area is justified and that a strong potential exists for tracing of specific mineral assemblages through the beneficiation processes and that these processes may be more efficiently designed and monitored. Such monitoring in the future could lead to multi-stream, multi-product plants with only a minimum amount of coal being subjected to more intensive cleaning processes. With careful planning, such a plant could provide a maximum fuel yield while providing maximum environmental protection at a minimum cost.

TABLE 1

MINERALS OF THE DISTRICT #3 PITTSBURGH COAL.
 SYMBOLS INDICATE ANALYTICAL PROCEDURES AVAILABLE FOR EACH
 MINERAL AND WHETHER THE PROCEDURE CAN BE USED FOR
 QUANTITATIVE, SEMIQUANTITATIVE, OR QUALITATIVE MINERAL ANALYSIS.

	<i>X-ray Powder Diffraction</i>	<i>Infrared Spectroscopy</i>	<i>Normative Calculations</i>	<i>Optical Petrography</i>	<i>Scanning Electron Microscopy</i>	<i>Formulae</i>
ILLITE	S		Q	S	I	variable
KAOLINITE	Q	Q	Q	S	I	$\text{Al}_4(\text{Si}_4\text{O}_{10})(\text{OH})_8$
QUARTZ	Q		Q	S	I	SiO_2
FELDSPARS	S				I	variable
MUSCOVITE				S	I	$\text{KA1}_4(\text{AlSi}_3\text{O}_{10})(\text{OH})_2$
CARBONATES		Q		S		variable
CALCITE	Q	Q	S	I	I	CaCO_3
DOLOMITE	Q		S	I	I	$\text{CaMg}(\text{CO}_3)_2$
BASSANITE	S				I	$\text{CaSO}_4 \cdot \frac{1}{2}\text{H}_2\text{O}$
GYPSUM		I		I		$\text{CaSO}_4 \cdot 2\text{H}_2\text{O}$
IRON DISULFIDES	Q		Q	S	I	FeS_2
PYRITE				S		FeS_2
MARCASITE				S		FeS_2
APATITE	S				I	$\text{Ca}_5(\text{F,Cl,OH})(\text{PO}_4)_3$
HEMATITE				S		Fe_2O_3
RUTILE				S	I	TiO_2

Q = Quantitative determinations ($\pm 10\%$)

S = Semiquantitative determinations ($\pm 10\text{--}30\%$)

I = Identification only possible

TABLE 2

Mineral weights in the products of the commercial preparation plant and the pilot plant scale coal cleaning equipment. Actual mineral weights are compared to weights predicted from the mineral washability curves of the Pittsburgh coal.

	Deister Table 3/16" X 100M		"Baum" J1g 1" X 3/16"		WEMCO HMS Drum Separator 2" X 10M		Heavy Media Cyclone 10 X 100M	
	Actual	Curve	Actual	Curve	Actual	Curve	Actual	Curve
YIELD	85%	83%	71%	93%	89%	85%	94%	95%
S.G.	?	1.35	?	>1.80	?	1.38	?	>1.80
ASH	5.9%	5.9%	7.7%	7.7%	6.2%	6.2%	8.4%	8.4%
M.M.	126#	120#	133#	185#	138#	135#	183#	210#
ILLITE	16#	29#	28#	46#	55#	31#	6#	58#
KAOLINITE	34#	30#	29#	38#	39#	31#	32#	41#
QUARTZ	21#	20#	25#	30#	23#	22#	26#	34#
CALCITE	13#	4#	12#	8#	10#	4#	9#	12#
PYRITE	30#	23#	28#	36#	0#	26#	36#	44#

= pounds of the mineral in the cleaned coal when one short tone of feed coal is cleaned.

M.M. = mineral matter.

S.G. = specific gravity of the washing medium.

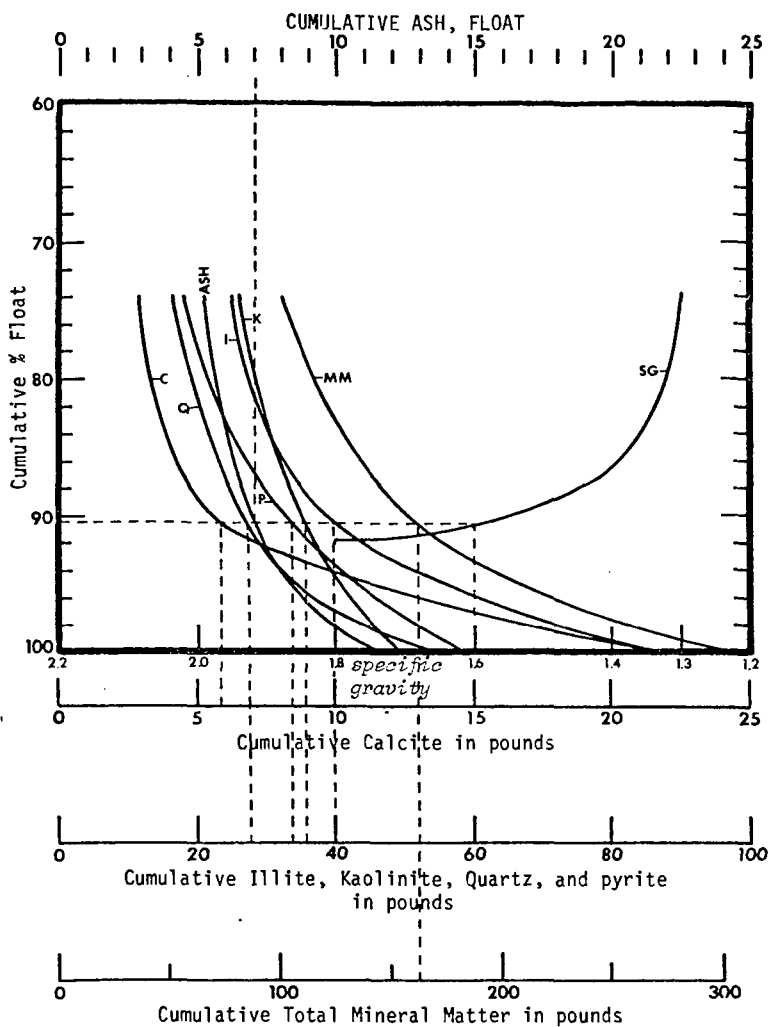


FIGURE 1

Washability curves for the minerals in the District 3 Pittsburgh coal (See the footnote on the next page for explanations of this diagram).

Automated Image Analysis of Mineral Matter
in Raw and Supercleaned Coals

Warren E. Straszheim and Richard Markuszewski

Ames Laboratory¹ and Department of Engineering Science and Mechanics
Iowa State University, Ames, IA 50011

The advent of highly sophisticated and automated microscopic techniques, together with powerful mini- and microcomputers, makes it now possible to characterize the mineral components of coal in-situ. Combined automated image analysis (AIA) and scanning electron microscopy (SEM) allows detailed characterization of minerals in coal for size, shape, composition, and relation to the coal matrix. For a statistically significant number of particles, both size distribution and volume fraction can be estimated and used to characterize independently the mineral matter content. The corresponding chemical analyses for the bulk coal samples, provided by more conventional techniques, may be related to the AIA-SEM data for comparison.

Conventional analytical techniques such as x-ray diffraction (XRD) and Fourier transform infrared spectroscopy (FTIR) can identify the mineral phases present in coal and can sometimes provide an estimation of the amount present. However, such techniques use bulk samples; they are limited to calculating only an "average" cleaning effectiveness and do not offer information on the size distribution of those mineral phases identified. On the other hand, AIA-SEM permits cleaning effectiveness to be evaluated with respect to both particle size and mineral phase. Thus, problems associated with removing a particle size or chemical class of particles can be detected and addressed. Such information is important for any coal preparation process, especially since it relates grinding and liberation of mineral particles to washability tests (1).

To evaluate coal particles produced by fine grinding for washability tests, the AIA-SEM technique provides information on the elemental distribution among the various mineral phases. The minerals are classified using a chemistry definition file based on the relative amounts of elements present as determined by energy-dispersive x-ray spectroscopy.

The AIA-SEM technique has been used in Ames Laboratory to study the effect of grinding on washability of fine coal. Several series of coals have been characterized by this technique in the past two years, thus demonstrating its usefulness. In this work, the AIA-SEM technique was applied to determine the coal mineral character before and after cleaning.

¹Ames Laboratory is operated for the U. S. Department of Energy by Iowa State University under Contract No. W-7405-Eng-82.

EXPERIMENTAL

Sample Description and Preparation

The analyses were performed on two bituminous coals being tested for washability by conventional means. The coals were from the Illinois No. 6 seam, Randolph county, Illinois, and from the Pittsburgh No. 8 seam, Lewis county, West Virginia. The coals were ground to a typical power plant grind (i.e., 70-80% less than 200 mesh or 75 μm). The coals were then supercleaned by float-sink separation (using halogenated hydrocarbons) at 1.3 specific gravity to produce a very low-ash, clean coal fraction (ash content <3%). The raw and clean coal fractions were analyzed for moisture, ash, and sulfur forms by the usual ASTM procedures (see Table 1).

Table 1. ASTM analyses of raw and supercleaned coal samples for moisture, ash, forms of sulfur, and mineral matter^a.

	Illinois No. 6		Pittsburgh No. 8	
	Raw	Clean	Raw	Clean
Moisture	16.90	1.95	1.97	1.12
Ash	16.11	2.61	6.75	2.97
Total S	5.10	2.54	3.17	1.82
Pyritic S	2.37	0.22	1.35	0.03
Sulfate S	0.36	0.04	0.41	0.12
Organic S	2.36	2.27	1.42	1.67
Mineral Matter ^b	19.32	3.05	8.26	3.37

^a Values are expressed as wt. % on a dry basis, except for moisture.

^b Mineral matter = $1.13 \times \text{ash} + 0.47 \times (\text{pyritic sulfur})$.

The raw and clean coal samples were prepared for AIA-SEM analyses by casting two grams of the sample with an epoxy resin into molds one inch in diameter. The hardened pellets were polished to reveal a cross section, with final polishing being done with 0.3 μm alumina powder. The pellets were coated with approximately 500 angstroms of carbon to render sample surfaces electrically conductive for examination in the electron microscope.

AIA-SEM Analysis

The AIA-SEM system consists of a JEOL (Japan Electron Optics Laboratory) model JSM-U3 scanning electron microscope, a LeMont Scientific B-10 image analyzer, and a Tracor Northern TN-2000 energy-dispersive x-ray analyzer. The image analyzer is a software-based system with associated electronics for SEM beam control, image amplification, and thresholding. The software base for image analysis allows the appropriate analysis algorithm to be selected for the particular sample and image conditions encountered. Particle extents are determined from the

points at which horizontal scans cross a feature, and particle outline is reconstructed from these adjacent chords of a particle. Once the outline has been determined, the x-ray data are collected from the center of the particles.

Samples were analyzed in the SEM using 25 kV beam voltage, 1-2 nA sample currents, 300x magnification, and backscattered electron imaging. A point density of 1024 pixels across the screen was used to provide $\pm 10\%$ accuracy on measurements as small as 1% of the field of view. X-ray data were collected for four seconds per particle at a typical counting rate of 1000 counts per second. Regions of interest were set to monitor the intensities of 30 elements; however, only these 11 elements occurred with significant frequency: Na, Mg, Al, Si, P, S, Cl, K, Ca, Ti, and Fe. Approximately 4000 particles were analyzed per sample at a rate of 200 particles per hour.

Data Handling

Based on the relative amounts of the elements present, the particles were classified into one of nine mineral categories according to the definitions given in Table 2. The categories derived from previously established guidelines (2,3) and included the common coal minerals pyrite, quartz, calcite, siderite, kaolinite, and illite. Several other minerals were identified, but they occurred in such small amounts that they were classified together into one common category titled "MINORS". This category included the minerals gypsum, dolomite,

Table 2. Chemical limits for mineral phase definitions

Mineral Phase	Chemical Definition in % Range ^a	Specific Gravity
PYRITE	S 10-80; Fe 10-70	5.00
KAOLINITE	Al 15-80; Si 15-85; Al/Si 0.33-3.0	2.65
ILLITE	Al 10-50; Si 20-85; Mg 0-15; Ca 0-35; Fe 0-40; Ti 0-15	2.75
QUARTZ	Si 65-100	2.65
CALCITE	Ca 70-100	2.80
SIDERITE	Fe 70-100; Mn 0-30; Ni 0-30	5.00
MINORS (includes the following categories)		
GYPSUM	S 10-80; Ca 10-70	2.30
DOLOMITE	Mg 10-60; Ca 60-100	2.90
RUTILE	Ti 70-100	4.50
ALUMINA	Al 65-100	4.00
APATITE	P 15-40; Ca 30-100	3.20
SILICATES	Si 20-80	2.70
MISCELLANEOUS	(no restrictions, all particles accepted)	2.00

^aSpecifications may be given for the amount of other elements that are allowed to be present. Such specifications allow minor amounts of elements not specifically listed in the class definition to be present, but they place an upper limit on the allowable amount.

rutile, alumina, and apatite. In addition, several other categories were defined to accommodate particles not corresponding to any of the above definitions. For example, a "SILICATES" category was defined to include particles with significant silicon content, yet with the balance of the elements in such proportions that the particle would not fit into either the quartz, kaolinite, or illite categories. A "MISCELLANEOUS" category was provided to include those particles whose composition did not allow them to fall into any of the above-mentioned categories. Further descriptions of the instrumental, statistical, classifying, and processing techniques will be given in another publication being readied for submission.

The AIA procedures classified mineral particles into both size and chemical classes. Area-equivalent diameter was used as the size parameter for data presentation. This measurement is the diameter of a circle with the same area as that measured for the mineral particle. Area-equivalent diameter was used instead of a simple length or width measurement because the outline of mineral particles in coal is often complex enough to render such measurements meaningless. The equivalent diameter measurement allows particles to be classified by the area of the particle and yet reported in terms of a linear dimension. Using available literature values for the specific gravity of the individual minerals, the data were then expressed as the weight fraction of the mineral matter within a given mineral/size category. The weight fraction data were then normalized using the mineral matter content to present the mineralogical estimates on a dry coal basis. Such a presentation provides a common base for comparing the coals before and after processing.

The data are presented in Tables 3a and 3b for the raw and clean Illinois coal respectively, and in Tables 4a and 4b for the raw and clean Pittsburgh coal, respectively. Percent removal of the mineral matter calculated for each mineral phase and size category for both coal samples is presented in Tables 3c and 4c.

RESULTS AND DISCUSSION

Conventional analytical data, obtained by ASTM procedures and presented in Table 1, indicate that the float-sink separation achieved an 84% and a 56% removal of ash from the Illinois and Pittsburgh coals, respectively, with corresponding decreases in total and pyritic sulfur of 50 and 91% and of 43 and 97%, respectively. If expressed as a reduction in the total mineral matter content, based on using a modified Parr formula (4), the corresponding values are 84% for the Illinois coal and 59% for the Pittsburgh coal.

The AIA data for the Illinois coal (Tables 3a-c) and for the Pittsburgh coal (Tables 4a-c) are much more interesting. Results for the raw Illinois coal show that pyrite, quartz, and two clays (kaolinite and illite in approximately equal proportions) make up the bulk (86%) of the mineral matter. The mineral phases are rather uniformly distributed over the entire range of particle size from less than 4 μm to more than 36 μm in diameter.

Table 3a. AIA results for Illinois No. 6 raw coal (200 x 0 mesh), expressed as weight percent of dry coal.

Mineral Phase	Particle Size						Totals
	<4 μm	<7 μm	<12 μm	<21 μm	<36 μm	>36 μm	
Pyrite	0.71	0.77	1.16	1.44	1.62	1.27	6.97
Kaolinite	0.57	0.67	0.65	0.38	0.36	0.20	2.83
Illite	0.32	0.38	0.42	0.42	0.45	0.47	2.47
Quartz	0.84	0.90	1.02	0.71	0.35	0.61	4.43
Siderite	0.10	0.10	0.08	0.14	0.00	0.00	0.42
Calcite	0.04	0.04	0.14	0.11	0.10	0.41	0.83
Silicates	0.23	0.16	0.17	0.10	0.03	0.19	0.89
Minors	0.02	0.03	0.05	0.01	0.04	0.00	0.15
Miscellaneous	0.05	0.06	0.11	0.03	0.07	0.00	0.32
Totals	2.87	3.12	3.79	3.36	3.02	3.15	19.32

Table 3b. AIA results for Illinois No. 6 coal floated at 1.3 specific gravity, as expressed as weight percent of dry coal.

Mineral Phase	Particle Size						Totals
	<4 μm	<7 μm	<12 μm	<21 μm	<36 μm	>36 μm	
Pyrite	0.19	0.28	0.42	0.21	0.07	0.00	1.17
Kaolinite	0.10	0.16	0.09	0.02	0.03	0.00	0.40
Illite	0.12	0.12	0.11	0.07	0.00	0.00	0.42
Quartz	0.16	0.19	0.18	0.09	0.01	0.00	0.63
Siderite	0.02	0.01	0.01	0.02	0.02	0.00	0.08
Calcite	0.00	0.00	0.00	0.00	0.00	0.00	0.01
Silicates	0.08	0.05	0.03	0.02	0.02	0.00	0.20
Minors	0.02	0.02	0.01	0.00	0.00	0.00	0.04
Miscellaneous	0.04	0.03	0.02	0.00	0.00	0.00	0.08
Totals	0.72	0.86	0.87	0.44	0.16	0.00	3.05

Table 3c. Use of AIA results to estimate percent removal of mineral matter from Illinois No. 6 coal. The numbers are based on values in Tables 3a and 3b before they were rounded off.

Mineral Phase	Particle Size						Totals
	<4 μm	<7 μm	<12 μm	<21 μm	<36 μm	>36 μm	
Pyrite	73	64	64	85	95	100	83
Kaolinite	83	77	86	94	91	100	86
Illite	61	69	74	82	100	100	83
Quartz	81	79	83	88	96	100	86
Siderite	81	85	86	89	--	100	80
Calcite	98	93	97	96	100	100	99
Silicates	67	67	81	77	45	100	77
Minors	38	51	75	100	100	100	72
Miscellaneous	30	58	83	100	100	100	75
Total	75	73	77	87	95	100	84

Table 4a. AIA results for Pittsburgh No. 8 raw coal (200 x 0 mesh), expressed as weight percent of dry coal.

Mineral Phase	Particle Size						Totals
	<4 μm	<7 μm	<12 μm	<21 μm	<36 μm	>36 μm	
Pyrite	0.13	0.62	0.72	0.81	1.00	1.19	4.47
Kaolinite	0.08	0.38	0.24	0.12	0.08	0.04	0.94
Illite	0.06	0.26	0.17	0.14	0.16	0.20	0.98
Quartz	0.03	0.13	0.12	0.08	0.01	0.15	0.52
Siderite	0.02	0.10	0.06	0.08	0.14	0.06	0.46
Calcite	0.00	0.02	0.01	0.02	0.00	0.00	0.05
Silicates	0.01	0.02	0.01	0.02	0.07	0.00	0.13
Minors	0.05	0.22	0.12	0.02	0.00	0.00	0.41
Miscellaneous	0.02	0.10	0.05	0.04	0.02	0.09	0.31
Totals	0.40	1.84	1.50	1.33	1.47	1.72	8.26

Table 4b. AIA results for Pittsburgh No. 8 Coal floated at 1.3 specific gravity, as expressed as weight percent of dry coal.

Mineral Phase	Particle Size						Totals
	<4 μm	<7 μm	<12 μm	<21 μm	<36 μm	>36 μm	
Pyrite	0.21	0.33	0.35	0.08	0.00	0.00	0.96
Kaolinite	0.28	0.45	0.21	0.04	0.00	0.00	0.98
Illite	0.24	0.35	0.11	0.01	0.00	0.00	0.70
Quartz	0.07	0.17	0.07	0.02	0.00	0.00	0.34
Siderite	0.00	0.01	0.01	0.03	0.00	0.00	0.05
Calcite	0.00	0.01	0.01	0.01	0.00	0.00	0.02
Silicates	0.02	0.02	0.01	0.00	0.00	0.00	0.05
Minors	0.02	0.03	0.01	0.04	0.00	0.00	0.10
Miscellaneous	0.06	0.08	0.03	0.00	0.00	0.00	0.17
Totals	0.91	1.43	0.80	0.22	0.00	0.00	3.37

Table 4c. Use of AIA results to estimate percent removal of mineral matter from Pittsburgh No. 8 coal. The numbers are based on values in Tables 4a and 4b before they were rounded off.

Mineral Phase	Particle Size						Totals
	<4 μm	<7 μm	<12 μm	<21 μm	<36 μm	>36 μm	
Pyrite	--	46	51	89	100	100	78
Kaolinite	--	--	12	64	100	100	--
Illite	--	--	37	96	100	100	28
Quartz	--	--	39	75	100	100	35
Siderite	76	95	80	63	100	100	88
Calcite	80	62	41	69	100	100	60
Silicates	--	--	32	100	100	100	62
Minors	57	86	89	--	100	100	75
Miscellaneous	--	17	42	100	100	100	45
Total	--	22	46	83	100	100	59

In the supercleaned Illinois coal, the levels of almost all minerals have been reduced by 60-85% somewhat uniformly for most of the particle size ranges up to 21 μm . Above that size, the removal increases sharply, with nearly complete removal for the larger sizes. The 21 μm cut-off seems reasonable for pyrite when the following calculation is considered. A 21 μm pyrite phase (specific gravity of 5.0) embedded in a 200 mesh (i.e. 75 μm) coal particle (specific gravity of 1.25) accounts for only 2.2% of the total volume. However, because it accounts for 8.2% of the total weight of such a particle, it increases the specific gravity of the total assemblage to over 1.33; it is thus rejected in the float-sink separation. A 12 μm pyrite phase, however, accounts for about 1% of the volume of the 74- μm assemblage, while the specific gravity is 1.29; thus it is carried along with the float fraction. Of course, since the size consist is 200 mesh x 0, there are many small pyrite particles completely liberated or attached to smaller sized coal particles; however, the cut-off at 21 μm is still remarkably sharp. Furthermore, since the specific gravities for the other minerals are lower than for pyrite, similar calculations for the other minerals should yield a higher value for the particle size at the cut-off point.

When the overall removal of 84% of the total mineral matter is broken down by particle size, it shows an expected trend of increasing with increasing particle size. The cleaning effectiveness ranges from about 75% for the smaller particles (4-12 μm) to 87% at 21 μm and to 100% for particles larger than 36 μm .

The AIA results for the Pittsburgh No. 8 coal (Tables 4a-c) show a distinctly different character of this coal. The mineral matter in the raw sample is more than 50% pyrite. Although the total amount of clay plus quartz is only one-fourth that of the Illinois No. 6 coal, the clay-to-quartz ratio is much higher. In addition, a substantially larger fraction of the mineral content is present in the larger size ranges. This coal exhibits a much sharper cut-off in the effectiveness of cleaning as a function of particle size. The superclean coal fraction contains no particles larger than 21 μm in diameter. The smaller size fractions show only small amounts of mineral matter removed. For the two smallest sizes, even a slight enrichment can be seen for several mineral phases. This apparent enrichment is partially the result of a mathematical anomaly of the normalization process and partially due to the decrease in the total weight by the removal of other mineral matter from the larger fractions. In any case, the absolute mineral content in these very small size fractions is so minute that the allowed analytical errors can account for the discrepancy, and the overall differences become negligible.

Another observation, however, should be scrutinized more closely. In both coals, the content of pyrite as determined by AIA is consistently higher than that calculated from the pyritic sulfur values obtained by ASTM. Since the accuracy (reproducibility between different labs) for ASTM analyses can be within 0.30 or 0.40% (for less than or more than 2.0% pyritic sulfur, respectively)(5), part of the discrepancy could be explained by the possible analytical error. A more plausible interpretation can be given if the ASTM leachings with nitric acid

do not remove all of the pyrite. Significant residues of pyrite have been observed previously in such leached coal samples (6). Another possible explanation can reside in the specific gravity of pyrite used. Although 5.0 is the literature value for mineral-grade pyrite, past work in this laboratory established that coal-derived pyrite can have a specific gravity significantly lower, ranging from about 3.60 for hand-picked samples to 4.25-4.50 for samples which have been extensively cleaned with hot hydrochloric acid (7). Although the absolute values for the pyrite content are divergent, the relative amounts removed (on a wt. % basis) are relatively comparable for both methods of analysis. However, further work is in progress to resolve this issue.

CONCLUSIONS

Automated image analysis used in conjunction with scanning electron microscopy and energy-dispersive x-ray analysis has been shown to be an effective tool to characterize in-situ the mineral matter in raw and cleaned coal. Both mineral phase analysis and particle size distribution were obtained for two coals (200 mesh x 0) before and after processing. For Illinois No. 6 coal, which contained mostly pyrite, quartz, kaolinite, and illite rather uniformly distributed among the various particle sizes, the cleaning effectiveness increased gradually with increasing particle size of the mineral phases. The levels of removal ranged from about 75% for the smallest particles to 100% for particles larger than 36 μm . For the Pittsburgh coal, more than half of the mineral matter was pyrite, and the pyrite was relatively coarse. The other minerals were smaller in size. During cleaning of the Pittsburgh coal, most of the large-sized mineral matter was removed, while the finer-sized mineral matter was relatively untouched. The cut-off size was approximately 21 μm .

ACKNOWLEDGEMENT

This work was supported by the Assistant Secretary for Fossil Energy, Division of Coal Utilization, through the Pittsburgh Energy Technology Center, Coal Preparation Branch. The authors wish to thank J. Cavallaro (PETC) for float-sink separation of the coal samples and D. L. Biggs (ISU) for sample collections.

REFERENCES

1. T. D. Wheelock and R. Markuszewski, "Coal Preparation and Cleaning," Chapter 3 in The Science and Technology of Coal and Coal Utilization, ed. by B. R. Cooper and W. A. Ellingson, Plenum Press, New York, 1984, pp. 47-123.
2. F. E. Huggins, B. A. Kosmack, G. P. Huffman, and R. J. Lee, "Coal Mineralogies by SEM Automated Image Analysis," Scanning Electron Microscopy/1980, Vol. I, pp. 531-540.
3. J. Lebedzik, LeMont Scientific, Inc., State College, PA, personal communication, Fall 1980.
4. P. H. Given and R. F. Yarzab, "Analysis of the Organic Substance of Coals: Problems Posed by the Presence of Mineral Matter," Chapter 20 in Analytical Methods for Coal and Coal Products, Vol. II, ed. by C. Karr, Jr., Academic Press, New York, 1978, pp. 3-41.
5. American Society for Testing and Materials, Annual Book of ASTM Standards, Section 5: Petroleum Products, Lubricants, and Fossil Fuels, Philadelphia, 1983, Method D2492.
6. R. T. Greer, "Organic and Inorganic Sulfur in Coal," Scanning Electron Microscopy/1979, Vol. I, pp. 477-485.
7. K. C. Chuang, M.-C. Chen, R. T. Greer, R. Markuszewski, Y. Sun, and T. D. Wheelock, "Pyrite Desulfurization by Wet Oxidation in Alkaline Solutions," Chem. Eng. Commun. 7, 79-94 (1980).

BEHAVIOR OF MINERAL MATTER DURING ALKALINE LEACHING OF COAL

C.-W. Fan, R. Markuszewski, and T. D. Wheelock

Chemical Engineering Department and
Energy and Mineral Resources Research Institute
Iowa State University
Ames, Iowa 50011

Introduction

A process for producing premium quality coal with a very low ash content was demonstrated recently (1). This process involves reacting the material with a hot alkaline solution to dissolve quartz and to convert clay minerals and iron pyrite into acid-soluble compounds which are removed in a second step by treatment with acid. To understand this process better, several minerals which generally make up a major portion of the ash-forming mineral matter in many coals were reacted individually with hot alkaline solutions, and the solid reaction products were characterized by X-ray diffraction (XRD). In this study, quartz, kaolinite, and iron pyrite were reacted individually with Na_2CO_3 , NaHCO_3 , and NaOH solutions using various concentrations and temperatures. The solid products were identified and their solubility in dilute mineral acids demonstrated. In addition, the extent of conversion of quartz and pyrite to acid-soluble species was demonstrated for various alkaline treatment conditions.

Experimental Methods

The materials used for this study, obtained from sources listed in Table 1, were checked for impurities by XRD. Using this method, no impurities were detected in the quartz, but the kaolin appeared to contain a significant amount of quartz and trace quantities of illite and titania. The iron pyrite was obtained as nodules by handpicking the refuse produced in cleaning coal from Mahaska County, Iowa. The nodules were crushed and ball-milled to $-38\ \mu\text{m}$ size. Part of the ground pyrite was treated for 1 hr. with excess 1.2 M HCl at 70°C under a nitrogen atmosphere (to remove acid-soluble impurities) and then washed and dried. This acid-cleaned material contained about 88% FeS_2 , based on total sulfur content, and significant amounts of quartz and kaolinite plus a trace of titania. In addition, it seemed to contain some amorphous material which may have been coal. The raw pyrite which had not been treated with acid contained all of these impurities plus significant amounts of calcite and iron oxides.

Table 1. Materials which were leached

Material	Source	Impurities
Quartz	Ottawa sand (Ill.)	None
Kaolin	Old Hickory No. 5 ball clay (Ky.)	SiO_2 , Illite, TiO_2
Raw pyrite	Coal, Mahaska County (Ia.)	CaCO_3 , iron oxides SiO_2 , kaolinite, TiO_2
Cleaned pyrite	Same as above	SiO_2 , kaolinite, TiO_2

For the leaching experiments, a weighed amount of finely divided mineral matter was mixed with 120 ml. of alkaline solution in a 300 ml. stainless steel autoclave equipped with a turbine agitator. The system was flushed with nitrogen and then heated to the desired leaching temperature. A nitrogen overpressure of 3.4 atm. was maintained throughout the leaching process. The mixture was stirred continuously while leaching was conducted at constant temperature and pressure for a specified period. After this treatment, the autoclave was cooled quickly, and the contents of the autoclave were filtered to recover any undissolved solids. The solids were washed with water, dried in an oven, weighed, and divided into two parts. One portion was analyzed by XRD with a Siemens D500 diffractometer using copper K α radiation. The other portion was usually subjected to an acid treatment and washing step in order to determine the proportion of acid-soluble material.

For the acid treatment step, up to 3 g. of alkali-leached material was mixed with 300 ml. of mineral acid (approximately 2.0 M) in a stirred, three-neck Pyrex reaction flask for 30 min. The treatment was conducted either at room temperature (25°C) or at the boiling point (100°C). After the treatment the mixture was filtered, and any undissolved solids were washed with water, dried, weighed, and analyzed by XRD.

Experimental Results

In one set of experiments, -38 μ m size quartz particles were leached with various hot alkaline solutions to study the effects of alkali type, alkali concentration, ratio of alkali to quartz, temperature, and leaching time on dissolution. After each leaching, the reactor contents were filtered with Whatman No. 40 filter paper using suction, and the residue was washed with cold water, dried at 350°C for 2 hr., and weighed. The percentage of material extracted was calculated using the following expression:

$$\text{Extraction (\%)} = 100 - \frac{\text{wt. of residue}}{\text{wt. of feed}} \times 100 \quad 1)$$

The results of leaching quartz with Na₂CO₃ solutions having different concentrations are shown in Figure 1. For each point, 2.0 g. of quartz was leached with 120 ml. of solution at 250°C for the indicated time. It can be seen that the amount of material extracted increased linearly with time for about the first hour. During this period the rate of extraction also increased with alkali concentration to approximately the 0.5 power. Following the constant rate period, the extraction stopped. Apparently the solubility limit was reached, and it seemed to be the solubility limit at room temperature rather than at the leaching temperature. The following evidence pointed to the lower temperature limit. The residue remaining after leaching quartz for 2 hr. or more was an amorphous, non-crystalline solid which was insoluble in hot HCl. The results suggested that quartz had dissolved in the hot solution, and upon cooling some of the silica and possibly some of the soda had reprecipitated as an amorphous or glassy material. On the other hand, the residue remaining after quartz had been leached for less than 1 hr. appeared to be largely quartz. Furthermore when quartz was leached for 1 hr. at 300°C with a 1.0 M solution, the amount of material extracted was only 69% which was no greater than the maximum amount extracted at 250°C. From published solubility data (2) for silica in various alkaline solutions, one would expect the solubility of quartz in a Na₂CO₃ solution to increase markedly with temperature.

Even though the amount of silica extracted seemed to be limited by the room temperature solubility limit, this limit was raised by increasing either the alkali concentration or the ratio of alkali to quartz. Thus by increasing the alkali concentration from 1.0 M to 2.0 M, the maximum amount extracted was raised from 70% to 98.5%. Moreover when the quantity of quartz leached in 1 hr. with a 1.0 M solution at 250°C was reduced from 1 g. to 2 g., the percentage extracted increased from 58% to 95%.

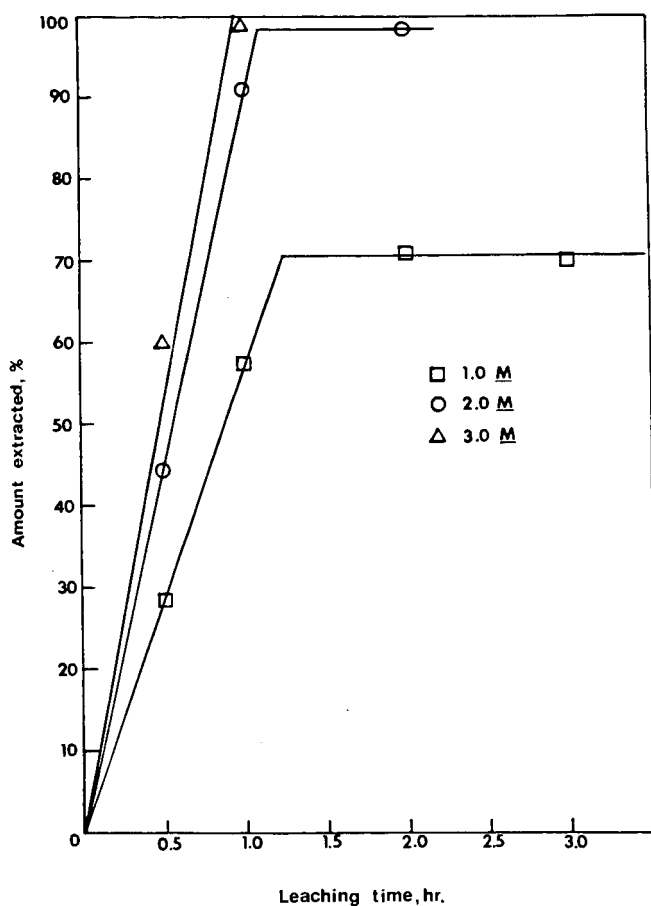


Figure 1. Dissolution of quartz (2.0 g.) by hot (250°C) sodium carbonate solutions (120 ml.) having different concentrations (1.0-3.0 M).

Quartz was also leached for 1 hr. at 250°C with either 2.0 M NaOH or NaHCO₃. In each case 2.0 g. of quartz was leached with 120 ml. of solution. Most of the quartz (99.5%) was converted to soluble sodium silicates and extracted by the hot caustic. On the other hand, only 10% of the quartz was extracted by the NaHCO₃ solution, and the residue appeared to be entirely quartz. These values were noticeably different from the 58% extracted by 1.0 M Na₂CO₃ under similar conditions. Therefore, these leachants were not equivalent even though each provided the same number of moles of sodium.

None of the residues remaining after leaching quartz with any of the alkalis were acid-soluble.

In a second set of experiments, -74 μ m size kaolin particles were leached with hot alkaline solutions to study the conversion of kaolinite to various sodium hydroaluminosilicate compounds (Table 2) under different leaching conditions. In each experiment, 15 g. of kaolin was leached with 120 ml. of alkaline solution. The solid reaction product was recovered by filtration, washed with water, dried in an oven at 95°C, and analyzed by XRD. Although this method of analysis identified the minerals present, it provided only an approximate indication of the relative proportions of the various minerals present. Quartz was particularly misleading because the method of detection was very sensitive to this mineral. Therefore, the results are reported only in terms of major, minor, and trace quantities present in the product as indicated by XRD (Table 3). Because the small amount of titania in the kaolin was apparently not affected by even the most rigorous leaching conditions, the product always contained a trace of this material so no further mention seems necessary.

When kaolin was leached with 1.0 M Na₂CO₃ at 200°C for 1 hr., most of the kaolinite was converted to the sodalite-type natrodavayne (NS) while the quartz and illite impurities were not affected noticeably (Table 3). Increasing the leaching temperature to 250°C resulted in the conversion of the kaolinite to a mixture of mixed-type natrodavayne (NCS) and analcime (A) and complete dissolution of the quartz impurity. The illite impurity was not affected. Leaching at 300°C and above resulted in the conversion of the kaolinite to the cancrinite-type natrodavayne (NC). Only at 350°C did the illite impurity appear to be affected.

A similar trend was observed when kaolin was leached for 1 hr. at 250°C with Na₂CO₃ solutions of different concentrations (Table 3). At the lowest concentration (0.2 M), part of the kaolinite was converted to the sodalite-type natrodavayne while the impurities were untouched. At the highest concentration (2.0 M), the kaolinite was converted to the cancrinite-type natrodavayne, and although the quartz was extracted, the illite remained.

Somewhat similar changes were observed when the leaching time was varied while holding the concentration of Na₂CO₃ at 1.0 M and the temperature at 250°C. With a leaching time of 0.5 hr. the kaolinite was converted to a mixture of analcime and sodalite-type natrodavayne, whereas with a leaching time of 2.0 hr. the kaolinite was largely converted to the cancrinite-type natrodavayne. Not all of the quartz was extracted when leaching was conducted for 0.5 hr., but all of the quartz appeared to be removed when leaching was conducted for longer periods. However, the illite remained even after 2 hr. of leaching.

When kaolin was leached with 1.0 M NaOH at 250°C for 1 hr., most of the kaolinite appeared to be converted to analcime (Table 3). Increasing the concentration to 2.0 M resulted in converting most of the kaolinite to hydroxycancrinite (HC). In either case the quartz impurity was extracted but the illite impurity remained.

Leaching kaolin with 2.0 M NaHCO₃ at 250°C for 1 hr. converted the kaolinite to the sodalite-type natrodavayne, but it had no apparent effect on the impurities.

Table 2. Various sodium hydroaluminosilicates produced in leaching kaolinite with hot alkaline solutions

Mineral	Chemical formula	Symbol
Analcime	$\text{Na}_2\text{O} \cdot \text{Al}_2\text{O}_3 \cdot 4(\text{SiO}_2) \cdot 2(\text{H}_2\text{O})$	A
Hydroxycancrinite	$\text{Na}_2\text{O} \cdot \text{Al}_2\text{O}_3 \cdot 2(\text{SiO}_2) \cdot \frac{2}{3}(\text{NaOH}) \cdot n(\text{H}_2\text{O})$	HC
Hydroxysodalite	(same as above)	HS
Natrodavynne (sodalite-type)	$\text{Na}_2\text{O} \cdot \text{Al}_2\text{O}_3 \cdot 2(\text{SiO}_2) \cdot \frac{1}{3}(\text{Na}_2\text{CO}_3) \cdot n(\text{H}_2\text{O})$	NS
Natrodavynne (cancrinite-type)	(same as above)	NC
Natrodavynne (mixed type)	(same as above)	NCS

Table 3. Results of leaching 15 g. kaolin (-74 μm) with 120 ml. alkaline solution

Leaching conditions				Mineral products excluding TiO_2 , type, (amount) ^a
Alkali	Conc., M	Temp., °C	Time, hr.	
Na_2CO_3	1.0	200	1.0	NS(maj), SiO_2 (maj), kaolinite(min), illite(tr)
Na_2CO_3	1.0	250	1.0	NCS(maj), A(maj), illite(tr)
Na_2CO_3	1.0	300	1.0	NC(maj), A(min), illite(tr)
Na_2CO_3	1.0	350	1.0	NC(maj)
Na_2CO_3	0.2	250	1.0	SiO_2 (maj), kaolinite(min), NS(min), illite(tr)
Na_2CO_3	0.5	250	1.0	SiO_2 (maj), NS(maj), illite(tr)
Na_2CO_3	1.0	250	1.0	NCS(maj), A(maj), illite(tr)
Na_2CO_3	2.0	250	1.0	NC(maj), illite(tr)
Na_2CO_3	1.0	250	0.5	A(maj), NS(maj), SiO_2 (min), illite(tr)
Na_2CO_3	1.0	250	1.0	NCS(maj), A(maj), illite(tr)
Na_2CO_3	1.0	250	2.0	NC(maj), A(min), illite(tr)
NaOH	1.0	250	1.0	A(maj), HS(min), illite(tr)
NaOH	2.0	250	1.0	HC(maj), A(min), illite(tr)
NaHCO_3	2.0	250	1.0	NS(maj), SiO_2 (maj), illite(tr)

^a Amount: maj = major quantity, min = minor quantity, tr = trace quantity.

To investigate the dissolution of the sodium hydroaluminosilicates produced by alkaline leaching, 3.0 g. portions of the leached product were treated with 300 ml. of acid in a stirred flask for 30 min. Either 2.0 M HCl or 1.8 M H_2SO_4 were utilized. While HCl was always used at the boiling point, H_2SO_4 was sometimes used at the boiling point and sometimes at room temperature. From XRD analysis of the solid residue remaining after the acid treatment, it was found that all of the sodalite-type and cancrinite-type compounds were dissolved by the acids whether hot or cold. On the other hand, analcime was completely dissolved only by the boiling acids.

In a third set of experiments, $-38\ \mu\text{m}$ pyrite particles were leached with hot alkaline solutions to study the conversion of iron pyrite to iron oxide and soluble sulfur species. In each experiment, 5 g. of acid-cleaned pyrite was leached with 120 ml. of alkaline solution for 1 hr. In addition to analyzing the solid residue by XRD, the total sulfur content of the leachate was determined in order to estimate pyrite conversion.

When iron pyrite was leached for 1 hr. with 1.0 M Na_2CO_3 at 250°C , only 12.7% of the pyrite was converted to iron oxide and soluble sulfur species (Table 4). Increasing the leaching temperature to 300°C raised the conversion to 26.4%, and increasing the temperature to 350°C raised the conversion to 44.8%. In each case the solid residue consisted principally of hematite and unreacted pyrite.

Increasing the Na_2CO_3 concentration, while maintaining the leaching time at 1 hr. and temperature at 250°C , increased the pyrite conversion only slightly (Table 4). On the other hand, when pyrite was leached with 2.0 M NaOH at 300°C for 1 hr., a conversion of 62% was achieved. Again, hematite appeared to be the principal solid reaction product.

When the pyrite residue from the alkaline leaching step was treated with acid, all of the hematite dissolved in either hot HCl or H_2SO_4 . However, the hematite appeared to dissolve incompletely or very slowly in cold H_2SO_4 . Unreacted pyrite was not touched by the acid whether hot or cold.

Conclusions

The solubilization of several of the most prevalent minerals in coal was demonstrated by a one- or two-step treatment process. The first step involves treatment with a hot alkaline solution while the second step involves treatment with a dilute mineral acid.

It was shown that fine-size quartz particles readily dissolve in 1-2 M Na_2CO_3 or NaOH at 250°C . However, when quartz is extracted by a hot Na_2CO_3 solution which is then cooled, an amorphous, acid-insoluble material is produced under some conditions. A likely possibility is that amorphous silica precipitates when the room temperature solubility limit of the material is exceeded. Formation of the amorphous material is prevented by using higher concentrations of alkali or a higher ratio of alkali to silica.

It was also shown that kaolinite reacts with hot alkaline solutions to form various sodium hydroaluminosilicates which are acid-soluble. The particular sodium hydroaluminosilicate formed depends on the type of alkali employed, the alkali concentration, the treatment temperature, and length of treatment. When Na_2CO_3 is employed, kaolinite is largely converted to the sodalite-type natrodavne under less rigorous conditions and to the cancrinite-type natrodavne under more rigorous conditions. Under intermediate treatment conditions, the mixed-type natrodavne and analcime are produced. When NaOH is employed, kaolinite is largely converted to analcime and hydroxycancrinite with the latter being favored by higher alkali concentrations.

Table 4. Results of leaching 5 g. acid-cleaned pyrite ($\sim 38 \mu\text{m}$) with 120 ml. alkaline solution for 1 hr.

Alkali	Leaching conditions		Conv., %	Residue
	Conc., M	Temp., °C		
Na_2CO_3	1.0	250	12.7	$\text{FeS}_2, \text{Fe}_2\text{O}_3$
Na_2CO_3	1.0	300	26.4	$\text{FeS}_2, \text{Fe}_2\text{O}_3$
Na_2CO_3	1.0	350	44.8	$\text{FeS}_2, \text{Fe}_2\text{O}_3$
Na_2CO_3	1.0	250	12.7	$\text{FeS}_2, \text{Fe}_2\text{O}_3$
Na_2CO_3	2.0	250	14.5	----
Na_2CO_3	3.0	250	15.8	----
NaOH	2.0	300	62.0	$\text{FeS}_2, \text{Fe}_2\text{O}_3$

It was further shown that iron pyrite reacts with hot alkaline solutions to form hematite and soluble sulfur species. NaOH is considerably more effective than Na_2CO_3 for this reaction. However, the effectiveness of Na_2CO_3 solutions can be increased by increasing the treatment temperature and to a lesser extent by increasing the alkali concentration. The hematite produced is readily dissolved by hot mineral acids.

Work is in progress to extend the described reactions to other minerals associated with coal. Further studies are also directed to leaching of coal itself. The results will be used to relate the behavior of the individual minerals when leached alone to their behavior when leached together in their natural occurrence with coal. The studies will shed light on the potential of demineralizing coal for use in low-ash, low-sulfur coal-water mixtures as fuel for replacing oil.

Literature Cited

1. Fan, C.-W., Markuszewski, R., and Wheelock, T. D., Process for producing low-ash, low-sulfur coal, Am. Chem. Soc. Div. of Fuel Chem. Preprints 29(1): 114-119 (1984).
2. Iler, R. K., The Chemistry of Silica, John Wiley and Sons, New York, 1979.

THE SEPARATION OF MINERAL MATTER FROM PITTSBURGH COAL BY WET MILLING

Douglas V. Keller, Jr.

Otisca Industries, Ltd.
P. O. Box 127, Salina Station
Syracuse, New York 13208

Introduction

The term "inherent mineral matter, or ash" is a commonly used phrase in the coal literature (1). The phrase refers to that fraction of the mineral matter bound organically to the carbonaceous structure of the coal and estimates of its content suggest that it is in the range of two weight percent of the whole mineral matter (1). Common classical physical separation schemes such as differential specific gravity separations or froth flotation which are directed at demineralizing the coal never approach that lower limit. For example, at the outset of this investigation one could receive a raw Pittsburgh seam coal at 30 weight percent ash and through careful float-sink processes reduce that ash content into the range of four to five weight percent. Practically reducing that ash content, however, to below three weight percent with a reasonable yield was quite unlikely (2). One consequence of the large weight fraction differential between the practical limit of demineralization, and if you like, the true "inherent" limit of demineralization was a total lack of understanding as to whether or not that mineral fraction could indeed be extracted by physical means. With this as a basis, further questions could be raised as to whether or not that retained mineral matter was a true distinct mineral phase, or if so, could it be bound chemically along the interfaces to the coal structure rendering those particles inseparable. Most simply, in all cases one could ask the question does a separation of mineral matter from the coal take place in all cases when coal is fractured and to what extent, or limit, can the fracture process be utilized in the demineralization of coal.

A series of experiments was assigned to explore the extraction of mineral matter from coal in the size ranges below 0.25 mm. The raw coal samples were obtained from three different sources in the Pittsburgh seam which permitted a degree of comparison over a rather large geographic area. The results are interesting in that they allow a new perspective in the demineralization of coal.

Experimental

The Pittsburgh seam coals used in this investigation has a nominal analysis as illustrated in Table 1.

Lots of Pittsburgh seam coal in excess of 1000 pounds each were received from three different sources in Washington County: Mine (A) was located about 20 miles west of Pittsburgh; Mine (B) was located just south of Pittsburgh; and Mine (C) was located about 40 miles south of Pittsburgh. Representative samples from each source were obtained by ASTM procedures and subjected to the following processing.

A raw coal sample was reduced to 250 μ m x 0 by dry mechanical crushing in a hammermill and then ground in a laboratory sample mill.

The mechanically ground coal was then mixed with water to form a slurry with 30 weight percent solids and placed in a standard laboratory ball mill. All of ball milling variables were held constant except for the duration of milling which permitted a variation of the particle size distribution. In the event that chemicals were employed during the ball milling operation those chemicals were incorporated in an excess of the amount of the standard mill content.

The coal water slurry was removed from the mill, diluted with water to ten weight percent solids and the coal fraction removed utilizing the Otisica T-Process (2,3). Separations by the T-Process are unique in that agglomeration results in the recovery of virtually 100% of the carbonaceous material leaving a full dispersed mineral phase in the residue water. Many detailed investigations of this type have concluded that mineral matter recovered with the coal phase is included in the coal that is the ash content of the product coal represents only that mineral matter mechanically attached to or enveloped by the coal.

Analytical procedures for ash (high temperature, HT) and sulfur contents were conducted according to ASTM procedures. Low temperature ash procedures were conducted at 550°C in an oven with an adequate supply of oxygen. The difference in mineral matter morphology and chemistry between this technique and the low temperature ashing method described by Gluskoter (3), can be anticipated from the paper by Mitchell and Gluskoter (4). Principally the higher temperature ashing process will convert pyrite to hematite and kaolinite to metakaolinite. Between 30% and 50% of the mineral matter in the Pittsburgh coal is considered to be kaolinite (5), and in this investigation we presumed that the 550°C ashing procedure did not significantly alter the particle size distribution of the original kaolinite particles.

A Micromeritics 5500L unit was used to obtain the particle size distribution data for this investigation. Data from the Micromeritics unit using a one μm mode sample was compared with the data developed by the manufacturer from a Coulter Counter on the same sample to within ten percent. Even with this in hand there was no attempt to characterize the particles on an absolute basis. The observed area percent data from the Micromeritics unit was transposed to a mass percent base at data points y (in μm) for all of the points $y = 2^x$ where $x = n + 0.5$ and $n = -3, -2.5, \dots, 0, \dots, +7, +7.5$. The data point at y represents that mass fraction of material lying in the size range $x \pm 0.25 \mu\text{m}$. Thus a summation of all of the data points represents the mass fraction of ash, or product coal, as the case might be.

The following particle size distribution data are given as a log distribution in particle diameter (μm) where the mass points are interconnected for convenience of comparison at the expense of rigor. Typical distributions are bell-shaped where the mode is defined as the particle diameter at that point of half width of the curve at the half height of the maximum. The Micromeritic unit is based on a Stokes' Law settling to the particles where one must choose an average specific gravity of particles under investigation before the data are recorded. In those cases where low temperature ash particles were investigated, the iron minerals with a density larger than 4 gms/cc were separated from the clay minerals with densities less than 3 gms/cc, the distributions measured individually and then the size distributions were recombined mathematically. The product coals demonstrated a very narrow specific gravity distribution in the range of 1.33.

Results and Discussion

Figure 1 illustrates the particles size distribution of the mineral matter that results from the low temperature ashing of three 5 cm cubes of bright coal that were hand-picked from the various samples. The ash contents were in the range of five weight percent. It is of interest to note that band of mineral matter particles that lie in the particle diameter range between one and 50 μm with a mode between four and eight μm . The particle size distribution data from the low temperature ashing of the 5 cm cubes of coal show that raw coal from each source has a unique "fingerprint" of mineral matter particles distributed in the particle size range below 0.25 mm.

Investigations of many other coal seams and coals within a particular seam indicate that indeed the mineral matter distribution varies widely both in shape and magnitude and as such cannot be anticipated from other coal properties. The mineral matter distribution is a fundamental property of that coal which is an uncontrolled natural variable in the extraction of mineral matter.

In order to demonstrate that the 5 cm cube was constituted of an accumulation of much smaller unit volumes each of which represented the whole coal in mineral matter particle size distribution a study of a series of size classified particles was undertaken. For example, if raw coal (C) were ground to 250 μm x 0, and then separated with standard sieves into the size fraction 53 x 44 μm , we would be afforded a dry mixture of raw coal particles and mineral particles with an average size of 48 ± 4 μm . Figure 2 illustrates the particle size distribution of the low temperature ash product of the product coal after the free mineral matter particles were removed. The free mineral matter particles in that size range must have evolved from larger coal particles. Again we have the characteristic curve very similar to the curve shown in Figure 1(C). In fact, that portion of the curve that lies below 3 μm can most usually be superimposed on other curves obtained in a similar manner from the other size fractions of coal (C). Providing, that is, that the coal particle diameters are larger than 10 μm .

The conclusion of that study indicated that product coal particles larger in diameter than the band of microparticles seemed to contain the whole particle distribution of the small microparticles of mineral matter. That is, there appeared to be a relatively homogenous distribution of particles throughout limited in top size by the largest particle in the test. To explore that aspect in more depth, a raw coal was wet milled to smaller sizes.

When a raw coal is wet ball-milled for a sufficient time to produce a slurry with a particle diameter mode in the range of 4 μm there results two forms of mineral matter: That fractured away from the coal and that which is still enveloped in the coal particles. Figure 3 illustrates a typical particle size distribution for the separated product coal as compared to the separated free mineral matter (90 weight percent ash) from one milling test. The separated mineral matter is clearly smaller in diameter than the coal which is probably due to its more brittle properties. Note that in Figures 3 and 4 an integration of the curves will yield 100% of the mineral matter (or ash) under consideration rather than the ash content of the coal as was the case in Figures 1 and 2.

When the product coal shown in Figure 3 was subjected to low temperature ashing as described above and that product subjected to particle size analysis, a curve as is illustrated in Figure 4 results. Clearly the enveloped mineral matter in the product coal particles is considerably smaller in diameter than the coal particles from which they came and as such are not released for separation.

Two very important points are illustrated in Figures 1-4: Firstly, it appears that as coal fracture takes place in this system, mineral matter particles are ejected from the fractured coal system and most without attached coal. Coal attached to mineral matter is recovered as product coal. The implication is that the coal-mineral matter interfaces are not chemically bound. If those interfaces were chemically bound one would observe mineral matter rejection with a large increase in the sub-micron particle population in the released mineral matter, cf. Figure 3, as well as that in the low temperature ash of the product coal. The latter is not observed as is illustrated below.

Secondly, given the low temperature ash distribution of the raw coal and a knowledge of the raw coal particle size distribution after wet milling, we are in a position to predict the ash content of the product coal. Consider Figure 5 where a hypothetical low temperature ash particle size distribution is superimposed on a T-Process product coal size distribution. The product coal particles with diameters lying between x and dx contain no mineral matter particles larger than dx as those particles were removed during the separation process. The mineral matter retained in the product coal particles is the cumulative mineral matter content represented by the low temperature ash curve. Since the mineral content given on the ordinate in Figure 5 is based on 100%, the ash content in each size range can be estimated by multiplying the mass fraction of that point by the total ash content in the raw coal sample, i.e. 250 m x 0, that was used to generate the low temperature ash curve.

A specific case is examined in Table 2 where the particle size distribution data from the low temperature ashing of a 5 cm cube of coal and 44-53 μ m coal was related to two product coal samples milled under different conditions all of which originated from the same source coal (C). The first column in Table 2 provides the average particle diameter points (y) at which the data were observed. A comparison of the low temperature ash data for the 5 cm cube, column 2, and for the 44-53 μ m coal, column 3, illustrate that the fracture of coal from a 5 cm cube to 48 μ m does not significantly disturb the mineral matter particles lying in the range of diameters below 6 μ m. Since a 4 μ m particle of product coal ought to have the complete mineral matter particle distribution smaller than 4 μ m enveloped in that particle, a cumulative ash fraction of the lesser particle diameter ash should be equivalent to the ash content within the 4 μ m particles, that is, 2.67 weight percent ash, cf. column 4 at 4 μ m.

A test of this relationship is afforded in column 5 where we observe the mass fraction of particles at various diameters of a product coal from a standard mill run with no chemicals added. The predicted ash content of the product coal is determined by a summation, over all particle diameters of the product of the ash content of each diameter cumulated by increasing diameter, (x) times the mass fraction of the product coal at that particular diameter (y). The predicted ash content for this case is 1.19 weight percent ash which can be compared to

the observed value using ASTM procedures of 1.12 weight percent ash. Following identical milling procedures, except for the addition of 20 pounds per ton ligninsulfonate, a dispersant, we obtain a much finer size distribution as is illustrated in column 6, Table 2. The predicted ash content in that case is 0.68 weight percent ash while the observed value was 0.91 weight percent ash. The large discrepancy in the finer coal case was probably due to imperfect separation procedures that were caused by the presence of the dispersant. The ability to predict ash contents using this procedure has been applied to several different coals from different seams and the same seam with results usually within ten percent. A careful examination of these data lends credence to the observation that for the most part the mineral matter included in coal to the micron particle size range is indeed a distinct separable phase capable of physical separation by fracture.

The extent to which milling can be carried out and still attain effective demineralization is to a degree limited by our knowledge of milling. Coal B was reduced in ash into the range of 0.5 weight percent, however, that limit appeared to be a function of milling phenomena rather than fracture phenomena. Clearly, according to the analysis shown in column 5 of Table 2 and the subsequent discussion, one might expect a monotonic decrease in product coal ash content with particle size distribution mode to zero mineral matter which has not been observed. What was not anticipated was the observation that that relation appeared to be insensitive to what might be considered as rather severe changes in the chemical environment during the milling process even though some of the chemical additives made significant changes in the milling efficiency, i.e., specific area increase per unit input energy. Consider the effect of three chemical additives: calcium hydroxide, sodium ligninsulfonate, and sodium sulfosuccinate, as compared to the case of no additives on the particle size distribution of the product coal from a standard mill run shown in Figure 6 where all conditions were identical. Clearly, there were no obvious effects. In the next series, shown in Figure 7, we investigated the additives ammonium hydroxide, sodium hydroxide, and a higher concentration of sodium ligninsulfonate. Clearly, a dynamic difference in specific surface area per unit input energy was observed. The explanation of the differences is beyond the scope of this paper, but what was interesting was the effect that the chemicals had on the fracture mechanism that effects the release of mineral matter. Figure 8 illustrates a plot of the ash content in the product coal versus the mode of the particle size distribution of the product coal. All of the tests utilizing chemical additives were milled under identical conditions utilized in the test which produced the "no additive" data with a 2 μ m mode. The three other "no additive" tests were milled for extended times to achieve smaller particle size distributions. The chemical additive calcium hydroxide when used at 20 pounds per ton is above the saturation limit and the solid particles have become imbedded in the coal structure, hence increasing the ash content of the product coal well removed from its anticipated location on the curve. A mild acid etch of that product coal to remove the calcium hydroxide allows recovery of its anticipated position in the scheme. Some of the chemical additives do alter the specific milling rate during the process, but that change does not alter the relationship between particle fracture and mineral matter released. Such lends support to the presumed model that the ultrafine mineral matter is to some degree homogeneously distributed and is only released with the fracture of the coal particle.

Conclusion

High ranked bituminous coals like those of the Pittsburgh seam contain a distribution of discrete mineral matter particles in the size range from 50 to 1 μm which can be released and physically separated from the coal by normal fracture mechanisms experienced in wet ball milling. Demineralization of coal by this mechanism appears to be a predictable process with an error in the range of 10 percent. The demineralization of Pittsburgh seam coal has been achieved to the range of 0.5 weight percent ash, a limit which appears to be controlled by the mechanics of the ball mill.

Acknowledgments

The author extends his sincere appreciation to W. Burry and D. S. Keller for their efforts in the development of the experimental procedures and data analysis.

References

1. Leonard, J. W., "Coal Preparation", Amer. Inst. Mining Met. Pet. Eng., Inc., New York (1979).
2. Keller, Jr., D. V., "Otisca T-Process, A New Coal Beneficiation Approach for the Preparation of Coal Slurries", Coal Gasification, Liquefaction, and Conversion to Electricity Conference, University of Pittsburgh, August 1982.
3. Keller, Jr., D.V., "Coal Refining by Physical Methods for the Preparation of Coal Slurries With Less Than 1 wt.% Ash", Fifth International Symposium on Coal Slurry for Combustion and Technology, Tampa, Florida, April 1983, U.S. DOE, Pittsburgh, p 269.
4. Gluskoter, H.L., Fuel, 44, 285 (1965).
5. Mitchell, R.S. and Gluskoter, H.L., Fuel, 55, 90 (1976).
6. O'Gorman, J.V. and Walker, P.L., "Mineral Matter and Trace Elements in U.S. Coals", U.S. Office of Coal Research, R& D Report No. 61, (1972).

TABLE 1

NOMINAL ANALYSIS OF PITTSBURGH SEAM COAL

	Weight Percent (Dry Basis)
Volatile Matter	35
Fixed Carbon	58
BTU/lb	14,200
Carbon	77.3
Hydrogen	5.2
Nitrogen	1.5
Chlorine	0.1
Sulfur	1.5
Oxygen (diff)	7.6
Ash	6.8

TABLE 2

PARTICLE SIZE DATA FOR LOW TEMPERATURE ASH PRODUCTS AND PRODUCT COALS

Data Point	Low Temperature Ash - Wt.%			Product Coal - Wt.%	
<u>μm</u>	<u>5 cm Cube</u>	<u>44-53μm</u>	<u>44-53μm</u> (Cumulative X)	Standard No Additives	Standard 20 pounds/ton Ligninsulfonate
(y)				(Y)	(Z)
0.35	0.03	0.06	0.06	0.08	0.14
0.50	0.06	0.1	0.16	0.05	0.08
0.71	0.19	0.18	0.34	0.085	0.13
1.00	0.35	0.28	0.62	0.13	0.20
1.41	0.49	0.38	1.0	0.2	0.14
2.0	0.67	0.52	1.52	0.18	0.10
2.83	0.63	0.60	2.12	0.145	0.05
4.0	0.66	0.55	2.67	0.06	0.03
5.66	0.66	0.55	3.22	0.04	0.01
No Additives		y = 5.66	$\Sigma (X_Y \times Y_Y) =$		
		y = 0.35			
Ligninsulfonate		y = 5.66	$\Sigma (X_Y \times Z_Y) =$		
		y = 0.35			
				1.19 Wt.% Ash Predicted	
				1.12 Wt.% Ash Observed	
				0.68 Wt.% Ash Predicted	
				0.91 Wt.% Ash Observed	

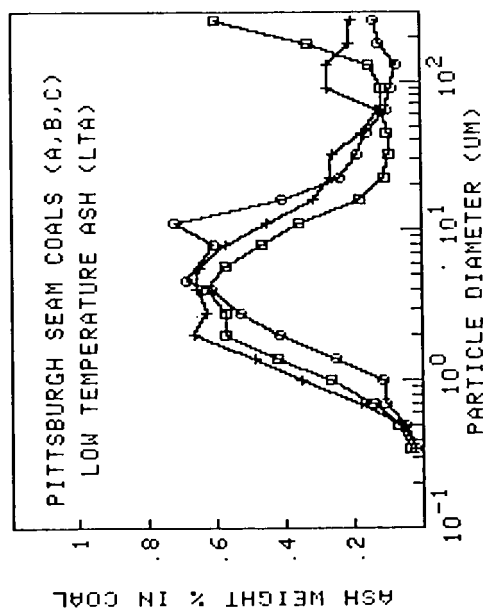


FIGURE 1: PARTICLE SIZE DISTRIBUTIONS OF THE LOW TEMPERATURE ASH PRODUCTS FROM THREE DIFFERENT 5 cm BLOCKS OF PITTSBURGH SEAM COAL: (*) Coal A; (□) Coal B; and (○) Coal C.

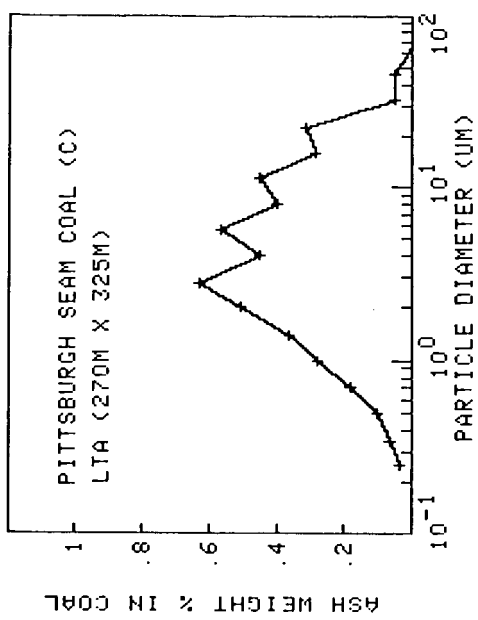


FIGURE 2: PARTICLE SIZE DISTRIBUTION OF THE LOW TEMPERATURE ASH PRODUCT OF A $48 \pm 4 \mu\text{m}$ PRODUCT COAL.

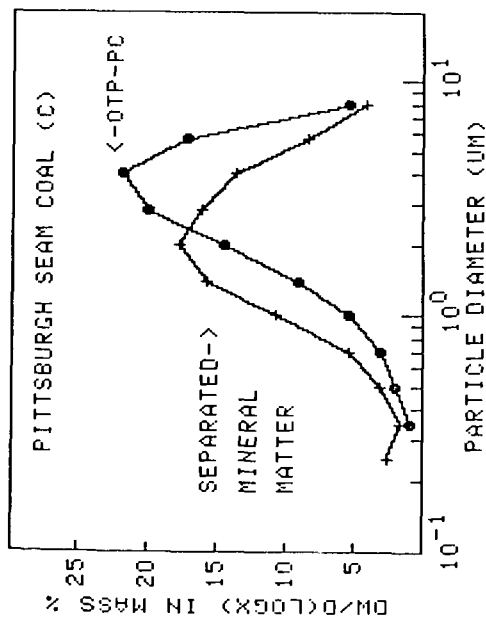


FIGURE 3: WHEN THE PRODUCTS OF WET MILLING 250 $\mu\text{m} \times 0$ PITTSBURGH COAL (C) ARE SEPARATED, TWO PRODUCTS EVOLVE: PRODUCT COAL AND SEPARATED MINERAL MATTER. THE PARTICLE SIZE DISTRIBUTIONS FOR EACH ARE ILLUSTRATED.

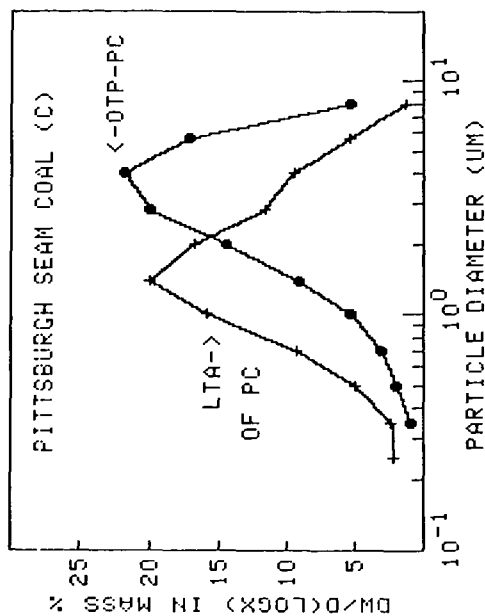


FIGURE 4: PARTICLE SIZE DISTRIBUTION OF THE LOW TEMPERATURE ASH PRODUCT FROM THE SAME PRODUCT COAL SAMPLE SHOWN IN FIGURE 3.

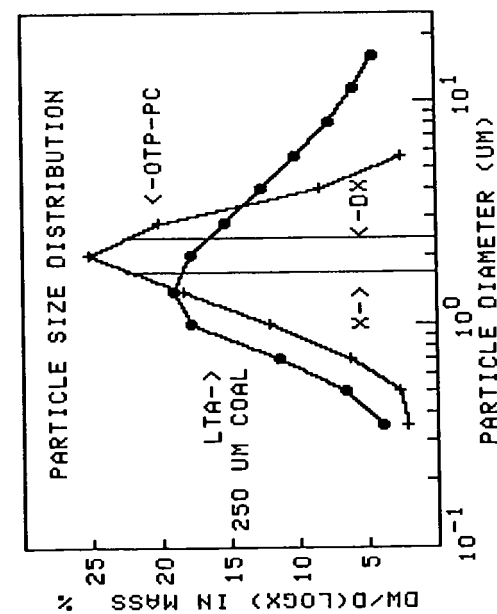


FIGURE 5: A HYPOTHETICAL PARTICLE SIZE DISTRIBUTION CURVE OF LOW TEMPERATURE ASH AND PRODUCT COAL.

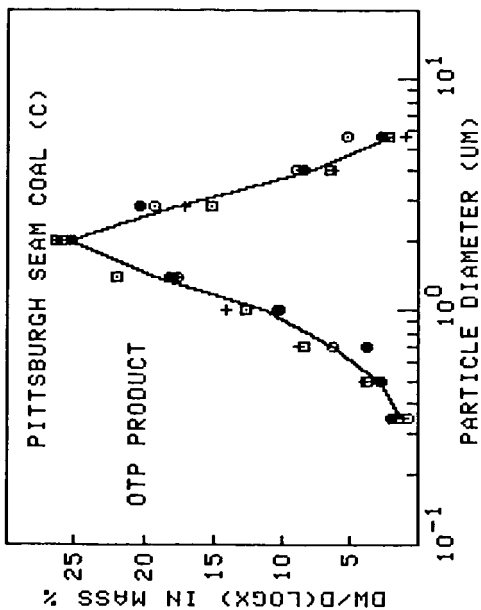


FIGURE 6: THE EFFECTS ON PRODUCT COAL PARTICLE SIZE DISTRIBUTION OF THREE CHEMICAL ADDITIVES WHILE MILLING AT CONSTANT CONDITIONS. (●) No Additives; (○) 2 lbs/ton Calcium Hydroxide; (□) 2 lbs/ton Sodium Ligninsulfonate; and (+) 20 lbs/ton Sodium Sulfosuccinate.

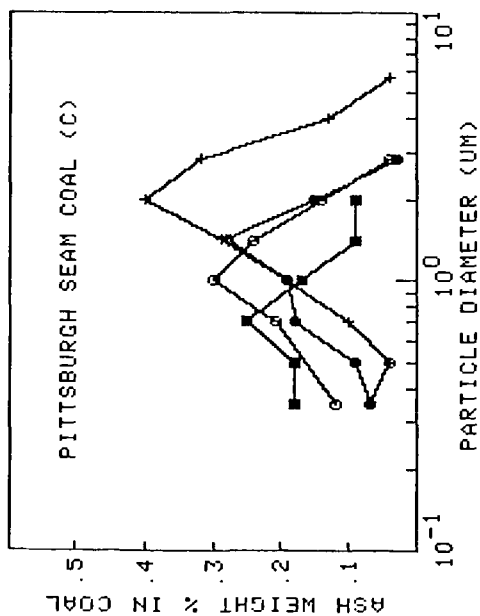


FIGURE 7: THE EFFECTS ON PRODUCT COAL PARTICLE SIZE DISTRIBUTION OF THREE CHEMICAL ADDITIVES WHILE MILLING AT CONSTANT CONDITIONS. (+) No Additives; (●) 36 lbs/ton Ammonium Hydroxide; (○) 7.9 lbs/ton Sodium Hydroxide; and (■) 20 lbs/ton Sodium Ligninsulfonate.

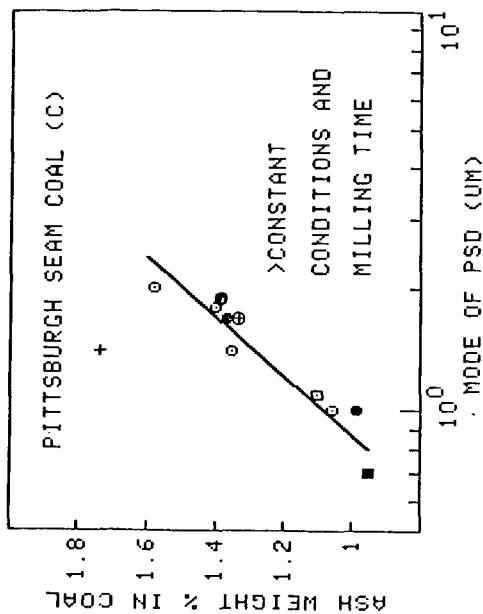


FIGURE 8: WEIGHT PERCENT ASH IN PRODUCT COAL VERSUS THE MODE OF THE PARTICLE SIZE DISTRIBUTION OF THE PRODUCT COAL. (○) No Additives; (●) 36 lbs/ton Sodium Hydroxide; (□) 7.9 lbs/ton Ammonium Hydroxide; (■) 20 lbs/ton Sodium Ligninsulfonate; (+) 20 lbs/ton Calcium Hydroxide; (●) 2 lbs/ton Sodium Ligninsulfonate; and (+) 20 lbs/ton Sodium Sulfosuccinate.

CHEMICAL TREATMENT PRIOR TO PHYSICAL COAL BENEFICIATION

A. B. Walters

Florida Power & Light Company
P.O. Box 14000
Juno Beach, Florida 33408

ABSTRACT

Conventional wisdom dictates that chemical treatment of coal should follow physical beneficiation. This ordering is expected to achieve reduced consumption and improved access of chemical reagents to the smaller, partially demineralized coal particles which result from physical cleaning. The advantages of reversing this conventional order of treatment, particularly for coal demineralization, are often overlooked. Chemical pretreatment can greatly improve the grindability of coal prior to the final size reduction required for physical beneficiation. The use of inexpensive chemical reagents can greatly reduce the disadvantage of higher reagent consumption. Prior chemical treatment can also selectively remove inorganic components which adversely affect coal ash behavior in combustion equipment. The effectiveness of subsequent physical coal demineralization can be improved by chemical pretreatment, especially for physical processes which exploit surface chemistry. Examples describing the advantages of chemical processing prior to physical coal beneficiation are included in this talk.

INTRODUCTION

Coal beneficiation research and development programs are commonly targeted to the dual objectives of sulfur and gross mineral matter removal. Many programs are primarily guided by environmental new source performance standards (NSPS) for coal-burning facilities. Attractive technical approaches to coal beneficiation which cannot meet NSPS are given limited attention. Beneficiation objectives in addition to sulfur and gross mineral matter removal, such as improved combustion behavior, reduced slagging and fouling, improved grindability, and compatibility with emission control equipment, are often ignored.

Earlier efforts to meet NSPS and restrictive oil-backout requirements concentrated on coal hydroliquefaction. These efforts yielded conceptual processes capable of producing highly desulfurized and demineralized coal-based fuels suitable for replacing petroleum-based fuels or feedstocks. High projected process capital costs and modest overall energy yields have discouraged the further development of these conceptual processes.

Relatively high energy yields and relatively low capital and operating costs are achievable with many commercially available coal beneficiation processes. Unfortunately, these processes are capable of only modest reductions in sulfur and gross mineral matter. Newer, conceptual processes are again embarking on the path of "super-clean" coal, the same path that led to

non-competitive product costs in the case of hydroliquefaction. Other, less ambitious approaches capable of improving the performance of coal-burning equipment via coal beneficiation may be more practical. In particular, inexpensive chemical treatment prior to near-conventional physical coal beneficiation may achieve many coal beneficiation objectives.

COAL BENEFICIATION OBJECTIVES

Coal can be beneficiated to meet a variety of objectives related to its use as a heat-producing fuel. These objectives include:

- ° reducing sulfur content for reduced SO_x emissions;
- ° reducing gross mineral matter content for reduced total particulate emissions and ash production;
- ° reducing moisture levels for improved efficiency;
- ° improving grindability for reduced grinding costs;
- ° preserving combustible volatiles content for needed combustion behavior;
- ° improving carbon burnout characteristics for improved efficiency and compatibility with particulate control equipment; and
- ° reducing selected mineral components to reduce slagging and fouling characteristics of the coal ash.

Many of these objectives are in conflict. Reduced SO_x in flue gases can reduce the efficiency of electrostatic precipitators due to high particulate electrical resistivities. Gross mineral matter reduction can change the composition of resulting coal ash leading to lower coal ash fusion temperatures and increased slagging and fouling; this may in some cases be the result of contamination by beneficiation aids, such as magnetite fines carried-over during heavy media separations. Severe chemical treatments to remove sulfur and mineral matter may significantly reduce the combustible volatiles content of the coal. Very low mineral matter levels can lead to high unburned carbon levels in fly ash particulates which may reduce the efficiency of electrostatic precipitators due to low particle electrical resistivity.

Despite these conflicts, a few general objectives can be selected for top priority. Coal pyrites contribute to increased SO_x and particulate emissions and to increased slagging and fouling due to increased iron in the coal ash. Pyrite removal is an important objective for coal beneficiation. Modern coal burning applications typically require fine coal grinding (ca. <200 mesh). This is true for dry, pulverized coal firing or for coal-water mixture fuels intended for oil-backout. Improved coal grindability would significantly reduce the subsequent costs of coal utilization. The preservation of combustible volatiles in the coal is also important. It is especially important for coal/water mixture fuels due to the high moisture levels (ca. 30-40 weight percent

water) in these fuels. The preservation of combustible volatiles limits the severity, particularly temperatures, which can be employed in coal beneficiation. Pyrite removal from many coals can be improved by fine grinding. It can also be improved if fresh pyrite particle surfaces can be rendered more hydrophilic prior to froth flotation for mineral matter removal. The selective removal of alkali and alkaline earth minerals would also be desirable due to the resulting increase in coal ash fusion temperatures which would reduce slagging and fouling. In the case of dry, pulverized coal firing, the high costs of dewatering fine coal prior to burning might preclude the application of froth flotation following fine grinding.

These refined coal beneficiation objectives point towards a chemical treatment aimed at coal mineral matter, particularly the interfaces between mineral matter and the carbonaceous coal macerals. This treatment, not so very distinct from developing chemical comminution technologies should greatly improve subsequent grindability, significantly increase coal ash fusion temperatures, and preserve combustible volatiles. An additional objective of low costs requires that inexpensive reagents and treatment equipment be employed. An approach which may achieve these coal beneficiation objectives is currently under investigation at the Brookhaven National Laboratory (BNL). A pressurized carbon dioxide/water mixture is used as the chemical reagent for chemico-physical coal beneficiation⁽¹⁾.

CHEMICO-PHYSICAL COAL BENEFICIATION

Gaseous carbon dioxide is known to penetrate coal⁽²⁾ and to improve coal grindability⁽³⁾. Unlike chemical comminution caused by ammonia⁽⁴⁾, water enhances the swelling and fracturing of coal caused by carbon dioxide⁽¹⁾. The carbon dioxide/water mixture is reported to have a synergy which enhances the carbon dioxide fracturing of coal while selectively removing alkali and alkaline earth minerals. Significant improvements in coal grindability with very high retention of overall energy content and coal volatiles are reported. Subsequent sink/float studies have indicated selective fracturing of the interfaces of the mineral matter and the carbonaceous coal macerals⁽⁵⁾. Treatment effects on pyrite surface hydrophilicity for coal ground in the pressurized carbon dioxide/water mixture remain to be determined. Such improvements in the hydrophilic nature of fresh pyrite surfaces have been reported for aqueous sodium carbonate treatment at the same temperatures used in the BNL chemico-physical treatment (ca. 80°C)⁽⁶⁾.

A major drawback to this potentially effective coal beneficiation treatment is the costs of achieving the treatment conditions (ca. 750 psi, 80°C). An investigation of the effects of treatment conditions on coal beneficiation is being initiated to allow for an engineering study to evaluate the commercial potential of the BNL approach to coal beneficiation.

CONCLUSIONS

The BNL carbon dioxide/water coal beneficiation treatment shows promise for meeting important coal beneficiation objectives. This treatment appears suitable for beneficiating coals for dry, pulverized coal firing without subsequent physical coal beneficiation or for coal/water mixture fuels with subsequent physical beneficiation, e.g. froth flotation. Froth flotation is already included in the processes for some of the proposed commercial coal/water mixture preparation facilities. The effectiveness of the BNL treatment for enhancing pyrite surface hydrophilicity needs further study. Also needed is further study of the commercial potential of this coal beneficiation approach. Engineering studies await the results of more detailed investigations of the effects of varied treatment conditions.

REFERENCES

1. Sapienza, R. S., Slegeir, W. A., Butcher, T., and Healy, F., I. Chem. E. Symp. Ser. No. 83, 85 (1983).
2. Fuller, E. L., Jr. "Coal Structure" M. L. Gorbaty and K. Ouchi, Eds., Adv. Chem. Ser., 192, 293 (1981).
3. Czaplinski, A., and Holda, S., Fuel, 61 (12), 1281-2 (1982).
4. Silveston, P. L., Hudgins, R. R., Spink, D. R., Smith, B., and Mathieu, G, "Coal: Phoenix '80's" A. M. Al Taweel, Ed., Proc. 64th CIC Coal Symp., 1, 277-83 (1982).
5. Sapienza, R. S., personal communication.
6. Patterson, E. C., Report No. IS-ICP-64, EMRRI, Iowa State University, Ames, Iowa, Sept. 1978.

DECOMPOSITION OF PYRITE IN A COAL MATRIX DURING PYROLYSIS OF COAL

I. Stewart and S. G. Whiteway
Atlantic Research Laboratory, National Research Council

AND

P. J. Cleyle and W. F. Caley
Technical University of Nova Scotia

The high sulphur content of Eastern Canadian coals has led to a number of studies aimed at reducing these sulphur levels¹. In general about two thirds of the sulphur is pyritic, often occurring as small inclusions, and therefore difficult to remove by conventional beneficiation techniques.

In general when coal is pyrolysed the pyrite decomposes to pyrrhotite and H_2S is emitted. It has been reported² that not all of the sulphur from the pyrite/pyrrhotite transformation is emitted; some becomes trapped in the organic matrix as 'bound' sulphur. In ₃ investigations of the pyrolysis of Nova Scotian coal, Brothers' noted that when 95% of the pyritic sulphur was removed prior to pyrolysis, the residual organic sulphur in the char decreased by about 50% in comparison to that of char formed from the raw coal.

The present study deals with the pyrolysis of coal from the Prince Colliery in Cape Breton Island, Nova Scotia (Table 1). This particular coal was chosen both because of its high sulphur content (~4 wt.% S) and because it is typical of much of the proven reserves of the field.

Experimental

The coal was crushed and sieved on Tyler screens to -8 + 16 mesh, (1-2.4 mm). Approximately 2 g of coal was placed in an alumina boat and pyrolysed under argon in a tube furnace at a variety of temperatures and times.

After pyrolysis pieces of the coal were mounted using Fisher Chemical Co. 'Quickmount' cold-mounting resin, and polished in preparation for scanning electron microscopy (SEM). Representative pyrite crystals about 20 μm in diameter, and not near macropores or other discontinuities, were selected for study.

A Jeol-35 SEM microprobe equipped with energy- and wavelength-dispersive spectrometers was used for elemental analysis. Point analyses were carried out; these covered approximately 0.5 μm for the

pyrite and 1 μm for the coal. The standard atomic number, absorption and fluorescence (ZAF) corrections were applied to all analysis, using counting times of 200 seconds, an accelerating voltage of 15 KV, and a pyrite crystal as standard.

Results

The extent of pyrite decomposition was followed by obtaining S/Fe atomic ratios at various points across selected pyritic inclusions. Figure 1 is a plot of this ratio vs. "distance from the edge of the inclusion" for seven particles pyrolysed at different temperatures. The duration of pyrolysis was 15 - 20 hours. It is apparent that the transformation from pyrite to pyrrhotite in Prince coal mainly occurs in the temperature range 500-550°.

Figure 2 is a plot of wt.% S as a function of distance from the inclusion/coal interface into the matrix. This demonstrates the constant background level of organic sulphur in the coal matrix surrounding undecomposed pyrite particles at 400 and 500°. In contrast, it is clear that the sulphur content is enhanced around pyrite particles that had been pyrolysed at 550, 600 and 700°C, and that sulphur transfer has occurred.

Figure 3 shows the effect of time on this sulphur transfer during pyrolysis at 600°C. It can be seen that the total amount of sulphur transferred remains approximately constant after 15.5 hours and that the depth of penetration of sulphur into the surrounding organic matrix does not increase with time of pyrolysis.

Discussion

A. Transformation Temperature

At 400°C and 500°C very little decomposition occurred, while at 600°C and 700°C transformation was virtually complete. At 550°C, however, the transformation was incomplete within the 20 hours given for pyrolysis, the results indicating a pyrite core surrounded by a pyrrhotite shell. These results indicate that pyrite in Prince coal begins to pyrolyse between 500 and 550°C; this is in general agreement with temperatures reported by other authors⁴.

B. Sulphur Transfer

The results of this study indicated that there was little transfer of sulphur from pyrite to the surrounding organic matrix of coal not heated beyond 500°C. This is similar to the findings of Raymond and Hagan⁵ who examined unreacted coal by SEM.

The extra sulphur observed around the decomposed pyrite in the present study therefore was formed as a result of the pyrolysis reactions. Radio-tracer work using ^{35}S -doped pyrite has shown that some of the sulphur released combines with the organic matrix with the formation of carbon-sulphur bonds⁶. It has been suggested⁷ that during pyrolysis sulphur migrates within the iron sulphide as S^{2-} . At the surface of the FeS charge transfer, reaction and desorption would lead to a variety of compounds.

Considering the hydrogen-rich environment presented by the decomposing coal matrix, one important sulphur compound would be H_2S , which would begin to diffuse away from the FeS/coal interface through the pores of the matrix. Active carbon sites, that are being generated simultaneously by devolatilization of the coal matrix, also could react with the sulphur trapping it as newly formed and strongly bound "organic" sulphur. In the ^{35}S tracer work referred to above, 38% of the overall sulphur liberated in the decomposition of the pyrite became fixed as "organic" sulphur.

Figure 1 shows that at 600°C a typical pyrite grain has decomposed entirely to pyrrhotite within 15.5 hours. Referring to Fig. 3 it is significant that the depth of penetration did not increase with increasing time, which indicates that the trapped sulphur was not mobile. In addition, therefore, we may conclude that diffusion in the matrix is not an important mechanism for migration of sulphur from the pyrite/coal interface. The main transfer mechanism for the sulphur that does escape probably is pore-diffusion of H_2S .

The data of Fig. 2 can be used to estimate the amount of sulphur trapped in a spherical shell around a pyrite particle, and to compare it with the amount of sulphur known to be released by the pyrite/pyrrhotite decomposition. Within the uncertainties of this order-of-magnitude calculation we concluded that all the sulphur released from a small, well-embedded, pyrite particle in Prince coal becomes trapped in the coal matrix. However, it should be pointed out again that during the pyrolysis of macro amounts of coal a considerable amount of pyritic sulphur is released into the gas phase as H_2S ; presumably this originates with pyrite of a more massive nature or which is not so well embedded in the matrix.

Summary

The decomposition temperature of pyrite in Prince coal was found to be between 500 and 550°C as determined using a SEM-microprobe. In addition, some of the sulphur liberated in this decomposition became trapped in the coal matrix surrounding the pyrite crystals. For small crystals, well embedded in the coal matrix, all the sulphur released by the decomposing pyrite becomes trapped as "organic" sulphur.

References

1. Tibbetts, T. E. and Montgomery, W. J.
Canmet Rep. 76-40 (publ. 1976).
2. Yergey, A. L., Lampe, F. W., Vestal, M. L., Day, A. G., Fergusson, G. J., Johnston, W. H., Synderman, J. S., Essenhigh, R. H. and Hudon, J. E.
Ind. Eng. Chem. Process. Des. Develop. 1974, 13, 233.
3. Brothers, J. A.
Proceedings of 1983 International Conference on Coal Science, Pittsburgh, 1983, p. 537.
4. Luganov, V. A. and Shabalin, V. I.
Can. Met. Quart. 1982, 21, 157.
5. Raymond, R. and Hagan, R. C.
Scanning Electron Microscopy. 1982, 2, 619.
6. Medvedev, K. P. and Petropolskaya
UKHIN. 1968, 19, 137.
7. Attar, A.
Fuel. 1978, 57, 201.

Table 1. Proximate Analysis and Sulphur Forms of Prince Coal

Constituent	Weight Percent (moisture free basis)
Moisture	5.5*
Volatiles	27.8
Ash	19.9
Carbon	52.4
Sulphur:	
Pyritic	3.33
Sulphatic	0.34
Organic	1.13
Total	4.80

* On "as received" basis

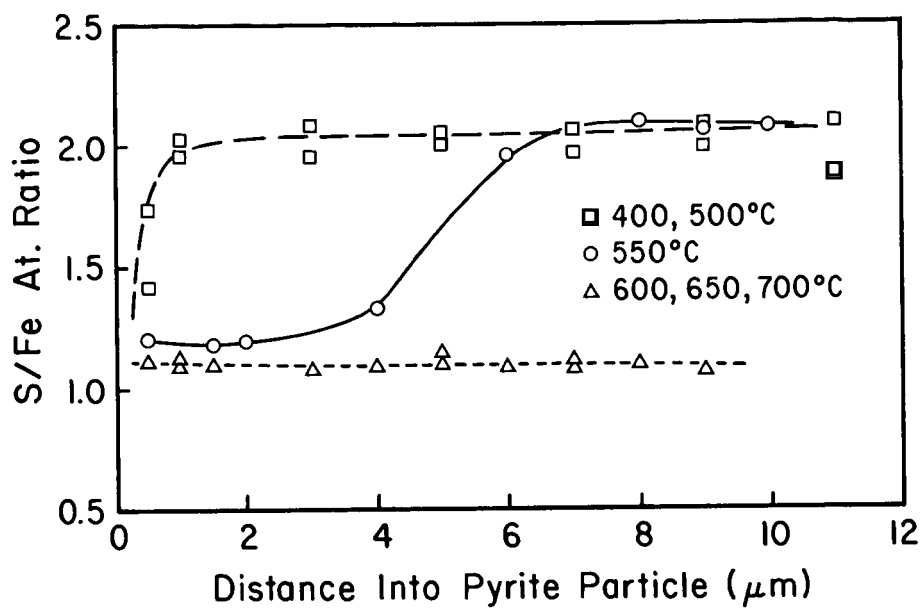


Fig.1 Decomposition of FeS_2 to FeS as coal is heated above 500° .

Fig.2 Sulphur from decomposed pyrite trapped in matrix of coal.

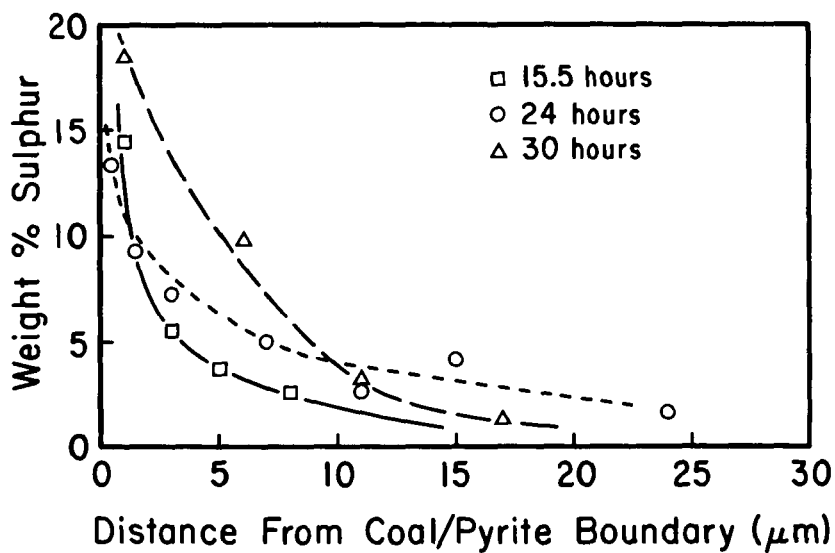
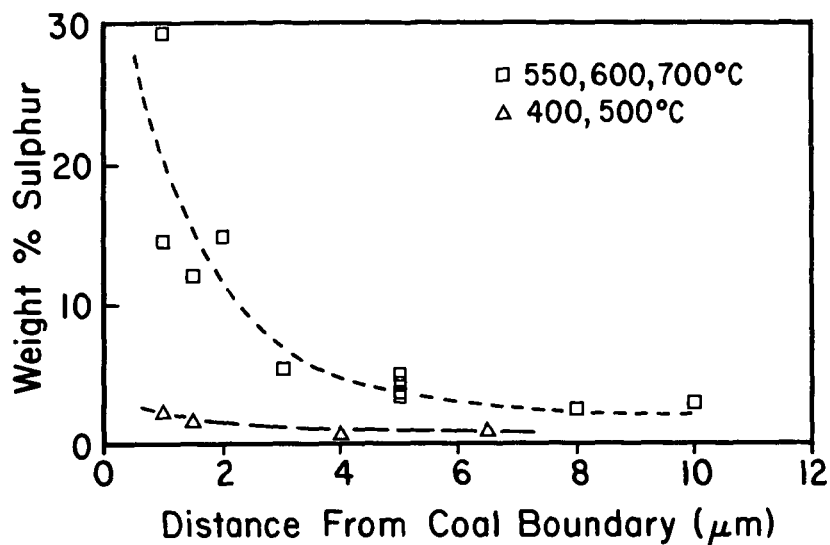


Fig.3 Stability with time of sulphur trapped in matrix of coal.